PROCEEDINGS

SEVENTH JAPAN-US CONFERENCE

ON

PHOTOCHEMICAL AIR POLLUTION

November 29-30, 1982
Tokyo, JAPAN

US DELEGATION

Dr. B. Dimitriades, Chairman
Environmental Sciences Research
Laboratory
USEPA

Dr. A. P. Altshuller
Environmental Sciences Research
Laboratory
USEPA

JAPANESE DELEGATION

Mr. Danjuro Miki, Chairman
Environment Agency

Mr. Saburo Kato
Environment Agency

Dr, Toshiichi Okita
National Institute for
Environmental Studies

Dr. Naoomi Yamaki
Saitama University

Dr. Hajime Akimoto
National Institute for
Environmental Studies

Mr, Tetsuhito Komeiji
Tokyo Metropolitan
Research Institute for
Environmental Protection

Dr. Haruo Tsuruta
Yokohama Research Institute for
Environmental Protection

Dr. Shinji Wakamatsu
National Institute for
Environmental Studies

COMPILED BY
AIR QUALITY BUREAU
ENVIRONMENT AGENCY
3-1-1, Kasumigaseki, Chiyoda-ku, Tokyo, JAPAN

PROCEEDINGS

SEVENTH JAPAN-US CONFERENCE

ON

PHOTOCHEMICAL AIR POLLUTION

November 29-30, 1982
Tokyo, JAPAN

US DELEGATION

Dr. B. Dimitriades, Chairman
Environmental Sciences Research Laboratory
USEPA

Dr. A. P. Altshuller
Environmental Sciences Research Laboratory
USEPA

JAPANESE DELEGATION

Mr. Danjuro Miki, Chairman
Environment Agency

Mr. Saburo Kato
Environment Agency

Dr, Toshiichi Okita
National Institute for Environmental Studies

Dr. Naoomi Yamaki
Saitama University

Dr. Hajime Akimoto
National Institute for Environmental Studies

Mr, Tetsuhito Komeiji
Tokyo Metropolitan Research Institute for Environmental Protection

Dr. Haruo Tsuruta
Yokohama Research Institute for Environmental Protection

Dr. Shinji Wakamatsu
National Institute for Environmental Studies

COMPILED BY
AIR QUALITY BUREAU
ENVIRONMENT AGENCY
3-1-1, Kasumigaseki, Chiyoda-ku, Tokyo, JAPAN

Printed in January 1983

by the

JAPAN ENVIRONMENT AGENCY

3-1-1, Kasumigaseki, Chiyoda-ku

Tokyo, JAPAN

PREFACE

This conference is a part of the activities fostered under the Japan-US Environmental Agreement negotiated between the two countries in August, 1975. The purpose of the Environmental Agreement and associated activities is to develop environmental awareness and to promote cooperation between the Japan and US in effort to reduce air pollution. Cooperative activities pertaining to photochemical air pollution were commenced in June, 1973, with the conduct of the first joint Japan-US Conference on Photochemical Air Pollution. As of todate such Conferences have been held as follows:

First Conference:	1973, Tokyo, Japan
Second Conference:	1975, Tokyo, Japan
Third Conference:	1976, Raleigh, NC
Fourth Conference:	1978, Honolulu, Hawaii
Fifth Conference:	1980, Tokyo, Japan
Sixth Conference:	1981, Research Triangle Park, NC
Seventh Conference:	1982, Tokyo, Japan

TABLE OF CONTENTS

Page

Introduction ---------- vi

Agenda of Meeting ---------- viii

Joint Communique ---------- x

Technical Papers

1. Countermeasures for Photochemical Air Pollution in Japan (Miki) ---------- 1
2. Atmospheric Reaction Mechanisms for Photochemical Ozone/ Oxidants (Dimitriades) ---------- 19
3. Smog Chamber Study of Photochemical Ozone Formation: Reactivities of Hydrocarbon-NO_x Mixtures and Sampled Ambient Air (Akimoto) ---------- 27
   [Ref.] Correlation of the Ozone Formation Rates with Hydroxyl Radical Concentrations in the Propylene-Nitrogen Oxide Dry Air System: Effective Ozone Formation Rate Constant ---------- 45
4. Further Development and Validation of EKMA (Dimitriades) ---------- 71
5. Acid Rain (Deposition) Chemistry and Physics (Altshuller) ---------- 77
6. Status of Recepter Models (Altshuller) ---------- 91
7. Recent Development of Aerosol Studies in Japan (Yamaki) ---------- 105

Appendices

Agenda of Joint Meeting ---------- 131

Technical Papers

1. The Problem of Acid Rain in Japan (Kato) ---------- 133
2. Progress in Photochemical Air Quality Simulation Modeling (Demerjian) ---------- 145
3. Researches on Acid Rain in Japan (Komeiji) ---------- 175
   [Ref.] A Numerical Model of Acidification of Cloud Water ---------- 229
4. Urban Ozone Modeling Developments in the U.S. (Dimitriades) ---------- 241
5. A Numerical Simulation of Local Wind and Photochemical Air Pollution (Kimura) ---------- 257
6. Transport and Transformation of Air Pollutants by Land and Sea Breezes (Tsuruta) ---------- 287
7. Evaluation of Eight Linear Regional-scale Sulfur Models by the Regional Modeling Subgroup of the United States/Canadian Work Group 2 (Demerjian) ---------- 315

8. Field Studies on Photochemical Air Pollution in Japan
(Wakamatsu) ---------- 333
[Ref.] A Lagrangian Observation of Polluted Air Mass
Using Aircraft ---------- 349
[Ref.] Distribution of Photochemical Pollutants and their
Three-Dimensional Behavior covering the Tokyo
Metropolitan Area ---------- 363
9. U.S. Studies on Stratospheric Ozone (Wiser) ---------- 393
10. Intrusion of Stratospheric Ozone into the Troposphere
(Muramatsu) ---------- 413
11. The Vertical Distributions of CF_2Cl_2, $CFCl_3$ and N_2O
over Japan (Hirota) ---------- 425

INTRODUCTION

Replacing Dr. Seigi Yoshizaki, Director of Air Quality Bureau, Environment Agency, who could not attend the meeting on urgent business, Mr. Danjuro Miki, Director of Planning Division, Air Quality Bureau, Environment Agency, welcomed the delegates. Dr. Basil Dimitriades, head of the U.S. delegation, thanked the organizers of the Seventh Conference.

SEVENTH JAPAN-US CONFERENCE ON PHOTOCHEMICAL AIR POLLUTION

Conference Room
Restaurant Castle
2-1-1 Uchisaiwai-cho, Chiyoda-ku
Tokyo, Japan

November 29–30, 1982

AGENDA

Monday, November 29, 1982

Acting Chairman: Mr. D. Miki

10:00 – 10:40	Opening Remarks	Dr. S. Yoshizaki (Director of Air Quality Bureau)
	Introduction of Participants Election of Session Chairman Approval of Conference Program	
10:40 – 11:00	Refreshments	

Session Chairman: Dr. B. Dimitriades

11:00 – 12:00	Countermeasures for Photochemical Air Pollution in Japan	Mr. D. Miki
12:00 – 13:30	Lunch	
13:30 – 15:00	Atmospheric Reaction Mechanisms for Photochemical Ozone/Oxidants	Dr. B. Dimitriades
	Smog Chamber Study of Photochemical Ozone Formation: Reactivities of Hydrocarbon-NO_x Mixtures and Sampled Ambient Air	Dr. H. Akimoto
15:00 – 15:30	Refreshments	
15:30 – 17:00	Further Development and Validation of EKMA	Dr. B. Dimitriades
	Acid Rain(deposition) Chemistry and Physics	Dr. A. P. Altshuller
17:30 – 19:30	Reception	

Tuesday, November 30, 1982 Session Chairman: Mr. D. Miki

10:00 - 10:45	Status of Receptor Models	Dr. A. P. Altshuller
10:45 - 11:15	Refreshments	
11:15 - 12:00	Pecent Development of Aerosol Studies in Japan	Dr. N. Yamaki
12:00 - 13:30	Lunch	
13:30 - 15:00	General Discussion Plans for Future Activities Preparation of Joint Communique Conclusion of Meeting	

Tokyo -----> Tsukuba

SEVENTH JAPAN-US CONFERENCE OF PHOTOCHEMICAL AIR POLLUTION JOINT COMMUNIQUE

The seventh Japan-US Conference on Photochemical Air Pollution was held in Tokyo, Japan, on November 29 - 30, 1982. The US delegation consisted of Dr. B. Dimitriades (Head of delegation) and Dr. A. P. Altshuller; the Japanese delegation consisted of Mr. D. Miki (Head of delegation), Mr. S. Kato, Dr. T. Ohkita, Dr. N. Yamaki, Dr. H. Akimoto, Dr. H. Tsuruta, Dr. S. Wakamatsu and Mr. T. Komeiji.

The two delegations discussed the following subjects:

- Countermeasures for photochemical air pollution in Japan
- Atmospheric reaction mechanisms
- EKMA Model
- Acid rain chemistry and physics (deposition)
- Studies on sampling, atmospheric chemistry/ removal, and source apportionment of ambient aerosol

Particular interest on the part of the US delegation was expressed in on-going and planned photochemical smog chamber studies in Japan and in recent Japanese developments regarding mechanism of photochemical ozone formation in the atmosphere. The Japanese delegation was interested in the latest EKMA Model for photochemical air pollution countermeasures, Source Apportionment Model for aerosol countermeasures, and acid rain studies in the US. Both delegations agreed to promote exchanging information in such areas furthermore.

The two delegations tentatively agreed to hold the next meeting of Photochemical Air Pollution Panel in the US. The date and agenda of the next meeting will be coordinated through future communications between the two Panel cochairmen.

Tokyo, November 30, 1982

Dr. Basil Dimitriades
Head of US delegation

Mr. Danjuro Miki
Head of Japanese delegation

COUNTERMEASURES FOR PHOTOCHEMICAL AIR POLLUTION IN JAPAN

Presented by D. Miki

Japan Environment Agency

Report on Curbing Hydrocarbons Emissions from Stationary Sources

In addition to promoting emergency measures to prevent photochemical air pollution, the Environment Agency has been striving to compile and analyze relevant knowledge and reduce the substances that cause the phenomenon.

Hydrocarbons are among the substances that trigger photochemical smog. The importance of measures to curb their emissions from stationary sources was stressed in a document on the "direction of measures against photochemical smog," which was approved by a relevant conference on April 8, 1975, and in a report which was submitted by the Central Council for Environmental Pollution Control on August 13, 1976.

The stationary sources discharging hydrocarbons and the way they are discharged are greatly diversified, as is emission control technology. Because of the need to take reduction measures according to cases, a panel of experts was set up in November 1979, to grasp the realities of emissions, appraise emission control technology, and consider other relevant matters.

The experts, led by Naoomi Yamaki, professor at the Faculty of Engineering of Saitama University, have recently presented a report. On the basis of the report, the Environment Agency will announce its policy on measures to curb hydrocarbons emissions from stationary sources and do its best to promote them. The gist of the report follows below.

I. PRESENT STATE OF PHOTOCHEMICAL AIR POLLUTION AND NECESSITY FOR CONTROLLING THE EMISSION OF HYDROCARBONS

1. Present state of photochemical air pollution

Danger to the health from photochemical air pollution became a problem after the event at Rissho High School in July, 1970. Since then serious studies have been made and preventive measures have been taken one after another. Thus, the situation of photochemical air pollution has tended to improve.

However, photochemical oxidant concentrations in most areas exceeded the ambient air quality standard and in addition, warnings based on the Article 23 of the Air Pollution Control Law are still often issued. In these last two years, the number of days when a warning was issued decreased remarkably (Fig. 1) partially due to the influence of the cool summer. But in view of the fact that many warnings were issued in May and in the beginning of June this year, the present condition seems to allow buildups of highly concentrated pollution in certain weather conditions. Furthermore, warnings have been issued also in the outer suburbs of large cities, and in a survey on the influence of photochemical smog on plants, the influence on plants was found to have spread. In these situations, photochemical air pollution has become a problem covering a wide area.

As can be seen, photochemical air pollution still remains a difficult problem, and in future the conditions of pollution must be carefully watched, and proper control measures taken.

2. Generation mechanism of photochemical air pollution

Photochemical air pollution refers to a phenomenon in which air containing hydrocarbons (HC) and nitrogen oxides (NOx) emitted from various sources reacts with sunlight (ultraviolet rays), affected by various weather conditions, to produce oxidants (Ox) such as ozone (O_3), and peroxyacylnitrates (PANs), nitrates, aldehydes, etc. To clarify such a complicated generation mechanism involves many difficulties. For this reason, research is being made energetically in two different approach, that is, in chamber studies to clarify the processes of reaction and in field studies to mainly clarify the processes of transport and diffusion, and information has been accumulating steadily.

(1) Chamber studies

Hitherto, various chambers have been used, to make studies concerning the photooxidation reactions in the environment and in an artificial atmosphere, and very accurate experiments are being made in low concentrations close to environmental conditions (Note 1). According to the information obtained from these chamber studies (Note 2), in order to lower the production of ozone in the region with excessive hydrocarbons like in the normal atmosphere, it is surmised to be necessary to take measures to (1) decrease the emission of nitrogen oxides to suppress the possible amount of ozone production by lowering the nitrogen oxide concentration, and (2) decrease the emission of hydrocarbons to suppress the rate of ozone production by lowering the non-methane hydrocarbon (NMHC) concentration.

(2) Field studies

Since the generation mechanism of photochemical air pollution in our country is closely linked with the land and sea breeze generated in coastal areas, it is important to clarify the processes of transport drift and diffusion as well as the reaction mechanism, to determine the relationship between oxidants and non-methane hydrocarbons. For this purpose, field studies have been made mainly in the Kanto Area, and as a result, precious information has been obtained. For example, it has been found necessary to investigate photochemical air pollution as a phenomenon over two or more continuous days, in an area where the circulation of air is poor.

Based on these results, efforts are being made to develop a simulation technique to secure the quantitative relationship between the emission of nitrogen oxides and hydrocarbons and the concentration of photochemical oxidants under various weather conditions in more detail.

3. Emergency urgent necessity for controlling stationary sources of hydrocarbons

As has been already pointed out, to prevent the generation of photochemical oxidants, it is necessary to decrease the emission of nitrogen oxides and hydrocarbons which generate such oxidants, and as mentioned in the previous section, the specific functions of both these materials in producing photochemical oxidants are gradually being elucidated. Of these, for nitrogen oxides, severe legal regulations have been enforced step by step for emission from stationary sources and motor vehicles.

For hydrocarbons, legal regulations for the emission of hydrocarbons from motor vehicles have also been intensified step by step since 1970, and control measures have been enacted against stationary sources by governments ordinances of local, etc. As a result, as shown in Table 1, the non-methane hydrocarbon concentration in the environment has tended to decrease a little.

However, in the present situations of photochemical oxidants, measures for preventing production are still insufficient, and efforts must be made successively to suppress the materials causing such production. Above all, control of hydrocarbons emitted from stationary sources is still lax compared with control against motor vehicles (Table 2), and the intensification of control measures is an urgent metter.

(Note 1)

In clarification of the processes of reaction of photochemical air pollution by the chamber studies, attention is being paid to the generation of ozone as a main component (usually 80 to 90%) of photochemical oxidants, for analysis. With regard to hydrocarbons as a primary pollutant, the non-methane hydrocarbons (NMHC) excluding methane, the reactivity of which can be neglected, are adopted as an index.

(Note 2)

According to studies concerning photo-oxidation reaction in the system of propylene (C_3H_6), nitrogen oxides and air, using the large chamber at the National Institute for Environmental Studies, it has been clarified that if propylene concentration is excessive ($[C_3H_6]_0/[NOx]_0 \gtrsim 3$), the maximum ozone concentration ($[O_3]$ max) caused by light irradiation continued until ozone has reached the maximum concentration is proportional to the square root of the initial nitrogen oxide concentration ($\sqrt{[NOx]_0}$) irrespective of the initial propylene concentration, that the maximum ozone production rate at that time is proportional to the initial propylene concentration ($[C_3H_6]_0$) and the maximum concentration of hydroxyl radicals ([OH] max) existing in the reaction system, and so on.

Furthermore, it has been proven that these relations derived for propylene are effective also for other hydrocarbons, and it has been almost confirmed that the same applies also in studies concerning photo-oxidation reaction in the environment using the Environment Agency's movable chamber.

II. REALITIES OF HYDROCARBONS EMISSIONS FROM STATIONARY SOURCES AND APPRAISAL OF EMISSION CONTROL TECHNOLOGY

It is an urgent problem to curb hydrocarbons emissions from stationary sources. But consideration of emission control measures must be preceded by overall knowledge of the realities of emissions and a precise appraisal of emission control technology.

1. Realities of Emissions

Hydrocarbons are used and handled in a great variety of fields in the form of crude oil, refined oil products, petrochemical products and the like. The industries and facilities, which discharged hydrocarbons, are also greatly diversified.

The amount of emissions, as surveyed by the Environment Agency, is given in Table 3. Emissions dropped from about 1.3 million tons in 1973 to 1.14 million tons in 1978, a difference of about 160,000 tons. In both years, industries using solvents accounted for about 80 percent of the total. Particularly, the industries having to do with coating accounted for about 50 percent of the total.

The survey dealt only with what seems to be principal emission sources. It did not cover all the industries and facilities which discharge hydrocarbons. The industries and facilities, which were not covered, need to be surveyed hereafter.

To check on the effect which the amount of emissions has on concentrations in the environment, the experts carried out case studies on the areas where data on emission sources and data on concentrations in the environment are in order.

Since a diffusion model, which reproduces environmental concentrations from the amount of emissions, has been developed, it now can be expected that a national picture will emerge as detailed data on emission sources and environmental concentrations become available.

2. Appraisal of Emission Control Technology

Technological measures to curb emissions are as varied as the diversity of the modes of emissions. Principal ones are given below.

(1) Control through equipment

a) Evaporation control equipment

This approach is designed to prevent the discharge of hydrocarbons from storage and other facilities by changing their structure. The relevant devices include floating roofs, inner floating roofs, and vapor return equipment.

b) Disposal equipment

This involves the use of devices to capture hydrocarbons emitted from various kinds of facilities for recovery or disposal by incineration. The devices come in five different kinds. They are respectively based on an absorption methods, an absorption method, a condensation method, a direct incineration method, and a catalytic oxidation method.

(2) Control through raw materials

Many of the conventional materials used for the production of paints, printing ink and the like contain hydrocarbons in the form of solvents and diluents. Consequently, hydrocarbons evaporate when paints, printing ink and the like are put to use. A good way to combat this is to switch from these conventional materials to materials which contain no hydrocarbons at all or only a little of them (referred to as low-pollution materials in the report presented by the experts).

Other case-by-case approaches in accordance with the modes of emissions are possible.

Control measures dealing with respective categories of emission sources are scheduled to be discussed in the next issue.

3. Emission Control Measures by Sources

Reflecting the great diversity of processes whereby hydrocarbons are discharged and the way they are discharged, emission control measures that can be applied are also greatly diversified.

Under the circumstances, the Environment Agency's panel of experts categorized emission sources by the kinds of facilities and industries and studied and assessed the control technology that is applicable to each category.

Their conclusions are shown in Tables 4 and 5, which list emission control measures by facilites and industries. The details of these measures were put together in the form of "Technological Guidelines for the Control of Hydrocarbon Emissions from Stationary Sources," so that they will serve as a manual. The guidelines are attached to the report from the panel.

III. DIRECTION OF EMISSION CONTROL MEASURES FOR STATIONARY SOURCES

1. Basic Direction of Control Measures

The rate of compliance for the environmental quality standard on photochemical oxidants is low. On the other hand, damage attributed to photochemical smog persists in the major cities and their environs, chiefly in summer. Under the circumstances, it is urgently necessary to curb hydrocarbon emissions from stationary sources as they are among the agents that trigger the smog.

In addition, some of the numerous substances which come under the category of hydrocarbons are feared to be toxic. For this reason and from the viewpoint of conserving resources, emission controls are also required.

Two approaches are conceivable. One is a realistic and technological approach. This involves making the most of the currently available technology to curb emissions and promoting technological development at the same time to achieve a further limitation.

The other is a total volume control approach. With a view to achieving the environmental quality standard on photochemical oxidants and keeping the environmental concentrations of hydrocarbons at levels that comply with the standard, this calls for emission controls to be based on the findings of research on the effects which individual emission sources have on the environmental concentrations of hydrocarbons.

With regard to the total volume control approach, the quantitative cause-and-effect relationship between photochemical oxidants and hydrocarbons in the atmosphere and the effects hydrocarbon emissions from respective sources have on the environmental concentrations of hydrocarbons in the area where they are located have to be cleared up. As has been stated earlier, these points are still in the process of being clarified.

As for the realistic and technological approach, the Environment Agency's panel of experts has drafted "Technological Guidelines for the Control of Hydrocarbon Emissions from Stationary Sources." The agency believes that this approach of making the most of the currently available technology to curb hydrocarbon emissions should be pursued for the time being.

There still remain aspects that require consideration before the introduction of legal controls to implement this approach, since data on individual factories and other business establishments are scarce and there are facilities and industries, whose emissions are still to be determined.

For the time being, therefore, the Environment Agency will promote maximum emission control efforts in line with local conditions on the basis of the report and "Technological Guidelines" which are attached to the report, particularly the control measures by facilities and industries, and at the same time, it will do its best to compile data on emission sources with the cooperation of local governments to work out specific methods to be employed when legal controls are introduced.

In addition, the agency will continue to compile knowledge to determine the quantitative cause-and-effect relationship regarding the mechanism whereby photochemical oxidants come into being and the environmental concentrations of hydrocarbons. It will also do its best to streamline the system to carry out anti-pollution measures in emergencies affecting wide areas.

2. Actions for Emission Control

In order to promote the control of hydrocarbon emissions from stationary sources on the basis of the basic direction discussed above, the following requests will be made to quarters concerned on improvement to be achieved through changes in equipment and raw materials, for which Tables 4 and 5 serve as guidelines, and other necessary emission control measures, and on the collection of data.

(1) To local governments; 1 to exercise emission control guidance on factories and other business establishments discharging hydrocarbons in line with the report; 2 to consider the introduction of regulatory measures or strengthen those already in place in accordance with local conditions; 3 to check on the degree of improvement brought about by emission controls, including measurement surveys; 4 to put in order data on principal emission sources and report them to the Environment Agency; 5 to adopt on a preferential basis low-pollution materials for the use of public enterprises over which local authorities have jurisdiction and give consideration to the timing of coating; 6 to strive to build a monitoring network on the environmental concentrations of non-methane hydrocarbons.

(2) To industrial organizations which have to do with factories and other business establishments discharging hydrocarbons; 1 to advance emission control measures in the related industries in line with the report; 2 to carry out research and development and work for the introduction of emission controls where their implementation is technically difficult now; 3 to cooperate in the periodic surveys the Environment Agency conducts to check on progress on the amount of emissions and emission control measures.

(3) To the related central government departments: to adopt positively low-pollution materials for public enterprises under their jurisdiction and give attention to the timing of coating. They will also be asked to cooperate by exercising guidance on industries which have closely to do with their operations and handle hydrocarbons and by helping them with remedial actions.

Table 1 Change in the concentration of non-methane hydrocarbons in the environment

(Simple mean values of 23 monitoring stations measured continuously from 1976 to 1980)

Fiscal year	1976	1977	1978	1979	1980
Annual mean (ppmC)	0.51	0.53	0.45	0.40	0.44

Table 2 Emission ratio of hydrocarbons between years (estimated)

	1978 fiscal year/ 1983 fiscal year
Mobile sources	0.61
Stationary sources	0.88

(Remarks) The figures for mobile sources were obtained for motor vehicles in Tokyo and three other prefectures (Chiba, Saitama, and Kanagawa) (hydrocarbons), and the figures for stationary sources were obtained over the whole country. The ratio of "mobile sources" to "stationary sources" in fiscal 1978 was estimated as 1 : 2 in Tokyo and the three prefectures.

Table 3 Hydrocarbons Emissions by Principal Stationary Sources

(Unit: ton)

Emission sources				FY 1973				FY 1978			
				Amount of emission	Ratio in total (%)	Total	Ratio in total (%)	Amount of emission	Ratio in total (%)	Total	Ratio in total (%)
Oil			Plants	100	-	198,000	(15.2)	100	-	162,800	(14.3)
			Refineries and storage facilities	67,000	(5.2)			42,400	(3.7)		
			Oil tanks and storage facilities	68,100	(5.2)			41,800	(3.7)		
			Gas stations	62,800	(4.8)			78,500	(6.9)		
Petro-chemicals			Plants	69,800	(5.4)	74,700	(5.8)	27,000	(2.4)	30,600	(2.7)
			Storage facilities	4,900	(0.4)			3,600	(0.3)		
Solvents	Coating		Paint production	1,600	(0.1)	623,500	(47.9)	1,500	(0.1)	616,500	(54.3)
		Coating processes	Automobiles	37,500	(2.9)			45,500	(4.0)		
			Ships	19,900	(1.5)			16,700	(1.5)		
			Others	564,500	(43.4)			552,800	(48.7)		
	Printing		Ink production	200	-	109,800	(8.4)	100	-	99,200	(8.7)
			Printing processes	109,600	(8.4)			99,100	(8.7)		
	Other Solvents		Solvents for adhesives	42,500	(3.3)	295,200	(22.7)	32,800	(2.9)	226,600	(20.0)
			Solvents for removal of grease from metals	85,000	(6.5)			52,800	(4.6)		
			Solvents for cleaning	116,500	(9.0)			106,000	(9.4)		
			Solvents for rubber production	51,200	(3.9)			35,000	(3.1)		
Grand total				1,301,200	(100.0)	1,301,200	(100.0)	1,135,700	(100.0)	1,135,700	(100.0)

Table 4. Emission Control Measures by Facilities

Facilities	Industries Discharging HC	Emission Control Measures
1. Storage facilities	Petroleum and coal products/Chemical and allied products/Food and tobacco/Electricity and gas/Mining/Wholesale and retail trade/Transport	(1) Floating roof tanks or inner floating roof tanks should be installed, with light colors, such as white and silver white. Or treatment apparatuses employing the condensation or absorption method or the like should be installed. (2) Particularly in the case of new large-scale facilities, tanks with floating roofs or inner floating roofs should be installed. (3) Where vehicles like tank cars and tank trucks are used for shipment, vapor return equipment or treatment apparatuses should be installed. Further studies are needed whether measures for loading into ships should be taken or not. (4) Vapor return equipment is applicable to facilities in certain conditions, such as underground storage facilities at gas stations. (5) Such other measures as the cooling of material in storage and the use of breather valves should be taken.
2. Transport facilities (ships, tank trucks, drum cans, and the facilities)	Petroleum and coal products/Chemical and allied products/Mining/Wholesale and retail trade/Transport	A close link should be established with storage facilities or treatment apparatuses through the use of vapor return equipment and the like. As for measures for ships, further studies are needed because there are such problems as ascertaining the anti-pressure resistance of the hull and the levels of oil in the holds.
3. Coating facilities (including drying facilities)	Lumber and wood products/Furniture and fixtures/Rubber products/Leather tanning and leather products/Ceramic, stone and clay products/Steel/Nonferrous metals and products/Fabricated metal products/General machinery/Electrical machinery, equipment and supplies/Transportation equipment/Precision instruments and machinery/Ordnance/Miscellaneous manufacturing industries/Services/Construction	(1) Less pollutive coatings should be used for outdoor coating or similar instances in which large machines and the like are coated indoors. (2) In other instances of indoor coating, less pollutive coatings should be used or treatment apparatuses employing the adsorption, catalytic incineration, or thermal incineration method or the like should be installed. (3) Coating efficiency should be raised through improvement in the coating methods, coating processes and the like.
4. Printing facilities (including drying facilities)	Publishing, printing and allied industries/ Pulp, paper, and paper products/Lumber and wood products/Textile mill products/ Ceramic, stone and clay products/Fabricated metal products/Nonferrous metals and products/Miscellaneous manufacturing industries	(1) Less pollutive printing ink should be used. (2) Treatment apparatuses employing the adsorption or catalytic incineration method or the like should be installed in the printing processes for metal plate printing and the like.
5. Degreasing facilities	Textile mill products/Furniture and fixtures/Nonferrous metals and products/ Fabricated metal products/General machinery/Electrical machinery, equipment and supplies/Transportation equipment/Precision instruments and machinery/Ordnance/Miscellaneous manufacturing industries/ Services	(1) Treatment apparatuses employing the adsorption or condensation method or the like should be installed. (2) Alkaline, emulsive or low-volatile solvents should be used in the degreasing process.
6. Adhesive coating facilities (including drying facilities)	Textile mill products/Lumber and wood products/Pulp, paper, and paper products/Rubber products/Leather tanning and leather products/Ceramic, stone and clay products/Steel/Nonferrous metals and products/Electrical machinery, equipment and supplies/Miscellaneous manufacturing industries/Construction	(1) Less pollutive solvent adhesives should be used. (2) Treatment apparatuses employing the adsorption or catalytic incineration method or the like should be installed.
7. Others	Hydrocarbons are also conceivably emitted from other sources, such as dry distillation, mixing, kneading, and extraction facilities, although the realities of emissions are not necessarily clear. To cope with this problem, the realities of emissions should first be cleared up and then appropriate ones should be selected from among the control technologies that are listed in Chapter 3 of the report from the panel. This procedure will probably be enough. In some cases, treatment apparatuses are already in place.	

(by the Japan Industrial Standards)

Table 5 Emission Control Measures by Industries

Facilities, Countermeasures / Industries	Facilities Discharging HC	Emission Control Measures
1. Petroleum industry		
Refineries	Storage facilities	(1) Floating roof tanks or inner floating roof tanks should be installed, with light colors used for the tanks, such as white and silver white. Or treatment apparatuses employing the condensation or absorption method or the like should be installed. (2) Particularly in the case of new facilities, tanks with floating roofs or inner floating roofs should be installed.
	Transportation facilities	(1) Treatment apparatuses employing the condensation or absorption method or the like should be installed.
	Production facilities	(1) Strict maintenance checks and management.
Oil storage yard	Storage facilities	(1) Floating roof tanks or inner floating roof tanks should be installed, with light colors, such as white and silver white. Or treatment apparatuses employing the condensation or absorption method or the like should be installed.
	Transportation facilities	(1) Treatment apparatuses employing the condensation or absorption method or the like should be installed.
Gas stations	Underground storage facilities	(1) Vapor return equipment or treatment apparatuses employing the condensation or adsorption method or the like should be installed. Or both of them should be installed.
2. Chemical industry	Production facilities	(1) Treatment apparatuses employing the thermal incineration or condensation method or the like should be installed. Or hydrocarbons should be recovered within the relevant processes. (2) Strict maintenance checks and management.
	Storage facilities	(1) Floating roof tanks or inner floating roof tanks should be installed, with light colors, such as white and silver white. Or treatment apparatuses employing the condensation or absorption method or the like should be installed.
3. Automobile industry	Degreasing facilities	(1) Treatment apparatuses employing the activated charcoal adsorption method or the like should be installed.
	Coating facilities (including drying facilities)	(1) Less pollutive coatings should be used. (2) Coating efficiecny should be raised. (3) Treatment apparatuses employing the catalytic incineration or thermal incineration method or the like should be installed.
4. Shipbuilding industry	Coating facilities	(1) Less pollutive coatings should be used. (2) Coating efficiency should be raised.
5. Construction industry	Coating facilities	(1) Less pollutive coatings should be used. (2) Coating efficiency should be raised.
	Adhesive coating facilities	(1) Less pollutive solvent adhesives should be used.
6. Printing industry	Printing facilities (including drying facilities)	(1) Less pollutive printing ink should be used. (2) Treatment apparatuses employing the adsorption or catalytic incineration method or the like should be installed.
7. Cleaning business	Cleaning facilities (including drying facilities)	(1) Treatment apparatuses employing the adsorption or absorption method should be installed.
8. Manufacture of rubber products	Production facilities (tires, rubber and other footwear, rubber belts, and the like)	(1) Manufacturers should switch from solvent-containing paste to non-solvent gruel-like paste, from solvent-type coatings to low pollutive coatings, and from solvent-type model-removing agents to water-based agents. (2) Treatment apparatuses employing the adsorption, catalytic incineration or thermal incineration method or the like should be installed. (3) Measures should be taken to raise the viscocity of rubber, seal facilities and containers, and improve operating methods.

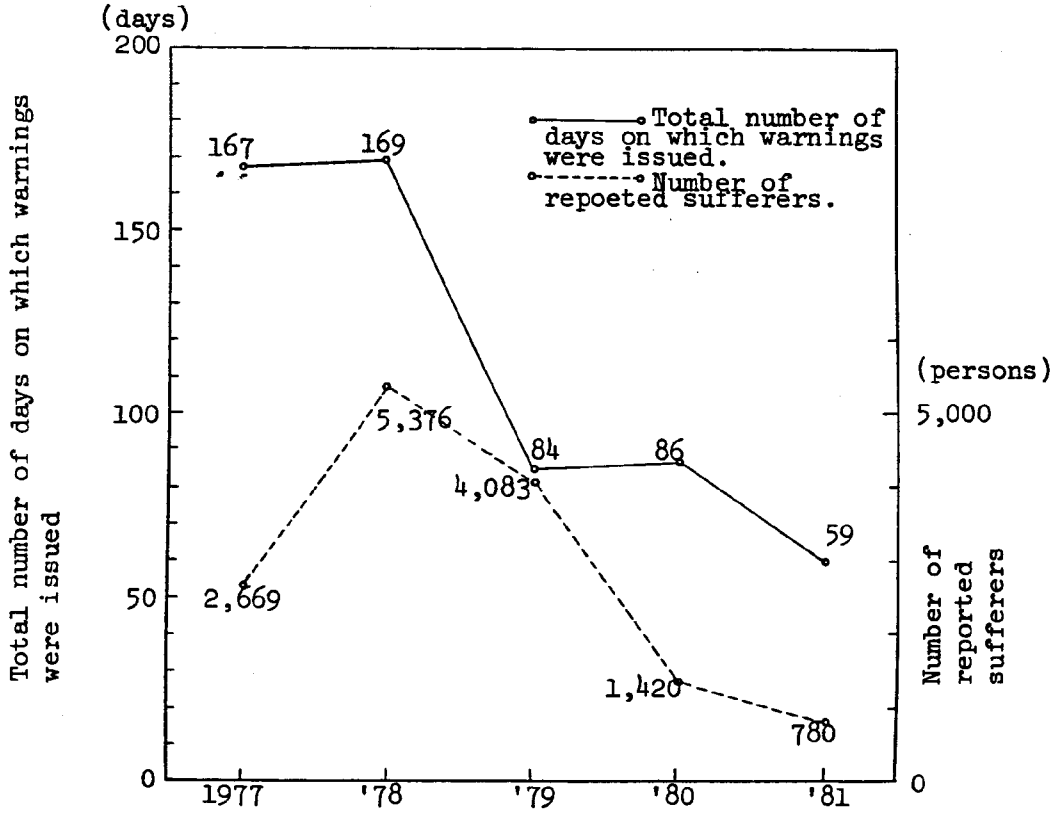

Fig. 1 Changes in the total number of days on which warnings were issued and in the number of reported sufferes (1977 to 1981)

ATMOSPHERIC REACTION MECHANISMS FOR PHOTOCHEMICAL OZONE/OXIDANTS

presented by B. Dimitriades

Environmental Sciences Research Laboratory

USEPA

Current U.S. research in the area of atmospheric reaction mechanisms for photochemical O_3/O_x formation is focussed on the following specific problems or information gaps:

(1) Large uncertainties of predictions of current mechanistic models for O_3 yields from single-day photochemical HC/NO_x systems.

(2) Lack of validated detailed mechanisms for use with regional O_3 air quality models (RAQSM).

(3) Lack of validated, detailed mechanistic models capable of predicting other-than-O_3 oxidants.

These problems/gaps are discussed, next, in some detail.

(1) Uncertainties in Current Mechanistic Model Predictions.

There are several mechanisms currently in existence in the U.S. explaining the atmospheric formation of O_3/O_x. These mechanisms include among others the EKMA, Carbon Bond, Demerjian, and Cal Tech mechanisms, and differ in several respects as shown in Table 1. Each of the four mechanisms was developed and validated independently, and until recently we had not intercompared them through parallel testing against a single set of data. Such an intercomparison was done recently using one set of smog chamber data and one set of field data, and results were presented and discussed in a workshop on EKMA, conducted on December 15-16, 1981, at Research Triangle Park, North Carolina (Proceedings Volume I has been sent to Japan; Volume II is forthcoming.).

The smog chamber data, from irradiated auto exhaust mixtures of constant HC composition, showed no large differences among the four mechanisms in their ability to predict smog chamber O_3 yields from given HC and NO_x concentrations. When the mechanisms, however, were coupled to a simple dispersion model and were used to predict ambient O_3 concentrations from emissions and meteorology input data, the predictions disagreed with observations substantially. Furthermore, the disagreement differed from mechanism to mechanism. Also, when the mechanisms were used, through isopleth diagrams, to compute HC control requirements for NAAQS-O_3 achievement, the results differed considerably from mechanism to mechanism. The conclusions from these mechanism intercomparison studies were (a) that most or all of the current mechanisms have substantial inaccuracies, and (b) that the existing smog chamber and real atmosphere data are not sufficiently diverse to permit a more informative evaluation of the various mechanisms.

Mechanistic inaccuracies can be either in the description of the chemical pathways or in the kinetic data used. Pathway errors occur either because pathways are not known in detail (e.g. photooxidation of aromatic HCs) or because they are used in an excessively condensed form (e.g. in lumped mechanisms). In Table 1, the four mechanisms shown consist each of 36 to 76 reaction steps. Considering that in actuality there are hundreds of operative steps, one may suspect that one cause of error in these four mechanisms is the lack of sufficient detail, particularly, with respect to the aromatic HC chemistry. It should be stressed here, however, that increasing the number of steps is not without penalty; it raises the computer capability demands of the model, a problem which can be prohibitive in the case of AQSMs.

Errors associated with the kinetic data used also may be significant. Table 2 shows the rate constant values used in the inorganic chemistry sections of the four mechanisms. It can be seen that only in four (out of 25 in all) cases the same value is used in the four mechanisms; in 20 cases, the values vary by factors of 1.1 to 6.3. A comparable situation exists in connection with the organic chemistry sections of the mechanisms.

Our viewpoint on this problem is that several, different-type research efforts need to be done before we can solve or minimize this problem. First, additional mechanism intercomparison studies should be conducted that would hopefully enable us to understand why the various mechanisms show these differences in behavior. It may be crucially important, for example, to have an in-depth understanding of the inaccuracies introduced by the different types of "lumping" in the lumped mechanisms versus the inaccuracies of the "surrogate" mechanisms. In these studies, it would be useful to include as many as possible <u>different</u> mechanisms, and it is for this reason that we would like to invite Japan to participate in the effort by conducting a study to compare the Akimoto/Carter mechanism (for propylene) with the other mechanisms in existence. In view of the much greater number of reaction steps that compose the Akimoto/Carter mechanism, inclusion of this mechanism in the mechanism intercomparison effort is more than justified.

A mechanism intercomparison effort has already been initiated in the U.S. and involves six mechanisms: Carbon Bond III (SAI), ELSTAR (ERT), LIRAQ, Photochemical Box Model mechanism (Demerjian), and EKMA (Dodge). We visualize a complementary effort to be conducted by Japan that will include one or more of the above mechanisms as well as those of Akimoto/Carter, of Derwent (England), and possibly others. If this is of interest to the Japanese delegation, we would be happy to arrange for communications between the Japanese and U.S. experts on the details of this cooperative effort.

Additional efforts are needed, in our viewpoint, (a) to scrutinize existing kinetic data and develop a standard set of such data to be used in all mechanisms, and (b) to develop standard sets of smog chamber data against which to evaluate all mechanisms. With respect to the latter need, again, we would invite Japan to discuss with us consideration of Dr. Akimoto's smog chamber data as one of the requisite standard sets of data.

(2) Lack of Validated Detailed Mechanisms for Use with Regional Air Quality Models (RAQSM).

Relative to the mechanisms used with the urban models, the regional model mechanisms must have two additional features: the ability to treat terpene chemistry, and the ability to treat multi-day chemistry. In response to this need there are laboratory and modeling studies on-going within ESRL addressed to the chemistry of terpenes, and also smog chamber and modeling studies addressed to multi-day chemistry. In the latter studies, the most difficult problem is caused by chamber wall-related interferences (e.g. adsorption/description of NO_2, HNO_3, PAN, N_2O_5, HCHO, etc.). Besides the mechanism of the multi-day chemical process, we need also to elucidate the mechanism by which "aged" pollutant mixtures affect the atmospheric chemistry of fresh pollutants. First indications are that such effects, to a large extent, can be explained in terms of effects of the aldehydes present in "aged" pollutant mixtures.

(3) Mechanistic Models for Non-Ozone Oxidants.

Recently, there has been an increasing concern in the U.S. about oxidants other than O_3, namely: NO_2, PAN, HNO_3, aldehydes, organic nitrates, and H_2O_2. While these species are products of the same atmospheric chemical process that produces O_3, it is not correct to assume that the same mechanistic models that predict O_3 can also predict (equally well) these other species. Development of models specific for those species requires an abundance of laboratory and field data on formation and fate of these species, as in the case of O_3. Acquisition of these data requires, in turn, availability of analytical methods for these species. ESRL is now conducting smog chamber and modeling studies for those oxidant species, and is also attempting to improve the analytical methodology required, especially for ambient HNO_3, particulate nitrates, and H_2O_2.

Table 1. Some characteristics of existing mechanisms

	Ekma	Carbon Bond-III	Demerjian	Cal Tech
No. of reactions:	76	75	37	52
(Inorganic):	(23)	(19)	(18)	(25)
(Organic):	(53)	(56)	(19)	(27)
	Fixed	Variable	Variable	Variable
Representative organic species used:	Propylene Butane Formald. Acetald. Propionald. Butyrald.	Ethylene Olef. Bond Para. Carbon Arom. Carbon	C_3-Olefin C_6-Paraffin C_8-Aromatic C_1-Aldehyde	Ethylene Olefin Aromatic Paraffin Formald. Aldehyde

Table 2. Comparisons of Inorganic Chemistries of Four Mechanisms

Rate Constant at 298K (ppm^{-1} min^{-1})

	Reaction	Carbon-Bond III	Dodge	Demerjian	Cal Tech	Variation, (highest/lowest)
1	$NO_2 \rightarrow NO + O$	k_1	k_1	k_1	k_1	--
2	$O + (O_2) + (M) \rightarrow O_3$	4.40×10^6	4.2×10^6	4.0×10^6	4.4×10^6	1.1
3	$NO + O_3 \rightarrow NO_2 + O_2$	26.6	25.0	22.0	23.5	1.2
4	$NO + O \rightarrow NO_2$	—	—	—	3.9×10^3	--
5	$NO_2 + O_3 \rightarrow NO_3 + O_2$	0.048	0.045	0.055	0.047	1.2
6	$NO_2 + O \rightarrow NO + O_2$	1.3×10^4	1.3×10^4	—	1.3×10^4	1.0
7	$NO_2 + O \rightarrow NO_3$	—	—	—	3.6×10^3	--
8	$OH + O_3 \rightarrow HO_2 + O_2$	100	84.0	87.0	82.3	1.2
9	$HO_2 + O_3 \rightarrow OH + 2O_2$	2.40	2.4	4.0	1.5	9.7
10	$OH + NO_2 \rightarrow HNO_3$	1.60×10^4	0.8×10^4	1.5×10^4	1.5×10^4	2.0
11	$OH + NO \rightarrow HONO$	9770	3,000	12,000	17,400	5.8
12	$NO + NO + (O_2) \rightarrow NO_2 + O_2$	1.50×10^{-4}	—	—	—	--
13	$OH + CO \rightarrow HO_2 + CO_2$	440	—	440	440	1.0
14	$NO + NO_3 \rightarrow NO_2 + NO_2$	2.80×10^4	1.3×10^4	1.1×10^4	2.7×10^4	2.5
15	$NO_2 + NO_3 + H_2O \rightarrow 2HNO_3$	Heterogen	—	68	—	--
16	$NO + HO_2 \rightarrow NO_2 + OH$	1.20×10^4	1.2×10^3	1.2×10^4	1.2×10^4	1.0
17	$NO_2 + NO_3 \rightarrow N_2O_5$	—	5.6×10^3	—	3.9×10^3	1.4
18	$N_2O_5 \rightarrow NO_2 + NO_3$	—	22.0	—	6.9	3.2
19	$N_2O_5 + H_2O \rightarrow 2HNO_3$	—	5×10^{-2}	—	29×10^{-2}	5.8
20	$NO_2 + NO + H_2O \rightarrow 2HONO$	—	2×10^{-5} (?)	—	—	--
21	$2HONO \rightarrow NO + NO_2 (+H_2O)$	—	1×10^{-3}	—	—	--
22	$HO_2 + HO_2 \rightarrow H_2O_2 + O_2$	1.50×10^4	0.84×10^4	1.0×10^4	0.37×10^4	4.1
23	$H_2O_2 + h\nu \rightarrow 2OH$	—	$0.0024 \times k_1$	—	$0.0026k_1$	1.1
24	$HONO \rightarrow OH + NO$	$(\approx 0.06\ k_1)^*$	$0.38 \times k_1$	$0.19\ k_1$	$0.18\ k_1$	6.3
25	$NO_2 + HO_2 \rightarrow HNO_2 + O_2$	—	—	4.3	1.7	2.5
26	$NO_2 + HO_2 \rightarrow HNO_4$	—	—	2.3×10^3	1.7×10^3	1.4
27	$HO + HNO_2 \rightarrow NO_2 + H_2O$	—	—	9.6×10^3	9.6×10^3	1.0
28	$HNO_4 \rightarrow HO_2 + NO_2$	—	—	9.0	4.4	2.0
29	$O_3 + h\nu \rightarrow O(^3P)$	—	$0.054 \times k_1$	—	$0.072\ k_1$	1.3
30	$O_3 \rightarrow O^1D$	$(\approx 10^{-3}\ k_1)^*$	$2.7 \times 10^{-3} \times k_1$	—	—	2.7
31	$O^1D \xrightarrow{+(M)} O$	4.44×10^{10}	8.7×10^4	—	—	500,000
32	$O^1D + H_2O \rightarrow OH + OH$	3.4×10^5	19×10^5	—	—	5.6
32	Total number of Steps	19	23	18	25	

SMOG CHAMBER STUDY OF PHOTOCHEMICAL OZONE FORMATION: REACTIVITIES OF HYDROCARBON-NO_x MIXTURES AND SAMPLED AMBIENT AIR

presented by H. Akimoto

National Institute for Environmental Studies
Japan EA

Smog Chamber Study of Photochemical Ozone Formation: Reactivities of Hydrocarbon-NO_x Mixtures and Sampled Ambient Air

Hajime Akimoto and Fumio Sakamaki

Division of Atmospheric Environment
The National Institute for Environmental Studies

P.O. Tsukuba-gakuen, Ibaraki 305 Japan

Introduction

Quantitative charactrization of photochemical ozone formation in organics-NO_x-air mixtures is of critical importance in planning ozone control strategy based on smog chamber data and computer simulation. Particularly, when one challenges the computer modeling of the photochemical processes of the ambient air, "photochemical reactivity" of the polluted atmosphere has to be defined by some means in a quantitative manner. It should be noted here that one can not a priori postulate that the photochemical reactivity of the ambient air can be predicted properly from the "known" pollutant composition at hand. Since polluted ambient air contains numerous organic and inorganic compounds all of which are not necessarily analyzed by conventional analytical techniques, some unknown factor might affect the reactivity of such systems. Thus, it is very interesting and important to see if the photochemical ozone formation rate

in the ambient air can be predicted from the conventionally analyzed hydrocarbon composition assuming the additivity of the reactivity. By this reason, a new method for analyzing the photochemical ozone formation rate in organics-NO_x-air mixture has been developed and the reactivity of the sampled ambient air is evaluated quantitatively in the present study.

As a rate parameter which could be representative of ozone formation, NO oxidation rate has been recognized as a useful measure of the photochemical reactivity of various hydrocarbons (1). More recently, Darnall et al (2) has proposed an OH-hydrocarbon reaction rate constant as a measure of hydrocarbon reactivity. While these parameters have been used as scales for the classification of numerous hydrocarbons based on the reactivity, no direct general relationship between these parameters and the actual ozone formation rate observed in a photochemical run of a selected organics-NO_x mixture has been proposed. The present study concerns with the method of analyzing the ozone formation rate in organics-NO_x-air system and proposes a phenomenological rate parameter which is useful for representing reactivity of mixtures of organics. The analysis was first made on the propylene-NO_x-air system for which both the systematic smog chamber data and a detailed reaction model for computer simulation are available. Based on the analysis a phenomenological rate parameter, "effective ozone formation rate constant" will be proposed. Smog chamber runs for various single hydrocarbons as well as hydrocarbon mixtures were next carried out, and the effective ozone formation rate constants of various hydrocarbons were determined and the additivity rule of the rate constants was established. Finally, the smog chamber runs of sampled

ambient air were carrried out and the reactivity of the ambient air was evaluated applying the method of analysis proposed here.

Experimental

Experiments were carried out at 30°C using an evacuble and bakable photochemical smog chamber ($6m^3$) at NIES (3). The light source consists of 19 of 1 kw high pressure Xe are lamps with approapriate Pyrex filters. Experimental procedures for the runs with single hydrocarbons and synthetic mixtures were the same as reported previously (3,4). For the runs with the sampled ambient air, a large air sampler which is made of two plastic bellow-type bags (about 3.5 m^3 each when inflated) housed in a container was used. The air was sampled at 8:00-8:30 a.m. at a nearly city, Tsuchiura, carried to the Institute, and introduced into the evacuated chamber.

Hydrocarbons and oxygen containing compounds were analyzed by GC's after concentration. The DNPH-GC method was also used for the analysis of formaldehyde and acetaldehyde. Carbon monoxide was analyzed by a long-path FTIR (L = 221.5m).

Computer simulation were performed for the C_3H_6-NO_x-dry air runs using the detailed reaction model reported before (5).

Results and Discussion

(1) C_3H_6-NO_x-dry air

Analysis was first made for propylene runs using two reaction

parameters, maximum ozone formation rate, $(d[O_3]/dt)_{max}$, and maximum OH concentration, $[OH]_{max}$. Here the experimental maximum ozone formation rate $(d[O_3]/dt)_{max}$ is defined as the maximum slope of the plot of $[O_3]$ vs. irradiation time for each run and the experimental maximum OH concentration, $[OH]_{max}$, was obtained from the decay rate of propylene by assuming that the reacting species for C_3H_6 are only OH and O_3 (6). Fig.1 shows the plot of $(d[O_3]dt)_{max}$ vs. $[OH]_{max}$ for the runs with various $[NO_x]$ and k_1 (NO_2 photolysis rate) but with the same initial concentration of C_3H_6 ($[C_3H_6]_0$ = 0.50 ppm). The linear plot implies that $(d[O_3]/dt)_{max}$ is linearly proportional to $[OH]_{max}$. The proportionality was also confirmed by computer simulation as depicted in Fig.1. A proportionality between $(d[O_3]/dt)_t$ and $[OH]_t$ within a single run was next checked by computer simulation. As shown in Fig.2, $(d[O_3]/dt)_t$ is in general proportional to $[OH]_t$ until $d[O_3]/dt$ and [OH] reach their maximums except during the very early stage of photooxidation. After $d[O_3]/dt$ and [OH] reach their maximums, the ozone formation rate decreases faster than the decrease of [OH].

Fig.3 shows the plot of $(d[O_3]/dt)_{max}$ vs. $[OH]_{max}[C_3H_6]_0$ for the runs with defferent $[C_3H_6]_0$ and k_1. The plots of both series of runs fall on a single linear line going through the origin verifying an approximate relationship.

$$(d[O_3]/dt)_{max} = k_e^{C_3H_6} [C_3H_6]_0[OH]_{max} \qquad (I)$$

where $k_e^{C_3H_6}$ is the effective rate constant of photochemical ozone formation. The value of $k_e^{C_3H_6}$ is obtained to be 6.0 x 10^4 ppm^{-1} min^{-1}. The relationship was confirmed by the computer simulation as shown in Fig.3. In order to check the validity

of $k_e^{C_3H_6}$, the experimental and calculated ratios $(d[O_3]/dt)/([OH]_{max}, [C_3H_6]_0)$ were plotted as a function of $[C_3H_6]_0/[NO_x]_0$ in Fig.4. Solid curve is drawn through the calculated data points. However, since it was found by the computer modeling that at low $[C_3H_6]_0/[NO_x]_0$ ratio, time for $(d[O_3]/dt)$ and [OH] to reach their maximum does not coincide but the latter is delayed, the ratio of $(d[O_3]/dt)_{max}$ to $[OH]_{tmax}$ $[C_3H_6]_0$ is also shown in a dashed curve. Here $[OH]_{tmax}$ is the OH radical concentration at the time when $d[O_3]/dt$ reaches the maximum. From the above results, the effective ozone formation rate constant $k_e^{C_3H_6}$ is found to be defined as an apparent constant in the hydrocarbon excess region. More detailed discussion will be found in our seperate paper (7).

(2) Single Hydrocarbon-NO_x-humid air

The effective ozone formation rate constants for various hydrocarbons are next determined experimentally in the NO_x-humid air mixture. Series of smog chamber experiments for five olefins, twelve paraffins and nine aromatics have been carried out. As an example, the experimental results for toluene are depicted in Figs.5 and 6. As shown in Fig.5, for the runs with constant $[NO_x]_0$ and k_1, ozone formation rate is proportional to $[Toluene]_0$ while the apparent first order decay rate of toluene which is equivalent to $k_{OH}^{Tol.} \cdot [OH]_{max}$ is constant being independent of $[Toluene]_0$ under our experimental conditions. This verifies that the relationship similar to Eq.(I),

$$(d[O_3]/dt)_{max} = k_e^{i}[HC]_0^{i}[OH]_{max} \qquad \text{(II)}$$

can hold for the hydrocarbon-NO_x-air system in general and the specific k_e value for each hydrocarbon can be determined.

Fig.6 confirms that the similar dependence of k_e on $[HC]_0/[NO_x]_0$ is seen for toluene as in the case of proplene shown in Fig.4.

Table I summarizes the experimentally determined k_e values for various hydrocarbons studied. For comparison, literature values (8) of the absolute rate constants of OH-hydrocarbon reactions, k_{OH}, are also cited in Table I. Fig.7 shows the correlation of experimentally determined k_e values with the k_{OH} values. It is interesting to note that the k_e values correlate linearly with k_{OH} and has the same order of magnitude as k_{OH}. As demonstrated in Fig.7, the k_e values fall between the values of k_{OH} and $2k_{OH}$ in most of the cases. Rationalization of this finding has been discussed in our separate paper (7).

(3) Synthetic Hydrocarbon Mixture-NO_x-humid air

In order to confirm the additivity rule of the k_e value, synthetic hydrocarbon mixture-NO_x-humid air runs were next carried out. Fig.8 shows the time profile of C_3H_6-toluene mixture runs. In this series of runs, initial concentration of toluene was varied keeping the initial concentration of C_3H_6 (0.5 ppm) and NO_x (0.09 ppm) to be constant. Fig.9 represents the maximum ozone formation rate obtained from Fig.8 and the maximum OH radical concentration calculated from the decay of toluene. From these data it is now possible to compare the experimental k_e value obtained from

$$(d[O_3]/dt)_{max} = k_e^{obs}([C_3H_6]_0+[\text{Toluene}]_0)\ [OH]_{max} \qquad \text{(II)}$$

with the calculated k_e value,

$$k_e^{calc} = \frac{[C_3H_6]_0 k_e^{C_3H_6} + [\text{Toluene}]_0 k_e^{\text{Toluene}}}{[C_3H_6]_0 + [\text{Toluene}]_0} \qquad \text{(III)}$$

where the values of $k_e^{C_3H_6}$ and $k_e^{Toluene}$ are available in Table I as 4.64×10^4 and 1.12×10^4 ppm^{-1} min^{-1}, respectively. The comparison of k_e^{obs} and k_e^{calc} is depicted in Fig.10 demonstrating a good agreement.

The additivity rule of the k_e value was further confirmed by using the hydrocarbon mixture sample consisting of 23 components simulating the ambient air sample which will be discussed below.

(4) Sampled Ambient Air

Finally, smog chamber runs for sampled ambient air have been carried out and the data were treated according to the above method of analysis. Table II shows the initial concentrations of the organics and NO_x for the sample studied. In this case, the effective ozone formation rate constant on C_1 base, k_e , defined by

$$(d[O_3]/dt)_{av}^{exp} = k_e'^{exp}[OH]_{av}[NMOG(ppmC)]_0^M \qquad (IV)$$

was determined experimentally for each run. Here, the average OH concentration was obtained from the decay of hydrocarbons and $[NMOG]_0^M$ is the initial non-methane organics concentration in ppmC unit as determined by a so called "non-methane hydrocarbon monitor". The obtained value of k'^{exp}_e can be compared with the average ozone formation rate constants calculated by

$$\bar{k}_e = \frac{\Sigma k_e^i [OG]_0^i}{\Sigma [OG(ppmC)]_0} \qquad (V)$$

using the values of k_e^i obtained before for indivisual hydrocarbons (Table I). For oxygen-containing compounds for which k_e values have not been determined experimentally, $k_e = 1.5\ k_{OH}$ was assumed

tentatively.

Table III summarizes the experimentally determined $(d[O_3]/dt)_{av}$, $[OH]_{av}$, $k'_e{}^{exp}$ as well as calculated k'_e according to Eq.(V). Average was taken for 0~1 hour after the start of irradiation since the maximum ozone formation rate was always observed during this period for these runs. In table III, k'_e(NMHC) is the value calculated using only the non-methane hydrocarbons neglecting all oxygen-containing compounds and CO, while k'_e(NMOG) is the value calculated taking into account all organics and CO analyzed in the present study. The results showed that the sampled ambient air has substantially higher reactivity than expected from the additivity of k_e values for hydrocarbons only, but the effective ozone formation rate constant of the ampled ambient air can well be represented when oxygen-containing compounds and CO, are taken into account. Among the oxygen- containig compounds, aldehydes were found to contribute predominantly thus demonstrating the importance of their analysis in the ambient air for the prediction of photochemical air pollution.

Fig.11 shows the plot of $(d[O_3]/dt)_{av}$ vs. $[OH]_{av}[NMOG]_0^M$. The experimental points fall on a single straight line implying that the Eq.(IV) holds for these systems and the effective ozone formation rate constant does not differ too much for these samples. The average ozone formation rate constant of the particular ambient air investigated in this study was determined from the slope of the line as 5.42×10^3 $ppmC^{-1}$ min^{-1}.

Summary

1. In hydrocarbon excess region, the relationship

$$(d[O_3]/dt)_{max} = k_e[OH]_{max}[HC]_0$$

can hold in general and the phenomenological second order rate constant, ke, may be called the effective ozone formation rate constant.

2. The k_e values for various hydrocarbons of atmospheric importance have been determined and their additivity rule was confirmed.

3. The photochemical reactivity of the ambient air as expressed by the ozone formation rate constant was determined to be 5.4 x 10^3 $ppmC^{-1}$ min^{-1} for the particular samples studied. The reactivity was predicted successfully from the k_e values of analyzed organics constituents including CO, and the substantial importance of aldehydes to account for the contribution to the ambient air reactivity has been noted.

References

(1) W.A. Glasson, C.S. Tuesday, Environ. Sci. Technol., 4, 37 (1970).

(2) K.R. Darnall, A.C. Lloyd, A.M. Winer, J.N. Pitts, Environ. Sci. Technol., 10, 693 (1976).

(3) H. Akimoto, F. Sakamaki, M. Hoshino. G. Inoue, M. Okuda, Environ. Sci. Technol. 13, 53 (1979).

(4) F. Sakamaki, H. Akimoto, M. Okuda, Environ. Sci. Technol., 15, 665 (1981).

(5) F. Sakamaki, M. Okuda, H. Akimoto, Environ. Sci. Technol., 16, 45 (1982).

(6) H. Akimoto, F. Sakamaki, G. Inoue, M. Okuda, Environ. Sci. Technol., 14, 93 (1980).

(7) H. Akimoto, F. Sakamaki, "Correlation of the Ozone Formation Rates with Hydroxyl Radical Concentrations in the Propene-Nitrogen Oxide Dry Air System: Effective Ozone Formatin Rate Constant, accepted for publication in Environ. Sci. Technol.

(8) R. Atkinson, K.R. Darnall, A.C. Lloyd, A.M. Winer, J.N. Pitts Jr., Adv. Photochem., 11, 375-488 (1979).

Table I Effective Ozone Formation Rate Constants, k_e, of Hydrocarbons as Compared with K_{OH}

No.	Hydrocarbon	$ke(\pm\sigma)x10^{-3}$ ($ppm^{-1}min^{-1}$)	$k_{OH}x10^{-3}$ (a) ($ppm^{-1}min^{-1}$)
O-1	Ethylene	19±4	14.8
O-2	Propylene	40±10	37.1
O-3	1-Butene	43±8	52.2
O-4	Isobutene	75	75.0
O-5	1-Pentene	53±13	43.1
P-1	n-Butane	6.4±2.1	4.03
P-2	Isobutane	5.9	3.73
P-3	n-Pentane	7.9±1.6	5.54
P-4	Isopentane	7.4	4.6
P-5	n-Hexane	9.9±2.7	8.6
P-6	2-Methylpentane	27	7.4
P-7	3-Methylpentane	18	10.1
P-8	2,2-Dimethylbutane	6.2	2.9
P-9	2,3-Dimethylbutane	11	6.4
P-10	n-Heptane	5.8±1.4	9.3
P-11	2-Methylhexane	15	9.1
P-12	3-Methylhexane	20	9.1
A-1	Benzene	2.0	1.78
A-2	Toluene	11.2±1.4	9.5
A-3	Ethylbenzene	13	11.1
A-4	o-Xylene	34	21.2
A-5	m-Xylene	49±3	34.9
A-6	p-Xylene	25	22.6
A-7	1,2,4-Trimethylbenzene	86	59.2
A-8	1,3,5-Trimethylbenzene	160	92.4
A-9	p-Ethyltoluene	20	18.1

(a) R. Atkinson, K.R. Darnall, A.C. Lloyd, A.M. Winer and J.N. Pitts, Jr., Adv. Photochem. 11, 375 (1979)

TableII Initial Concentrations of the Constituents of the Sampled Ambient Air

Run	Data 1981	$[NMOG]_0^M$ ppmC	$[NO_x]_0$ ppm	CO ppm	R.H. %	Hydrocarbon Composition (mole %) Paraf.	Olef.	Arom.	Acet.	Unknown	$\Sigma[HC]_0$ ppb
9	3/16	0.26	0.032	0.79	6	44.7	20.2	18.1	14.5	2.6	43.1
10	3/18	0.40	0.052	1.19	8	43.8	18.5	20.3	15.1	2.4	66.6
11	3/23	0.44	0.063	1.33	27	39.6	21.8	19.5	17.3	1.8	80.3
12	7/27	0.37	0.055	0.42	50	37.6	14.4	37.6	9.0	1.3	25.6
13	7/29	0.40	0.032	0.43	60	34.3	11.7	46.8	6.0	1.2	40.7

-Continued

Run	Initial Concentrations (ppb v/v) HCHO	CH_3CHO	CH_3OH	C_2H_5OH	CH_3COCH_3	$\Sigma[NMOG]_0$ ppmC	$\frac{\Sigma[NMOG]_0}{\Sigma[NMOG]_0^M}$
9	11	12.0	5.6	3.1	4.8	0.20	0.82
10	14	11.8	8.3	6.9	4.9	0.32	0.80
11	13	14.6	4.3	1.7	4.3	0.37	0.84
12	39	24.3	26.9	8.8	45.6	0.31	0.84
13	24	11.0	17.3	3.4	11.8	0.28	0.70

Table III Experimental Results of the Sampled Ambient Air Runs

Run	$(d[O_3]/dt)_{av}^{exp}$ ppm min^{-1}	$[OH]_{av}$ 10^{-7} ppm	$k_e'^{exp}$ $ppmC^{-1}min^{-1}$	$\bar{k}_e'(NMHC)$ $ppmC^{-1}min^{-1}$	$\bar{k}_e'(NMOG)$ $ppmC^{-1}min^{-1}$
9	2.60×10^{-4}	2.09×10^{-7}	4.8×10^3	3.2×10^3	6.5×10^3
10	2.80	1.37	5.1	3.1	5.6
11	4.98	2.03	5.6	3.3	5.8
12	8.50	3.66	6.6	2.6	6.2
13	7.10	3.56	5.0	2.4	5.0

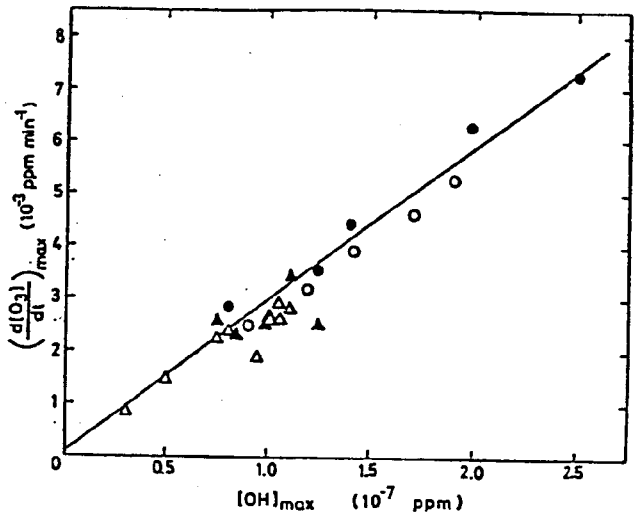

Fig.1
plot of $(d[O_3]/dt)_{max}$ vs. $[OH]_{max}$. Filled and open symbols are for observed and calculated values, respectively. $[C_3H_6]_0$=0.50 ppm. Variable $[NO_x]_0$ runs (▲,△), k_1=0.16 min^{-1}; variable k_1 runs (●,○) $[NO_x]_0$=0.09 ppm.

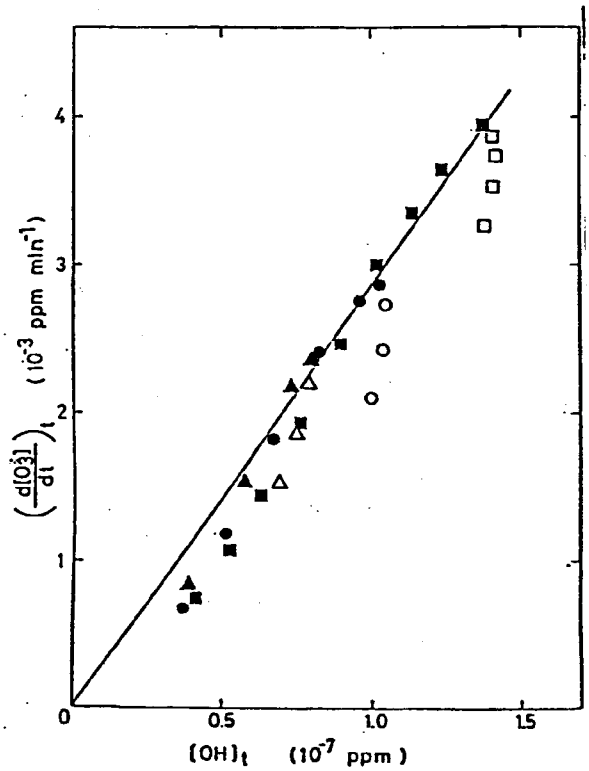

Fig.2
Plot of $(d[O_3]/dt)$ vs. $[OH]_t$ in three computer simulation runs. Filled and open sympols correspond to values before and after the $d[O_3]/dt$ reaches the maximum. $[C_3H_6]_0$=0.5 ppm

	$[NO_x]_0$	k_1
▲ △	0.045 ppm	0.16 min^{-1}
● ○	0.090	0.16
■ □	0.083	0.25

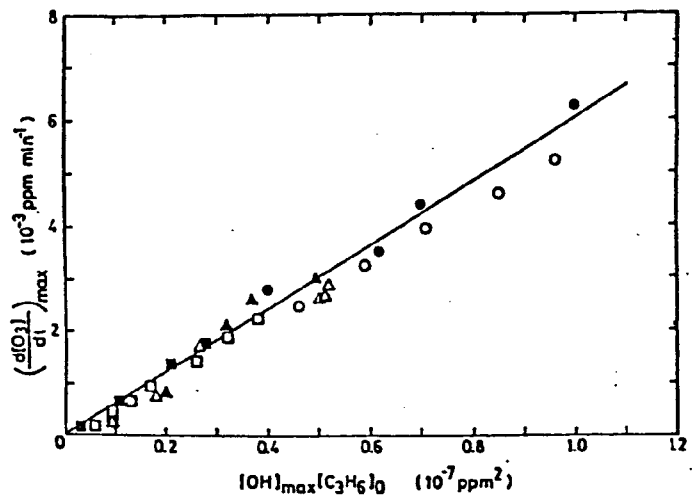

Fig.3
Plot of $(d[O_3]/dt)_{max}$ vs. $[OH]_{max} \cdot [C_3H_6]_0$. Filled and open symbols are for observed and calculated values, respectively. Variable $[C_3H_6]_0$ runs for $[NO_x]_0$=0.04 ppm (■,□) $[NO_x]_0$=0.09 ppm (▲,△), k_1=0.16 min^{-1}, Variable k_1 runs for $[C_3H_6]_0$=0.50 $[NO_x]_0$=0.09 ppm (●,○).

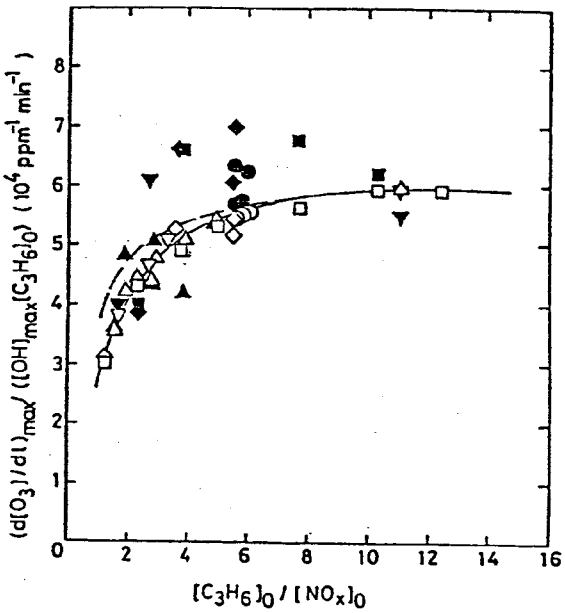

Fig.4
Plot of $(d[O_3]/dt)_{max}/[OH]_{max}\cdot[C_3H_6]_0$ vs. $[C_3H_6]_0/[NO_x]_0$ in the C_3H_6-NO_x-dry air system.

Dashed line shows the ratio of $(d[O_3]/dt)_{max}/([OH]t_{max}\cdot[C_3H_6]_0)$

Filled symbols are for the experimental and open symbols are for the calculated data points.

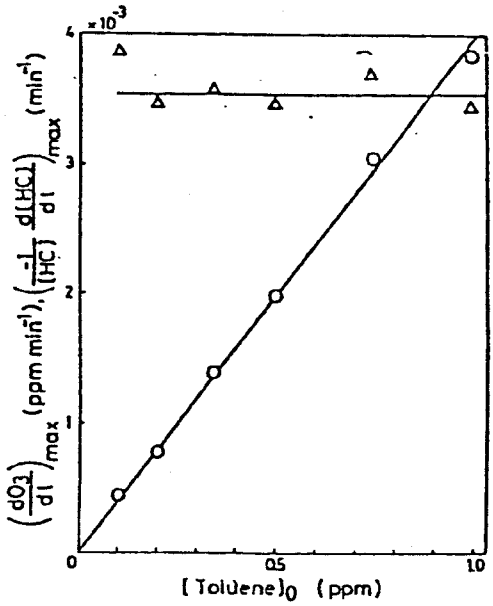

Fig.5.
Maximum ozone Formation rate (○) and maximum hydrocarbon decay rate (△) vs. $[Toluene]_0$ in the toluene-NO_x-humid air system. $[NO_x]_0 = 0.09$ ppm, $k_1 = 0.26$ min^{-1}.

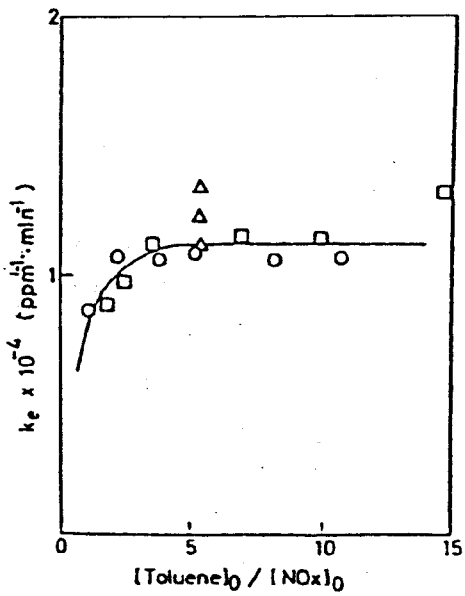

Fig.6.
Experimental values of k_e as a function of $[Toluene]_0/[NO_x]_0$ in the toluene-NO_x-humid air system.

○ : $[Toluene]_0$-varied run
□ : $[NO_x]_0$-varied run
△ : k_1-varied run

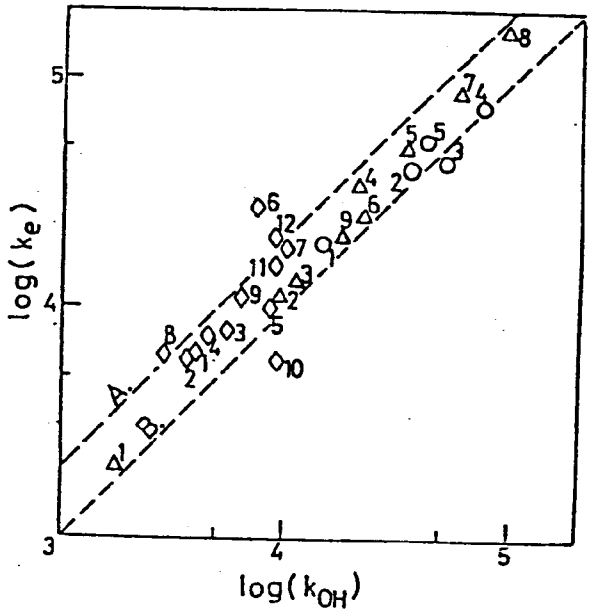

Fig.7
Correlation of k_e and k_{OH}.
line A; $k_e=2k_{OH}$, B; $k_e=k_{OH}$
○ olefins, ◇ paraffins
△ arromatics
Numbers correspond to those in Table I.

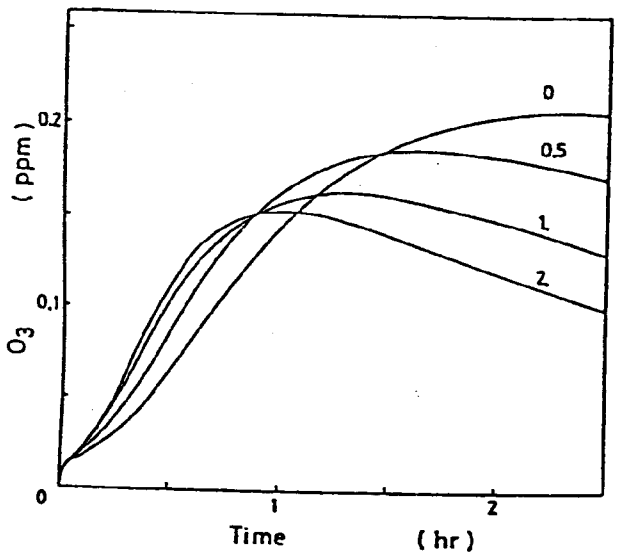

Fig.8
Time profile of ozone formation in the C_3H_6-toluene-NO_x-humid air runs.
$[C_3H_6]_0$=0.5 ppm, $[NO_x]_0$=0.09 ppm, k_1=0.19 min^{-1}.
Numerals in the figure are $[Toluene]_0$ in ppm.

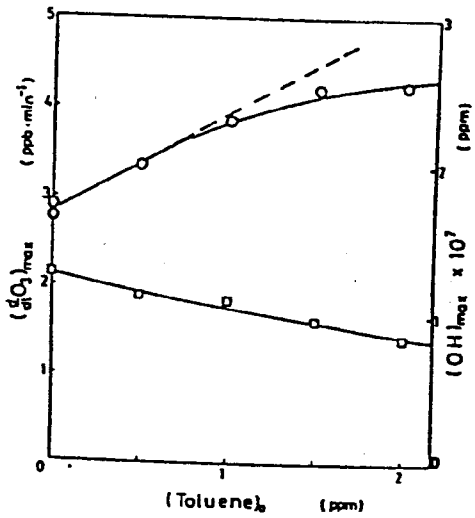

Fig.9
Maximum ozone formation rate and maximum OH concentration vs. $[Toluene]_0$ in the C_3H_6-toluene-NO_x-humid air runs.
Experimental conditions are the same as in Fig.8.

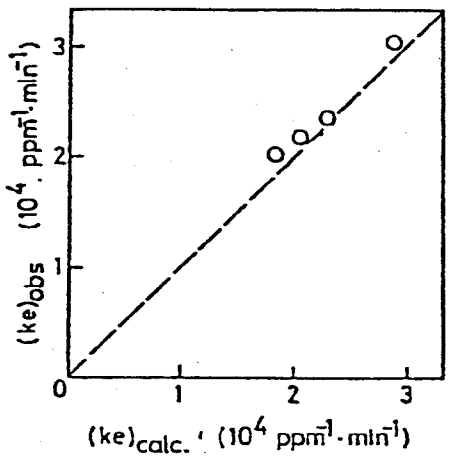

Fig.10
Comparison of the observed and calculated overall effective ozone formation rate constant in the C_3H_6-toluene-NO_x-humid air runs.

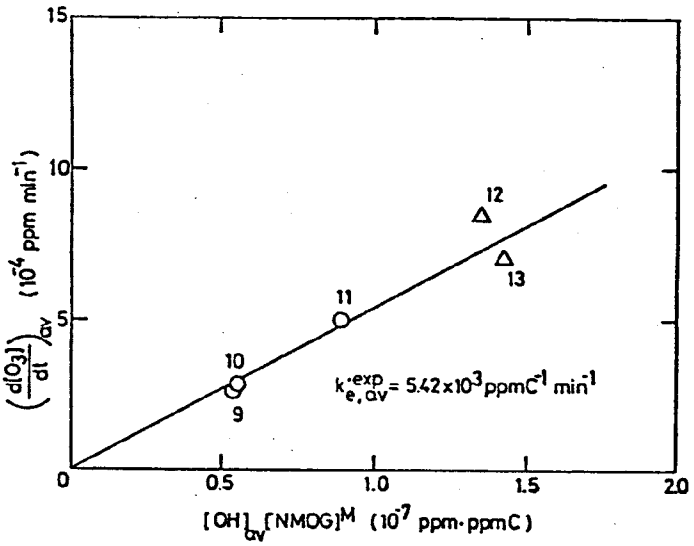

Fig.11
$(d[O_3]/dt)_{av}$ vs. $[OH]_{av}[NMOG]_0^M$ in the sampled ambient air runs. Average was taken for 0-1 hour after irradiation. Numerals in the figure correspond to run numbers in Table II and III.

[Ref.]

Correlation of the Ozone Formation Rates with Hydroxyl Radical Concentrations in the Propylene-Nitrogen Oxide Dry Air System: Effective Ozone Formation Rate Constant

Hajime Akimoto* and Fumio Sakamaki
Division of Atmospheric Environment
The National Institute for Environmental Studies
P.O. Tsukuba-gakuen, Ibaraki 305 Japan

Ozone formation rates obtained in smog chamber experiments for the C_3H_6-NO_x-dry air system were analyzed with the aid of computer simulation using a detailed reaction model. In the region of $[C_3H_6]_0/[NO_x]_0 \geq 5$, the ozone formation rate was found to be approximately proportional to the product of the OH-radical concentration and the initial concentration of C_3H_6 in the earlier stage of photooxidation until the $d[O_3]/dt$ reaches a maximum. The proportionality constant was defined as an effective ozone formation rate constant and is proposed to be a useful parameter to represent photochemical reactivity of hydrocarbon mixtures based on the ozone formation rate. The effective ozone formation rate constant for C_3H_6 in the dry air-NO_x mixture was determined to be $6.2 \pm 1.1 \times 10^4 ppm^{-1} min^{-1}$.

Quantitative characterization of photochemical ozone formation in organics-nitrogen oxide-air mixtures is of critical importance in planning ozone control strategy based on smog chamber data and computer simulation. From this viewpoints, an "ozone formation potential" was proposed as one of the generalized reaction parameter in our previous studies (1-5). While the "ozone formation potential" governs the maximum amount of ozone formed ultimately after prolonged irradiation, the "ozone formation rate" is another even more important parameter which characterizes the photochemical ozone formation in organics-nitrogen oxide air mixtures. The purpose of this study is to present a method for analyzing the ozone formation rate and to propose a phenomenological rate parameter which would be useful for representing reactivity of mixtures of hydrocarbons and other organics whose components are not necessarily known.

As for the rate parameters which could be representative of ozone formation rate, the NO oxidation rate has been recognized as a useful measure of the photochemical reactivity of various hydrocarbons and most extensively studied by Glasson and Tuesday (6). More recently, Darnall et al. (7) have proposed OH-hydrocarbon reaction rate constant as a measure of hydrocarbon reactivity. However, although these parameters has been used for classification of numerous hydrocarbons based on a reactivity scale, no direct general

relationship between these parameters and the actual ozone formation rate observed in a photochemical run of a selected organics- nitrogen oxide mixture has been proposed on an absolute rate basis.

This study presents an analysis of ozone formation rate data for the propylene-nitrogen oxide-dry air system carried out in an evacuable photochemical smog chamber. An approximately proportional relationship between the ozone formation rate and the product of the maximum OH-radical concentration and initial concentration of propylene was found to hold. The relationship was further confirmed in terms of computer simulation using a detailed kinetic reaction model.

Experimental and Computation

All the experimental data used in the present study were obtained in C_3H_6-NO_x-dry air runs using the evacuable and bakable photochemical smog chamber at NIES. Experimental procedures and details of these runs have been reported previously (1). The experiments were carried out at 30°C. The initial conditions and light intensity expressed as k_1 (NO_2 photolysis rate) are given in Table I. Typical wall loss rate of ~0.04 ppm of ozone in the chamber was 0.07 ± 0.01 hr^{-1}. The experimental maximum ozone formation rate, $(d[O_3]/dt)^{obs}_{max}$ is defind as the maximum slope of the plot of ozone concentration vs. irradiation time. The experimental maximum OH-

radical concentration, $[OH]_{max}^{obs}$ was obtained from the maximum slope of the semi-log plot of the decay of propylene after subtracting the decay of propylene due to ozone reaction. The rate constants used for the C_3H_6-OH and C_3H_6-O_3 reactions were 2.51×10^{-11}(8) and 1.30×10^{-18}(9) $cm^3 molecule^{-1} s^{-1}$, respectively. The data reduction techniques to obtain the maximum OH-radical concentration have been reported in our earlier paper (10). The obtained $[OH]_{max}^{obs}$ for each run is cited in Table I. The estimated error in $[OH]_{max}^{obs}$ is $\pm 25\%$ for the runs with $[C_3H_6]_0$=0.50 ppm. For lower $[C_3H_6]_0$ runs, the error tends to get larger due to the larger scattering error in the C_3H_6 concentration measurement and a larger contribution of the correction term of C_3H_6-O_3 reaction.

Computer simulations were performed for the C_3H_6-NO_x-dry air runs using the reaction model reported before (4). The model consists of 158 chemical equations and 89 species, and was used without modification. Wall loss rate of O_3, 0.058 hr^{-1} was used throughout the computation runs. Calculated maximum ozone formation rate, $(d[O_3]/dt)^{calc}$ and maximum OH concentration, $[OH]_{max}^{calc}$ were obtained directly from the computer output of these values. The integration program used was the same as described previously (4, 11).

The initial conditions of the computer runs were the same as those of corresponding experimental runs. A few supplemental computer runs were also performed under initial conditions for which experimental runs were not available.

Results

Table I summarizes the observed and calculated maximum ozone formation rates and maximum OH concentrations for all the C_3H_6-NO_x-dry air runs studied in this work. The deviation of the calculated values from the observed ones is the largest for the runs with high light intensity (Runs 23 and 24). Although the agreement between the calculated and observed values is thought to be satisfactory except for these runs, it should be noted that the present reaction model predicts much slower initial oxidation rate than observed experimentally. For example, the simulation for Run 1 predicts the maximum ozone formation rate at 120 min, whereas the experimental run gives the maximum rate at 80 min after the irradiation began. Although this deviation would be due to the presence of unknown radical sources as discussed by Carter et al. (12, 13), this problem was not pursued further in the present study since the following discussion on the relationship between $(d[O_3]/dt)_{max}$ and $[OH]_{max}$ will not be affected by the delay of photooxidation.

Since it was generally found both experimentally and by the computer simulation that the maximum ozone formation rate and maximum OH concentration are observed at nearly the same time after irradiation in most of the runs it is expected that the $(d[O_3]/dt)_{max}$ is correlated to $[OH]_{max}$ quantitatively. Figure 1 shows a plot of $(d[O_3]/dt)_{max}$ vs.

$[OH]_{max}$ for the runs with various $[NO_x]_0$ and k_1 but with the same initial concentration of propylene ($[C_3H_6]_0$ = 0.50 ppm). The linear plot implies that $(d[O_3]/dt)_{max}$ is linearly proportional to $[OH]_{max}$ even though $(d[O_3]/dt)_{max}$ and $[OH]_{max}$ vary with the $[NO_x]_0$ and k_1. The proportionality was also confirmed by computer simulation as demonstrated in Figure 1. Deviation from the linear line can be noted for the run with a low $[C_3H_6]_0/[NO_x]_0$ ratio. Thus, both the experimental and calculated points for Run 15 are much lower than the linear line. This is because the initial concentration ratio, $[C_3H_6]_0/[NO_x]_0$=1.7, for Run 15 does not fall into the hydrocarbon excess region as will be discussed later.

A proportionality between $(d[O_3]/dt)_t$ and $[OH]_t$ within a single run was next checked by computer simulation. Figure 2 depicts examples for Runs 10, 11 and 25. $(d[O_3]/dt)_t$ is, in general, proportional to $[OH]_t$ until $d[O_3]/dt$ and [OH] reach their maximums except during the very early stage of photooxidation. After $d[O_3]/dt$ and [OH] reach their maximums, the ozone formation rate decreases faster than the decrease of [OH].

For the runs with different $[C_3H_6]_0$, a plot of $(d[O_3]/dt)_{max}$ vs. $[OH]_{max} \cdot [C_3H_6]_0$ was attempted. Figure 3 shows the plot for all the runs with different $[C_3H_6]_0$, $[NO_x]_0$ and k_1. The plots of most of the runs except for those with low $[C_3H_6]_0/[NO_x]_0$ ratio fall on a single linear line going through the origin. Verifying an approximate proportionality

between $(d[O_3]/dt)_{max}$ and $[OH]_{max} \cdot [C_3H_6]_0$, i.e.,

$$\left(\frac{d[O_3]}{dt}\right)_{max} = k_e^{C_3H_6} [OH]_{max} [C_3H_6]_0 \qquad (1)$$

where $k_e^{C_3H_6}$ is the effective rate constant of photochemical ozone formation for propylene. From a least square fit to the all experimental points, the value of $k_e^{C_3H_6}$ is obtained to be $6.0 \times 10^4 ppm^{-1} min^{-1}$ as a slope of Fig.3. The relationship can be confirmed by the computer simulation as demonstrated in Figure 3 and the calculated $k_e^{C_3H_6}$ value agreed with the experimental one within 10%.

In order to check the validity of $k_e^{C_3H_6}$, the experimental and calculated ratios $(d[O_3]/dt)_{max}/([OH]_{max} \cdot [C_3H_6]_0)$ for all runs were plotted as a function of $[C_3H_6]_0/[NO_x]_0$ in Figure 4. Solid curve is drawn through the calculated data points. However, since it was found by the computer modeling that at low $[C_3H_6]_0/[NO_x]_0$ ratio, time for $(d[O_3]/dt)$ and $[OH]$ to reach their maximum does not coincide but the latter is delayed, the ratio of $(d[O_3]/dt)_{max}$ to $[OH]_{t_{max}} \cdot [C_3H_6]_0$ is also shown by a dashed curve. Here, $[OH]_{t_{max}}$ is the OH radical concentration at the time when $d[O_3]/dt$ reaches the maximum. The deviation of the two curves is apparent at low $[C_3H_6]_0/[NO_x]_0$ ratio. As shown in Figure 4, both ratios decrease as the $[C_3H_6]_0/[NO_x]_0$ ratio decreases. Although the experimental points scatters appreciably, they also tend to decrease as the $[C_3H_6]_0/[NO_x]_0$ ratio decreses in accordance with the prediction of the computer simulation. The region

where the ratio gives nearly a constant value, which can be defined as $k_e^{C_3H_6}$, can be called a hydrocarbon excess region for the ozone formation rate. The hydrocarbon excess region for the C_3H_6-NO_x-dry air system may be defined as $[C_3H_6]_0/[NO_x]_0 \gtrsim 5$ from the plot of Fig. 4, if one takes the 90 % line of the calculated limiting value. The average of experimental data only in the region of $[C_3H_6]_0/[NO_x]_0 \gtrsim 5$ gives the observed k_e value of 6.2 ± 1.1 (2) $ppm^{-1}min^{-1}$.

Discussion

The importance of OH-radicals in the reaction of photochemical air pollution is well recognized (14-21) and efforts have been made to correlate OH-radical rate constants with ozone formation both in experimental (23) and assessment studies (24). However, no direct correlation between the OH-radical concentration and ozone formation rate has been verified experimentally. The results of the present study shown in Figures 1-3 reveal that the ozone formation rate and the OH-radical concentration can be correlated in the hydrocarbon excess region by the equation,

$$\left(\frac{d[O_3]}{dt}\right)_t = k_e^{C_3H_6}[OH]_t \cdot [C_3H_6]_0 \qquad (2)$$

and an effective rate constant, $k_e^{C_3H_6}$. is defined as an apparent constant during the early stage of photooxidation until the ozone formation rate reaches its maximum. Equation

(1) is a special case of Equation (2). Similarly, time-averaged values, $(d[O_3]/dt)_{av}$ and $[OH]_{av}$ for a certain time interval may also be used to obtain the value of k_e when these quantities changes slowly with irradiation time. It is interesting to note that the ozone formation rate can be expressed in terms of OH-radical concentration and hydrocarbon concentration being independent of nitrogen oxides concentration and light intensity. The latter two parameters only affect the OH-radical concentration and do not appear explicitly in Equation (2). Further, the phenomenological effective rate constant, $k_e^{C_3H_6}=6.2 \times 10^{-4} ppm^{-1} min^{-1}$, has the same order of magnitude as the OH-C_3H_6 elementary rate constant, $k_{OH}^{C_3H_6}=3.64 \times 10^{4} ppm^{-1} min^{-1}$ (9).

In order to check the validity of the proportionality between the maximum ozone formation rate and the initial concentration of C_3H_6 as represented by Eq.(1), numerical evaluations of the terms contributing to the ozone formation rate are made by means of the computer simulation. The ozone formation rate and the NO decay rate in the photooxidation processes can be written as,

$$\frac{d[O_3]}{dt} = k_2[O][O_2] - k_3[NO][O_3] - \Sigma L_i(O_3) \qquad (3)$$

and

$$-\frac{d[NO]}{dt} = -k_1[NO_2]+k_3[NO][O_3]+\Sigma k_i[RO_2][NO]+\Sigma k_j[RO][NO] \qquad (4)$$

where k_1, k_2 and k_3 are the rate constants of reactions, $NO_2+h\nu \longrightarrow NO+O$ (i), $O+O_2+M \longrightarrow O_3+M$ (ii) and $NO+O_3 \longrightarrow NO_2+O_2$

(iii), respectively. The $L_i(O_3)$ stands for every loss term of O_3 except the reaction (iii), RO_2 and RO represent all peroxy- and oxy- type radicals which can react with NO, respectively. At the time when the maximum ozone formation rate is observed, the inequalities, $(d[O_3]/dt) \gg (d[NO]/dt)$ and $\Sigma k_j[RO][NO] \ll k_1[NO_2]$, $k_3[NO][O_3]$, and $\Sigma k_i[RO_2][NO]$ hold, which lead to the approximation, $d[NO]/dt \approx 0$ and thus,

$$k_1[NO_2] - k_3[NO][O_3] \approx \Sigma k_i[RO_2][NO] \qquad (5)$$

Next the steady state approximations for [O] and $[RO_2]$ are assumed

$$\frac{d[O]}{dt} \approx k_1[NO_2] + (k_4 + k_5)[O_3] - k_2[O][O_2] \equiv 0 \qquad (6)$$

$$\frac{d[RO_2]}{dt} \approx \Sigma S_i(RO_2) - \Sigma k_i[RO_2][NO] \equiv 0 \qquad (7)$$

where k_4 and k_5 are the photolysis rate constants of O_3, $O_3 + h\nu \longrightarrow O_2 + O(^3P)$ (iv) and $O_3 + h\nu \longrightarrow O_2 + O(^1D)$ (v), respectively, and $S_i(RO_2)$ stands for every source term of RO_2. Oxygen atom loss other than the reaction with O_2, and RO_2 loss due to radical-radical reactions can be neglected at the earlier stage of photooxidation and are not included in Eqs.(6) and (7). From Eqs.(3)-(7), the ozone formation rate can be expressed as,

$$\frac{d[O_3]}{dt} = \Sigma S_i(RO_2) - \Sigma' L_i(O_3) \qquad (8)$$

where $\Sigma' L_i(O_3)$ is the summation of net ozone loss terms excluding the terms of O_3 photolyses (reactions (iv) and (v))

which mostly regenerate O_3. Further, each term of $S_i(RO_2)$ and $L_i(O_3)$ can be written as,

$$\Sigma S_i(RO_2) = \sum_{OH-C_3H_6} S_i(RO_2) + \sum_{RCHO} S_i(RO_2) + \sum_{O_3-C_3H_6} S_i(RO_2) \quad (9)$$

$$\Sigma' L_i(O_3) = k_6[O_3][C_3H_6] + k_7[NO_2][O_3] + k_w[O_3] \quad (10)$$

and all other terms are found to be negligible. Here $\sum_{OH-C_3H_6} S_i(RO_2)$ and $\sum_{O_3-C_3H_6} S_i(RO_2)$ are the RO_2 production rate in the $OH-C_3H_6$ reaction sequence and $O_3-C_3H_6$ reaction sequence, respectively. $\sum_{RCHO} S_i(RO_2)$ is the RO_2 production rate in the sequences of aldehydes (HCHO and CH_3CHO) photolysis and OH-aldehydes reactions. Contributions of other aldehydes have been neglected. In Eq.(10), k_6, k_7, and k_w are the rate constant of the reactions $O_3+C_3H_6 \rightarrow$ products (vi), $NO_2+O_3 \rightarrow NO_3+O_2$ (vii) and O_3 wall decay.

Table II summarizes numerical values of the terms which contributes to $\Sigma S_i(RO_2)$ and $\Sigma L_i(O_3)$ obtained in the computer simulation for variable $[C_3H_6]_0$ runs ($[NO_x]_0 \approx 0.04$ ppm and $k_1 = 0.16\ min^{-1}$). The given values are for the time giving the maximum rate of ozone formation for each run. As shown in Table II, the ozone formation rate calculated by Eq.(8) from each terms, $(d[O_3]/dt)_{max}^{Eq(8)}$, agrees well with $(d[O_3]/dt)_{max}^{calc}$ obtained directly in each computer runs within 10% for these runs. Figure 5 depicts the dependence of source terms of RO_2 on $[C_3H_6]_0$ and Figure 6 shows that of loss terms of O_3 and $(d[O_3]/dt)_{max}$ obtained by the difference of $\Sigma S_i(RO_2)$ and $\Sigma' L_i(O_3)$. Figure 6 also shows the concentration of OH at the time of maximum ozone formation rate. It is seen in

Figure 5 that the RO_2 production rate due to $OH-C_3H_6$ and $O_3-C_3H_6$ reactions increases linearly with $[C_3H_6]_0$ while that of aldehydes reaction is nearly constant being independent of $[C_3H_6]_0$. This is because the maximum ozone formation rate appears at prolonged irradiation time as the $[C_3H_6]_0$ decreases and the absolute concentration of aldehydes at the time of maximum ozone formation are kept nearly constant even at the lower $[C_3H_6]_0$. The sum of all production rates of RO_2 is approximately proportional to $[C_3H_6]_0$ as shown in Fig.5. Figure 6 shows that a loss term of O_3 due to $O_3-C_3H_6$ reaction is a linear function of $[C_3H_6]_0$ while that due to NO_2-O_3 reaction and wall loss of O_3 is nearly independent of $[C_3H_6]_0$ and contribute only a minor extent except at very low $[C_3H_6]_0$. The maximum ozone formation rate resultant from the difference of $\Sigma S_i(RO_2)$ and $\Sigma' L_i(O_3)$ is a linear function of $[C_3H_6]_0$ but has a small negative intercept as shown in Fig.6. Thus, the approximate proportionality between $(d[O_3]/dt)_{max}$ and $[C_3H_6]_0$ as expressed by Eq.(1) and the decrease of k_e value at the low ratio of $[C_3H_6]_0/[NO_x]_0$ can be rationalized by the analysis of computer simulation runs.

The reason that the effective ozone formation rate constant is in the same order of magnitude as k_{OH} is also apparent from the analysis shown in Table II and Figs.5 and 6. The major term contributing to $d[O_3]/dt$ is the $S(RO_2)$ due to $OH-C_3H_6$ reaction sequence which produces about twice as much RO_2 radicals as reacted C_3H_6. Contribution of all

other production and loss terms in Eq. (10) are a fraction of the term value of $\sum_{OH-C_3H_6} S(RO_2)$, yielding the $k_e^{C_3H_6}$ value between $k_{OH}^{C_3H_6}$ and $2k_{OH}^{C_3H_6}$.

The above discussion suggests that the relationship of Equation (2) may be applicable to any type of hydrocarbon-NO_x-air system in the hydrocarbon excess region during the earlier stage of photooxidation

$$\left(\frac{d[O_3]}{dt}\right)_t = k_e [OH]_t \ [HC]_0 \tag{11}$$

For a practical purpose the time averaged form of Eq. (11) would be more useful, i.e.,

$$\left(\frac{d[O_3]}{dt}\right)_{av} = k_e [OH]_{av} \ [HC]_0 \tag{12}$$

The average should be taken for a time interval near the maximum of $d[O_3]/dt$. Therefore, if the value of k_e is determined for each hydrocarbon and also for hydrocarbon mixtures, it can offer a new useful scale of hydrocarbon reactivity based on the ozone formation rate. It should be noted that the k_e value determined in smog chamber experiments is free from the error due to possible presence of unknown radical sources in the chamber (10, 11), since k_e is defined by the ratio of the ozone formation rate to the OH-radical concentration. Therefore, the quantitative evaluation of the photochemical reactivity of ambient air in terms of the ozone formation rate can be accomplished by irradiating sampled air in a smog chamber. The determina-

tion of k_e for various types of hydrocarbons and for the sampled ambient air is underway in our laboratory.

Literature Cited

(1) Akimoto, H., Sakamaki, F., Hoshino, M., Inoue, G., Okuda, M., Environ. Sci. Technol., 1979, 13, 53.

(2) Sakamaki, F., Akimoto, H., Okuda, M., Environ. Sci. Technol., 1980, 14, 985.

(3) Sakamaki, F., Akimoto, H., Okuda, M., Environ. Sci. Technol., 1981, 15, 665.

(4) Sakamaki, F., Okuda, M., Akimoto, H., Environ. Sci. Technol., 1982, 16, 45.

(5) Shibuya, K., Nagashima, T., Imai, S., Akimoto, H., Environ. Sci. Technol., 1981, 15, 661.

(6) Glasson, W.A., Tuesday, C.S., Environ. Sci. Technol., 1970, 4, 37.

(7) Darnall, K.R., Lloyd, A.C., Winer, A.M., Pitts, J.N., Environ. Sci. Technol., 1976, 10, 693.

(8) Japer, S.M., Wu, C.H., Niki, H., J. Phys. Chem., 1974, 78, 2318.

(9) Atkinson, R., Pitts, J.N., Jr., J. Chem. Phys., 1975, 63, 3591.

(10) Akimoto, H., Sakamaki, F., Inoue, G., Okuda, M., Environ. Sci. Technol., 1980, 14, 93.

(11) Whitten, G.Z., Hogo, H., "Modeling of Simulated Photochemical Smog with Kinetic Mechanisms Vol.2 CHEMK: A Computer Modeling Scheme for Chemical Kinetics, EPA-600/3-80-0286, Feburuary 1980.

(12) Carter, W.P.L., Lloyd, A.C., Sprung, J.L., Pitts, J.N.Jr.,Int. J. Chem. Kinet., 1979, 11, 45.

(13) Carter, W.P.L., Atkinson, R., Winer, A.M., Pitts, J.N.Jr., Int. J. Chem. Kinet., 1982, 14, 813.

(14) Heicklen, J., Westberg, K., Cohen, N., "Chemical Reaction in Urban Atmospheres", Tuesday, C.S., Ed., American Elsevier Press, New York, 1971, p.55.

(15) Niki, H., Daby, E.E., Weinstock, B., Adv. Chem. Ser., 1972, 113, 16.

(16) Demerjian, K.L., Kerr, J.A., Calvert, J.G., Adv. Environ. Sci. Technol., 1974, 4, 1.

(17) Doyle, G.J., Lloyd, A.C., Darnall, K.R., Winer, A.M., Pitts, J.N.Jr., Environ. Sci. Technol., 1975, 9, 237.

(18) Calvert, J.G., McQuigg, R.D., Int. J. Chem. Kinet. Symp., 1975, 1, 113.

(19) Darnall, K.R., Lloyd, A.C., Winer, A.M., Pitts, J.N.Jr., Environ. Sci. Technol., 1976, 10, 692.

(20) Wu, C.H., Japar, S.M., Niki, H., J. Environ. Sci. Health, Ser. A, 1976, 11, 191.

(21) Calvert, J.G., Environ. Sci. Technol., 1976, 10, 257.

(22) Wang, C.C., Davis, L.I.Jr., Wu, C.H., Japar, S., Niki, H., Weinstock, B., Science, 1975, 189, 797.

(23) Winer, A.A., Darnall, K.R., Atkinson, R., Pitts, J.N.Jr., Environ. Sci. Technol., 1979, 13, 822.

(24) Singh, H.B., Martinez, J.R., Hendry, D.G., Jaffe, R.J., Johnson, W.V., Environ. Sci. Technol., 1981, 15, 113.

Figure Captions

Figure 1. Plot of $(d[O_3]/dt)_{max}$ vs. $[OH]_{max}$. Filled and open symbols are for observed and calculated values, respectively. $[C_3H_6]_0$ = 0.50 ppm. Variable $[NO_x]_0$ runs (▲,△), k_1 = 0.16 min^{-1}; variable k_1 runs (●,○), $[NO_x]_0$ ≈ 0.09 ppm.

Figure 2. Plot of calculated $(d[O_3]/dt)_t$ vs. $[OH]_t$ in the computer simulation for Runs 10 (▲,△), 11 (■,□) and 25 (●,○). Filled and open symbols correspond to values before and after the $d[O_3]/dt$ reach the maximum.

Figure 3. Plot of $(d[O_3]/dt)_{max}$ vs. $[OH]_{max} \cdot [C_3H_6]_0$. Filled and open symbols are for observed and calculated values, respectively. Variable $[C_3H_6]_0$ runs for $[NO_x]_0$ ≈ 0.04 (■,□) and 0.09 ppm (◆,◇), k_1 = 0.16 min^{-1}; Variable $[NO_x]_0$ runs for $[C_3H_6]_0$ = 0.10 (▲,△) and 0.50 ppm (▼,▽); Variable k_1 runs for $[C_3H_6]_0$ = 0.50, $[NO_x]_0$ ≈ 0.09 ppm (●,○).

Figure 4. Plot of $(d[O_3]/dt)_{max}/([OH]_{max} \cdot [C_3H_6]_0)$ vs. $[C_3H_6]_0/[NO_x]_0$. Symbols are the same as in Figure 1. Dashed line shows the ratio of $(d[O_3]/dt)_{max}/([OH]_{t_{max}} \cdot [C_3H_6]_0)$ (see text).

Figure 5. Production rate of RO_2 due to C_3H_6-OH, C_3H_6-O_3 and RCHO-OH, hν reaction sequences, and the sum. $[NO_x]_0$ ≈ 0.04 ppm, k_1 = 0.16 min^{-1}.

Figure 6. Loss rate of O_3 due to C_3H_6-O_3, NO_2-O_3 and wall reaction, and the sum. $(d[O_3]/dt)_{max}$ calculated from Eq.(8) and $[OH]_{t_{max}}$ are also shown as a function of $[C_3H_6]_0$. $[NO_x]_0 \simeq 0.04$ ppm, $k_1 = 0.16$ min^{-1}.

Table 1 Experimental and Calculated Ozone Formation Rates and OH-Radical Concentrations in the C_3H_6-NO_x-Dry Air System

Run	$[C_3H_6]_0$ ppm	$[NO_x]_0$ ppm	k_1 min^{-1}	$\left(\frac{d[O_3]}{dt}\right)_{max}^{obs}$ 10^{-3}ppm min^{-1}	$\left(\frac{d[O_3]}{dt}\right)_{max}^{calc}$ 10^{-3}ppm min^{-1}	$[OH]_{max}^{obs}$ 10^{-7} ppm	$[OH]_{max}^{calc}$ 10^{-7} ppm
1	0.10	0.009	0.16[a)]	0.12	0.38	—	0.64
2	0.10	0.020	0.16	0.30	0.43	0.56	0.80
3	0.10	0.026	0.16	0.33	0.42	0.79	0.83
4	0.10	0.034	0.16	0.37	0.41	0.73	0.87
5	0.10	0.036	0.16	0.41	0.39	0.94	0.86
7	0.10	0.052	0.16	0.38	0.38	0.78	0.90
8	0.10	0.063	0.16	0.35	0.33	0.95	0.91
S1	0.50	0.010	0.16	—	0.84	—	0.28
S2	0.50	0.020	0.16	—	1.46	—	0.48
10	0.50	0.045	0.16	2.31	2.37	0.84	0.80
S3	0.50	0.150	0.16	—	2.78	—	1.10
14	0.50	0.187	0.16	3.40	2.58	1.11	1.10
15	0.50	0.291	0.16	2.48	1.84	1.25	0.96
16	0.05	0.038	0.16	0.13	0.16	0.42	1.07
6	0.10	0.043	0.16	0.35	0.38	0.88	0.88
17	0.15	0.039	0.16	0.71	0.64	0.71	0.86
18	0.20	0.040	0.16	1.00	0.92	—	0.89
19	0.30	0.039	0.16	1.40	1.45	0.69	0.86
20	0.40	0.039	0.16	1.74	1.90	0.70	0.80
S4	0.50	0.040	0.16	—	2.22	—	0.75
9	0.10	0.086	0.16	0.19	0.30	—	0.96
21	0.20	0.086	0.16	0.78	0.77	0.99	0.88
22	0.33	0.091	0.16	2.10	1.73	0.96	0.99
11	0.50	0.090	0.16	2.97	2.86	0.97	1.06
13	0.50	0.090	0.16	2.59	2.65	0.74	1.01
12	0.50	0.089	0.16	2.50	2.60	—	1.00
23	0.50	0.085	0.37	7.27	5.26	2.50	1.91
24	0.50	0.090	0.31	6.25	4.60	1.97	1.69
25	0.50	0.083	0.25	4.38	3.94	1.40	1.42
26	0.50	0.088	0.19	3.50	3.22	1.23	1.18
27	0.50	0.089	0.13	2.82	2.47	0.80	0.91

(a) Typical uncertainty in k_1 is 0.16 ± 0.02 min^{-1}.

Table II. Calculated RO_2 Formation Rates, O_3 Loss Rates at the time giving the Maximum Ozone Formation Rate[a]. $[NO_x]_0 = 0.09$ ppm $k_1 = 0.16\ min^{-1}$

Reaction Term \ $C_3H_6{}_0$(ppm)	0.10	0.20	0.30	0.40	0.50
RO_2 Formation Rate (10^{-3}ppm min^{-1})					
C_3H_6-OH Reaction Sequence					
$C_3H_6+OH \xrightarrow{O_2} CH_3CH(O_2)CH_2OH$	0.099	0.296	0.496	0.633	0.825
$C_3H_6+OH \xrightarrow{O_2} CH_3CH(OH)CH_2O_2$	0.053	0.106	0.159	0.267	0.443
$CH_3CH(O)CH_2OH \xrightarrow{O_2} CH_3CHO+HCHO+HO_2$	0.095	0.282	0.473	0.671	0.783
$CH_3CH(OH)CH_2O \xrightarrow{O_2} CH_3CHO+HCHO+HO_2$	0.051	0.100	0.252	0.336	0.417
$\sum_{C_3H_6\text{-}OH} S_i(RO_2)$	0.30	0.89	1.49	1.99	2.47
Aldehyde Reaction Sequence					
$HCHO+OH \xrightarrow{O_2} HO_2+CO+H_2O$	0.038	0.050	0.047	0.044	0.045
$CH_3CHO+OH \xrightarrow{O_2} CH_3CO_3+H_2O$	0.058	0.080	0.076	0.073	0.074
$CH_3CO_2 \xrightarrow{O_2} CH_3O_2+CO_2$	0.023	0.016	0.011	0.008	0.007
$CH_3O \xrightarrow{O_2} HCHO+HO_2$	0.046	0.063	0.073	0.087	0.106
$HCHO+h\nu \xrightarrow{2O_2} 2HO_2+CO$	0.012	0.014	0.013	0.013	0.014
$CH_3CHO+H \xrightarrow{2O_2} CH_3O_2+HO_2+CO$	0.014	0.017	0.016	0.016	0.017
$\sum_{RCHO} S_i(RO_2)$	0.22	0.27	0.27	0.27	0.26
C_3H_6-O_3 Reaction Sequence					
$C_3H_6+O_3 \longrightarrow CH_3CHO_2+HCHO$	0.014	0.046	0.069	0.094	0.124
$\longrightarrow CH_2O_2+CH_3CHO$	0.014	0.046	0.069	0.094	0.124
$CH_3CHO_2 \xrightarrow{O_2} CH_3O_2+OH+CO$	0.004	0.012	0.019	0.025	0.033
$\xrightarrow{2O_2} CH_3O_2+HO_2+CO_2$	0.005	0.016	0.024	0.033	0.043
$\xrightarrow{O_2} CH_3O+CO+HO_2$	0.001	0.003	0.005	0.006	0.008
$CH_2O_2 \xrightarrow{2O_2} CO_2+2HO_2$	0.001	0.004	0.006	0.008	0.011
$\sum_{C_3H_6\text{-}O_3} S_i(RO_2)$	0.05	0.15	0.22	0.30	0.40
$\sum_{all} S_i(RO_2)$	0.56	1.31	1.98	2.56	3.12
O_3 Loss Rate (10^{-3}ppm min^{-1})					
$O_3+C_3H_6 \longrightarrow$ products	0.056	0.182	0.278	0.376	0.496
$O_3+NO_2 \longrightarrow NO_3+O_2$	0.084	0.114	0.112	0.114	0.132
$O_3+wall \longrightarrow O_3$ Loss	0.060	0.073	0.066	0.069	0.066
$\Sigma' L_i(O_3)$	0.20	0.37	0.46	0.56	0.69
O_3 Formation Rate (10^{-3} ppm min^{-1})					
$\left.\frac{d[O_3]}{dt}\right|_{max}^{Eq.(8)} \equiv \sum_{all}{}' S_i(RO_2) - {}' L_i(O_3)$	0.36	0.94	1.52	2.00	2.43
$\left.\frac{d[O_3]}{dt}\right|_{max}^{Calc}$	0.38	0.92	1.45	1.90	2.22

(a) Calculations for $[C_3H_6]_0$ = 0.10-0.50 ppm correspond to Runs 6, 18, 19, 20, and 21, presented in Table 1, respectively so that $[NO_x]_0$ value for each run varied slightly. For the reactions which produces two RO_2 radicals, the reaction rates were multiplied by two to obtain RO_2 formation rates.

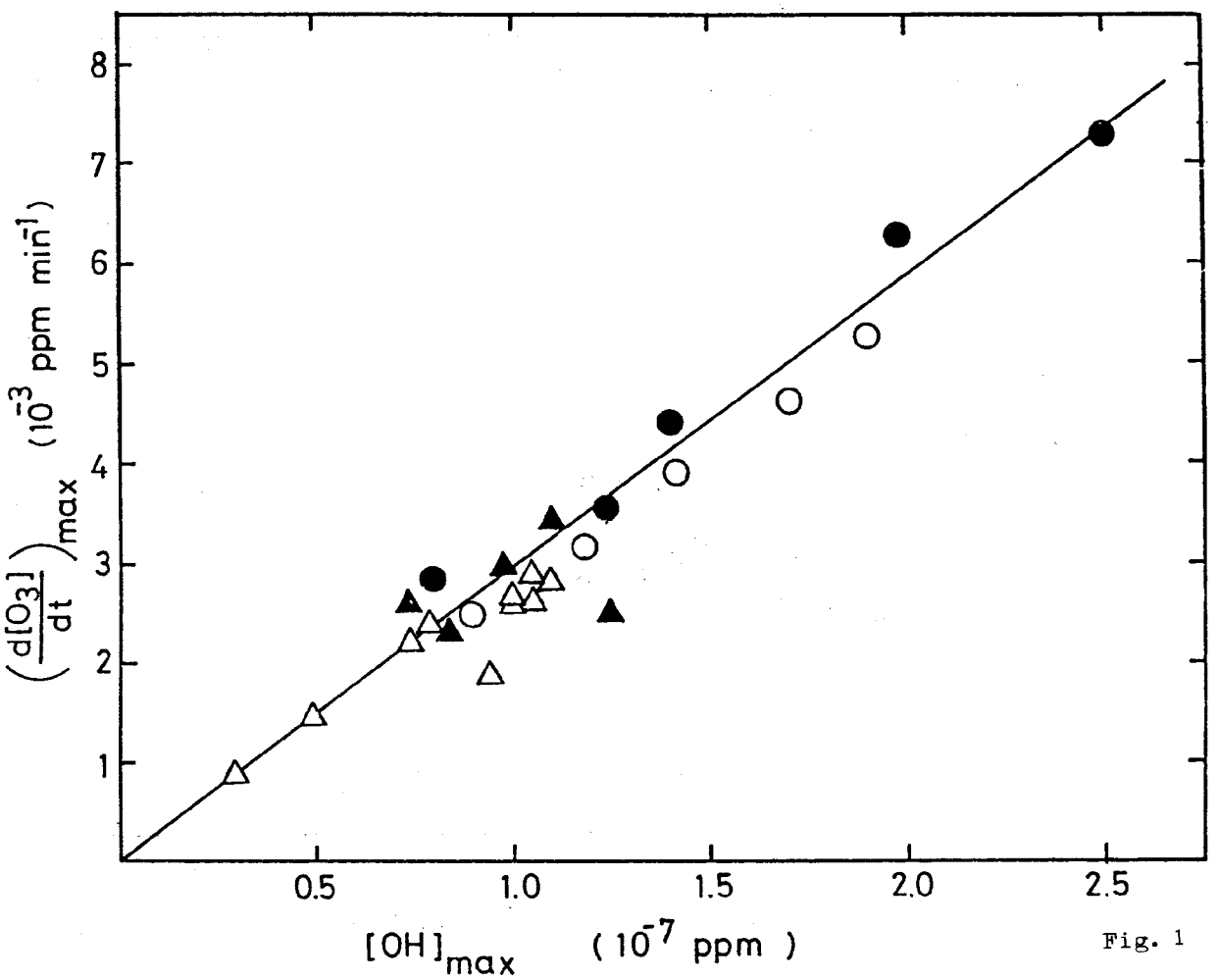
$\left(\frac{d[O_3]}{dt}\right)_{max}$ (10^{-3} ppm min^{-1})
8
7
6
5
4
3
2
1
0.5
1.0
1.5
2.0
2.5
$[OH]_{max}$ (10^{-7} ppm)

Fig. 1

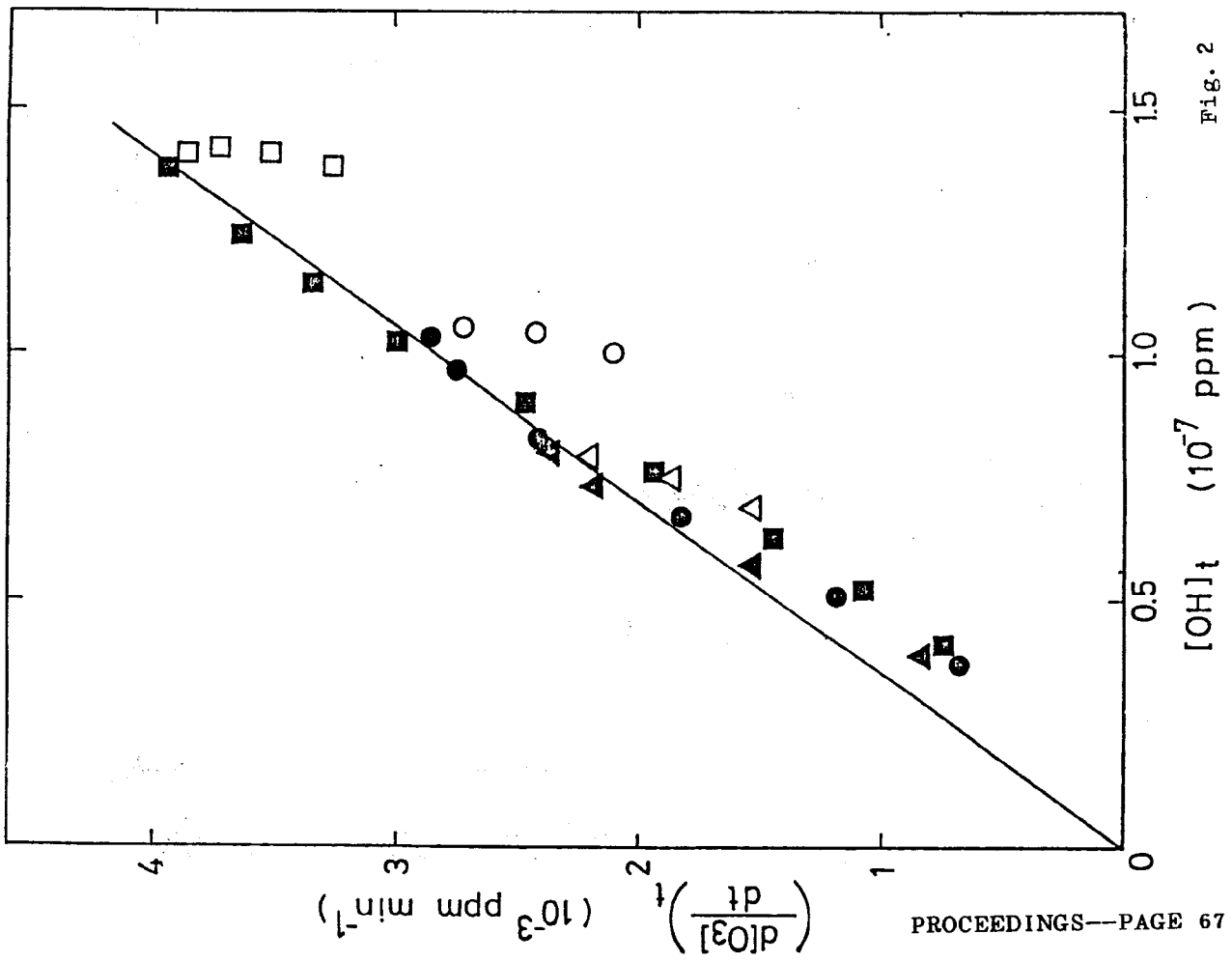
$\left(\frac{d[O_3]}{dt}\right)_t$ (10^{-3} ppm min^{-1})
4
3
2
1
0
0.5
1.0
1.5
$[OH]_t$ (10^{-7} ppm)

Fig. 2

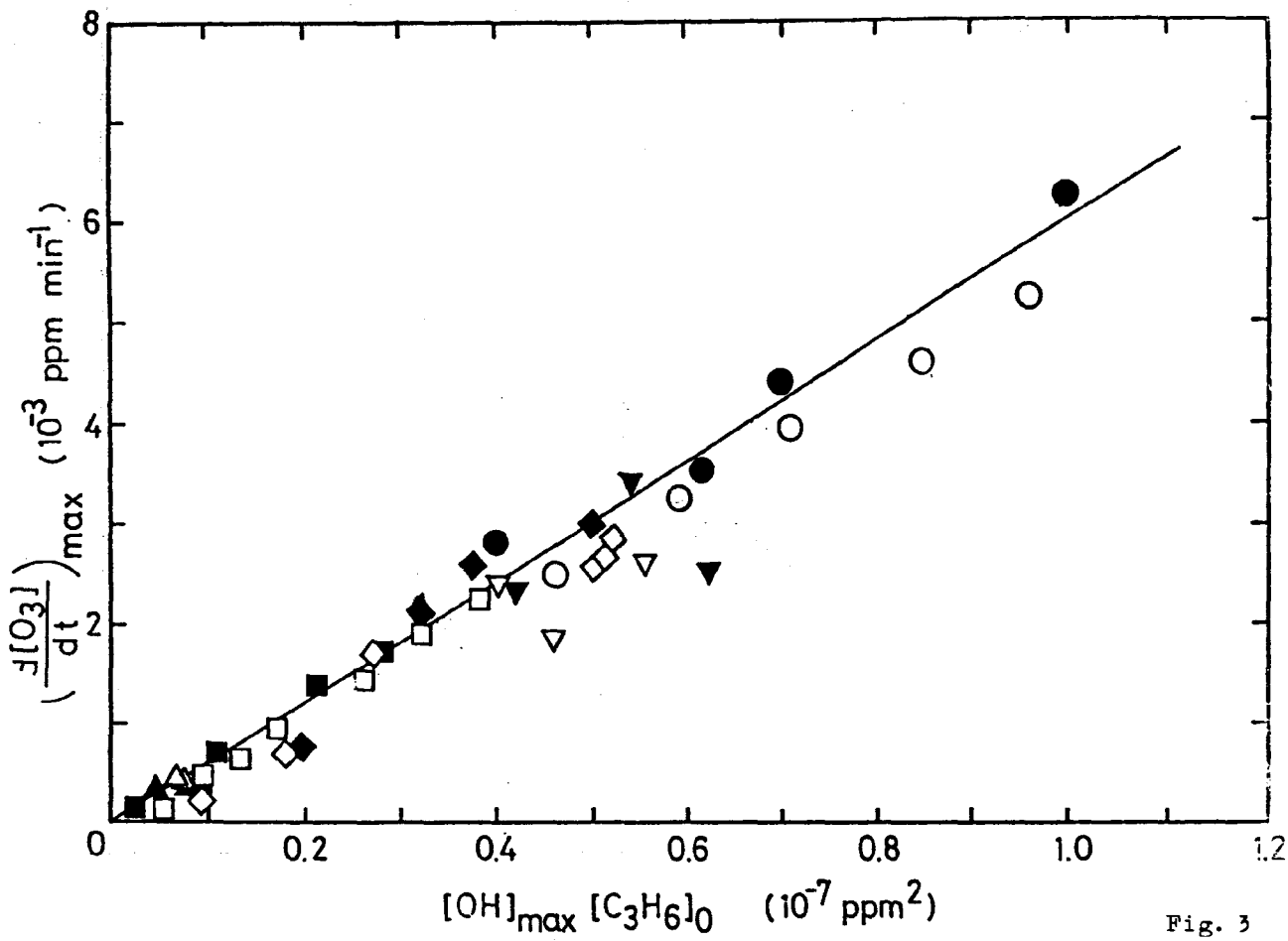
$\left(\frac{d[O_3]}{dt}\right)_{max}$ (10^{-3} ppm min^{-1})
$[OH]_{max}\,[C_3H_6]_0$ (10^{-7} ppm^2)
0
0.2
0.4
0.6
0.8
1.0
1.2
2
4
6
8

Fig. 3

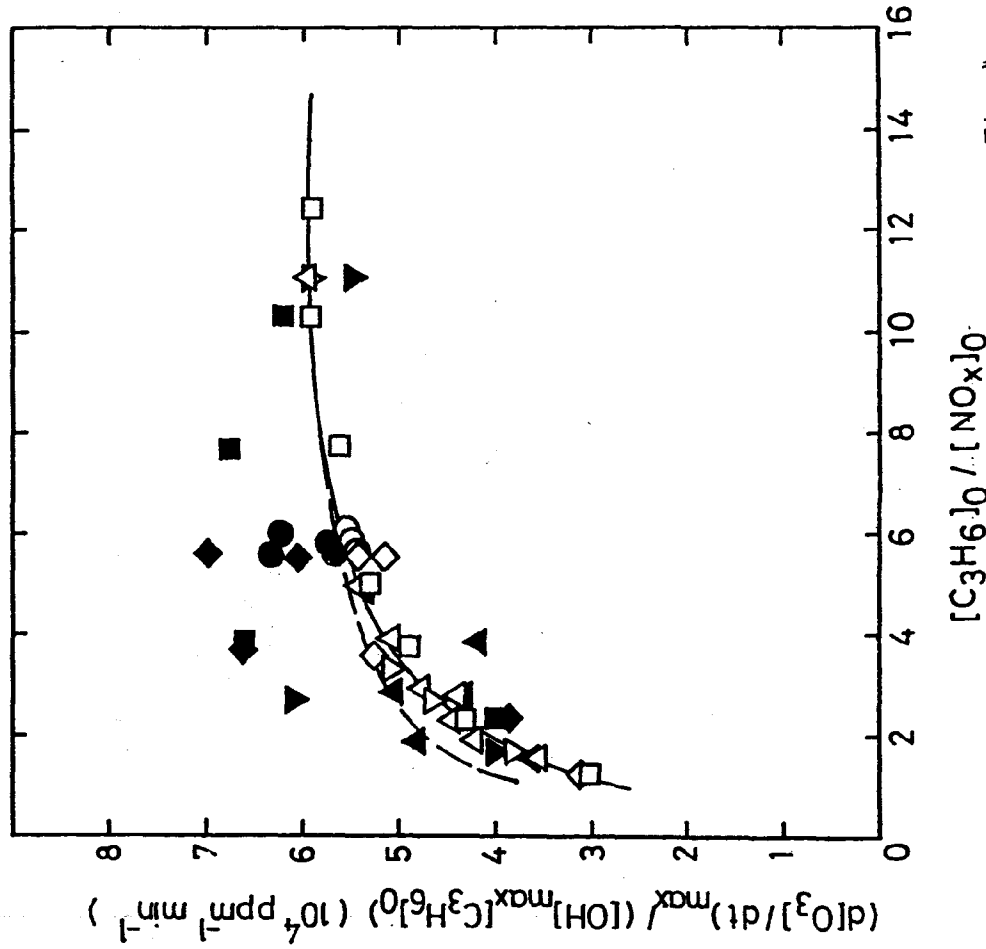
$(d[O_3]/dt)_{max}/([OH]_{max}[C_3H_6]_0)$ (10^4 ppm^{-1} min^{-1})
$[C_3H_6]_0/[NO_x]_0$
0
1
2
3
4
5
6
7
8
2
4
6
8
10
12
14
16

Fig. 4

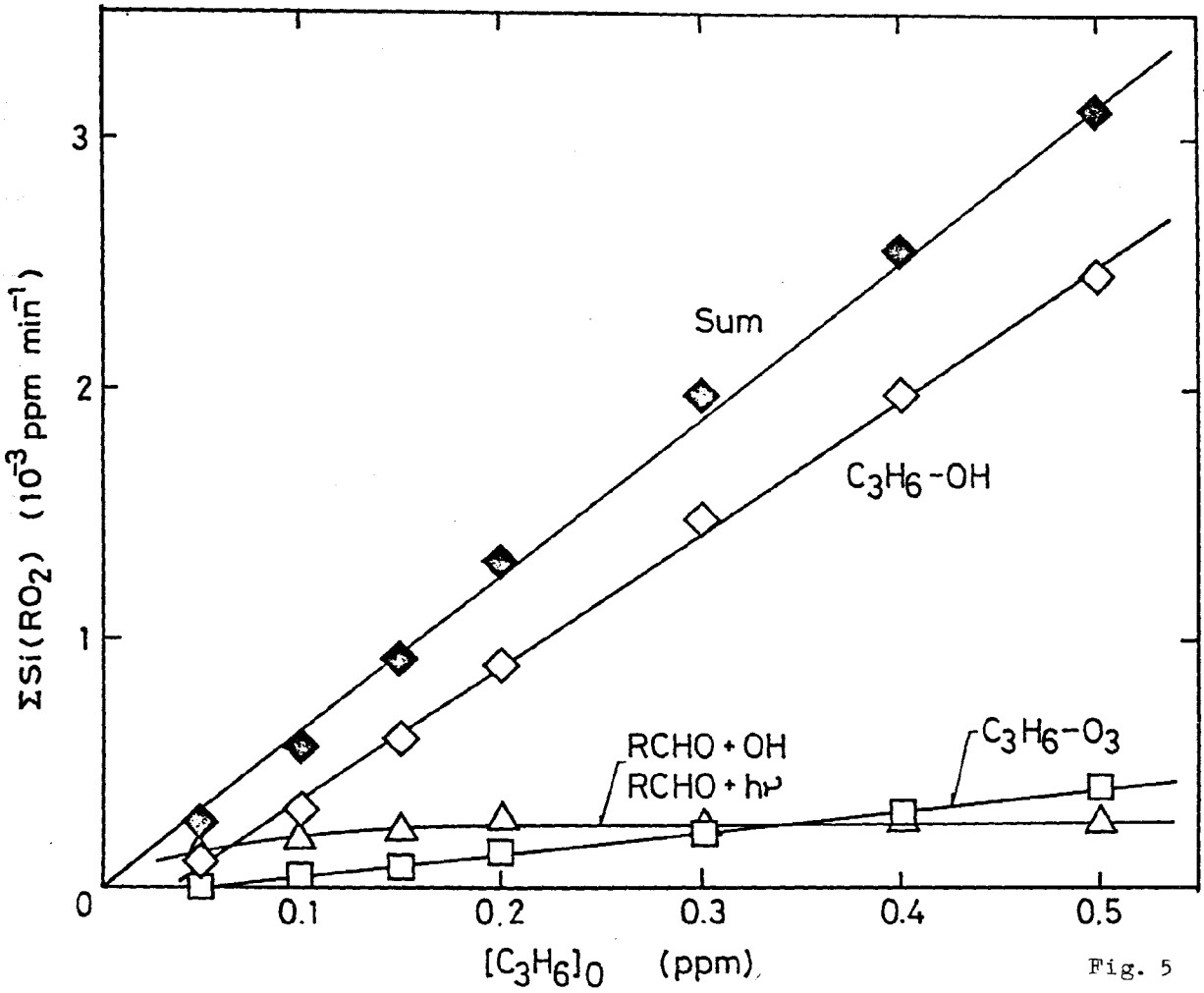
ΣSi(RO2) (10-3 ppm min-1)
Sum
C3H6-OH
RCHO + OH
RCHO + hν
C3H6-O3
[C3H6]0 (ppm)

Fig. 5

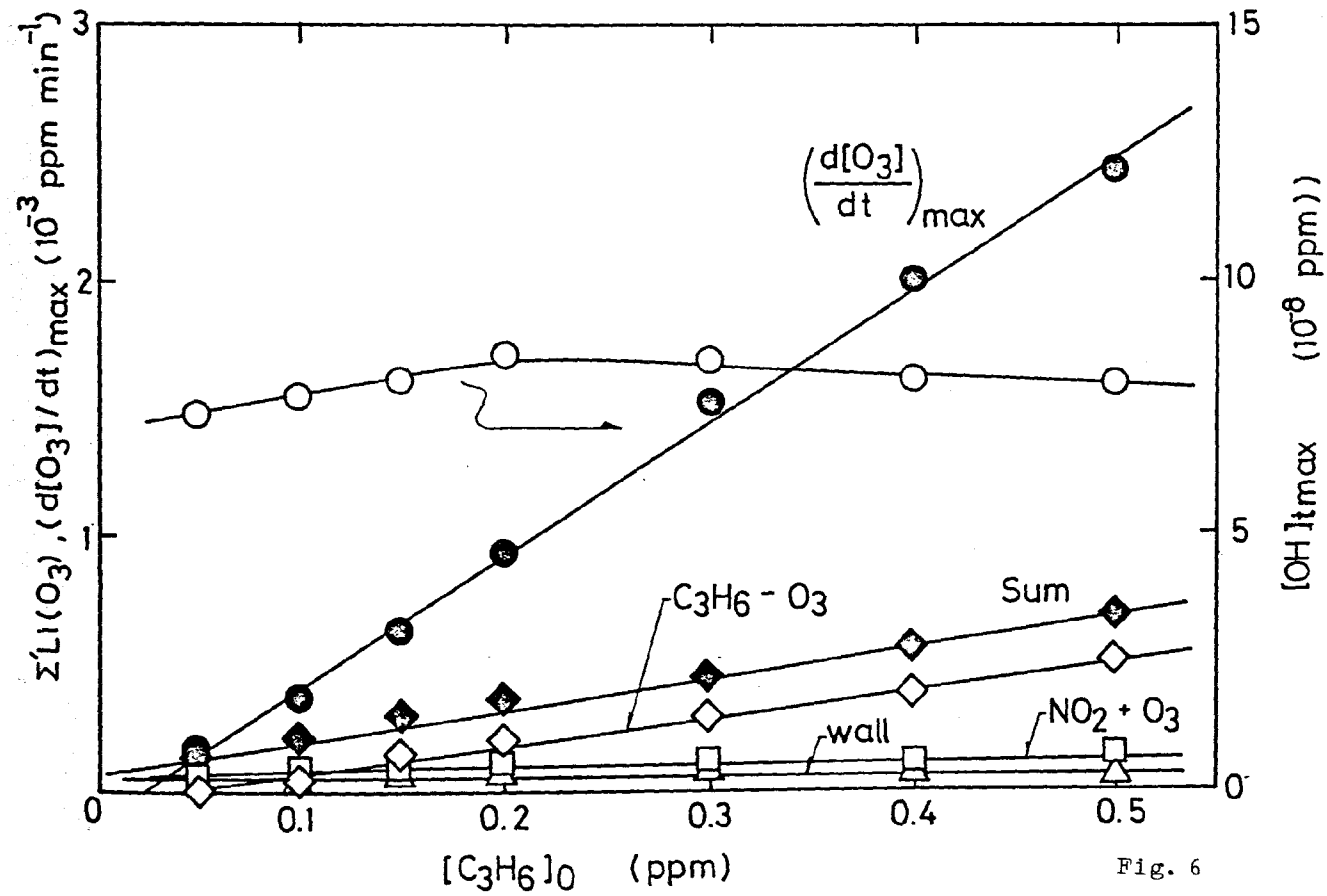
Σ'Li(O3), (d[O3]/dt)max (10-3 ppm min-1)
[OH]tmax (10-8 ppm))
(d[O3]/dt)max
C3H6 - O3
Sum
wall
NO2 + O3
[C3H6]0 (ppm)

Fig. 6

FURTHER DEVELOPMENT AND VALIDATION OF EKMA

presented by B. Dimitriades

Environmental Sciences Research Laboratory

USEPA

The discussion presented earlier on further development of atmospheric reaction mechanisms applies, of course, to EKMA also. The discussion to follow, therefore, will focus on the field validation component only of the EKMA development effort in the U.S.

At first glance, it would appear that for a purely mechanistic scheme such as EKMA, the only validation needed is against laboratory data. EKMA, however, is used as a complete air quality predictive model, and as such, according to an all-accepted rule, it should be validated against field data also. Field validation of mechanistic models is extremely difficult because of the problem in separating out the meteorological influences. Nevertheless, there are some techniques that, in concept or partially at least, circumvent this problem. These techniques, and some comments they received from the EKMA Workshop experts are as follows:

(1) Trend Analysis of Historical Emissions and Air Quality Data (J. Trijonis)

Historical precursor trends are constructed for an urban area using emissions data and ambient 6-9-am data for NMHC and NO_x. The precursor trends are entered into the standard EKMA model to predict historical ozone trends. The predicted ozone trends are then compared to actual ozone trends to test the EKMA model.

This method, while simple in concept, is complicated by the large uncertainty in the precursor data. For example, emissions inventory figures for the Los Angeles area during 1964-1978 show 29% decreases in reactive hydrocarbons and 35% increases in oxides of nitrogen but corrections of various inventorying errors over this same time period are at least of this same order. Also, the model predictions are extremely sensitive to the $NMHC/NO_x$ ratio and, hence, to the errors of the ratio estimates.

Results from one application of the method showed that the method underestimated observed ozone levels by as much as 35% for peak hourly ozone levels at Azusa. The discrepancy was greatly alleviated by the use of the more robust statistic, the 95th percentile ozone level. The disagreement seemed to be comparable between the case of precursor-derived $NMHC/NO_x$ ratios and that of emission-derived $NMHC/NO_x$ ratios. Although attempts were made to outline the source areas the emissions of which had most influence on each ozone monitoring station and to correct ozone formation for meteorology, no account was made for day-to-day differences in initial chemical composition, mixing depth composition at the upper boundary or path differences over the emissions pattern.

One important conclusion from such studies was that the emissions changes during relatively short periods (3-4 years) are not large enough to provide an adequate test of the EKMA model. Also, the method requires an accurate knowledge of the $NMHC/NO_x$ ratio as well as reliable emissions and ambient air quality data. With improvements in these areas, the trend analysis approach can be a useful one.

(2) Statistical Evaluation of EKMA (J. Martinez, C. Maxwell, H. S. Javitz, and R. Bawol)

The method entails computation of maximum daily O_3 from 6-9-am NMHC and NO_x and statistical comparison of such predictions with daily maximum O_3 observations. A central theme to this approach is the probability that the ratio (R) of observed-to-estimated ozone lies within the range 0.8 to 1.2. The graphical representation of the output is represented as accuracy probability isopleths on the NMOC/NO_x plane. The method was used to compare the Carbon Bond II, Demerjian and Dodge chemical mechanisms using data from St. Louis, Houston, Philadelphia, Los Angeles, and Tulsa. Results showed that qualitatively all three mechanisms give similar shapes for the over-($R<0.8$) and underprediction ($R>1.2$) regions, but the Dodge mechanism is represented best of all of the mechanisms in the $0.8<R<1.2$ range. The use of this technique for future conditions could generate ozone frequency distributions from input joint frequency functions for NMVOC and NO_x. The method could be improved by extension to use day-specific meteorological air quality and emissions conditions.

(3) Predicting Ozone Frequency Distributions from Ozone Isopleth Diagrams and Air Quality Data (H. Jeffries and G. Johnson)

The method entails computation of O_3 from morning NMHC and NO_x concentration values and comparison of resultant frequency distribution of predicted O_3 concentrations with frequency distribution of observed concentrations. Application of this method upon Sydney (Australia) data from some 800 hourly measurements of NMHC, NO_x during 6-10 am resulted in excellent agreement between predictions and observations.

The method was extended to parameterize the max-O_3-NMHC-NO_x surface using seven parameters representing relevant precursor, chemistry, and meteorology factors. Parameters were determined so as to maximize agreement between predicted and observed O_3 frequency distributions. Thus, effects of emission controls were translated not in terms of max O_3 concentration changes but in terms of changes in O_3 frequency distribution. This method, as the preceding one, is particularly appealing because it lends itself to computing error probability and risk distributions.

(4) Simplified Trajectory Analysis Approach for Evaluating OZIPP/EKMA (G. Gibson and E. Meyer)

Back air parcel trajectories are calculated from the site observing the highest hourly ozone concentration in an urban area. The EKMA model is then used to simulate the chemistry that occurs within a uniformly mixed parcel of air as the parcel moves along the calculated trajectory. The resulting peak ozone concentration predicted at the site is compared to the actual observed maximum value. The method, using the different forms of the EKMA model, was applied to St. Louis and Philadelphia data. Results showed that the more complex form of EKMA, i.e. the one that uses wind trajectory data, is not necessarily the more accurate one; errors in wind trajectory estimates cause substantial errors in the model predictions.

Also, the method suffers from the limitation that it does not use statistical samples; its performance depends on selection of one worst-case hour or day.

(5) Comparison of EKMA with AQSMs (G. Whitten)

This method for field-validating EKMA is an indirect one, based on comparison with other field-validated models e.g. the SAI airshed model. Results from parallel applications of the EKMA and SAI models showed good agreement except when the NMHC/NO_x ratio is defined differently (based on emissions for SAI and on ambient concentrations for EKMA) and in situations in which background pollutant concentrations are important.

(6) Deriving EKMA Isopleths from Experimental Data: The Los Angeles Captive Air Study (D. Grosjean, R. Countess, K. Fung, K. Ganesan, A. Lloyd and F. Lurmann)

The method involves sampling and irradiation of urban air inside Teflon bags and comparing resultant O_3 concentration to those estimated by EKMA. An application of the method is under way in LA, but results are not available yet. The method is realistic but, unless shown to the contrary, it suffers from the usual uncertainty problems associated with chamber wall effects.

Discussion

All the above techniques for field-validating EKMA are being considered by USEPA as candidates for subjects of future research. At this time we have no final choices but we do favor those of the existing techniques (or new ones) that provide statistical measures of the model's accuracy. Furthermore, we are interested in the "Captive Air Experiment" concept but not for precisely the same reasons as those of Grosjean and co-workers. Since our reasons may be of interest to Japan also, I wish to elaborate further on this concept and to invite the Japanese delegation to consider this as another subject for cooperative research with the U.S.

The captive air experiments we would propose would be for the purpose of testing the common technique of simulating urban atmospheres using smog chambers and synthetic pollutant mixtures. The main question posed here is whether such simulations are indeed realistic or useful. More specifically, the proposed experiments would be for the purpose of comparing the photochemical behavior of real atmosphere pollutant mixtures with that of synthetic mixtures presumably representative of the ambient mixtures. Briefly, these experiments would entail parallel outdoor irradiation of bags containing ambient (urban) air and bags containing synthesized "ambient" VOC/NO_x mixtures. If the two sets of bag mixtures display substantial differences in photochemical behavior, we would have to reconsider all AQSM techniques that assume no such differences.

METHODS FOR VALIDATING EKMA AGAINST FIELD DATA

1. TREND ANALYSIS OF HISTORICAL EMISSIONS AND AIR QUALITY DATA
2. STATISTICAL EVALUATION
3. COMPARISON OF OZONE FREQUENCY DISTRIBUTIONS
4. SIMPLIFIED TRAJECTORY ANALYSIS APPROACH
5. COMPARISON WITH AQSMS
6. COMPARISON WITH SMOG CHAMBER DATA FROM AMBIENT AIR IRRADIATIONS

ACID RAIN (DEPOSITION) CHEMISTRY AND PHYSICS

presented by A.P. Altshuller

Environmental Sciences Research Laboratory

USEPA

Acid deposition often referred to as "acid rain" results from the combined effects of wet scavenging by rain, snow, sleet, or hail, by fogs and dry deposition of gases and particles. The substances usually considered of concern are sulfur dioxide, sulfur aerosols, nitrogen dioxide and nitric acid and hydrochloric acid.

The concern biologically is not only with the acidity of the deposited substances, but with the total sulfur and nitrogen deposited. With respect to the background pH level, this level often has been assumed in the past to be that of natural rainwater containing only dissolved CO_2. Such an aqueous solution has a pH of 5.6. However, the pH of rain in remote areas has been measured below 5.6. Charlson and Rodhe (1982) have discussed the concentration levels of sulfur compounds, ammonia and carbon dioxide possible in cloud water in remote areas. They conclude that pH values could range from 4.5 to 5.6 in remote locations. Therefore, the pH values obtained in populated rural areas or cities should be evaluated compared to this wider background pH range.

Natural and Anthropogenic Emissions for the United States

Estimates of the natural and anthropogenic emissions of sulfur compounds in the United States are summarized in Table 1. In the eastern United States, the natural emissions summing to about 0.2 Tg S yr^{-1} (10^{12} grams S yr^{-1}) are insignificant compared to the anthropogenic emissions of 12 to 13 Tg S yr^{-1} (Robinson and Homolya, 1982). The natural emissions appear to be more significant in the western United States compared to anthropogenic sources. However, the method of estimation is such as to possibly overestimate natural emissions of sulfur from the more arid and alkaline soils of the western United States.

For the eastern United States, the natural emissions of nitrogen compounds based on two different methods of estimation (Robinson, 1982) sum to a lower estimate of 0.24 Tg N yr^{-1} or an upper estimate of 1.9 Tg N yr^{-1} (Table 1). The upper estimate of natural emissions of nitrogen compounds would constitute about 18% of the sum of natural and anthropogenic emissions in 1978 for the

eastern United States. Natural emissions would have constituted a much larger percentage of total emissions of nitrogen in earlier years because the anthropogenic emissions of NO_x have increased rapidly with time. In the western United States, natural emissions of nitrogen compounds may be substantial compared to anthropogenic emissions. However, the range of uncertainty in estimating natural emissions of nitrogen is so wide as to make the estimates of natural emissions particularly in the western United States preliminary.

Coal-fired emission sources burning coals with substantial chlorine contents are major contributors to the anthropogenic emissions of HCl in the atmosphere (Homolya, 1982). However, the natural emissions of chlorine appear to exceed the anthropogenic emissions in the eastern United States (Table 1).

Sulfates or sulfur in particle form can arise either from primary emissions of particle sulfur from fossil-fueled sources or be formed from sulfur dioxide through atmospheric reactions. In some areas of the northeastern United States primary particle sulfur is significant compared to secondary particle sulfur particularly in the winter months (Homolya, 1982). These higher emissions of particle sulfur are associated with oil-fired sources burning fuel oils under operating conditions leading to higher percentages of particle sulfur than usual. In parts of New England ant the mid-Atlantic states particle sulfur can constitute 5 to 10% of total sulfur emissions.

Emissions of sulfur oxides from coal-fired sources in the United States have been high for the last century. However, there was a shift away from use of coal after World War I for residential and commercial heating and for railroad travel. Almost concurrently, there was a substantial growth in coal-fired power plants in the midwestern and southeastern United States. As a result, anthropogenic sulfur emissions today in the United States are emitted from many large sources with tall stack heights in rural areas in addition to urban sulfur emissions.

Nitrogen oxide emissions in the United States increased about four-fold between 1940 and 1978 from anthropogenic sources (Homolya, 1982). This increase was associated with large increases in emissions from both highway vehicles and from electric utilities. The relative contribution of highway vehicles compared to electric utilities varies substantially from region to region in the United States.

Air Quality Measurements

Sulfur oxide concentrations are highest in urban areas of the eastern United States (Altshuller, 1982). However, the sulfur oxide concentrations have decreased substantially because of reductions in the sulfur content of fuels during the late 1960's and 1970's. Although sulfur dioxide is appreciably lower in rural areas of the eastern United States than in urban areas, the differences in concentrations between urban and rural areas has decreased.

Sulfate aerosols occur at substantial concentration levels compared to sulfur dioxide both in rural and urban areas. These aerosols are mainly in the submicron particle size range although lower concentrations of supermicron sulfur particles can be measured. Sulfate concentrations have decreased in eastern cities in the United States in the winter months, but not in the summer months. In rural areas, sulfate concentrations have not decreased throughout the year and they have increased in summer months. Sulfate areosols can contribute one-third to one-half of the sulfur burden in rural areas in the summer.

The concentrations of nitrogen oxides are comparable to the concentration of sulfur oxides in both urban and rural areas of the eastern United States (Altshuller, 1982). However, the concentration of nitrogen in aerosol form is substantially lower than that of sulfur in aerosol form in the eastern United States.

Sulfate aerosols not only make a contribution to acid deposition in the United States, but also to visibility reduction. Sulfate aerosols appear to be the most important species contributing to visibility reduction in rural areas in eastern North America.

Transport of Acid Compounds

The flow field in the planetary boundary layer (PBL) within which the acid substances are emitted is affected by a broad spectrum of atmospheric motions (Gillani, 1982). These factors include wind shear with height, strong diurnal and seasonal effects, as well as complex flows in river valleys, on mountain slopes, or on the shores of lakes or oceans.

Within the Midwestern United States prevailing winds, on the average are from the southwestern quadrant in summer, but are more westerly in winter (Gillani, 1982). The vertical transport layer from longer-range transport varies from the ground up to 1 or 2 km in the summer and about half these heights in the winter. Diurnal variability of the flow field is especially large in the summer when a "nocturnal jet" with strong wind shear is a frequent occurrence particularly in the midwestern United States. Plumes undergo sequences of sheared stratification and distortion at night followed by rapid vertical mixing during the day. As a result, emissions can be rapidly dispersed over a regional scale.

The diurnal and seasonal variations in mixing height are important also (Gillani, 1982). Because of substantially lower mixing heights in winter than summer, a significant part of the emissions from tall stacks may remain elevated and relatively undispersed to the surface over distances in excess of 500 km. Such diurnal and seasonal aspects should have an important influence on the atmospheric residence times, range of transport before deposition, of emissions from elevated compared to near surface sources. For example, nitrogen oxide emissions from tall stacks should have significantly longer residence times than the nitrogen oxide emissions from highway vehicles. The emissions from highway vehicles can undergo substantial dry deposition especially during the night-time hours. Therefore, the relative contributions of various types of sources to biologically sensitive areas downwind should vary substantially with season of the year.

Transformation Processes

It is reasonably certain that OH radicals predominate in the gas-phase reactions that transform sulfur dioxide to sulfate aerosols and nitrogen dioxide to nitric acid (Miller, 1982). The rate of transformation of nitrogen dioxide to nitric acid is substantially faster than the rate of conversion of sulfur dioxide to sulfate. The concentrations of OH radicals show large diurnal, seasonal and geographical variations. The reactions associated with OH radicals should be most significant during the daylight hours, warmer months of the year and at lower latitudes. In polluted air, the concentration of OH is strongly related to the concentrations of hydrocarbons, aldehydes and of nitrogen oxides. The same sets of atmospheric reactions of importance in determing the formation of ozone and other photochemical products are involved in determining the net OH radical concentrations.

Various chemical reactions must be considered with respect to reaction in cloud and rain drops (Hegg and Hobbs, 1982). However, available evidence indicates that the primary source of nitric acid and hydrochloric acid in cloud and rain drops are either the homogeneous atmospheric gas-phase reactions discussed above or the direct emissions of hydrochloric acid. Production of sulfuric acid in solution within raindrops or other hydrometeors can occur by several different chemical reactions. The oxidation of sulfite by hydrogen peroxide appears to be the single most important of these reactions producing sulfuric acid. However, the amounts of hydrogen peroxide available in solution is not well characterized at present.

Neutralization by ammonia absorption is an important process (Hegg and Hoggs, 1982). However, the acidity of raindrops appears to remain higher than the acidity of suspended particles in the atmosphere.

A wide range of rates of conversion of sulfur dioxide to sulfate have been reported in urban plumes (0 to 32% hr^{-1}) (Miller and Whitbeck, 1982). The rates appear to be appreciable higher in urban plumes within or near cities than in power plant plumes or in rural areas. Rates of conversion of nitrogen dixoide

ranging from 5 to 24% hr^{-1} have been computed. Most of the products of reaction of nitrogen dioxide in plumes are gaseous rather than aerosol species.

A wide range of rates of conversion of sulfur dioxide also have been obtained from measurements within power plant plumes (Miller and Whitbeck, 1982) (0 to 15% hr^{-1}). However, the rates of conversion of sulfur dioxide are moderate, 0 to 3% hr^{-1}, in a number of studies. The rates are dependent on time of day, season of year and availability of "background" hydrocarbon concentrations to mix into plumes from ambient air. The latter factor may explain the higher rates of conversion for sulfur dioxide frequently reported for plumes in the eastern compared to the western United States. Where concurrent measurements of sulfur dioxide and of nitrogen dioxide rates are made, the rates of nitrogen dioxide conversion were several times faster than those for sulfur dioxide conversion.

It is difficult to separate out the contributions of gas-phase and liquid phase reactions in plumes (Gillani, 1982). However, based on measurements in power plant plumes the following 24 hour average estimates of sulfur dioxide conversion rates have been suggested: July, gas-phase $0.8 \pm 0.3\%$ hr^{-1}, liquid phase, $0.4 \pm 0.2\%$ hr^{-1}; January, gas phase, <0.1% hr^{-1}; liquid phase, about 0.2% hr^{-1}. Similar parameterizations are not yet available for nitrogen dioxide conversions in power plant plumes. Also, similar parameterization values have not been suggested in urban plumes.

Precipitation Scavenging Processes

Precipitation scavenging may be defined as the composite process by which airborne gases and particles attach to precipitation elements and subsequently deposit on the Earth's surface (Hales, 1982). The processes involve many intermeshed pathways. Different storm types, differ in the significance of the processes leading to deposition; nevertheless, there is a substantial overlap in the characteristics of storm types. Important storm types include cyclonic or "frontal" storm systems and convective storms.

The results of field studies on precipitation scavenging lead to the following conclusions (Hales, 1982).

(1) Sulfur oxides and nitrogen oxides are removed with low efficiences short distances downwind of power plant stacks.

(2) In urban plumes, moderate percentage removals of sulfur oxides have been observed out to 100 km. Removal of nitrogen oxides from urban plumes is less than sulfur oxides, but still significant.

(3) On a regional scale the removal of nitrogen oxides is greater in proportion to its regional emission rate than the removal sulfur oxides.

Dry Deposition Processes

The rates of dry deposition from the air to surfaces depend on a large number of chemical, physical and biological factors (Hicks, 1982). The relative importance of these factors vary according to the nature of the surface, characteristics of the chemical and the meteorological conditions. Despite such complexities it is useful to consider a deposition velocity, V_d, for gases and submicron particles which can be used along with airborne concentrations, C, to estimate fluxes, F, by the expression $F = V_d{}^{\circ}C$. For particles larger than about 5 um diameter deposition is primarily determined by Stokes' law, while for submicron particles turbulent transfer tends to dominate. Deposition of gases is often limited by diffusive properties close to the receptor surface. Surface effects can be very important. Uptake rates of vegetation is often determined by stomatal resistance. Surface wetness also is important on biological and man-made surfaces.

For a specific surface such as a lake, air moving from land over water will equilibrate at a rate dependent on the stability regime involved. Henry's law constants and chemical reactivity of substances are important to exchange between air and water.

Wind tunnel experiments indicate very low deposition rates for submicron particles. Over water, the role of waves can substantially increase particle transfer by several possible processes.

Several micrometeorological measurement methods have been used to calculate deposition velocities. These methods include eddy-correlation, concentration gradient techniques, a "modified Bowen ratio" method and high-frequency variance methods.

A substantial number of field investigations have been carried out to obtain the deposition velocities for sulfur dioxide (Hicks, 1982). Deposition rates of 0.1 to 0.2 cm s^{-1} have been reported over snow. Measurements available over pasture, wheat and soybeans result in deposition velocities usually ranging from 0.4 cm s^{-1} to 1.3 cm s^{-1}. Most of these results are for daylight conditions. One set of field experiments over a forested area (pine plantation) demonstrated the wide variation possible in deposition velocities over the diurnal cycle. Relatively few measurements are available for the deposition velocity of nitrogen dioxide. One set of measurements over soybeans during daylight hours provided values of V_d comparable to those of sulfur dioxide over field crops. The resistance to deposition of nitric oxide, NO, is high. While no direct experiments are available for nitric acid a very low resistance to transfer is estimated with a substantial similarity to HF which has a high deposition velocity.

Deposition velocities for sulfate particles are greater than obtained for other particles in the submicron range (Hicks, 1982). An explanation suggested was the presence of sufficient amounts of larger sulfate particles to result in higher deposition velocities. However, in recent dry deposition measurements submicron particles were specifically considered in which sulfur dominated the chemical composition. Deposition velocities of about 0.5 cm s^{-1} were obtained.

Deposition Monitoring

Methods for monitoring dry deposition are inadequate (Hicks, 1982). Results obtained from use of collection vessels and from surrogate surfaces are not easily related to the actual behavior of natural surfaces with respect to deposition.

A wide variety of precipitation chemistry sampling networks have been operated in the United States because of the ease of collecting rain and snow (Stensland, 1982). Bulk samplers often have been used which do not permit

the separation of wet from dry deposition. Many networks in the past lacked the spatial and temporal extent necessary to assessing national or even regional trends and patterns. More recent networks in the United States and in Canada use automatic samplers and have sufficient geographical extent to give useful information over eastern North America. The highest concentrations of sulfate, nitrate and hydrogen ions in precipitation occur in the midwestern United States east of the Mississippi River, into the mid-Atlantic states and in parts of southern Ontario and Quebec. These concentrations fall off the west, south and east of this geographical area. The highest ammonium ion concentrations in precipitation are in the midwest, west of the Mississippi River. The highest calcium ion in precipitation are in approximately the same geographical area as ammonium. Therefore, the depositions of alkaline species, ammonium and calcium are displaced somewhat to the west of those for hydrogen ion, sulfate and nitrate.

An increase of nitrate in precipitation in the United States since the 1950's can be demonstrated (Stensland, 1982). However, there are serious questions as to the evidence to support a similar increase in acidity.

Air parcel trajectory analyses have been used to link precipitation chemistry patterns to emission source regions (Stensland, 1982). While general directional characteristics have been obtained in several investigations, such techniques need to be further developed and verified with field experiments.

Other aspects relating to deposition measurement ~~invoice~~ involve direct impaction of cloud water within mountains at cloud heights and fog water. Munger and coworkers (1982) report at urban locations in California the pH of fog water to be lower than rainwater (Liljestrand and Margan, 1978). The pH of a number of samples of fog water was as low as the 2.0 to 3.0 range. This behavior in urban areas appears different than in rural areas where the concentration of ions of fog water has been reported as comparable to that in cloud and rainwater. The composition of the fog water was such that nitrate ions exceeded sulfate ions and ammonium ions usually exceeded hydrogen ions in concentration. The authors concluded that "the chemistry of fog water in the samples they analyzed was dominated by the composition of the haze-forming aerosol that preceeded it".

References

Charlson, R.J. and Rodhe, H. (1982) Factors controlling the acidity of natural rainwater. Nature 295, 683-685.

Waldman, J.M., Munger, J.W., Jacob, D.J., Flagan, R.C., Morgan, J.J. and Hoffmann, M.R. (1982). Chemical composition of acid fog. Science 218, 677-680.

Liljestrand, H.M. and Morgan, J.J. (1978). Chemical Composition of Acid Precipitation in Pasadena, California. Environ. Sci. Technol. 12, 1271-1276.

From Critical Assessment Draft Document
The Acidic Deposition Phenomenon and its Effects Volume 1. Prepared for : U.S. Environmental Protection Agency through North Carolina State Univ. Acid Precipitation Program, October 1982.

Robinson, E., in Chapter 2 - Natural and Anthropogenic Emissions Sources
Homolya, J. in Chapter 2 - Natural and Anthropogenic Emissions Sources
Altshuller, A.P. in Chapter 3 - Atmospheric Concentrations and Distributions of chemical Substances
Gillani, N. in Chapter 4 - Transport Processes
Miller, D in Chapter 5 - Transformation Processes
Hegg, D. and Hobbs, P. in Chapter 5 - Transformation Processes
Gillani, N. and Whitbeck, M.R. in Chapter 5 - Transformation Processes
Hales, J. in Chapter 6 - Precipitation Scavenging Processes
Hicks, B. in Chapter 7 - Dry Deposition Processes
Hicks, B. in Chapter 9 - Deposition Monitoring
Stensland, G. in Chapter 9 - Deposition Monitoring

Source	Element	Emissions, TgX yr^{-1} Contiguous U.S.	U.S. East of Mississippi River plus Texas
Anthropogenic (1978)	S	13	12
electric utility	S	-	8
Anthropogenic (1970)	S	14	13
electric utility	S	-	7.5
Natural Sources	S	∿.5	∿.2
biogenic onland	S	≤.23	.07
oceanic	S	.2	.1
volcanic	S	small[a]	neg
Anthropogenic (1978)	N	10.7	8.9
electric utility	N	-	2.9
Anthropogenic (1970)	N	9.3	7.9
electric utility	N	-	2.4
Natural Sources	N	.84[b], 6.9[c]	.24[b], 1.9[c]
NO_x biogenic onland	N	0.23, 2.5	0.04, 0.7
NO_x by lightening	N	0.01 - 0.1	0.01
NH_2 biogenic onland	N	0.6, 4.3	0.19, 1.2
Anthropogenic (1974)	Cl	-	≥.45
Natural Sources	Cl	-	1.6

[a]may be important in certain areas for short time periods

[b]estimated from approach based on results of Adams and coworkers See Robinson (1982)

[c]estimated from approach based on results of Galbally See Robinson (1982)

STATUS OF RECEPTOR MODELS

presented by A.P. Altshuller

Environmental Sciences Research Laboratory

USEPA

Status of Receptor Models

Robert K. Stevens, Charles W. Lewis and A. P. Altshuller
U.S. Environmental Protection Agency
Research Triangle Park, NC 27711

Introduction

The development of receptor-based models has progressed significantly in the past few years (see Report of First Quail Roost Workshop, Watson et al., 1981). Mathematical receptor models presently in use can be classified into several categories: chemical mass balance (CMB), multivariate, microscopic, and source-receptor hybrids. For the sake of brevity, we will only discuss two types of receptor models, tracer (CMB) and factor analysis models (multivariates) in detail. We also distinguish receptor models from conventional dispersion modeling.

DISPERSION MODELS

Dispersion models are the conventional means of predicting the environmental impact of an emission source on air quality. In general, the dispersion model states that the contribution of source j to a receptor, S_j, is the product of an emission rate, E_j, and a dispersion factor, D_j, so that

$$S_j = D_j E_j$$

Dispersion formulae are usually classified by the geometric form of the emission source, giving rise to expressions for point, line, and area sources. A basic goal of air quality meteorology is to relate the dispersion factor for a given source goemetry to known meteorological parameters such as wind speed and direction and atmospheric stability. The available dispersion models have been classified and described in various EPA reports.* Current development of dispersion models focuses on modeling dispersion in rough terrain, long-range transport, wet and dry acidic deposition, and complex atmospheric chemistry.

RECEPTOR MODELS

In contrast to dispersion models, receptor models start with observed ambient airborne particle concentrations of many elements at a receptor and seek to apportion the observed concentrations between several source types based upon knowledge of the composition of the source and receptor material. Receptor models and their application have been reviewed by Gordon (1980).

The foundation of all receptor-based models of particulate source assignment is a simple mass conservation argument. If a number of sources, p, exists, and if there is no interaction between their aerosols that causes mass removal or formation, the total airborne particulate mass measured at the receptor, C, will be a linear sum of the contributions of the individual sources S_j:

$$C = \sum_{j=1}^{p} S_j \qquad (1)$$

*Dispersion models usually provide predictions involving a single pollutant such as sulfur dioxide, carbon monoxide or ozone. The models are designed to satisfy the emission, transport and transformation characteristics of the selected pollutant.

Similarly, the mass concentration of aerosol property i,* C_i, will be

$$C_i = \sum_{j=1}^{p} a_{ij} S_j \qquad (2)$$

where a_{ij} is the mass fraction of source contribution j possessing property i at the receptor.

The Chemical Mass Balance Receptor Model

When the property i is a chemical property, Equation (2) represents a chemical mass balance. If one measures n chemical properties of both source and receptor, n equations of the form of Equation (2) exist. If the number of source types contributing those properties is less than or equal to the number of equations, that is, if $p \leq n$, then the source contributions S_j can be calculated by solving the overdetermined system of linear Equations (2). Five methods of performing this calculation have been applied: the tracer property, linear programming, ordinary linear least-squares fitting, effective variance least-squares fitting, and ridge regression. Effective variance least-squares is the most widely used CMB method (Watson, 1979).

Tracer Method --

The tracer element method is the simplest and will be the only receptor model discussed in detail. Tracer models assume that each aerosol source type possesses a unique property that is common to no other source type. Equation (2) then reduces to

$$S_j = \frac{c_t}{a_{tj}} \qquad (3)$$

for each source j with its own tracer t (using the same notation as in Equation (2). It works well when the tracers meet the following requirements:

(1) a_{tj} perceived at the receptor is well known and invariant between source and receptor,
(2) C_t can be measured accurately and precisely in the ambient sample, and
(3) the concentration of property t at the receptor comes only from source type j.

These conditions cannot be completely met in practice, and limiting the model to only one tracer property per source type means that valuable information contained in the other aerosol properties is discarded. However, in some instances, one can use a tracer approach as a first-approximation, upper-limit estimate of source impact. Thus, solutions to the set of Equations (2) have been developed to make use of the additional information provided by more than one unique chemical property of a source type, and even by properties not so unique. The other methods of solution must deal with the case of a number of constraints, n, greater than the number of unknowns, p.

*examples of aerosol properties are chemical composition and particle size distribution.

Multivariate Models

The CMB uses the aerosol property of chemical composition. If source and ambient samples are taken in more than one size range, the size property can be used to separate the contribution of one source from another. However, the CMB solutions discussed above have no way to incorporate the variability of ambient concentrations and source emissions. The multivariate methods can do this. Multivariate methods include factor analysis, target transformation factor analysis, extended Q-mode factor analysis, and multiple linear regression, which is often used in conjunction with factor analysis. Only factor analysis will be discussed here.

While the CMB receptor model is easily derivable from the source model and the elements of its solution system are fairly easy to present, multivariate receptor models are not as simple. Watson (1979) has carried through the calculations of the source-receptor model relationship for the correlation and principal component models.

The apparent mathematical complexity of these models does not remove the requirement that every receptor model be representative of and derivable from physical reality as represented by the source model. A statistical relationship between the variability of one observable and another is insufficient to define cause and effect unless this physical significance can be established and is the same restriction as imposed on the CMB model.

The multivariate models (except the extended Q-mode model) deal with a series of m measurements of aerosol component i during sampling period or at sampling site k. From Equation (2),

$$C_{ik} = \sum_{j=1}^{p} a_{ij} S_{jk}, \quad k=1...m \tag{4}$$

The multivariate models deal only with C_{ik} with the objective of predicting the number of sources, p, and of predicting which a_{ij} is associated with which S_j (or, more ambitiously, estimating a_{ij} and S_{jk}).

Factor Analysis --

Factor analysis, a special type of multivariate model, generally begins with a cross-product matrix of the data; frequently, by calculating the correlation coefficient:

$$r_{C_iC_j} = \frac{1}{m-1} \sum_{k=1}^{m} \left(\frac{C_{ik} - \bar{C}_i}{\sigma_i} \right) \left(\frac{C_{jk} - \bar{C}_j}{\sigma_j} \right) \tag{5}$$

where m is the number of observations, $\bar{C}_i$ and $\bar{C}_j$ are the average values of C_i and C_j, and σ_i and σ_j are the standard deviations of C_i and C_j. The correlation coefficient is a measure of the extent that ambient concentrations C_i and C_j vary in the same way.

The classical factor analysis model transforms Equation (2) to

$$C_{ik}^{s} = \sum_{j=1}^{p} \alpha_{ij} S_{jk}^{s} + d_j U_{ij} \tag{6}$$

where

$$C_{ik}^{s} = \frac{C_{ik} - \bar{C}_i}{\left(\overline{C_i^2} - \bar{C}_i^2\right)^{\frac{1}{2}}} \tag{7}$$

$$S_{jk}^{s} = \frac{S_{jk} - \bar{S}_j}{\left(\overline{S_j^2} - \bar{S}_j^2\right)^{\frac{1}{2}}} \tag{8}$$

and

$$\alpha_{ij} = a_{ij}\left(\frac{\overline{s_j^2} - \bar{S}_j^2}{\overline{C_i^2} - \bar{C}_i^2}\right)^{\frac{1}{2}} \tag{9}$$

where α_{ij} (the "factor loading") is related to the source compositions through Equation (9) and S_{jk}^{s} (the "factor score") is related to the source contributions through Equation (8). The d_j and U_{ij} are unique factor loadings and scores, respectively, and often left out of the analysis. The result is a principal component analysis:

$$c_{ik}^{s} = \sum_{j=1}^{p} \alpha_{ij} S_{jk}^{s} \tag{10}$$

The factor model treats the C_{ik}^{s} as components of a vector for each chemical component i in an n-dimensional space. If Equation (4) is true, then only p vectors, where $p \leq n$ in a less complex p-dimensional space, are required to produce the vectors of C_i^{s}. This p-space is defined by the eigenvectors of the correlation matrix of the C_i^{s}. The p eigenvectors merely define the space, however, and are not necessarily representative of the sources, the S_j^{s} vectors. They must be linearly combined to form the new source vectors. This is typically done by a procedure known as "VARIMAX" rotation. The classical factor analysis can be used to screen a data set for potential error identification as well as for source recognition.

MULTICOLLINEARITY IN SOURCE APPORTIONMENT

An important aspect of source apportionment concerns the handling of sources with similar signatures, that is, sources whose aerosols are chemically and physically similar. Large errors can result if source apportionment by conventional regression or weighted regression analysis is attempted when two or more sources with very similar signatures are included. It is not uncommon for negative aerosol contributions with large magnitudes to

be estimated for some sources under these conditions. Another symptom is the calculation of uncertainties that are larger than the calculated source contributions themselves.

In statistical terms, the problem of similar souce signatures is one of "multicollinearity." More generally, multicollinearity exists when one source signature is nearly a linear combination of any subset of the other signatures. Details of how one can perform source apportionment studies when source signatures are similar are discussed in detail in the EPA Receptor Model Validation Workshop Report (Quail Roost II).

Considerations in Design of Source Apportionment Studies: A group of the participants headed by Dr. Glen Gordon, University of Maryland, examined and evaluated the preliminary results presented at the Quail Roost II Workshop and prepared reports that contained (1) an assessment of the value of the real and simulated sets and (2) a series of recommendations which serve as a basis for design of source apportionment studies which may be conducted by private or governmental institutions. The section, prepared principally by Gordon with input from Quail Roost II participants, will appear in an EPA report entitled "Mathematical and Empirical Receptor Models: Quail Roost II". Some of the key issues of this section dealt with the development of protocols to perform different levels of source apportionment. For example, it was recommended that source apportionment studies could be divided into three levels of intensity based principally on resource availability.

Level I Minimal Resources Requirements. This effort uses existing source signature libraries, existing ambient air quality data (mass and elemental composition of fine and coarse particles), local emission inventories, and literature values for soil composition. With this data one can perform chemical mass balance and factor analysis to determine if there are sources contributing to the receptor site which are not accounted for in the emission inventory.

Level II Moderate Resources are available: This level of effort includes all of the Level I work plus source elemental profiles from "grab" samples of fugitive sources, soil and major primary particle emitters in the airshed. These grab samples are resuspended and recollected in the same manner and on the same filter material as used to collect particles at the receptor site(s).

Level III Maximum Resources: This level III effort calls for (1) collection of aerosols at receptor sites where maximum plume fumigation may occur; (2) collection of particle emissions from the major emission sources with a dilution sampler that is coupled with a sampler similar to those used at the receptor sites; (3) both X-ray fluorescence (XRF), and instrumental neutron activation analysis (INAA) are used to analyze filters from the sources and receptor sites; (4) X-ray diffraction (XRD), scanning electron microscopy (SEM) and optical microscopy are also used to resolve sources with similar emission profiles.

Gordon included in his section a list (Table I) of aerosol sampling and gas measurement methods that should be part of a complete receptor model station. Figure 1 depicts the aerosol sampling analysis and data obtained for a complete aerosol apportionment study. We note from this figure at least 4

different sampling procedures may be necessary to perform reliable source apportionments. Gordon further recommended that multivariate and wind trajectory receptor models be used whenever there is a need to obtain source signatures not readily available by conventional source sampling procedures. These models are capable of providing source signatures by their unique treatment of air quality data. However, multivariate statistical models require large data sets (40 or more observations) and wind trajectory methods require short sampling periods (6 hours or less) and appropriate meteorological measurements.

Recommendations for Future Research: Table II is a list of marker elements used by the Quail Roost II participants in their various receptor models to report the Houston emission sources contributing to ambient particles impacting our Houston receptor site. The sulfate and nitrate listed in Table II do not, in the absence of appropriate source signatures, have marker elements which could reliably deduce their origins. At present, we can only speculate as to the origin(s) of the sulfate and nitrate. Even analysis of the Houston filters by SEM and optical microscopy failed to deduce their origin. Parenthetically, ancillary analysis of the aerosol samples by SEM, XRD and optical microscopy expands the number of sources beyond what can be identified by CMB methods alone (see Figure 2). In most airsheds in the United States sulfate and nitrate and their associated cations represent a substantial portion of the particle mass below 10 μm. Procedures must be developed to determine the origins of sulfate and nitrate that impact a given receptor site if source apportionment methodology is to adequately address urban and rural particulate problems.

At Quail Roost I and II there was no attempt by the participants to incorporate within the receptor modeling framework procedures to deal with questions of non-conserved species, particularly sulfates and nitrates. In view of the dominance of these species in urban and rural aerosols, it seems clear that this issue requires resolution.

Recent work by EPA scientists (1982) has been directed at addressing the problem of source apportionment of the non-conserved species, namely secondary products of SO_2 and NO. One solution they propose is the application of the following general formula:

$$T_j = S_j \cdot A_j \cdot M \qquad (11)$$

where:

T_j = Mass Concentration of Secondary Particles (e.g., $SO_4^{=}$) from Source J.

S_j = Mass Concentration of Primary Fine Particles from Source j determined to impact at Receptor Site. This term is derived from CMB calculations.

A_j = Ratio of SO_2 to Fine Particle Emissions measured at Source j.

M = Transformation Function [e.g., rate of conversion of SO_2 to $SO_4^{=}$ enroute from Source j to Receptor Site]

Assumptions: 1. Transport mechanism for sulfate and fine particle marker elements from Source J to Receptor Site is nearly the same.
2. Back trajectory meteorological data available.

This general equation has several features which need further discussion. For example, using the ratio of SO_2 to fine particle emissions eliminates the need to know absolute emission rates from source j. Also, the transformation function which will be described in a future publication is decoupled from the dilution of the primary emissions during transport. The only parameters we need to know are the rate of conversion of the primary gas to secondary particles, a relatively crude estimate for the additional deposition of SO_2 compared with the fine particles, and the time from source to receptor. The time function can be obtained through back trajectory analysis. The longer the distance from source to receptor the more uncertain will be the apportionment. We have estimated that with this model it should be feasible to estimate the impact of a coal or oil fired power plant on a receptor site downwind as far away as 500 km under meteorological stability class D, with the theoretical limitation being the dilution of the CMB marker species reaching the receptor site to a concentration below the detection limit of existing analytical methods.

We offer this novel approach to receptor measurements not as an ultimate solution to handling the apportionment of the secondary particles but to stimulate other investigators to examine this issue and put forth substantive alternative models. Perhaps by the time we hold our Quail Roost III Receptor Modeling Workshop, field experiments will have been conducted and new source apportionment models will have been tested to resolve the sources of the sulfate and nitrate particles.

REFERENCES

Gordon, G. (1980) "Receptor Models" Environ. Sci. Technol. 14:792.

Watson, J.G. Chemical Element Balance Receptor Model Methodology for Assessing the Sources of Fine and Total Suspended Particulate Matter in Portland, Oregon. Ph.D. Dissertation, Oregon Graduate Center, Beaverton, Oregon. 1979.

Watson, J.G. Receptor Models Relating to Ambient Suspended Particulate Matter to Sources. EPA-600/2-81-039, Research Triangle Park, NC. 1981.

Although the research described in this article has been funded wholly or in part by the United States Environmental Protection Agency, it has not been subjected to Agency review and therefore does not necessarily reflect the views of the Agency and no official endorsement should be inferred.

TABLE I. TYPICAL SAMPLERS FOR COMPLETE RECEPTOR-MODEL STATION

Particulate Sampler	Flow rate (l/min)	Filter Medium	Species Measured	Method
Dichotomous	17	Teflon	Mass	β-gauging
			Elements	XRF, INAA
		Quartz	Carbon	Combustion
			Ionic species (SO_4^{2-}, NO_3^-, etc.)	Ion chromatography/chemistry
		Nuclepore	Individual particles	SEM/XRF
Dichotomous	50	Teflon	Crystals, minerals	XRD, LM
Hi-Vol (with cyclone) 2.5 μm cutpoint	500-1000	Quartz	Organic compounds	GC/MS,LLC, etc.

Gas sampler	Gases measured	Output
Total sulfur	SO_2 and other S-containing gases	Real time, need data-logging system
NO_x	NO, NO_2	Real time, need data-logging system
O_3	O_3	Real time, need data-logging system
Polyurethane	Organic vapors	Later extraction and analysis in laboratory

Meteorological	Parameter	Output
Wind Speed	cm/sec	Data Logger-Real Time
Direction	compass Heading	Data Logger-Real Time
Temperature	°C	Data Logger-Real Time
Humidity	Dew Point °C	Data Logger-Real Time

TABLE II. SOURCE CATEGORIES AND MARKER ELEMENTS FOR HOUSTON AEROSOL

Marker Elements	General Source Categories	Specific Source Categories
Na, Cl	Marine	Marine
Al, Si, K, Ca, Mn, Fe	Crustal	Wind erosion of soil Paved and unpaved roads Construction Limestone crushing and handling Cement Lime Kiln Fly ash Slag
C, Br, Pb	Transportation	Noncatalyst vehicles Catalyst cars Diesels
Mn, Fe	Steel	Iron and steel production Steel finishing and handling
Cu, Zn, As, Sm, Sb	Nonferrous metals	
NH_4^+, SO_4^{2-}	Sulfate	Primary emissions in Houston airshed Conversion of SO_2 in Houston airshed Regional background
C	Carbonaceous	Refineries Botanical Vegetative burning Tire wear
NO_3^-	Nitrate	Photochemical

Fig. 1

RECEPTOR MODELING
AMBIENT AIR SAMPLING PROTOCOL

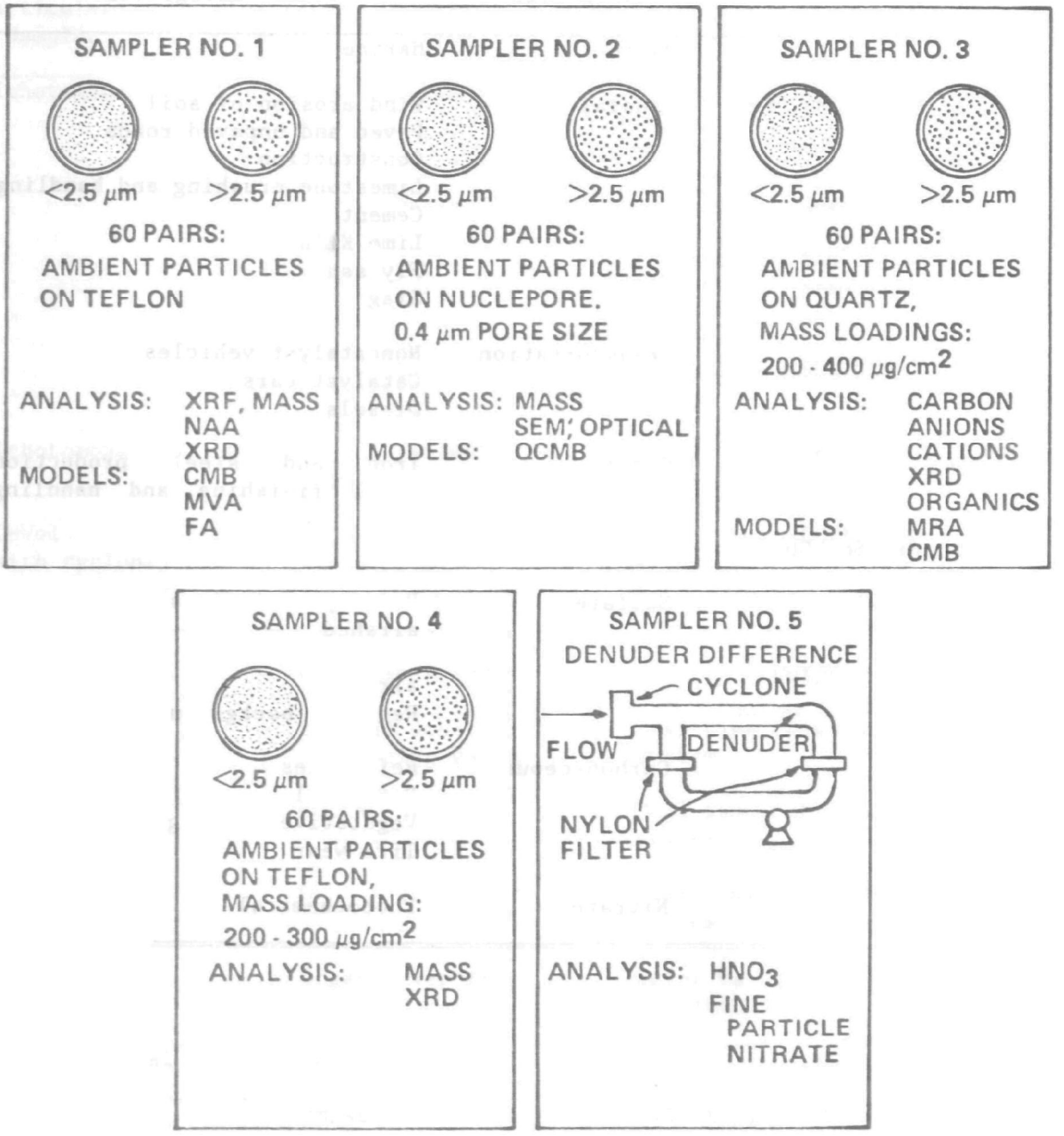

Fig. 2

FINE PARTICULATE SOURCE APPORTIONMENT RESULTS
HOUSTON AEROSOL DEVELOPED BY QUAIL ROOST II WORKSHOP

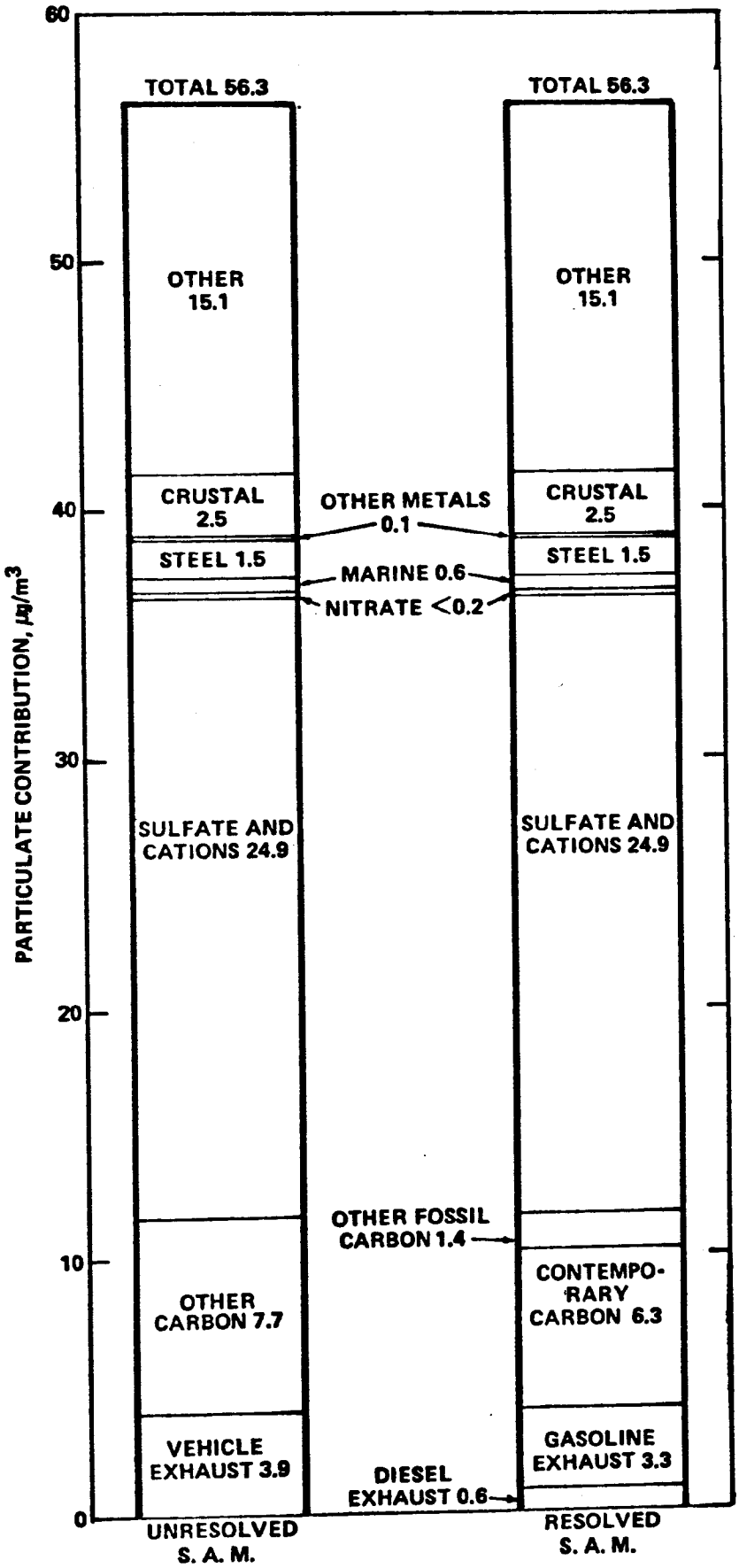

Fig. 2

COARSE PARTICULATE SOURCE APPORTIONMENT RESULTS

HOUSTON AEROSOL DEVELOPED BY QUAIL ROOST II WORKSHOP

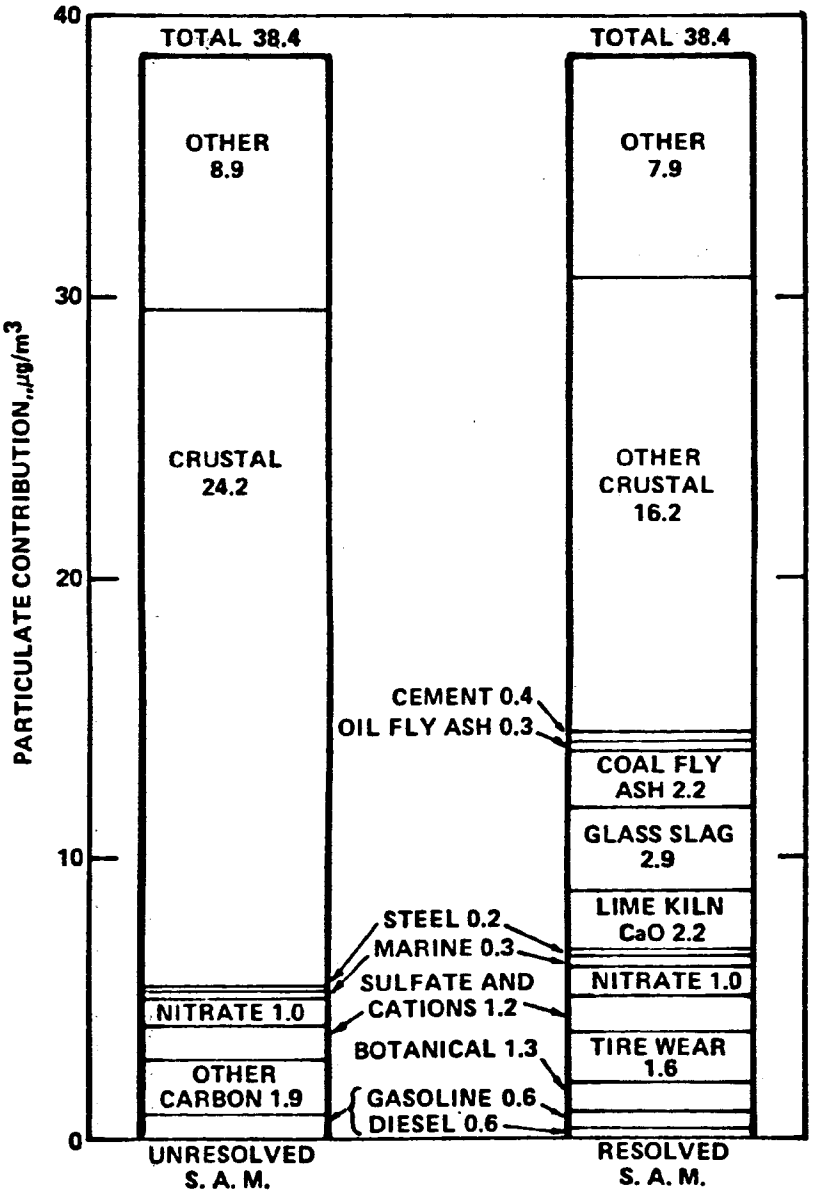

RECENT DEVELOPMENT OF AEROSOL STUDIES IN JAPAN

Naoomi Yamaki

Issei Iwamoto

Kazuhiko Sakamoto

Department of Environmental Chemistry, Faculty of Engineering, Saitama University

Presented by N. Yamaki

Saitama University

Japan

In the 1970's, aerosol studies have been considered important as one of serious problems of air pollution and recently a lot of studies have been actively conducted.

We present here briefly the aerosol studies conducted in Japan for these 2~3 years, particularly with respect to estimation of the contribution to atmospheric particulate matter from various emission sources, secondary formation of atmospheric particulate matter, and artifacts at filter collection of atmospheric particulate matter.

I. Estimation of Contribution to Atmospheric Particulate Matter in Urban Areas from Various Emission Sources

Friedlander first reported(1973) the CEB method to estimate emission sources of particulate matter. Recently, a large number of studies have been performed to estimate the contribution to atmospheric particulate matter in urban areas from emission sources(Dzubay(1979), Cooper et al.(1980),Gordon(1980), Matsuo et al.(1978),[1] Mizohata et al.(1980)[2]).

Contribution to Total Suspended Particulate Matter(TSP) from Automobile Exhausts

Mizohata et al. tried to estimate the contribution to TSP from each main source according to the CEB method, based on the results of neutron activation analysis of TSP collected at Sakai in Osaka(Table 1).[2] The change in the contribution to TSP from the automobile exhaust during 5 years from 1975 to 1980 was also estimated with respect to TSP samples at Osaka monitoring station of NASN.[3] The sum of the percentage contributions from the six main sources(soil, marine aerosol, iron and steel industry, refuse incineration, fuel oil combustion, automobile) with respect to the 10 index elements(Na,Al,K,Sc,V,Mn,Fe,Zn,Br, Pb) was calculated to be ca. 50%(Table 2). The percentage contribution from the automobile was estimated as ca. 10% and the percentage contribution from diesel engine vehicles to the automobile increased from 88% to 95% year by year; most of particulate matter from automobiles arises from the diesel engine vehicles and is the most important primary man-made source.

The results were obtained according to the CEB method by choosing inert elements as the index element. Recently, the introduction of decay factors for reactive materials to the CEB method was reported by Friedlander(1980) and in Japan, the possibility of introduction of PAH as the index material is now discussed.

The Contribution to TSP from Natural Sources

From estimation by Mizohata et al.(1979)(Table 2), the contribution to TSP from the natural sources(soil and marine aerosol) was about 30%, the contribution from other four sources was 25%, and the remaining 45% was from the other various small particulate-generating factories and secondary aerosols formed in the atmosphere.

Kadowaki[4] reported that according to the bimodal model the percentage contribution to TSP from the natural sources was estimated to be 50% in spring when yellow sand phenomena often appeared and 35 to 40 % in the other seasons.

These values of contribution were calculated with respect to the particulate matter of smaller than 10μm in size. To know real influences of particulate matters on human environment, the contribution from emission sources as a function of particle size(for example, 2μm>, 2μm≤)will be more useful. As the result, the contribution from the natural sources to coarse particles and the contribution from automobile exhausts and secondary aerosol formed in the atmosphere to fine particles are to be much higher. This approach will be very useful to propose a more reasonable emission control for particulate matter. Furthermore, the estimation of environmental effect of suspended particulate matter(SPM) should be done by taking into consideration the quality of SPM besides the quantity of SPM. Kasahara suggested[5] that to estimate the environmental effect the size and the chemical composition of SPM should be taken into account as well as the concentration.

Analysis of Carbon of Particulate Matter

It is expected the contribution to fine particles arises mainly from secondary aerosols formed from gas-particle transformation and diesel exhausts. To make this clear,

characterization of size-segregated samples and determination of appropriate index element or index material for particles from diesel exhausts will be required. It is considered that the main components of the secondary aerosols are SO_4^{2-}, NO_3^-, Cl^-, NH_4^+ and organics. While analytical methods for inorganic ions are almost established, for organics improved methods making it possible to determine the quantity of organics by using only a little amount of samples are desired, since the conventional solvent extraction method needs a significant amount of samples and the quantity of extract depends on the kind of solvent used. In this connection, various analytical methods for particulate carbon were reported * that the quantity of organic carbon in stead of that of total organics were measured, together with the quantity of elemental carbon which was considered as the main component of diesel exhaust particles and as one of the important substances relating to climate change.

Such kind of studies have been performed also in Japan. Ohta et al.[6] determined the quantities of total carbon(C_t), elemental carbon(C_{el}) and organic carbon(C_{org}) with an NC-analyzer and a FID-GC. C_t was obtained from direct analysis of a quartz fiber filter of SPM, C_{el} was analyzed after pre-treatment of the filter at the temperature of 300°C for 30 minutes (organic carbons were removed), and $C_{org}=C_t-C_{el}$.

Sakamoto et al.[7] determined both C_{org} and C_{el} by using a Thermal Carbon Analyzer consisting of a NDIR for detection of CO_2 and a thermal volatilization apparatus(C_{org} : thermal volatilization at 450°C, C_{el} : combustion at 850°C). The time required for heating in this method is only several minutes which is extremely shorter than the other methods. This makes it possible to reduce the possibility that organic carbons are changed to elemental carbons owing to carbonization. The diurnal variations of C_{org} and C_{el} of SPM determined by using the Thermal Carbon Analyzer are shown in Fig.1.

---

* Cf. "Particulate Carbon - Atmospheric Life Cycle -", ed. G.T.Wolff and R.L.Klimisch, 1982.

The contribution from automobile exhausts has been determined from the ratio of particle emission from gasoline powered vehicles to that from diesel engine ones,according to the CEB method where Pb emitted from gasoline powered vehicles used as index element. Since the ratio of leaded gasoline to all gasoline decreases to only 3 % at the present time, another new index material will be required. The possibility of adoption of C_{el} as the index material is now being discussed, since ca. 70 % of fine particles from diesel exhausts is C_{el}.

II. Secondary Formation of Particulate Matter

Gas-Particle Equilibrium for NH_4NO_3 and NH_4Cl

Eq.1 shows the reaction of gaseous HNO_3 with gaseous NH_3 to form particulate NH_4NO_3. However, since it has been pointed out by Stelson et al.(1979) that there is an equilibrium for this reaction, studies on a relationship between concentration of HNO_3 or NO_3^- in the atmosphere and ambient temperature have widely been performed in Japan.

Kadowaki[8] suggested major reactions for HNO_3 and NO_3^- formation in the atmosphere(Table 3) and the formation pathway of the secondary aerosols was explained as shown in Fig.2. For particulate NH_4Cl, an equilibrium of eq.2 probably exists. Oka et al.[9] observed the same relationship between $[NH_3][HCl]$ and 1/T as that reported for NH_4NO_3 by Stelson et al.(1979).

$$HNO_3(g) + NH_3(g) \longrightarrow NH_4NO_3(s) \quad --- \quad (1)$$

$$HCl\ (g) + NH_3(g) \longrightarrow NH_4Cl\ (s) \quad --- \quad (2)$$

Hara et al.[10] considered NO_3^- and Cl^- in the range of fine particles as NH_4NO_3 and NH_4Cl, respectively, and defined the f-value for NO_3^- or Cl^- as shown in eq.3. The temperature

$$\text{f-value} = \frac{[\text{fine-particles}]}{[\text{gaseous}] + [\text{fine-particles}]} \quad --- \quad (3)$$

dependence of each f-value was interpreted in terms of equilibrium of eqs. 1 and 2 (Figs.3~5).

Measurement of $[NH_4^+]$ and $[NH_3]$ as notified in eqs. 1 and 2 was carried out by Iwase et al.[11] The temperature dependence was found similar to that for $[NO_3^-]$ and $[Cl^-]$, that is; in summer the concentration of gaseous NH_3 was relatively high and that of particulate ammonium salts was high in winter.

Since the product of the reaction(eq.1), NH_4NO_3 is deliquescent at around 25°C and a relative humidity of ca.65% because of its hygroscopic nature, the equilibrium may strongly depend on the value of relative humidity in the range of relative humidity higher than 65%. Iwamoto et al.[12]

examined the temperature and humidity dependences of NH_3 and HNO_3 in air after passing through a NH_4NO_3 impregnated filter. It was found that loss of NH_4NO_3 occured stoichiometrically according to eq.1 and that HNO_3 concentration remained constant regardless of the wide change in the air flow-rate and a strong humidity dependence was observed over 60% of relative humidity. The result of the temperature and humidity dependences was in good agreement with that derived from thermodynamic analysis of an aqueous NH_4NO_3 solution which was considered as an non-ideal solution by Stelson and Seinfeld (1982)(Figs.6~7). Consequently, when field measurement data are analyzed, not only temperature but also relative humidity should be taken into account. Since in most of the field studies above mentioned, the collection of samples was done by means of dual filter method and the collection period was very long(a half day ~ one week), it is likely not to estimate accurately the effect of the artifact arising from the variation in temperature and relative humidity during the sampling periods.

Formation of NO_3^- from Reaction of NO_2 with Marine Salt

With respect to atmospheric particulate matter collected with an Andersen air sampler in Kobe(Kobayashi et al.[13]) and in Nagoya(Kadowaki[8]), it was estimated from the value of Cl^*_{loss} that NaCl particles were partly converted to $NaNO_3$ particles. Kobayashi et al. found a positive relation between Cl_{loss} and NO_2 concentration as Martens et al.(1973) did and suggested the possibility of NO_3^- formation through the following reactions(eqs.4~6).

$$3NO_2 + H_2O \longrightarrow 2HNO_3 + NO \quad \text{---(4)}$$

$$NaCl + HNO_3 \longrightarrow NaNO_3 + HCl \quad \text{---(5)}$$

$$3NO_2 + H_2O + 2NaCl \longrightarrow 2NaNO_3 + 2HCl + NO \quad \text{---(6)}$$

---

* Cl_{loss}(μmol/m^3) was calculated according to the following equations.

$$Cl_{theor} = 1.17 \times Na_{c-obs}$$

$$Cl_{loss} = Cl_{theor} - Cl_{c-obs}$$

$$1.17 = (Cl^- \text{ of seawater}/Na^+ \times 1.8) \times (\text{Na atomic weight}(23.0)/\text{Cl atomic weight}(35.5))$$

However, Kadowaki pointed out[8] that the remarkable increase in Cl_{loss}, especially in summer may be due to acceleration of the reaction in eq.5, accompanied by the evaporation of HNO_3 from particulate nitrates and the increase of HNO_3 formed in photochemical and heterogeneous reactions at higher temperature.

Conversion of Nitrogen Oxides to Nitric Acid and Nitrates

In Fig.8, a simplified mechanism for nitrates(HNO_3 and NO_3^-) formation from NO_x is shown.

The formation path has been explained in terms of f_N (conversion from NO_x to NO_3^-)(Grosjean and Friedlander(1975)) or in terms of $f(NO_3^-/NO_x)$(Appel et al.(1978)). As mentioned above, however, because of the equilibrium between particulate NO_3^- and gaseous HNO_3, it is more reasonable to consider the sum of NO_3^- and HNO_3 than to consider each species. Sakamoto et al.[14] defined f_N' as shown in eq.9 and measured the diurnal variations of f_N'(Figs.9~10). It is noted that for

$$f_N = \frac{[NO_3^- - N]}{[NO_x - N] + [NO_3^- - N]} \quad \text{---(7)}$$

$$f = \frac{[NO_3^- - N]}{[NO_x - N]} \quad \text{---(8)}$$

$$f_N' = \frac{[NO_3^- - N] + [HNO_3 - N]}{[NO_x - N] + [NO_3^- - N] + [HNO_3 - N]} \quad \text{---(9)}$$

the date in summer shown in Fig.9 the contribution of PAN to f_N' is considered small since the concentration of PAN measured at some intervals was always lower than 1 ppb. In general, f_N' is high at daytime and becomes low at night, and a positive relationship between f_N' and O_3 concentration is obtained. This suggests the possibility that the conversion of NO_x to HNO_3 and/or NO_3^- occurs(NO_x+OH,O_3 $\longrightarrow$ HNO_3) at daytime when the photochemical potential is high.

If the values of f_N' with respect to the same air mass at different sites along the trajectory are measured, the conversion rate from NO_x to HNO_3 and NO_3^- can be calculated from f_N' and the transportation time of the air mass. On the assumption that the each result in Fig.9 or 10 was obtained for the same air mass, the conversion rate was obtained to be ca. 6 % h^{-1} for the summer data(Fig.9) and ca.

3 % h^{-1} for the data in May(Fig.10). These values are considered reasonable, taking account of the difference in the intensity of sunlight and in O_3 concentration. In addition, the value of 6 % h^{-1} is similar to the value of ca. 5 % h^{-1} obtained from the data in September~October for urban plume by Spicer et al.(1978).

In Japan there are little isolated urban plume of sufficient residence time, but some studies have been carried out to obtain the conversion rate by chasing a polluted plume over big cities with airplane. From measurement of NO_3^- concentration in air over southern Kanto areas by Suzuki et al.[15] (August,1980), the formation rate was obtained to be 0.5~1.0 % h^{-1} and the formation rate of HNO_3(g) was obtained as ca. 20 % h^{-1} on the basis of OH radical concentration estimated from HC composition. This formation rate is between the values of 24 % h^{-1}(Spicer(1979)) and 13 % h^{-1}(Meagher et al. (1981)).

Secondary Formation of Organic Particles

Not a lot of studies have been done with respect to organic composition in atmospheric particulate matter, but a few studies about secondary formation of organic particles by photochemical reaction have been done. The ratio of primary organic particles to the secondary ones varies with areas and seasons, but it is estimated that the ratio of secondary organic particles to total organic particles will increase in summer at urban areas with high photochemical potential.

Sakamoto et al.[16] thought most of secondary organic particles formed by a photochemical reaction were carbonyl compounds, and suggested that a relative values($R_{C=O}$),the ratio of integrated intensity of carbonyl ir peak($\nu_{C=O}$)to that of methylene ir peak(ν_{CH_2}) can be used as a parameter showing the contribution of secondary organic particles. This is also applicable to organic nitrates.[17] Grosjean and Friedlander(1975) suggested a positive relation between $\nu_{C=O}$ intensity of organic particles and O_3 concentration. The value of $R_{C=O}$ here is in a good correlation with O_3 concentration, which is one of parameters showing photochemical potential (Table 4). Moreover, with regards to samples in the fine

particle regions, a correlation coefficient between $R_{C=O}$ and O_3 concentration was obtained as 0.83(n=15)(significant), but for the coarse particles such a correlation was not found. This may suggest the possibility of heterogeneous nucleation that organic carbonyl compounds formed in a photochemical reaction condense on the fine particles with large surface areas.[18] From organic acidic components in the atmospheric particulate matter collected on August, 1978, several kinds of α,ω-dicarboxylic acids(succinic acid, glutaric acid and adipic acid) were identified,which were considered as final products of HC and O_3 or OH reactions(Table 5).[19]

$$R_{C=O} = \frac{\varepsilon_{max}(C=O)\cdot\Delta\nu_{1/2}(C=O)}{\varepsilon_{max}(CH_2)\cdot\Delta\nu_{1/2}(CH_2)} = \frac{1/cl\cdot\log I_0/I(C=O)\cdot\Delta\nu_{1/2}(C=O)}{1/cl\cdot\log I_0/I(CH_2)\cdot\Delta\nu_{1/2}(CH_2)} = \frac{\log I_0/I(C=O)\cdot\Delta\nu_{1/2}(C=O)}{\log I_0/I(CH_2)\cdot\Delta\nu_{1/2}(CH_2)} \quad \text{---(10)}$$

Formation of Particles from Cyclohexenes

Bandow et al.[20] and Sakamoto et al.[21,22] studied a chemical reaction mechanism for formation of particles from cyclohexenes in photoirradiation of cyclohexenes-NO_x-air system. Hexanedialdehyde($OHC(CH_2)_4CHO$) in dry air system and adipic acid($HOOC(CH_2)_4COOH$) in a humidified air system were formed from cyclohexene. Glutaric acid($HOOC(CH_2)_3COOH$) and PAN were formed from 1-methylcyclohexene. This suggests not only the scission of 1,2-double bond but also that of 1,6-single bond can easily occur in 1-methylcyclohexene(Fig.11).[22] These products can be explained by the reaction pathways almost same to that proposed by Grosjean and Friedlander(1980), that is ; at the initial reaction stage HC is consumed mainly with OH radical addition to the double bond.

Even if equimolar NO_x,SO_2 and cyclohexene are completely transformed to particulate matter, the weight ratio of the particulate matter is not equivalent but is calculated as 1 : 1.5 : 2.4(=NO_3^- : SO_4^{2-} : adipic acid). It is thus considered that because of the largest value of 2.4 the contribution to secondary particles from organic particles will be important. It is necessary to study the photochemical particle formation ability for various kinds of HC which may be emitted from sources.

Formation of Particles from Reduced Sulfur Compounds

In addition to a lot of studies on photooxidation of SO_2, there has been growing interest in photochemical reaction of reduced sulfur compounds which are biologically generated and are important compounds in consideration of sulfur balance in the atmosphere(Cox et al.(1980),Niki et al.(1980,1982)).

Hatakeyama et al.[23~25] studied a photochemical reaction of dimethyl sulfide, methane thiol, or dimethyl disulfide-NO-air system and found H_2SO_4 and CH_3SO_3H which was detected in atmospheric pariculate matter by Panter et al.(1980). A possible formation pathway was shown in Fig.12 where the reaction was initiated by addition of OH to S.[24] In this reaction, the simultaneous formation of SO_2 in addition to CH_3SO_3H and H_2SO_4 is of interest.

Formation of Particles in Photoirradiation of HC-NO-SO_2-Air System

By means of a rotatable aerosol chamber which makes the residence time of particles in air longer(Volume $4m^3$,$S/V=4.8m^{-1}$), Izumi et al.[26,27] conducted the photoirradiation experiments of C_3H_6-NO-SO_2-dry air system to study photochemical oxidation of SO_2 and particles formation. The SO_2 oxidation rate can not be explained only in terms of the reaction of SO_2 with OH radical and a good correlation was found between SO_2 decay rate and the amount of C_3H_6 consumed in O_3-C_3H_6 reaction.[26] In a dark reaction of O_3-C_3H_6-SO_2-dry air,[27] at the initial stage very fine particles were mainly formed and they grew with reaction time(Fig.13). By use of steady state method with respect to an active intermediate(P*) formed from O_3 and C_3H_6 and from a series of experiments with different SO_2 concentrations, they have shown that about a half of P*(k'/k= 0.92) was consumed for oxidation of SO_2 to SO_3(eq.12).

$$C_3H_6 + O_3 \longrightarrow P^* \qquad \text{---(11)}$$

$$P^* + SO_2 \xrightarrow{k} SO_3 + \text{Products} \qquad \text{---(12)}$$

$$P^* + SO_2 \xrightarrow{k'} SO_2 + \text{Products} \qquad \text{---(13)}$$

Transport and Removal of Particulate Matter

Since all big cities and industrialized zones in Japan are located along coasts, the air pollutants from emission sources are transported by sea-land breezes etc., transformed with chemical and physical processes and removed with various processes. Several studies on fate of gaseous pollutants have been done by NIES group and others, but only a few studies have been done with respect to particulate matter.

Kadowaki et al.[28] studied the change in the composition of particulate matter by comparing that of an urban area with that of mountainous and coastal areas which were about 70 km distant from the urban area. They found that in the course of the transport process from the urban area to mountainous area, soil particles and marine-salt particles in the range of coarse particles were selectively removed. They also pointed out some transformation during the transport process since SO_4^{2-} existed as NH_4HSO_4 in the urban area and did as $(NH_4)_2SO_4$ in the mountainous area.

Oka et al.[9] collected atmospheric particulate matter with an NH_3 denuder and measured quantitatively H_2SO_4 mist and SO_4^{2-} concentrations of size-segregated particulate matter. From the particle size distribution observed, they suggested the possibility that fine particle H_2SO_4 mist reacted with NH_3 in the course of condensation to become large size particle of SO_4^{2-}.

Tamaki and Hiraki[29] studied the effect of rainfall on the concentrations of gaseous NO_X and particulate NO_3^- in the atmosphere. The average concentration of NO_3^- during rainfall decreased to about a half of its initial concentration by about 10 mm rainfall and to about a quarter just after rainfall. This was explained from the fact that NO_3^- is contained mainly in coarse particles and is not produced in air during rainfall, since it is formed photochemically.

III. Artifacts in Sampling Atmospheric Particulate Matter with Filter Collection

Since the middle of 1970's, it has been reported in succession that the positive interference in sampling atmospheric particulate sulfate and nitrate resulted from adsorption of SO_2 and HNO_3 on or reaction with the filter materials. As a result of many active studies on positive and negative artifacts in sampling sulfate and nitrate, it was found that several (quartz-fiber and Teflon) filters gave relatively little artifact.

The polycyclic aromatic hydrocarbon(PAH) content of particulate matter emitted into the air by combustion of fossil fuels is receiving increasing attention. Furthermore, due to better fuel economy of diesel engines than that of gasoline engines, the increase in dieselized fraction of automobile will increase the emission of particulate originating in vehicular engines. Recently, many studies on the filter collection of PAH and its carcinogenic nitro-derivatives, which present mostly in respirable size and may constitute a significant inhalation health hazard to the human population, have been reported.

Sampling Atmospheric PAH with Polyurethane Foam Plugs

It is difficult to determine the real ambient concentration of PAH with collection of a particulate matter on filters by using conventional high-volume air sampler due to its high vapor pressure. Yamasaki et al.[30] determined the concentrations of 3- to 6-ring PAHs both in the vapor phase(PAH_{xvap}) and in the particulate phase(PAH_{xpat}) with the collection method using a combination of glass-fiber filters(GFs) and two layers-polyurethane foam plugs(PUFPs) as back-up. This method permitted a higher flow rate in sampling particles than the collection method using various polymer beads (Broddin et al.(1980), Robertson et al.(1980), Lindgren et al. (1980)) and cooling collection systems(Handa et al.(1980)[31]). In their result, at ambient temperature levels substantial amounts of 3- to 5-ring PAHs were found in the vapor phase depending upon temperature(T,K) and 6-ring PAHs were all found in the particulate phase(Table 6). Aspects of the formers in ambient air were considered to be explained by the

Langmuir adsorption concept(eq.14). thus, it was suggested that correction of various PAH data obtained by conventional methods might be possible using the concept.[32]

$$\log \frac{[PAH_{xvap}]}{[PAH_{xpat}]/[TSP]} = -A/T + B \quad ---(14)$$

$[PAH_{xvap}]$: PAH_x concentration(ng/m^3) in the gas phase
$[PAH_{xpat}]$: PAH_x concentration(ng/m^3) in the particulate phase
[TSP] : TSP concentration(ng/m^3)
A,B : Constant

Formation of Nitropyrene as Artifact during Collection of Particulate Matter

It has been reported by Pitts et al.(1978) that formation of nitro-derivatives by the possible reactions between PAHs and nitrogen oxides, which were representative atmospheric pollutants, on filter for collection of particulate matter. Carcinogenicity of 1-nitropyrene and 3-nitrofluoranthene recently reported by Kawashi et al.(1981) induced the great concern about the possible health effects by these compounds in diesel exhaust particles collected.

Since the first report by Pitts et al. appeared in 1978, an increasing number of papers have been published on both the increase in mutagenicity and the amount of nitro-derivatives by the exposure of diesel exhaust particulate matter and/or PAHs on filters to diesel exhaust gas or controlled gas containing NO_2, SO_2, HNO_3, etc. Also, identification of 1-nitropyrene in atmospheric and diesel exhaust particulate matter was reported by several workers. However, the study on the collection method without artifact nitration of PAHs during sampling will be very significant since nitro-derivatives of PAHs are formed by the reaction of PAHs even with several ppb of HNO_3 due to the result reported by Pitts et al.(1978).

Sakamoto et al.[33] reported the conversion efficiency of pyrene to nitro-derivative by exposure of controlled humidified gas containing 50 ppm of NO_2(Table 7) and indicated that the conversion efficiency decreased significantly by the treatment of quartz-fiber filter with K_2CO_3(Table 8). Recently, the systematic study on collection and analytical methods for nitro-derivatives of PAHs in atmospheric and diesel exhaust particulate matter was started in Japan.

REFERENCES

1) Y.Matsuo, M.Fujiwara, and T.Higuchi, J.Environ.Pollut.Control., 14, 951 (1978).
2) A.Mizohata and T.Mamuro, J.Jpn.Soc.Air Pollut., 15, 198 (1980).
3) A.Mizohata,"Contribution Rate of Automobile Exhaust in Urban Atmospheric Particulates", 23th Conference Abstracts of Jpn.Soc. Air Pollut., p.119, Nov. 1982.
4) S.Kadowaki, J.Jpn.Soc.Air Pollut., 13, 252 (1978).
5) M.Kasahara, "Atmospheric Aerosol -Properties and Evaluation of Pollution Level-", 23th Conference Abstracts of Jpn.Soc.Air Pollut., p.81, Nov.1982.
6) T.Ohta and T.Okita,Annual Meeting Abstracts of Jpn.Soc.Meteorology, No.339, May 1982;idem , 23th Conference Abstracts of Jpn.Soc.Air Pollut., No.839, Nov.1982.
7) K.Sakamoto, S.Hara, S.Otsuka, I.Iwamoto, N.Yamaki,and T.Kimoto, ibid., No.840, Nov.1982;K.Sakamoto, N.Harayama, S.Otsuka, I.Iwamoto, N.Yamaki, and K.Yamashita,ibid., No.411, Nov. 1982.
8) S.Kadowaki, J.Environ.Pollut.Control., 18, 553, 667 (1982).
9) K.Oka, K.Inoue, and T.Taguchi, 23th Conference Abstracts of Jpn. Soc.Air Pollut., No.827, Nov. 1982.
10) H.Hara, T.Kato, and H.Matsushita, ibid., No.822, Nov. 1982.
11) Y.Iwase et al., ibid., No.244, Nov. 1982.
12) I.Iwamoto, H.Yoshida, H.Matsuda, S.Otsuka, K.Sakamoto, and N.Yamaki, ibid., No.816, Nov. 1982.
13) T.Kobayashi, T.Ikezawa, and H.Watanabe, J.Jpn.Soc. Air Pollut., 14, 401(1979).
14) K.Sakamoto, K.Takahashi, S.Otsuka, I.Iwamoto, and N.Yamaki, 43th Annual Meeting Abstracts of Chem. Soc. Jpn., No. 3011, Apr. 1981; K.Sakamoto,H.Kojima,S.Otsuka, I.Iwamoto,and N. Yamaki, 22th Conference Abstracts of Jpn. Soc. Air Pollut., No. 805, Oct. 1981; idem, 23th Conference Abstracts of Jpn. Soc. Air Pollut., No. 817, Nov. 1982.
15) M.Suzuki,I.Uno,S.Wakamatsu, and K.Murano,ibid., No.212, Nov.1982.
16) *K.Sakamoto, S.Sasaki, S.Otsuka, I.Iwamoto, and N.Yamaki, J. Jpn. Soc. Air Pollut., 15, 426(1980).
17) *K.Sakamoto, S.Sasaki, K.Takahashi, M.Mizuochi, S.Otsuka, I. Iwamoto, and N.Yamaki, ibid., 15, 429(1980).
18) K.Sakamoto, S. Otsuka, I. Iwamoto, and N. Yamaki, 22th Conference Abstracts of Jpn. Soc. Air Pollut., No. 275, Oct. 1981.

19) K. Sakamoto, S. Sasaki, S. Otsuka, I. Iwamoto, and N. Yamaki, 41th Spring Annual Meeting Abstracts of Chem. Soc. Jpn., No. 3C10, Apr. 1980.

20) H.Bandow and H. Akimoto, 23th Conference Abstracts of Jpn. Soc. Air Pollut., No. 439, Nov. 1982.

21) K. Sakamoto, T. Sutoh, S. Otsuka, I. Iwamoto, and N. Yamaki, 21th Conference Abstracts of Jpn. Soc.Air Pollut., No. 420, Nov. 1980; K. Sakamoto, T. Sutoh, N. Fukushima, Y. Matsuda, S. Otsuka, I. Iwamoto, and N. Yamaki, 43th Spring Annual Meeting Abstracts of Chem. Soc. Jpn., No. 3007, Apr. 1981.

22) K. Sakamoto, T. Sutoh, S. Otsuka, I. Iwamoto, and N. Yamaki, 22th Conference of Jpn. Soc. Air Pollut., No. 724, Oct. 1981.

23) *S. Hatakeyama, M. Okuda, and H. Akimoto, Geophys. Res. Lett., 9, 583(1982).

24) *S. Hatakeyama and H. Akimoto, Int. Sympos. Abstracts on Chem. Kinet. related to Atmos. Chem., No. 16, June 1982, Jpn.

25) S. Hatakeyama and H. Akimoto, 23th Conference Abstracts of Jpn. Soc. Air Pollut., No. 442, Nov. 1982.

26) K. Izumi, M. Mizuochi, T. Fukuyama, K. Murano, and M. Okuda, 45th Spring Annual Meeting Abstracts of Chem. Soc. Jpn., NO. 3S15, Apr. 1982.

27) K. Izumi, M. Mizuochi, K. Murano, and T. Fukuyama, 23th Conference of Jpn. Soc. Air Pollut., No. 837, Nov. 1982.

28) S. Kadowaki, S. Imai, and K. Yoshimoto, ibid., No. 353, Nov. 1982.

29) M. Tamaki and T. Hiraki, J. Chem. Soc. Jpn., 1982, 1252.

30) H. Yamasaki, K. Kuwata, and H. Miyamoto, Bunseki Kagaku, 27, 317(1978).

31) *T. Handa, Y. Kato, T. Yamamura, T. Ishii, and K. Suda, Environ. Sci. Technol., 14, 316(1980).

32) *H. Yamasaki, K. Kuwata, and H. Miyamoto, ibid., 16, 189(1982).

33) K. Sakamoto, K. Mita, N. Harayama, S. Otsuka, I. Iwamoto, and N. Yamaki, 23th Conference Abstracts of Jpn. Soc. Air Pollut., No. 852, Nov. 1982.

* These literatures are English and the others are Japanese.

Table 1. Contributions of major sources to TSP.

Component	Predicted TSP contribution (μg/m³)	Percentage contribution (%)
Main components taken into concideration		
Soil particles	26.1	33.0
Marine aerosols	1.5	1.9
Iron-and-steel industry	4.3	5.4
Refuse incineration	2.4	3.0
Fuel oil combustion	1.9	2.4
Gasoline engine automobile	2.8	3.5
Total primary aerosol predicted	39.0	49.4
Observed TSP	79.0	100.0
Balance not accounted for by resolution	40.0	50.6
Remaing components		
Diesel engine	14.2	18.0
Secondary aerosol components		
Sulfur dioxide — SO_4^{2-}	9.3	11.8
Nitrogen oxides — NO_3^-	?	
Hydrocarbons ——— particulates	?	20.8
Various small aerosol generating factories	?	

Table 2. Contributions of major sources to TSP.

Year	1975		1976		1977		1978		1979	
Leaded-/all gasoline(%)	18		13.5		10.5		8.0		5.5	
TSP(μg/m³)	49.4		57.5		43.1		53.7		39.0	
Source \ Contribution	μg/m³	%	μg/m³	%	μg/m³	%	μg/m³	%	μg/m³	%
Soil particles	10.1	20.5	13.0	22.7	8.4	19.5	11.0	20.6	10.4	26.8
Marine aerosols	1.5	3.0	0.7	1.2	0.8	2.0	1.4	2.6	1.4	3.6
Iron-and-steel industry	2.3	4.6	2.6	4.6	2.1	4.8	2.6	4.9	1.6	4.2
Refuse incineration	2.1	4.2	2.8	4.9	3.9	9.0	1.8	3.4	2.0	5.0
Fuel oil combustion	3.2	6.5	2.8	4.8	1.9	4.5	1.9	3.6	1.4	3.5
Automobile exhaust (diesel and gasoline)	4.8	9.8	5.4	9.4	3.9	9.1	7.3	13.6	4.6	11.8
Others	25.4	51.4	30.2	52.5	22.0	51.1	27.6	51.3	17.6	45.0

Table 3. Major reactions of nitric acid and nitrate aerosols in the atmosphere.

Paths of formation	Reaction
Formation of nitric acid by photochemical oxidation	$NO_2+O_3 \longrightarrow NO_3+O_2$ $NO_2+NO_3 \longrightarrow N_2O_5$ $N_2O_5+H_2O \longrightarrow 2HNO_3$ $NO_2+OH \longrightarrow HNO_3$
Formation of nitric acid by thermal reaction	$2NO_2+H_2O \longrightarrow HNO_2+HNO_3$ $3NO_2+H_2O \longrightarrow 2HNO_3+NO$
Vaporization of nitric acid droplet	$HNO_3(l) \longrightarrow HNO_3(g)$
Formation of nitrate aerosol by homogeneous nucleation	$HNO_3(g)+NH_3(g) \longrightarrow NH_4NO_3(s)$
Formation of nitrate aerosol by heterogeneous nucleation	$HNO_3(l)+NH_3(g) \longrightarrow NH_4NO_3(s)$ $HNO_3(g)+NaCl(s) \longrightarrow NaNO_3(s)+HCl(g)$
Dissociation of nitrate aerosol by Harker loss	$NO_3^-(s)+H_2SO_4 \longrightarrow HNO_3(g)+HSO_4^-(s)$

Table 4. Correlation between $R_{C=C}$ value and O_3 concentration[a)]

Sampling time	Correlation coefficient(r)	(Number of sample (n))	O_3 concentration
8/2～8/13,1978 (24h)	0.95**	(7)	$[O_3]_{24h\text{-}ave}$ b)
	0.79	(7)	$[O_3]_{12h\text{-}ave}$ b)
	0.85	(7)	$[O_3]_{max}$
8/7～8/8, 1978 (2 or 3h)	0.84**	(10)	$[O_3]_{2\ or\ 3h\text{-}ave}$
7/24～8/4, 1979 (24h)	0.85**	(9)	$[O_3]_{24h\text{-}ave}$ b)
	0.58	(9)	$[O_3]_{12h\text{-}ave}$ b)
7/31～8/3, 1979 (4 or 6h)	0.83** (below 1.8μm)	(15)	$[O_3]_{4\ or\ 6h\text{-}ave}$
	0.24 (above 1.8μm)	(15)	$[O_3]_{4\ or\ 6h\text{-}ave}$

a) Sampling site: Saitama Univ. Sampling method : high-volume air sampler or Andersen high-volume air sampler.
b) 12h-averaged O_3 concentration during 6:00 am～6:00 pm.

Table 5. Dicarboxylic acids and aliphatic acids identified in the atmospheric aerosols.

Dicarboxylic Acid	Authors			
	Grosjean *et al.* (1978)	Cronn *et al.* (1977)	Schuetzle *et al.* (1975)	Sakamoto *et al.* (1980)
Malonic Acid	O		O	
Methylmalonic Acid	O			
Succinic Acid	O		O	O
Methysuccinic Acid	O			
Glutaric Acid	O	O	O	O
2-,3-Methylglutaric Acid	O			
Adipic Acid	O	O	O	O
Dimethylglutaric Acid	O			
2-,3-Methyladipic Acid	O	O		
Pimelic Acid	O		O	
Suberic Acid	O			
Azelaic Acid	O			O
Sebacic Acid	O			

Table 6. PAHs in the ambient air trapped on the GF and PUFPs.

PAH	PAHs trapped (μg/1000 m³)			Total (μg/100 m³)	% on GF	Ring number
	GF	PUFP-1	PUFP-2			
Phenantrene+Anthracene	1.16	69.8	34.6	105.6	1.1	3
Fluoranthene	0.95	24.6	0.13	25.7	3.7	4
Pyrene	0.99	18.5	0.07	19.6	5.1	4
Benzo(a)fluorene+Benzo(b)fluorene	0.20	3.58	n.d.	3.78	5.3	4
Chrysene+Benzo(a)anthracene+Triphenylene	2.34	3.05	n.d.	5.39	43.4	4
Bezo(a)pyrene+Benzo(e)pyrene	2.99	0.17	n.d.	3.16	94.6	5
o-Phenylenepyrene+Unknown**	2.91	n.d.	n.d.	2.91	100	6
Benzo(ghi)perylene+Anthanthrene	3.05	n.d.	n.d.	3.05	100	6

* Sampling site : Environmental Pollution Control Center(1-3-62, Nakamichi, Higashinari-ku, Osaka-shi, Osaka), Sanpling date : July 6-7, 1977, Temperature : (22.9~32.4°C), Volume of air sample : 1114 m³; ** Unknown substance was surmised benzo(b)chrysene due to reference (6). PUFP-1; First PUFP, PUFP-2 : Second PUFP, n.d. : Not detected (below 0.05μg/1000 m³)

Table 7. Conversion of pyrene to nitropyrene.

Filter(pH)		Time	Conversion
1st	2nd	(h)	(%) (n)
—	TQ (5.9)	20	24 (4)
PA	TQ		6 (2)
—	AE (9.5)		16 (2)
PA	AE		3 (2)
—	TBG (5.1)		6 (2)
—	TCG (5.4)		6 (2)
—	FP (4.9)	21	0
		72	0

Amount of pyrene/47mmφ filter: 10mg

Table 8. Conversion of pyrene to nitropyrene on several treated filters.

Exposure method	Tissuquartz filter	pH	Conversion (%) (n)
Through filter	HCl-treated	5.1	47 (2)
		4.9	49 (2)
	Non-treated	6.9	35 (5)
	K_2CO_3-treated	10.1	0.1 (2)
On filter	Non-treated	6.9	39 (4)
	K_2CO_3-treated	10.1	0.1 (2)
		10.3	0.1 (2)

Amount of pyrene/47mmφ filter: 5mg.

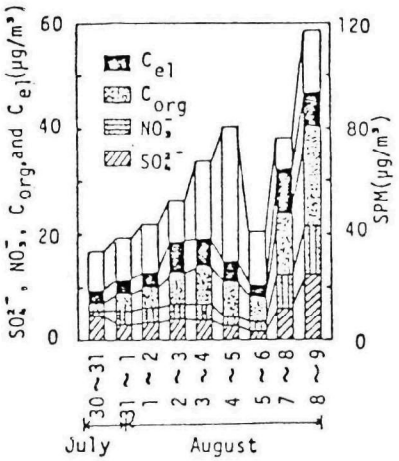

Fig.1. Chemical composition of SPM.
Sampling date: summer in 1981.
Sampling site: Saitama Univ.
Sampling method: high-volume air sampler.

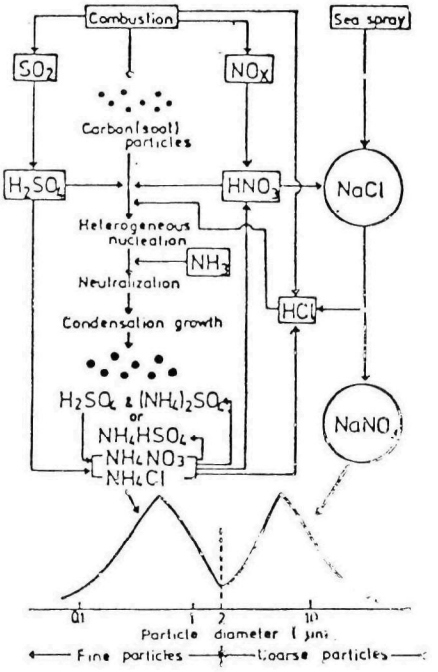

Fig.2. Schematic diagram of suggested mechanisms for sulfate, nitrate, and chloride formation in urban air at Nagoya.

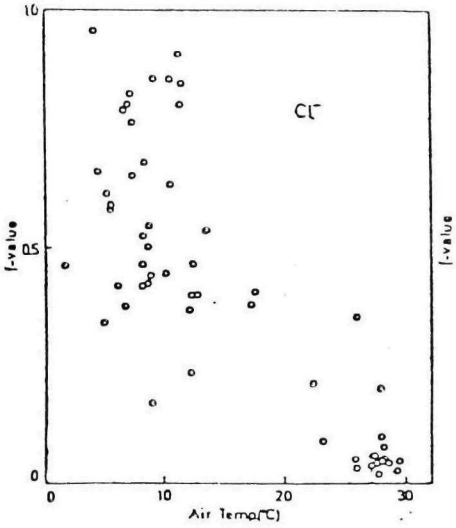

Fig.3. Ambient temperature vs. f-value of Cl^-.

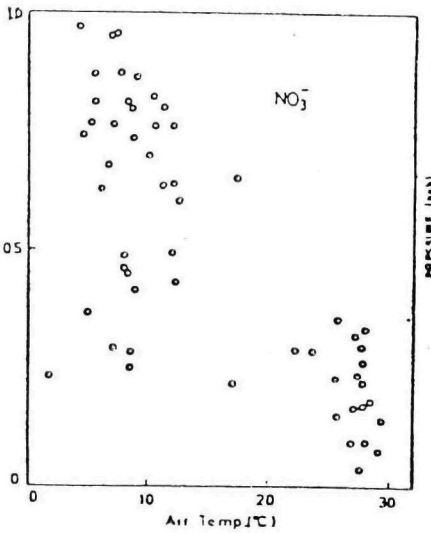

Fig.4. Ambient temperature vs. f-value of NO_3^-.

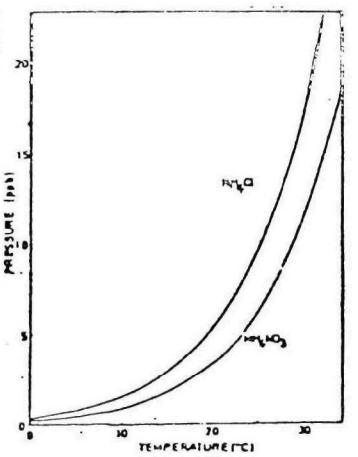

Fig.5. Dependence of theoretical vapor pressure (P_{HCl} and P_{HNO_3}) on ambient temperature in eqs. 1 and 2.

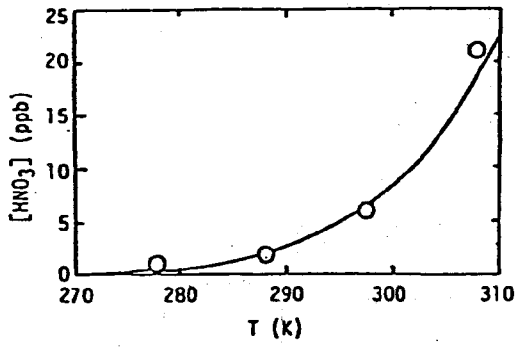

Fig.6. Temperature dependence of $[HNO_3]$ in the purified air passed through NH_4NO_3 loaded TQ filter;at R.H.0%,face velocity 4.7cm/sec, 10mg impregnated,(——) calculated from Stelson's equation.

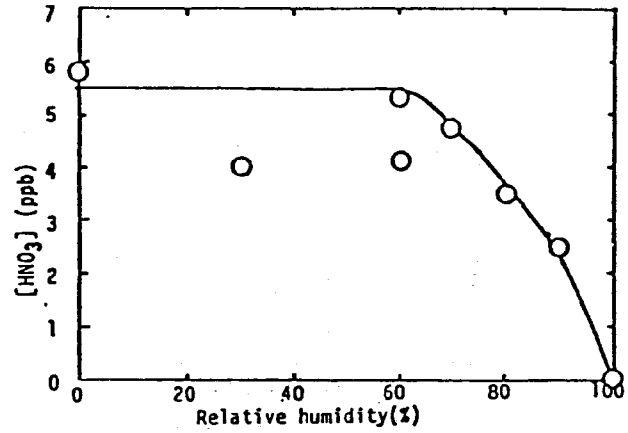

Fig.7. Relative humidity dependence of $[HNO_3]$ in the purified air passed through NH_4NO_3 impregnated TQ filter;at 25°C,face velocity 4.7cm/sec,10mg impregnated,(——) calculated values from Stelson's equation.

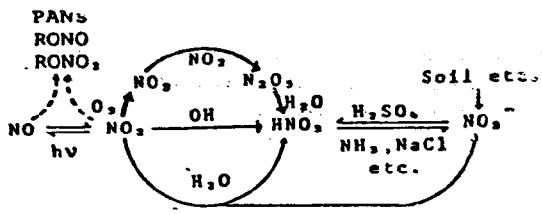

Fig.8. Mechanism for nitrates formation in the atmosphere.

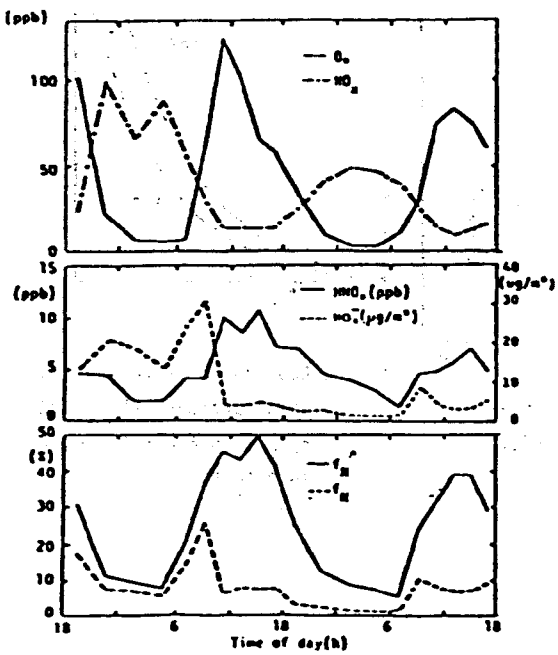

Fig.9. Diurnal variations of f_N', f_N, and selected pollutants at Saitama Univ.(July 31~August 2,.1979).

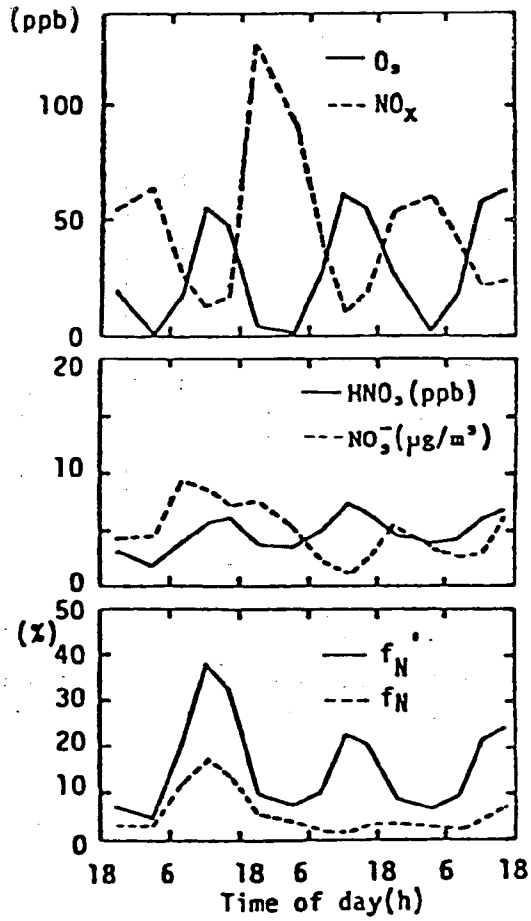

Fig.10. Diurnal variations of f_N', f_N, and selected pollutants at Saitama Univ.(May 27~30,1980).

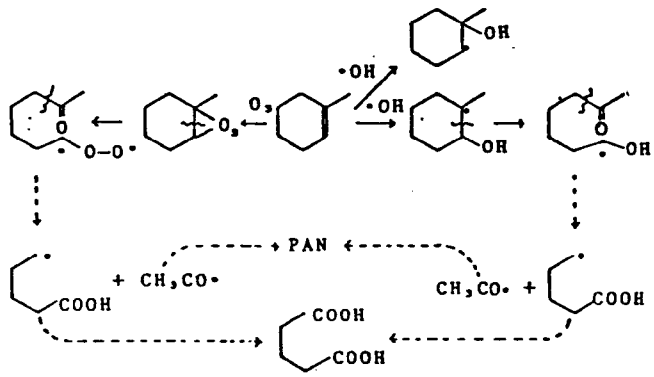

Fig.11. Possible formation pathways for glutaric acid and PAN.

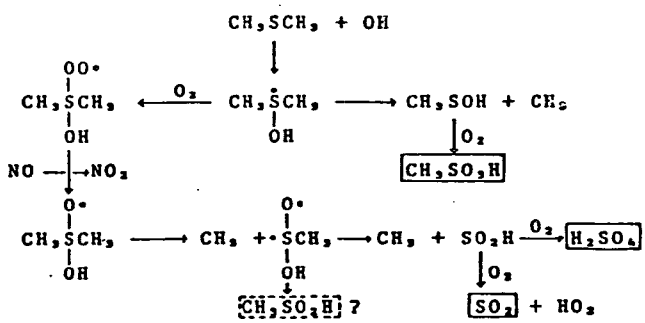

Fig.12. Possible formation pathways for methylsulfonic acid, sulfuric acid, and sulfur dioxide.

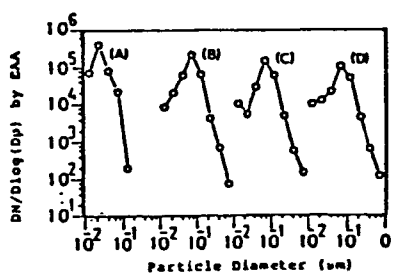

Fig. 13. Particle size distribution of photochemical aerosol formed from C_3H_6(1.0ppm)/NO(0.2ppm)/SO_2 (0.1ppm)/dry air (H_2O<1ppm) system by EAA; k_1 = 0.27 min^{-1}.

	Elapsed time (min)	σ_g (-)	Med. Diam. (μm)
(A)	97	1.45	0.029
(B)	150	1.52	0.075
(C)	211	1.75	0.081
(D)	275	1.86	0.079

APPENDICES

JAPAN-US JOINT CONFERENCE
ON
PHOTOCHEMICAL AIR POLLUTION AND
AIR POLLUTION-RELATED METEOROLOGY

Conference Room
National Institute for Environmental Studies
16-2 Onogawa, Yatabe-cho, Tsukuba-gun
Ibaragi Prefecture, Japan

December 1–2, 1982

AGENDA

Wednesday, December 1, 1982

Acting Chairman: Dr. T. Okita

10:00 – 10:40	Opening Remarks	Dr. J. Kondo (Director of NIES)
	Introduction of Participants Election of Session Chairman Approval of Conference Program	
10:40 – 11:00	Refreshments	
		Session Chairman: Dr. H. L. Wiser Wiser
11:00 – 12:00	The Problems of Acid Rain in Japan	Mr. S. Kato
12:00 – 13:30	Lunch	
13:30 – 15:00	Progress in Photochemical Air Quality Simulation Modeling	Dr. K. L. Demerjian
	Researches on Acid Rain in Japan	Mr. T. Komeiji
15:00 – 15:30	Refreshments	
15:30 – 17:00	Urban Ozone Modeling Developments in the U. S.	Dr. B. Dimitriades
	A Numerical Simulation of Local Wind and Photochemical Air Pollution	Dr. F. Kimura
17:00 – 17:45	Transport and Transformation of Air Pollutants by Land and Sea Breezes	Dr. H. Tsuruta

Thursday, December 2, 1982 **Session Chairman: Dr. N. Murayama**

9:00 – 10:30	Evaluation of Eight Linear Regional-scale Sulfur Models by the Regional Modeling Subgroup of the United States/Canadian Work Group 2	Dr. K. L. Demerjian
	Field Studies on Photochemical Air Pollution in Japan	Dr. S. Wakamatsu
10:30 – 11:00	Refreshments	
11:00 – 12:30	US Studies on Stratospheric Ozone	Dr. H. L. Wiser
	Intrusion of Stratospheric Ozone into the Troposphere	Dr. H. Muramatsu
	The Vertical Distributions of CF_2Cl_2, $CFCl_3$ and N_2O over Japan	Dr. M. Hirota
12:30 – 14:00	Lunch	
	Tsukuba – – – ➔ Tokyo	

THE PROBLEMS OF ACID RAIN IN JAPAN

Presented by S. Kato

Environment Agency

Japan

I. Actual occurrence of acid rain found to date in Japan

1. Damage caused by acid rain in Japan

In Japan, no damage by acid rain to the ecosystem; forest, agricultural products, fish, etc., has been reported, though it has become a problem in North Europe and North America. Therefore, in this field, acid rain is not a social problem yet in Japan. The problem of acid rain occurring in Japan to date is irritation to the eyes and the skin due to mist and drizzle occurring in the metropolitan area, etc. from 1973 to 1975 (see Table 1).

Since this was considered to be caused by irritants such as hydrogen ions (H^+) contained in mist and drizzle, it became necessary to clarify the mechanism of pollution generation by these materials. The Environment Agency designated this kind of pollution "wet-air pollution" (health hazard due to contaminated precipitation) and carried out relevant studies for the 5 years from 1975 to 1979 fiscal year.

(Note) Differences in adverse effects due to acid rain between Japan and USA found to date.

- o Japan ..... Irritation caused to humans (irritation to the eyes and the skin)
- o USA ..... Damage to the ecosystem (lakes and marshes, forest, etc.)

2. On wet-air pollution studies

Studies on wet-air pollution are intended to clarify the generation mechanism. When this is considered, it is necessary to clarify (1) weather conditions liable to cause mist or drizzle, (2) the production of irritants and absorbtion into precipitation, and (3) the production mechanism of irritants during precipitation.

To clarify the conditions causing actual damage, it is necessary to know (4) the concentrations of irritants in precipitation and (5) the concentrations of those irritants which cause damage.

To clarify the above points, a series of studies were made.

Irritation to the eyes and the skin was surmised to be caused not only by the action of acid materials in precipitation but also the mutual action of such coexisting materials as formaldehyde (HCHO), formic acid (HCOOH), and hydrogen peroxide (H_2O_2), etc. and the production mechanism of these materials was taken to be as shown in Fig. 1.

3. Results of researches

(1) Weather conditions liable to cause wet air pollution

Weather conditions on days when reports were made were investigated, and it was found that irritation occurred under certain weather conditions (when a weak front with high humidity slowly approached a stagnant high pressure area and humidity was high.

(2) Results of rainwater analysis

Rainwater was analysed from 1975 to 1979 fiscal year. Especially, pH showed a very low value of about 4 on average (see Table 2).

(3) Relation between the concentrations of irritants and its effects

In an experiment using rabbits, irritation to the eyes could be confirmed only at very high concentrations of irritants.

(4) Generation, diffusion and production of irritants in the atmosphere

Among irritants and their precursors, the distributions of the generation sources of those other than sulfur dioxide and nitrogen oxides were not known, and sufficient data could not be obtained on the drift and diffusion of these materials. For this reason, the relation between sources and effect could not be clarified. Furthermore, also with regard to the production of irritants in the atmosphere, the actual production mechanism and production rates could not be determined by field studies. Especially the transformation at high humidity in cloudy weather was not clarified, being left as a problem to be solved in the future.

(5) Absorbtion of irritants into precipitation and production mechanism during precipitation

The pH of rainwater was found to relate to sulfate ions and nitrate ions, and low pH is presumed to be caused by the absorbtion of sulfate mist and gaseous nitric acid.

(6) Change of wet-air pollution

Adverse effects on human health from wet-air pollution occurred often in the period from 1973 to 1975, but since then, none were reported except one case in 1976. However, recently in June, 1981, a case where several persons reported adverse effects occurred in Isezaki City, Gunma Pref.

II. Planning future research

The Environment Agency is planning to conduct studies concerning acid rain from fiscal 1983 for 5 years. The outline is as follows (for the entire flow, see attached sheet).

1. Atmosphere system

To find measures to prevent influences on the ecosystem, etc., the actual conditions of acid rain and the balance of pollutants must be clarified, and the production mechanism of acid rain must be known. For these purposes, the studies with the following contents will be made.

(1) Analysing pollutants and rainwater

Pollutants and rainwater will be sampled at 12 places throughout the country, to analyze pH, sulfate ions, nitrate ions, chlorine ions and ammonium ions, to determine the conditions of pollution.

(2) Measuring the distributions of pollutants by altitude, and arranging and analysing meteorological data

The concentrations of pollutants (sulfur dioxide, nitrogen oxides, ozone, sulfate ions, nitrate ions and nitric acid) in the sky will be investigated by altitude, to determine their distribution, and meteorological data (wind direction, wind velocity, temperature and humidity) will be arranged and analyzed.

(3) Measuring the settling rates of pollutants

To clarify the balance of pollutants in the atmosphere, the settling rates of pollutants (sulfur dioxide, nitrogen oxides, sulfate ions, nitrate ions and nitric acid) on the ground surface will be examined.

(4) Studies concerning the process of absorbtion of pollutants into rainwater, and so on

Studies concerning the process of absorbtion into rainwater of various pollutants (sulfur dioxide, nitrogen oxides, sulfate ions, nitrate ions and nitric acid) causing the production of acid rain will be made.

2. Land water system

(1) Survey of actual conditions

To determine the actual conditions of land water pollution due to acid rain throughout the country, the pH, electrical conductivity, metal concentrations, etc. will be measured in lakes, marshes, rivers, etc. in mountainous areas little affected by artificial pollution, and the species and numbers of fish, shells, and other animals living there will be investigated.

(2) Studies to clarify the acidifying mechanism

Based on the results of the survey of actual conditions, studies will be made successively in the land water areas of lakes, marshes, rivers, etc. where acidifying continues, to clarify the acidifying mechanism of land water.

3. Soil system

Considering the weather conditions such as precipitation, land use, and so on, 5 typical areas will be selected throughout the country, and studies will be made on the physicochemical natures of rainwater and soil, and biological natures of soil, vegetation, etc. to determine the actual conditions of soil environment worsened by acid rain, and to clarify the influences on the soil ecosystem and vegetation.

Table 1 Number of reported sufferers

Fiscal year	Month and date	Number of reported sufferers	pH of rainwater
1973	6.28 ∿ 6.29	540	2 ∿ 3
	9.13	7	-
		Subtotal 547	
1974	7.3 ∿ 7.4	32,546	3 ∿ 4
	7.18	506	3 ∿ 4
	Others	129	
		Subtotal 33,181	
1975	6.25	143	3 ∿ 4
	Others	101	
		Subtotal 244	
1976	8.16	1	5.6
		Grand total 33,973	

Table 2 pH of rainwater in Kanto Area
(3 mm from initial rainfall)

Place \ Fiscal year	1975	1976	1977	1978	1979	Mean	n
Mito	3.3 ∿ 5.8 (4.8)	4.0 ∿ 5.2 (5.0)	4.6 ∿ 6.8 (5.0)	4.2 ∿ 6.0 (5.4)	4.3 ∿ 6.7 (5.0)	4.8 ∿ 5.4	54
Shimodate	3.4 ∿ 6.6 (-)	3.8 ∿ 5.4 (4.3)	4.0 ∿ 7.4 (4.7)	4.2 ∿ 5.9 (4.8)	4.2 ∿ 6.7 (5.1)	3.9 ∿ 5.1	52
Utsunomiya	3.2 ∿ 6.3 (3.9)	3.3 ∿ 4.0 (3.9)	4.1 ∿ 6.3 (4.6)	3.3 ∿ 6.2 (4.0)	3.9 ∿ 6.5 (4.4)	3.9 ∿ 5.1	80
Tochigi	3.6 ∿ 6.3 (4.0)	3.6 ∿ 5.2 (4.0)	3.9 ∿ 6.2 (4.6)	3.7 ∿ 6.3 (4.2)	4.3 ∿ 7.0 (4.9)	4.0 ∿ 6.3	75
Maebashi	4.4 ∿ 6.5 (5.0)	3.9 ∿ 4.0 (3.9)	4.6 ∿ 6.1 (5.0)	3.6 ∿ 4.6 (3.9)	4.3 ∿ 6.3 (4.7)	3.9 ∿ 5.0	33
Tatebayashi	3.3 ∿ 6.1 (3.9)	3.6 ∿ 4.2 (3.9)	5.2 ∿ 5.8 (5.5)	3.7 ∿ 4.9 (4.3)	4.5 ∿ 6.2 (5.2)	3.9 ∿ 5.2	82
Urawa	3.1 ∿ 4.4 (3.7)	3.6 ∿ 4.7 (4.0)	3.7 ∿ 6.0 (4.3)	3.5 ∿ 6.1 (4.0)	4.1 ∿ 6.3 (4.7)	3.7 ∿ 4.7	71
Kumagaya	3.1 ∿ 6.7 (3.7)	4.7 ∿ 6.5 (5.0)	3.8 ∿ 6.5 (4.7)	3.9 ∿ 6.6 (4.3)	4.6 ∿ 6.6 (5.1)	3.7 ∿ 5.1	53
Ichihara	3.7 ∿ 5.7 (4.3)	4.4 ∿ 6.8 (4.9)	3.7 ∿ 5.7 (4.3)	3.6 ∿ 6.4 (4.2)	3.8 ∿ 5.0 (4.0)	4.0 ∿ 4.9	99
Togane	3.9 ∿ 6.0 (4.3)	4.3 ∿ 6.4 (5.0)	4.0 ∿ 5.8 (4.6)	3.3 ∿ 6.1 (5.2)	4.5 ∿ 5.5 (4.8)	4.3 ∿ 5.8	74
Chiyoda	3.9 ∿ 6.6 (4.4)	4.1 ∿ 5.9 (4.8)	4.0 ∿ 5.6 (4.4)	3.5 ∿ 7.0 (4.1)	4.0 ∿ 6.5 (4.5)	4.1 ∿ 4.8	61
Tama	3.5 ∿ 6.6 (4.3)	4.7 ∿ 6.8 (5.2)	3.5 ∿ 6.9 (4.0)	3.4 ∿ 4.4 (3.8)	4.2 ∿ 6.1 (4.7)	3.8 ∿ 5.2	72
Kawasaki	3.5 ∿ 6.4 (3.9)	3.6 ∿ 5.3 (4.1)	4.0 ∿ 4.8 (4.3)	3.5 ∿ 4.7 (3.9)	3.3 ∿ 5.3 (3.6)	3.6 ∿ 4.3	70
Yokohama	3.3 ∿ 4.4 (3.7)	3.3 ∿ 4.0 (3.6)	3.0 ∿ 3.6 (3.3)	3.4 ∿ 4.5 (3.8)	4.0 ∿ 6.5 (4.5)	3.3 ∿ 4.5	60
Hiratsuka	3.4 ∿ 5.4 (4.0)	3.7 ∿ 4.8 (4.0)	3.8 ∿ 4.2 (4.0)	3.1 ∿ 5.6 (3.6)	4.5 ∿ 5.8 (4.9)	3.6 ∿ 4.9	62
Mean	3.1 ∿ 6.7	3.3 ∿ 6.8	3.0 ∿ 7.4	3.1 ∿ 7.0	3.3 ∿ 7.0	3.3 ∿ 6.3	998

(Note) 1) The values in parenthese are mean values.

2) The period of survey was from the latter half of June to the first half of July.

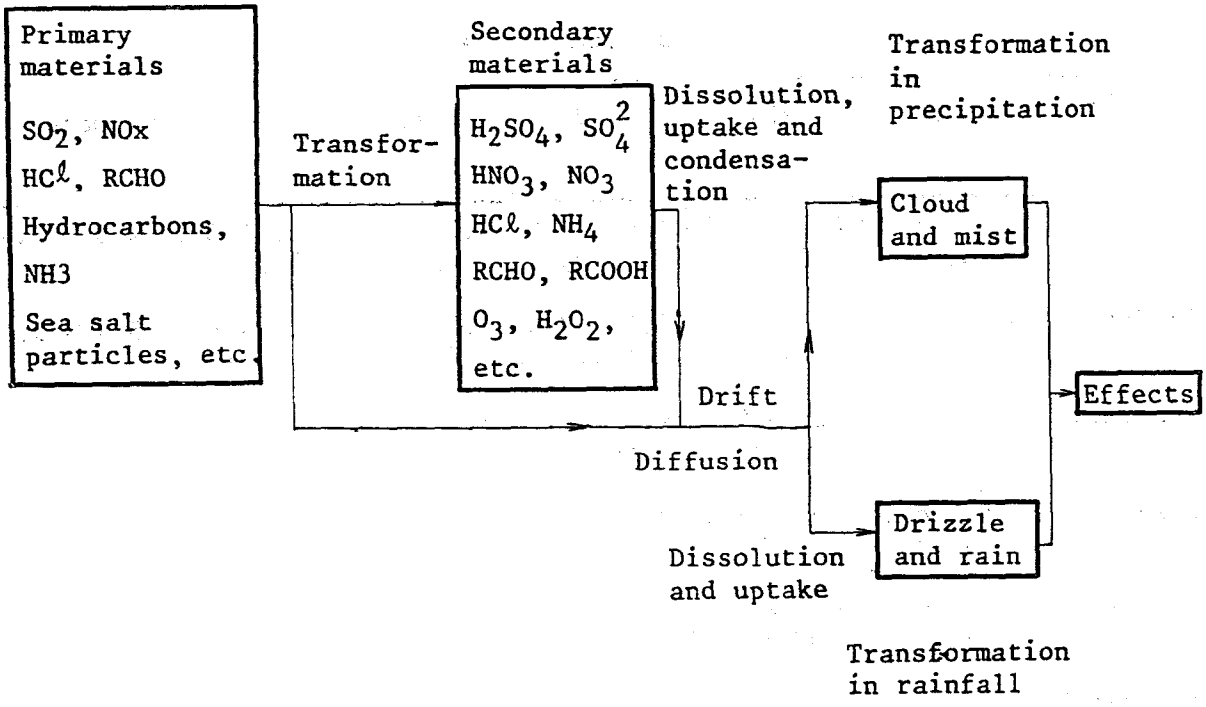

Fig. 1 Assumed production mechanism of wet-air pollution

Fig. 2 Surveyed places

(ATTACHED SHEET) Acid rain research flow

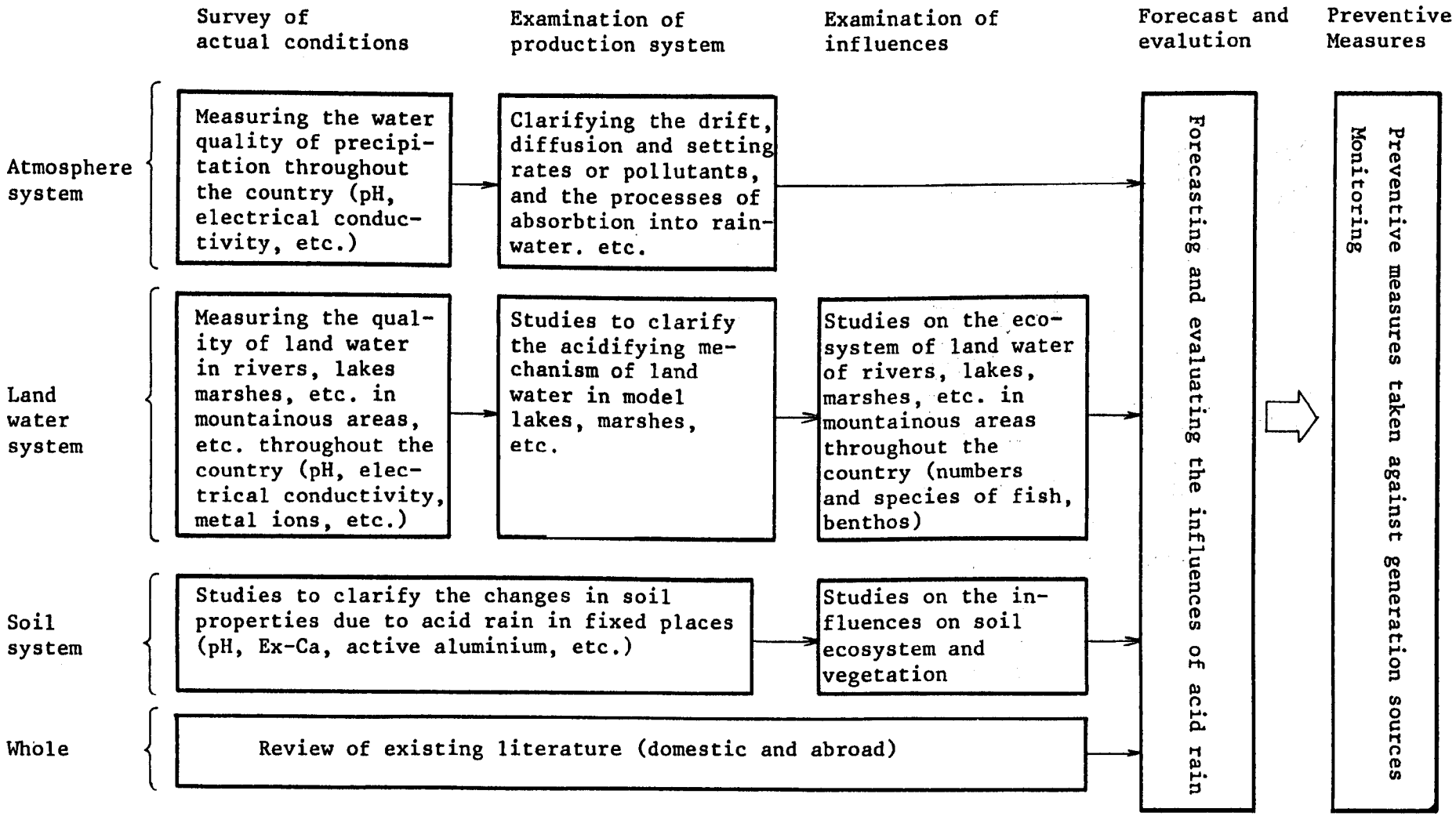

PROGRESS IN PHOTOCHEMICAL AIR QUALITY SIMULATION MODELING

presented by K.L. Demerjian

Environmental Sciences Research Laboratory

USEPA

PROGRESS IN PHOTOCHEMICAL AIR QUALITY SIMULATION MODELING

J.H. Shreffler, K.L. Schere, and K.L. Demerjian[1]

Environmental Sciences Research Laboratory
U.S. Environmental Protection Agency
Research Triangle Park, NC 27711 U.S.A.

INTRODUCTION

Over the past 15 years we have witnessed the development of atmospheric dispersion models which include increasingly complex approximations of photochemistry. Unlike existing Gaussian or analytic schemes, the models simulate atmospheric chemical reactions, some of which act at very rapid rates, and therefore involve time steps much shorter than are generally regarded as necessary for transport and dispersion of inert species. The computational demands rise rapidly with the number of chemical species considered, and it is not unusual to see present-day models for urban and regional scales having computer simulation speeds comparable to the real-world events. Computer restrictions have tended to engender decisions to diminish the spatial resolution of the models in order to increase the number of species and reactions treated.

We have recognized for a number of years that within the class of existing or conceived photochemical air quality simulation models (PAQSM's) there are only several basic approaches. The United States Environmental Protection Agency (U.S. EPA) in the mid-1970's reviewed the various urban scale models which were in existence and chose three, embodying distinct approaches, for further refinement, development, and evaluation. In the case of the EPA, the ultimate goal was to provide regulatory tools for control of photochemical pollutants, O_3 in particular. The models

---

[1]All authors are on assignment from the National Oceanic and Atmospheric Administration, U.S. Department of Commerce.

were to be used to predict the problems created by new sources or the benefits of controlling existing sources. Shortly thereafter, work also began on a regional-scale (1000 km) photochemical model to be used initially in the northeastern U.S. Interest in larger scales derived from a growing awareness that elevated O_3 levels may be found over large regions and at considerable distances from urban centers (Wolff et al., 1977). The goal of the regional modeling effort was again to allow defensible regulatory decisions, but the complexity of the problem and its immense resource requirements precluded study of several alternate approaches as was done with the urban models.

The purpose of this paper is to describe the PAQSM's emerging from research and development projects of the U.S. EPA. The presentation will not attempt a detailed discussion of chemical mechanisms or numerical schemes. Rather, emphasis will be placed on the models' basic structures, data requirements, computer requirements, and problems encountered in applying them. Also, we will describe the two major field programs which have been conducted by EPA to support testing and evaluation of the models.

COMPONENTS OF MODEL SIMULATIONS

PAQSM's may differ in complexity and therefore data and resource requirements through deliberate choices of the builders. For example, restriction to a simple box-model makes spatial resolution of emissions and winds unnecessary. Furthermore, data requirements will vary greatly depending on the goal of the simulations. If model development and evaluation are planned, then the data needs are extensive. On the other hand, if the model is already viewed as a reliable operational tool, data needs are greatly reduced as climatological scenarios may be used for worst-case and average events. In the latter case, predicted pollutant levels are only checked for reasonableness against previous records and not against specific observations. Photochemical air quality simulations share similar attributes, and requirements, regardless of the particular model used. Generally, all PAQSM's are logical frameworks which synthesize information from meteorology, sources, and air quality and predict the photochemical pollutant concentrations consistent with expressions for governing physical laws. The simulation is therefore an interplay of four equally important components.

PHYSICAL LAWS: Physical laws are expressed as mathematical equations governing atmospheric motions (transport and diffusion) and the chemical kinetics. The equations enforce mass conservation and promote appropriate chemical transformations in a manner consistent with theoretical considerations and observational data.

Kinetic mechanisms generally have been developed by comparing numerical predictions to concentrations resulting from carefully controlled smog chamber experiments. It is important to note that equations of both the meteorological and chemical aspects of the problem are approximations. For example, mixing rates are usually difficult to prescribe, and hydrocarbon (HC) species must be lumped in terms of reactivity classes.

SOURCE EMISSIONS: Pollutant emissions are an important component in the application of a PAQSM and must be compiled on spatial and temporal scales comparable to the resolution inherent in the model structure. Photochemistry involves a strong diurnal cycle which dictates a temporal resolution on the order of 1-h in the emissions inventory. Inventories usually are divided into the source types of area, point, and line. Area sources include many diffuse, population-related sources such as those associated with space heating or residential automotive traffic. Point sources are large, identifiable sources such as power plants, and line sources refer to major automotive thoroughfares. A typical inventory for a large city may include several hundred point sources. Unless the model has the unusual capacity to treat line sources, they may be incorporated into the area source inventory. For PAQSM's the emphasis is usually on developing emissions for HC, NO_x, and CO, although mechanisms generally include other species such as SO_2 and SO_4. The HC emission is broken into reactivity classes consistent with the kinetic mechanism (e.g., olefins, paraffins, aromatics, formaldehyde, and other aldehydes). Also, the NO_x must be appropriately split between NO and NO_2.

METEOROLOGICAL FACTORS: Meteorological factors account for the transport and diffusion of pollutants and influence reaction rates in the chemical mechanism. These data are introduced into the model from observations and are not predicted. Important parameters include the wind field, inversion height, atmospheric stability, solar radiation, water vapor, and temperature.

AIR QUALITY MEASUREMENTS: Ambient concentration measurements are needed to set initial conditions, boundary conditions, and as evaluation data. Photochemical simulations usually begin with an initial set of observations used to assign concentrations of important O_3 precursors, HC and NO_x, within the modeled domain. As an alternate strategy, the model could generate its own initial state by allowing sufficient time for emissions to establish suitable concentration levels. However, this strategy is usually impracticable when considering other aspects of the problem such as ventilation rates, especially on the urban-scale. Boundary conditions refer to the concentrations assigned at the extremities of the modeled region, both in the horizontal and vertical. Concentrations at the upwind boundary of a grid-model domain are of obvious impor-

tance. Moreover, the concentrations aloft may also play a role as they are entrained during the diurnal growth of the mixed layer. Ambient data must have a spatial and temporal resolution at least comparable to the model output if evaluation of the model is to be attempted.

URBAN MODELS

The U.S. EPA currently has interest in three urban models embodying distinctly different approaches and levels of complexity. Those models are:

Photochemical Box Model (PBM) - a single cell Eulerian model constructed by EPA.

Lagrangian Photochemical Model (LPM) - a multi-level parcel model originally developed by Environmental Research and Technology, Inc.

Urban Airshed Model (UAM) - a multi-level, Eulerian grid model originally developed by Systems Applications, Inc.

The versions of the models at EPA have been structured to easily use urban data compiled during the Regional Air Pollution Study (RAPS) and have been subject to continuing modifications. The RAPS will be discussed in a later section. In this section, the basic frameworks and requirements of the models will be surveyed.

Photochemical Box Model

The Photochemical Box Model (PBM) is a single cell Eulerian air quality model whose purpose is to simulate the transport and chemical transformation of air pollutants in smog prone urban atmospheres. The model's domain is set in a variable-volume, well-mixed reacting cell where the physical and chemical processes responsible for the generation of O_3 by its HC and NO_x precursors are mathematically created. These processes include the transport and dispersion of pollutant species through the cell, the injection of primary precursor species by emission sources, and the chemical transformation of the reactive species into intermediate and secondary products. They are schematically illustrated in Figure 1. In a typical application of the model, the horizontal length scale of the single cell is about 20 km and the vertical scale is time-varying, equivalent to the depth of the mixed layer. The model domain is centered on the city such that the area encompasses most of the major emissions sources. Source emissions are assumed to be distributed uniformly across the surface face of the cell.

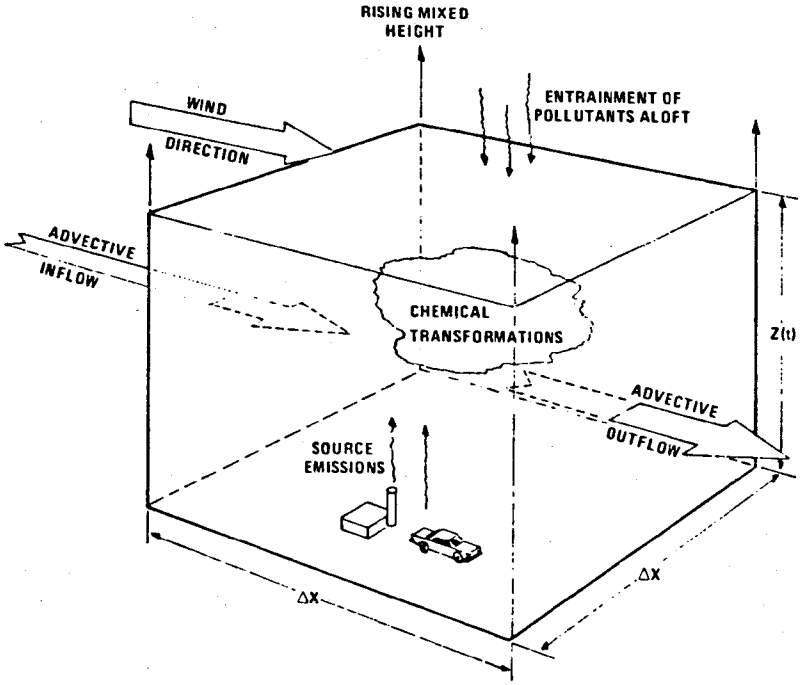

Fig. 1. Schematic of the domain and processes in the Photochemical Box Model.

While the data requirements of the PBM are not particularly rigorous, three data preprocessors must be executed prior to each model simulation. The first accesses the 1-h average air quality and meteorological data base forming the initial concentrations of participating species, determining the 1-h average wind vectors that guide transport through the model domain, and choosing the hourly updated concentration of species at the upwind boundary of the box. The first preprocessor also forms similar spatial averages of concentrations of monitored pollutant species for comparison with model predictions.

A function of the second preprocessor is to determine 10 min average values of total solar radiation from pyranometer measurements. From these values the time-varying photolytic rate constants can be determined through a series of empirical and theoretical relationships. The temporal resolution of these data is greater than for most other data because of the rapid chemical reactions which are associated with these rate constants. This preprocessor also calculates the diurnal growth pattern of the mixed layer, or the depth of the model domain. To perform this calculation, the morning minimum and afternoon maximum mixed layer heights are provided by the user. These heights were determined in the RAPS application by studying the vertical structure of the temperature and moisture from radiosondes. Releases occurred

throughout the day at 6-h intervals beginning 1 h before sunrise. The model fits a piece-wise linear function between the specified minimum and maximum depths that simulates the actual mixed layer growth as observed by acoustic sounder, lidar, and radiosonde techniques. Ten-minute averages of mixed layer height are formed for the PBM; photolytic rate constants for the corresponding time period are integrated through this depth.

The third preprocessor is responsible for forming hourly emissions source terms for CO, NO, NO_2, and non-methane HC. Even though the emissions may have spatial resolution, all source emissions, both area and point, within the model domain are summed to provide a total emission rate for each primary pollutant species at every hour of simulation.

The PBM may be executed when the data files from the three preprocessors have been created. The only other relevant information needed at this time is the concentration of O_3 at the top boundary of the modeling domain, that pollutant having been transported into the area by winds aloft during the night. This concentration is determined from the O_3 measurements at the far upwind surface monitoring sites after the nocturnal temperature inversion has eroded and the air aloft mixes down through the atmosphere to the surface. Concentrations of other pollutants at the top of the modeling region are assumed to be negligible. The simulation is typically started at 0500 CST and continues through 1700 CST.

The PBM contains a chemical kinetic mechanism with 36 reactions and 27 reactive species (Demerjian and Schere, 1979). The set of equations describing the rates of change of the concentrations of these species is numerically solved at time steps on the order of 10 min. From these solutions the model determines the 1-h average predicted concentration of each modeled species.

Lagrangian Photochemical Model

The Lagrangian Photochemical Model (LPM) was developed by Environmental Research and Technology, Inc. of Westlake Village, California and adapted under contract with EPA for use with the RAPS data base. (The LPM is essentially identical to the general-use model named ELSTAR.) The LPM envisions a portion of the atmosphere as an identifiable parcel which can be tracked from early morning to the late afternoon. As the parcel moves over the various emissions sources, pollutants are assimilated, vertically mixed, and subjected to photochemical reactions in the presence of solar radiation (see Figure 2). The LPM is attractive relative to grid models in that it is fairly simple to execute and uses a moderate amount of computer time. On the other hand, the LPM

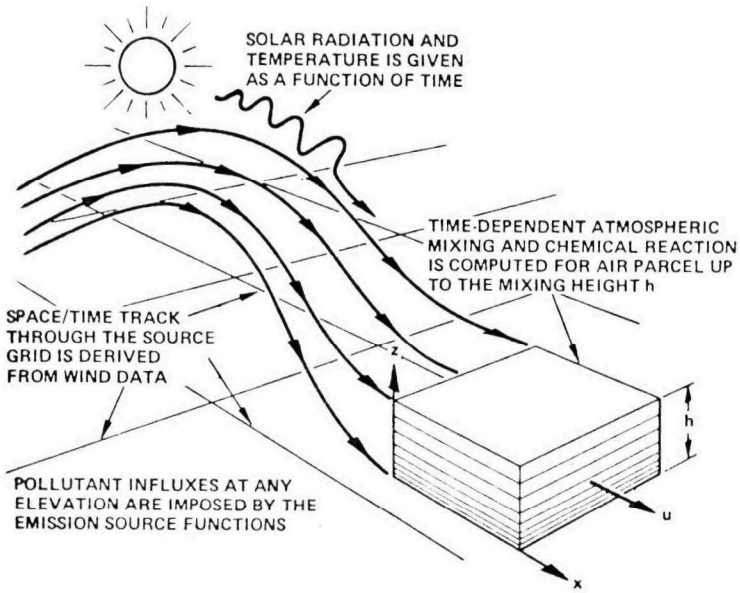

Fig. 2. Schematic of the modeling concepts of the Lagrangian Photochemical Model.

calculates concentrations only within a parcel and not over a complete spatial field.

The LPM is executed using a series of program modules. They are METMOD, EMMOD, and KEMOD, sequentially performing calculations on meteorology and air quality, emissions, and photochemistry. The input and running procedures described by Lurmann et al. (1979) have been generally followed, although some modifications were deemed necessary as more experience with the model was acquired (Lurmann, 1980; 1981).

The first step in setting up a simulation is to determine the starting point of a parcel so that it will arrive at a specified point at an assigned time. A backward trajectory can be generated by the METMOD. The parcel trajectory is usually determined by $1/R^2$ weighting of winds from the closest three stations. However, experience with wind data suggests that even closely situated stations can show large, unexplained differences in wind vectors from time to time. Reliance on a single anomalous station, if the parcel has a close approach, can create an erratic trajectory. To eliminate the possibility of such vagaries, it may be prudent to compute a single resultant wind vector from the wind station network and assign it to all stations for a given hour. The resultant gives a general movement of the air mass over the region.

Because of the difficulty in solving the chemistry set with minimal solar radiation, the start time of a parcel (which is on the hour) must be at least 10 min past local sunrise. Once the start position is set, the METMOD is run in a forward-trajectory mode until 1800 CST or the parcel leaves the region.

Mixing heights are computed from radiosondes released approximately 1 h before sunrise and at 6-h intervals thereafter. The temperature and wind profiles from the balloons are processed automatically by the model to give vertical eddy diffusivities throughout the day. The trajectory information from METMOD is stored and is available to EMMOD to enable that module to obtain the emissions that the parcel will encounter. METMOD also stores the observed pollutant concentrations along the trajectory using a $1/R^2$ weighting scheme on the closest three stations. These observations are available for setting initial conditions in the parcel and later comparisons with the model predictions. In most cases, the parcel starts in a relatively clean rural environment, and levels of HC, NO, and NO_2 are assumed to decrease with height according to an assigned formula. On the other hand, ozone is depleted near the ground at night; thus, the initial O_3 increases from the surface to a value at 400 m which is equal to the observed 1000-1200 CST surface concentration upwind of the city (Shreffler and Evans, 1982).

The EMMOD creates a record of the emissions entering the parcel as it traverses its trajectory. These emissions are used by the KEMOD to simulate the photochemical reactions which will take place as a function of time, yielding concentrations of 39 chemical species at 30-min intervals. A total of 65 reactions are modeled.

Urban Airshed Model

The Urban Airshed Model (UAM) is a three-dimensional (3-D) grid-type, or Eulerian, PAQSM developed by Systems Applications, Inc. (SAI) of San Rafael, California. The structure of the model consists of a latticework array of cells (see Figure 3), the total volume of which represents an urban-scale domain and in which the physical and chemical processes responsible for photochemical smog are mathematically simulated. These processes include the advection of pollutant species through the modeling domain, the species entrainment from aloft by a growing mixed layer, the diffusion of material from cell-to-cell, the injection of primary source emissions into the modeled volume, and the chemical transformations of reactive species into intermediate and secondary products. The horizontal dimensions of each cell are constant but the heights of the cells vary throughout a model simulation as the depth of the mixed layer in the UAM changes accordingly.

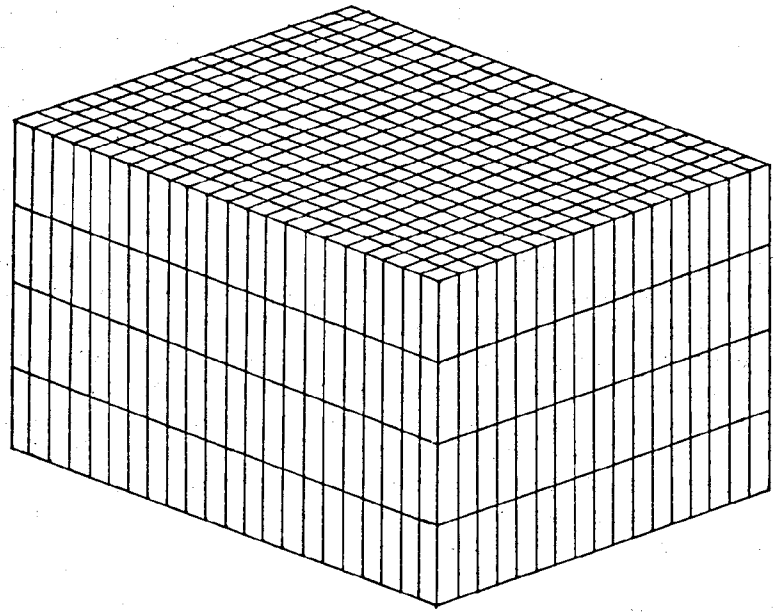

Fig. 3. Schematic of the grid domain used in the Urban Airshed Model.

In typical applications, the area modeled is about 60 x 60 km, and each individual cell is 4 km on a side in the horizontal. Vertically, there are four layers of cells in total; the bottom two layers simulate the mixed layer and the top two represent the region immediately above the mixed layer. The 3-D grid model is a sophisticated type of PAQSM and provides both spatially and temporally resolved concentration predictions. Thus, the UAM attempts to estimate the 1-h average observed concentration of a pollutant species at each monitoring site within the model domain.

The package of computer programs constituting the UAM actually contains 12 data preprocessing programs as well as the simulation model. The data requirements for applying the model are rather intensive. The preprocessors (PP's) access surface-based, hourly air quality and meteorological data base, the upper air pibal and radiosonde data, and the source emissions inventory for the necessary parameters, and process the parameters as required by the simulation model. A brief description of the PP's follows in order to convey a sense of the UAM data requirements.

The chemistry PP sets up the rate constants and other parameters related to the chemical kinetic mechanism within the model. This mechanism, named Carbon Bond II, is a state-of-the-art set of chemical reactions describing the NO_x-HC-O_3 species interactions

within a photochemically active atmosphere. The mechanism was developed at SAI by Whitten et al. (1980). The terrain PP describes the spatially varying types of surfaces within the modeling domain, reflecting the transition from urban to suburban and finally to rural land uses. The spatial resolution of these land forms should be on the same scale as the grid cell size. Both the chemistry and terrain PP's need only be executed once for a particular model application. All of the remaining PP's, however, must be executed prior to each model simulation within the application.

The diffusion-break and region-top PP's describe the variations in the mixing heights and modeling region depths, respectively, over the domain during the course of the simulation. Hourly values of the mixing height must be supplied at representative locations on the grid. It is the responsibility of the user to specify these depths in a meaningful manner from upper air soundings or equivalent data. The meteorological PP describes the temporal variation of vertical temperature gradient, stability class, atmospheric pressure, water vapor concentration, and the NO_2 photolysis rate constant. Values for these parameters do not vary spatially in the model. The top-concentration PP specifies the concentrations of principal species at the top of the modeled region throughout the simulation. In most cases these concentrations will be close to the clean air background values for these species, although substantial concentrations of O_3 can result from advection over the region. Its value is determined from the O_3 measurements at the far upwind surface monitoring sites after the nocturnal temperature inversion has eroded and the air aloft mixes to the surface.

The air quality, temperature and wind speed PP's all require data from a surface monitoring network. Hourly averages of observed species concentrations are objectively interpolated across the model grid by the air quality PP to produce a field of initial concentrations for the UAM. Typically this initial field is applied near sunrise. As the density of monitoring locations increases, the reliability of the objective interpolation does likewise. The temperature PP produces gridded fields of surface temperature at each hour of model simulation. These are required for both the wind and point source PP's. Finally, the wind PP assimilates all available surface and upper air wind speed and direction measurements and produces a gridded field of u and v wind components at each of the model's four vertical levels. This objective wind field analysis routine was developed by Anderson of SAI (Killus et al., 1977). Vertical wind velocities are calculated internally by the UAM from mass continuity considerations. Anderson's interpolation routine smooths the data in such a way so as to eliminate unrealistic vertical motions. It simulates the mesoscale urban circulation patterns through the use of the surface temperature

patterns. The boundary concentration PP determines the modeled species concentrations along each of the domain's borders for each hour of model simulation. A vertical concentration gradient is also described.

The last two PP's needed before the model is executed deal with source emissions. The area sources, including highway and line sources, and the point sources are treated separately. Hourly emission rates of all primary pollutants for each grid are calculated. Organic HC emissions must be distributed into particular structural classes.

Each PP generates a data file required by the UAM. Model simulations begin at 0500 CST and continue through 1700 CST. The model numerically calculates the rates of change of species concentrations at time steps on the order of several minutes, and from these determines the 1-h average predicted concentrations.

Status of the Urban Models

The three models discussed in this section are viewed by EPA as being in final form. That is, substantial breakthroughs in chemical mechanisms or the compilation of a clearly superior data base will be needed before revisions would be considered. Although the model preprocessors are geared to easy use of the RAPS data, it would not be difficult to adapt the models to other locations and other forms of data. In the next section the RAPS data set will be described along with some results of model applications. Before proceeding, we review some problems which arose during the testing of the models and look at estimated resource requirements.

Because of its relative simplicity, the PBM is attractive for use where resources are limited and results do not need to be highly detailed. With this model, it should be noted that emissions control strategies are difficult to target on particular sources because of the lack of spatial resolution. Also, the highest O_3 concentrations in the domain, upon which decisions may be more critically centered, are lost in the averaging assumptions. Finally, the simplified wind field (a single vector for each hour) and large size to the Eulerian domain make the model best suited for low-wind or stagnation episodes. These, of course, are usually conditions most favorable to high O_3 concentrations.

Compared to the UAM, the LPM may seem less resource intensive. However, the data requirements are nearly identical. The LPM may be used along a single trajectory, perhaps that trajectory encountering the observed maximum concentration, and therefore use much less computer time. If multiple trajectories are executed to display

concentrations over the region, such as the UAM does in a single simulation, then computer resources and preparation time will grow accordingly.

A number of problems have become apparent in the development and testing of the models. For example, the LPM seems quite sensitive to initial conditions since the parcel retains all pollutants. Thus, care must be taken to put realistic vertical distributions of precursors in the parcel at the beginning of the simulation day. The LPM has five vertical levels in which to distribute the pollutants. As originally conceived the model did not include any lateral diffusion, and this produced unrealistically high O_3 concentrations since all emissions were retained in a fixed volume. The model now allows the parcel to expand laterally in a manner commensurate with empirically determined diffusion. Whereas this feature considers dilution of a parcel when beyond the high emissions area, it introduces a problem in setting side boundary condition concentrations representative of the air that is entrained into the parcel. Our approach has been to set the initial parcel size about equal to the downtown area of highest emissions (5 x 5 km for RAPS) and treat the entrained air as having background values of HC and NO_x. The parcel is viewed as a segment of the urban plume. However, large power plant sources are liable to present conditions seriously in conflict with that assumption from time to time. This example evinces a fundamental truth about all of the PAQSM's; there is an element of art in their application which is unlikely to be eliminated without jeopardizing the models' flexibility in treating different situations.

The UAM as originally constructed suffered from substantial numerical diffusion. We believe this potential problem should be thoroughly investigated in any grid model of this sort. The tendency of the UAM to underestimate ozone maxima in our tests (see results in next section) was suspected of being due to the spurious diffusion. However, the underestimation was only slightly improved by a new and accurate numerical scheme, which, incidentally, increased computer time by 15 percent (Schere, 1982).

The choice of which particular model to use in a specific application involves not only the accuracy of the model but also the resources required to operate it. The models discussed here have resource requirements correlated with their level of complexity. In terms of man-months needed to set up a single day simulation and computer time expended (minutes of CPU on a Univac 1100/82) the approximate requirements are:

PBM	0.15 man-month	1 minute CPU
LPM	0.20 man-month	10 minutes CPU
UAM	0.50 man-month	110 minutes CPU

The initial man-month investment needed to become adequately familiar with the model perhaps exceeds the simulation set-up time by at least a factor of 10.

The three models discussed here have all shown themselves to be acceptable tools for analysis of urban O_3 air quality. The specific configuration of an application along with the quantity and quality of related data and resources available to the user must all be considered in the final selection of a model. For an indication of average O_3 air quality in an urban area under stagnation conditions or as a screening method for a more complex model, the PBM is appropriate. The choice of a trajectory model, such as the LPM, or a grid model, like the UAM, might well be decided by resource requirements or by the number of proposed simulations. In any event, the user of any of these models must have a strong scientific background and exercise extreme care in implementing the air quality simulations.

THE RAPS AND URBAN MODEL EVALUATION

Beside the physical laws expressed in the PAQSM, essential components of air quality simulations include emissions, meteorological and ambient concentration data. In this section we describe an extensive field effort for gathering data on an urban scale and some of the modeling results based on that data.

The Regional Air Pollution Study (RAPS) was carried out in the St. Louis area during 1974-1977. St. Louis is a city of negligible topographic relief in the central U.S.; about 2.3 million people reside in the metropolitan area. Although augmented by a variety of special studies, the principal data base was gathered by a 25 station network comprising the Regional Air Monitoring System (RAMS). Measurements included both meteorological parameters and pollutant concentrations. The purpose of RAPS was to develop a data base for testing numerical air quality simulation models and especially models involving the complex photochemical reactions leading to O_3 formation. The RAPS expenditures totaled about $25 million over a five-year period, and the data base remains the most comprehensive available.

RAMS measurements, recorded as 1-min averages, included wind speed and direction, temperature, vertical temperature difference, solar radiation and concentrations of O_3, CO, HC, NO_x and SO_2. The sampling manifold used by all gaseous monitors had an intake at about 4 m from the ground. Figure 4 shows the layout of the RAMS network. A more detailed description of the RAPS program and the RAMS instrumentation is given by Schiermeier (1978).

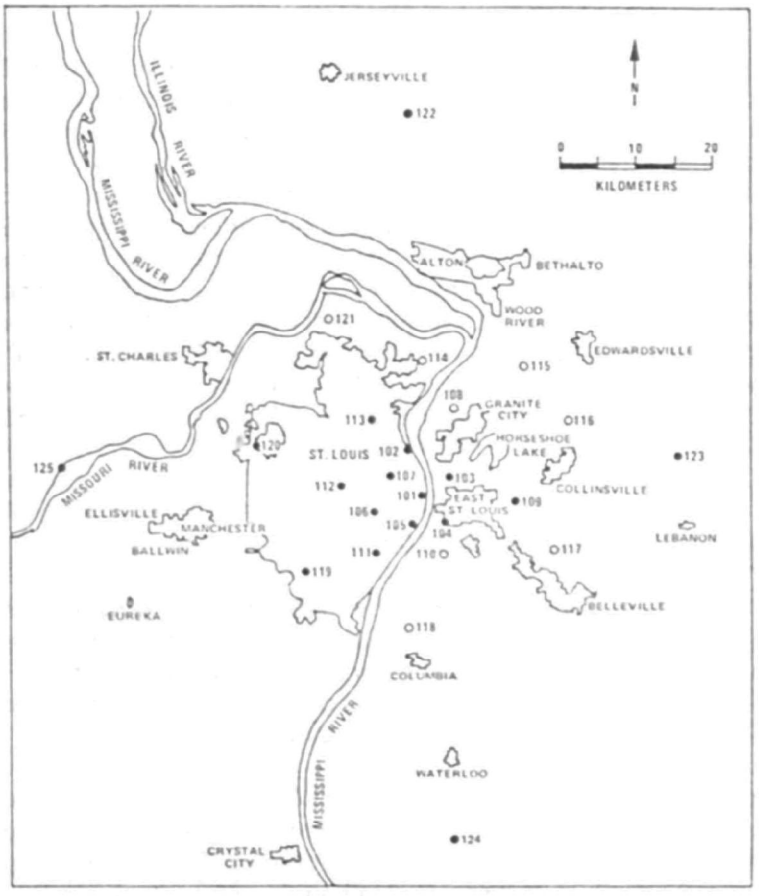

Fig. 4. The St. Louis area with locations of the RAPS stations 101-125.

The 1-min average values of all parameters were objectively screened. The screening excluded values which were null, part of a calibration set, taken during a period of excessive drift, outside instrument limits, taken under abnormal instrument status, or indicating persistence. The remaining data were used to form 1-h averages, and the 1-h average archive was generally the one used in model evaluation.

Overviews of the RAPS O_3 and NO_x data are given by Shreffler and Evans (1982) and Shreffler (1982). Figure 5 displays a 4-mo record of ozone taken in mid-1975. The time series are for the inflow concentration (that from upwind rural areas) and the maximum 1-h concentration recorded at any station in the network. The locations of the maxima, especially the strong peaks, usually show

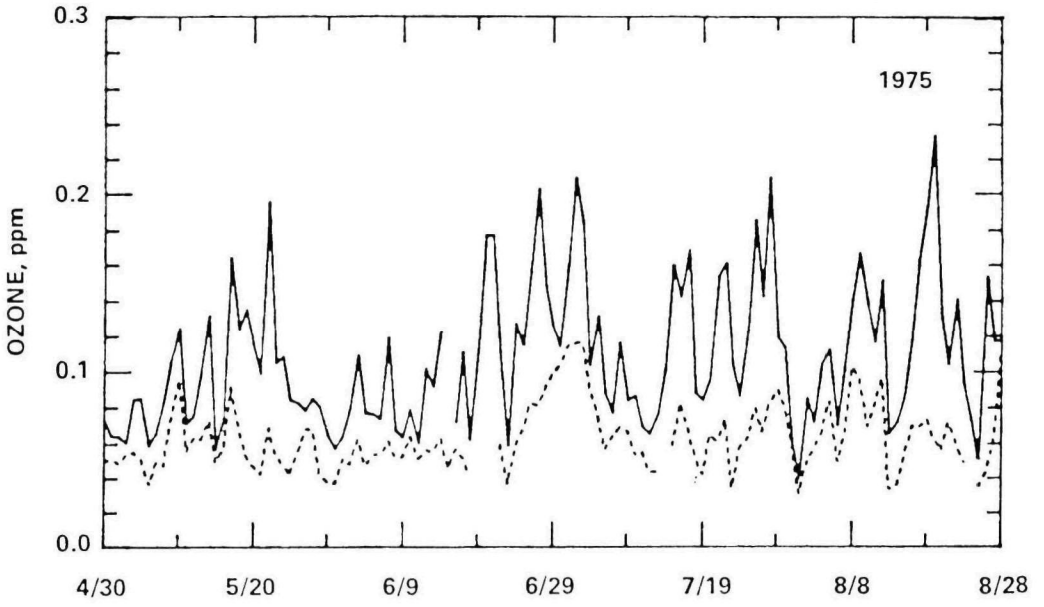

Fig. 5. Time series of the daily maximum 1-hr ozone concentration (solid) and the daily rural inflow ozone concentration (dashed) for May - August 1975 as measured in the RAPS.

clear downwind relations to high emissions areas. The differences between concentrations in the two series may be ascribed to net enhancement of O_3 levels due to the urban emissions.

In preparation for model evaluation, the entire data base was examined to establish suitable case-study days. In all, 20 days were selected for simulations based on high observed O_3 maxima and adequate availability of data. The maximum observed O_3 on these days ranged from 160 to 260 ppb.

The three urban models (PBM, LPM, and UAM) were adapted to access the RAPS data archive, which included a detailed emissions inventory with resolution to 1 h and 1 km (Littman, 1979). Although precise input requirements differ among the models, effort was made to supply information in a consistent form for all. Thus, the simulations were done in parallel, using the same basic data sets, and the results give a comparison among models as well as an indication of accuracy against observed concentrations.

As examples of model results, Figures 6 and 7 show observed and predicted O_3 values for the PBM and LPM on a single day, 1 October, 1976. Stagnation conditions prevailed on that day. For the PBM, the time series show concentrations within a fixed box 20 km x 20 km over the city center. Maximum and minimum observed

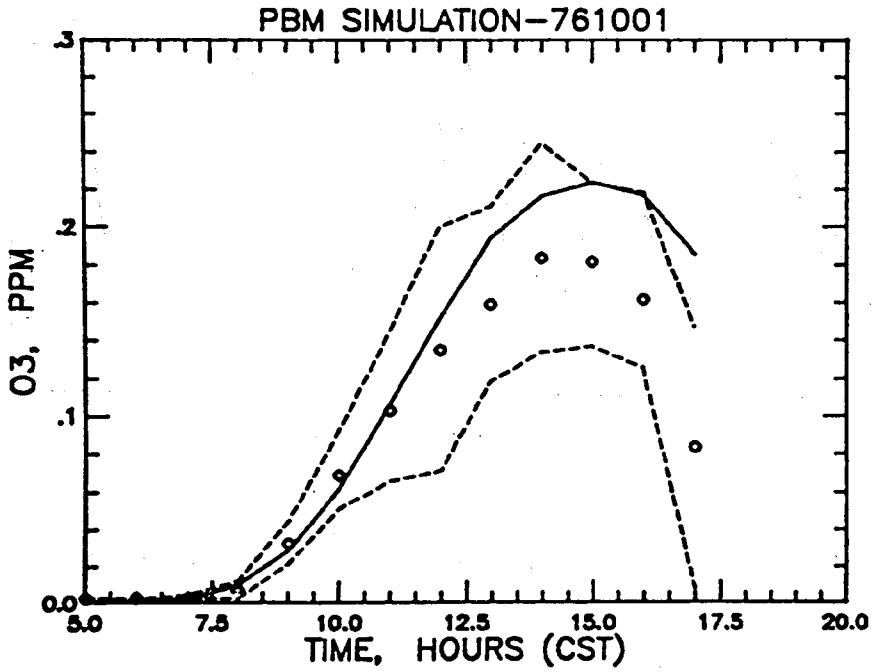

Fig. 6. PBM predicted ozone (solid) compared to measured domain average (circles) and maximum and minimum within the domain (dashed). This result is for the 1 October 1976 RAPS simulation.

concentrations over all the stations (13) in the box are given by the dashed lines. The average observed concentration is given by circles, and the model prediction is given by the solid line. For the LPM, the concentrations refer to a moving parcel with initial horizontal dimensions 5 km x 5 km. Predicted values are given for two vertical levels in the parcel, the surface (L-1) and about 200 m (L-3). This particular parcel arrives at the station (102) observing the maximum 1-h O_3 value at the time of that observation (1400 CST).

The ability of the models to reproduce observed O_3 maxima over the 20 test days is summarized by statistics given in Table 1. Complete results of the urban model evaluation are now available in report form (Schere and Shreffler, 1982).

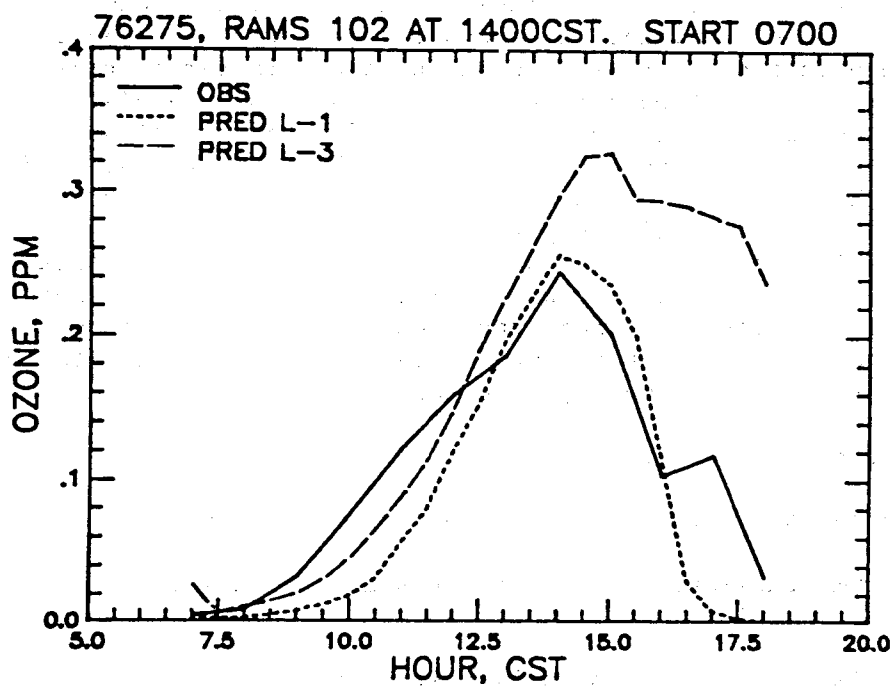

Fig. 7. LPM predicted ozone at the surface (L-1) and 200 m (L-3) compared to the observed ozone. This result is for the 1 October 1976 RAPS simulation.

Table 1. Statistics on residual concentrations (observed minus predicted) of maximum ozone (ppb) from 20 days of RAPS data. The observed maxima ranged 160-260 ppb.

	PBM	LPM	UAM
$\overline{\Delta C}$	-12	5	62
s.d.(ΔC)	39	58	35
$\overline{\lvert\Delta C\rvert}$	29	50	62

A REGIONAL SCALE (1000 KM) MODEL

The U.S. EPA is presently developing a model that can guide the formulation of regional emissions control strategies by estimating the effect of sources on concentrations in remote regions, determining the pollution burden that cities impose on distant neighbors, and eventually analyzing the effect of emissions on acid rain, visibility and fine particles. The utility and credibility of the model will be determined primarily by the extent to which it accounts for all the governing physical and chemical processes. Accordingly, the model is formulated, in principle, to treat all of the chemical and physical processes that are known, or presently thought, to affect the concentrations of air pollutants over several day/1000 kilometer scale domains. Among these processes are (not necessarily in order of importance):

1. Horizontal transport;

2. Photochemistry, including the very slow reactions;

3. Nighttime chemistry of the products and precursors of photochemical reactions;

4. Nighttime wind shear, stability stratification, and turbulence "episodes" associated with the nocturnal jet;

5. Cumulus cloud effects - venting pollutants from the mixed layer, perturbing photochemical reaction rates in their shadows, providing sites for liquid phase reactions, influencing changes in the mixed layer depth, perturbing horizontal flow;

6. Mesoscale vertical motion induced by terrain and horizontal divergence of the large scale flow;

7. Mesoscale eddy effects on urban plume trajectories and growth rates;

8. Terrain effects on horizontal flows, removal, diffusion;

9. Subgrid scale chemistry processes resulting from emissions from sources smaller than the model's grid can resolve;

10. Natural sources of HC, NO_x and stratospheric O_3;

11. Wet and dry removal processes, e.g., washout and deposition.

Of the eleven processes listed above, only the first and last have been treated in any detail in the regional scale models of air pollution developed to date. In fact, a review of these models (see, for example, reviews by Drake and Bass in Henderson et al.

1980) reveals that virtually all of the Eulerian type models are in essence simply expanded urban scale models. They account for the physical processes that are active during daylight hours and within 10 km or so of a source, but they neglect both the processes that are important beyond this distance and those that are active at night.

The U.S. EPA has taken the approach of developing a truly regional model, allowing the processes described above to influence the structure of the model, rather than trying to force the processes into an existing urban structure. The original goal of this work was to develop a specific model of regional scale photochemical air pollution. However, as the work progressed and new developments and ideas continually emerged, the need was seen for a general modeling framework within which the various physical and chemical processes that play important roles could be treated in modular form. This would permit ongoing incorporation into the model of state-of-the-art techniques without the need to overhaul the model each time. The structure and modular form of the Regional Oxidant Modeling System (ROMS) are unique for studying regional scale pollution. Complete documentation of the ROMS is being prepared (Lamb, 1982a, 1982b).

When this model development work was initiated some four years ago, an attempt was made to derive from the observational evidence available at that time an estimate of the minimum vertical and horizontal resolutions necessary to describe regional scale air pollution phenomena. The aim was to arrive at the best compromise between the restrictions imposed upon the model by computer time and memory limitations and the need to describe as accurately as possible all of the governing processes cited above. Careful review was made of the NO, O_3 and meteorological data reported in Siple (1977) by the participants of the 1975 Northeast Oxidant Transport Study. The characteristics of the O_3 distribution described in those reports would require at the very least a three-level model--one level assigned to the surface layer, another level to the remainder of the daytime mixed layer, and an additional layer atop the mixed layer. The top level would be used in conjunction with the mixed layer to account for downward fluxes of stratospheric O_3 as well as upward fluxes of O_3 and its precursors into the subsidence inversion layer above. Material that entered this top layer could be transported by winds aloft to areas outside the modeling region; it could enter precipitating clouds and be rained out of the atmosphere; or it could undergo chemical transformation. Representing the subsidence inversion, where cumulus clouds often form under stagnant high pressure conditions, the top level of the model would be instrumental in simulating the chemical sink effect of heterogeneous (within cloud droplets) reactions among O_3, its precursors, and other natural and pollutant species. Including

cloud effects in the model would be especially important in future simulation of SO_2 and sulfates.

Having three layers in a model is insufficient in itself to simulate all relevant phenomena. For example, three layers of constant thickness are incompatible with the spatial and temporal variability that the radiation inversion and mixed layer thickness are known to have. What is needed in the model is three "dynamic" layers that are free to expand and contract locally in response to changes in the phenomena they are intended to treat. The model discussed here possesses this property. Figure 8 illustrates the vertical structure of this model and the physical phenomena that each layer is intended to simulate. The surfaces that comprise the interfaces of adjacent layers in our model are variable in both space and time in order that each layer can keep track of the changes that occur in the particular set of phenomena that layer is designed to describe (summarized in Figure 8). A consequence of this structure is that the volumes of the grid cells vary in both space and time. By contrast, in conventional models the grid network and cell volumes remain fixed and surfaces such as the mixed layer top move through the grid system. In the following several paragraphs, we elaborate on some of the phenomena cited in Figure 8 that our model will take into account.

During the day the highest layer shown in Figure 8a represents the synoptic scale subsidence inversion, which may or may not contain cumulus clouds. Stratospheric O_3 is transported downward through this layer and anthropogenic O_3 and its precursors can be carried into it by cumulus clouds or penetrative convection. The base of this layer is normally 1 to 2 km above ground level. Below it pollutants are kept well mixed vertically by turbulent convection. If the winds are strong or the surface heat flux is weak, wind speed and direction may vary appreciably within the first several hundred meters above ground. There is usually also a marked difference in the wind speed and direction between the inversion layer and the mixed layer below. Over large lakes and along sea coasts there is frequently a second inversion layer below that generated by synoptic scale subsidence. This lower inversion is produced by sea or lake breeze regimes, and it restricts the vertical mixing of pollutants emitted over the water and within several kilometers inland from the water's edge.

Air drawn into young cumulus clouds originates primarily in the lower portion of the mixed layer. Fresh emissions of NO_x and HC can be transported by the vertical currents that feed these clouds from ground-level to altitudes well above the top of the mixed layer in one steady, upward motion. In the process little or no mixing with aged pollutants in the mixed layer occurs. At night, cumulus clouds usually evaporate, and when they do they

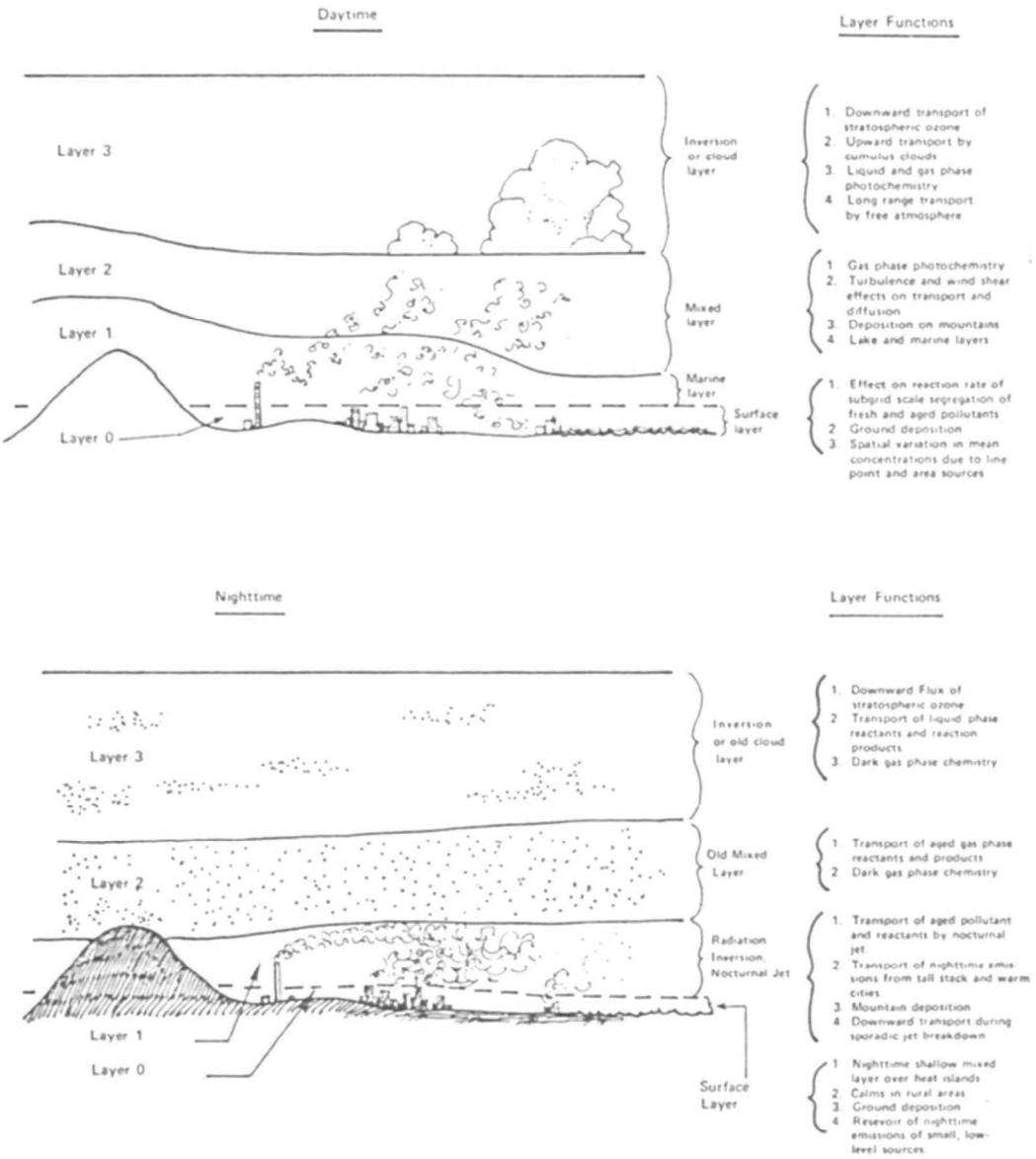

Fig. 8. Schematic illustration of the dynamic layer structure of the regional model and phenomena each layer is designed to treat: (a) daytime, (b) nighttime.

leave behind products of liquid phase reactions that can be transported hundreds of kilometers before sunrise.

Dramatic changes occur in the mixed layer at night. With the onset of surface cooling following sunset, a stable layer of air forms near the ground that quenches the vertical momentum fluxes that give rise to frictional drag on the horizontal flow. With retardation forces eliminated, the wind just above the stable layer accelerates giving rise to the phenomenon known as the nocturnal jet. Wind speeds in the core of the jet, which usually lies between 300 and 500 meters above ground, may be 10-15 m/s while at the same time the air is nearly calm at the surface. Emissions from tall stacks and from sources within the urban heat island enter the jet region at night. There they react with aged pollutants from the previous day and are transported considerable distances by the strong flow. The remnant of the previous day's mixed layer above the jet is isolated from the influence of fresh emissions and it moves at a slower speed than air below.

Sporadic episodes of turbulence in the shear layer beneath the nocturnal jet are a mechanism by which O_3 and constituents of urban plumes are brought to ground-level at night. There, deposition on surfaces and reactions with emissions of small, low-level sources occur. This sporadic mixing process is perhaps the only mechanism by which the reservoir of aged pollutants aloft can be depleted at night.

One point that we wish to emphasize here is that one-layer regional scale air pollution models are incapable of simulating the effects on pollutants like O_3 of the vertical segregation of aged and fresh emissions that occurs at night. Being cut-off from contact with the ground and fresh NO_x emissions, O_3 above the nighttime radiation inversion is free to travel great distances before it is mixed vertically by convection the following day. The effect of this nighttime segregation of pollutants is to extend greatly the effective residence times of species like O_3 in the lower troposphere. Consequently, a multi-layered model seems to be essential to simulate accurately the long range transport of photochemical air pollutants.

As now planned, the horizontal resolution of the model is about 18 km. The resolution should be as high as possible to mitigate the effects of subgrid scale concentration fluctuations. A scheme to treat subgrid chemistry is implemented in Layer 0, adjacent to the ground. Layer 0 is treated diagnostically in the governing equations, and also handles surface depletion. In modeling atmospheric processes over 1000 km scale regions, effect of the earth's curvature must be taken into account. Model equations are transformed into a curvilinear frame in which latitude, longitude and

elevation are coordinates and the basis vectors point north, east and vertically upward at every point on the earth. We have chosen this frame because it is a natural one from which transformations to any rectilinear system are easily performed. Also, is the frame in which worldwide meteorological data are reported.

There are three basic problems that must be overcome to make operational a model as large and comprehensive as the one we are developing.

First, due to the large number of processes that we plan to treat, our model is rather complicated. In order to alleviate the problems that this might cause in operating the model and in making future refinements, we have structured it so that its central core consists solely of a set of algorithms for solving the coupled set of generalized finite difference equations that describe processes in each of its layers. The modeling functions of describing the mixed layer dynamics; topographic effects on winds; chemistry; cloud fluxes, etc. will be handled by a set of special processors that are external to the central model and which feed the model key variables through a computer file. Within this framework the techniques used to describe the various physical processes can be altered without overhauling the model itself. An additional advantage is that execution times are greatly reduced when several runs of a given scenario are to be performed in which only one or a few parameter values are altered.

A second problem is limitations of computer storage capacity. To simulate air quality over the northeastern United States with the horizontal resolution we desire, our model has roughly 10^4 grid points and treats 25 (eventually more) chemical species. Thus, the concentration variables alone require 250K words of storage and this is just under the working limit of 260K words of memory on EPA's Univac computer. To accomodate a model of the anticipated size we have developed special techniques for handling the modeling domain in piecewise fashion.

Finally, the empirical data needed to parameterize some of the physical phenomena cited earlier are not presently available. To remedy this, EPA initiated project NEROS (Northeast Regional Oxidant Study) to collect during the summers of 1979 and 1980 the meteorological and chemical data required to formulate the model. A second goal of NEROS was to gather the data required to perform comprehensive test runs and evaluation exercises of the model (see Clark and Clarke, 1982; Clarke et al. 1982).

Aircraft sampling during NEROS was designed to gather evaluation data for the regional model. Using a trajectory model and radiosonde data, flight tracks were directed to obtain Lagrangian

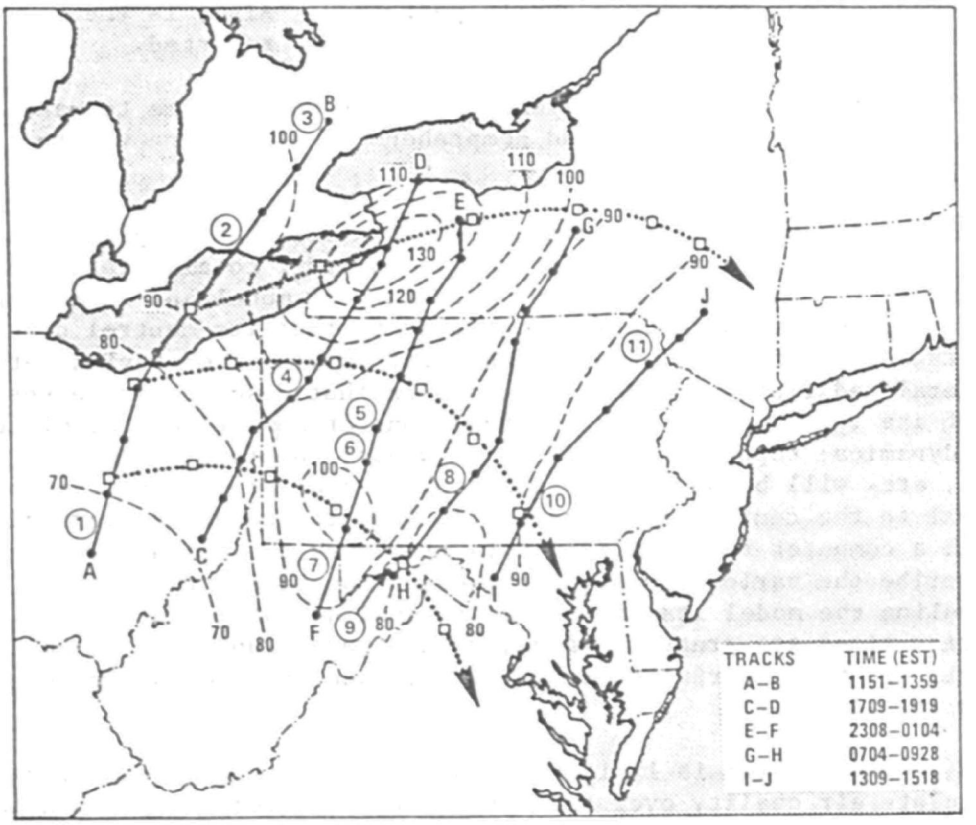

Fig. 9. Aircraft flight tracks, ozone concentrations (ppb), and air trajectories (6-hr segment given by (□)) for 3-4 August 1979.

sampling of an air mass. Figure 9 shows computed trajectories and corresponding aircraft flight tracks with O_3 concentration isopleths on one day. Figure 10 gives the O_3 concentrations in a vertical cross-section along one of the flight tracks (E-F). The significant O_3 concentrations at the level of the nocturnal jet are evident in these data taken near midnight.

The model is currently set up with a 60 x 42 array of grid cells. Figure 11 shows the region of the northeast U.S. being modeled as well as NO_2 isopleths resulting from a short test run. Although the model is functioning, substantial development work must yet be accomplished. Preprocessors must be thoroughly checked for accuracy, a refined emissions inventory (including biogenics) must be finished, and the NEROS data base must be analyzed. We

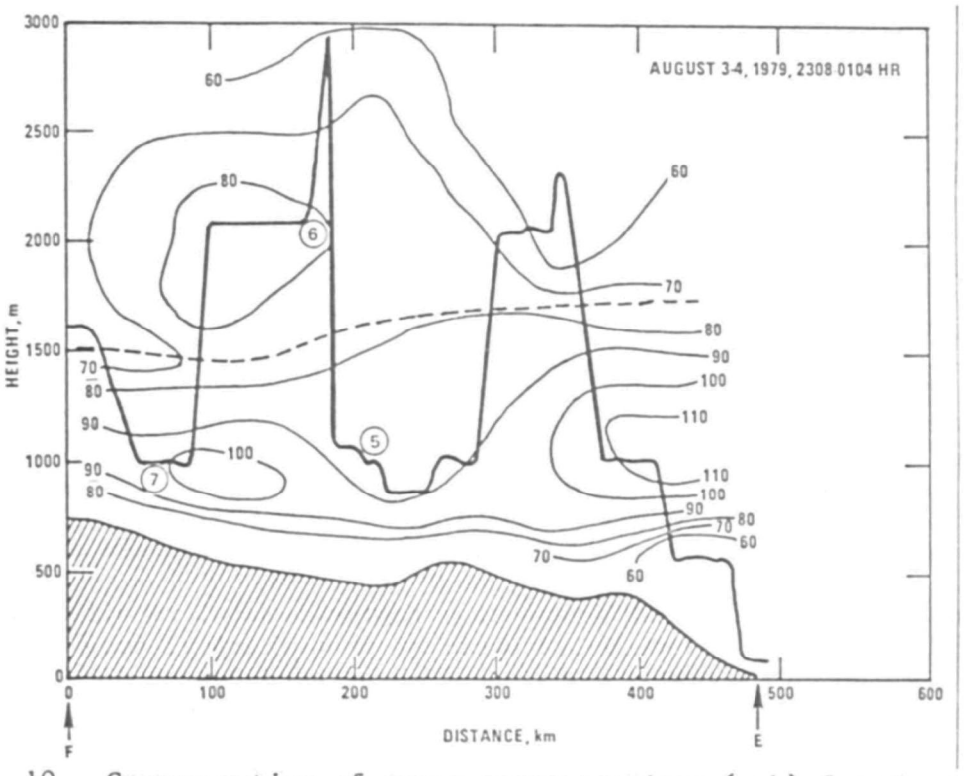

Fig. 10. Cross-section of ozone concentrations (ppb) for the track E-F in Fig. 9. Aircraft path is given by solid line, and the dashed line shows an elevated inversion.

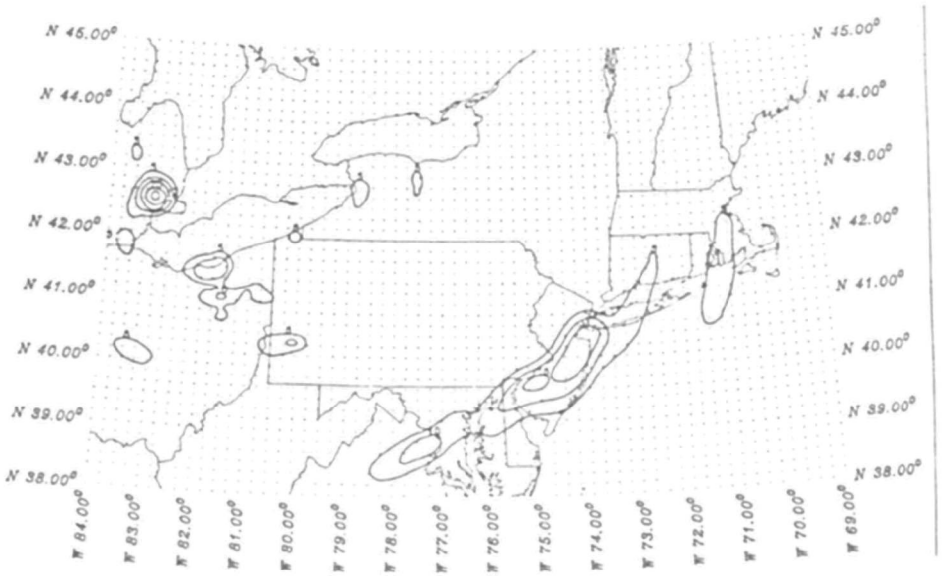

Fig. 11. The grid of the regional model and NO_2 isopleths from a test run. The isopleths are for 0800 local time and reflect sources about urban areas.

believe these tasks can be completed in mid-1983. After that we would need about another year of model running and evaluation before the model would be operational and could conceivably be transferred to other user groups (perhaps mid-1984).

CONCLUDING REMARKS

Over the past decade, focus of research, development, and evaluation efforts concerning photochemical models has been initially on the urban O_3 problem and more recently on the regional O_3 problem. Because of the earlier emphasis on the urban scale, there now exist in operational form several PAQSM's which are designed to simulate urban photochemistry and which have been applied in the U.S., Europe, and Australia. We have summarized the attributes of three such models which have emerged from programs of the U.S. EPA and been evaluated with a comprehensive urban data base. The models have been shown to be effective in predicting urban O_3 concentrations. The choice of which model to use will depend, in part, on the spatial resolution required and the computer resources available.

The impetus for development of a regional model resulted from a growing awareness that constituents of photochemical smog travel long distances, and control of locally generated O_3 may not be sufficient to alleviate air quality problems. On the regional scale, the multi-day nature of long-range transport necessitates consideration of factors which may be neglected for a one-day episode on the urban scale. These processes include slow photochemical reactions and segregation of surface and upper layers at night. Testing and evaluation of the regional model using data of the NEROS program will begin in 1983.

In confining our review to progress with EPA models, we do not mean to exclude other approaches which are being considered but believe that whatever choices are made the number of basic frameworks must remain quite limited due to the large resource requirements of PAQSM's. Thus, refinement of a single approach is preferred over a proliferation of models with slightly different characteristics. We have emphasized that successful application of a PAQSM involves the use of an extensive, and usually expensive, data base including information on meteorology, air quality, and source emissions. We believe that commitment to gathering such data should stand equally with efforts at developing the mathematical constructs and computer programs which constitute the PAQSM.

REFERENCES

Clark, T.L., and J.F. Clarke, 1982: Boundary layer transport of NO_x and O_3 from Baltimore, Maryland-A case study. Proceedings of Third Joint Conference on Applications of Air Pollution Meteorology, San Antonio, Texas, American Meteorological Society.

Clarke, J.F., J.K.S. Ching, R.M. Brown, H. Westburg, and J.H. White, 1982: Regional transport of ozone. Proceedings of Third Joint Conference on Applications of Air Pollution Meteorology, San Antonio, Texas, American Meteorological Society.

Demerjian, K.L. and K.L. Schere, 1979: Application of a photochemical box model for O_3 air quality in Houston, Texas. In Proceedings of Ozone/Oxidants: Interactions with the Total Environment II, Houston, Texas, October 1979, Air Pollution Control Association, pp. 329-352.

Henderson, R.G., R.P. Pitter and J. Wisniewski, 1980: Research Guidelines for Regional Modeling of Fine Particulates, Acid Deposition and Visibility, Report of a Workshop held at Port Deposit, MD October 29-November 1, 1979.

Killus, J.P., J.P. Meyer, D.R. Durran, G.E. Anderson, T.N. Jerskey and G.Z. Whitten, 1977: Continued research in mesoscale air pollution simulation modeling: Volume V--Refinements in numerical analysis, transport, chemistry, and pollutant removal. Report No. ES77-142, Systems Applications, Inc., San Rafael, CA 94903.

Lamb, R.G., 1982a: A Regional Scale (1000 km) Model of Photochemical Air Pollution, Part I: Model Formulation. EPA Report (in press), U.S. Environmental Protection Agency, Research Triangle Park, North Carolina.

Lamb, R.G., 1982b: A Regional Scale (1000 km) Model of Photochemical Air Pollution, Part II: Procedures for Model Operations, Validation and Refinement, EPA Draft Report (June 1982), U.S. Environmental Protection Agency, Research Triangle Park, North Carolina.

Littman, F.E., 1979: Regional Air Pollution Study-Emission inventory summarization. Report No. EPA-600/4-79-004, U.S. Environmental Protection Agency, Research Triangle Park, NC 27711.

Lurmann, F., D. Godden, A.C. Lloyd, and R.A. Nordsieck, 1979: A Lagrangian Photochemical Air Quality Simulation Model. Vol. I-Model Formulation, Vol. II-Users Manual. EPA-600/8-79-015a,b (available NTIS).

Lurmann, F., 1980: Modification and Analysis of the Lagrangian Photochemical Air Quality Simulation Model for St. Louis. Environmental Research and Technology, Inc. Document No. P-A095. Westlake Village, CA. 25pp.

Lurmann, F., 1981: Incorporation of Lateral Diffusion in the Lagrangian Photochemical Air Quality Simulation Model. Environmental Research and Technology, Inc. Document No. P-A748. Westlake Village, CA. 32pp.

Schere, K.L., 1982: An evaluation of several numerical advection schemes. Submitted to Atmospheric Environment.

Schere, K.L. and J.H. Shreffler, 1982: Final Evaluation of Urban-Scale Photochemical Air Quality Simulation Models. EPA Report (in press), 249 pp.

Schiermeier, F.A., 1978: Air monitoring milestones: RAPS field measurements are in. Environmental Science and Technology, 12, 664-651.

Shreffler, J.H., 1982: Observations and modeling of NO_x in an urban area. Proceedings of the U.S.-Dutch Symposium on NO_x. Maastricht, The Netherlands, May 24-28, 1982.

Shreffler, J.H. and R.B. Evans, 1982: The surface ozone record from the Regional Air Pollution Study, 1975-1976. Atmospheric Environment, 16, 1311-1321.

Siple, G.W., 1977: Air Quality Data for the Northeast Oxidant Transport Study, EPA-600/4-77-020, Environmental Protection Agency, Research Triangle Park, North Carolina.

Whitten, G.Z., J.P. Killus, and H. Hugo, 1980: Modeling of Simulated Photochemical Smog with Kinetic Mechanisms - Vol. 1. report No. EPA-600/3-80-028a, U.S. Environmental Protection Agency, Research Triangle Park, NC 27711.

Wolff, G.T., P.J. Lioy, G.D. Wight, R.E. Meyers and R.T. Cederwall 1977: An investigation of long-range transport of ozone across the midwestern and eastern United States. Atmospheric Environment, 11, 797-802.

RESEARCHES ON ACID RAIN IN JAPAN

Presented by T. Komeiji

Tokyo Metropolitan Research Institute for Environment Protection

Japan

1. INTRODUCTION

Increases of acidity in precipitation and its influences have posed serious environmental problems in various countries in the world, and there is now an urgent requirement to clarify the actual conditions and to take preventive measures. In Japan, many people had reported pains in the eyes, sore skin and other irritation; in 1973 in Shizuoka and Yamanashi Prefectures, and in 1974 and 1975 in the Kanto Area. These occurrences forced many people to recognize that pollution from precipitation and its influences were serious in Japan, and subsequently, local private organisations and the Environment Agency started research [1), 2)].

The problem of acid rain in Japan characteristically showed itself as a direct influence on the human body, unlike the increase in acidity in lakes and marshes which influenced fish and decreased forest productivity as observed in Northern Europe and North Eastern America. For this reason, the major subject in the researches into acid rain in Japan has been to clarify the actual pollution level of the initial precipitation which caused irritation to the human body.

Since this irritation showed itself, many studies have been made, and a large amount of information has been obtained. This report introduces the present situation of the problem of acid rain in Japan, mainly in reference to the reports of those studies.

2. OCCURRENCE OF IRRITATION CAUSED TO THE HUMAN BODY BY ACID RAIN IN JAPAN

The occurrence of irritation to humans from acid rain is shown in Tables 1 and 2[1), 3)]. As can be seen from Table 1, 31,815 persons reported irritation on July 3, 1974 mainly in the south of Tochigi Prefecture. Symptoms were irritation of the eyes and sore areas on the skin. On July 4, the affected area spread to the south of Kanto.

On July 18, there were similar reports mainly in the south of Tochigi Prefecture and also in Saitama Prefecture. In 1975, on June 25 reports came from the widest area in the year, and many people were affected.

To investigate the causes, precipitation was sampled and the components measured in the Kanto Area. The sampling method and measurement methods were standardized in the Environment Agency's wet air pollution survey in 1975[2)].

This wet air pollution survey was carried out for 5 years from 1975 to 1979, for 10-day periods from the latter part of June to the early part of July when reports of irritation seemed most frequent. The precipitation sampler used in the survey is shown in Fig. 1. It is designed to allow sampling, especially of the initial precipitation, separately since the irritations were said to have occurred especially at the beginning of precipitation. Places surveyed are given in Fig. 2, and the items and methods of measurement are shown in Table 3.

The resultant pattern of irritation caused by acid rain in 1974 and 1975 obtained by the wet air pollution survey by the Environment Agency and other surveys are shown in Tables 1 and 2. The measured results of precipitation components are shown in Tables 4 and 5.

As can be seen from Table 4, the pH of the precipitation on July 3, 1974 was as low as 3.1 in Ome and Utsunomiya, and sulfate ion concentrations were respectively 30 and 37 μg/mℓ. In the case of the precipitation on July 4, the measured pH values were 3.5 in Chiyoda, 3.0 in Chofu, 3.7 in Kawasaki and 3.6 in Tatebayashi, respectively, being low. The sulfate ion concentration measured simultaneously was as high as 23 μg/mℓ both in Chiyoda and Chofu. As shown in Table 5, the pH values of precipitation on June 25, 1975 in the respective places were low, being 3.3 in Ome, 3.1 in Kumagaya and 3.3 in Tatebayashi. Sulfate ion concentration was

very high, being 34.2 μg/mℓ in Kumagaya and nitrate ion concentration, too, was as high as 26.4 in the same area. As mentioned, the pH values of precipitation sampled in places where the irritations caused by acid rain were reported, on the days when it occurred were low, and sulfate ion and nitrate ion concentrations were very high.

For the precipitation of June 25 1975, sulfate ions, nitrate ions and chloride ions were taken up as components relating to the drop in the pH of precipitation, and the relation between the ratios of the three components and pH ranges is shown in Figs. 3 and 4[4]. From Fig. 3, it can be estimated that sulfate ion and nitrate ion concentrations contribute to the drop in pH since these concentrations in the anion concentration of precipitation with pH4 or less are high while chloride ion concentration is low. However, as for the cause of irritation, we cannot conclude that irritation is caused by acid substances in the precipitation only, and it is surmised that irritants such as formic acid and formaldehyde are also having an effect[4), 5)].

3. PRESENT SITUATION OF RESEARCH INTO PRECIPITATION IN JAPAN

Studies on precipitation in Japan have been made systematically since the reports of the irritations from acid rain in 1974 and 1975, but research into the causes of acid precipitation have only just begun. Studies made in Japan are introduced below in reference to the category of the research.

3.1 Chemical components of precipitation

The places in Japan where chemical components of precipitation quoted in this report were measured are shown in Fig. 5.

3.1.1 pH

The pH of precipitation was continuously measured for several years in Yokkaichi and Kumamoto in the early 1960s[6), 7)].

Figs. 6 and 7 show the results of those measurements. According to Fig. 6, the pH of precipitation in Yokkaichi was about 6 in 1961, and suddenly dropped thereafter, reaching about 4 in 1966. In the case of Kumamoto City in Fig. 7, the pH, which had remained at about 7 in the period from 1963 to 1966, tended to drop from 1967, to about 4.5 in 1972.

In addition to the above, event precipitation was sampled over a long period of time to enable measurement of the components of precipitation. The Tokyo Metoropolitan Research Institute for Environmental Protection (TMRIEP) has sampled the initial 1 mm precipitation, initial 5 mm precipitation and event precipitation since 1973, for measurement[8]. The results of Ph measurement are shown in Table 6. The changes in the annual mean value of pH in 4 places in Tokyo are shown in Figs. 8, 9 and 10. According to Fig. 8 (1) which shows the yearly changes in the annual mean pH to initial (0 to 1 mm) precipitation, the pH can be said to have remained almost the same in the 4 places, showing no large yearly variation. By place, the pH values (4.8 to 5.2) in Chiyoda were found to be obviously higher than the values of 4.2 to 4.5 in the other three places.

According to Fig. 8 (2) which shows the minimum pH values of (0 to 1 mm) precipitation, the minimum value did not show any large yearly variation, either.

As for the difference between places, as in case of the mean values, the pH in Chiyoda tended to be higher than that in the other places.

According to Fig. 8 (3) which shows the maximum pH values of (0 to 1 mm) precipitation, unlike the former two cases, the maximum value changed greatly between years, and large changes were observed in Chiyoda and Chofu.

As shown in Figs. 8 (1), (2) and (3), the pH of (0 to 1 mm) precipitation became low in the outer suburbs and the hilly areas compared with Chiyoda which is in the center of Tokyo.

According to Fig. 9 (1) which shows the yearly changes in the annual mean pH value of (0 to 5 mm) precipitation, the pH tended to drop in the period from 1974 to 1978, but rose a little in 1979 and 1980. It can be said that throughout the period, the pH remained at almost the same level. By place, as for (0 to 1 mm) precipitation, the values in Chiyoda were high, and those in Chofu and Ome were low.

According to Fig. 9 (2) which shows the yearly changes in the minimum value, the pH dropped most in Chofu and Ome in 1974 and 1975, and tended to rise a little thereafter.

According to Fig. 10 (1) which shows the yearly changes in the annual mean pH of event precipitations at one time, observed for (0 to 1 mm) and (0 to 5 mm) precipitations, the annual mean pH of event precipitation tended to rise in 1979 and 1980. By place, the pH values in Chiyoda in 1978 and 1979 were lower than those in the other places, showing that the differences in the pH of event precipitation between the respective places were different from that for the above mentioned pH of initial precipitation.

The TMRIEP took measurements in control places, in addition to the survey made in Tokyo[8]. The results are shown in Fig. 11. According to Fig. 11 (1), in the case of Ogasawara by the sea, the monthly mean pH values of (0 to 1 mm) precipitation were distributed around neutral (pH 7), being from 5.6 to 9.4. The pH values in Yagisawa, a mountainous area in Fig. 11 (1) ranged from 4.0 to 4.9, being on the same level as those in the outer suburbs and the hilly areas of Tokyo. This shows that the

acid precipitation covered a very wide area. Also the pH values for (0 to 5 mm) precipitation in Fig. 11 (2) show the same trend as for (0 to 1 mm) precipitation.

Among the precipitation surveys made in the Kanto Area, a year-long survey was made in Urawa[9]. Fig. 12 shows the results of measurement. According to Fig. 12, the annual mean pH values of (0 to 1 mm) precipitation in Urawa were lower than the pH values in places in Tokyo, being especially low in 1975. As for the yearly change, the pH of precipitation in Urawa tended to rise.

Measurement was made also in Koenji, Tokyo[10]. The results are shown in Table 7. According to Table 7 which shows the yearly change in the pH of precipitation, the pH values remained almost the same at about 4.5. The mean pH value of event precipitation for the 6 years from 1973 to 1978 in Koenji was 4.52, which is the same as the mean pH value 4.52 of event precipitation in the period from 1978 to 1980 in Chiyoda. Though there may have been some differences in measuring conditions, etc., the mean pH value of precipitation in Tokyo Ward was about 4.5.

The Meteorological Agency measured the components of precipitation in Ryori, Iwate Prefecture as part of an WMO background survey[11]. The results are shown in Fig. 13. According to Fig. 13, the monthly mean pH values of precipitation in Ryori were almost 4.5 or higher, and the annual mean pH value is estimated to be 5.0 or higher.

The pH values of precipitation measured in other cities in Japan are shown in Table 8, together with components of precipitation[12), 13), 14), 15), 16)]. According to Table 8, all the mean pH values for the measurements were 4.9 or lower. From this, it can be estimated that acid precipitation is increasing also in local cities.

3.1.2 Electric conductivity

Measurement of electric conductivity has been more frequently made since the reports of irritations from acid rain in 1973.

The results of measurements done by the TMRIEP[8)] are shown in Table 9. Yearly changes in electric conductivity are shown in Figs. 14, 15 and 16.

According to Fig. 14 (1) which shows the yearly changes in the annual mean electric conductivity of (0 to 1 mm) precipitation, the values show a slight downward trend in respective places. By place, the values are decreasing in the order Chiyoda/Chofu, Ome and Okutama.

According to Fig. 14 (2) which shows the yearly changes in the minimum electric conductivity of (0 to 1 mm) precipitation, the values tended to increase in Chiyoda, but have remained almost the same in Ome and Okutama. As for the differences by place, clear differences in the descending order of Chiyoda, Chofu, Ome and Okutama are observed. The clear differences in the minimum value by place show the background values of pollution of precipitation.

According to Fig. 14 (3) which shows the changes in the maximum electric conductivity of (0 to 1 mm) precipitation, it changed greatly between years as with the pH values, and both the yearly changes and the differences between places showed no clear trends.

According to Fig. 15 (1) which shows the yearly changes in the annual mean electric conductivity of (0 to 5 mm) precipitation, the values in Chiyoda and Ome tended to decrease gradually. Differences between places in the descending order of Chiyoda, Chofu, Ome and Okutama was indicated very clearly. From this,

a close relationship between the electric conductivity of precipitation and human activities can be estimated.

According to Fig. 15 (2) which shows the changes in the minimum electric conductivity of (0 to 5 mm) precipitation, the values tended to decrease until 1977, but from then remained almost the same.

Figs. 16 (1), (2) and (3) show that the mean and minimum electric conductivities of event precipitation remained the same, and that differences in the descending order of Chiyoda, Ome and Okutama clearly existed between the places.

The yearly changes in the electric conductivity in Urawa are shown in Fig. 17 as for pH[9]. As shown in Fig. 17, the electric conductivity of initial (0 to 3 mm) precipitation in Urawa tended to decrease in the period from 1975 to 1980, but has increased in the last year. With increase in precipitation from 1 mm to 2 mm, then to 3 mm, the electric conductivity showed a clear decrease. The difference between the electrical conductivity for initial 1 mm precipitation and that for initial 2 mm precipitation was observed to be especially large.

The TMRIEP also took measurements in control places, and the results are shown in Fig. 18[8]. According to Fig. 18, the electric conductivities in Ogasawara as a control place by the sea were large, and the mean values throughout the period were 90.2 for (0 to 1 mm) precipitation and 60.6 for (0 to 5 mm) precipitation, showing the same level of values as in Chiyoda. In Yagisawa, a mountainous area, the mean electric conductivity of (0 to 1 mm) precipitation was 30.6, and that of (0 to 5 mm) precipitation was 18.9, being a little lower than the values in Okutama.

3.1.3 Sulfate ions, nitrate ions, chloride ions and ammonium ions

Survey results on the concentrations of sulfate ions, nitrate ions, chloride ions and ammonium ions which were measured most frequently in the surveys on the components of precipitation are introduced below.

The results of measurements made by the TMRIEP are shown in Figs. 19, 20, 21, 22 and 23 and Table 10. According to Fig. 19, the highest ion concentration among the components of initial (0 to 1 mm) precipitation in Chiyoda was sulfate, being followed by chloride, nitrate and ammonium in this order.

According to Fig. 20 which shows the yearly changes in the chemical components of (0 to 5 mm) precipitation, the concentrations of sulfate ions and chloride ions showed similar changes, decreasing until 1978, and increasing a little in 1979 and 1980. The concentration of nitrate ions showed a slight upward trend from about 1976. The concentration of ammonium ions remained almost the same. Sulfate ions showed the highest concentration, being followed by chloride, nitrate and ammonium in this order (in μg/mℓ). Taking the mean values from 1974 to 1980, the respective component ion concentration can be arranged in the order sulfate 8.6 (μg/mℓ), chloride 4.9, nitrate 4.1 and ammonium 1.3.

According to Fig. 21, the concentrations of components of event precipitation in Chiyoda showed the same order as in Fig. 19. However, with respect to yearly changes, sulfate ion and chloride ion concentrations changed greatly, and nitrate ion and ammonium ion concentration changed little.

The concentrations of components by place in 1980 will be compared. For (0 to 5 mm) precipitation, as shown in Fig. 22, sulfate ion and chloride ion concentration showed a similar

downward trend, and this trend increased according to movement from urban center to inland area in the order Chiyoda, Ome and Okutama. The rate of decrease in ammonium ion concentration was smaller than for the former two, but the downward trend was the same. Nitrate ion concentration was the highest in Ome, unlike the three other components. For the event precipitation shown in Fig. 23, the differences in the concentrations of components among the three places were observed to be small, excluding nitrate ion concentrations.

As can be seen from Figs. 19 to 23, the change in pattern of sulfate ion and chloride ion concentration are similar in the same places and between different places. Both are estimated to be similar with regard to transport and diffusion in the air and the mechanism of absorption in precipitation. Ammonium ion concentration showed the smallest yearly change and the difference between places. Nitrate ion concentration showed the highest in the intermediate position between urban center and mountainous area, and this is surmised to be caused by the difference in transport, diffusion and process of reaction from sulfate ions.

Takeuchi measured the chemical components of precipitation in Kichijoji, Tokyo and reported the yearly and monthly changes in sulfate ion and chloride ion concentrations[17]. These measured values are shown in Tables 11 and 12. According to Table 11, sulfate ion concentration was high in 1970 and chloride ion concentration was high in 1972. But clear yearly changes could not be seen. In reference to the monthly mean values for 7 years in Table 12, both sulfate ion and chloride ion concentrations tended to drop in August, September and October. The mean value of sulfate ion concentration over 7 years was reported to be 4.8 (μg/mℓ), and this coincided well with the mean value of 4.82 for sulfate ion concentration for the 3 years from 1978 to 1980 reported by the TMRIEP. The mean value of chloride ion concentration for 7 years in Kichijoji was 0.9, and this is smaller than

the 1.27 for event precipitation in 1980 in Ome shown in Table 10. It was reported that chlorine compounds in the air increased in Tokyo during this period[18].

Saitama Prefectural Pollution Center measured the components of initial precipitation in Urawa. The results are shown in Figs. 24, 25, 26 and 27[9]. These graphs show that sulfate ion and chloride ion concentrations were lower than those in Chiyoda (Fig. 19), but that nitrate ion concentration was about the same, and that ammonium ion concentration was higher. With regard to yearly changes, sulfate ion and nitrate ion concentrations tended to decrease until 1979, but increased again 1980. Chloride ion and ammonium ion concentrations remained almost the same. As for the rates of decrease of component concentrations of 1 mm, 2 mm and 3 mm precipitation in Urawa, very large rates of decrease were observed between 1 mm precipitation and 2 mm precipitation.

Kanagawa Prefectural Pollution Center measured the components of precipitation and reported the results[19]. The results are shown in Tables 13 and 14. The ion concentrations of the three components, sulfate, nitrate and chloride were lower than those of Chiyoda shown in Table 10.

The concentrations of sulfate ions and nitrate ions in precipitation measured in various places in Japan shown in Table 8 were lower than the concentrations of event precipitation in 1980 in Chiyoda and Ome, Tokyo shown in Table 10.

A survey of inland regions made by Tamaki, et al. in Hyogo Prefecture was reported[20]. The results are shown in Table 15. The TMRIEP took measurements in control places, and the results[8] are shown in Table 15. In Ogasawara a control place by the sea, as shown in Table 16, chloride ion concentration was 9.9 (μg/mℓ), about double that of Chiyoda, sulfate ion concentration about

1/3, nitrate ion concentration about 1/5 and ammonium ion concentration about 1/15. In Moshi, as shown in Table 15, sulfate ion concentration was about 1/3 of that of Chiyoda, nitrate ion concentration about 1/2, chloride ion concentration about 1/5 and ammonium ion concentration about 1/3. Similarly, in Yagisawa, compared with Chiyoda, sulfate ion concentration was about 1/11, nitrate ion concentration about 1/7, chlorine ion concentration about 1/10 and ammonium ion concentration about 1/11.

3.1.4 Other substances

Organic acids, aldehydes, etc. can all be considered as possible irritants in addition to inorganic acid materials. They were also measured, and the results were reported. Measured values obtained so far are shown in Table 17. A case where formaldehyde showed a high value of 2.7 (μg/mℓ) in Chiyoda was reported[2]. Acrolein concentration was reported to be 0.23 in Kanagawa Prefecture[5]. The mean value in Hiratsuka was reported to be 0.045[23]. Formic acid concentrations were reported to be 0.11 to 0.9 in Kobe[21]. Hydrogen peroxide concentrations measured by Yoshizumi were found to be 0.0001 to 1.06[22] (in μg/mℓ).

The concentrations of formaldehyde and formic acid shown here are high enough to induce irritation in the eyes, according to Kurokawa, et al.[5].

3.3 Mutual relations between components of precipitation

The composition ratios in equivalent of sulfate ions, nitrate ions and chlorine ions in precipitation obtained in the wet air pollution survey by the Environment Agency are shown in Figs. 28 and 29[24]. Triangle diagrams indicating cases of irritation are shown in Figs. 3 and 4.

Fig. 4 shows high sulfate ion rates, and Fig. 3 shows high nitrate

ion ratios. Fig. 3 shows cases of reported irritation in the Kanto Area on June 25, 1975, with low chloride ion ratios and much precipitation of 4 or lower pH. Fig. 28 shows a case where precipitation of 4 or lower pH was little observed, and in this case, the chloride ion ratios tended to be high.

In the composition of anions in precipitations of 4 or lower pH, as can be seen in Figs. 3 and 29, the chloride ion concentration considered to have originated from the sea was low, and the concentrations of sulfate ions[25)] and nitrate ions reported to have artificially originated were high. As indicated here, the pH of precipitation in the Kanto Area was found to drop when sulfate ions and nitrate ions were contained in high ratios in precipitation.

Correlation coefficients obtained between hydrogen ion concentration and other ion concentrations in Urawa[26)] are shown in Tables 18 and 19.

Table 18 shows that the correlation of hydrogen ion concentration with other ion concentrations in (0 - 1 mm) precipitation in Urawa was relatively good. Table 19 shows correlation coefficients obtained similarly for precipitation of 4 or lower pH, and it can be seen that the correlation in 1972 in Table 19 is far better than that in Table 18.

3.4 Relation between the increase in precipitation and concentrations of components of precipitation

In general, it is recognized that according to the increase in precipitation from the beginning of precipitation, concentrations of components in the precipitation drop.

Continuous samples of fractions of a single precipitation and concentrations of components[27)] measured in Chiyoda are shown in Fig. 30. As shown in Fig. 30, the pH of precipitation in Chiyoda became

high once initially with the increase in precipitation and showed a gradual decrease thereafter. Electrical conductivity decreased relatively constantly with increase in precipitation. Chloride ion concentration decreased very much in the beginning, and almost dropped lower than the detection limit for a precipitation higher than 20 mm. The rate of decrease in sulfate ion concentration is surmised to be about the same as that of chloride ion concentration, but at a precipitation higher than 20 mm, the concentration remained higher than for chloride ions. The component with the smallest rate of decrease was nitrate, and the ion concentration tended to drop gradually with increase in precipitation.

From the results of measurement made by the TMRIEP[8] annual mean values of pH and electric conductivity per 1 mm of precipitation were obtained for one year of precipitation by amount of precipitation, to determine the relations between the increase in precipitation with pH values and electric conductivities in the respective places. They are shown in Figs. 31 and 32. According to Fig. 31, in Chiyoda in the urban center, pH was rather high in the (0 to 1 mm) precipitation of 1978 and the beginning of 1979, and dropped with increased precipitation. In event precipitation, it showed a rising trend again. As mentioned above, in the beginning of precipitation in Chiyoda in the urban center, as can be seen also in Fig. 30, pH was rather high and tended to drop with increased precipitations, showing a relationship opposite to the decrease of general components of precipitation with increased precipitation. This phenomenon is assumed to have been caused by the fact that the precipitation in the urban center contained large amounts of buffer substances such as dust acting to neutralize the pH toward the alkali side[28]. With regard to this matter, in the cases of Ome and Okutama shown in Fig. 31, pH showed a rise consistently with increased precipitation.

The electric conductivity shown in Fig. 32 decreased consistently in all places.

With regard to the rates of decrease of electric conductivity against precipitation in respective places, the values for Chiyoda and Chofu were larger than Ome which was larger than Okutama. The rate of decrease was observed to drop according to the increase in the distance from the source of artificial ion generation.

In order to show that, in the urban center, there are many buffer substances which are believed to suppress the drop of pH of precipitation for initial precipitation, the relationship between hydrogen ion concentration and electric conductivity are shown in Figs. 33, 34 and 35.

Fig. 33 shows that electric conductivity was very large for hydrogen ion concentration in (0 to 1 mm) precipitation in Chiyoda, in the city center and Chofu, a suburb town, and that electric conductivity decreased for hydrogen ion concentration in Ome and Okutama with increased distance from the city center.

As shown in Fig. 34 for (0 to 5 mm) precipitation and Fig. 35 for event precipitation, with increased precipitation, electric conductivity showed a trend approaching a linear relationship between the hydrogen ion concentration of hydrochloric acid and electric conductivity in all places.

In Fig. 35, it can be seen that many electrolytes in precipitation existed as acids in Okutama, the farthest place from the city center. Furthermore in all places irrespective of the amount of precipitation, with the increase in hydrogen ion concentration, the relation between hydrogen ion concentration and electric conductivity approached that of hydrochloric acid.

3.5 Amounts of chemical components falling due to precipitation

The quantities of chemical components contained in the precipitation[8)] are shown in Table 20.

As shown in Table 20, the amounts of chemical components in the precipitation were 0.91 to 1.3 (g/m^2 year) of sulfate ions, 0.45 to 0.67 of nitrate ions, 0.62 to 0.85 of chloride ions and 0.12 to 0.18 of ammonium ions. The amount of sulfate ions was the largest, followed by chlorine ions, nitrate ions, ammonium ions and hydrogen ions in this order. Also for (0 to 5 mm) precipitation and overall precipitation, the order of ion component content was the same as for (0 to 1 mm) precipitation.

Though the sampling times were different, mean values were calculated to calculate the ratios of the amounts in (0 to 1 mm) and (0 to 5 mm) precipitation to those in event precipitation, as shown in Table 21. According to Table 21, irrespective of precipitation, the component showing the largest amount was sulfate ions, accounting for about 50% of the whole, followed by chloride ions, nitrate ions, ammonium ions and hydrogen ions in this order. As for the ratios of the quantities of chemical components in (0 to 1 mm) and (0 to 5 mm) precipitation to the quantities in event precipitation, nitrate ions showed the highest value in (0 to 1 mm) precipitation, followed by chloride ions, sulfate ions or ammonium ions, and hydrogen ions in this order, and nitrate ions showed the highest value in (0 to 5 mm) precipitation, followed by ammonium ions, sulfate ions, chloride ions and hydrogen ions.

This shows that in Chiyoda, the quantity of sulfate ions contained in precipitation was the largest of the chemical components of precipitation, and that nitrate ions were removed at the highest rate at the beginning of precipitation.

The TMRIEP measured sybstances falling when dry (during non-precipitation) and falling when wet (during precipitation), and the results[29] are shown in Tables 22, 23 and 24.

According to the tables, anions such as sulfate ions fell mostly during precipitation, and this trend was more clearly observed in

Ome and Okutama with increased distance from the city center, rather than in Chiyoda, in the city center. Furthermore, as can be seen in Table 24, in Chiyoda and Ome, the ratios of anions as a percentage of the weight falling were very high. It was clarified that anions such as sulfate ions, which are closely relating to hydrogen ions as mentioned, fell in very large quantities to the ground during precipitation.

3.6 Frequency distribution of component concentrations of precipitation

The frequency distribution of measured electric conductivities of precipitation completed by Kanagawa Prefectural Pollution Center[23)] is shown in Fig. 36. The frequency distributions obtained from the results of precipitation measurement made by the TMRIEP and plotted on log-linear paper are shown in Figs. 37 and 38.

In Fig. 37 (1), two distributions separated at pH5 were observed. In Fig. 37 (2), electric conductivities showed a logarithmic-normal distribution.

In Chiyoda, hydrogen ions show a distribution with high frequencies in concentrations lower than those of the logarithmic-normal distribution type. Electric conductivities showed a logarithmic-normal distribution. From these results, the distribution of component concentrations in precipitation is surmised to be close to a logarithmic-normal distribution.

3.7 pH distribution by raindrop size

To clarify the causes of irritations due to acid rain in Japan, individual raindrops must be sampled, to measure components such as the pH of the raindrop, to determine the distribution, aside from bulk sampling as done hitherto for precipitation sampling.

A method of examination was contrived. In this method, a raindrop is received on parafilm, and the pH of the raindrop is measured in reference to the color due to the dissolution of the pH indicator uniformly dispersed on the parafilm into the raindrop[30].

The discoloration ranges of the indicator used are shown in Fig. 39, and pH distributions of raindrops are shown in Fig. 40. As shown in Fig. 40, the sizes of raindrops were less than 1.0 mm.

As for the pH distributions by particle size, low pH values (1.2 to 1.8) appeared at a frequency of 65% in the particle size range of 0.2 mm or less. With the increase in size of the raindrops, low pH values appeared less, and high pH values appeared more. In the largest particle size range from 0.8 to 1.0 mm, pH values lower than 3.9 did not appear, and most values were 4 or higher.

From this example, it was clarified that when the mean pH of bulk rainwater was about 3.8, the pH values by raindrop sizes were distributed in the range 1.2 or lower and the in the range 4.8 or higher. There was observed a trend for the width of the distribution of the pH raindrops to be wide in a place where artificial pollution was high, and narrow in a place with low pollution[30].

4. PROBLEMS IN THE FUTURE

As introduced here, research into acid rain in Japan has just started, and there remain many problems yet to be solved.

Problems to be solved are:

1) Clarifying the causes of the increase in acid precipitation

   Relations with artificial sources

   Transport dispersion and reaction in air, and the mechanism of absorption into precipitation

2) Surveys of actual conditions

Sampling, measuring methods, survey items

Field survey techniques such as selection of survey areas

Distribution of areas covered by acid precipitation (local and national)

3) Examination of models

Material balance

4) Influences

Atmosphere

Hydrosphere

Biosphere including ground surface, soil, etc.

With regard to the above, mutually related studies must be promoted.

5. CONCLUSION

Studies concerning acid rain in Japan have been mostly done individually, and only a few systematic studies have been made. The latter includes the Wet-Air Pollution Survey by the Environment Agency and a Joint Survey by Tokyo and six prefectual government in the Kanto Area.

Studies to be promoted in future must more specifically and systematically aim at solutions of problems with clear objectives.

Efforts must be made in this direction.

REFERENCES

1) "Acid Rain (Wet-Air Pollution) in the Kanto Area", Council for Prevention of Pollution in Tokyo and Three Prefectures, Air Pollution Section of Pollution Control Promotion Headquarters of Governments in Kanto Area, March, 1975

2) "1975 Report on the Wet Air Pollution Survey", Wet Air Pollution Examination Committee, Air Quality Bureau of Environment Agency, March, 1976

3) "Acid Rain (Wet-Air Pollution) in the Kanto Area in 1975", Council for the Prevention of Pollution in Tokyo and Three Prefectures, Air Pollution Section of Pollution Control Promotion Headquarters of Governments in the Kanto Area, October, 1976.

4) Toshikazu Ohtaki: "Wet-Air Pollution - Acid Rain -, Pollution and Control Measures", 13, 732-750 (1977)

5) Michiko Kurokawa, et al.: Formaldehyde concentration in rainfall and irritation to the eyes", Air Pollution Study, 10, 86 (1975)

6) Katsumi Yoshida: "Acid rain and the Morning Glory", Air Pollution News, No. 66 (1971)

7) Teiji Nishi: "Air Pollution in reference to pH of rainwater", Air Pollution News, No. 64 (1971)

8) "Results of investigations concerning acid rain" (1), (2), (3) and (4), Tokyo Metropolitan Research Institute for Environmental Protection Institute, (1975 - 1982)

9) Kazuko Mizukami: "A survey on the components of rainwater (4th report)", Annual Report of Saitama Prefectural Pollution Center, 60-66 (1981)

10) Katsuko Saruhashi and Teruko Kanazawa: "pH of precipitation, Weather", 25, 784-786 (1978)

11) Report of Ocean Pollution Observation by the Meteorological Agency, Marine Department of Meteorological Agency, (1976-1980)

12) Yoko Kitamura, et al.: "A study on the distribution of air pollutants in the environment - Properties of rainwater in Miyagi Prefecture", Report of Miyagi Prefectural Pollution Control Technical Center, No. 8 (1979)

13) Hikaru Satsumabayashi and Kazutoshi Sasaki: "Chemical components of precipitation in Nagano City", Report of study by Nagano Prefectural Sanitation and Pollution Research Institute (1979)

14) Kanji Masamichi, et al.: "A study on components of rainwater (3rd report)", Annual Report of Fukui Prefectural Pollution Center, 7, (1977)

15) Tsunao Suetsugu, et al.: "A survey of actual conditions of acid rain"

16) National Council on Studies of Pollution: "A study on the distribution of air pollutions in the environment", (1977)

17) Nobuyuki, Nakai and Ushio Takeuchi: "Chemistry of rain and air pollution, Chemistry", 29, 418-426

18) Tetsuhito Komeiji, Isao Koyama, Mie Kyoda, Tatsukichi Ishiguro, Morio Kadoi and Yoshiyuki Oinuma: "Examination on the use of the corrosion of metallic materials as an index of air pollution", Pollution Study Report of Tokyo Metropolitan Research Institute for Environmental Protection Institute, 63-89 (1976)

19) Kanagawa Prefectural Pollution Center: "A survey on wet-air pollution", Research Report on Air Pollution by Kanagawa Prefectural Government, 19th report, 110-120 (1977)

20) Motonori Tamaki and Takatoshi Hiraki: "Ion composition in rainwater in the hinterland of an urban area", Environment Technology, 9, 865-871 (1980)

21) Hiroshi Sakurada, Kozo Shintani and Hiroshi Watanabe: "Concentrations of formaldehyde and formic acid in air and rainwater", A collection of summaries of lectures at the 23rd meeting of the Air Pollution Society, 265 (1982)

22) Kunio Yoshizumi: Private letter

23) Kanagawa Prefectural Pollution Center: "A survey on wet-air pollution", Research Report on Air Pollution by Kanagawa Prefectural Government, 18th report, 46-66 (1976)

24) 1976 Research Report on Wet-Air Pollution, Committee for the Examination of Wet-Air Pollution, Air Quality Bureau of Environment Agency (1977)

25) Nobuyuki Nakai, Naoko Takahashi and Ushio Takeuchi: "Sources of sulfate ions in precipitation and air pollution", Geochemistry (Special issue for environmental problems), 118-124 (1975)

26) Kazuko Mizukami and Yasuo Kaneko: "A survey on the components of rainwater (3rd report)", Annual Report of Saitama Prefectural Pollution Center, 60-65 (1978)

27) Tetsuhito Kameiji, Tadashi Sawada, Toshio Ohira, Kazuyoshi Hirosawa and Morio Kadoi: "A survey on the components of rainwater", Annual Report of Tokyo Metropolitan Research Institute for Environmental Protection, 6, 104-112 (1975)

28) Tetsuhiko Komeiji, Saburo Fukuoka, Yoshitsugu Nakano, Kunihiko Asakino and Toshio Ohira: "A study on the pollution of rainwater and its mechanism", Annual Report of Tokyo Metropolitan Research Institute for Environmental Protection, 7, 27-37 (1976)

29) Tetsuhito Komeiji, Isao Koyama, Nobuko Watanabe and Tatsukichi Ishiguro: "Pollution characteristics of falling matter in precipitation, etc. by place", Annual Report of Tokyo Metropolitan Research Institute for Environmental Protection, 81-88 (1982)

30) Tetsuhito Komeiji, Isao Koyama, Tatsukichi Ishiguro and Morio Kadoi: A collection of summaries of lectures at the 23rd meeting of the Air Pollution Society, 258 (1982)

Table 1 Reported influences of acid rain on the human body

(1974)

Month/ date	Prefecture	Number of reporters	Time of occurrence	Symptoms
7/3	Tochigi	28,762	14:00∿18:00	Irritation of the eyes, soreness to the skin, offensive odor
	Ibaragi	1,793	15:30∿20:00	Irritation of the eyes, painful arms
	Saitama	1,120	15:30∿17:00	Eyes smarting, hoarseness of the throat
	Gunma	140	17:30∿18:00	Pain in the eyes
	Total			
7/4	Ibaragi	321	15:00∿20:00	Irritation in the eyes
	Tokyo	203	11:00∿20:00 (Especially between 16:00 and 18:00)	"
	Kanagawa	187	15:00∿18:00	" smarting on the arms
	Chiba	20	13:00∿15:00	Irritation in the eyes
	Total	731		
7/5	Ibaragi	3	Unknown	Irritation in the eyes
	Chiba	9	11:00	Irritation in the eyes, inflamed part above the eyes
	Total	12		
7/6	Chiba	4	8:50∿ 9:00	Irritation in the eyes
7/13	Saitama	3	19:30∿21:30	"
7/14	Saitama	1	11:00	"
7/17	Tochigi	71	10:30∿15:15	"
7/18	Tochigi	225	10:00∿16:00	"
	Saitama	281	10:00∿16:00	" eyes bloodshot
	Total	374		
7/20	Saitama	506	21:00	
	Grand Total	33,144		

Table 2 Reported influences of acid rain on the human body

(1975)

Month/ date	Prefecture	Number of reporters	Time of occurrence	Symptoms	Remarks
5/3	Saitama	1	7:10∿ 7:30	Pain in the eyes, watering eyes.	1 in Kawaguchi
5/19	Ibaragi	72	7:00∿ 14:10	Pain in the eyes, watering eyes.	72 in Koga
6/24	Saitama	9	13:05∿ 19:50	Pain in the eye=	7 in Kumagaya, 2 in Chichibu
6/25	Tochigi	90	8:00∿ 17:00	Rain in the eyes	90 in Kanuma
	Saitama	43	11:20∿ 12:30	Rain in the eyes	30 in Fukaya, 12 in Enamimura, 1 in Asaka
	Tokyo	9	16:00∿ 23:00	Pain in the eyes, watering eyes.	4 in Nerima, 1 in Chuo, 1 in Chofu, 1 in koganei, 1 in Tanashi, 1 in Tachikawa
	Kanagawa	1	15:00	Skin smarting	1 in Totsuka
	Total	143			
6/26	Gunma	18	17:00	Pain in the eyes	18 in Oizumi
7/10	Saitama	1		Pain in the eyes	1 in Omiya
	Grand total	244			

Table 3 Measurement items and methods for precipitaton[3)]

Item	Method
pH	Glass electrode method
Electrical conductivity	Conductivity meter (25°C)
Sulfate ions (SO_4^{2-})	Barium chloride turbidimetry (glycerol-alcohol method)
Nitrate ions (NO_3^-)	Sodium salicylate method
Chlorine ions (Cl^-)	Mercury (II) thiocyanate method
Ammonium ions (NH_4^+)	Indophenol method
Formaldehyde (HCHO)	m-aminophenol method

Table 4 Results of analyzed components of rainwater in July, 1974

Place sampled		Date of sampling	pH	SO_4^{-2} (ppm)	NO_3^- (ppm)	Cl^- (ppm)	Remarks
Tokyo	TMRIEP	2 ∿ 3	423	-	-	-	
	Ome City	3	3.1	30.0	8.7^B	10.0	
Tochigi	Prefectural Office	3	3.1	37		-	
Tokyo	Ota-ku	4 ∿ 5	3.9	16.7	7.4^B	5.0	
	Itabashi-ku	4 ∿ 5	4.3	3.0	3.6^B	5.0	
	TMRIEP	4	3.5	22.6	8.1^B	-	
	Shinagawa-ku	4	4.5	26.6	7.9^B	-	
	Ome City	4	4.2	3.0	2.4^B	2.4	
	Chofu City	4 ∿ 5	3.0	22.6	8.5^B	7.0	
	Musashino City	4 ∿ 5	4.9	7.9	-	-	
	Mitaka City (Mure)	4	3.8	16.7	-	-	
Kanagawa	Pollution Center (Head Office)	4	3 ∿ 4	-	-	-	
	Pollution Center (Heihin Branch)	4	4.2	6.5	-	-	
	Pollution Center (Shonan Branch)	4 ∿ 5	4.5	4.5	0.5^A	-	
	Yokohama City (Sanitation Research)	4	3 ∿ 4	-	-	-	
	Yokosuka City (Sanitation Research)	4 ∿ 5	4.0	-	-	-	
	Kawasaki City (Pollution Research)	4 ∿ 5	3.7	27.0	-	-	
	Kawasaki City (Monitor Center)	4 ∿ 5	4.2	-	-	-	
	Kawasaki City (Saiwai-ku)	4 ∿ 5	4.2	-	-	-	
	Kawasaki City (Tama Ikuta)	4 ∿ 5	3.8	-	-	-	
Chiba	Funabashi City	4 ∿ 5	39.5	-	-	-	
	Chiba City	4 ∿ 5	4.00	-	-	-	
	Pollution Research Institute)	4 ∿ 5	6.7	14.0	-	-	
Saitama	Honjo Public Health Center	4 ∿ 5	4.5	-	-	-	

Place sampled		Date of sampling	pH	SO_4^{-2} (ppm)	NO_3^- (ppm)	Cl^- (ppm)	Remarks
Gunma	Maebashi City	4	7.0*	-	-	-	
	Kiryu City	4	7.0*	-	-	-	
	Ota City	4	5.6*	-	-	-	
	Isezaki City	4	5.6*	-	-	-	
	Tatebayashi City	4	3.6	-	-	-	
	Annaka City	4	4.2**	-	-	-	
Ibaragi	Koba City	4 ∿ 5	3.9*	-	-	-	
Tokyo	TMRIEP	18 ∿ 19	6.07	42.2	9.6[B]	11.4	
	Ota-ku	18	6.59	30.6	3.4[B]	4.8	
	Ome City	18	3.61	7.3	13.0[B]	6.1	
	Chofu City	18	4.5	24.0	-	18.9	
Kanagawa	Pollution Center (Head Office)	18	3.8	25.0	11.0[A]	4.1	
	Pollution Center (Shonan Branch)	18	3.6	11	14[A]	-	
	Yokohama City (Sanitation Research)	18	3.7	15	20[A]	6.3	
	Yokosuka City (Sanitation Research)	18	4.3**	-	-	-	
Chiba	Kisarazu City	18	6.2	77.5	14.1[A]	-	
Saitama	Honjo Public Health Center	18	3 ∿ 4	-	-	-	
	Kumagaya City	18	3.2	-	-	-	
Gunma	Takasaki City	18	3.9	-	-	-	
	Maebashi City	18	7.0*	-	-	-	
	Ota City	18	3.6*	-	-	-	
	Tatebayashi City	18	4.2*	-	-	-	
	Annaka City	18	3.4**	-	-	-	
Ibaragi	Ishioka City	18	4.0	-	-	-	
	Mito City	18	4.2	-	-	-	
Tochigi	Prefectural Office	18	3	-	-	-	

Table 5 Concentrations of rainwater components for the initial 1 mm rainfall on June 25, 1975

Place sampled \ Item		pH	SO_4^{2-} (μg/mℓ)	NO_3^- (μg/mℓ)	Cl^- (μg/mℓ)	NH_4^+ (μg/mℓ)	HCHO (μg/mℓ)	Time of sampling	Remarks
Tokyo	Chiyoda-ku	4.2	49.0	21.3	10.2	1.3	0.2	11:15	
	Tama New Town	3.5	36.1	20.3	13.2	2.6	1.2	13 ∿	
	Ota-ku	6.6	44.8	16.5	5.8	1.8	1.0	10:00	
	Chofu City	3.4	31.8	19.7	10.6	1.8	1.1	13:00	
	Ome City	3.3	13.2	13.2	3.2	4.3	0.3	20:00	
	Itabashi-ku	5.9	12.5	3.7	1.9	2.6	-	22:00	
Kanagawa	Yokohama City (Asahi-ku)	3.7	27.3	17.4	3.3	8.2	1.1	13:10	
	Kawasaki City	3.7	30.3	17.6	6.4	8.2	1.1	12:15	
	Yokohama City (Sanitation Research)	3.8	15.0	11.0	3.5	-	0.4	-	
	Hiratsuka City	3.6	18.0	17.0	6.9	3.6	0.7	16:30	
Chiba	Kisarazu City	4.1	7.2	5.6	5.5	2.1	0.2	11:00	
	Ichihara City	4.6	6.8	6.7	1.3	1.4	0.3	10:00	
	Yachiyo City	3.9	12.4	13.0	3.8	1.5	0.3	22:00	
	Ichikawa City	3.7	15.5	14.8	3.7	4.2	0.4	12:00	
	Sahara City	4.0	3.5	3.7	1.6	0.3	0.2	14:00	
	Togane City	4.0	ND	4.5	2.5	0.2	0.2	10:30	
Saitama	Urawa City	3.5	40.0	17.2	8.3	7.5	0.9	16:00	
	Kumagaya City	3.1	34.2	26.4	4.0	4.7	1.1	13 ∿ 16	
Tochigi	Utsunomiya City	3.5	30.1	5.8	3.2	3.8	0.6	12 ∿ 21	
	Tochigi City	3.6	20.0	4.9	0.9	2.2	0.5	12 ∿ 15	
Ibaragi	Mito City	3.3	17.0	19.7	1.4	1.6	0.9	9 ∿ 10	
	Koga City	3.4	25.0	30.2	1.8	1.9	0.9	9 ∿ 10	
Gunma	Tatebayashi City	3.3	21.0	12.0	ND	2.6	ND	13 ∿ 16	

Places where irritations were reported:

Kashima, Tochigi Pref.	8:00 ∿ 17:00	90 persons
Fukaya, etc., Saitama Pref.	11:00 ∿ 13:00	43 persons
Chofu, etc., Tokyo	16:00 ∿ 23:00	9 persons
Totsuka, Kanagawa Pref.	15:00 ∿	1 person

Table 6 (1) pH of (0 to 1 mm) precipitation in Tokyo

	Chiyoda			Chofu			Ome			Okutama		
Year	Mean	Number of samples	Min.-Max.	Mean	Number of samples	Min.-Max.	Mean	Number of samples	Min.-Max.	Mean	Number of samples	Min.-Max.
1975	4.8	63	3.8-7.8	4.5	89	3.4-10	4.4	99	3.5-7.7	-	-	-
1976	4.8	70	3.6-7.1	4.3	123	3.3-6.9	4.5	112	3.6-6.3	-	-	-
1977	4.8	67	3.9-6.9	4.5	61	3.6-6.9	4.3	106	3.6-6.5	4.3	90	3.3-7.2
1978	4.8	75	3.6-4.8	4.2	79	3.5-7.2	4.3	69	3.4-6.1	4.2	95	3.5-7.5
1979	5.2	79	4.0-7.2	-	-	-	4.4	99	3.9-7.6	4.5	120	3.5-7.5
1980	4.9	76	3.6-8.2	-	-	-	4.4	122	3.4-6.8	4.5	113	3.3-7.8

Mean: Arithmetic mean

Table 6 (2) pH of (0 to 5 mm) precipitation in Tokyo

	Chiyoda			Chofu			Ome			Okutama		
Year	Mean	Number of samples	Min.-Max.	Mean	Number of samples	Min.-Max.	Mean	Number of samples	Min.-Max.	Mean	Number of samples	Min.-Max.
1973	4.6	8	3.9-6.3	4.4	14	3.9-5.0	4.5	16	3.7-5.6	-	-	-
1974	4.9	63	3.5-7.2	4.5	96	3.0-7.4	4.8	87	2.5-8.0	-	-	-
1975	4.5	63	3.6-7.9	4.4	89	3.4-10	4.4	99	3.1-7.7	-	-	-
1976	4.6	70	3.6-7.1	4.4	123	3.3-6.9	4.5	112	3.6-6.3	-	-	-
1977	4.5	67	3.6-6.9	4.4	61	3.6-7.1	4.3	106	3.4-6.5	4.4	40	3.3-7.2
1978	4.4	75	3.3-9.2	4.2	79	3.4-7.2	4.2	69	3.3-6.2	4.3	95	3.5-7.4
1979	4.5	79	3.6-7.2	-	-	-	4.5	99	3.3-7.6	4.5	120	3.5-7.7
1980	4.7	76	3.6-8.2	-	-	-	4.5	122	3.4-6.8	4.5	113	3.3-7.8

Mean: Arithmetic mean

1) In 1973 and 1974, 0-4.6 mm was regarded as 0-5.0 mm.

Table 6 (3) pH of event precipitation in Tokyo

	Mean	Number of samples	Min.-Max.	Mean	Number of samples	Min.-Max.	Mean	Number of samples	Min.-Max.
1978	4.3	75	3.3-9.2	-	-	-	4.5	95	3.5-7.4
1979	4.6	79	3.6-7.2	4.7	99	3.3-7.6	4.8	120	3.5-7.7
1980	4.8	76	3.6-8.2	4.7	122	3.4-6.8	4.7	113	3.3-7.8

1) Calculated from the measured values for every 1 mm precipitation. Min.-Max. values were also extracted from the measured values for every 1 mm precipitation.

Table 7 pH of precipitation in Koenji, Tokyo (Meteorological Research Institute)

Period	Number of samples	pH	
		Mean	Range
Jul to Dec, 1973	26	4.57	3.60 ~ 6.80
Jan to Dec, 1974	86	4.65	3.48 ~ 6.60
Jan to Dec, 1975	68	4.42	3.34 ~ 6.30
Jan to Dec, 1976	83	4.47	3.71 ~ 6.34
Jan to Dec, 1977	69	4.57	3.64 ~ 6.86
Jan to Jul, 1978	32	4.51	3.90 ~ 5.80
Jul, 1973 to Jul, 1978	364	4.52	

Table 8 Analytical results of rainwater components in local cities
(The values indicate the mean values of all measured values)

Prefecture \ Item	Place	Period	Rainwater sampling method	pH	SO_4^{2-} (μg/mℓ)	NO_3^- (μg/mℓ)	Cl^- (μg/mℓ)	NH_4^+ (μg/mℓ)
Miyagi	Sendai City (General Sanitation Center)	Jul to Nov, 1979	Rainwater sampler which allows sampling every 1 mm rainfall	4.75	4.73	1.3	3.71	0.32
Nagano	Nagano City (Sanitation and Pollution Research Institute)	Aug, 1975 to Jul, 1976	Sampling by a dust jar for every rainfall	4.62	2.9	1.16	0.76	0.54
Fukui	Fukui City (Pollution Center)	May, 1977 to Feb. 1978	Rainwater sampler which allows sampling every 1 mm rainfall	4.39	4.2	1.68	3.94	0.83
Gifu	Gifu City (Pollution Research Institute)	Apr to Oct, 1976	ditto	4.52	5.5	2.4	1.9	
Saga	Karatsu City (Pollution Center)	May to Nov, 1975	Rainwater sampler which allows sampling every 0.5 mm rainfall	4.90	2.70	0.52	0.85	

Table 9 Electric conductivities of precipitation in Tokyo

Table 9 (1) Electric conductivities of (0 to 1 mm) precipitation

(at 25°C)

Year	Chiyoda			Chofu			Ome			Okutama		
	Mean	Number of samples	Min.-Max.	Mean	Number of samples	Min.-Max.	Mean	Number of samples	Min.-Max.	Mean	Number of samples	Min.-Max.
1975	120	72	10-510	98	90	11-580	73	99	2.3-450	-	-	-
1976	82	74	8.8-200	84	125	4.3-830	55	73	4.1-170	-	-	-
1977	83	67	16-250	89	62	9.8-200	62	106	4.9-250	36.6	91	2.2-200
1978	84	75	25-280	94	78	14-280	65	68	5.4-280	34.7	95	2.4-130
1979	92	79	21-670	-	-	-	44	99	3.4-310	35	120	2.5-310
1980	72	76	20-190	-	-	-	57	122	3.6-270	34	113	2.3-280

Table 9 (2) Electric conductivities of (0 to 5 mm) precipitation

Year	Chiyoda			Chofu			Ome			Okutama		
	Mean	Number of samples	Min.-Max.	Mean	Number of samples	Min.-Max.	Mean	Number of samples	Min.-Max.	Mean	Number of samples	Min.-Max.
1973	69	8	5.5-125	37		12-62	41	16	12-130			
1974	57	63	7.4-192	40		70-660	51	87	3.6-330			
1975	69	72	12-510	62	90	3.0-580	44	99	2.3-490			
1976	48	74	9.2-200	40	12.5	2.6-830	35	73	3.8-170			
1977	49	67	5.3-250	54	62	5.0-200	40	106	1.3-250	25	91	1.7-200
1978	43	75	5.3-280	51	78	3.7-280	37	68	3.3-280	22	95	1.3-130
1979	49	79	5.1-670				30	97	2.8-310	23	120	1.6-310
1980	39	76	5.1-190				38	122	2.4-300	23	113	1.4-280

Table 9 (3) Electric conductivities of event precipitation

Year	Mean	Number of samples	Min.-Max.	Mean	Number of samples	Min.-Max.	Mean	Number of samples	Min.-Max.
1978	26	75	5.3-280	-	-	-	13	95	1.4-130
1979	32	79	4.8-670	22	99	2.8-310	12	120	1.6-310
1980	28	76	5.1-190	21	122	2.4-300	15	130	1.4-280

Table 10 Chemical Components of precipitation in Tokyo

Precipitation / Year	SO_4^{2-}			NO_3^-			Cl^-			NH_4^+		
	(0-1mm)	(0-5mm)	Total	(0-1mm)	(0-5mm)	Total	(0-1mm)	(0-5mm)	Total	(0-1mm)	(0-5mm)	Total
Chiyoda												
1974		9.25 (300)			4.18 (295)			5.26 (280)				
1975	18.7 (71)	10.1 (270)		9.36 (71)	4.09 (270)		12.2 (71)	6.14 (268)		1.68 (71)	1.38 (229)	
1976	18.0 (73)	8.15 (270)		6.73 (73)	3.36 (270)		8.96 (73)	4.62 (272)		2.42 (73)	1.20 (270)	
1977	13.6 (52)	7.81 (207)		6.72 (52)	4.33 (212)		9.30 (52)	4.80 (212)		1.98 (52)	1.34 (210)	
1978		6.75 (282)	3.12 (972)		3.95 (282)	1.79 (972)		3.32 (281)	1.78 (972)		0.87 (281)	0.55 (972)
1979		8.34 (267)	4.01 (1247.5)		4.84 (266)	2.06 (1249.1)		6.10 (265)	4.58 (1247.1)		1.47 (273)	0.54 (1250.1)
1980		9.18 (316)	6.64 (1452.7)		4.29 (316)	1.62 (1452.7)		4.22 (316)	2.04 (1452.7)		1.39 (316)	0.79 (1452.7)
Mean	17.1 (196)	8.57 (1912)	4.82 (3672.2)	7.68 (196)	4.14 (1911)	1.81 (3673.9)	10.2 (196)	4.90 (1894)	2.83 (3671.9)	2.04 (196)	1.26 (1579)	0.64 (3674.9)
Ome												
1980		6.04 (411)	4.25 (1026.9)		5.03 (411)	2.96 (1026.9)		2.06 (411)	1.27 (1026.9)		1.11 (411)	0.56 (1026.9)
Okutama												
1980		4.28 (424)	3.82 (1123.5)		2.27 (424)	1.32 (1123.5)		0.83 (424)	0.47 (1123.5)		0.31 (424)	0.21 (1123.5)

Concentration in μg/mℓ. The values in the parentheses indicate the amounts of precipitation.

Table 11 Yearly changes in the concentrations of sulfate ions and chloride ions in precipitation (1967-1973, Kichijoji, Tokyo)

Year	1967	1968	1969	1970	1971	1972	1973
SO_4^{2-} (μg/mℓ)	4.0	5.9	4.8	7.1	4.4	4.1	3.8
$Cℓ^-$ (")	0.5	0.1	0.5	1.2	0.8	1.6	0.1

Table 12 Monthly mean values of the concentrations of sulfate ions and chloride ions in precipitation (1967-1973, Kichijoji, Tokyo)

Month	Jan.	Feb.	Mar.	Apr.	May.	Jun.	Jul.	Aug.	Sept.	Oct.	Nov.	Dec.	Mean value over 7 years
SO_4^{2-} (μg/mℓ)	4.0	6.0	4.6	4.7	4.9	4.8	5.4	3.3	4.0	3.3	4.7	4.3	4.8
$Cℓ^-$ (")	0.9	2.1	1.1	1.2	1.0	1.2	0.9	0.4	0.4	0.3	1.2	1.9	0.9

Table 13 Mean values and variations (Jan to Dec, 1975)
(Initial 1 mm precipitation)

Component	Place of measurement	Arithmetic mean value $\bar{x}$	Geometrical mean value x_α	Standard deviation σ	Standard deviation percent A	Number of samples n
pH	Yokohama	4.48	4.40	0.90	20	62
	Kawasaki	5.18	5.10	0.96	19	85
	Hiratsuka	4.73	4.66	0.80	17	81
Electric conductivity (μmho/cm)	Yokohama	104	85.0	62.9	60	59
	Kawasaki	94.3	78.8	55.4	59	85
	Hiratsuka	-	-	-	-	-
SO_4^{2-} (ppm)	Yokohama	9.0	5.3	13	144	62
	Kawasaki	12.3	8.9	10.0	81	52
	Hiratsuka	12.1	9.7	8.2	68	59
NO_3 (ppm)	Yokohama	6.4	4.4	5.7	89	61
	Kawasaki	6.1	3.4	5.7	95	53
	Hiratsuka	8.9	5.6	8.6	97	53
$Cℓ^-$ (ppm)	Yokohama	9.7	7.2	6.8	70	61
	Kawasaki	9.5	6.3	8.8	93	51
	Hiratsuka	11.1	7.7	9.7	87	59
HCHO (ppm)	Yokohama	0.24	0.13	0.27	113	62
	Kawasaki	0.25	0.15	0.26	102	54
	Hiratsuka	0.37	0.38	0.25	68	42

Table 14 Ranges

Component	Place of measurement	Min. and max. values		Range
		Max. value	Min. value	R
pH	Yokohama	7.4	3.3	4.1
	Kawasaki	7.3	3.5	3.8
	Hiratsuka	6.7	3.4	3.3
Electric conductivity (μmho/cm)	Yokohama	367.0	15.1	351.9
	Kawasaki	295.0	6.4	288.6
	Hiratsuka	-	-	-
SO_4^{2-} (ppm)	Yokohama	91	0.3	90.7
	Kawasaki	48	0.9	47.1
	Hiratsuka	42	2.0	40.0
NO_3^- (ppm)	Yokohama	23	0.0	23.0
	Kawasaki	24	0.1	23.9
	Hiratsuka	45	0.3	44.7
Cl^- (ppm)	Yokohama	27	0.6	26.4
	Kawasaki	46	0.8	45.2
	Hiratsuka	50	0.1	49.9
HCHO (ppm)	Yokohama	1.1	0.00	1.10
	Kawasaki	1.1	0.01	1.09
	Hiratsuka	1.1	0.00	1.10

Table 15 Average concentrations of main ions in the rain water

(Mita City 1976)

	Summer (No. 1 6)	Autumn (No. 7 14)	Total
SO_4^2 (μg/mℓ)	1.73 (6)	0.78 (2)	1.49 (8)
NH_4 (μg/mℓ)	0.40 (6)	0.13 (8)	0.25 (14)
NO_3 (μg/mℓ)	1.34 (6)	0.42 (8)	0.82 (14)
NO_2 (μg/mℓ)	<0.001 (6)	<0.001 (8)	<0.001 (14)
Cℓ (μg/mℓ)	0.54 (6)	0.54 (8)	0.54 (14)
Ng (μg/mℓ)	0.18 (6)	0.22 (7)	0.20 (13)
pH	4.43 (6)	5.07 (8)	4.80 (14)
E.C. *) (μ℧/cm)	22.78 (6)	11.10 (8)	16.10 (14)

The numbers of samples are in parentheses.

*) Electric conductivity

Table 16 Concentrations of precipitation components in control places

1978	SO_4^{2-}		NO_3^-		Cℓ		NH_4^+	
	Yagisawa	Ogasawara	Yagisawa	Ogasawara	Yagisawa	Ogasawara	Yagisaga	Ogasawara
Jun.	0.57 (36)	2.3 (16)	0.49 (36)	1.4 (16)	0.26 (36)	6.3 (16)	0.12 (31)	0.08 (16)
Jul.	0.69 (19)	-	0.82 (19)	-	0.12 (19)	-	0.092 (19)	
Aug.	1.02 (24)	2.8 (12)	0.86 (24)	-	0.63 (24)	8.4 (12)	0.18 (24)	0.09 (12)
Sept.	0.63 (35)	-	0.26 (35)	-	0.64 (35)	-	0.086 (35)	-
Oct.	1.05 (16)	3.7 (13)	0.94 (10)	0.3 (13)	0.85 (16)	15.7 (13)	0.097 (16)	0.07 (13)
Mean	0.75 (130)	2.9 (41)	0.58 (124)	0.91 (29)	0.48 (130)	9.9 (41)	0.11 (125)	0.08 (41)

In Yagisawa, (0 to 6 mm) precipitation was taken as one sample.

In Ogasawara, (0 to 5 mm) precipitation was taken as one sample.

The values in parentheses indicate amounts of precipitation in mm.

Note:	SO_4^{2-}	NO_3	$Cℓ^-$	NH_4^+
Mean of Chiyoda (73-80) (0 to 5 mm)	8.57	4.14	4.90	1.26
Total precipitation (78-80)	4.82	1.81	2.83	0.64

Table 17 Examples of measured components of precipitation

(μg/mℓ)

Place	Period	Formaldehyde	Acrolein	Formic acid	Hydrogen peroxide	Measurer
Tatebayashi	June, 1975 to July, 1979	<0.05 ∿ 0.76				Survey by Environment Agency[2]
Urawa	ditto	<0.1 ∿ 2.2				"
Kumagaya	ditto	<0.1 ∿ 2.0				"
Chiyoda	ditto	<0.1 ∿ 2.6				"
Kanagawa		1.9	0.23			Kurokawa, et al.[5]
Kobe	November, 1981 to July, 1982	0.017 ∿ 0.21		0.11 ∿ 0.9		Sakurada, et al.[21]
Chiyoda	June to September 1982				0 ∿ 1.06	Yoshizumi[22]
Hiratsuka	July to December, 1974	0.53	0.045			Kanagawa Prefectural Pollution Center[23]

Table 18 Correlation coefficients between hydrogen ion concentration and respective materials (initial 1 mm precipitation)

Year \ Item	Electric conductivity	SO_4^{2-}	NO_3^-	Cl^-	NH_4^+	N
1975	0.93	0.59	0.78	0.25	0.59	41
1976	0.87	0.78	0.82	0.35	0.75	48
1977	0.51	0.27	0.26	0.12	0.04	44

Table 19 Correlation coefficients between hydrogen ion concentration and respective materials (rainfall of pH 4 or lower)

Year \ Item	Electric conductivity	SO_4^{2-}	NO_3^-	Cl^-	NH_4^+	N
1975	0.84	0.45	0.73	0.33	0.48	48
1976	0.91	0.79	0.89	0.41	0.79	51
1977	0.66	0.54	0.43	0.36	0.22	27

Table 20 Amounts of chemical components falling in precipitation (Amount in g/m^2 year, precipitation in mm)

	Chemical component	Chiyoda 1974	1975	1976	1977	1978	1979	1980	Ome 1980	Okutama 1980
(0 to 1 mm) Precipitation	SO_4^{2-}		1.33 (48)	1.31 (59)	0.913 (55)					
	NO_3^-		0.665 (60)	0.478 (52)	0.450 (49)					
	Cl^-		0.845 (51)	0.636 (50)	0.623 (61)					
	NH_4^+		0.120 (32)	0.177 (54)	0.133 (40)					
	H^+		0.00113 (13)	0.00116 (17)	0.00119 (16)	0.00119 (11)	0.00050 (5.8)	0.00096 (15)		
	Precipitation		71	73	67	75	79	76		
(0 to 5 mm) Precipitation	SO_4^{2-}	2.78	2.77	2.22	1.66	1.90 (62)	2.28 (46)	2.90 (30)	2.48 (57)	1.81 (42)
	NO_3^-	1.254	1.104	0.913	0.918	1.11 (64)	1.32 (52)	1.36 (47)	2.07 (68)	0.964 (65)
	Cl^-	1.58	1.66	1.26	1.02	0.94 (55)	1.67 (29)	1.33 (46)	0.847 (65)	0.353 (67)
	NH_4^+	-	0.372	0.326	0.284	0.245 (46)	0.401 (77)	0.439 (39)	0.456 (79)	0.133 (56)
	H^+	0.00369	0.00815	0.00668	0.00718	0.0126 (26)	0.00787 (25)	0.00675 (29)	0.0139 (63)	0.0128 (52)
	Precipitation	300	270	272	212	282	273	316	411	424
Complete Precipitation	SO_4^{2-}					3.03	5.01	9.65	4.36	4.29
	NO_3^-					1.74	2.57	2.35	3.04	1.49
	Cl^-					1.700	3.73	2.91	1.30	0.528
	NH_4^+					0.537	0.524	1.14	0.579	0.236
	H^+					0.0487	0.0314	0.0230	0.0220	0.0246
	Precipitation					972	1250	1453	1027	1124

Note: The values in parentheses of (0 to 1 mm) precipitation are ratios (%) to (0 to 5 mm) precipitation.
The values in parentheses of (0 to 5 mm) precipitation are ratios (%) to complete precipitation.

Table 21 Amounts of chemical components falling in Chiyoda, Tokyo (1974 - 1980)

Precipitation	Chemical component	Mean amount	% to the total chemical components	% to the corresponding amount of overall precipitation
(0 to 1 mm) precipitation	SO_4^{2-}	1.19	46	19
	NO_3^-	0.532	21	24
	Cl^-	0.702	27	20
	NH_4^+	0.144	5.6	19
	H^+	0.000992	0.04	3.0
	Total	2.57		
(0 to 5 mm) precipitation	SO_4^{2-}	2.40	47	38
	NO_3^-	1.15	22	51
	Cl^-	1.22	24	34
	NH_4^+	0.349	6.8	45
	H^+	0.00752	0.15	23
	Total	5.13		
Overall precipitation	SO_4^{2-}	6.32	49	
	NO_3^-	2.26	18	
	Cl^-	3.55	28	
	NH_4^+	0.771	6.0	
	H^+	0.0327	0.25	
	Total	12.9		

Table 22 Amounts of respective components falling by place (wet and dry)

(In $mg/m^2/month$)

	Chiyoda		Ome		Okutama	
	Fine	Rainy	Fine	Rainy	Fine	Rainy
SO_4^-	664.3	901.6	357.6	735.3	55.1	204.2
NO_3^-	187.1	238.6	165.4	255.6	70.8	136.4
Cl^-	127.1	231.7	57.2	139.4	28.4	56.0
NH_4^+	44.0	117.4	19.0	119.1	21.0	67.6
K^+	12.2	7.9	17.2	7.7	14.2	13.1
Na^+	38.9	66.8	22.2	39.2	15.5	31.0
Ca^{2+}	120.2	78.1	50.8	452.9	22.1	232.6
Mg^{2+}	12.5	14.2	5.9	7.4	2.7	4.6
Fe^{2+}	2.7	4.1	1.5	3.0	1.2	2.3
Mn^{2+}	0.98	1.2	0.28	0.58	0.12	0.36
Pb^{2+}	0.27	2.7	0.033	0.76	0.058	0.15
Zn^{2+}	5.2	8.2	1.7	4.0	0.76	1.6
Ni^{2+}	0.059	0.050	0.023	0.22	0.026	0.18

Table 23 Ratios of the respective components by place

(in %)

		Chiyoda	Ome	Okutama
SO_4^{2-}	Fine	42.4	32.7	21.2
	Rainy	57.6	67.3	78.8
NO_3^-	Fine	44.0	39.3	34.2
	Rainy	56.0	60.7	65.8
Cl^-	Fine	35.4	29.1	33.6
	Rainy	64.6	70.9	66.4
NH_4^+	Fine	27.3	13.8	24.2
	Rainy	72.7	86.2	75.8
K^+	Fine	60.7	69.1	52.0
	Rainy	39.3	30.9	48.0
Na^+	Fine	36.8	36.2	33.3
	Rainy	63.2	63.8	66.7
Ca^{2+}	Fine	60.6	10.1	8.7
	Rainy	39.4	89.9	91.3
Mg^{2+}	Fine	46.8	44.4	37.0
	Rainy	53.2	55.6	63.0
Fe^{2+}	Fine	39.7	33.3	34.3
	Rainy	60.3	66.7	65.7
Mn^{2+}	Fine	45.0	32.6	40.0
	Rainy	55.0	67.4	60.0
Pb^{2+}	Fine	9.1	4.2	27.9
	Rainy	90.9	95.8	72.1
Zn^{2+}	Fine	38.8	29.8	32.2
	Rainy	61.2	70.2	67.8
Ni	Fine	54.1	9.5	12.6
	Rainy	45.9	90.5	87.4

Table 24 Concentrations of the respective components by place

(In %)

	Chiyoda		Ome		Okutama	
	Fine	Rainy	Fine	Rainy	Fine	Rainy
SO_4^{2-}	54.6	53.9	51.2	41.7	23.7	27.2
NO_3^-	15.4	14.3	23.7	14.5	30.4	18.2
C^-	10.5	13.8	8.2	7.9	12.2	7.5
NH_4^-	3.7	7.0	2.7	6.8	9.3	9.0
K^+	1.0	0.5	2.5	0.4	6.1	1.8
Na^+	3.2	4.0	3.2	2.2	6.7	4.1
Ca^{2+}	9.9	4.7	7.3	25.7	9.5	31.0
Mg^{2+}	1.0	0.8	0.8	0.4	1.2	0.6
Fe^{2+}	0.2	0.2	0.2	0.2	0.5	0.3
Mn^{2+}	0.1	0.1	0	0	0.1	0.1
Pb^{2+}	0	0.2	0	0	0	0
Zn^{2+}	0.4	0.5	0.2	0.2	0.3	0.2
Ni^{2+}	0	0	0	0	0	0

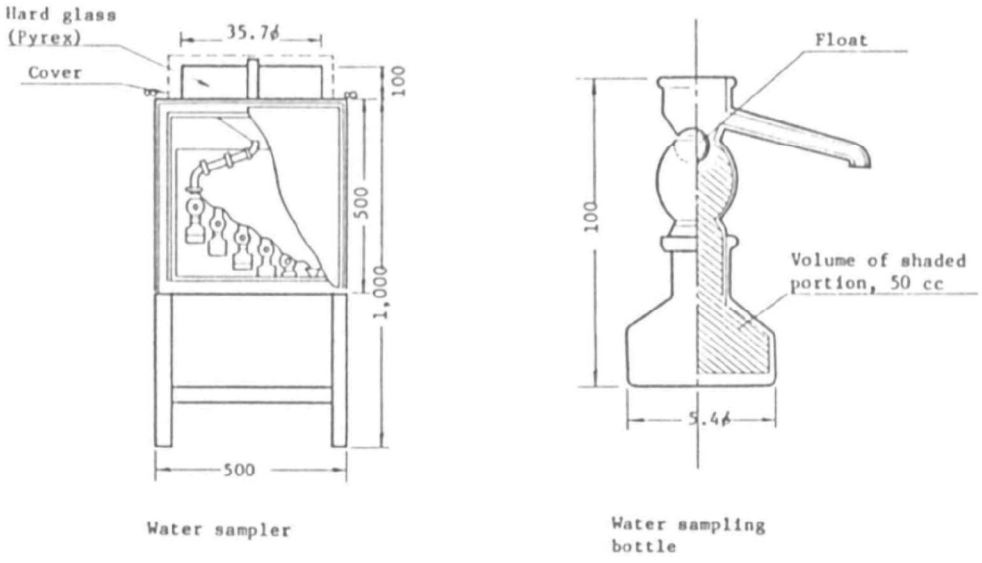

Fig. 1 Precipitation sampler

Fig. 2-(2) Surveyed places

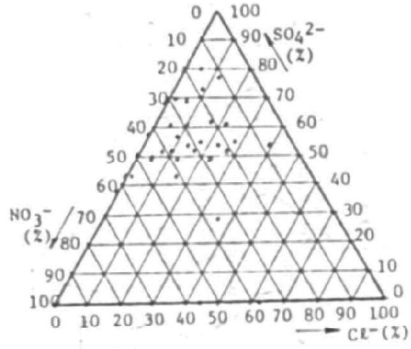

Fig. 3 Composition ratios in equivalent of anions in rainwater (June 25, 1975)

· ≤pH4 x ≤ pH6 ≤ pH5

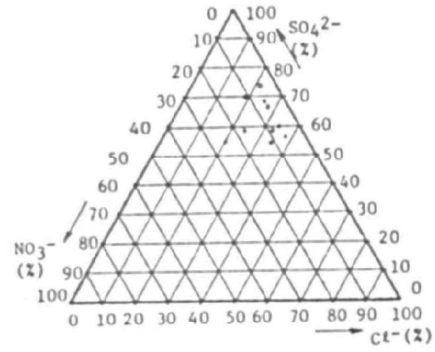

Fig. 4 Composition ratios of anions in rainwater (June 30, 1976)

· ≤pH4 0 ≤ pH5

Fig. 5 Surveyed areas

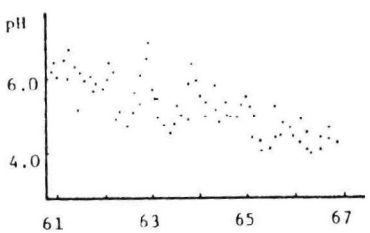

Fig. 6 Changes in the pH of rainwater in Yokkaichi City (Mean values of 18 places in the city, by Yoshida)

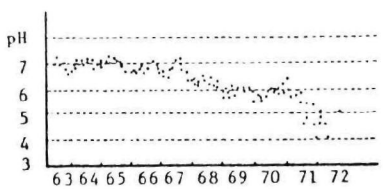

Fig. 7 Changes in the pH of rainwater in Kumamoto City (Mean values of 5 to 7 places in the city, Surveyed by Nishi, Sanitation Bureau of Kumamoto Municipal Office)

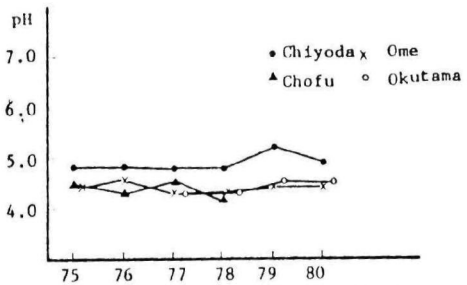

(1) Changes in the annual mean pH of (0 to 1 mm) precipitation

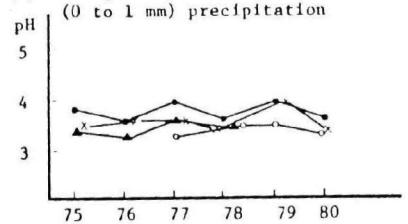

(2) Changes in the minimum pH value of (0 to 1 mm) precipitation

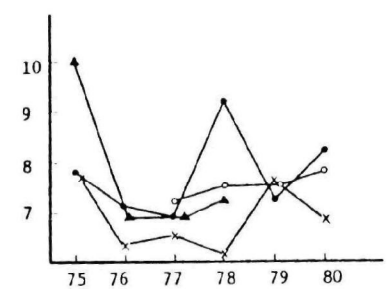

(3) Changes in the maximum pH values of (0 to 1 mm) precipitation

Fig. 8 Changes in the pH of initial (0 to 1 mm) precipitation

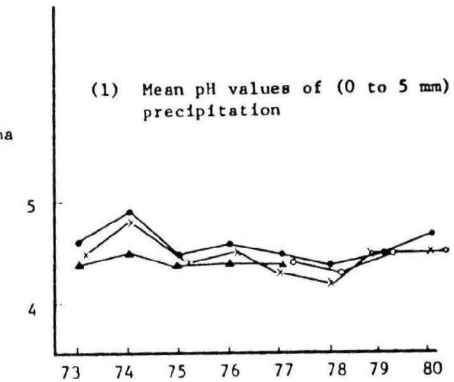

(1) Mean pH values of (0 to 5 mm) precipitation

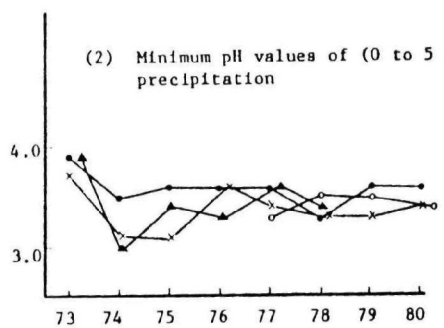

(2) Minimum pH values of (0 to 5 mm) precipitation

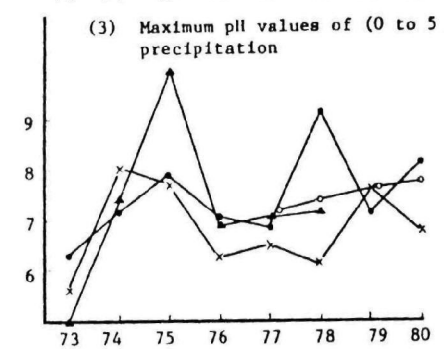

(3) Maximum pH values of (0 to 5 mm) precipitation

Fig. 9 Changes in the pH of (0 to 5 mm) precipitation

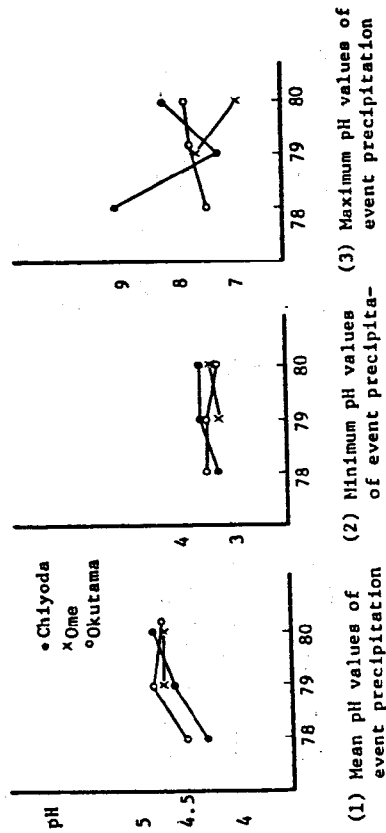

Fig. 10 Changes in the pH of event precipitation

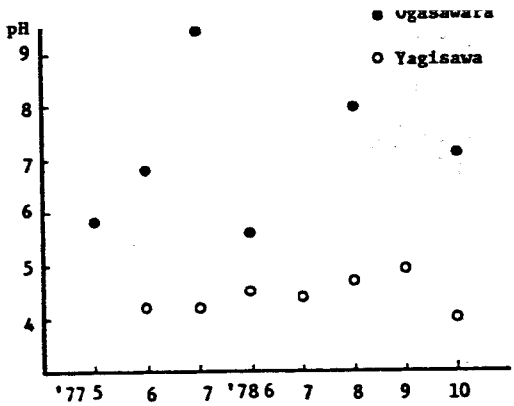

(1) Mean pH values of (0 to 1 mm) precipitation in control places

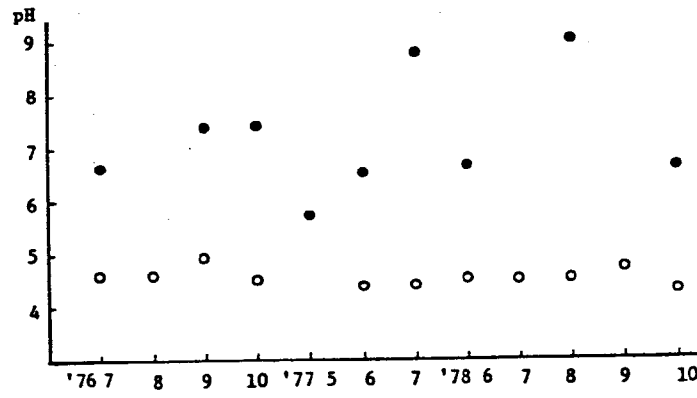

(2) Mean pH values of (0 to 5 mm) precipitation in control places

Fig. 11 pH values of precipitation in control places

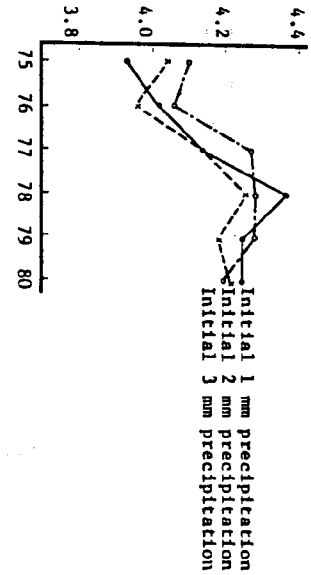

Fig. 12 Yearly changes of pH (Urawa)

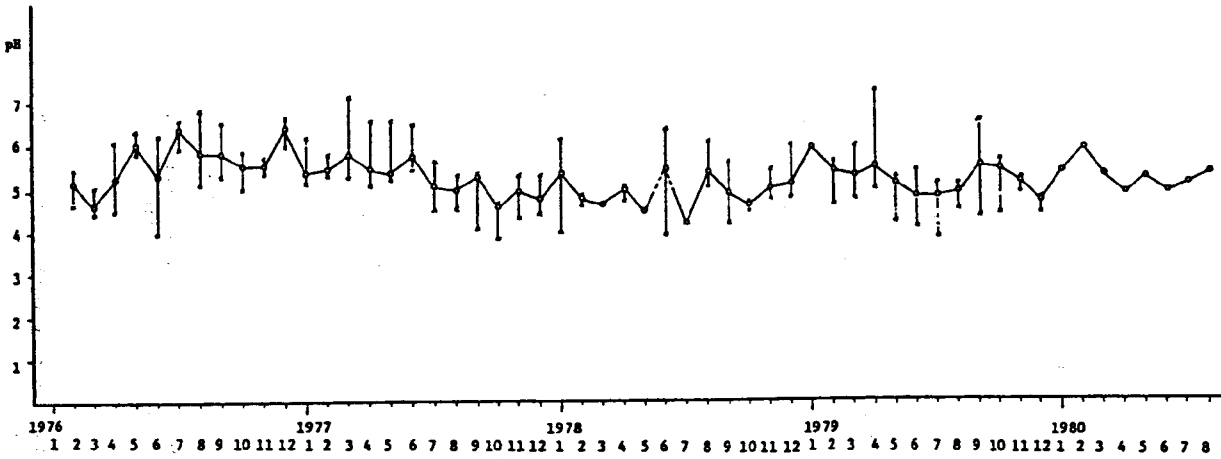

Fig. 13 pH of rainwater in a background area (Ryori, Sanriku-cho, Iwate Pref., Surveyed by Meteorological Agency)[11]

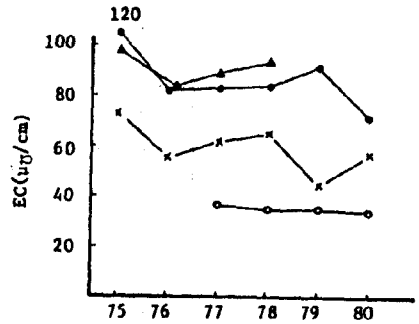

(1) Changes in the mean electric conductivity of (0 to 1 mm) precipitation

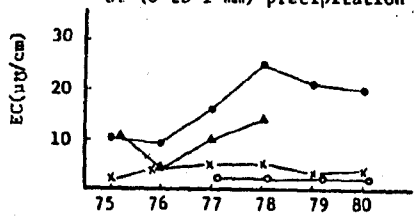

(2) Changes in the minimum electric conductivity of (0 to 1 mm) precipitation

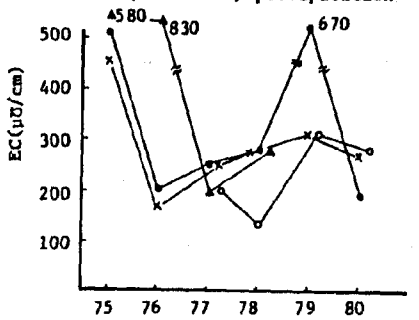

(3) Changes in the maximum electric conductivity of (0 to 1 mm) precipitation

Fig. 14 Changes in the electric conductivity of (0 to 1 mm) precipitation

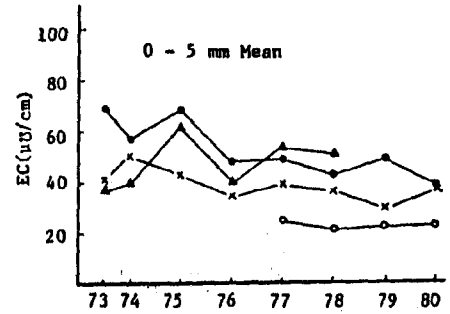

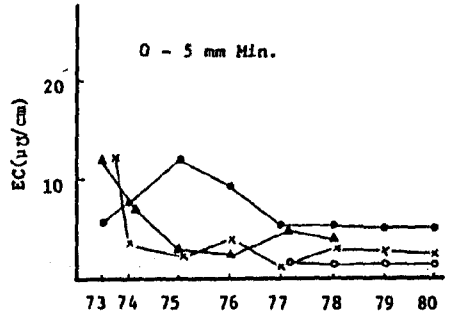

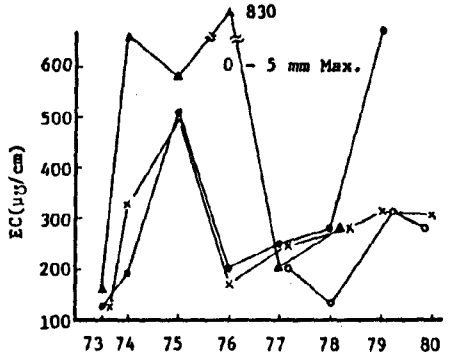

Fig. 15 Changes in the electric conductivity of (0 to 5 mm) precipitation

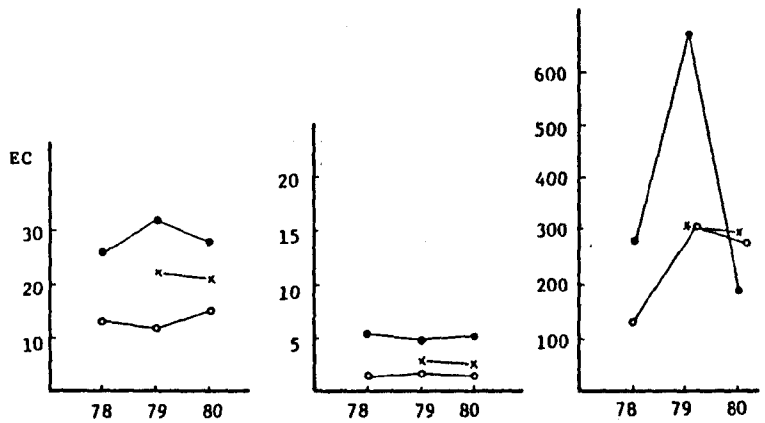

(1) Mean electric conductivities of event precipitation

(2) Minimum electric conductivities of event precipitation

(3) Maximum electric conductivities of event precipitation

Fig. 16 Changes in the electric conductivity of event precipitation

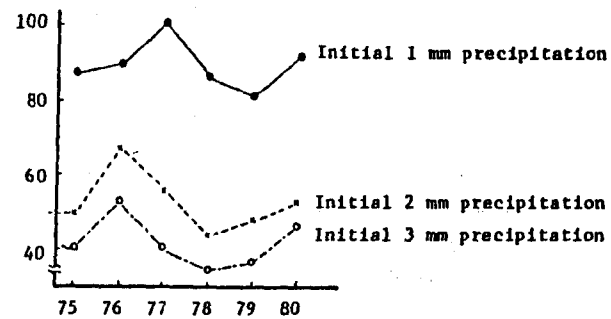

Fig. 17 Annual changes in electric conductivity (Urawa)

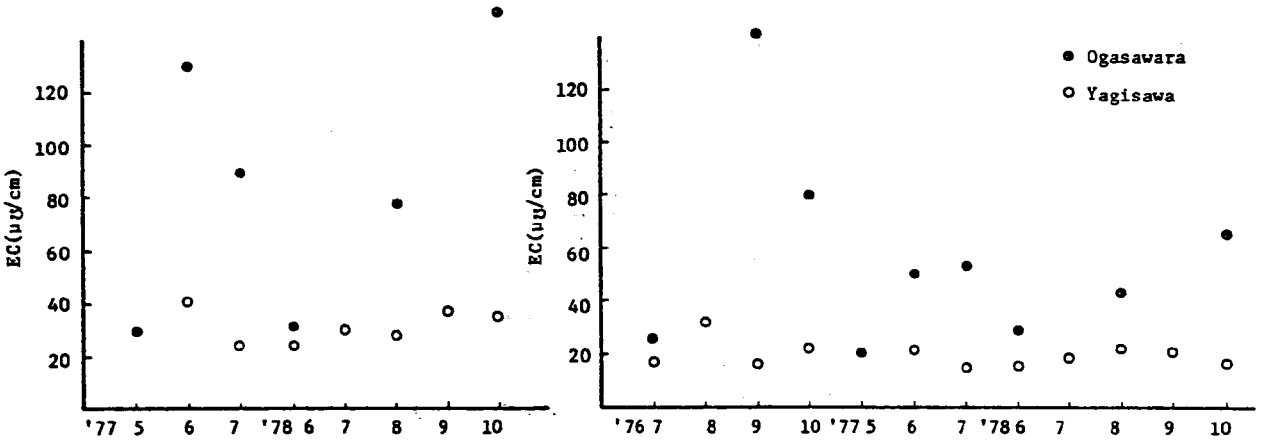

Mean electric conductivites of (0 to 1 mm) precipitation in control places

Mean electric conductivities of (0 to 5 mm) precipitation in control places

Fig. 18 Electric conductivities of precipitation in control places

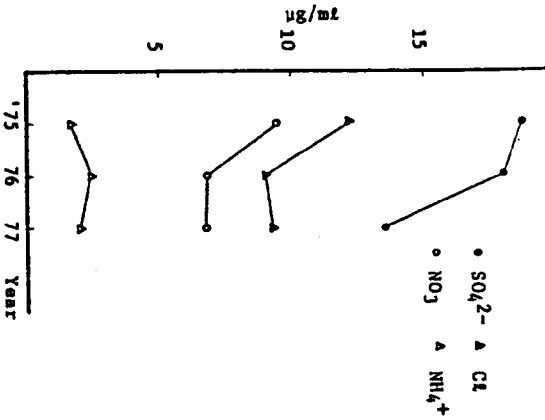

Fig. 19 Mean values of components of (0 to 1 mm) precipitation (Chiyoda)

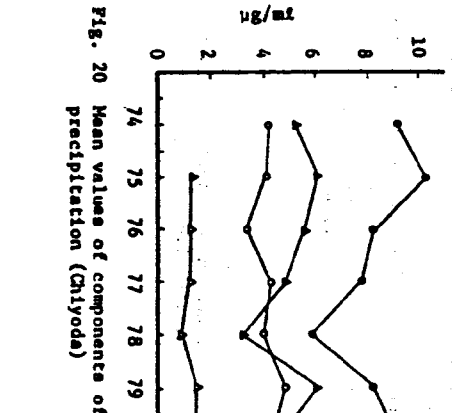

Fig. 20 Mean values of components of (0 to 5 mm) precipitation (Chiyoda)

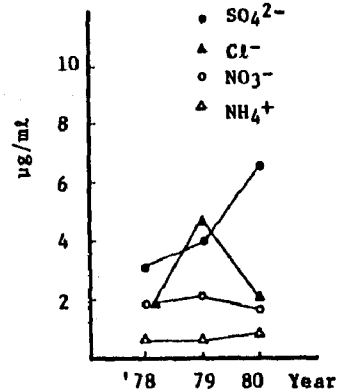

Fig. 21 Mean values of components of event precipitation

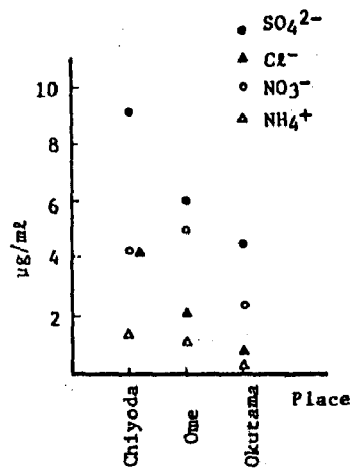

Fig. 22 Mean values of components of (0 to 5 mm) precipitation (1980)

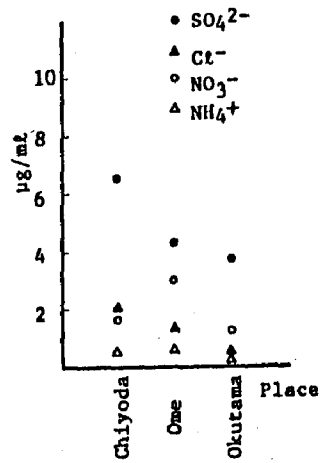

Fig. 23 Mean values of components of event precipitation (1980)

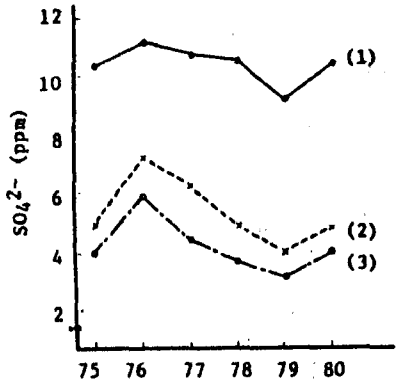

Fig. 24 Yearly changes in sulfate ion concentration (Urawa)

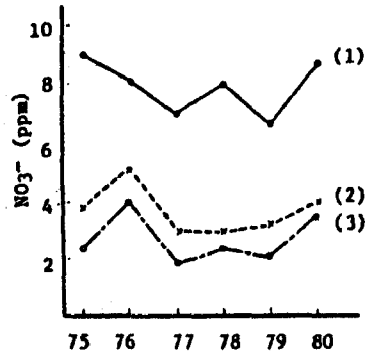

Fig. 25 Yearly changes in nitrate ion concentration (Urawa)

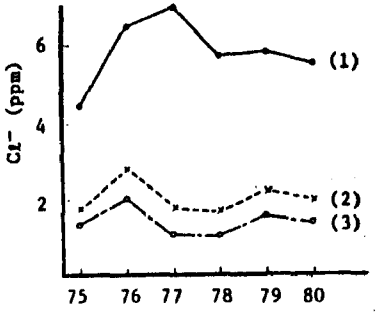

Fig. 26 Yearly changes in chloride ion concentration (Urawa)

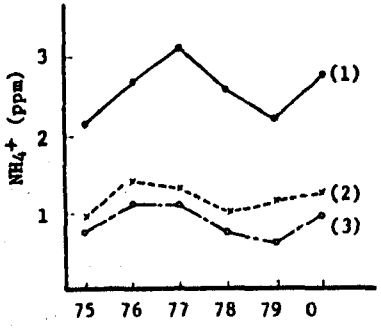

Fig. 27 Yearly changes in ammonium ion concentration (Urawa)

Notes (1) Initial 1 mm precipitation

(2) Initial 2 mm precipitation

(3) Initial 3 mm precipitation

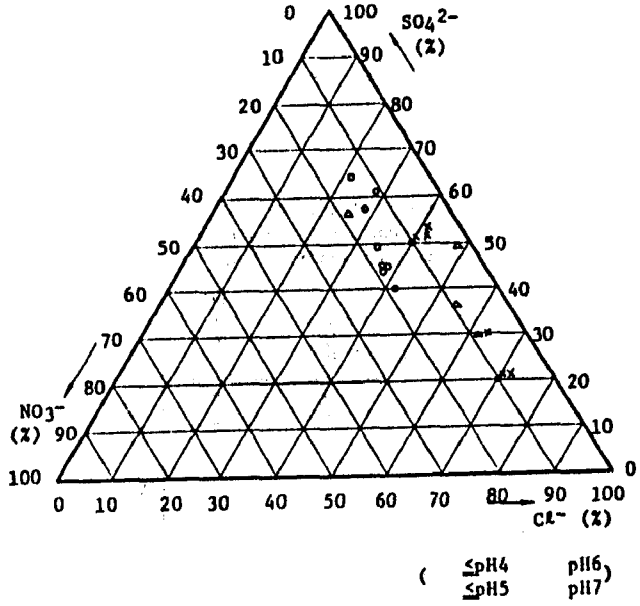

Fig. 28 Composition ratios in equivalent of anions in rainwater (July 3)

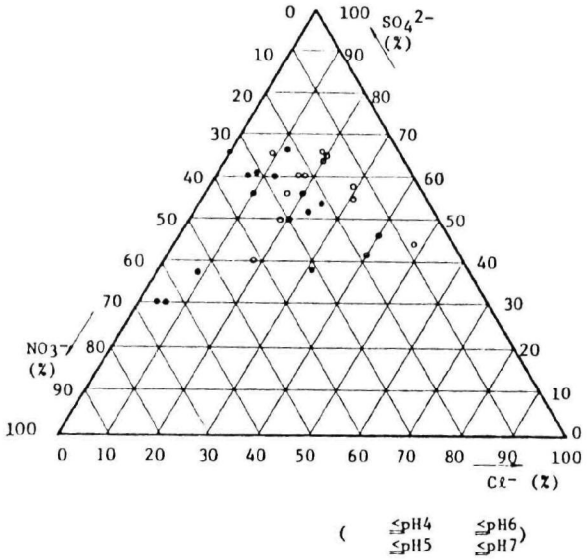

Fig. 29 Composition ratios in equivalent of anions in rainwater (June 29)

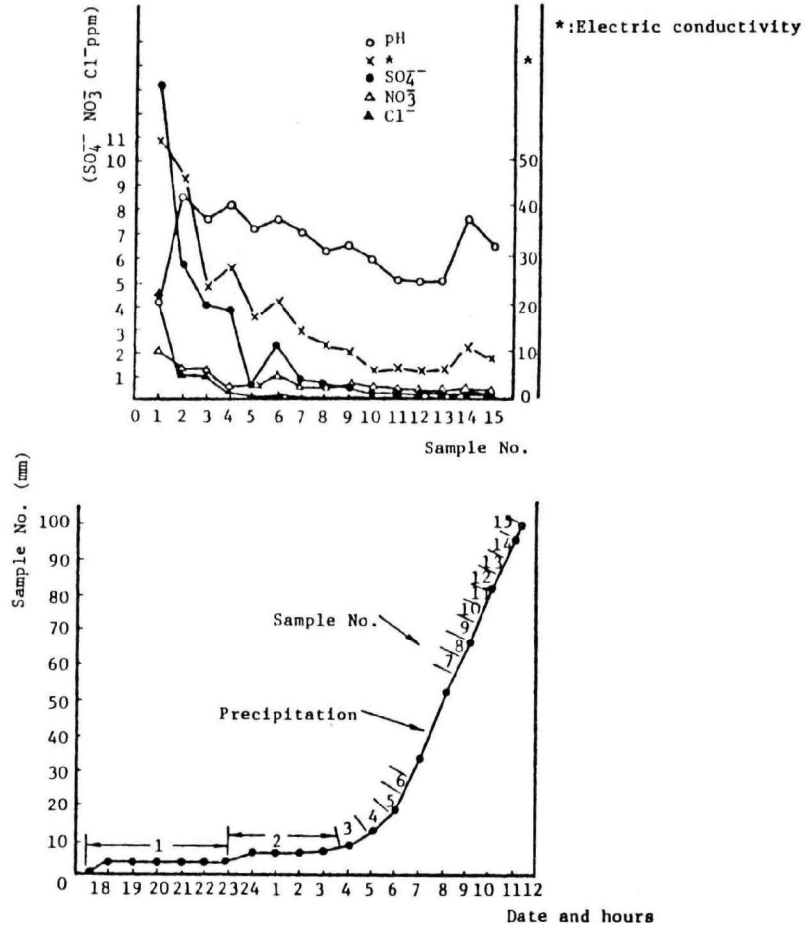

Fig. 30 Continuous precipitation diagram for Chiyoda

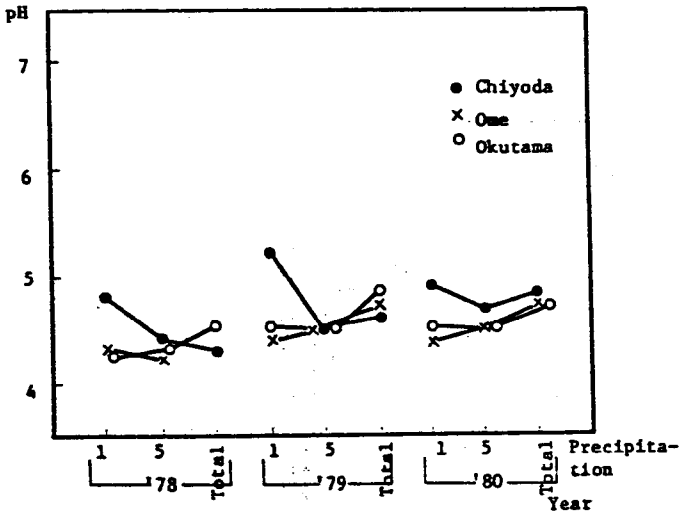

Fig. 31 Relation between precipitation and pH

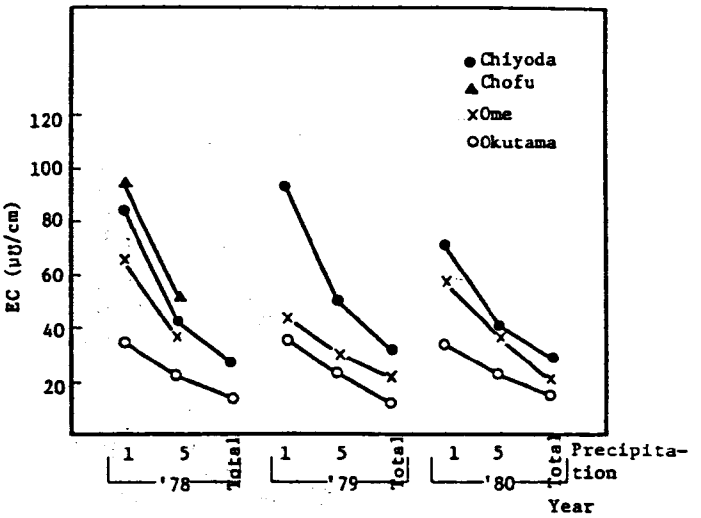

Fig. 32 Relation between precipitation and electric conductivity

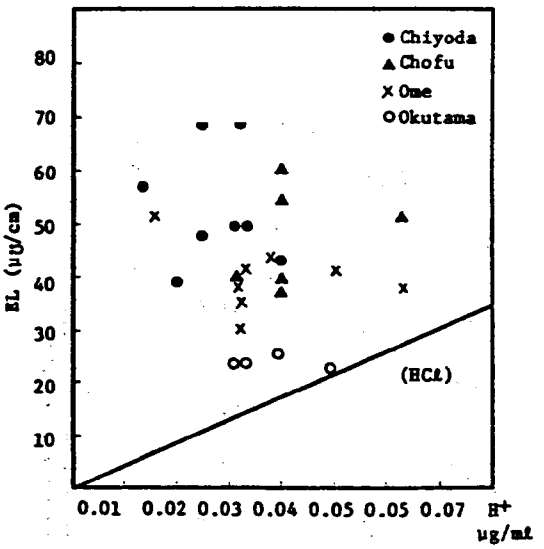

Fig. 34 Relation between hydrogen ion concentration and electric conductivity in (0 to 5 mm) precipitation

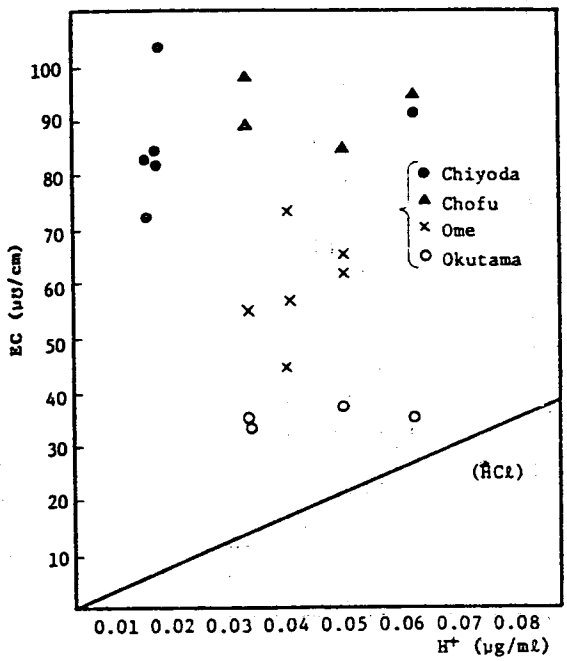

Fig. 33 Relation between hydrogen ion concentration and electric conductivity in (0 to 1 mm) precipitation

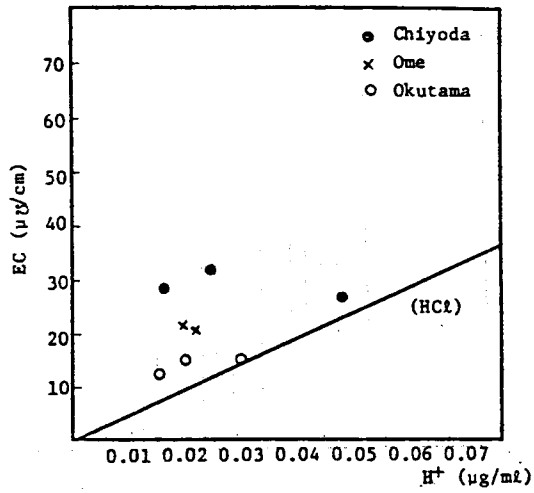

Fig. 35 Relation between hydrogen ion concentration and electric conductivity in event precipitation

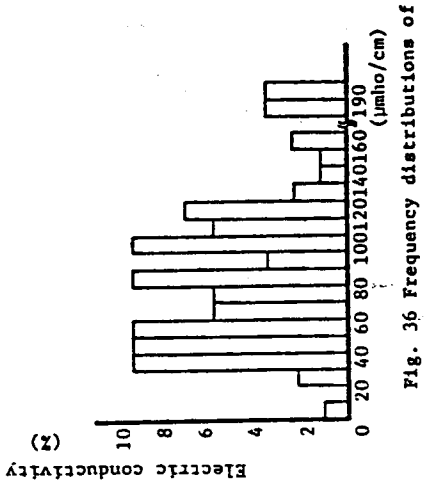

Fig. 36 Frequency distributions of hydrogen ion

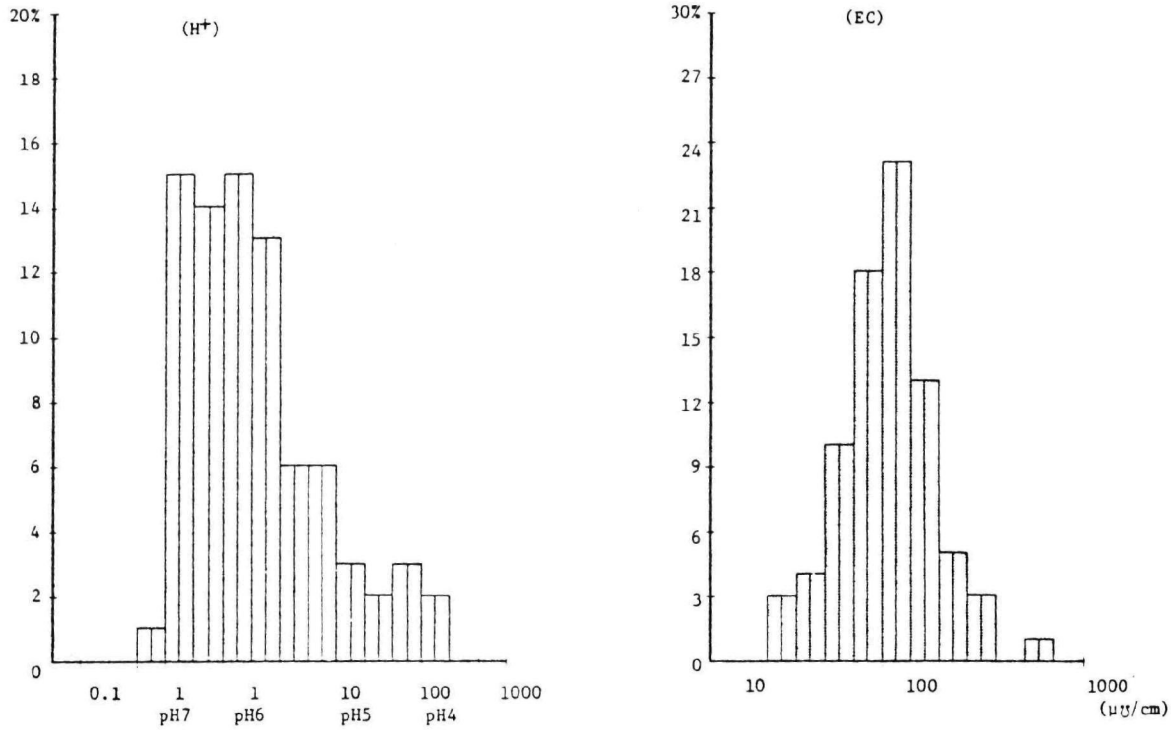

Fig. 37 Frequency distributions of hydrogen ion concentrations and electric conductivities (1979, (0 to 1 mm) precipitation)

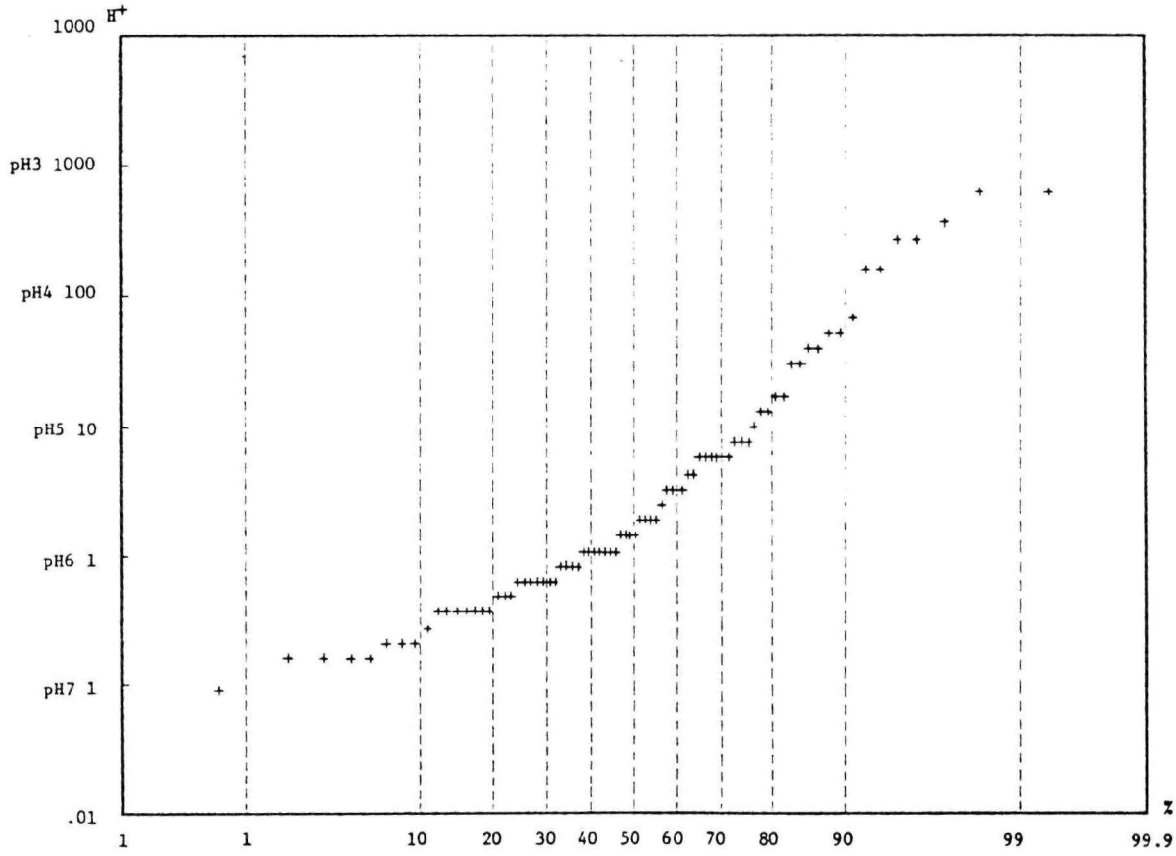

Fig. 38 (1) Frequency distribution of hydrogen ion concentrations in Chiyoda (1979, (0 to 1 mm) precipitation)

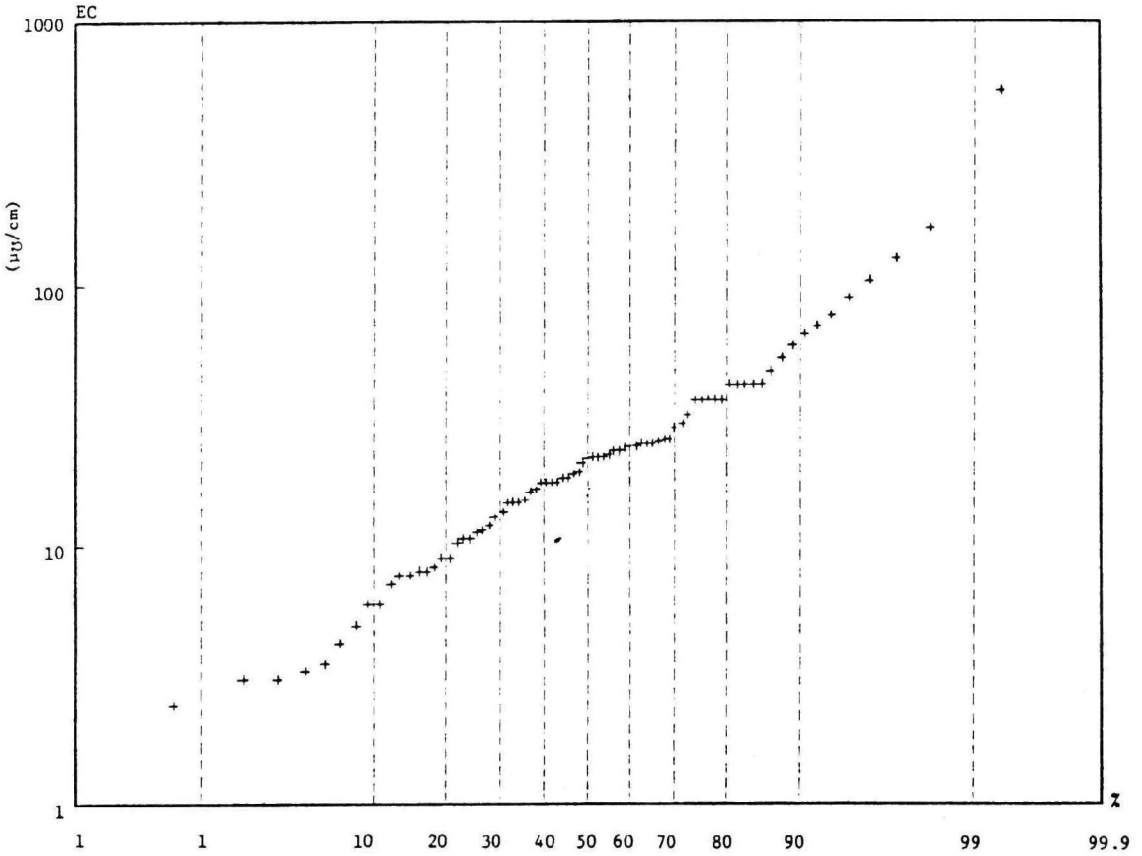

Fig. 38 (2) Frequency distribution of electric conductivities in Chiyoda (1979, (0 to 1 mm) precipitation)

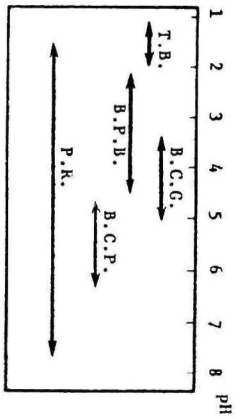

Fig. 39 Discoloration ranges of ph indicator

July 4, 1981; Tokyo Metropolitan Pollution Research Institute; Light Rain; Rain started at 10:30, and sampling started at 10:35; mean pH 3.80

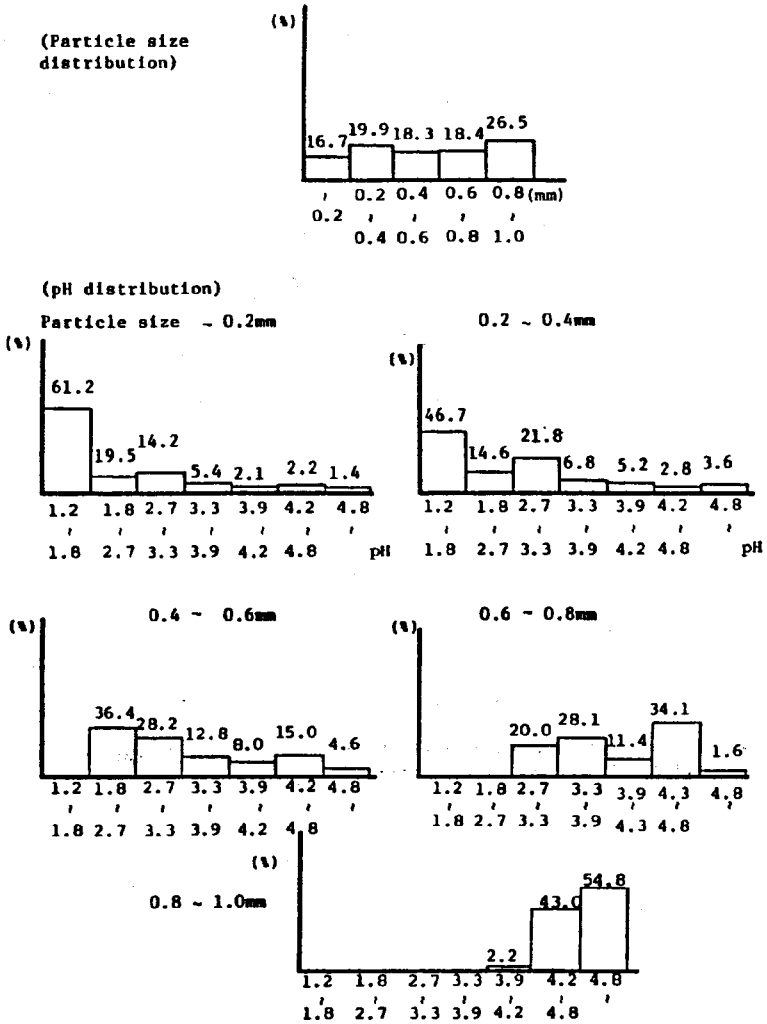

Fig. 40 Raindrop size distribution and pH distributions by raindrop sizes.

[Ref.]

A Numerical Model of Acidification of Cloud Water

By Sachio Ohta and Toshiichi Okita

Department of Sanitary Engineering, Hokkaido University, Sapporo 060

and Chiaki Kato

Sumitomo Denko Ltd., Konohana-ku, Osaka
(Manuscript received 22 April 1981, in revised form 21 September 1981)

Abstract

The numerical model calculation was conducted cf pH of cloud water on the assumption that the cloud droplets formed on H_2SO_4 and other sulfate and nitrate nuclei dissolve acidic and alkaline gases to achieve gas-liquid equilibrium in a very short time. With the initial concentration of gases and particulate components as found in the real atmosphere the pH of the clcud water is calculated to be three. The calculation inetrprets pH, and the concentrations of SO_4^{2-}, NO_3^- and other species in cloud water observed on a mountain fairly well.

1. Introduction

The acidification of the precipitation was reported from Europe, U.S.A. and Canada. In Japan three episodes occurred in which people, particularly students who were cycling, walking and working in outside air were suffered from eye- and skin-irritation as a result of the attack of contaminated drizzle droplets. The dates of the episodes, the places where the episodes occurred (c.f. Fig. 1) and the number of those who complained the irritation are as shown in Table 1.

Since the pH of the drizzle droplets was as low as about three, we assumed that hydrogen ion in the droplets might be responsible for the irritation as well as formaldehyde and other irritants. For the study of the cause of the irritating precipitation Japanese Environment Agency organized a study group and since 1975 during rainy season of June and July three dimensional study of atmospheric gaseous and particulate species and the species in precipitation have been made in the Kanto area (Fig. 1). As members of the group we made measurements of acidic and alkaline gaseous and particulate species and of pH and the concentration of various species in cloud water on the top of Mt. Tsukuba (altitude 870 m).

Then in order to know the effect of the gaseous and particulate species on the pH of the cloud water, an equilibrium model was formulated to describe the pH of the cloud water in terms of the concentration of gaseous and particulate species in the atmosphere. It was also found that the dissolution of NO_2 into water is unimportant for the formation of NO_3^- in the water.

2. Determination of concentration of chemical species in cloud water

In the rainy season the top of Mt. Tsukuba was frequently covered with a cap cloud. In June and July of 1975 through 1978 sampling of the cloud water was made. The concentrations of the species in the cloud water are reproduced from the reference of Okita and Ohta (1979) as shown in Fig. 2 in which the data are arranged in the order of diminishing H^+ concentration. It was found that high H^+ concentration was accompanied by high NO_3^- concentration and high SO_4^{2-} concentration exceeding NH_4^+ concentration on normality basis in range A. Cl^- concentration was independent of H^+ concentration. It was also found that in case of high H^+ concentration (range A) the ionic balance was approximately established between H^+, NH_4^+, SO_4^{2-}, NO_3^- and Cl^- ions. Therefore it seems that the incorporation of acidic particulate and

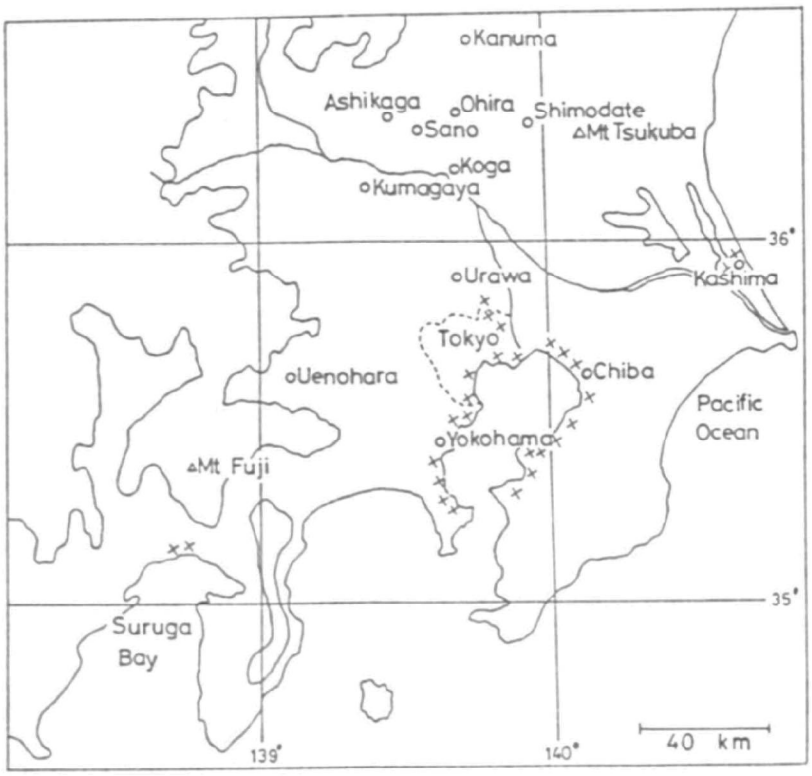

Fig. 1 Map of Kanto area. ×: Industrial area.

Table 1 Dates, places and number of people who complained eye- and skin-irritation due to contaminated drizzle.

Date	Place	Number of people
June 28 and 29, 1973	Several cities and towns on the coast of Suruga Bay Uenohara	441
July 3 and 4, 1974	Area covering Ashikaga, Sano, Ohira, Koga and Kumagaya Tokyo and Yokohama area	32,730
June 25, 1975	Kanuma Kumagaya	144

gaseous species such as H_2SO_4 and HNO_3 into the cloud droplets would give rise to acidic droplets. In the ranges of less H^+ concentration (B and C ranges) SO_4^{2-} concentration was usually the same as NH_4^+ concentration or slightly lower, which presupposes that most of the SO_4^{2-} was incorporated into the droplets in the form of $(NH_4)_2SO_4$. In these ranges NO_3^- concentration was usually much lower than in range A.

3. Determination of equilibrium vapor concentration of NO_2 over its dilute aqueous solution

Since gaseous HNO_3, HCl, NH_3 etc. may dissolve into cloud droplets to have influence on the pH of the cloud water, the solubilities of these gases into water are important data for the formulation of the equilibrium model. The solubilities of SO_2, HCl and CO_2 were summarized by Orel *et al.* (1977). The solubilities of low concentrations of HNO_3 and NH_3 were respectively measured by Davis and de Bruin (1964) and by Hales and Drewes (1979).

The experimental setup for the measurement of air-water equilibrium of NO_2 is as shown in Fig. 3. 0.6-600 ppm of NO_2 prepared in a tedlar

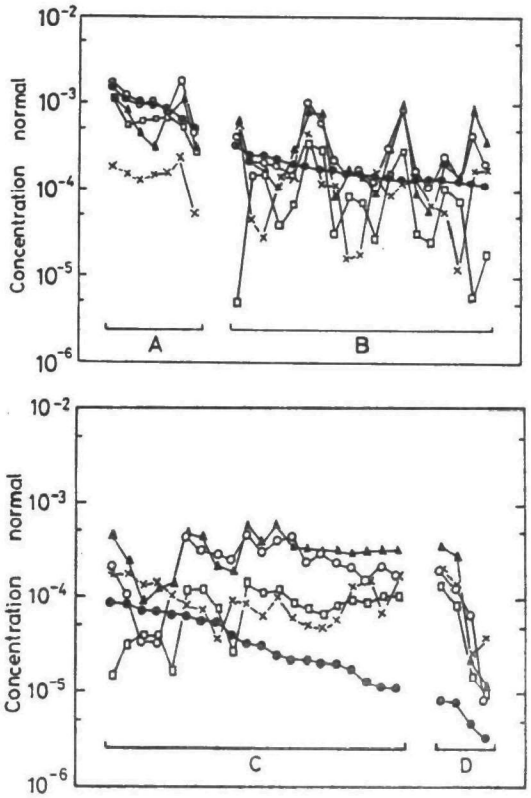

Fig. 2 Concentrations of species in cloud water arranged in the order of diminishing H^+ concentration.
A: pH<3.3, B: 3.3≤pH<4.0,
C: 4.0≤pH<5.0, D: 5.0≤pH
● H^+, ▲ NH_4^+, ○ SO_4^{2-}, □ NO_3^-, × Cl^-.

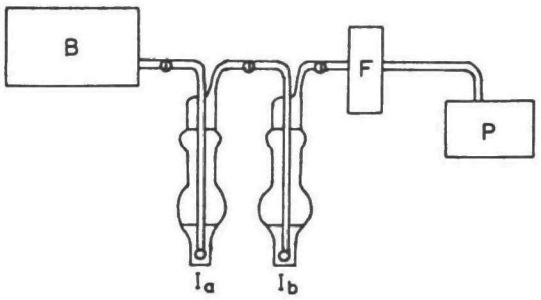

Fig. 3 Experimental setup for measurement of NO_2 solubility.
B: Tedlar bag, I_a: Bubbler containing distilled water, I_b: Bubbler containing Saltzman solution, F: Rotameter, P: Pump.

bag was passed through the bubblers I_a and I_b with flow rate of 0.33 L min^{-1}. 40 mL of distilled and deionized water and Saltzman's reagent were put into I_a and I_b respectively. Whether the air-water equilibrium was attained in I_a was checked by successive measurements of the concentration of NO_2 sampled in I_b. It was found that within 20 minutes the concentration of NO_2 became invariant. The high and low concentrations of NO_2^- in I_a were respectively determined by NO_2^- ion electrode and naphthylethylene diamine (NEDA) colorimetric method. High NO_3^- concentration was determined by NO_3^- ion electrode. In the case of low concentration of NO_3^- it was reduced to NO_2^- by cupper-cadmium column and then determined by NEDA method. pH was measured on a pH meter.

Orel *et al.* (1977) expressed the air-water equilibrium of NO_2 as follows,

$$2NO_2+H_2O \rightleftharpoons HNO_2+H^++NO_3^-$$

$$K_{NO_2}=\frac{[HNO_2][H^+][NO_3^-]}{P^2_{NO_2}}$$

where P_{NO_2} is the pressure (atm) of NO_2. HNO_2 is dissociated as follows,

$$HNO_2 \rightleftharpoons H^++NO_2^-$$

$$K_{HNO_2}=\frac{[H^+][NO_2^-]}{[HNO_2]}=5.1\times10^{-4}\ \mathrm{mol\ L^{-1}}$$

at 25°C.

In their simulation model Orel *et al.* assigned a value of $4.3\times10^5\ \mathrm{mol^3\ L^{-3}\ atm^{-2}}$ as K_{NO_2} which was obtained by Pick. As a result they concluded that the dissolution of NO_2 into water is a major route for the formation of NO_3^-. However, we raised a doubt that the above K_{NO_2} value might be too large in low NO_2 concentration range.

Our experimental relation between K_{NO_2} and NO_2 concentration in the air is as shown in Fig. 4 indicating a steep decrease of K_{NO_2} with decreasing NO_2 concentration. A cross in the figure is an experimental result obtained by Kato *et al.* (1978). These experimental results show that K_{NO_2} is not constant but a function of the concentration of NO_2. The relation shown in the figure may approximately be expressed by

$$K_{NO_2}=10^{1.95\log NO_2+3.08}$$

where NO_2 concentration and K_{NO_2} are in terms of atm and $\mathrm{mol^3\ L^{-3}\ atm^{-2}}$ respectively.

From above two equilibrium equations, the equation

$$[NO_3^-]=\frac{K_{HNO_2}K_{NO_2}P^2_{NO_2}}{[H^+]^2[NO_2^-]}$$

is obtained. As NO_2^- concentration is an order of 10^{-6} mol L^{-1} in cloud or rain water, on substituting the values of K_{HNO_2}, K_{NO_2} and $P_{NO_2}=10^{-8}$ atm and pH=5.0 into this equation, NO_3^-

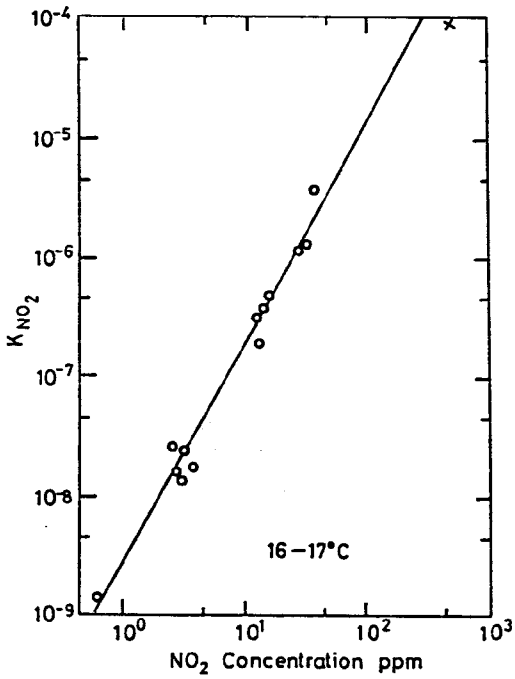

Fig. 4 Relation between K_{NO_2} and NO_2 concentration.

concentration becomes to be an order of 10^{-16} mol L^{-1} which is very small in comparison with the NO_3^- concentration in cloud water as shown in Fig. 2.

4. A numerical model of acidification of cloud water

In order to interprete the pH and the concentration of gaseous and aerosol species in the atmosphere the following numerical simulation is conducted.

It may primarily be assumed that in the atmosphere the gaseous species SO_2, CO_2, NO_2, HNO_3, NH_3 and HCl, and aerosol components H_2SO_4, $(NH_4)_2SO_4$, Na_2SO_4, NH_4NO_3 and $NaNO_3$ are the major species affecting the pH and content of ionic species of the cloud droplets.

As described in the previous section our experiment shows that the solubility of NO_2 in water is so low that its effect may be neglected. Na_2SO_4 and $NaNO_3$ may be produced by reacting H_2SO_4 and HNO_3 with NaCl in sea-salt particles, so that most of them would be in the micron-size range. However, since the size distribution of SO_4^{2-} measured on Mt. Tsukuba showed that most of the SO_4^{2-} was submicron in size (Okita, 1978), therefore in inland area the presence of Na_2SO_4 and $NaNO_3$ may be neglected.

It is assumed that the air parcel containing above mentioned gaseous and aerosol species ascends along a side of a mountain and that the cloud of water content of W (g m^{-3}) is formed at a level which is somewhat lower than the top of the mountain. The initial supersaturation in the cloud is difficult to measure, but Scott *et al.* (1979) estimated that it is greater than 0.2%. Therefore in the present calculation the initial supersaturation is assumed to be 0.2%. It is further assumed that no entrainment of gaseous and aerosol components occurs after the formation of the cloud.

The radius r of solution droplets containing m (g) of solute which is in equilibrium with the air of relative humidity H is given by (Mason, 1971)

$$\frac{H}{100}=\left[\exp\left(\frac{2\sigma' M_w}{\rho_L' R' T r}\right)\right] \times\left[1+\frac{imM_w}{M_m\left(\frac{4}{3}\pi r^3\rho_L'-m\right)}\right]^{-\rho_L/\rho_L'} \quad (1)$$

where M_m and M_w are respectively molecular weight of solute and water, ρ_L and ρ_L' respectively the density of water and solution, σ' surface tension of solution, i van't Hoff's factor, R' gas constant and T is absolute temperature. Fig. 5 is the relation between m and r derived from equation (1) for the solution of $(NH_4)_2SO_4$, H_2SO_4 and NH_4NO_3. The measurements of the size distributions of SO_4^{2-} and NO_3^- conducted on the top of Mt. Tsukuba (Okita, 1978) and at Nagoya (Kadowaki, 1976 and 1977) indicated that more than 95% by weight of SO_4^{2-} and NO_3^- is in the range above 0.1 μm in particle radius. Since the relative humidity during the measurements was usually below 80% most aerosol mass might be consisted of particles with mass of H_2SO_4, $(NH_4)_2SO_4$ or NH_4NO_3 larger than 10^{-15} g.

The equilibrium radius r of solution droplet when relative humidity exceeds 100% as calculated using equation (1) is shown in Fig. 6. This figure indicates that the particles containing more than 10^{-15} g of H_2SO_4, $(NH_4)_2SO_4$ and NH_4NO_3 can be activated as condensation nuclei with the supersaturation exceeding 0.2%.

In view of the above conclusion it may be assumed that almost all the aerosol mass of H_2SO_4, $(NH_4)_2SO_4$ and NH_4NO_3 may be incorporated into cloud droplets as condensation nuclei.

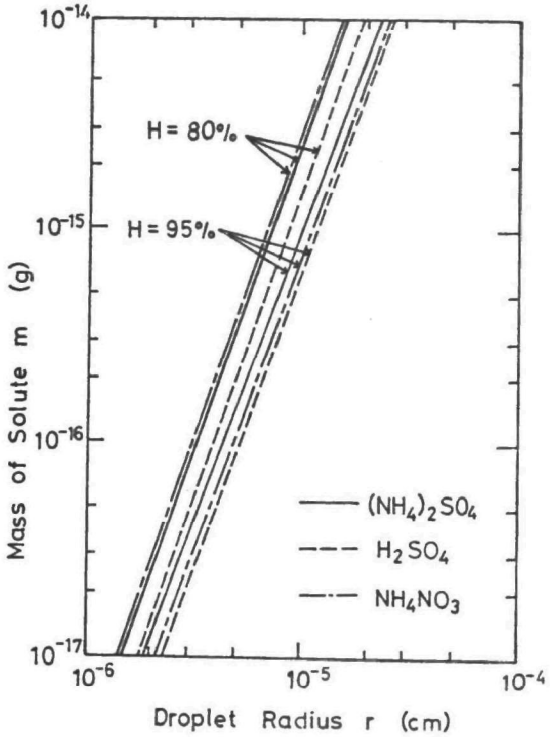

Fig. 5 Mass of solute as a function of equilibrium radius of solution droplet and relative humidity H.

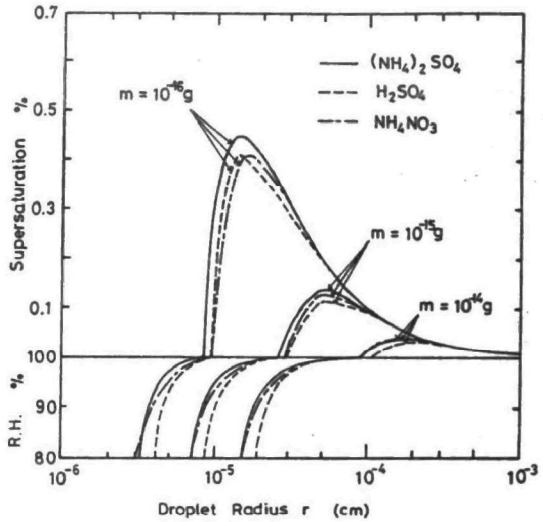

Fig. 6 The equilibrium relative humidity (or supersaturation) as a function of droplet radius for solution droplets containing indicated mass by m.

On forming a cloud droplet around the nucleus it seems that water soluble gases are also incorporated into aqueous phase in a very short time to establish gas-liquid phase equilibrium of these gases.

The equations for the chemical equilibrium of SO_2-NH_3-CO_2-HCl-HNO_3-H_2O system are given in Table 2. The values of K_{hh} and K_{1h} were measured by Davis and de Bruin (1964). K_{ha} was measured by Hales *et al.* (1979). Other Henry's constants and dissociation constants are those described in Table III of Orel *et al.*'s paper (1977). γ_+, γ_- and γ_{2-} are the activity coefficients which are given by the following equations according to the Debye-Hückel theory,

$$\log_{10}\gamma_{z+}=\log_{10}\gamma_{z-}=-A\sqrt{I}z^2/(1+\sqrt{I})+0.2AIz^2, \quad (z=1,2,\cdots), \qquad (2)$$

where $A=0.509$ and I is ionic strength which is given by

Table 2 Chemical equilibria in SO_2-NH_3-CO_2-HCl-HNO_3-H_2O system.

Reaction	Equilibrium constant expression	Value of equilibrium constant at 20°C
$H_2O \rightleftarrows H^+ + OH^-$	$K_w=[H^+][OH^-]\gamma_+\gamma_-$	1.008×10^{-14}
$SO_2(g)+H_2O \rightleftarrows SO_2\cdot H_2O$	$K_{hs}=[SO_2H_2O]/P_{SO_2}$	1.24
$SO_2\cdot H_2O \rightleftarrows H^+ + HSO_3^-$	$K_{1s}=[H^+][HSO_3^-]\gamma_+\gamma_-/[SO_2\cdot H_2O]$	1.27×10^{-2}
$HSO_3^- \rightleftarrows H^+ + SO_3^{2-}$	$K_{2s}=[H^+][SO_3^{2-}]\gamma_+\gamma_{2-}/[HSO_3^-]\gamma_-$	6.24×10^{-8}
$NH_3(g)+H_2O \rightleftarrows NH_3\cdot H_2O$	$K_{ha}=[NH_3\cdot H_2O]/P_{NH_3}$	92.9
$NH_3\cdot H_2O \rightleftarrows NH_4^+ + OH^-$	$K_{1a}=[NH_4^+][OH^-]\gamma_+\gamma_-/[NH_3\cdot H_2O]$	1.774×10^{-5}
$CO_2(g)+H_2O \rightleftarrows CO_2\cdot H_2O$	$K_{hc}=[CO_2\cdot H_2O]/P_{CO_2}$	3.4×10^{-2}
$CO_2\cdot H_2O \rightleftarrows H^+ + HCO_3^-$	$K_{1c}=[H^+][HCO_3^-]\gamma_+\gamma_-/[CO_2\cdot H_2O]$	4.45×10^{-7}
$HCO_3^- \rightleftarrows H^+ + CO_3^{2-}$	$K_{2c}=[H^+][CO_3^{2-}]\gamma_+\gamma_{2-}/[HCO_3^-]\gamma_-$	4.68×10^{-11}
$HCl(g)+H_2O \rightleftarrows HCl\cdot H_2O$	$K_{hl}=[HCl\cdot H_2O]/P_{HCl}$	19.0
$HCl\cdot H_2O \rightleftarrows H^+ + Cl^-$	$K_{1l}=[H^+][Cl^-]\gamma_+\gamma_-/[HCl\cdot H_2O]$	1.3×10^{6}
$HNO_3(g)+H_2O \rightleftarrows HNO_3\cdot H_2O$	$K_{hh}=[HNO_3\cdot H_2O]/P_{HNO_3}$	2.1×10^{5}
$HNO_3\cdot H_2O \rightleftarrows H^+ + NO_3^-$	$K_{1h}=[H^+][NO_3^-]\gamma_+\gamma_-/[HNO_3\cdot H_2O]$	15.4

$$I=\frac{1}{2}\sum_i [i]\cdot z_i^2\,, \qquad (3)$$

in which $[i]$ and z_i are the concentration and valency of i ions respectively.

In the cloud water the following electroneutrality is also established, that is

$$[H_+]+[NH_4^+]=[OH^-]+[HSO_3^-]+2[SO_3^{2-}]+[HCO_3^-]+2[CO_3^{2-}]+[Cl^-]+[NO_3^-]+2[SO_4^{2-}] \qquad (4)$$

Substituting the expressions for the equilibrium constants in Table 2 the equation (4) can be written as

$$[H^+]+\frac{K_{1a}K_{ha}[H^+]P_{NH_3}}{K_w}=\frac{K_w}{[H^+]\gamma_+\gamma_-}+\frac{K_{1s}K_{hs}P_{SO_2}}{[H^+]\gamma_+\gamma_-}+\frac{2K_{2s}K_{1s}K_{hs}P_{SO_2}}{[H^+]^2\gamma_+^2\gamma_{2-}}+\frac{K_{1c}K_{hc}P_{CO_2}}{[H^+]\gamma_+\gamma_-}+\frac{2K_{2c}K_{1c}K_{hc}P_{CO_2}}{[H^+]^2\gamma_+^2\gamma_{2-}}+\frac{K_{1h}K_{hh}P_{HNO_3}}{[H^+]\gamma_+\gamma_-}+\frac{K_{1l}K_{hl}P_{HCl}}{[H^+]\gamma_+\gamma_-}+2[SO_4^{2-}]\,. \qquad (5)$$

Since only a small amount of SO_4^{2-} is produced by the oxdation of SO_2 in cloud droplets within several minutes (for example, Larson *et al.* (1978)) it may be assumed that all the SO_4^{2-} in the droplets comes from aerosol SO_4^{2-}. If the pressure P_k of the gases k under equilibrium condition are known, equation (5) may be solved with respect to $[H^+]$ for specified values of γ_+, γ_- and γ_{2-}. According to the calculation, P_k in the cloud are expressed by

$$P_{NH_3}=\frac{\dfrac{P^0_{NH_3}\times 10^6}{24.04W}+\dfrac{2000m_{s2}}{M_sW}+\dfrac{1000m_n}{M_nW}}{\dfrac{K_{1a}K_{ha}[H^+]}{K_w}+K_{ha}+\dfrac{10^6}{24.04W}}\,, \qquad (6)$$

$$P_{SO_2}=\frac{\dfrac{P^0_{SO_2}\times 10^6}{24.04W}}{\dfrac{K_{2s}K_{1s}K_{hs}}{[H^+]^2\gamma_+^2\gamma_{2-}}+\dfrac{K_{1s}K_{hs}}{[H^+]\gamma_+\gamma_-}+\dfrac{10^6}{24.04W}}\,, \qquad (7)$$

$$P_{CO_2}=\frac{\dfrac{P^0_{CO_2}\times 10^6}{24.04W}}{\dfrac{K_{2c}K_{1c}K_{hc}}{[H^+]^2\gamma_+^2\gamma_{2-}}+\dfrac{K_{1c}K_{hc}}{[H^+]\gamma_+\gamma_-}+\dfrac{10^6}{24.04W}}\,, \qquad (8)$$

$$P_{HCl}=\frac{\dfrac{P^0_{HCl}\times 10^6}{24.04W}}{\dfrac{K_{1l}K_{hl}}{[H^+]\gamma_+\gamma_-}+\dfrac{10^6}{24.04W}}\,, \qquad (9)$$

$$P_{HNO_3}=\frac{\dfrac{P^0_{HNO_3}\times 10^6}{24.04W}+\dfrac{1000m_n}{M_nW}}{\dfrac{K_{1h}K_{hh}}{[H^+]\gamma_+\gamma_-}+\dfrac{10^6}{24.04W}}\,, \qquad (10)$$

where P_k^0 is the initial pressure of the gas k, W liquid water content (g m^{-3}), $m_{s2}=m_sb/(a+b)$, and m_s and m_n are the concentrations (g m^{-3}) of aerosol SO_4^{2-} and NO_3^- components in the atmosphere respectively. The letters a and b are respectively the concentrations (mol m^{-3}) of H_2SO_4 and $(NH_4)_2SO_4$, and M_s and M_n are respectively molecular weight of SO_4^{2-} and NO_3^-.

The SO_4^{2-} concentration in cloud water is given by

$$[SO_4^{2-}]=1000m_s/M_sW\,. \qquad (11)$$

Substituting equations (6)-(11) into equation (5), then using equations (2) and (3), $[H^+]$ may be obtained. The concentrations of the various ions may then be calculated from equations shown in Table 2. More details of the principles of the model calculation has been described elsewhere (Okita 1974, Okita and Ohta 1980).

The model calculation was conducted for the four cases shown in Table 3, where $R=a/(a+b)$

Table 3 Initial concentrations of gases and aerosol components.

Case		I	II	III	IV
$P^0_{SO_2}$	(atm)	2×10^{-9}	2×10^{-9}	2×10^{-9}	2×10^{-9}
$P^0_{NH_3}$	(atm)	2×10^{-9}	2×10^{-9}	5×10^{-9}	2×10^{-9}
P^0_{HCl}	(atm)	10^{-9}	10^{-9}	10^{-9}	10^{-9}
$P^0_{CO_2}$	(atm)	3.3×10^{-4}	3.3×10^{-4}	3.3×10^{-4}	3.3×10^{-4}
$P^0_{HNO_3}$	(atm)	variable	5×10^{-9}	5×10^{-9}	variable
m_s	(μg m^{-3})	20	20	20	10
m_n	(μg m^{-3})	0.6	0.6	0.6	0.6
R	$\{=a/(a+b)\}$	0.5	variable	variable	0.5
W	(g m^{-3})	0.2	0.2	0.2	0.2

which shows the contribution of H_2SO_4 on total sulfate.

5. Results of calculation

The results of the model calculations are shown in Figs. 7-10.

Case I: Fig. 7 indicates that with increasing $P^0_{HNO_3}$ both $[NO_3^-]$ and $[H^+]$ increase. The computed pH are 2.73 and 2.54 with $P^0_{HNO_3}$ of 5×10^{-9} and 10^{-8} atm respectively. On the other hand, there is little dependence of $[SO_4^{2-}]$, $[NH_4^+]$ and $[Cl^-]$ upon $P^0_{HNO_3}$.

Case II: Fig. 8 indicates the increase of $[H^+]$ and decrease of $[NH_4^+]$ with increasing R. There is little variation of $[SO_4^{2-}]$, $[NO_3^-]$ and $[Cl^-]$ with R. If all the sulfate is sulfric acid, pH is calculated to be 2.54.

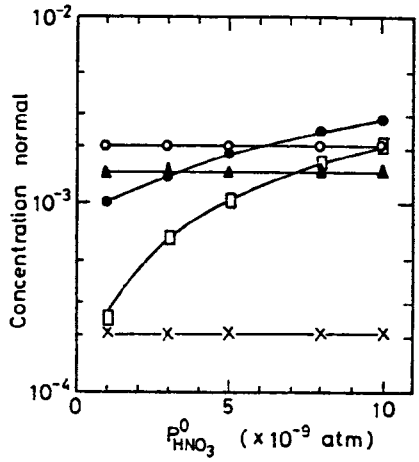

Fig. 7 Calculated concentrations of species in cloud water in case I of Table 3. ● H^+, ▲ NH_4^+, ○ SO_4^{2-}, □ NO_3^-, × Cl^-.

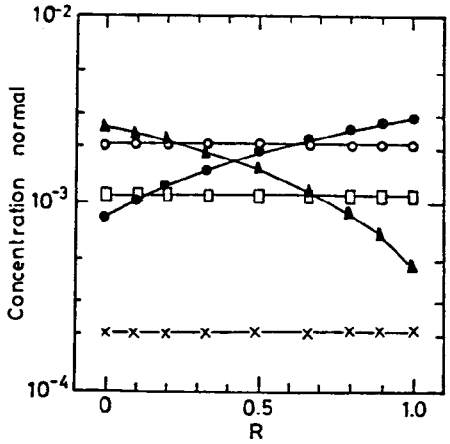

Fig. 8 Calculated concentrations of species in cloud water in case II of Table 3. Symbols in the figure are the same as in Fig. 7.

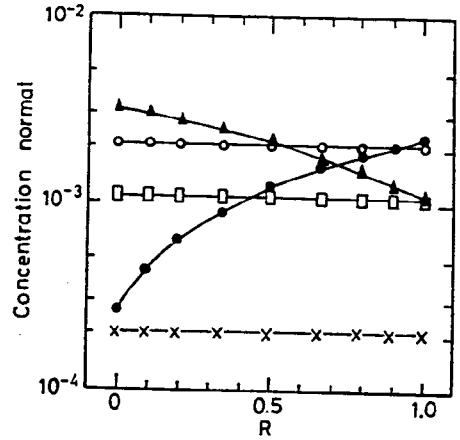

Fig. 9 Calculated concentrations of species in cloud water in case III of Table 3. Symbols in the figure are the same as in Fig. 7.

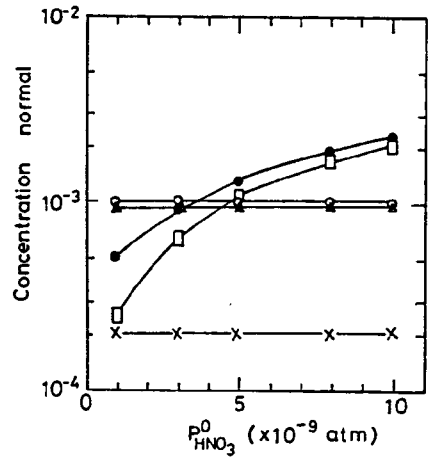

Fig. 10 Calculated concentrations of species in cloud water in case IV of Table 3. Symbols in the figure are the same as in Fig. 7.

Case III: In comparison with Fig. 8, Fig. 9 indicates that with the increase of $P^0_{NHO_3}$ $[NH_4^+]$ increases and $[H^+]$ decreases whereas little change occurs of $[SO_4^{2-}]$, $[NO_3^-]$ and $[Cl^-]$. The figure also indicates that the pH values are 2.90 and 2.64 with R of 0.5 and 1.0 respectively.

Case IV: In comparison with Fig. 7, Fig. 10 shows that when the initial concentration of SO_4^{2-} is reduced by half $[SO_4^{2-}]$, $[NH_4^+]$ and $[H^+]$ decrease whereas $[NO_3^-]$ and $[Cl^-]$ are not subject to change. The values of pH are

respectively 2.87 and 2.62 with $P^0_{HNO_3}$ of 5×10^{-9} and 10^{-8} atm.

6. Comparison of calculation with measured concentrations

The minimum pH of the cloud water collected at Mt. Tsukuba was 2.80 (Fig. 2). The measurement at Mt. Tsukuba (Okita, 1968) indicated that the mean cloud water content was about 0.2 g m^{-3}. The estimaiton of the cloud water content from the amount of water collected on wire net during the 1975-1978 observation period gave about the same content as the previous measurement.

On the top of Mt. Tsukuba the highest HNO_3 concentration was 1.5×10^{-9} atm, but it was as high as 6.5×10^{-9} atm at height of 700 m near Mt. Tsukuba as measured on board a helicopter (Okita and Ohta, 1979). On the top of Mt. Tsukuba NH_3 concentration was as high as $(2\text{-}8)\times10^{-9}$ atm probably due to its generation on the mountain, but the measurements using helicopter and tethered balloons indicated that it was about 2×10^{-9} atm at height of 500-1000 m in the free atmosphere (Okita and Ohta,

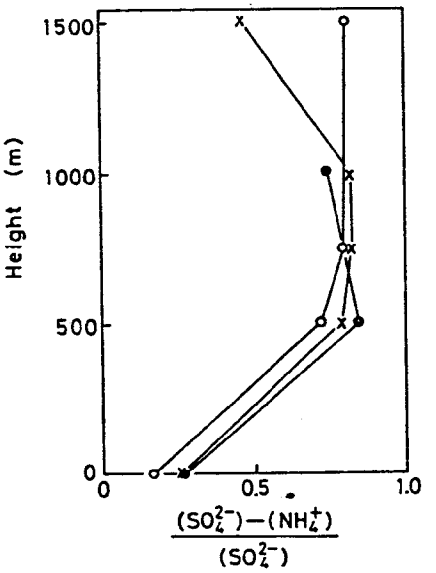

Fig. 11 The vertical distributions of the ratio of difference of equivalent concentrations of SO_4^{2-} and NH_4^+ to that of SO_4^{2-} measured in July 5-7, 1978 using a helicopter over the Kanto plain.
● July 5, ○ July 6, × July 7.

Table 4 Comparison of calculated and measured concentrations of species in cloud water.

Initial values in air			Calculated values			Measured values in cloud water		
			in cloud air					
SO_2	2×10^{-9}	atm	SO_2	1.9999×10^{-9}	atm			
NH_3	2×10^{-9}	〃	NH_3	4.91×10^{-12}	〃			
HNO_3	5×10^{-9}	〃	HNO_3	5.46×10^{-13}	〃			
HCl	10^{-9}	〃	HCl	1.37×10^{-14}	〃			
CO_2	3.3×10^{-4}	〃	CO_2	3.30×10^{-4}	〃			
W	0.2 g m^{-3}		in cloud water					
SO_4^{2-}	20 μg m^{-3}							
R	0.5		pH	2.73		pH	2.80	
NO_3^-	0.6 μg m^{-3}		H^+	1.87×10^{-3}	mol L^{-1}	H^+	1.59×10^{-3}	mol L^{-1}
			OH^-	6.21×10^{-12}	〃			
			HSO_3^-	1.94×10^{-8}	〃			
			SO_3^{2-}	8.62×10^{-13}	〃			
			SO_4^{2-}	1.04×10^{-3}	〃	SO_4^{2-}	0.89×10^{-3}	〃
			NO_3^-	1.09×10^{-3}	〃	NO_3^-	1.10×10^{-3}	〃
			NH_4^+	1.51×10^{-3}	〃	NH_4^+	1.11×10^{-3}	〃
			Cl^-	2.08×10^{-4}	〃	Cl^-	1.83×10^{-4}	〃
			HCO_3^-	3.08×10^{-9}	〃			
			CO_3^{2-}	1.02×10^{-16}	〃			
			I	4.42×10^{-3}	〃			
			γ_{+,γ_-}	0.9305				
			$\gamma_{2+,\gamma_{2-}}$	0.7497				

1979). The measurements on the top of Mt. Tsukuba indicated that the maximum SO_2 and HCl concentrations were about 2×10^{-9} and 10^{-9} atm respectively. The maximum SO_4^{2-} concentration was 21 $\mu g\,m^{-3}$ on the top of Mt. Tsukuba. No measurement has been made of the concentration of H_2SO_4 particles, but at Mt. Tsukuba SO_4^{2-} concentration was, on the average, about 30% higher than that of NH_4^+ on normality basis (Okita and Ohta, 1979). Further, it may be presumed that some H_2SO_4 collected on filter was reacted with NH_3 gas to produce $(NH_4)_2SO_4$ or NH_4HSO_4. The concentrations of SO_4^{2-} and NH_4^+ components of aerosols in the atmospheric boundary layer was measured over the Kanto plain 50 km west of Mt. Tsukuba in July 5-7, 1978 by using a helicopter. The vertical distributions of the ratio of difference of equivalent concentrations of SO_4^{2-} and NH_4^+ to that of SO_4^{2-} are shown in Fig. 11. Above the height of 500 m, this ratio becomes 0.80, but at Mt. Tsukuba the ratio seems to decrease slightly on account of the generation of gaseous NH_3 from the surface of the mountain. Therefore, there is a possibility that more than a half of the SO_4^{2-} would be H_2SO_4. The concentration of NO_3^- was usually much lower than that of SO_4^{2-}.

The above measurements indicated that there is a possibility of the formation of cloud of liquid water content of 0.2 g m^{-3} in the air of $P^0_{SO_2}=2\times10^{-9}$ atm, $P^0_{HNO_3}=5\times10^{-9}$ atm, $P^0_{NH_3}=2\times10^{-9}$ atm, $P^0_{CO_2}=3.3\times10^{-4}$ atm, $P^0_{HCl}=10^{-9}$ atm, $m_s=20\ \mu g\,m^{-3}$, $R=0.5$, $m_n=0.6\ \mu g\,m^{-3}$. The calculated gas-liquid equilibrium concentrations are as shown in Table 4, which correspond to the case of $P^0_{HNO_3}=5\times10^{-9}$ atm in Fig. 7.

Table 4 indicates that HNO_3 and HCl gases are almost completely dissolved into cloud droplets and more than 99.7% of NH_3 is also absorbed into the droplets. On the other hand, SO_2 and CO_2 are scarcely absorbed and thus the concentrations of HSO_3^-, SO_3^{2-}, HCO_3^- and CO_3^{2-} are very low. The pH value is 2.73 which is slightly lower than the minimum pH of 2.80 observed at Mt. Tsukuba. In addition, the calculated concentrations of SO_4^{2-}, NH_4^+, NO_3^- and Cl^- are close to their measured concentrations in the cloud water of pH 2.80.

Therefore it may be concluded that low pH of cloud water observed on Mt. Tsukuba may be interpreted by the incorporation of acidic aerosol such as H_2SO_4 and acidic gases such as HNO_3 and HCl into the cloud droplets even in the presence of neutralizing gases such as NH_3.

7. Discussion and conclusion

Our model calculation indicates that the pH of cloud water of less than three may be interpreted by the formation of cloud droplets upon H_2SO_4 nuclei and dissolution of HNO_3 into the droplets if both species are present in the atmosphere with concentration of about ten ppb or $\mu g\,m^{-3}$ even in the presence of NH_3.

The measurements of gaseous and particulate species and of the species in cloud water on the summit of Mt. Tsukuba and in the free atmosphere near Mt. Tsukuba confirmed the validity of our model calculation.

However, our equilibrium model may only be applied to the cloud which elapses within 20 minutes after its formation. When the cloud stays longer the chemical reaction within the cloud droplets such as those between HSO_3^- and O_3 and between NO_2^- and O_3 would produce additional H_2SO_4 and HNO_3. Further closed model may not be applied to long-lived cloud. In addition our model may be applied only to the A range in Fig. 2 and for the interpretation of higher pH value other mechanism must be incorporated.

Moreover, more detailed knowledge of the vertical and horizontal distributions of H_2SO_4 particles and HNO_3 gas and the mechanism of their formation in the atmosphere are necessary in order to more clearly understand the mechanism of the formation of acid precipitation.

Acknowledgements

The authors express their thanks to the Japanese Environment Agency for their financial support of their work.

References

Davis, W., Jr., and H. J. de Bruin, 1964: New activity coefficients of 0-100 percent aqueous nitric acid. *J. Inorg. Nucl. Chem.*, **26**, 1069-1083.

Hales, J. M., and D. R. Drewes, 1979: Solubility of ammonia in water at low concentrations. *Atmospheric Environment*, **13**, 1133-1148.

Kadowaki, S., 1976: Size distribution of atmospheric total aerosols, sulfate, ammonium and nitrate particles in the Nagoya area. *Atmospheric Environment*, **10**, 39-43

———, 1977: Size distribution and chemical composition of atmospheric particulate nitrate in the Nagoya area. *Atmospheric Environment*, **11**, 671-675.

Kato, S., N. Ono, and H. Tohata, 1978: A basic

study of treatment of NOx in wet system (Absorption of NOx into and subsequent reaction with water). Abstracts of 19th Annual Meeting of the Japan Air Pollution Soc., 469 (in Japanese).

Larson, T. V., N. R. Horike, and H. Harrison, 1978: Oxidation of sulfer dioxide by oxygen and ozone in aqueous solution: a kinetic study with significance to atmospheric rate processes. *Atmospheric Environment*, **12**, 1597-1611.

Mason, B. J., 1971: The physics of clouds, Oxford Univ. Press, p. 26.

Okita, T., 1968: Concentration of sulfate and other inorganic materials in fog- and cloud-water and in aerosol. *J. Meteor. Soc. Japan*, **46**, 120-127.

———, 1974: Mechanism of formation of acid rain (II). *Taikiosen-kenkyu*, **9**, 176 (in Japanese).

———, 1978: Recent investigation of transformation and deposition of atmospheric constituents. *Tenki*, **25**, 110-119 (in Japanese).

Okita, T., and S. Ohta, 1979: Measurement of nitrogeneous and other compounds in the atmosphere and in cloud-water: A study of the mechanism of formation of acid precipitation. Nitrogeneous Air Pollutants, Chemical and Biological Implications. Grosjean, D. ed., Ann Aabor Science, 289-305.

———, 1980: Acid Rain. Analysis of Mechanism of Air Pollution. Suzuki, T. ed., Sangyo Toshyo, 203-231 (in Japanese).

Orel, A. E., and J. H. Seinfeld, 1977: Nitrate formation in atmospheric aerosols. *Envir. Sci. Technol.*, **11**, 1000-1007.

Scott, B. C., and N. S. Laulainen, 1979: On the concentration of sulfate in precipitation. *J. Appl. Meteor.*, **18**, 138-147.

雲水の酸性化機構の数値モデル

太田幸雄・大喜多敏一
北海道大学工学部衛生工学科

加藤千明
住友電気工業株式会社

雲水の酸性化機構について数値計算を行った。雲粒は粒子状硫酸，硫酸塩，硝酸塩を凝結核として形成されるものとし，また，酸性及びアルカリ性ガスを吸収して非常に短い時間で気液平衡状態に達するものと仮定した。実際に観測によって求められた環境大気中のガス及びエアロゾル成分の濃度を初期濃度として計算を行ったところ，pH 3 の雲水が得られた。このモデル計算によって，筑波山頂において観測された雲水の pH，雲水中の SO_4^{2-}, NO_3^- 及び他成分の濃度を非常によく再現することができる。

URBAN OZONE MODELING DEVELOPMENTS IN THE U.S.

presented by B. Dimitriades

Environmental Sciences Research Laboratory

USEPA

This discussion will deal (a) with the results from recent efforts in the U.S. to develop and evaluate urban O_3 models, (b) with the main imperfections in the O_3 models currently in existence in the U.S., and (c) with some suggestions for additional research needed in this area that could be done independently or cooperatively with Japan.

There are three types of urban O_3 models now in use or contemplated in the U.S.:

(A) Mechanistic or EKMA-Type Models

These models predict O_3 concentrations from VOC and NO_x concentrations in ambient air. The precursor concentrations are either measured directly or are estimated from emission rates through simple dilution calculations. The relationships between O_3 and precursor concentrations are used in the form of O_3 isopleth curves derived from the chemical mechanism. Dispersion is not treated by the model but advection effects are treated in the "trajectory" form of the EKMA model. For application, we need to know primarily the max. O_3 concentration (or 90-percentile or etc.) and the VOC/NO_x ratio during 6-9 am. For more accuracy, we need to input also information on background pollutant concentrations, diurnal mixing height variation, and post-9-am hourly emission rates. The model is used in a relative sense, that is, to predict O_3 changes from precursor changes. Ideally, therefore, the model should be evaluated by comparison against observations of O_3 air quality changes. There are several USEPA documents describing the EKMA model, which have been sent to Japan.

(B) Air Quality Simulation Models (AQSM)

Unlike EKMA, the AQSMs treat emission dispersion in detail, which enhances model validity but it also adds considerable complexity. The AQSMs treat chemistry with detail which currently is comparable to that of the EKMA chemistry. Unlike EKMA, however, the computer capacity demands associated with the greater spatial detail of the AQSMs put a limit to the detail with which AQSMs can treat chemistry. The AQSM models are designed to predict absolute air qualities, and their evaluation, therefore, is done by comparison against absolute air quality observations.

(C) Photochemical Box Models (PBM)

These are models which with respect to conceptual validity and complexity lie between EKMA and AQSM. They treat chemistry with detail comparable to that of EKMA, and advection as with the "trajectory" form of EKMA; they do not treat horizontal or vertical dispersion. Unlike EKMA, the PBM does not use O_3-isopleths to compute O_3 from VOC and NO_x inputs; it relies instead on built-in mathematics. Also, unlike EKMA, it has been designed to predict absolute air quality; its evaluation, therefore, is based on comparison against absolute air quality observations.

Evaluation status and availability of these models is as follows. Three AQSMs and one PBM have been evaluated against field data taken in the St. Louis area during 1974-1977 (RAPS data). This evaluation and results are discussed in detail in the EPA Report "Final Evaluation of Urban Scale Photochemical AQSMs" (sent to Japan), and in a summary form in a report by Schere and Shreffler (attached here). Briefly, the three AQSMs were a Langrangian model developed by ERT (ELSTAR) , and two Eulerian, grid-type models developed by Lawrence Livermore Laboratory (LIRAQ) and by Systems Applications, Inc. (SAI), respectively. The fourth model was a PBM using a chemical mechanism developed by Demerjian. First results from the LIRAQ evaluation showed such a poor model performance that they discouraged further evaluation of the model. Results from the other model evaluations are illustrated in Figure 1 and Tables 1 and 2. Of these models, the ELSTAR is now available for use; the SAI and PBM will take a few more months before they are completely documented and ready for use by others.

Evaluation of the EKMA model was discussed in detail in a previous presentation in this Conference (Photochemical Pollution Panel). Briefly, evaluation efforts in the last two years included a comparison of the EKMA mechanism with other mechanisms currently in existence in the U.S., and evaluations against field data. The mechanism intercomparison effort revealed substantial disagreements suggesting that most or all of the intercompared chemical mechanisms have inaccuracies, a problem that, obviously, affects not EKMA only, but all models that include an O_3-chemistry component. The field validations were all of limited conclusiveness for a number of reasons, discussed in detail in an EKMA Workshop conducted by USEPA in December, 1981 (Workshop Proceedings have been sent to the Japanese Environment Agency). The EKMA model and guidelines for its use are currently available for use.

Imperfections in the current models exist in all their components, that is, in the emissions, emission dispersion, and chemistry modules. The chemical composition of the VOC emissions, as measured currently, has uncertainties, one problem being that the currently available emission composition data were taken for the most part from laboratory testing of emissions and do not necessarily reflect actual composition in the ambient air. The horizontal advection model component also is subject to errors because of "artificial diffusion" caused by the finite difference numerical advection algorithm. Lastly, the chemistry module is subject to uncertainties, as revealed from the EKMA mechanism intercomparison study.

While some research is being conducted in the U.S. in response to the above problems, we believe that additional efforts done cooperatively by Japan and the U.S. will be of considerable value. Specifically, as we have already discussed in the Photochemical Pollution panel meeting, we propose a cooperative mechanism intercomparison study that will include this time the Carter/Akimoto (and other) mechanism(s) not included in the U.S. studies. We would propose, further, testing of existing urban O_3 models against air quality data for Japanese urban areas (such as Tokyo). In a more general sense, we would invite our Japanese colleagues to participate in efforts to develop standard sets of chemical kinetic data, of smog chamber data, and of field data, against which existing and new urban O_3 models could be evaluated.

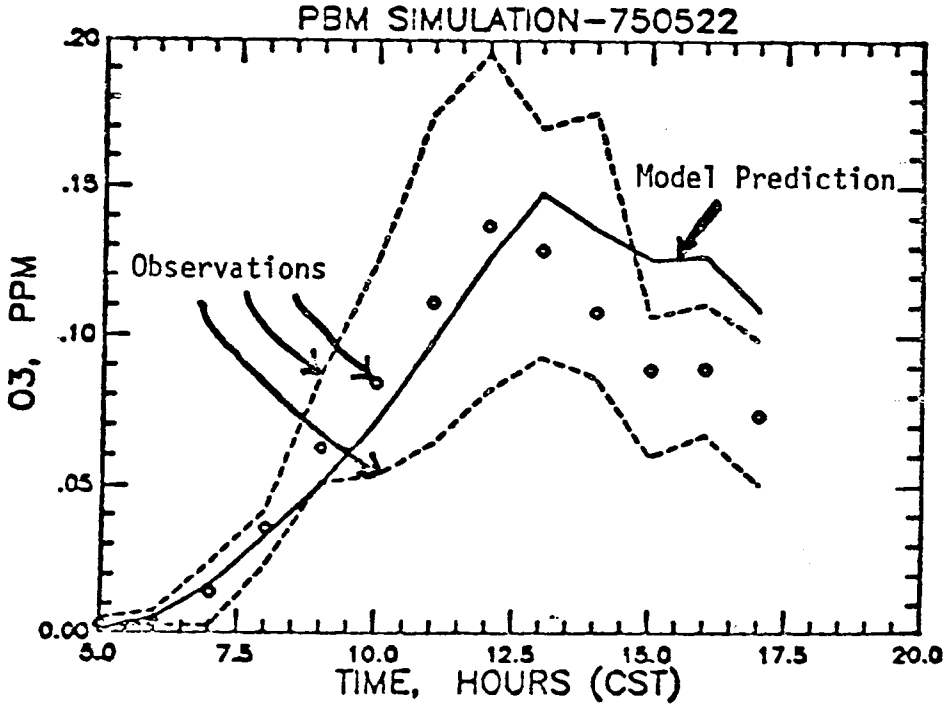

Figure 1. PBM simulation results for O_3 - Day 142 of 1975.

TABLE 1. A SUMMARY OF PREDICTED AND OBSERVED O_3 MAXIMA FROM THE ELSTAR FOR 20 DAYS SELECTED FROM 1975-1976.

Day	Hour	Station	Observed 4-meters (ppm)	LPM Predicted Level-1 (ppm)	LPM Predicted Level-3 (ppm)
142 (1975)	12	101	0.20	0.07	0.13
178	14	112	0.20	0.15	0.31
182	12	125	0.16	0.25	0.24
183	15	124	0.21	0.18	0.18
184	13	118	0.18	0.21	0.22
207	14	113	0.18	0.11	0.13
209	11	118	0.21	0.14	0.15
221	15	121	0.17	0.16	0.16
230	13	121	0.19	0.18	0.17
231	14	121	0.23	0.19	0.19
251	14	122	0.26	0.29	0.30
159 (1976)	15	122	0.20	0.18	0.18
160	16	115	0.22	0.21	0.23
195	15	114	0.22	0.15	0.15
211	15	120	0.16	0.11	0.12
212	12	108	0.17	0.10	0.11
225	13	117	0.17	0.08	0.09
226	13	109	0.23	0.20	0.22
237	11	120	0.18	0.30	0.29
275	14	102	0.24	0.26	0.30

TABLE 2. A SUMMARY OF PREDICTED AND OBSERVED O_3 MAXIMA FOR THE SAI

Julian date[a]	Hour (CST)	Station	Observed at 4-meters (ppm)	UAM Predicted Specific (ppm)	UAM Predicted Independent (ppm)
142 (1975)	12	101	0.195	0.116	0.238
178	14	112	0.202	0.156	0.243
182	11	121[b]	0.142	0.083	0.166
183	10	119[b]	0.171	0.154	0.209
184	13	118	0.184	0.132	0.234
207	14	113	0.185	0.141	0.252
209	11	118	0.209	0.128	0.195
221	15	121	0.166	0.118	0.149
230	13	121	0.193	0.095	0.214
231	14	121	0.233	0.133	0.205
251	12	121[b]	0.179	0.146	0.178
159 (1976)	14	114[b]	0.172	0.142	0.312
160	16	115	0.221	0.121	0.190
195	15	114	0.223	0.160	0.174
211	15	120	0.155	0.143	0.169
212	12	108	0.170	0.128	0.155
225	13	117	0.166	0.050	0.073
226	13	109	0.225	0.077	0.124
237	11	120	0.176	0.119	0.203
275	14	102	0.244	0.220	0.246

[a]Twenty days selected from 1975 and 1976.
[b]Overall maximum at 122, 123, 124, or 125; outside SAI domain.

URBAN-SCALE PHOTOCHEMICAL MODEL EVALUATIONS FOR OZONE USING RAPS DATA

Kenneth L. Schere and Jack H. Shreffler

Meteorology and Assessment Division
Environmental Sciences Research Laboratory
Environmental Protection Agency
Research Triangle Park, North Carolina 27711

1. INTRODUCTION

The Regional Air Pollution Study (RAPS) was conducted in the St. Louis area over the period 1974-1977 (Schiermeier, 1978). RAPS was designed to provide a comprehensive data set for the testing and evaluation of numerical air quality simulation models on an urban scale. This paper describes some of the evaluation tests that have been performed by EPA on three such models. One, a relatively simple box-type model, was constructed at EPA's Meteorology Laboratory. The second, a Lagrangian model, was developed by Environmental Research and Technology, Inc. of Santa Barbara, California, and the third, a 3-D grid model, was developed by Systems Applications, Inc. of San Rafael, California.

This paper summarizes the results of simulations for 20 days where maximum 1-hr ozone concentrations were observed at 0.16 to 0.26 ppm in St. Louis. Generally these days exhibited stagnation conditions with little cloud cover and represented the situations conducive to production of photochemical smog from local emissions (Table 1). The simulations were designed to evaluate the ability of the 3 models to reproduce the observed ozone maxima.

2. PHOTOCHEMICAL BOX MODEL

The Photochemical Box Model (PBM) is a single cell Eulerian air quality simulation model whose purpose is to simulate the transport and chemical transformation of air pollutants in smog prone urban atmospheres. The model's domain is set in a variable volume, well mixed reacting cell where the physical and chemical processes responsible for the generation of ozone by its hydrocarbon and nitrogen oxides precursors are mathematically created.

In the application of the model to the St. Louis RAPS data

TABLE 1. A SUMMARY OF WIND SPEED (WS), WIND DIRECTION (WD), TEMPERATURE, SOLAR RADIATION (ALL WAVELENGTHS), AND MAXIMUM AFTERNOON MIXING HEIGHT (MH) FOR THE 20 DAYS EXAMINED.*

Date	Day (Julian)	WS (m/s)	WD (deg)	Temp (°C)	Solar (ly/min)	Max MH (m)
5/22/75	142	1.1	224	29	1.12	1504
6/27/75	178	0.4	245	29	0.96	1822
7/01/75	182	1.4	70	29	0.99	2606
7/02/75	183	1.4	15	30	0.92	2488
7/03/75	184	1.8	324	30	0.85	1875
7/26/75	207	1.0	139	26	0.98	1477
7/28/75	209	2.0	18	30	0.98	1909
8/09/75	221	0.4	88	26	0.98	1195
8/18/75	230	1.6	167	27	0.96	1488
8/19/75	231	1.3	168	28	0.95	1052
9/08/75	251	1.8	181	25	0.89	1797
6/07/76	159	1.0	129	25	1.06	1972
6/08/76	160	1.3	284	27	1.01	1772
7/13/76	195	2.3	145	28	1.02	1853
7/29/76	211	0.3	251	26	0.53	1706
7/30/76	212	1.7	205	30	0.82	1304
8/12/76	225	2.3	253	29	0.70	730
8/13/76	226	1.1	273	30	0.86	1427
8/24/76	237	1.3	110	28	0.82	2124
10/01/76	275	0.6	222	22	0.78	527

*Meteorological variables (except MH) are network averages over the period 0700-1359 CST.

base the horizontal length scale of the single cell was 20 km and the vertical scale was time-varying, proportional to the depth of the mixed layer. The model domain was centered on downtown St. Louis such that the 20x20 km area encompassed most of the major emissions sources on either side of the Mississippi River. Source emissions were assumed to be distributed uniformly across the surface face of the cell. Twelve of the surface monitoring stations as well as one upper air sounding location were also located within the cell's boundaries.

The PBM contains a chemical kinetic mechanism with 36 reactions and 27 reactive species. The set of equations describing the rates of change of the concentrations of these species is numerically solved at time steps on the order of 10 minutes. Model simulation is started at 0500 CST and continues through 1700 CST. From these solutions the model then determines the hour-average predicted concentrations of all modeled species. The simulated concentrations from the PBM represent spatial averages over the volume of the box.

Table 2 presents a summary of the predicted and PBM domain-average observed ozone maxima and an elementary statistical analysis of the results for all 20 modeled days. The 'specific' model predictions are those that correspond to the same hour as the observed maximum and the 'independent' predictions represent the peak at any hour of the simulation. The specific and independent predictions may not coincide, indicating a phase lag between observed and predicted ozone peaks. This lag often appears when the maximum observed ozone within the model domain occurs before noon. Statistics on the residual concentration have been computed for both the specific and independent predictions. Both the average signed residual and absolute residual, and standard deviation (s.d.) are presented for the analyses.

The average residual is negative in both the specific and independent cases, indicating an overprediction of ozone, although the specific value is half the independent value. The value of the average absolute residuals are both different than the signed residuals. This implies that there were underpredictions as well as overpredictions among the individual days. The magnitude of the s.d. is slightly greater than the average residual. The discrepancy on Day 251 accounts for a good portion of the s.d. The average value of the model's overprediction for ozone over all 20 days is 23%.

3. LAGRANGIAN PHOTOCHEMICAL MODEL

The Lagrangian Photochemical Model (LPM) envisions a portion of the atmosphere as an identifiable parcel. As the parcel moves over the region, pollutants are assimilated, vertically mixed, and subjected to photochemical reactions in the presence of solar

TABLE 2. A SUMMARY OF PREDICTED AND OBSERVED O_3 MAXIMA FOR THE PBM

Julian date[a]	Hour (CST)	Observed at 4-meters (ppm)	PBM Predicted Specific (ppm)	PBM Predicted Independent (ppm)
142 (1975)	12	0.137	0.125	0.148
178	14	0.159	0.162	0.173
182	13	0.094	0.128	0.140
183	13	0.115	0.070	0.097
184	13	0.114	0.182	0.182
207	14	0.140	0.144	0.145
209	10	0.108	0.087	0.122
221	13	0.132	0.125	0.125
230	13	0.072	0.096	0.119
231	10	0.084	0.059	0.101
251	15	0.084	0.205	0.205
159 (1976)	13	0.125	0.203	0.210
160	14	0.162	0.166	0.170
195	15	0.151	0.132	0.137
211	15	0.094	0.084	0.088
212	12	0.127	0.114	0.121
225	12	0.111	0.088	0.092
226	15	0.144	0.171	0.171
237	11	0.115	0.132	0.156
275	14	0.183	0.216	0.223

[a]Twenty days selected from 1975 and 1976.

For the data displayed above:

ΔC = Obs - Specific

$\overline{\Delta C} = -0.012$

s.d.(ΔC) = 0.039

$\overline{|\Delta C|} = 0.029$

ΔC = Obs - Independent

$\overline{\Delta C} = -0.024$

s.d.(ΔC) = 0.036

$\overline{|\Delta C|} = 0.031$

radiation. The parcel expands along its trajectory at a rate proportional to a Gaussian sigma-y derived from the stability class. The LPM is attractive relative to grid models in that it is fairly simple to execute and uses a moderate amount of computer time.

The model is executed using a series of modules, sequentially performing calculations on meteorology and air quality, emissions and photochemistry. The input and running procedures described by Lurmann et al. (1979) have been followed generally, although some modifications were deemed necessary as more experience with the RAPS data base was acquired.

The first step in setting up a simulation is to determine the starting point of a parcel so that it will arrive at a specified point at an assigned time. A backward trajectory is generated by inverse-distance squared weighting of winds from the closest 3 monitoring stations. However, experience with wind data suggests that even closely situated stations can show large unexplained differences in wind vectors from time to time. Reliance on a single, anomalous station, if the parcel has a close approach, can create an erratic trajectory. To eliminate the possibility of such vagaries, it was decided to compute a single resultant wind vector from the network and assign it to all stations for the hour. The start time of a parcel (which is on the hour) must be at least 10 min past local sunrise. Once the start position is set, the model is run in a forward-trajectory mode until 1800 CST or the parcel leaves the region.

In most cases, the parcel starts in a relatively clean rural environment, and levels of hydrocarbons, nitric oxide and nitrogen dioxide are assumed to decrease with height according to an assigned formula. On the other hand, ozone is depleted near the ground at night; thus, the initial ozone profile increases with height.

Table 3 presents a summary of the predicted and observed ozone maxima and a statistical evaluation of the results for the 20 days of the study. The prediction refers to the model prediction at the time and position of the observed ozone maximum. The residuals are calculated for both the first (L-1) and the third (L-3) vertical model level predictions. The average residual for L-1 indicates slight underprediction, while the average residual for L-3 is essentially zero. For both levels, the s.d.'s are identical, and the average absolute deviations are nearly so.

4. URBAN AIRSHED MODEL

The Urban Airshed Model (UAM) is a 3-D grid-type, or Eulerian, photochemical air quality simulation model (PAQSM). The structure of the model consists of a latticework array of cells, the total volume of which represents an urban-scale domain and in which the

TABLE 3. A SUMMARY OF PREDICTED AND OBSERVED O_3 MAXIMA FROM THE LPM FOR 20 DAYS SELECTED FROM 1975-1976.

Day	Hour	Station	Observed 4-meters (ppm)	LPM Predicted Level-1 (ppm)	LPM Predicted Level-3 (ppm)
142 (1975)	12	101	0.20	0.07	0.13
178	14	112	0.20	0.15	0.31
182	12	125	0.16	0.25	0.24
183	15	124	0.21	0.18	0.18
184	13	118	0.18	0.21	0.22
207	14	113	0.18	0.11	0.13
209	11	118	0.21	0.14	0.15
221	15	121	0.17	0.16	0.16
230	13	121	0.19	0.18	0.17
231	14	121	0.23	0.19	0.19
251	14	122	0.26	0.29	0.30
159 (1976)	15	122	0.20	0.18	0.18
160	16	115	0.22	0.21	0.23
195	15	114	0.22	0.15	0.15
211	15	120	0.16	0.11	0.12
212	12	108	0.17	0.10	0.11
225	13	117	0.17	0.08	0.09
226	13	109	0.23	0.20	0.22
237	11	120	0.18	0.30	0.29
275	14	102	0.24	0.26	0.30

For the data displayed above:

ΔC = Obs minus L-1 Pred

$\overline{\Delta C} = 0.023$

s.d.(ΔC) = 0.058

$\overline{|\Delta C|} = 0.052$

ΔC = Obs minus L-3 Pred

$\overline{\Delta C} = 0.005$

s.d.(ΔC) = 0.058

$\overline{|\Delta C|} = 0.050$

physical and chemical processes responsible for photochemical smog are mathematically simulated. The horizontal dimensions of each cell are constant but the heights of the cells vary throughout a model simulation as the depth of the mixed layer in the UAM changes accordingly.

In the application of the model to the St. Louis data base, the area modeled was 60 km wide and 80 km long. Each individual cell was 4 km on a side in the horizontal. Vertically, there were 4 layers of cells in total; the bottom 2 layers simulated the mixed layer and the top 2 represented the region immediately above the mixed layer. The domain of the UAM was centered just west of downtown St. Louis and included the entire metropolitan area.

The package of programs constituting the UAM actually contains 12 data preprocessing programs as well as the simulation model. The data requirements for applying the model are rather intensive. The preprocessors access the RAPS surface-based hour-average air quality and meteorological data base, the upper air pibal and radiosonde data, and the source emissions inventory for the necessary parameters, and process the parameters as required by the simulation model. Simulations begin at 0500 CST and continue through 1700 CST. The model numerically calculates the rates of change of species concentrations at time steps on the order of several minutes, and then determines from these the hour-average predicted concentrations.

Table 4 presents a summary of the predicted and observed ozone maxima and a statistical analysis of the UAM results for all 20 modeled days. The 'specific' model predictions are those that correspond to the same location and time as the observed maximum and the 'independent' predictions represent the maximum hour-average ozone generated by the model at any lowest layer grid cell at any time during the simulation. The specific and independent model predictions, as seen in Table 4, typically do not coincide. This indicates that the maximum value of ozone produced by the model did not correspond either in space or time, or both, to the maximum value observed in the atmosphere. Statistics on the residual concentration, as shown below, have been computed for both the specific and independent predictions. Moreover, the average signed residual and s.d. are presented for the analysis.

Values of the average residual for the specific and independent cases, 0.062 and -0.006 ppm respectively, differ noticeably. The independent predictions show more promise toward maximum ozone simulation. The average absolute residual is much larger than the average signed residual in the independent case, indicating both over- and underpredictions among the 20 days tested. In the specific case however, the average signed and absolute residuals are identical, signifying that the model has underpredicted consistently over all 20 days. The s.d.'s of the specific and independent residuals are 0.035 and 0.053 ppm respectively. The model's average performance for maximum ozone

TABLE 4. A SUMMARY OF PREDICTED AND OBSERVED O_3 MAXIMA FOR THE UAM

Julian date[a]	Hour (CST)	Station	Observed at 4-meters (ppm)	UAM Predicted Specific (ppm)	UAM Predicted Independent (ppm)
142 (1975)	12	101	0.195	0.116	0.238
178	14	112	0.202	0.156	0.243
182	11	121[b]	0.142	0.083	0.166
183	10	119[b]	0.171	0.154	0.209
184	13	118	0.184	0.132	0.234
207	14	113	0.185	0.141	0.252
209	11	118	0.209	0.128	0.195
221	15	121	0.166	0.118	0.149
230	13	121	0.193	0.095	0.214
231	14	121	0.233	0.133	0.205
251	12	121[b]	0.179	0.146	0.178
159 (1976)	14	114[b]	0.172	0.142	0.312
160	16	115	0.221	0.121	0.190
195	15	114	0.223	0.160	0.174
211	15	120	0.155	0.143	0.169
212	12	108	0.170	0.128	0.155
225	13	117	0.166	0.050	0.073
226	13	109	0.225	0.077	0.124
237	11	120	0.176	0.119	0.203
275	14	102	0.244	0.220	0.246

[a]Twenty days selected from 1975 and 1976.
[b]Overall maximum at 122,123,124, or 125; outside UAM domain.

For the data displayed above:

ΔC = Obs - Specific

$\overline{\Delta C}$ = 0.062

s.d.(ΔC) = 0.035

$\overline{|\Delta C|}$ = 0.062

ΔC = Obs - Independent

$\overline{\Delta C}$ = -0.006

s.d.(ΔC) = 0.053

$\overline{|\Delta C|}$ = 0.041

over all simulations shows a 32.4% underprediction in the specific case and a 4.4% overprediction in the independent.

5. CONCLUSIONS

The evaluation of the PBM, LPM and UAM for ozone is now completed by the Meteorology Division of EPA. A full report documenting the study is currently being prepared (Schere and Shreffler, 1982).

Evidence shows the PBM to be a useful tool in assessing area-wide urban air quality for photochemically reactive pollutants, especially in stagnation conditions. In order for this model to be a better aid to the regulatory community, the relationship between the average ozone concentration predicted within the model domain and the maximum ozone level observed at a single station must be studied.

The LPM also shows promise to be an effective aid in understanding urban ozone production. The model is relatively easy to use, inexpensive to execute, and seems immune to various execution errors which tend to arise unexpectedly in complex computations of this sort.

From the work performed on the UAM it is clear that the potential use of a grid-type PAQSM such as this one is great, although the complexity of the model often makes the solution of problems that arise more difficut. The model evaluation effort discussed here has shown the UAM to simulate ozone maxima in an independent sense in St. Louis quite well, although generally underpredicting in a specific sense.

REFERENCES

Lurmann, F., D. Godden, A.C. Lloyd, and R.A. Nordsieck, 1979: A Lagrangian Photochemical Air Quality Simulation Model. Vol. I-Model Formulation, Vol. II-User's Manual. EPA-600/8-79-015a,b (available from NTIS as PB 300470 and PB 300471).

Schere, K.L. and J.H. Shreffler, 1982: Final Evaluation of Urban-Scale Photochemical Air Quality Simulation Models. EPA Report, U.S. Environmental Protection Agency, Research Triangle Park, NC (in press).

Schiermeier, F.A., 1976: Air monitoring milestones: RAPS field measurements are in. Environ. Sci. Technol., 12, 644-651.

A NUMERICAL SIMULATION OF LOCAL WIND AND PHOTOCHEMICAL AIR POLLUTION

presented by F. Kimura

Meteorological Research Institute

Japan MA

A Numerical Simuration of Local Wind and Photochemical Air pollution

Fujio Kimura

Meteorological Research Institute, Tsukuba, Japan

Presented at 7th Japan-US Joint Meeting on Air Pollution Related Meteorology and Photochemical air pollution (Nov.29-Dec.2,1982, in Tokyo and Tsukuba)

1. Introduction

A number of different numerical models on the photochemical smog have been developed during the last ten years in the U.S.A. and also in Japan. Some models among them have fairly succeeded to simulate ozone or other pollutants concentration.
At the same time, however, many difficult problems to be solved have been pointed out. One of the most important common problem of these models is a lack of meteorological data such as upper wind, vertical diffusivity, mixing depth etc. It is well known that the accuracy of these data has a very strong effect on the results. This problem is more important in case of air pollution in complex local wind system including land and sea breeze and mountain and valley wind. However, it is very high cost to make field observation of three dimensional wind system.

In this study, numerical simulation on the photochemical air pollution under an idealized local wind system is carried out by a two step numerical model in order to make clear the fundamental characteristics of the effect of the local wind upon the photochemical air pollution.

Fig.1 is a flow-chart of the model. The first step is a three-

dimensional time-dependent local wind model, which calculates wind velocity and vertical diffusion coefficient under the given condision such as large scale wind, topography and ground surface condition. The second step is a photochemical air pollution model which is also three dimensional model by using the result of the first step model as input data. The second step model is further constructed with two sub-models, a diffusion and advection model and a photochemical reaction model.

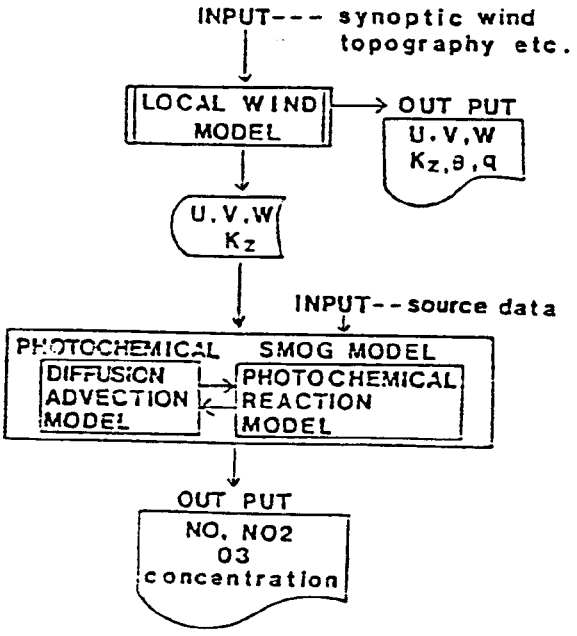

Fig.1 A flow-chart of the two step model

We assumed an idealized photochemical reaction in place of the actual reaction which is very complex. Some models of the photochemical reaction have been developed well, but not compleatly established yet. Moreover, they need detail infomation on the emission data espetially on non-CH4 hydrocarbons, which is difficult to obtain. In this study, we do not intend to simulate the reaction process in detail, but outline of the reaction process. The idealized photochemical reaction model is simple,

but the feature of it, espetialy ozone concentration behaviour, is very close to the artual reaction. The idealized reaction model is derived from more complex photochemical reaction model by a kind of mathematical apploximation.

2. Numerical model

1) Local wind model

The governing equations and numerical integration scheme of the model are almost the same as the local wind model developed by Kikuchi et.al(1981). The equations are Boussinesq hydrostatic equations which are written in the terrain-following coordinate system.

Equations of mortion:

$$\frac{\partial hu}{\partial t}+\frac{\partial huu}{\partial x}+\frac{\partial huv}{\partial y}+\frac{\partial huw^*}{\partial z^*}=fhv-h\theta\frac{\partial x'}{\partial x}+gh\frac{\theta'}{\theta}\frac{z_T-z^*}{z_T}\frac{\partial z_G}{\partial x}+h\frac{\partial}{\partial x}\left(K_H\frac{\partial u}{\partial x}\right)+h\frac{\partial}{\partial y}\left(K_H\frac{\partial u}{\partial y}\right)+\frac{z_T^*}{h}\frac{\partial}{\partial z^*}\left(K_m\frac{\partial u}{\partial z^*}\right) \quad (1)$$

$$\frac{\partial hv}{\partial t}+\frac{\partial huv}{\partial x}+\frac{\partial hvv}{\partial y}+\frac{\partial hvw^*}{\partial z^*}=-fhu-h\theta\frac{\partial x'}{\partial y}+gh\frac{\theta'}{\theta}\frac{z_T-z^*}{z_T}\frac{\partial z_G}{\partial y}+h\frac{\partial}{\partial x}\left(K_H\frac{\partial v}{\partial x}\right)+h\frac{\partial}{\partial y}\left(K_H\frac{\partial v}{\partial y}\right)+\frac{z_T^*}{h}\frac{\partial}{\partial z^*}\left(K_m\frac{\partial v}{\partial z^*}\right) \quad (2)$$

Equation of thermodynamics:

$$\frac{\partial h\theta'}{\partial t}+\frac{\partial h\theta' u}{\partial x}+\frac{\partial h\theta' v}{\partial y}+\frac{\partial h\theta' w^*}{\partial z^*}=h\frac{\partial}{\partial x}\left(K_H\frac{\partial\theta'}{\partial x}\right)+h\frac{\partial}{\partial y}\left(K_H\frac{\partial\theta'}{\partial y}\right)+\frac{z_T^2}{h}\frac{\partial}{\partial z^*}\left(K_h\frac{\partial\theta'}{\partial z^*}\right) \quad (3)$$

Continuity equation:

$$\frac{\partial hu}{\partial x}+\frac{\partial hv}{\partial y}+\frac{\partial hw^*}{\partial z^*}=0 \quad (4)$$

Equation of mixing ratio:

$$\frac{\partial hq}{\partial t}+\frac{\partial hqu}{\partial x}+\frac{\partial hqv}{\partial y}+\frac{\partial hqw^*}{\partial z^*}=h\frac{\partial}{\partial x}\left(K_H\frac{\partial q}{\partial x}\right)+h\frac{\partial}{\partial y}\left(K_H\frac{\partial q}{\partial y}\right)+\frac{z_T^2}{h}\frac{\partial}{\partial z^*}\left(K_h\frac{\partial q}{\partial z^*}\right) \quad (5)$$

where z^* is the terrain-following vertical coordinate defined as

$$z^*=z_T\frac{z-z_G}{h} \qquad h=z_T-z_G$$

in which z_T and z_G are the level of the top and the ground surface of the model atmosphere respectively. w^* is the vertical z^*-velocity, and other symbols are of usual.

The considered area is 450 km square and coverd by 30x30 grid points at the interval of 15 km in the horizontal plane. The vertical thichness of the model atmosphere is 6000m and divided into 15 layers with larger interval in upper layers.

The ground surface temperature θ_0 is predicted by the force restore method(Bhumralker,1975), which agrees very well to the multiple soil layers model(Deardorff,1978). θ_0 is written as follows:

$$\frac{\partial \theta_0}{\partial t} = \frac{1}{C_1}(S+L-H-\ell E) - \frac{1}{C_2}(\theta_0 - \theta_1) \qquad (6)$$

Where, S is total solar radiation, L is net long wave radiation, H is sensible heat flux, ℓE is latent heat flux, θ_1 is the soil temperature to be constant in the certain depth, and C_1 and C_2 are the soil characteristic parameters.

The vertical diffusion coefficient, which is very important to vertical transport of heat and pollutants, is calculated from the turbulent closure model (level 2) by Mellor and Yamada.

2) Diffusion and advection model

The equation is written in the terrain followins coordinate system which is the same as the local wind model.

$$\frac{\partial hC_i}{\partial t} + \frac{\partial hC_i u}{\partial x} + \frac{\partial hC_i v}{\partial y} + \frac{\partial hC_i w^*}{\partial z^*} = \frac{z_T^*}{h}\frac{\partial}{\partial z^*}K\frac{\partial C_i}{\partial z^*} + hQ_i + hR_i \ (i=1,2\cdots n) \qquad (7)$$

where, C_i, Q_i and R_i are concentration, source emission and formation rate by the reaction of the i-th pollutant, respectively. Boundary condition at the ground surface is given by the following equation which means surface dry deposition.

$$F_i \equiv \left(K\frac{\partial C_i}{\partial z}\right)_{z=0} = -v_{di}(z_1)\ C_i(z_1) \qquad (8)$$

where $v_{di}(z_1)$ is the deposition velocity definded at the level of 1m. As the lowest level of the model is z_1=25m, concentration at z=1m is

calculated by the followind equation under the assumption of a constant flux layer of pollutans.

$$C(z_1) = C(z_2) - \frac{F}{ku^*} \ln z_2/z_1 \qquad (9)$$

where u* is friction velocity and k is Karman constant.

3) Idearized photochemical reaction model

It is well known that formation of ozone by photochemical reaction depends on initial concentration of NOx and non-CH4 hydrocarbon, composition of the hydrocarbon and also light intensity. In the case of hydrocarbon excess, the maximum ozone concentration does not strongly depend on the initial hydrocarbon. Since observed data in a city or near a city usually shows high hydrocarbon concentration, we assumed that hydrocarbon concentration is always sufficient high and it can be eliminate form independent variables of the reaction model.

From this point of view, we further simplify photochemical reaction models and constract an idearized reaction model. At the first, we evaluate the budget of NO, NO2, O3 and O by the reactions. The most important reactions are the follows:

$$NO_2 + h\nu \xrightarrow{k_1} NO + O \qquad [1]$$

$$O + O_2 + M \xrightarrow{k_2} O_3 + M \qquad [2]$$

$$NO + O_3 \xrightarrow{k_3} NO_2 + O_2 \qquad [3]$$

The other reactions are classified following 8 groups:

Sum of the oxidation reactions of NO except reaction [3] are represented by $R_1[NO]$, where,

$$R_1 = k_8[HO_2] + k_{12}[RO_2] + k_{13}[RO_2'] + 2k_{28}[NO_3] + \cdots \qquad (10)$$

Total rate of decay reactons of NO2, O3, NO, O are represented by $R_2[NO]$ $R_3[O_3]$, $R_4[NO]$, and $R_5[O]$, respectively and total formation rates of NO, NO2

and O3 are represented by F_1, F_2 and F_3 respectively.

$$R_2 = k_4[NO][H_2O] + k_6[HO][M] + k_{14}[RO_2] + k_{24}[O_3] + k_{25}[NO_3] + \cdots \quad (11)$$

$$R_3 = k_{19}[HC] + k_{21}[HO_2] + k_{24}[NO_2] + \cdots \quad (12)$$

$$R_4 = k_4[NO_2][H_2O] + k_{20}[HO] + \cdots \quad (13)$$

$$R_5 = k_7[RCHO] + k_{15}[HC] + \cdots \quad (14)$$

$$F_1 = k_5[HNO_2] + \cdots \quad (15)$$

$$F_2 = k_{27}[N_2O_5] + k_{28}[NO_3][NO] + \cdots \quad (16)$$

$$F_3 = k_{18}[RO_2] + \cdots \quad (17)$$

Conservetion equations of NO, NO2, O3 and O are written as follows.

$$\frac{d}{dt}\underset{10^{-4}}{[NO]} = -\underset{10^{-1}}{k_3[NO][O_3]} + \underset{10^{-1}}{k_1[NO_2]} - \underset{10^{-2}}{R_1[NO]} - \underset{5\times10^{-5}}{R_4[NO]} + \underset{2\times10^{-4}}{F_1} \quad (18)$$

$$\frac{d}{dt}\underset{10^{-3}}{[NO_2]} = \underset{10^{-1}}{k_3[NO][O_3]} - \underset{10^{-1}}{k_1[NO_2]} + \underset{10^{-2}}{R_1[NO]} + \underset{10^{-2}}{F_2} \quad (19)$$

$$\frac{d}{dt}\underset{10^{-10}}{[O]} = \underset{10^{-1}}{k_1[NO_2]} - \underset{10^{-1}}{k_2[O]} - \underset{10^{-4}}{R_5[O]} \quad (20)$$

$$\frac{d}{dt}\underset{3\times10^{-3}}{[O_3]} = -\underset{10^{-1}}{k_3[NO][O_3]} + \underset{10^{-1}}{k_2[O]} - \underset{3\times10^{-3}}{R_3[O_3]} + \underset{10^{-7}}{F_3} \quad (21)$$

Althosh the value of each term stronsly depends on the initial concentration and the elapsed time, the order of them are shown under the equations in a case of typical initial concentration and reaction time.

Terms of reaction[1] - [3] which are larger than others, can be eliminated and we obtain the following equations which include only slow reaction.

$$\frac{d}{dt}\underset{10^{-3}}{[NO_x]} = -\underset{10^{-2}}{R_2[NO_2]} + \underset{10^{-2}}{F_2} - \underset{5\times10^{-5}}{R_4[NO]} + \underset{2\times10^{-4}}{F_1} \quad (22)$$

$$\frac{d}{dt}\underset{10^{-3}}{[PO]} = \underset{10^{-2}}{R_1[NO]} - \underset{10^{-2}}{R_2[NO_2]} + \underset{10^{-2}}{F_2} - \underset{10^{-4}}{R_2[O]} - \underset{3\times10^{-3}}{R_3[O_3]} - \underset{10^{-7}}{F_3} \quad (23)$$

where,

$$[NOx] = [NO] + [NO_2]$$

$$[PO] = [NO_2] + [O] + [O_3]$$

Equations (22) and (23) express the most important process of the photochemical reaction. We neglect smaller terms of eqs. (20)~(23) and get the following equations after some substitution.

$$\frac{d}{dt}[NOx] = -R_2'[NO_2] \tag{24}$$

$$\frac{d}{dt}[PO] = R_1[NO] - R_2'[NO_2] - R_3[O_3] \tag{25}$$

$$\left.\begin{aligned} [NO_2] &= S/2 - \sqrt{S^2/4 - [PO][NOx]} \\ [NO] &= [NOx] - S/2 + \sqrt{S^2/4 - [PO][NOx]} \\ [O_3] &= k_1/k_3\,[NO_2]/[NO] \end{aligned}\right\} \tag{26}$$

where

$$S = [PO] + [NOx] - k_1/k_3$$

$$R_2'[NO_2] = R_2[NO_2] - F_2$$

This set of equations must be good approximation of the reaction, but it is not closed, because R_1, R_2' and R_3 are complex functions of unknown concentrations. Then, we introduce new assumption: R_1, R_2 and R_3 are assumed to be parameters instead of functions of unkown concentrations and to be approximated as follows:

$$\left.\begin{aligned} R_1 &= r_1[O_3] \\ R_2' &= r_2[O_3] \\ R_3 &= r_3[NOx] \end{aligned}\right\} \tag{27}$$

These equations must be the simplest form which do not spoil the fundamental charactereristics of the reactions. The order of the constant r_1 - r_3 can be estimated by more detail reaction model, i.e., $(r_1, r_2, r_3) = (1, 10^{-1}, 10^{-1})$, but optimum values of them must be decided by comparison with experiments.

Fig.2 shows the relationship of the maximum ozone concentration and the intial NOx concentration under hydrocarbon excess

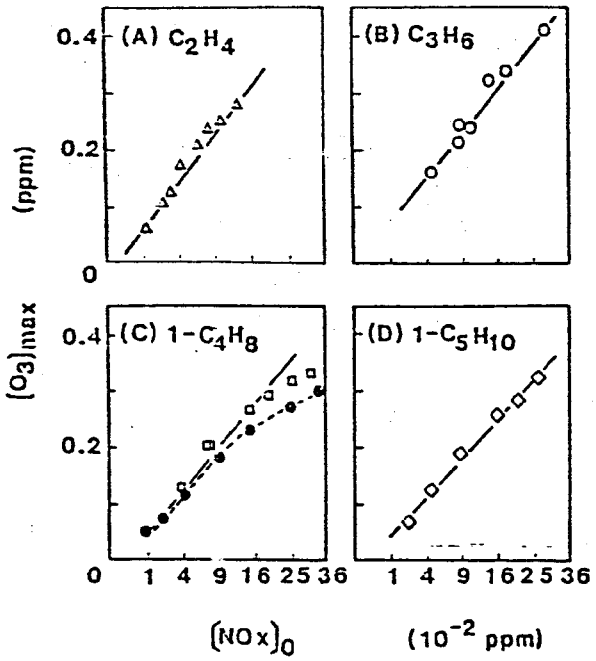

Fig.2 Maximim ozone concentration and initial NOx in HC excess case given by a chamber simulation after Sakamaki, et al.(1981) Black circles are calculated value by the idalized reaction model

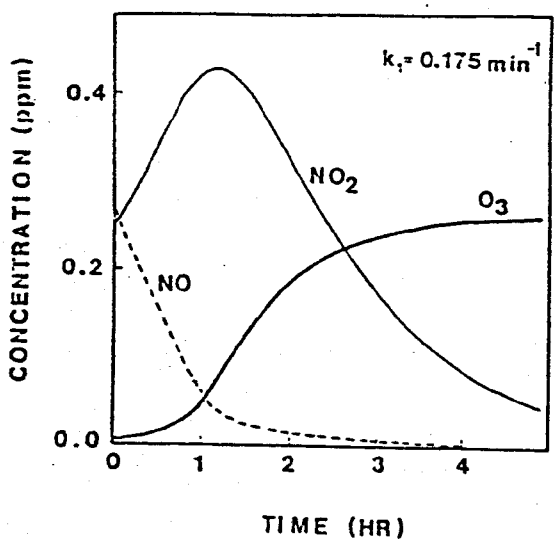

Fig.4 One of the solution of the idealized photochemical reactio model

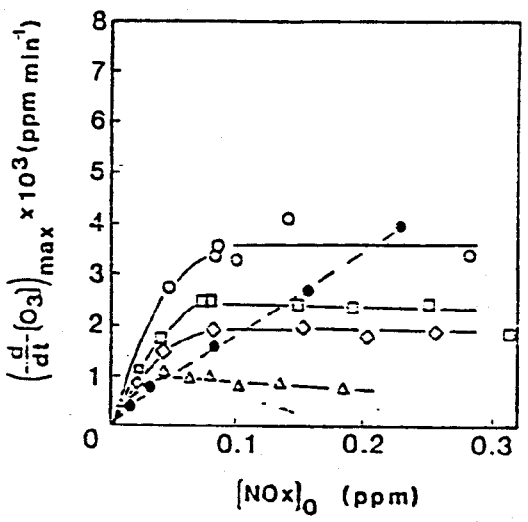

Fig.3 The same as Fig.2, but the maximum ozone fomation rate

condition given by a chamber experiment by Sakamaki et al.(1981). Black circles are calculated value by the idealized reaction model, when the pararameters r_1, r_2 and r_3 are assumed to be 3.6,0.1 and 0.08 Calculated ozone concentration is almost proportoinal to square root of initial NOx concentration. This agrees with the experimental result. The experiment also shows week dependency of the maximum ozone concentration on a species of hydrocarbon.

Fig.3 shows the maximum formation rate of ozone. Althogh the experimental result depends on a species of hydrocarbon, calculated values are seemed to agree well to the typical value in the low NOx level. The experimental maximum formation rate of ozone is almost proportional to K_1 value, and the calculated one shows the same manner as the experimental result. A solution of the ideaized reaction model is shown in Fig.4. Time variations of concentrations have similar feature as those of the chamber experiments.

3. Photochemical air pollution in the two dimensional land and sea breeze

At the first, we discuss the photochemical air pollution in a two dimensional land and sea breeze, which must be the simplest local wind. Simulated area is 225km in horisontal scale and divided into 30 grid points with interval of 7.5 km. We assume the source area which exists from the coast to 30 km inland. Emission rate is assumed to be 200 $m^3h^{-1}(7.5km)^{-2}$ for each of NO and NR (non-reactive pollutant) from 0700 until 2000 and zero in the other period. On the ground surface, the deposition velocity of ozone is assumed to be 0.3 cm/sec. And k_1 value

is assumed as follows:

$$k_1 / k_3 = 0.013\ S \quad (ppm)$$

where S ($cal/cm^2 min$) is total solar radiation.

At the first, zero synoptic wind is assumed over all area.

Fig.5 shows distributions of wind velocity, ozone, NOx and NR at 0600 on the second day, i.e., 30 hours after numerical integration started. Week land breeze exists broadly in the lowest 500m layer and weeker counter flow appears above the land breeze layer.

Ozone concentration is low near the ground, but high in the layer of 500m to 1500m above the source area. This ozone is due to the primary pollutant emitted on the day before. NOx and NR concentrations in the figure are also due to the day before, and difference of them means removal by the reaction, because the emission rate of them are same each other.

At 1200 (Fig.6), sea breese appeares near the coast and mixing layer develops on the land, which enhances vertical diffusion. O3 is formed by the reactions and mixing with ozone in the upper layer, so that very high concentration appeares on the source area, but NOx concentration is not high because of vertical diffusion and decay.

At 1500 (Fig.7) sea breeze penetrates over 50 km inland with strong horizontal velocity (over 5 m/sec) and a sea breeze front is formed with notable upward motion. As a result, concentrations of ozone and non-reactive pollutant decrease in the low level on the source area, but inclease on the downwind. Concentration in the upper layer on the source area is still high and it is slowly moving toward the sea.

At 1800 (Fig.8), sea breeze penetrates further inland, but

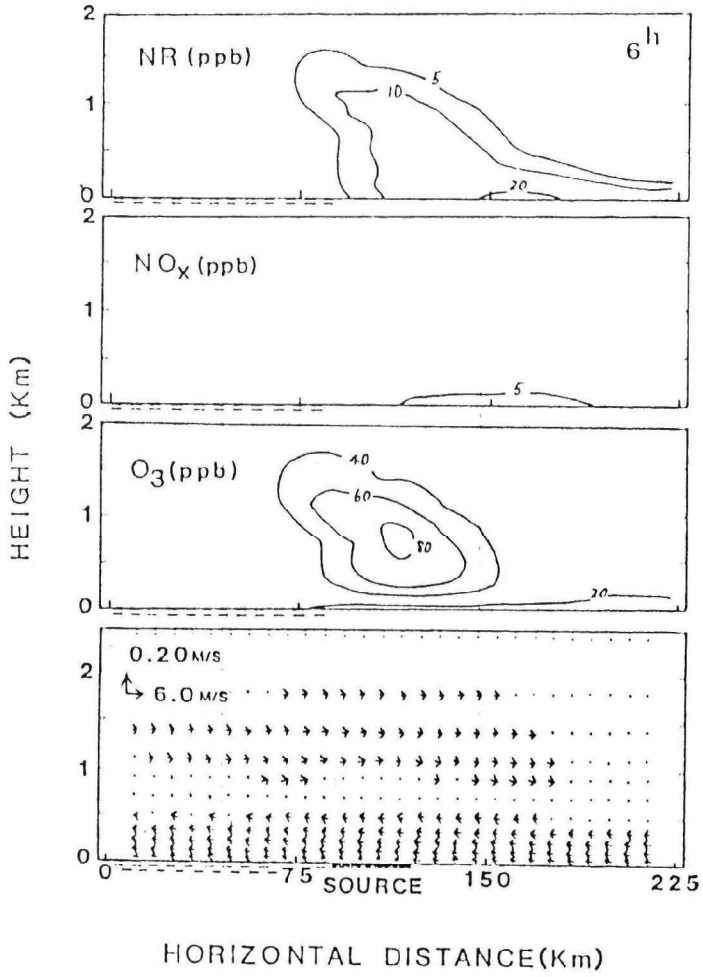

Fig.5 Distribution of wind velocity, ozone, NOx and NR (non-reactive pollutant) given by the model

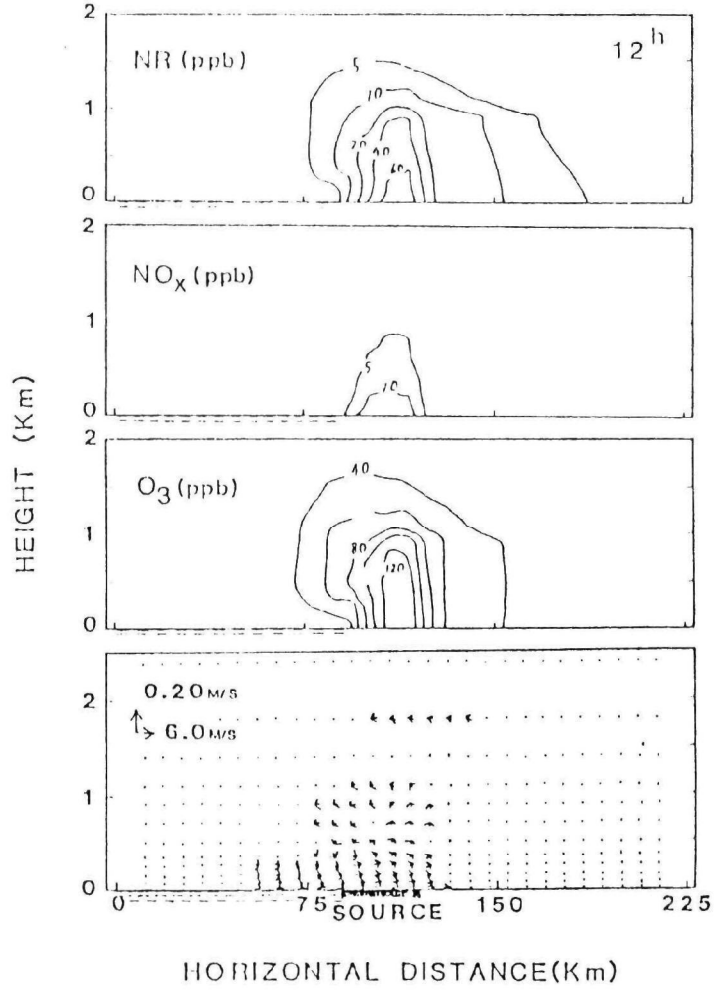

Fig.6 The same as Fig.5, but at 1200.

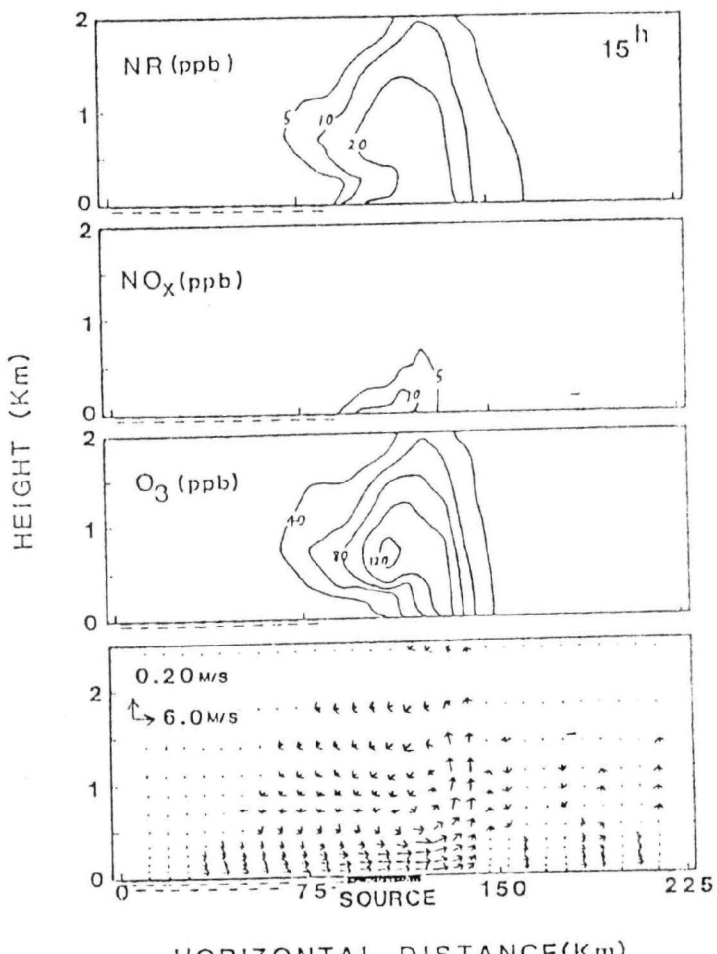

Fig.7 The same as Fig.5, but at 1500.

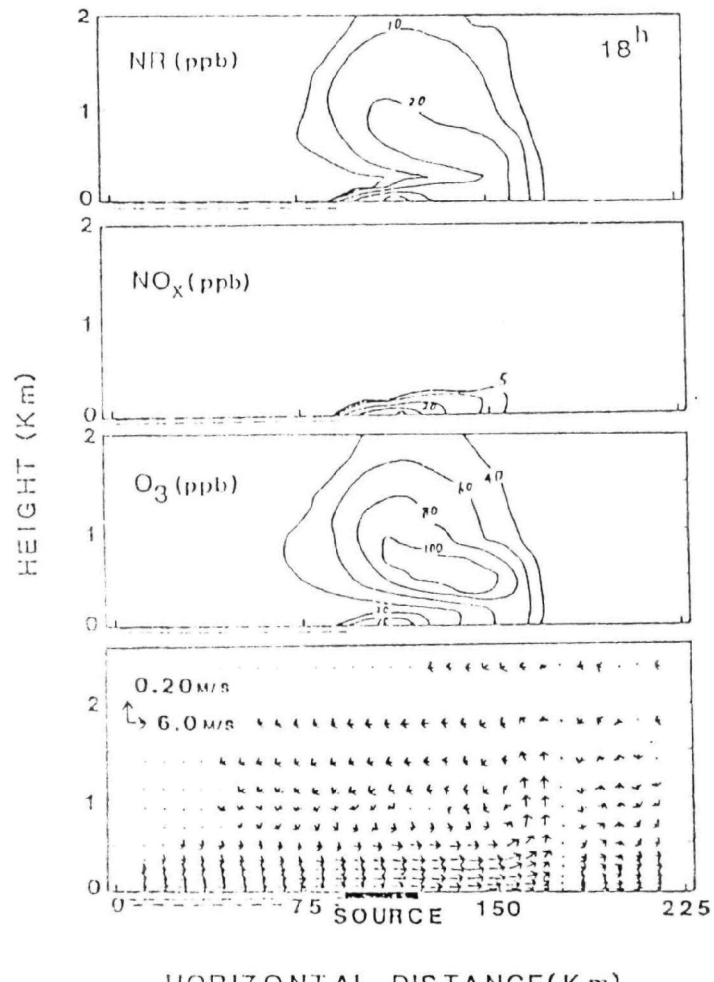

Fig.8 The same as Fig.5, but at 1800.

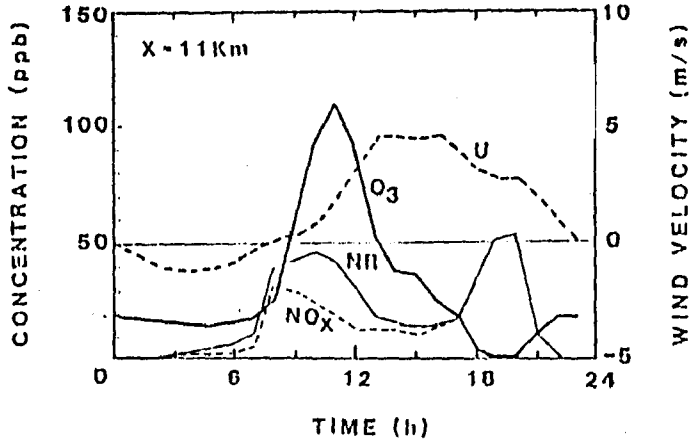

Fig.9 Diurnal variation of wind velocity and concentrations at the level of 25m, X is the distance from the coast

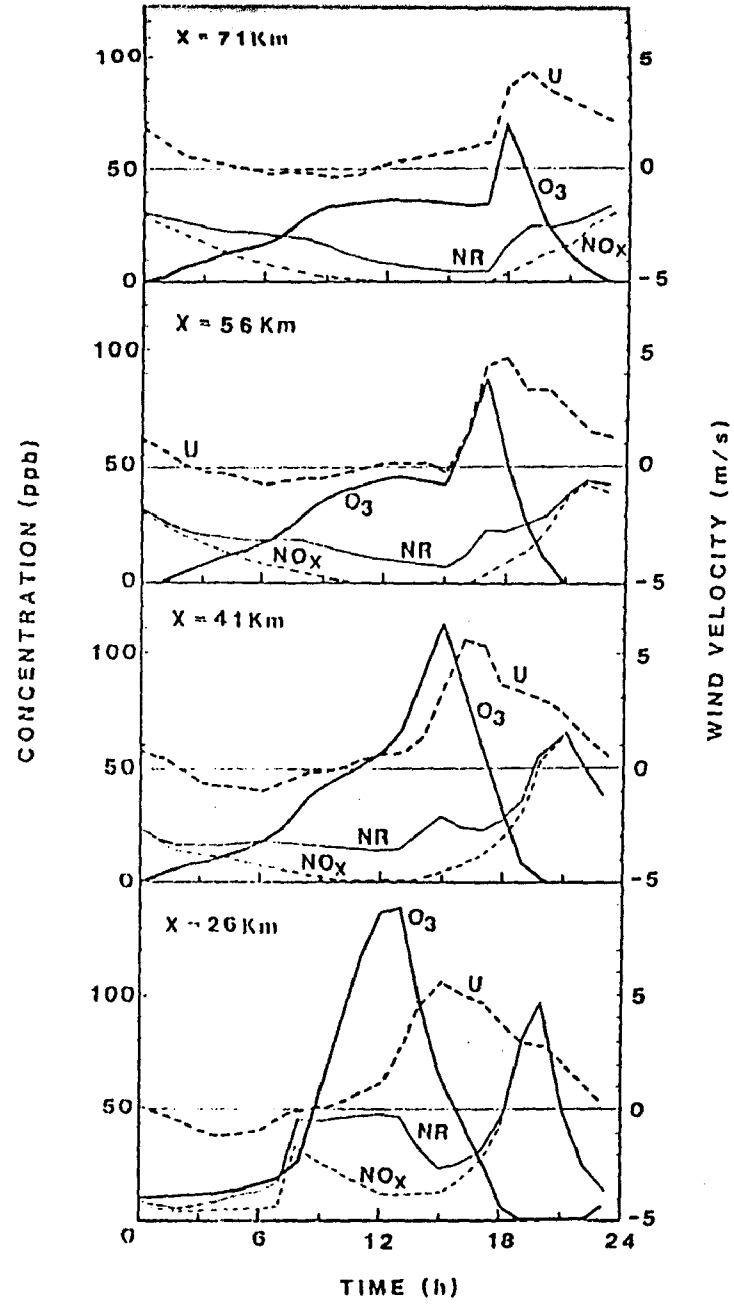

Fig.10 The same as Fig.9, but varios distance from the coast

the mixing layer changes gradually to stable layer. It makes high NOx concentration and further low O3 concentration, or sometime zero ozone, in the low level on the source area. In the upper layer, however, high O3 concentration is kept until the next morning. Simiar phenomenon is often observed actualy.

Fig.9 shows diurnal variation of wind velocity and concentration at the lowest level (25m) in the source area. Ozone concentration has a peak at about 1100, and NOx and NR have bi-modal variation with two peaks in the morning and eveing. These diurnal variation are commonly observed in urban area. At about 0800, land breeze changes to sea breeze, which becomes stronger at about noon when ozone concentration begins to decrease. The maximum velocity of sea breeze is about 5 m/s, and sea breeze continue until midnight.

Fig.10 shows the same as Fig.9, but at the other points. X in the figure is the distance from the coast. Peak time of ozone concentration shifts afterward with increasing distance from the source area, and at far points, we can fined another small peaks at about noon. The small peak at noon is due to the effect of the previous day.

The figure shows also that the diunal variation of wind velocity also shifts afterward with incleasing X. This is one of the common characteristics of land and sea breezes.

The effect of week large scale wind is investigated. Large scale wind modifies both of land and sea breeze and distribution of concentrations. Fig.11a shows the lowest level wind velocity at point x=11 km in three cases: large scale wind U_ℓ = 0, -0.3 and -1.0 m/sec. Minus of U_ℓ means direction of the large scale wind is the same as land breeze. Modification of the lowest level wind is small, but O3 concentration is

strongly modified (Fig.11b). Week sea-ward large scale wind enhances ozone concentration and shifts the peak time afterward in the source area.

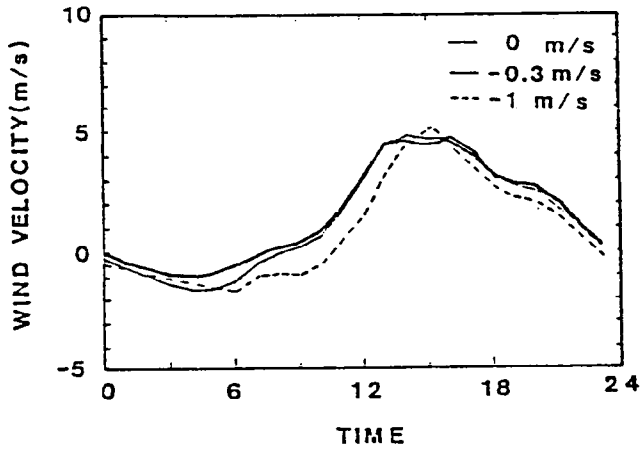

Fig.11a The effect of week large scale wind on the wind speed at X=11 km.

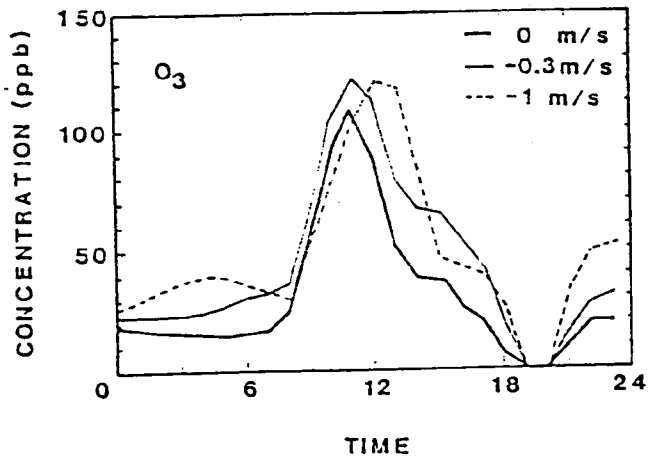

Fig.11b The effect of week large scale wind on ozone conentrstion.

4. Application to Tokyo metropolitan area

Many researchers have been pointed out that the photochemical air pollution of Tokyo metropolitan area is strongly affected by the local winds. It is also suggested that horizontal distributions of the maximum ozone concentration in a polluted day can be classified into the following three types.

Type I: High ozone concentration appeares broadly in Kanto plains.

Type II: High ozone concentration appeares only in the southan part of the plains.

Type III: High ozone concentration appeares only in the northan part of the plains.

For examle, Figs.12 and 13 show the maximum ozone concentrations in a typical day of type I (17,Jun,1979) and Type II (5,Jul,1978), respectively.

All of three types appear under such the almost same meteorological condision as mild synoptic wind on a clear day. But the local wind systems are appricably different each other. Fig.14 and 15 show observed surface wind on the same days as Figs. 12 and 13, respectively. On the days of type I, wind is usually calm all over Kanto plains in the early morning, and southerly sea breezes begin to blow from Sagami bay and Tokyo bay in the before noon. The maximum velocity of the sea breezes reaches about 5 m/sec. On the northan part of the plains, wind direction shifts to south-easterly in the before noon. This pattern often continues until night. On the days of type II, northerly wind prevails over the plains in the early morning, but it is not strong. After that, easterly sea breeze from the eastan ocean

prevails over the plains. The southerly sea breeze from Sagami bay begins to blow later than that of type I. It often begin in the afternoon, and usualy covers only the south-west part of the plains. On the days of type III, wind system is quite similar to the case of type I, unless the southerly component is stronger.

Numerical simulation is carried out in the area shown by Fig. 16, which is much larger than the Kanto plains. Because it has been suggested that the local wind system in the plains is affected by the mountain area in central Japan. The figure also shows an area source (shadowded area) and elevated point sources (black circles). The emission rate is given by rough estimation with diurnal variation. Figs. 17 and 18 show calculated wind velocities in the height of 25 m for the cases that the large scale wind is zero (case A) and NNW 3 m/sec (case B), rewpectively. Cases A and B are corresponding to the Types I and II respectively. Characteristics of the wind systems in the cases A and B agree fairly with the those of the type I and II, respectively, which are mentioned above.

Figs 19 (a),(b),(c) and (d) are calculated ozone concentration in the case A for 0900, 1200, 1500 and 2100, respectively. Ozone concentration begins to inclease at about 0900 on the source area, and it reaches the maximum value at about 1200. The polluted air mass is transported toward north by the southerly sea breeze, but the ozone concentration slowly decreases in the afternoon.

Figs 20 (a)-(d) are the same as Figs 19 (a)-(d), but in the case B. On the Sagami bay, ozone concentration begins to inclease at about 0900, because NOx emitted from the source has been transported to south by the northerly wind in the early morning.

Although high ozone concentration covers the southern part of Kanto plains, it does not so to the northan part until night. This agrees with the fundamental characteristics of the type II.

Fig.12 The maximum ozone concentration in a typical day of type I (17,Jun,1979).

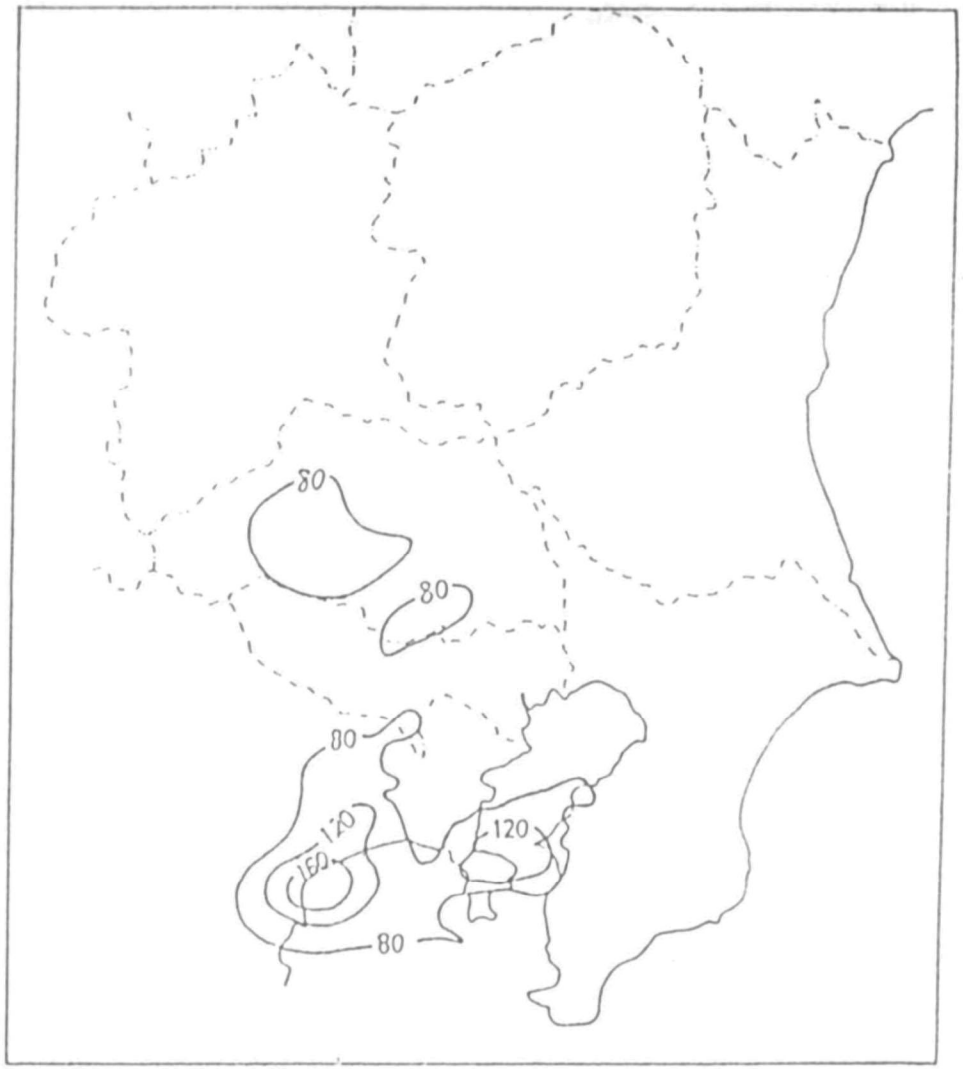

Fig.13 The same as Fig.12, but type II (5,Jul,1978)

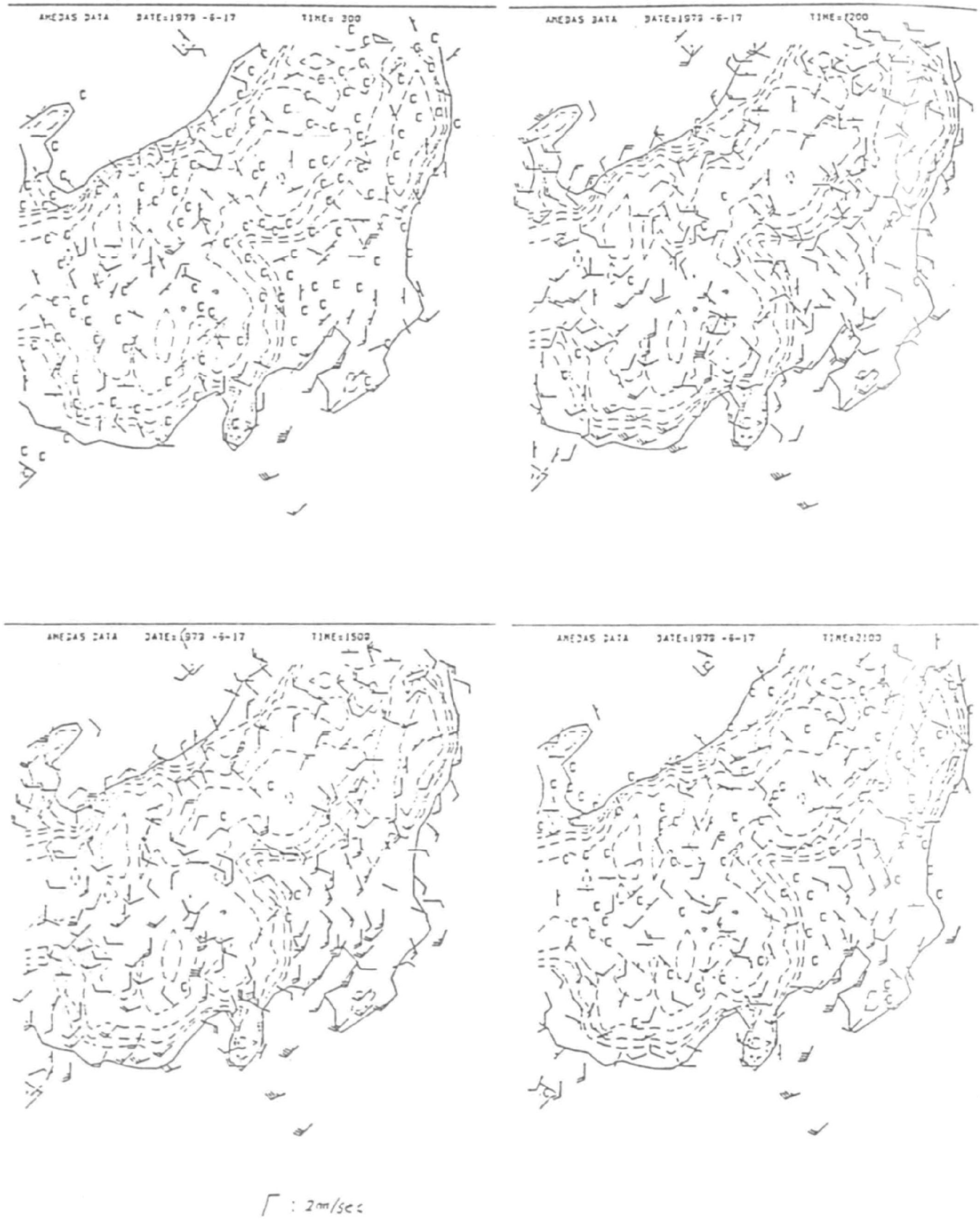

Fig.14 Observed wind velocity on 17 Jun,1979 (type I).

Fig.15 Observed wind velocity on 5 Jul,1978 (type II).

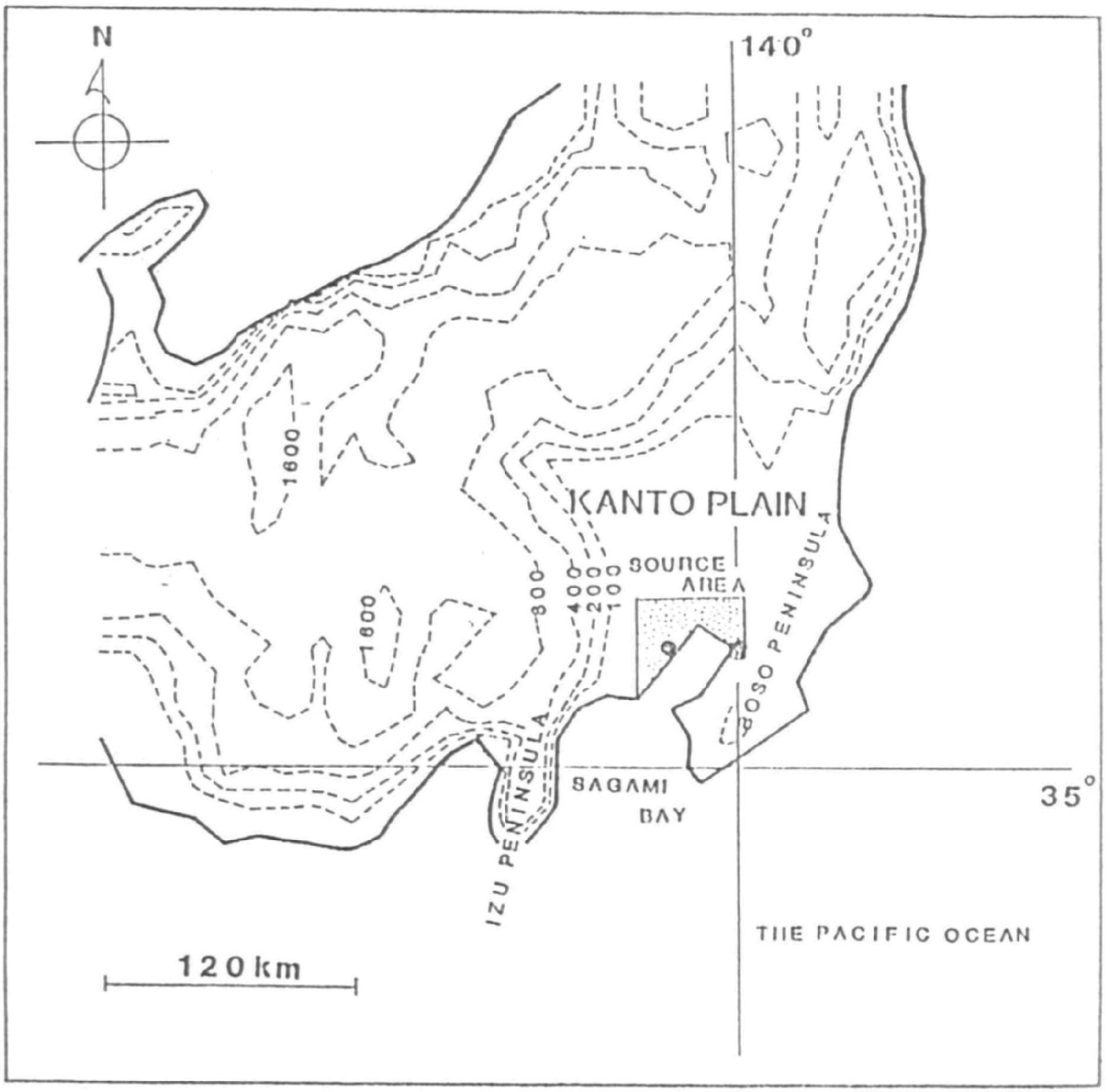

Fig.16 The numerical simulation applied area. Shadowded area is an area source and black circles are alevated point source (h = 500m).

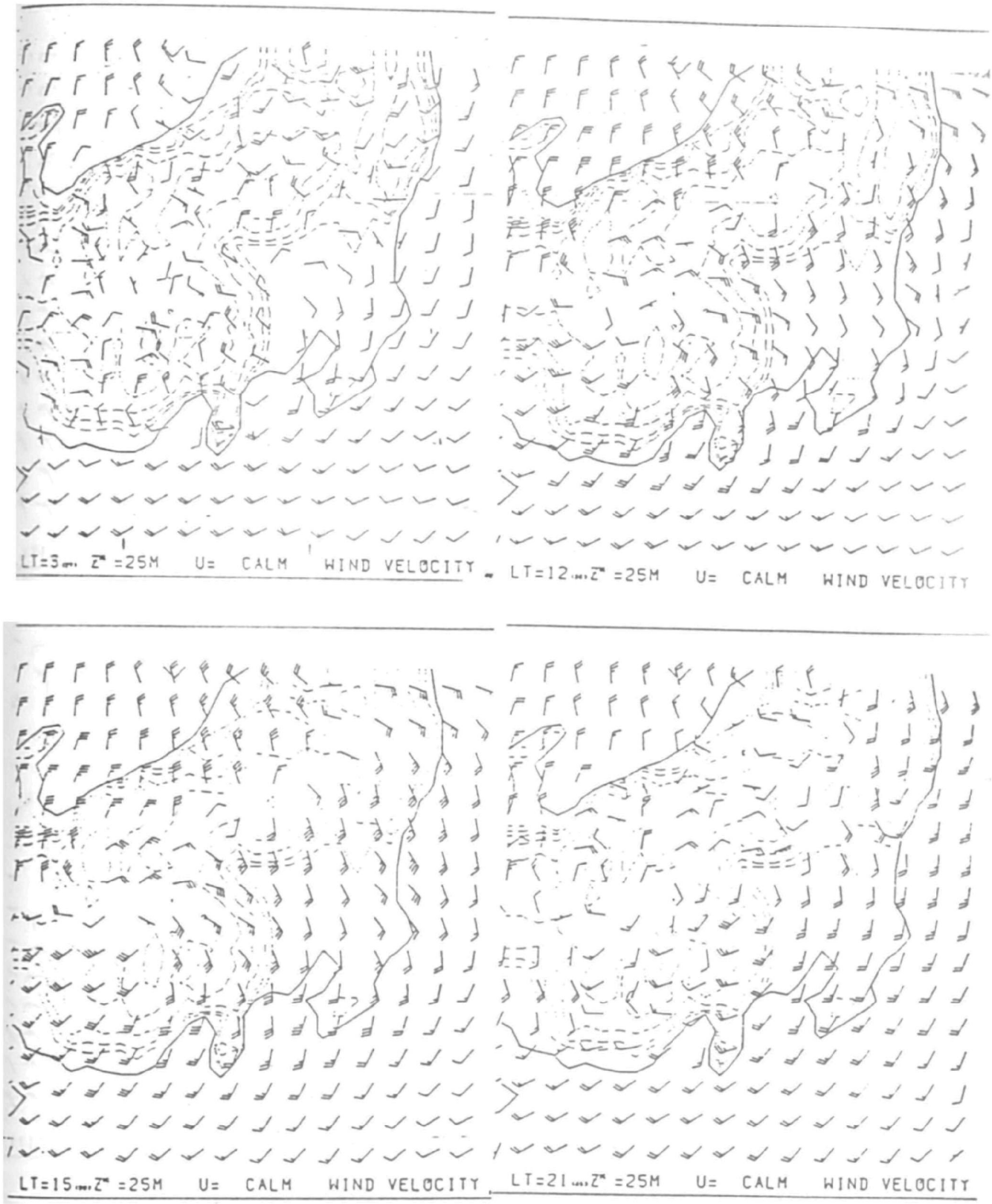

Fig.17 Calculated wind velocity in the case A, which is corresponding to type I.(see Fig.14) Γ: 2m/sec

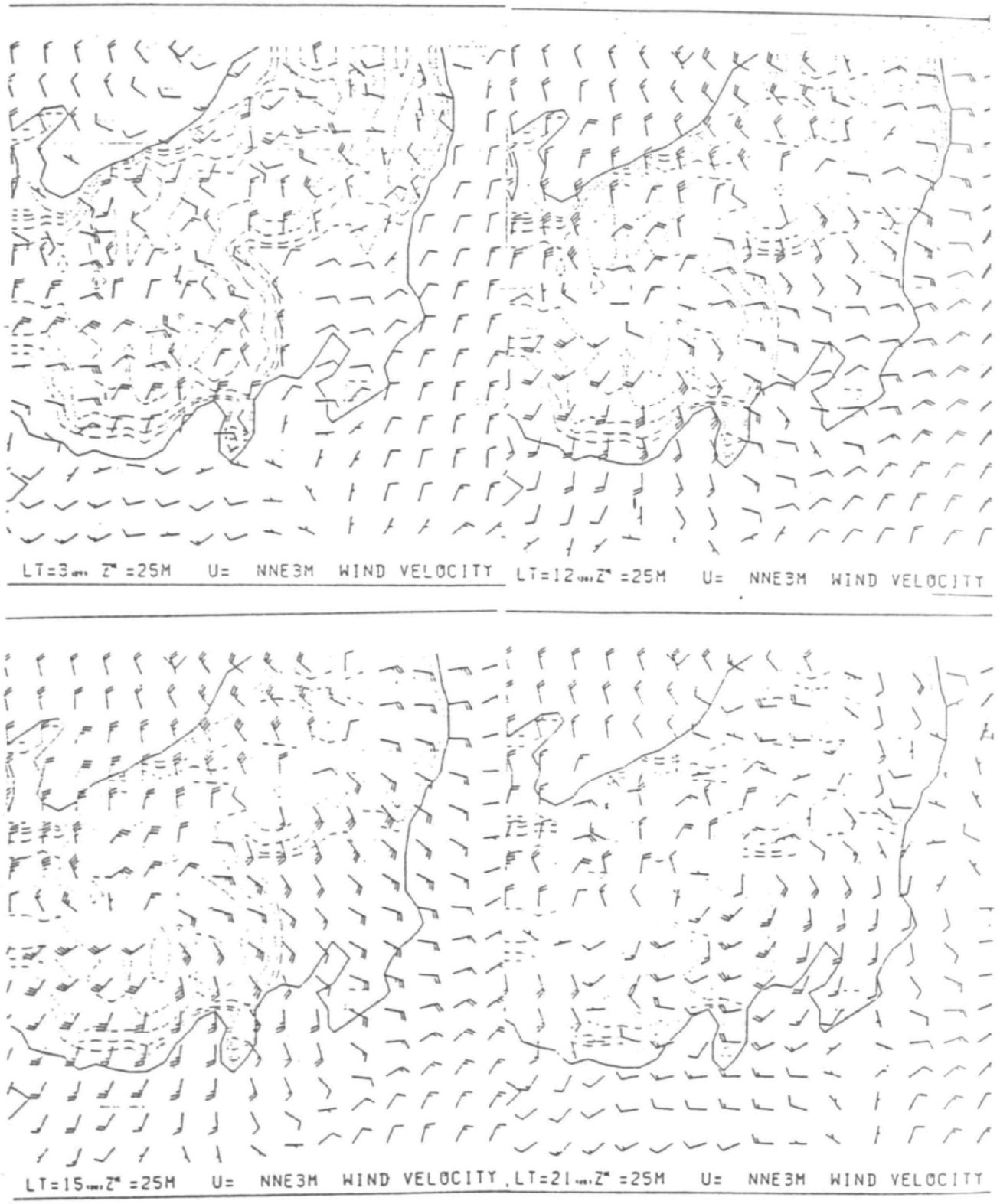

Fig.18 Calculated wind velocity in the case B, which is corresponding to type II. (see Fig.15)

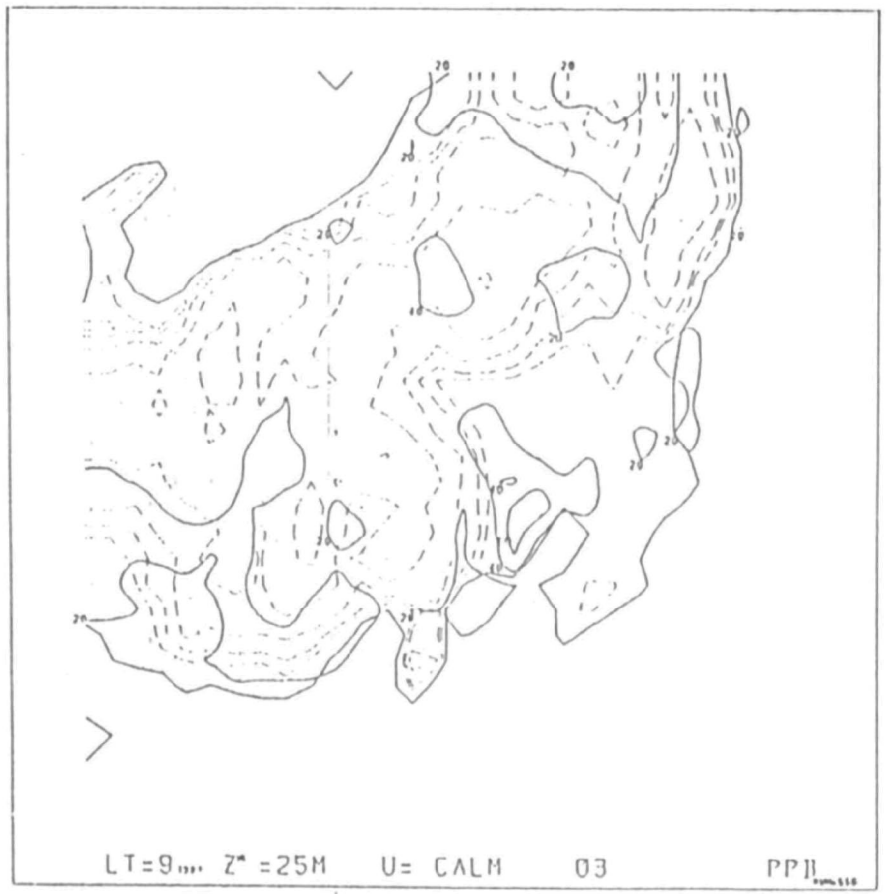

Fig.19 (a) Calculated ozone concentration at 0900 in the case A

Fig.19 (b) Calculated ozone concentration at 1200 in the case A

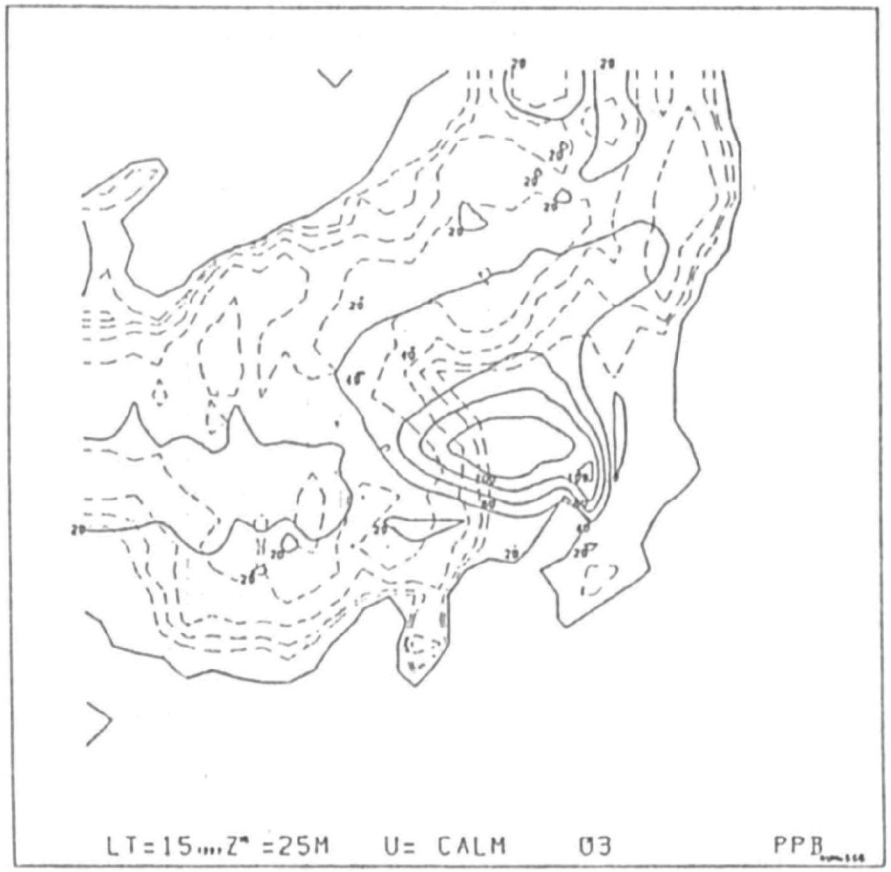

Fig.19 (c) Calculated ozone concentration at 1500 in the case A

Fig.19 (d) Calculated ozone concentration at 2100 in the case A

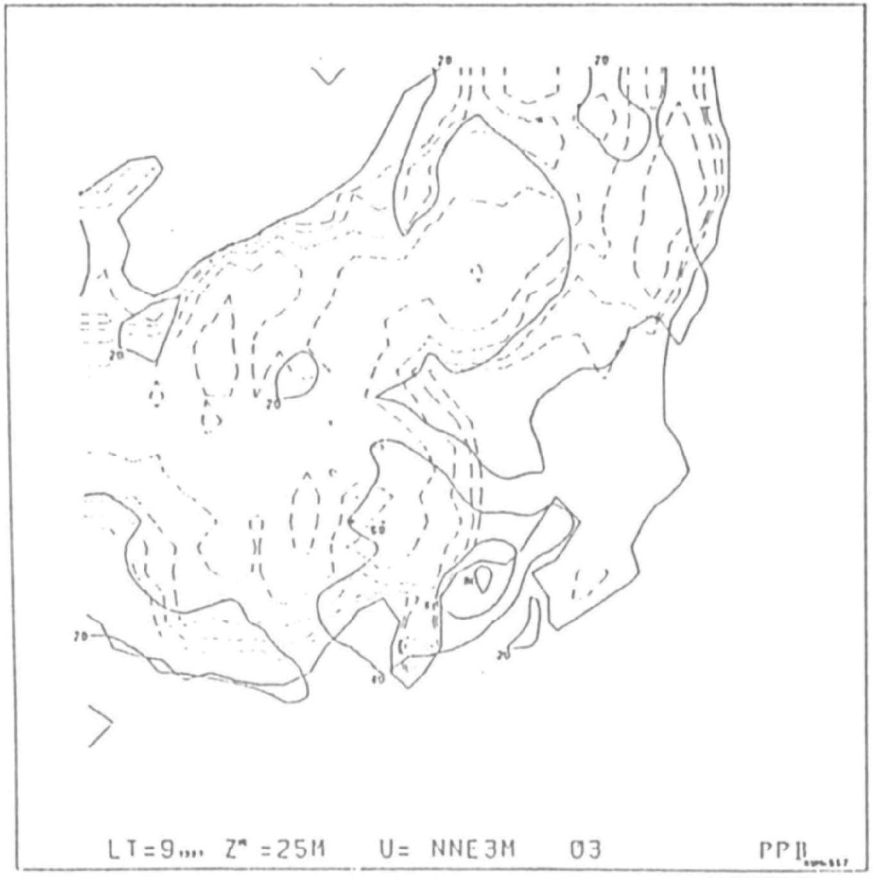

Fig.20 (a) Calculated ozone concentration at 0900 in the case B

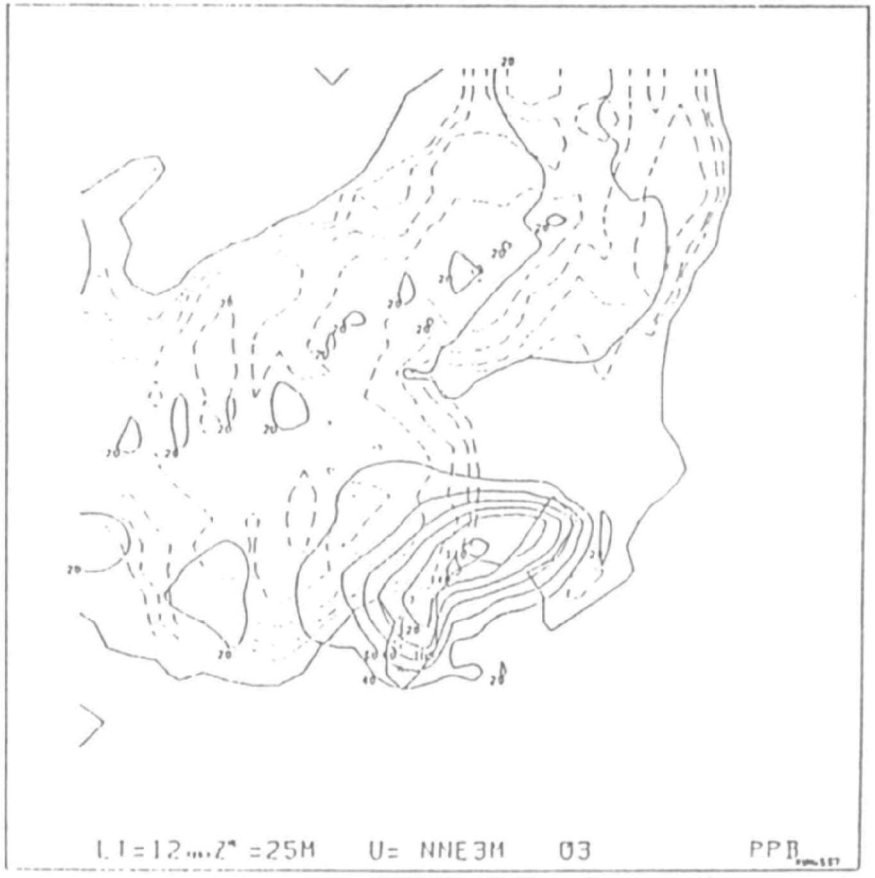

Fig.20 (b) Calculated ozone concentration at 1200 in the case B

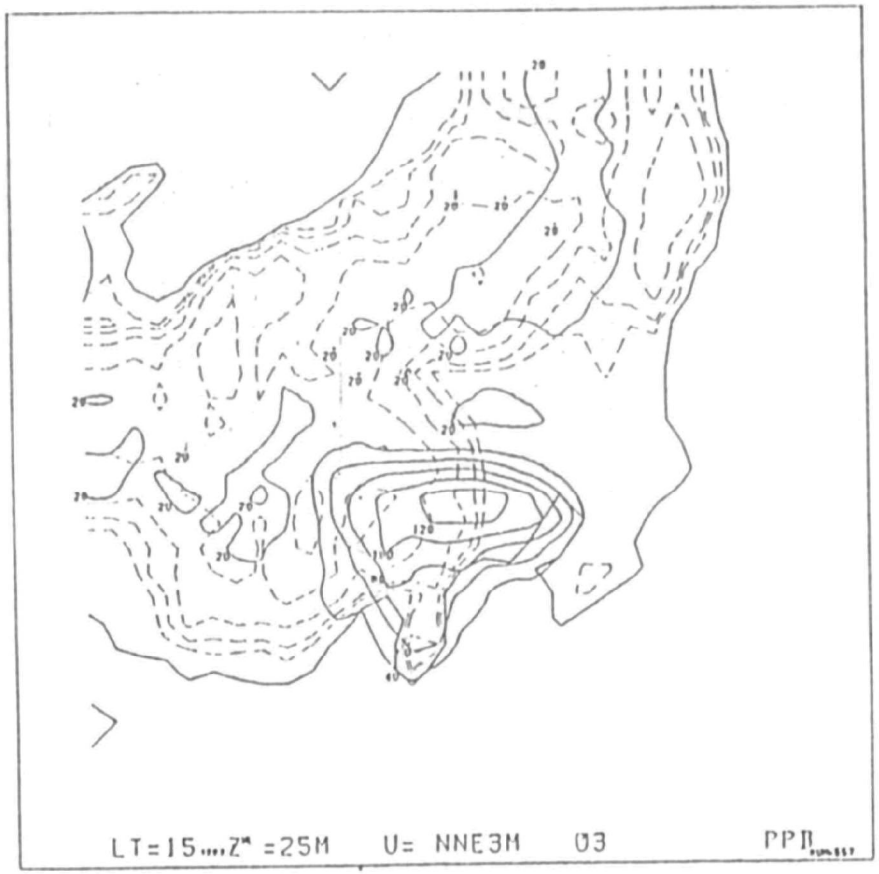

Fig.20 (c) Calculated ozone concentration at 1500 in the case B

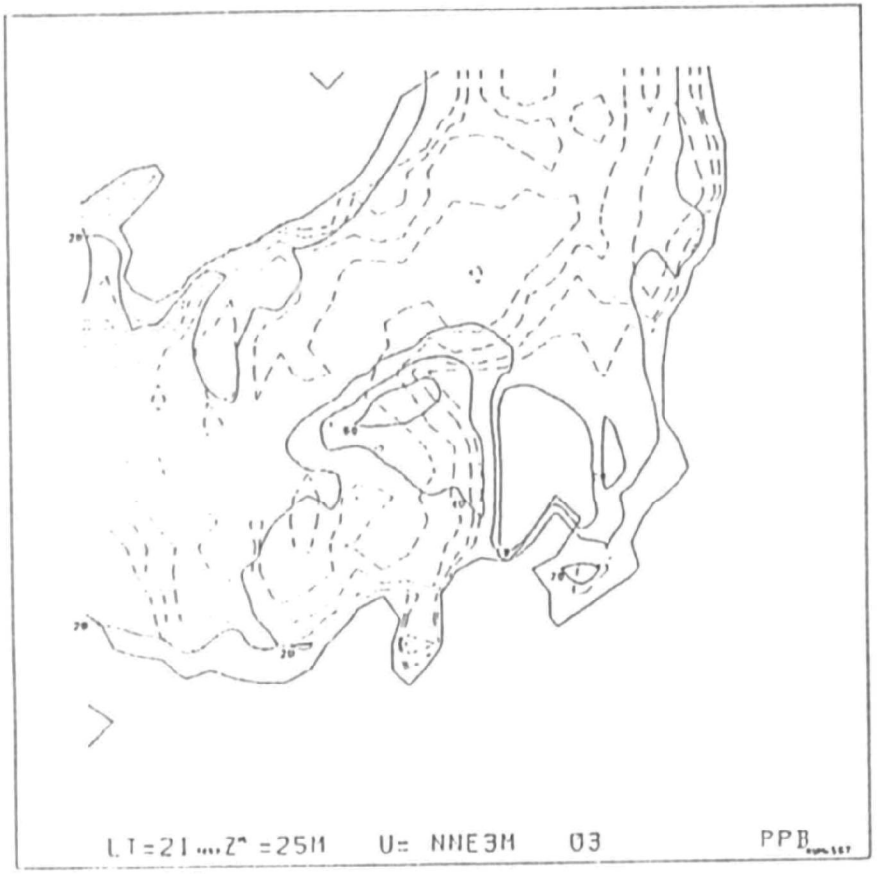

Fig.20 (d) Calculated ozone concentration at 2100 in the case B

TRANSPORT AND TRNSFORMATION OF AIR POLLUTANTS BY LAND AND SEA BREEZES

Presented by H. Tsuruta

Yokohama Research Institute for Enviromental Protection

Japan

TRANSPORT AND TRNSFORMATION OF AIR POLLUTANTS BY LAND AND SEA BREEZES

1. INTRODUCTION

Most of urban or industrial areas in Japan are located along the coastal region, and mountain areas are located close to the rural or urban area. Air pollutants, emitted from those source areas, are expected to be transported by meso-scale wind circulation, such as land and sea breeze, mountain and valley wind, and larger-scale one coupled between the two systems.

In the Kanto region, it has been reported that the polluted air mass with with high oxidant concentration above 100ppb formed in the Tokyo Metropolitan area has been transported as far as Tochigi or Nagano area, 100 km north from Tokyo, by southerly winds (Fig. 1).

In the coastal region in Japan, high oxidant concentration has been also measured during the sea breeze especially in the summer season, as shown in Fig. 2 and Fig. 3 . Lyons and Olsson[1)] have studied the transport mechanism of air pollutants during the lake breeze along the Lake Michigan. Lyons and Cole[2)] have recently reported that the same phenomena as mentioned above in Japan have been observed in the coastal area of Lake Michigan. The transport mechanism of air pollutants by meso-scale circulation, however, was hardly known due to the lack of continuous data over the sea. Photochemical reaction must be considered in the course of transport of the polluted air mass.

We have challenged to reveal its mechanism using the research vessel. Results of preliminary surveys conducted in 1976 and 1977 were reported

at this fifth Conference.[3] In those experiments, it has been revealed that the primary pollutants emitted mainly from Keihin industrial area are transported to Sagami Bay by offshore flow from midnight to early morning, and high oxidant concentrations are observed over Sagami Bay in the daytime when it becomes calm after offshore wind. In this report, a brief outline of the results obtained from two experiments conducted in 1980 and 1981.

2. EXPERIMENTAL

A two-day field program around Sagami Bay area was planned in the summer of 1980 and 1981, by the observational group in the special research project, " Study of meso-scale atmospheric pollution in Kanto District". Ocean Research Institute of Tokyo University observed vertical wind structure over Sagami Bay at the fixed station, the research vessel " Tansei-Maru " , belonging to Ocean Research Institute, as shown in Fig. 4. National Institute for Environmental Studies launched pilot balloons at six locations, Yokohama National University also observed vertical wind profile at another six locations. Yokohama Research Institute for Environmental Protection measured concentrations of gases and aerosols in ambient air at the fixed station in Sagami Bay, using the research vessel. National Institute for Environmental Studies and Yokohama Research Institute for Environmental Protection measured with light airplane, three dimensional distribution for meteorological parameters (including real wind field), air pollutants, respectively. Ozone sonde was used to measure the diurnal variation on vertical distribution of ozone concentration at one station only in the summer of 1981.

These field studies were conducted, 12-13 August 1980, 9-11 August 1981, respectively. The results on the overall field and theoretical studies, and on the three-dimensional wind structure and its diurnal variation on meso-scale circulation will be reported elsewhere, and the results on measurements of air pollutants will be shown hereafter.

3. RESULT AND DISCUSSION

3-1 Diurnal Variation of Gaseous Pollutants over Sagami Bay

Measurements for gaseous pollutants were made in ambient air over Sagami Bay, which were NO_x, CH_4, NMHC, C_2-C_5 light hydrocarbons, CO, HCHO, O_3, HNO_3 and H_2O_2 (H_2O_2 and HNO_3 were measured in cooperation with Dr. Yoshizumi, Tokyo Metropolitan Research Institute for Environmental Protection). The data obtained in the summer of 1980 and 1981 are shown in Fig. 5 and Fig. 6, respectively.

Meso-scale wind circulation was developed during both period for observation, as shown Fig. 7. It was clearly found that the offshore wind continued to blow during the morning, the onshore wind during the afternoon, as shown in Fig. 5 and Fig. 6. In the coastal area of Sagami Bay, warnings against photochemical air pollution were issued as a result of high oxidant concentrations (more than 0.12 ppm hourly average value) only on two days of 9 Aug. and 10 Aug., in 1981. The following discussion will be made mainly on the data obtained in the summer of 1981.

The concentrations of primary pollutants, such as NO_x, CH_4, NMHC and CO, were higher during the land breeze than during the sea breeze. On the other hand, levels of the secondary pollutants such as O_3, were higher during the sea breeze than during the land breeze.

The O_3 concentrations, after reaching to the maximum in the early afternoon, were gradually decreased, but were higher than the background level of O_3, about 20-30 ppb observed in the marine atmosphere. These phenomena mean that, as the air with the primary pollutants advects further offshore, O_3 is formed in the air with photochemical reaction, and that in the afternoon, the air with its burden of O_3 advects landward because there is almost no scavenging process over the sea. Just after the offshore wind begins to blow, the O_3 values are drastically decreased below the background level due to the reaction with NO emitted at the urban area. During a few hours after sunrise, the photochemical equilibrium is established between NO, NO_2 and O_3 as shown in Fig. 5, if the O_3 concentration is not relatively high levels. In the late morning when the solar radiation energy is increasing rapidly, this equiliblium can be no longer maintained as the reaction of hydrocarbons with NO_x becomes more active, and the O_3 formation rate increases rapidly as shown in Fig. 5.

The concentration of HNO_3 was higher during the onshore flow than during the offshore flow, as presented in Fig. 6, shows that HNO_3 is formed with the reaction (1),

$$NO_2 + OH \xrightarrow{(M)} HNO_3 \qquad (1)$$

which is one of the net loss reaction for NO_x.

H_2O_2 was measured with the equipment on board, which was made by Yoshizumi[4] after improving the Kok's measurement system.[5] The H_2O_2 concentrations were presented in Fig. 6. The ambient H_2O_2 values were very higher during the sea breeze than during the land breeze, as well as the HNO_3 values. As the diurnal variation of the H_2O_2 values were similar

to that of O_3 and the ratio of O_3 to H_2O_2 is about ten, H_2O_2 is produced from the following photochemical reactions:

$$HCHO + hv \longrightarrow H + CHO \qquad (2)$$

$$CO + OH \longrightarrow H + CO_2 \qquad (3)$$

$$H + O_2 \xrightarrow{(M)} HO_2 \qquad (4)$$

$$HO_2 + HO_2 \longrightarrow H_2O_2 + O_2 \qquad (5)$$

Kok[6] has already measured the ambient H_2O_2 concentrations in the California South Coast Air Basin in the daytime during the summer season, and has discussed the correlation of the H_2O_2 values with the O_3 values with great ambiguity.

The HCHO concentration, which is not only a primary pollutant but also a secondary produced pollutant, was slightly higher during the offshore flow than during the onshore flow.

C_2-C_5 hydrocarbons were analyzed in real time with FID-GC on board during the 2nd survey in 1981. As the ratio of the concentration of C_3H_6 and C_2H_4 to that of C_2H_2 were very lower in the daytime than in the nighttime, it is assumed that most of C_3H_6 and C_2H_4 were consumed with the reaction of OH or O_3, near the source area or in the course of transport.

3-2 DIURNAL VARIATION OF AEROSOLS OVER SAGAMI BAY

Aerosols in ambient air over Sagami Bay were collected and analyzed for SO_4^{2-}, NO_3^-, Cl^-, NH_4^+ and metals (Na^+, Mg^{2+}, K^+, Ca^{2+}, Fe, Mn, Zn, Pb, Ni, V) and PAH (BaP, BghiP). Fig. 8 and Fig. 9 show the diurnal variation of the concentrations of these species in aerosols. Diurnal pattern of total mass concentrations (TSP) were so similar to that of such a primary pollutants in gases as CH_4 or CO.

But the SO_4^{2-} concentrations in aerosols were much higher during the

sea breeze than during the land breeze as well as that of HNO_3. It is reasonable that SO_4^{2-} in aerosols was formed mainly with photochemical reaction in the day of high oxidant levels. NO_3^- and Cl^-, on the other hand, showed the pattern of primary pollutant, but the ratio of these concentrations during sea breeze to those during land breeze was very lower than in the case of trace gases such as CO or CH_4. From these phenomena, loss mechanism for NO_3^- and Cl^- must be considered:

$$2NO_3^- + H_2SO_4 \longrightarrow 2HNO_3(g) + SO_4^{2-} \quad (6)$$

$$2Cl^- + H_2SO_4 \longrightarrow 2HCl\ (g) + SO_4^{2-} \quad (7)$$

Sea salt particles are expected to be found in the samples during the onshore flow. As shown in Fig. 9, that the ratio of Mg^{2+} to Na^+ was almost nearly the value of 0.13 in the sea water during the onshore flow, is the demonstration of generation of sea salt particles. Therefore, chlorine loss also occurs with the reaction between NaCl and H_2SO_4 (7) or $HNO_3(g)$ during the onshore flow.[7)]

Fe was used to be the index for soil particles in the first approximation. Enrichment factors for Mn and Zn were calculated to be about 2 and 100, respectively, over Sagami Bay. It is clear that the origin of Mn and Zn are soil and anthropogenic sources respectively.

4. DIURNAL VARIATION OF SURFACE OXIDANT CONCENTRATIONS IN MONITORING STATIONS AND TRANSPORT OF POLLUTED AIR MASS

Fig. 10 shows the surface oxidant concentrations near the shore line and the inland areas, on 9-10 August, 1981. After sunrise, oxidant concentration increased gradually. Just after the front of sea breeze passed by, the levels of primary pollutants such as SO_2, CH_4 and CO increased stepwise, and oxidant value reached to the maximum 1-3 hours

later. With trajectory analysis as shown in Fig. 11, the polluted air mass with its burden of primary pollutants, starting from Keihin industrial area in the late morning to the south by northerly wind, were transported over Sagami Bay at about noontime, and was advected to the shoreline with its burden of photochemical oxidants such as O_3, HNO_3, H_2O_2 and SO_4^{2-} aerosols obsserved on the research vessel, by onshore flow.

In the evening, the oxidant concentration near the surface rapidly decreased with the reaction of NO, and the cooled air sloping down the mountain areas moved slowly from the northwest, reached to the shoreline at midnight. The oxidant concentration resulted in the drastic decrease over Sagami Bay just after the offshore flow with its burden of fresh NO_x. Fig. 12 shows the schematic pattern of the diurnal variation of NO_x and O_3 near the surface of the inland and the sea, on the day when the land and sea breeze is developed and on the day when the southerly wind is prevailing, respectively.

5. DIURNAL VARIATION OF VERTICAL DISTRIBUTION OF OXIDANT CONCENTRATIONS

Measurements on vertical distribution of oxidant concentrations were made at the station Y in Fig. 11, from noon on 9 August to noon on 11 August, in 1981, using the ozone zonde. Fig. 13 shows the vertical profile on wind, temperature and oxidant concentrations at station Y.

During the nighttime, oxidant concentrations at the height of 500-800 m remained to be the value above 100 ppv observed after the front of sea breeze passed through, while the oxidant value was recorded in minimum below the 300m height.

Vertical distribution of oxidant was uniform in the mixing layer, in the morning after breaking up of temperature inversion and when the offshore wind was blowing. This phenomena is due to the vertical mixing of aged pollutants above the temperature inversion layer with the fresh air pollutants near the surface, with the thermal convection.

6. THREE DIMENSIONAL PROFILE OF THE O_3 AND NO_x CONCENTRATIONS IN THE FOUR STAGE OF MESO-SCALE CIRCULATION

During two experiments,measurements for O_3 and NO_x were made with airplane to obtain the horizontal distribution at the constant height of 300m and 1,000m, and the vertical distribution over the three points of bay,shoreline and inland. The flight was done in the four stage of the day, which means the offshore flow stage, alternative stage from offshore flow to onshore flow, the onshore flow stage and alternative stage from the onshore flow to the offshore flow, respectively.

Fig. 14 and Fig. 15 show examples of vertical cross section of O_3 and NO_x concentrations and the wind structure analyzed by Fujibe[8], in the onshore flow stage and in the alternative stage from the onshore flow to the offshore flow.

Fig. 16 shows the schematic pattern on the vertical cross section for the O_3 and NO_x concentrations in the four stage of the meso-scale circulation, perpendicular to the shoreline.

In the first stage, the primary pollutants are advected from inland to the sea,and the level of NO_x are higher in the land than over the sea, and than above the mixing layer. On the other hand, the levels of O_3 are lower in the land than over the sea and than that above the mixing

layer which is 20-30 ppb of O_3. The mixing layer is of a few hundred meters height.

In the 2nd stage, the photochemical process is predominant. The O_3 concentration is increased rapidly both over the land and the sea, and mixing layer is developed to the 1,000m height or so over the land by strong thermal convection

In the 3rd stage, as the onshore flow advects the secondary pollutants to the inland horizontary and aloft especially near the front of sea breeze, the concentration of O_3 in the lower layer over the sea is decreased. If the return flow is present, O_3 alofted is advected to the sea gradually. The NO_x levels are lower than in the first stage as NO_x is consumed with photochemical reaction.

In the 4th stage, as the large scale offshore wind begins to blow the higher concentration of O_3 alofted is advected to the upper part of the sea, and the layer of the higher O_3 level is formed both over the land and the sea. But the O_3 levels near the surface in the land is decreased by the reaction with NO.

Then, in the first stage on next day, it is characteristic that the aged pollutant layer with the high O_3 level is present above the mixing layer. After breaking up of the inversion, these aged pollutants influence the photochemistry and the O_3 level near the surface with vertical mixing.

7. SUMMARY

In the summer of 1980 and 1981, a field study for diurnal variation of air pollutants over Sagami Bay and three dimensional stucture of air pollutants on meso-scale circulation was conducted using the research vessel and the aircraft.

The high concentrations of O_3, H_2O_2, HNO_3 and SO_4^{2-} were observed during the sea breeze in the afternoon. As the diurnal variation of their concentrations are very similar, all of them are mainly produced with photochemical reactions in the daytime of summer.

O_3, which is formed in the urban and industrial areas, are transported three-dimensionally with meso-scale circuration induced by land and sea breezes, and the aged pollutants with its burden of O_3 were present above the mixing layer in the next morning after the day when land and sea breezes were generated.

REFERENCES

1) Lyons, W.A. and L.E. Olsson: Mesoscale air pollution transport in the Chicago Lake breeze, J. Air Poll. Cotrol Assoc., 22, 876-881 (1972).

2) Lyons, W.A. and H.S. Cole: Photochemical oxidant transport: Mesoscale lake breeze and synoptic-scale aspects, J. Appl. Meteor., 15, 733-743 (1976).

3) Tsuruta, H., H. Maeda and M. Ohta: Observation on transport and background concentrations of atmospheric pollutants over Sagami Bay and the Izu Islands Sea, Papers presented at the fifth US-Japan Conference on Photochemical Air Pollution, 1980.

4) Yoshizumi, K.: in preparation.

5) Kok, G.L., T.P. Holler, M.B. Lopez, H.A. Nachtrieb and M. Yuan: Chemiluminescent method for determination of hydrogen peroxide in the ambient atmosphere, Environ. Sci. Technol., 12, 1072-1076(1978).

6) Kok, G.L., K.R. Darnall, A.M. Winer, J.N. Pitts,Jr. and B.W. Gay: Ambient air measurements of hydrogen peroxide in the California South Coast Air Basin, Environ. Sci. Technol., 12, 1077-1080 (1978).

7) Kadowaki, S.: Behavior of sea salt particles in urban air, Chemical Society of Japan, 141-146 (1980).

8) Fujibe, F.: in preparation.

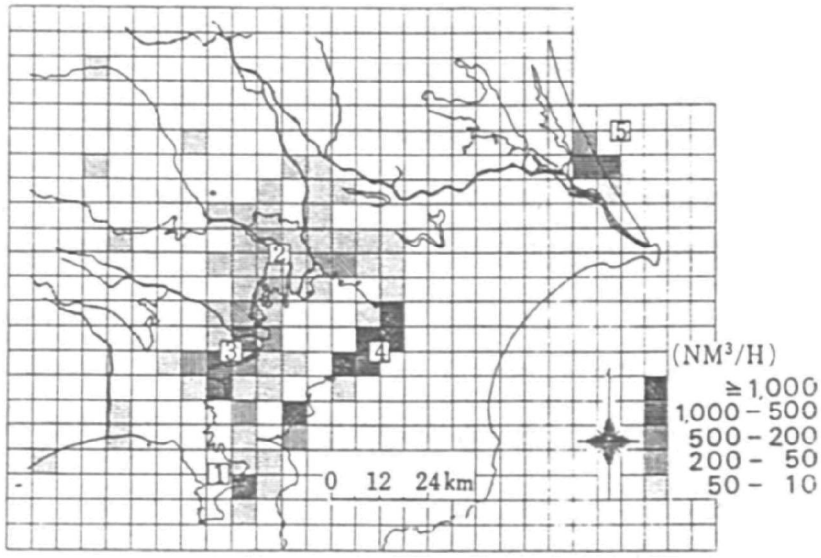

Fig. 1 Map of NO_x emission rate in the Southern part of Kanto area[9]

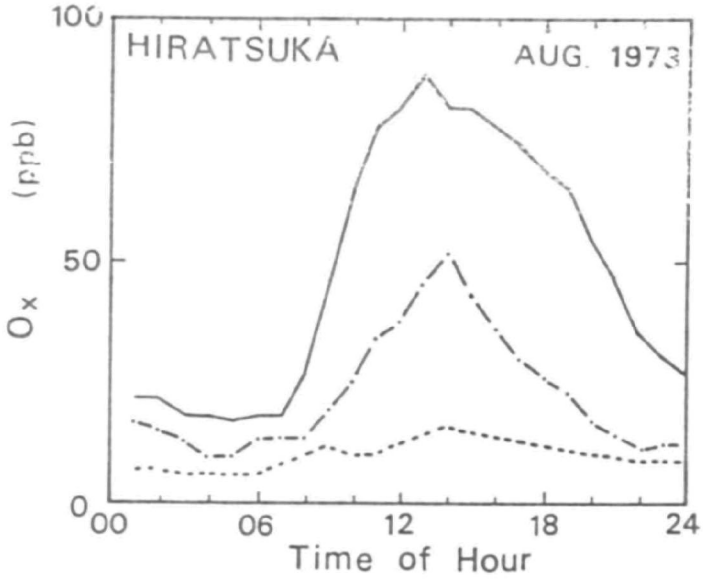

Fig. 2 Diurnal variation of oxidant concentration when the land and sea breeze are generated (——) when northerly wind is prevailing (·—·—·) and when southerly wind is prevailing (·····) .

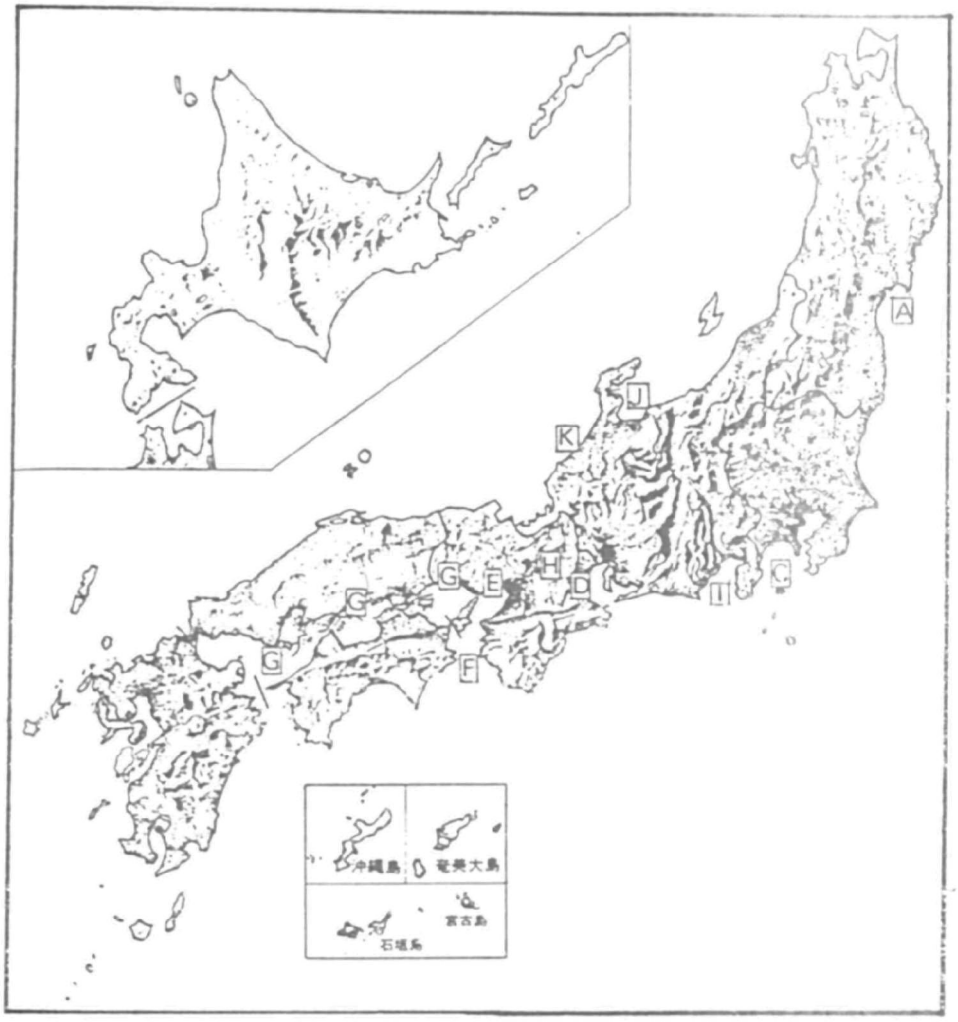

Fig. 3 Areas where high oxidant concentrations have been measured during sea breeze, in Japan.

A -- Sendai Bay, B -- Tokyo Bay,
C -- Sagami Bay, D -- Ise Bay,
E -- Ohsaka Bay, F -- Kii Channel,
G -- Seto Inland Sea, H -- Lake Biwa,
I -- Suruga Bay, J -- Toyama Bay,
K -- Fukui coastal area.

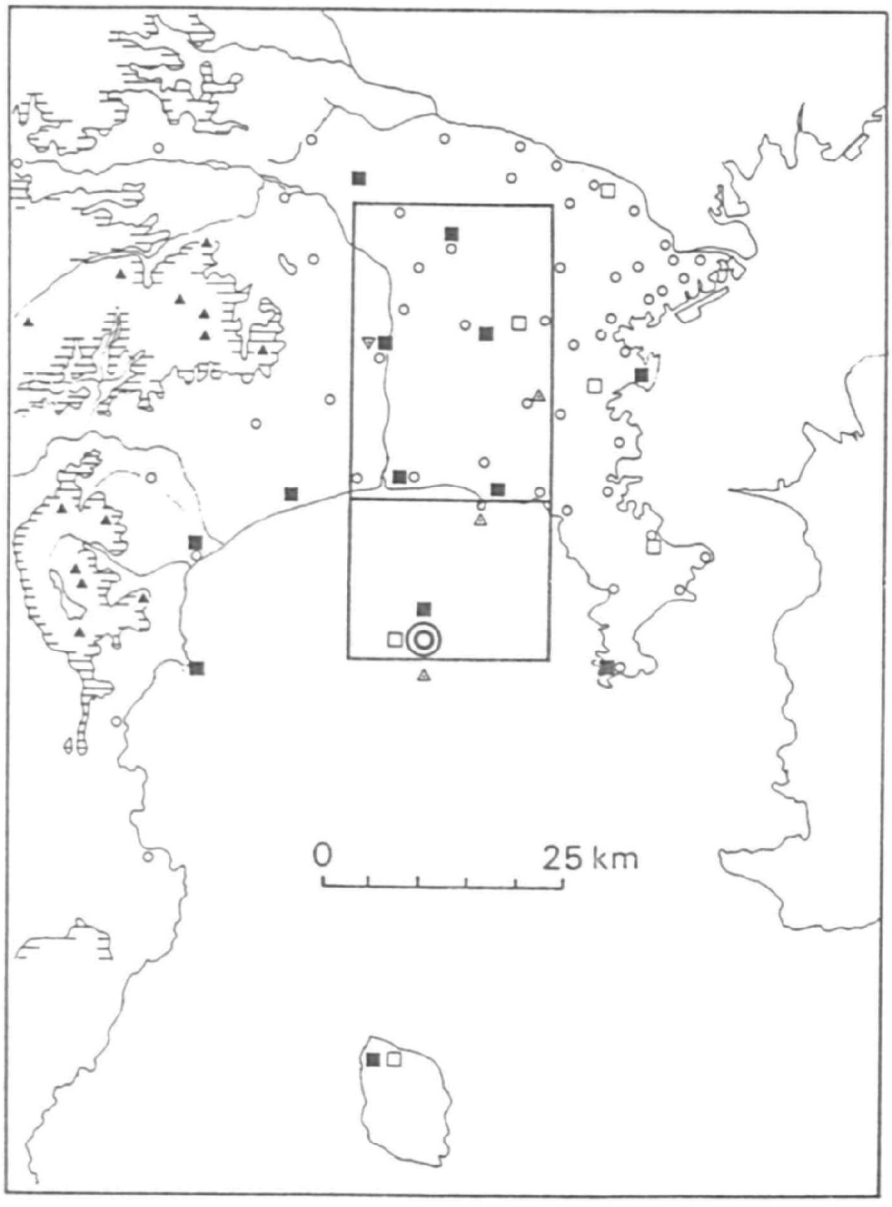

Fig. 4 Map of experimental area.

◎ Fixed station, " Tansei-Maru "

■ station for pilot balloon

○ Monitoring station for air pollutants

□ Point for O_3 measurement

▽ Station for O_3 sonde

△ Point for vertical flight

—— Course for horizontal flight

Area abive 600m height.

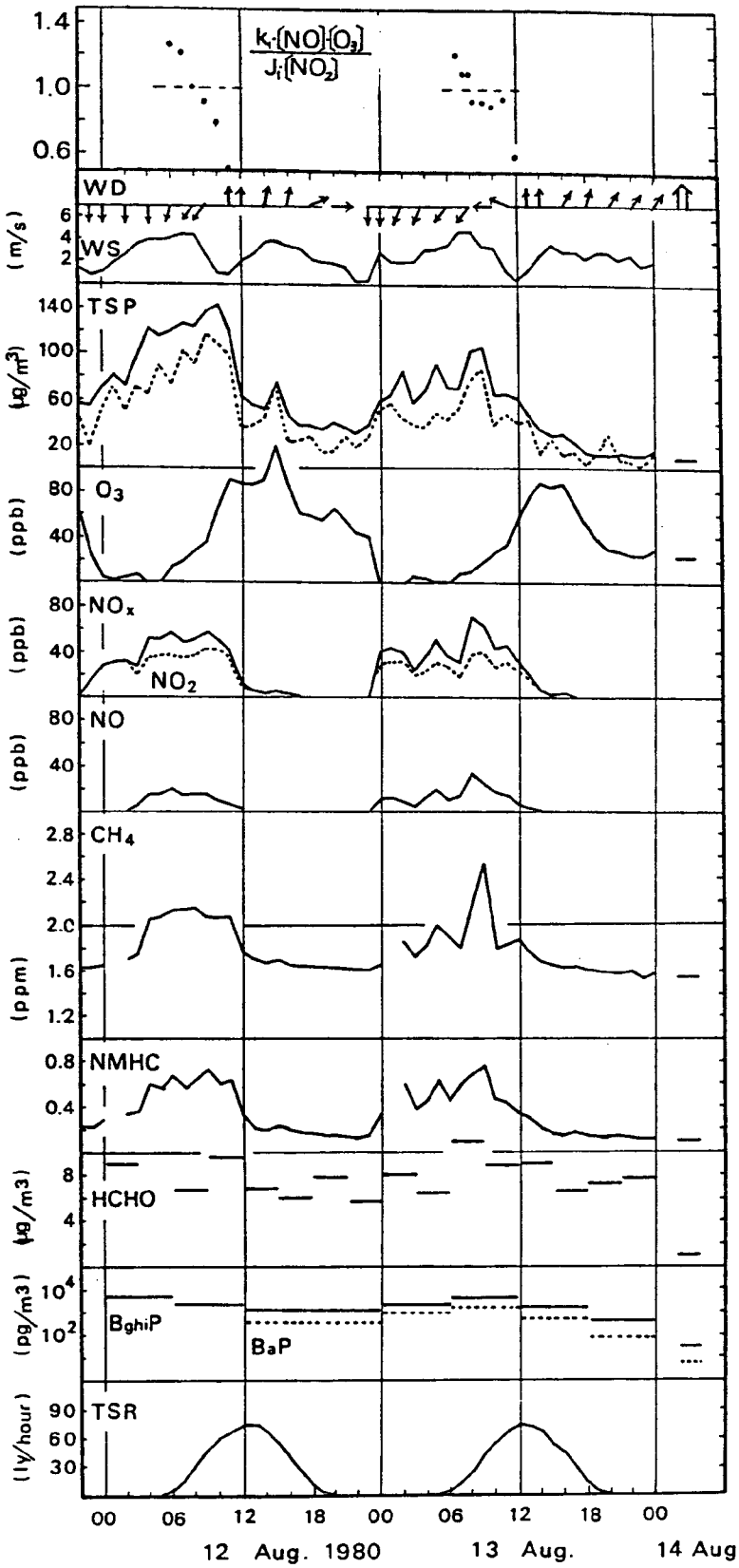

Fig. 5 Diurnal variation of air pollutants.
(12 - 13 August, 1980)

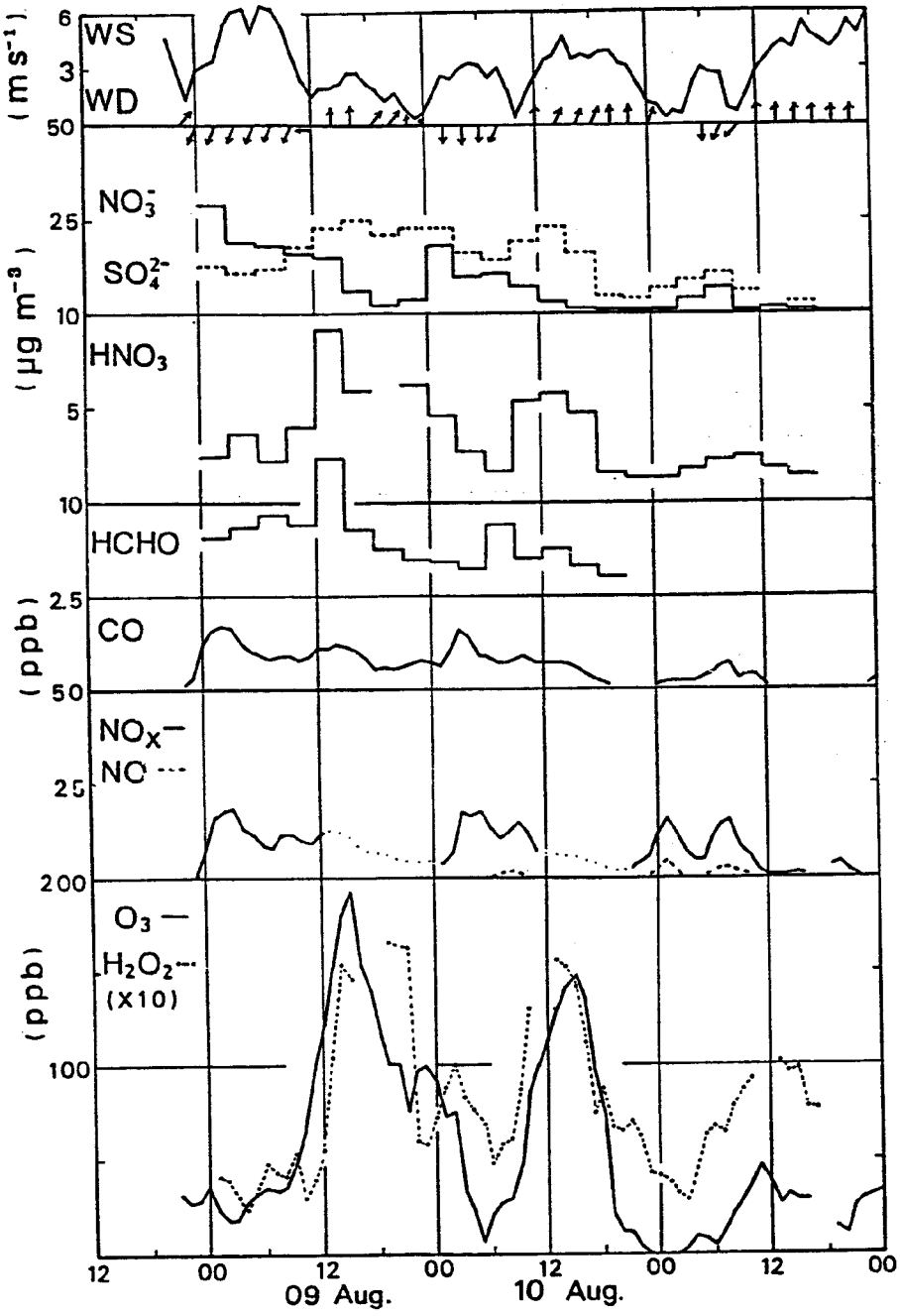

Fig. 6 Diurnal variation of air pollutants
(09 - 11 August, 1981)

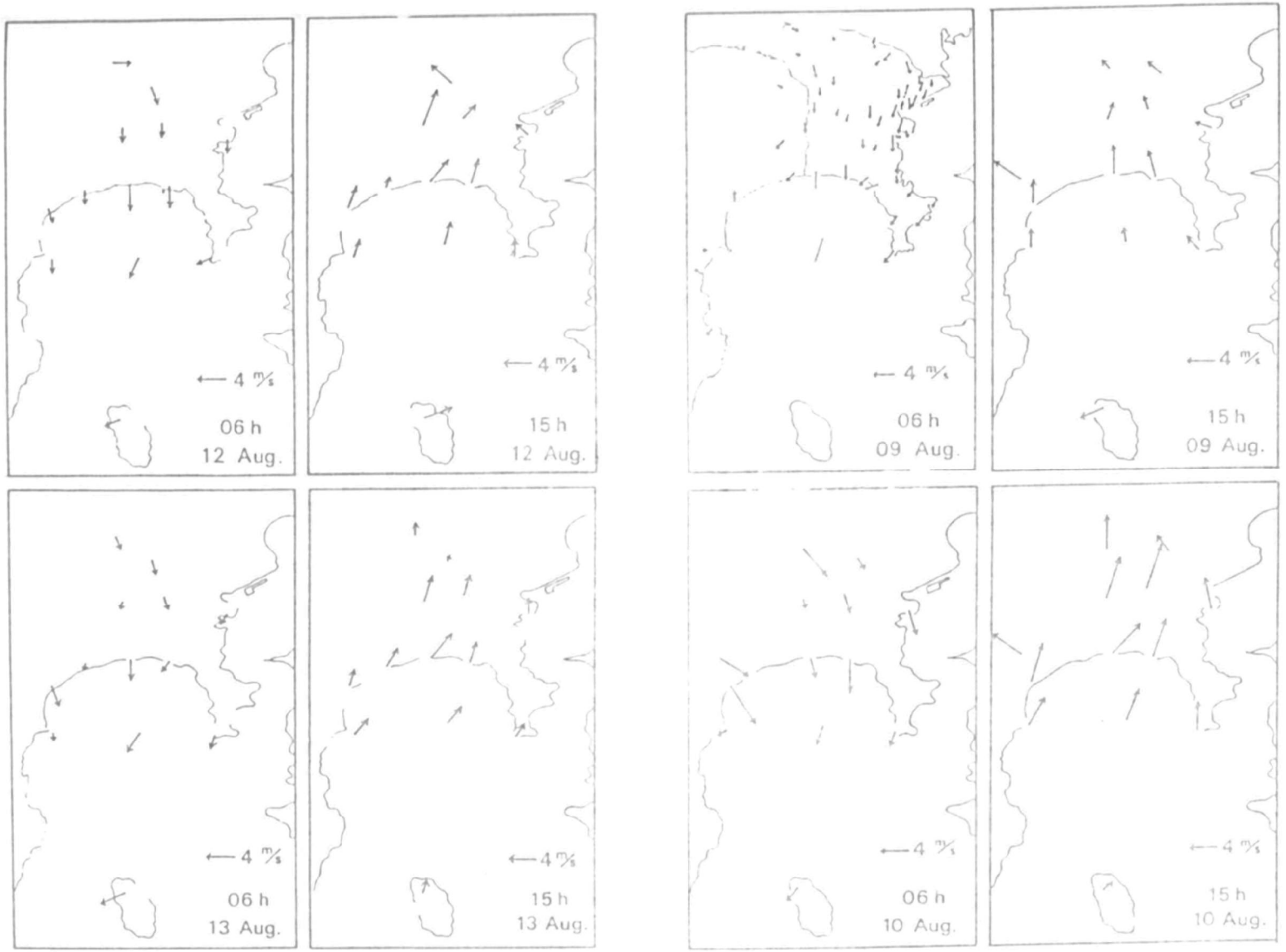

(1) 12 - 13 August 1980

(2) 09 - 10 August 1981

Fig. 7 Surface wind vectors during the two experiments.

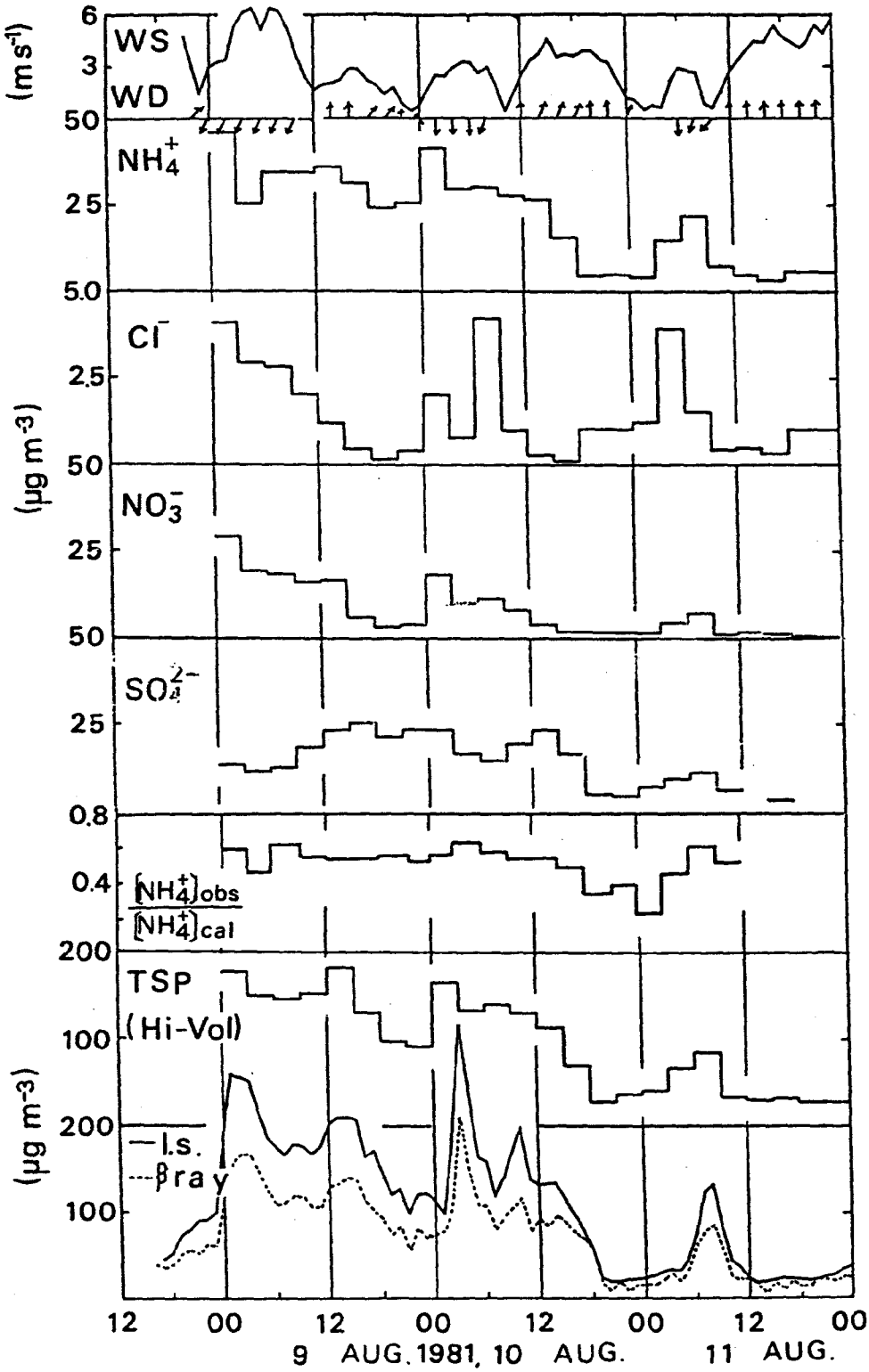

Fig. 8 Diurnal variation of aerosols over Sagami Bay.

(9 - 11 August 1981)

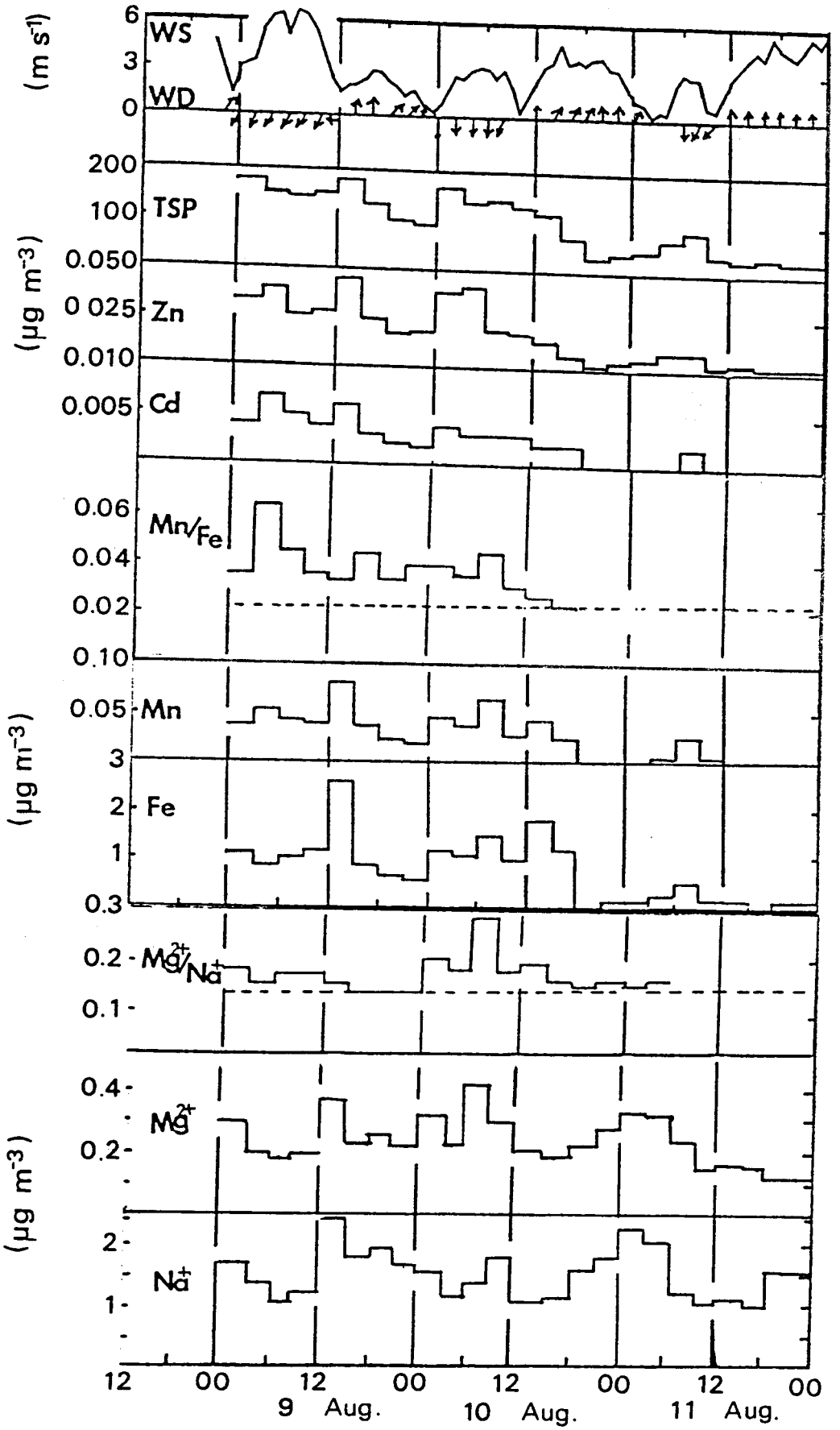

Fig. 9 Diurnal variation of aerosols over Sagami Bay.

(9 - 11 August 1981)

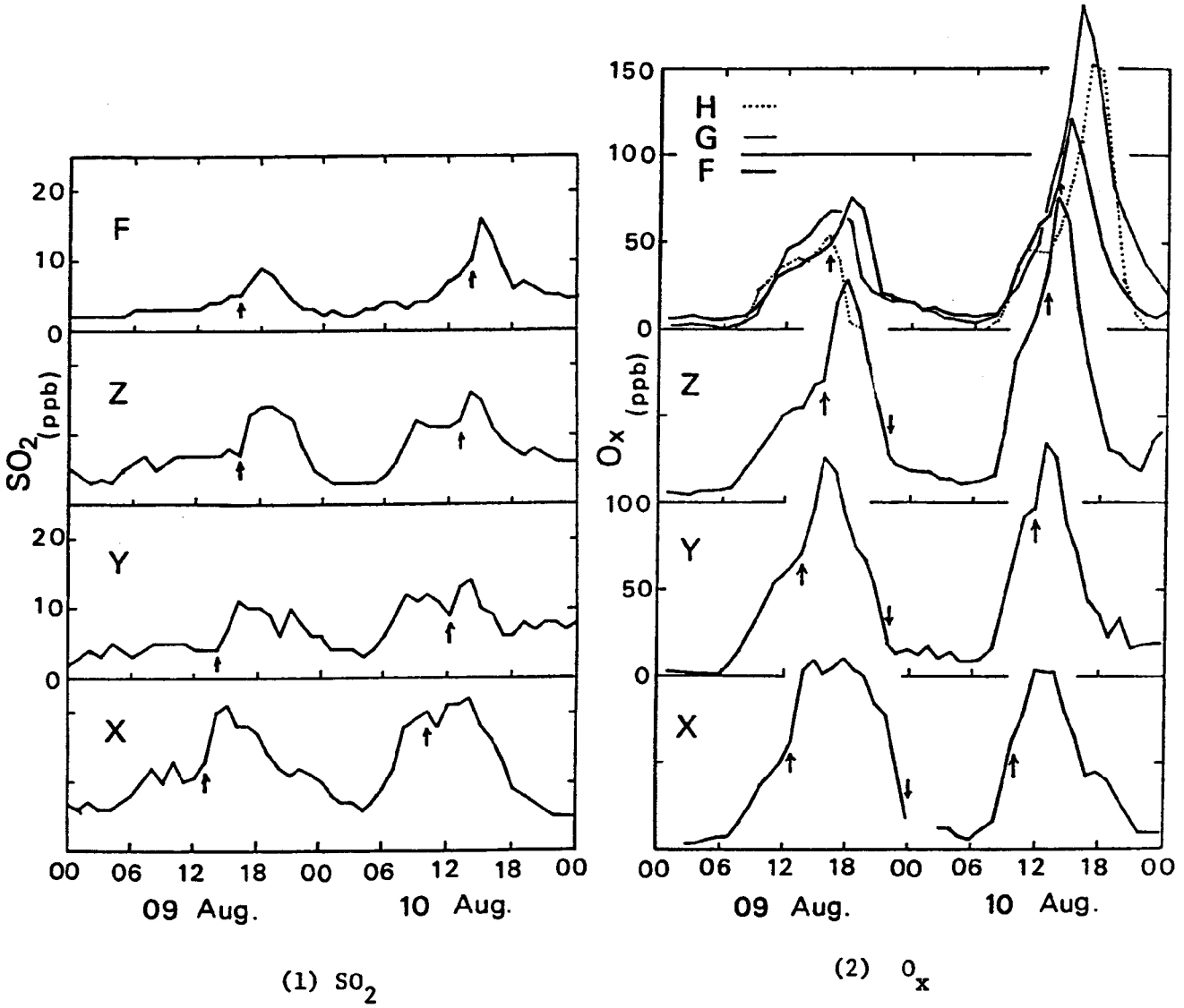

Fig. 10 Diurnal variation of SO_2 and O_x concentrations around the coastal area.

(9 - 10 August 1981)

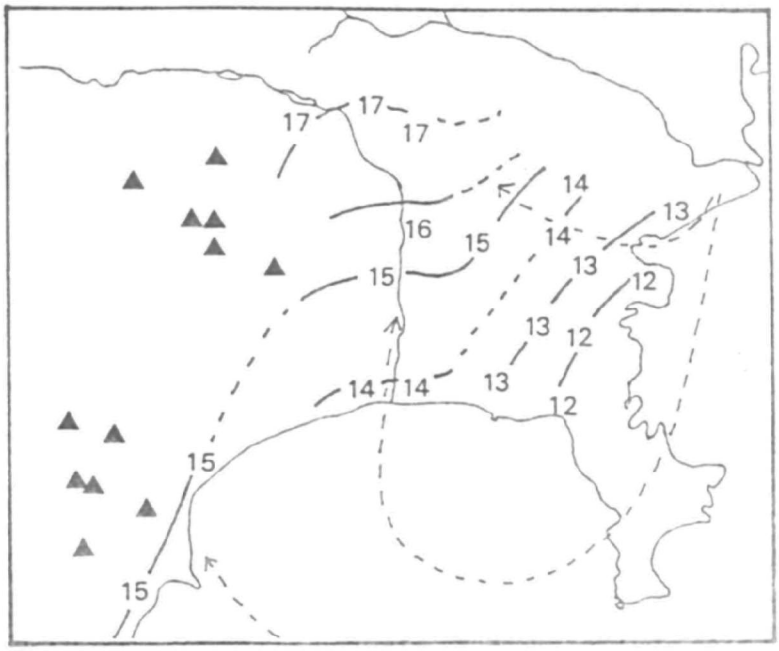

(1) The hour where the onshore flow passed by

and the trajectory of the air reached to shoreline at 14 h.

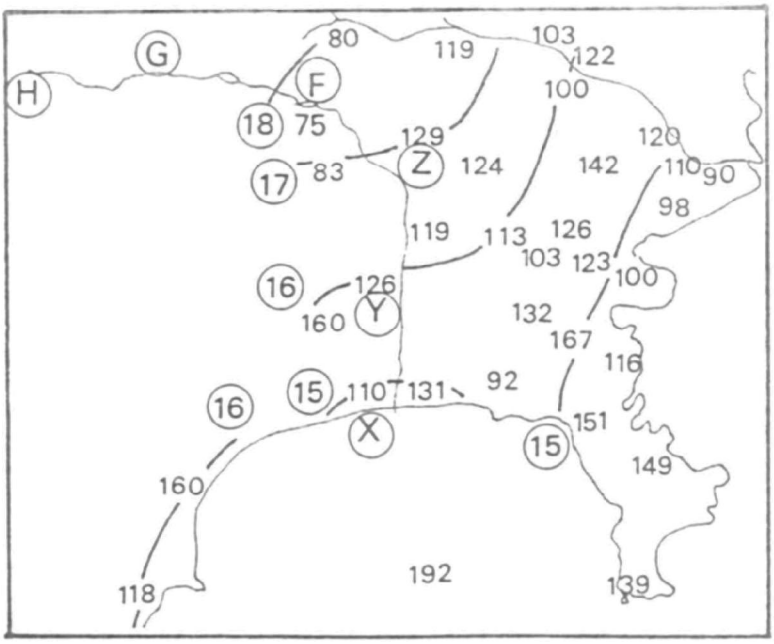

(2) Maximum O_x concentration

and the hour where maximum concentration was recorded.

Fig. 11 Analysis of monitoring data on 9 August 1981.

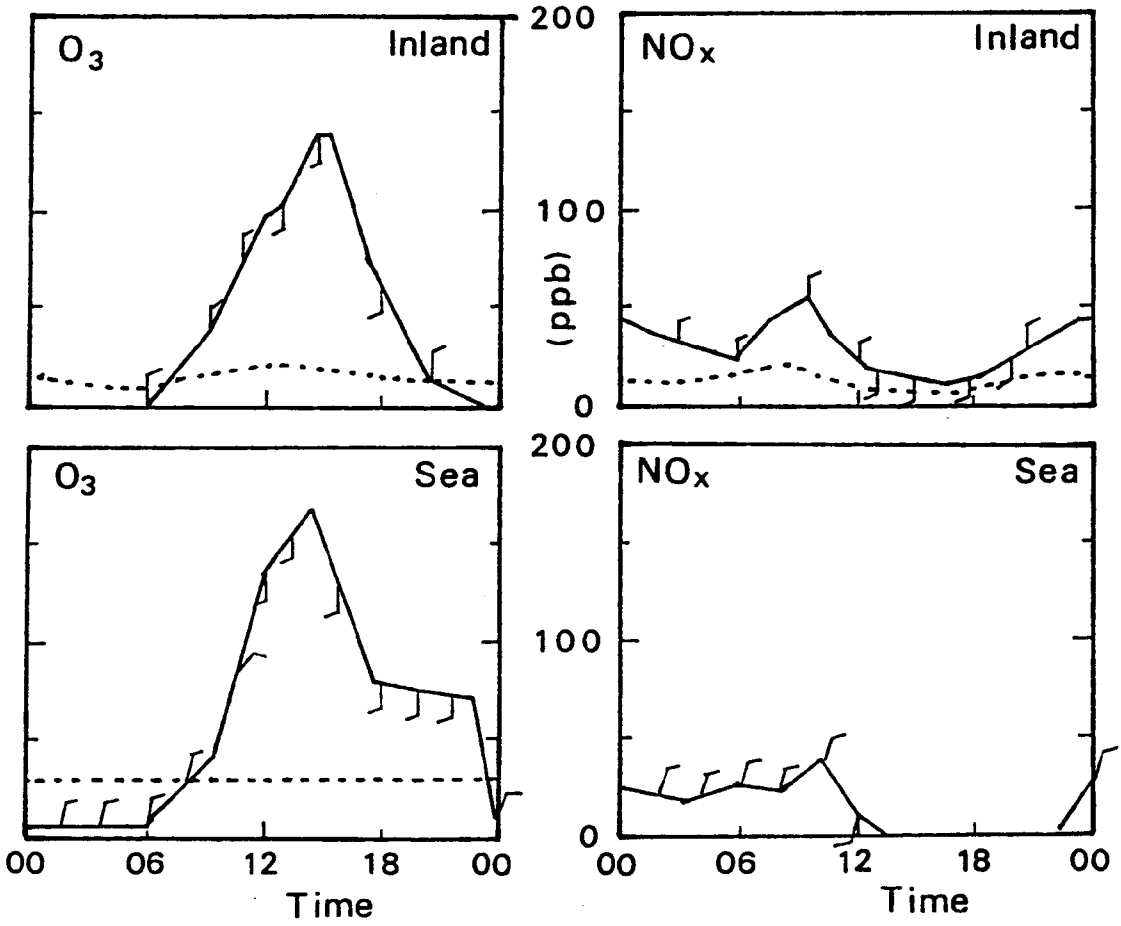

Fig. 12 Schematic diurnal variation of O_3 and NO_x concentrations over the land and the sea.

Solid line (——) corresponds with the day when the land and sea breeze occurs and dot line (----) with the day when the southerly wind blows all day.

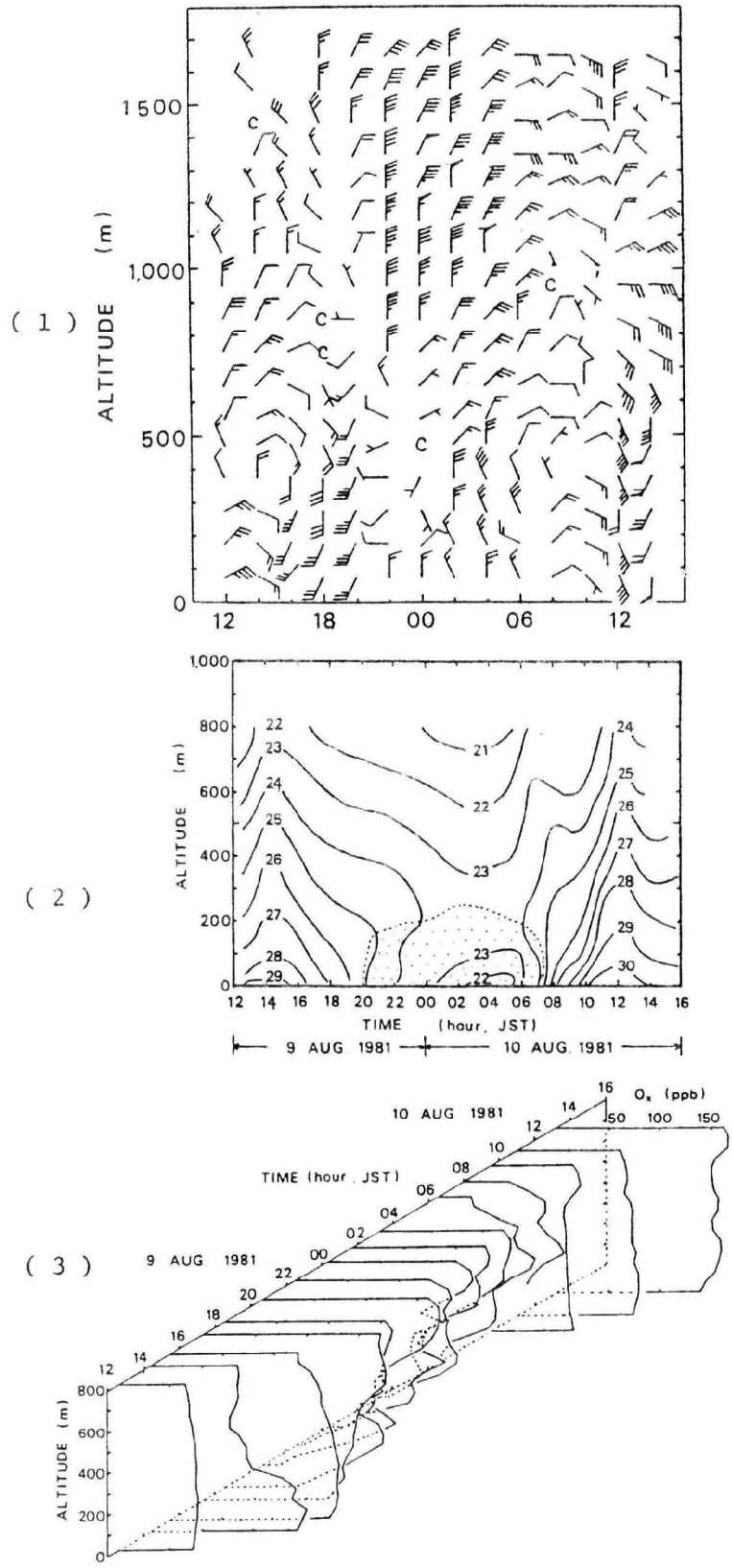

Fig. 13 Diurnal variation of vertical profile of (1) wind, (2) temperature and (3) Oxidant at station Y on 9-10 August , 1981.

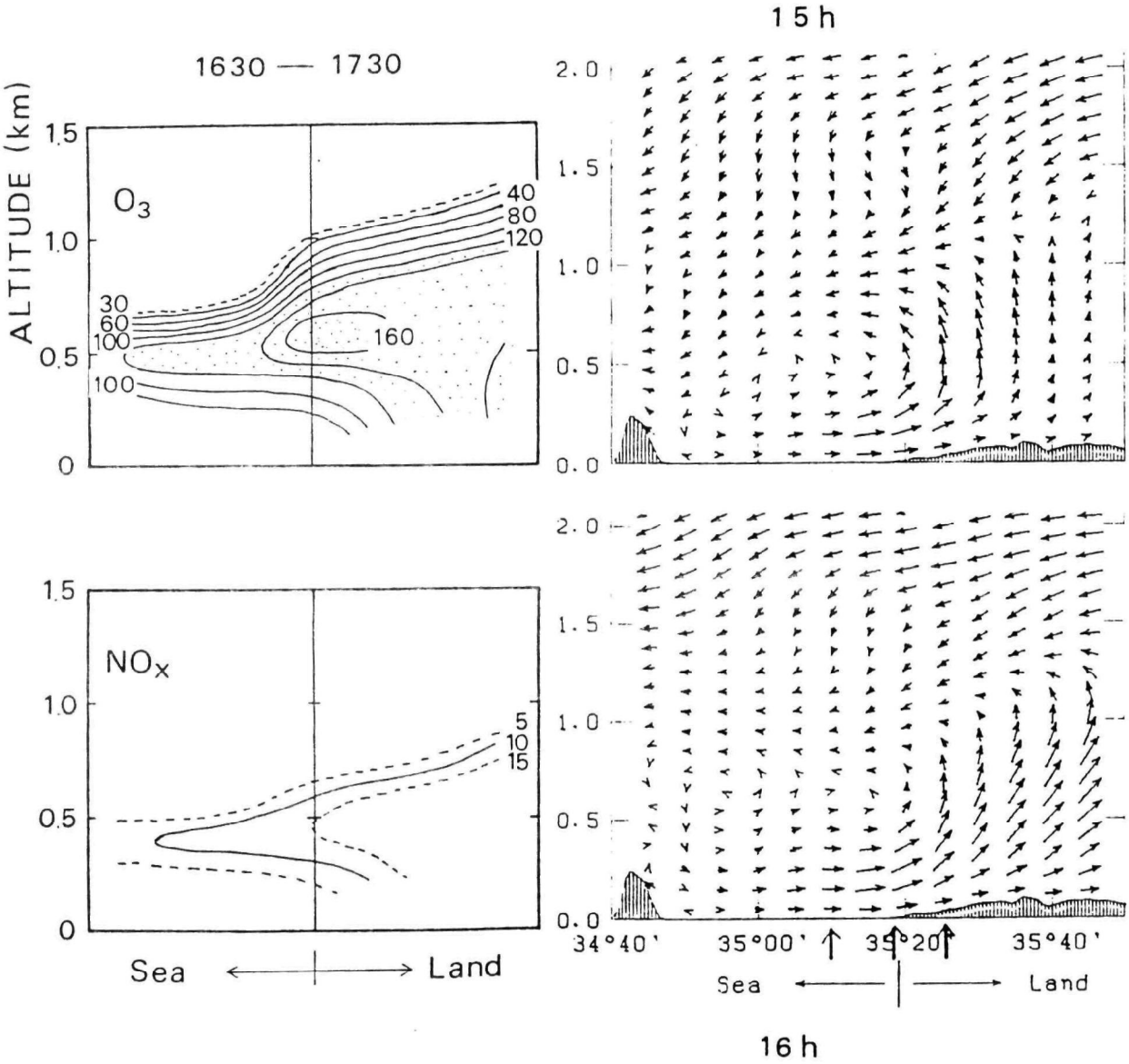

Fig. 14 Vertival cross section of O_3 and NO_x concentrations and the wind structure in the 3rd stage.

(9 August 1981)

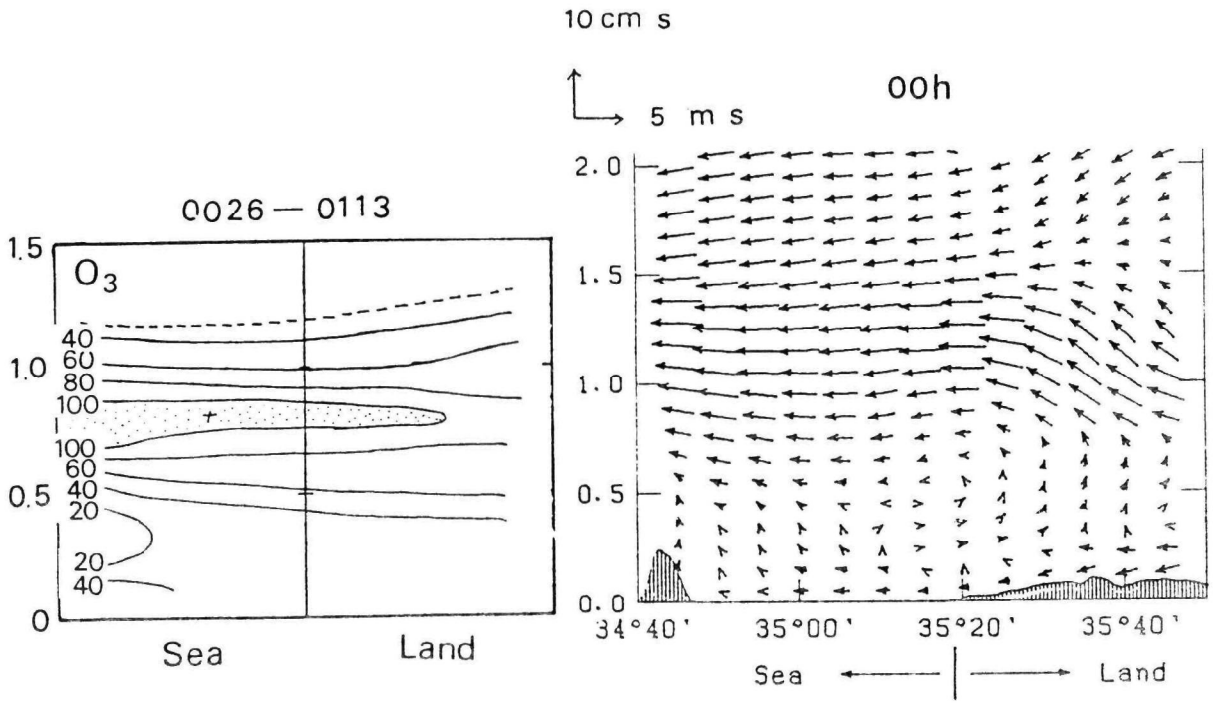

Fig. 15 Vertical cross section of O_3 and NO_x concentrations and the wind struture in the 4th stage.
(10 August 1981)

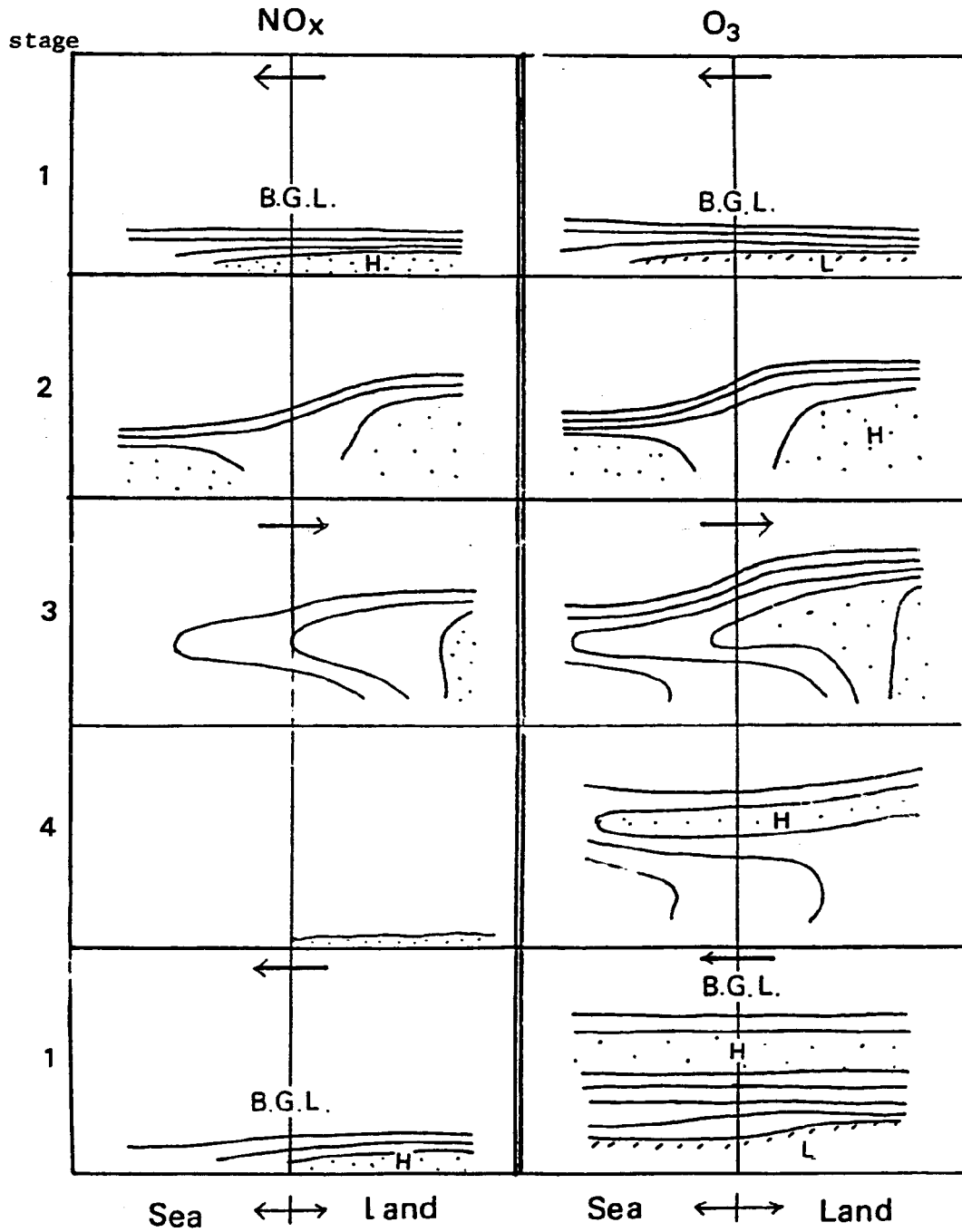

Fig. 16 Schematic pattern of the vertical cross section for the O_3 and NO_x concentrations in the four stage of the meso-scale circulation.

EVALUATION OF EIGHT LINEAR REGIONAL-SCALE SULFUR MODELS BY THE REGIONAL MODELING SUBGROUP OF THE UNITED STATES/CANADIAN WORK GROUP 2

presented by K.L. Demerjian

Environmental Sciences Research Laboratory

USEPA

EVALUATION OF EIGHT LINEAR REGIONAL-SCALE SULFUR MODELS BY THE REGIONAL MODELING SUBGROUP OF THE UNITED STATES/CANADIAN WORK GROUP 2

Francis A. Schiermeier
United States Subgroup Co-Chairman
U.S. Environmental Protection Agency
Research Triangle Park, NC 27711

Prasanta K. Misra
Canadian Subgroup Co-Chairman
Ontario Ministry of the Environment
Toronto, Ontario M5S 1Z8

The Atmospheric Sciences and Analysis Work Group 2, formed under the United States/Canadian Memorandum of Intent on Transboundary Air Pollution, was charged with describing the transport of air pollutants from their sources to final deposition, especially in ecologically sensitive areas. Eight linear regional-scale models developed by Canadian and United States scientists were applied by the Regional Modeling Subgroup of Work Group 2 using standardized 1978 emissions and precipitation input data sets. Model results were evaluated with currently-available January, July, and annual 1978 observational data sets.

Concentrations and depositions of sulfur compounds as well as source-receptor relationships (transfer matrices) were calculated by the eight long-range transport models using simplified formulations. These were state-of-the-art linear models in which scavenging and chemical transformation processes were treated linearly as a first approximation.

For the 1978 data set, most of the models appeared to perform relatively better in predicting the deposition of sulfur in precipitation than in predicting sulfate concentrations in ambient air. Based on available 1978 wet deposition measurements, the models were able to reproduce the correct order of magnitude of the large time and space-scale features of measured wet sulfur deposition patterns. In the construction of unit transfer matrices, the models examined by the Regional Modeling Subgroup predicted generally similar relative impacts on receptor regions in terms of ranked order of importance, although variations existed among models in the absolute magnitudes of the transfer matrix elements.

Introduction

The Atmospheric Sciences and Analysis Work Group 2 was one of five work groups established under the Memorandum of Intent (MOI) on Transboundary Air Pollution, signed by the governments of Canada and the United States on August 5, 1980. The objectives of the work groups were to synthesize available knowledge about the causes and effects of transboundary air pollution, with initial emphasis on acid deposition, for use by the governments of the two countries in negotiating a bilateral air quality agreement.

Under the auspices of Work Group 2, the Regional Modeling Subgroup conducted the Phase III evaluation of eight linear regional-scale sulfur transport models using standardized input and validation data sets. The Modeling Subgroup consisted of some members of Work Group 2 (restricted to employees of the Canadian federal or provincial governments and the United States federal government) and participating modelers. The participating modelers included non-government scientists directly involved in the operation of the Phase III selected models and those interested in advancing the science of model evaluation and intercomparison.

It was not possible (due to practical modeling considerations as well as our incomplete understanding of the phenomena) to provide models for all of the pollutants of interest or to incorporate all the processes mathematically into operational regional models. For example, deficiencies in both emission inventories and in our comprehension of transformation and deposition processes precluded the development of quantitative models for acid nitrate deposition. Nor was it possible to incorporate the detailed atmospheric chemical reactions between SO_2, NO_x, volatile organic compounds (VOC), oxidants, and their acidic reaction products. The models used by Work Group 2, therefore, contained simplifying assumptions which were based upon our current understanding of the phenomena of long-range pollutant transport.

The results of the Phase III evaluation of the eight long-range transport models are described in the Regional Modeling Subgroup Final Report[1] and are summarized in the Atmospheric Sciences and Analysis Work Group 2 Final Report.[2] The information contained in the Subgroup Report is representative of the current state of knowledge in modeling long-range transport of air pollution, given the limited time and resources available to conduct the evaluation and to prepare the report.

Model Profiles

Eight regional-scale sulfur transport models (Table I) developed by Canadian and United States scientists were selected by Work Group 2 based on criteria established during earlier phases of the MOI. These models were applied by the Regional Modeling Subgroup using standardized input and validation data sets to fulfill the MOI terms of reference. The techniques of simulating the transport, diffusion, transformation, and deposition of pollutants among the models were quite varied since: (1) the best modeling techniques were not clearly discernable; (2) the natures of all relevant physical and chemical processes were not well understood; (3) each modeler made various assumptions to simplify the complex processes; and (4) each model was developed independently.

The models are "linear" in the sense that chemical transformations and scavenging are expressed as first-order processes where the rate constants are assumed to be independent of emissions and co-pollutant concentrations. This assumption of linearity that is incorporated into all eight models used in the Phase III effort may be questioned. However, nonlinear parameterizations for models have either not been available or have not been feasible for incorporation into regional-scale transport models of the types used here at the present state of the art. The question that is subject to individual scientific judgment is whether the linear sulfur models represent a reasonable first approximation in the absence of operational nonlinear models. It is not clear that nonlinear effects would invalidate the general monthly and annual results of these linear models.

Each of the models simulated the transport, diffusion, transformation, and deposition of sulfur compounds. Monthly-averaged concentrations and depositions, as well as monthly source-receptor relationships (transfer matrices), were generated for central and eastern North America. The AES, ASTRAP. CAPITA, MOE, and RCDM models also included varying portions of western North America in the model domain. The ASTRAP, CAPITA, ENAMAP, MEP, MOE, and RCDM models were source-oriented, which facilitated generation of concentration and deposition fields, while the AES and UMACID models computed the concentrations and depositions at user-specified receptor points.

Most of the models utilized gridded SO_2 point and area source emissions as input and, with the exception of the ASTRAP and MEP models, treated the SO_2 emissions within a given grid cell as one virtual point source emitting pollutants at one level or within one layer. The ASTRAP and MEP models distributed the emissions vertically as a function of stability and stack characteristics. The emission grid resolution varied from model to model within the range of 70 to 190 km. In addition to SO_2, the AES, ASTRAP, CAPITA, ENAMAP, MOE, and UMACID models were capable of including primary sulfate emissions. During Phase III, the MOE model assumed a constant SO_4^{2-}/SO_2 ratio of 0.02, while the CAPITA model assumed that 1% of the total sulfur emitted was sulfate. The UMACID model varied the percentages of sulfur emitted in the form of sulfate from 1% in the winter to 5% in the summer. The AES, ASTRAP, and ENAMAP models required sulfate emissions input; if none were available (as was the case in Phase III), sulfate emissions were not considered.

Six of the models required objectively-analyzed meteorological observations, while the other two (MOE and RCDM) used the statistical characteristics of long-term climatological data. For example, the MOE model made assumptions regarding long-term wind statistics and the RCDM model used monthly and seasonal resultant wind vectors at each source emissions area to define the pollutant transport process. The MEP model used 6-hourly surface pressure data to generate wind fields, while the remaining five models used analyses of actual wind data (surface and/or upper air) observed at 3- to 24-hourly intervals. Precipitation data input requirements ranged from 3-hourly analyses to the average durations of wet and dry periods over seasonal or annual time periods. The analyses of the wind and precipitation data were performed by preprocessors and were not modules within the models.

The mixing heights parameterized in the AES, ENAMAP, RCDM, and UMACID models were treated as seasonally dependent constants. In these models, no diurnal fluctuations were considered; the heights reflected the estimated average mixing height over the simulation period. Only the AES model used monthly gridded values of the mixing height based on seasonally stratified climatological data. The CAPITA model used seasonally dependent mixing height values but also considered a nocturnal lowering of the mixing height to 300 m, thus simulating the release of nocturnal emissions above the surface layer. The ASTRAP and MEP models considered a diurnally fluctuating mixing height as well as the occurrence of a nocturnal inversion. A user-specified, fixed mixing height of 1000 m was used in the MOE model for the Phase III application.

The MOE and RCDM models used analytical functions to determine the distribution of mass in space and time after emission, while the other models treated the emissions as discrete puffs. The mass of sulfur in each puff was determined from the time increment (3 to 12 hours) and the emission rate. The AES model allowed input of pollutants to boxes which were transported across emission areas at 3-hourly time steps, while the other five models actually simulated the transport of individual pollutant puffs.

Horizontal dispersion was simulated in different ways. The AES and ASTRAP models calculated long-term dispersion directly through the distribution of simulated trajectories. The MEP model assumed a Gaussian distribution about the simulated plume centerline. The CAPITA model used constant daytime and nighttime horizontal dispersion rates, plus vertical shear overnight. The RCDM model assumed a constant horizontal dispersion rate, while the ENAMAP, MOE, and UMACID models used time-dependent dispersion parameters.

Vertical dispersion in all the models except ASTRAP occurred instantaneously within the specified mixed layer, resulting in a homogeneous distribution of pollutants in the vertical. Additionally, the MEP model allowed pollutant input above the mixed layer. The vertical dispersion in ASTRAP, which considered nine sublayers within the boundary layer, was dependent upon a diurnally varying stability profile.

The rate of transformation of SO_2 to sulfate was defined to be a constant 1% per hour in the AES, ENAMAP, MOE, and RCDM models. The transformation rate varied seasonally in the remaining models. In addition to the seasonal variations, the ASTRAP, MEP, and UMACID models also considered diurnal variations in the transformation rates.

Dry deposition of sulfur compounds was simulated using a constant deposition rate for SO_2 and another for sulfate in the AES, MOE, and RCDM models. The CAPITA and ENAMAP models used seasonally dependent dry deposition rates, while the remaining models used diurnally and seasonally dependent rates. The RCDM model also used the total dry time (total time in a period minus the total precipitating time) to calculate dry deposition.

All but the CAPITA and MOE models simulated wet sulfur deposition based on the actual precipitation rate over a specific period times a scavenging coefficient. The CAPITA model computed wet deposition using the 6-hourly probability of the occurrence of various intensities of precipitation across each 127-km grid square. The MOE model used an average precipitation rate

based on climatological data times a scavenging coefficient, and assumed that the probability of precipitation scavenging was related to the durations of wet and dry periods along the pollutant trajectory. Wet deposition in the RCDM model was simulated by the product of the scavenging coefficient, the total precipitation for the simulation period, and the ratio of total time to wet periods. The MEP model also considered the pH of the precipitation based on seasonal pH observations and the ambient temperature as factors for determining the amount of wet sulfur deposition. The AES, MEP, and MOE models systematically added a constant background sulfur contribution to the annual wet sulfur deposition.

These descriptions of the model input data requirements, model parameterizations, and model output address specific Phase III applications of Work Group 2. In a series of applications of different scenarios, the nature of the available input data, the time and cost constraints, and the desired model output often dictate the form of model parameterizations. Thus the features used in the Phase III model parameterizations may differ from those used in previous phases and are subject to change for subsequent applications.

It should be noted that these eight long-range sulfur transport models represent the various types of currently available models capable of simulating sulfur transport, diffusion, transformation, and deposition. The variations in techniques and parameterizations of the models reflect a breadth of scientific opinions and judgment amongst the modelers. As the pertinent physical and chemical processes and relationships become better understood, these models will likely be modified to reflect the resulting gains in knowledge.

Phase III Input Data Bases

The standardized 1978 input data sets for the Phase III modeling effort included sulfur emissions and precipitation data. In the Phase III Canadian SO_2 emissions inventory representative of 1978, point sources were located by latitude/longitude while area source emissions were gridded on a 127-km spacing. The area emissions were calculated for 1976, but were not expected to differ greatly from 1978. All large point sources, specifically major power plants and smelters, were updated to their 1978 emission levels while smaller point sources were reported for 1976, the most recent year for which data were available.

The United States SO_2 emissions inventory for 1978 was given for each eastern state as total emissions for the utility and non-utility sectors. The utilities inventory was based on 1978 fuel consumption, plant flue gas desulfurization equipment, and other fuel characteristics. Although the non-utility emissions estimates were derived from 1980 data, their use was recommended by Work Group 3B in the absence of better information.

A further disaggregation of the emissions for the eastern United States was performed by the Regional Modeling Subgroup. Emissions from the 200 largest utility emittors for 1978 were gridded based on the source latitude/longitude. The remaining utility emissions were distributed as state wide percentage changes in the 1979 emissions of plants not included in the top emittors for 1978. The non-utility emissions were disaggregated within each state by scaling the non-utility source totals to

the emissions inventory prepared for the Multistate Atmospheric Power Production Pollution Study (MAP3S). In the MAP3S inventory, point sources were located by latitude/longitude and area source emissions were presented as county totals located at the area centroid of each county.

The western United States emissions distributions were provided by Work Group 3B. The emissions from large point sources, except utilities emitting more than 25,000 (short) tons per year, were taken from the 1978 National Emissions Data System (NEDS) files and were identified by latitude/longitude. The large power plant emissions were estimated separately by an EPA contractor. All other emissions were extracted from NEDS and provided by Air Quality Control Region. Because of this piecemeal approach, standardized western United States emissions were not available in model compatible form in time for incorporation into the Phase III model runs. Thus, different emissions estimates for the western states--if any--were used by the participating modelers.

To facilitate analysis of some modeling results, the 40 emissions source regions in the United States and Canada (Figure 1) were grouped into 11 aggregate regions (Table II). The uncertainties in the emissions data were not available at the time of model evaluation. It is not unlikely that these uncertainties are functions of source regions, which would affect the model results significantly since a constant uncertainty factor would only introduce a bias. Furthermore, since emissions were only available as annual totals, model predictions cannot be expected to accurately simulate monthly or seasonal emissions variations. To properly analyze the behavior of model predictions, one would need to know the magnitudes and spatial variability of all the emissions uncertainties.

The amount of sulfur deposition predicted by the models was a function of the estimates of precipitation used as input. Therefore, it was important to make independent, rigorous estimates of actual precipitation at the targeted sensitive receptors as well as at the sites used to evaluate model performance. In addition, since the meteorological representativeness of the period of simulation was of special interest, the precipitation amounts for 1978 were compared with 30-year normals to determine how precipitation amounts for this year compared with statistical averages.

At the thirteen model evaluation sites in eastern North America, the precipitation data obtained from rain gauge values were corrected for biases in rain gauge type and for wind effects. At the nine targeted sensitive receptors used for construction of transfer matrices, areal estimates of the monthly and annual precipitation amounts were determined by averaging the daily total observed precipitation from all recording sites in an 80 by 80 km grid cell centered on the receptor. These values were similarly adjusted to reflect unbiased precipitation amounts.

The observed precipitation during 1978 at the ten Canadian evaluation sites was on the average 50% above the 30-year normal in January, 20% below the normal in July, and about normal for the year. At the targeted sensitive receptors (Figure 2), five of the areas had January 1978 totals that exceeded the 30-year average by more than one standard deviation, showing that the month was exceedingly wet. For the month of July 1978

and for the year 1978, only two sites had values that fell outside (below) one standard deviation from the average values.

Phase III Network Observations

The evaluation of model estimates with observations was a critical aspect of assessing model performance. The Regional Modeling Subgroup agreed in Phase III to compare results from the selected models with network data in eastern North America for January, July, and annual 1978. Different networks were surveyed and evaluated based on availability of data, sampling period, geographical coverage, data capture and the degree of local effects. The Electric Power Research Institute's Sulfate Regional Experiment (EPRI SURE) and the MAP3S sampling networks in the northeastern United States and the Canadian Network for Sampling Precipitation (CANSAP) network in Canada were selected for the model evaluation.

In order to proceed with the model evaluation within the Phase III report deadline, the Regional Modeling Subgroup decided on criteria for data representativeness and capture, and on methods for estimating uncertainties in the data. The criteria, methodology, and resulting evaluation data for each network are described in detail in the Regional Modeling Subgroup Final Report.[1]

The only network meeting the selection criteria for air quality data was the EPRI SURE, which measured SO_2 and sulfate concentrations in the eastern United States on hourly and 24-hourly intervals, respectively. During the period under consideration, the nine Class I sites operated for the entire year while the 45 Class II sites only operated during four intensive periods (January 10 to February 10, April, July, and October 1978). It was agreed not to use the SO_2 data because these measurements were subject to influence by local sources, and because 50% of the SO_2 measurements were below the detection limit of 3 ppb.

Sulfate measurements for both Class I and Class II EPRI SURE sites were used to generate evaluation data sets for January and July of 1978 while only Class I sites were considered for the annual average estimates. To generate a monthly average concentration, a site was required to have a minimum data capture of 65% for the month except for the Class II sites in January, where data capture was relaxed to 55% (since these sites only operated a maximum of 22 days during that month). At least nine months of data were required for valid annual estimates. No regionally representative air quality measurements were available in Canada, except for one site in the EPRI SURE network.

The CANSAP network measured concentrations of sulfur in precipitation and precipitation amounts, permitting estimates of sulfur deposition for the sampling period (usually monthly). CANSAP had 20 sites operating within the region east of Manitoba. Ten of these were rejected because of poor handling, insufficient data, location in urban or industrial areas, or influence by local sources. Three of the remaining sites were considered questionable and flagged as such, but were included in the model evaluation exercise. For the ten acceptable sites, it was required that for the monthly sample, the monitor must have operated a minimum of 20 and a maximum of 35 days per sampling month and have a minimum collection efficiency of 25%. Collection efficiency is defined as the ratio, expressed

in percent, of the precipitation amount recorded by the sampler to the actual amount estimated from the catch in a co-located rain gauge, where the catch was adjusted based on collector type, site exposure, and wind effects.

CANSAP wet deposition samples at coastal sites were corrected for contributions from sea salt, while corrections for under-catch and evaporation were made at all ten sites. Resulting values for wet deposition were expressed as kilograms of sulfur per hectare. Annual amounts were obtained by simply scaling the collection period (9 to 11 months) amounts to the annual precipitation at the site.

The MAP3S network sampled on a daily basis. Samples with a catch of less than 50% of the nearby rain gauge volume were not used for deposition calculations. When the daily sampler catch exceeded 50% of the rain gauge catch, the volume of the rain gauge was used for deposition calculations. Total deposition for a specific month was calculated only when the total sampler catch for the month was a minimum of 90% of the rain gauge volume. Only four sites reported wet deposition for July 1978, but one of these was rejected because of an unresolvable difference of precipitation between the reported sample catch and the official rain gauge report at the same site. January and annual 1978 wet deposition estimates were only available for one MAP3S site and hence, were not included in the data set for model evaluation.

The data from the CANSAP, MAP3S, and EPRI SURE networks are believed insufficient for conclusive model evaluation. The periods chosen, two sample months and the entire year, were too short, while the spatial distribution of the data was also poor. Air quality data were only available in the eastern United States while the precipitation chemistry data were mainly for Canada. The uncertainty, especially in the CANSAP data, was high, being about a factor of two in many cases based on under-catch alone. In addition, a bias in the annual estimates is likely when only nine months are required for the annual sample and when the missing months fall completely within one season. Based on these considerations, the model evaluations to be described below can only serve as a demonstration of the statistical methodology to be used and as a preliminary indication of model performance.

Transport Winds and Precipitation Fields

An attempt was made to compare the methods which were used by each model to analyze the transport winds and precipitation fields, and to compare the dispersion which was either explicitly expressed or was inherent in the scatter of sequential trajectories. The purpose was to offer insight into the manipulation of the standardized meteorological data by the different models in the hope of explaining some of the differences in results between the models.

Each modeler was requested to calculate trajectories at time steps of 12 hours up to a total of 96 hours for January and July 1978. The origins of the trajectories were chosen to be Sudbury, Ontario and St. Louis, Missouri. The former site was selected because it represented a significant point source in a region with relatively sparse wind data, while the latter represented an area of relatively good wind data availability in all directions. The resulting mean displacements for the various models

varied considerably, both in distance and direction, depending upon the type of data used to generate the wind flow. Such discrepancies in the calculation of mean trajectories were a definite factor in producing differences in model concentrations and depositions.

Some of the models displayed westward displacements after long eastward travel times; this was an attribute of the analyses for this trajectory exercise and did not represent what was used in the model evaluation effort. Pollutant puffs transported to the northern or eastern boundaries were dropped since computation of trajectories outside the modeling domains were terminated, thereby biasing the trajectory statistics toward the lower wind speeds used in this exercise.

The dispersion over the extended period of analysis caused by shifting wind patterns was computed explicitly by two of the models, but was implicit in the sequential trajectory calculations of the remaining models. To compare the effective dispersion in January and July 1978 from Sudbury and St. Louis, calculations were performed of the square root of the sum of the variances in the x (east) and y (north) directions. As with the trajectories, the values of the standard deviations from model to model varied widely, depending on the methodology that was employed to calculate the transport field.

An analogous test was made for the second meteorological input common to the models, namely precipitation. The precipitation gridding process is quite dissimilar between models, which can lead to significantly different results. For example, some models gridded hourly precipitation data to compatible time steps and grid configurations. Since these gridding processes and configurations were dissimilar, the precipitation amounts derived for grid cells encompassing wet sulfur deposition receptors usually differed between models. Other models relied on a statistical treatment of the stochastic properties of precipitation to estimate the precipitation occurrence and amounts along the trajectories. This analysis involved specification of the probabilities of changing from wet to dry periods and vice versa, and the frequency distribution of precipitation amounts. Therefore, similar precipitation data sets obtained and gridded independently can lead to discrepancies in the modeling results.

Model Evaluation

The physical and chemical processes associated with the long-range transport and deposition of pollutants are extremely complex and, at the present time, our understanding of them is limited. Because of this limitation, the framework of long-range transport models will have to be modified to accommodate new information as it becomes available. This suggests that our confidence in model simulation is directly related to the amount of evaluation that has been performed.

A set of criteria for model evaluation was formulated by the Regional Modeling Subgroup, based on the recommendations of the Workshop on Dispersion Model Performance sponsored by the American Meteorological Society. The criteria were based on the differences between observed and model-predicted monthly and annual values for ambient sulfate concentrations and for wet sulfur deposition. The sulfate concentrations used for model evaluation were obtained from the EPRI SURE monitoring network as shown in

Figure 3; the number of values available were 29, 47, and 9 for January, July, and annual 1978, respectively. All but one of the sites were located in the United States. The networks of CANSAP (ten sites in Canada) and MAP3S (three sites in the United States) were used as the source of wet sulfur deposition values for the model evaluation exercise (Figure 4); the number of values available were 7, 13, and 8 for January, July, and annual 1978, respectively. The statistical tests and evaluation results are described in detail in the Regional Modeling Subgroup Report.[1]

Although significant limitations exist in the input emissions and precipitation data as well as in the measurement data used for evaluation, some conclusions can be drawn regarding the overall performance of the models. Collectively, the models appeared to perform better for wet sulfur deposition than for ambient sulfate concentration prediction. This is somewhat surprising because wet sulfur deposition is episodic in nature, whereas the model results were aggregated as non-episodic or longer-term. Ambient SO_2 was not considered for the evaluation exercise due to unavoidable contamination of data from nearby sources and errors in measurements at very low concentrations.

The evaluation data set for annual 1978 contained only eight points for wet sulfur deposition and nine points for sulfate concentrations. This did not constitute a sufficient data set from which to draw statistical conclusions on the relative performance of models. Therefore, although some models appear individually to perform better than others, no firm conclusions should be drawn without more extensive evaluations. Clearly, while a start has been made toward developing evaluation statistics, further testing must be done to provide reliable quantitative information about model performance.

Transfer Matrices

The MOI terms of reference required Work Group 2 to recommend tools for preliminary assessment activities. This included the evaluation of observations and the estimation of emissions reductions that would be needed in source regions in order to achieve proposed reductions in air pollutant concentrations and deposition rates necessary to protect sensitive areas. The principal tools available for this assessment are air quality simulation models (including the long-range transport models used in this exercise), local and mesocale models, and transfer matrices. Transfer matrices should be viewed primarily as a convenient form for either representing the results of a model or for applying those results to the study of emissions reduction scenarios.

The effect that emissions of pollutants from any source (or group of sources in a region) will have in producing ambient concentrations and deposition of pollutants at some other receptor location is known as the source-receptor relationship. That relationship is determined by the directions that pollutants are carried by the winds and also by the dispersal, chemical transformation, and removal of pollutants along the way. It should be understood, however, that nonlinear processes and interactions among pollutants are important to the actual, absolute source-receptor relationships. To the extent that such nonlinear processes are important, one cannot define a simple relationship among the regions because the effect that emissions from one source have on any receptor depends somewhat on various pollutants emitted from other sources.

Transfer matrices are based on the principle of linear superposition of pollutant emissions from various sources. This means one assumes that concentrations and/or depositions at a receptor location are the sum of partial contributions, where each contribution is proportional to emissions from a source or group of sources in an upwind region. Thus, a coefficient of proportionality exists connecting each source region with each receptor. The array of these coefficients connecting all sources with all receptor locations of interest constitutes a normalized or unit transfer matrix.

The eight long-range transport models were used to calculate transfer matrices for ambient sulfate and for wet and dry sulfur deposition for the periods of January, July, and annual 1978. Nine targeted sensitive receptors were originally selected by the Canada/United States Research Consultation Group as receptors sited in regions of northeastern North America which are sensitive to acidic deposition. Figure 2 shows the locations of these receptors. The 40 by 9 matrices of Phase III pertained to groups of all SO_2 sources over 40 source regions (Figure 1) and to the nine targeted sensitive receptor areas. Smaller 11 by 9 matrices were also produced by aggregating the 40 source regions into 11 larger source regions (Table II). Tables of normalized transfer coefficients (matrices) for wet and dry sulfur deposition and for ambient sulfate concentration calculated by the eight long-range transport models are presented as Appendices to the Regional Modeling Subgroup Final Report.[1]

The Phase III matrices showed substantial variation in the absolute size of transfer coefficients from one model to another which is to be expected since the annual matrices are based on various meteorological periods and different analysis methods using the 1978 input data. Hence it is difficult to ascertain correct values for the absolute size of source-receptor relationships.

If emissions reduction studies are not based on absolute values of source-receptor relationships, the demands on accuracy from matrix elements are less critical. For example, if prescribed emission reductions were established for large regions, then matrix elements might be used for only a qualitative indication of the relative importance of different source regions to given receptor areas. For purposes of qualitative assessment, perhaps only the relative position of rank orders among source regions would be of concern. Rank order simply means that the source regions are placed in order according to the value of the matrix elements pertaining to a given receptor. Thus, if the value for source A exceeds that for source B, it is ranked above B irrespective of the absolute size of the difference. Preliminary analysis indicated that the eight models produced matrices with reasonably consistent rank orderings.

Transfer matrices represent the results of model calculations and generally suffer from any limitations in the model and input data used to calculate them. Some additional limitations are inherent in the matrices as a result of definitions and approximations made in their calculation, which include the lumping of emissions sources in each source region and averaging pollutant values over space and time in the receptor area. These specific matrix limitations are not at issue, but need to be accounted for when attempting to use the matrices in practical applications.

More controversial questions about matrices relate to interpretation of the significance of matrix elements and to their validity as assessment tools. Normalized matrix elements explicitly identify quantitative relationships between source regions and receptor regions and tend to imply a linear relationship between emissions and air quality or deposition. While those relationships are also imbedded in the parent model if it is one of the linear types used in Phase III, the source-receptor relationship is not so obvious in aggregate model results. Predictions of absolute values of concentrations and depositions can be compared with observed data, but neither the linearity nor the partial contributions from each source region can be directly verified by comparison with currently available data. In the absence of such direct validation, there is disagreement about the degree of confidence that can be placed in the linearity of prediction and in the inferred source-receptor relationships based upon given level of agreement between model calculations and current absolute observations.

Conclusions

While differing opinions persist within the modeling community as to the proper method and the statistics to be used for evaluation and intercomparison of model results, the Regional Modeling Subgroup designated specific evaluation criteria for performing this task for the eight selected models used in the Phase III MOI application.

It is generally accepted that one should expect model predictions to deviate from measurements because a practical model cannot incorporate even our current understanding of the relevant chemical and physical processes involved in long-range transport and deposition of pollutants, and because available observational data are insufficient to estimate the ensemble average which the model is designed to predict. Due to these deficiencies, it is not possible to quantify the uncertainties in model predictions based on the differences between model predictions and observations (residuals).

One of the original tasks for the Regional Modeling Subgroup was to recommend the best model(s) for future use in emission reduction scenarios. Towards this end, the input parameters of the models were displayed and model evaluation criteria were standardized to ascertain model accuracies. However, due to uncertainties in the emissions inventory and precipitation data used by the models as well as in the measurement data used for evaluation, a ranking of models in terms of their absolute performance could not be made during the Phase III effort.

Furthermore, the assumption of linearity by the models provides for rate constants that are independent of emissions and co-pollutant concentrations. The question is raised as to whether the linear models of sulfur transport represent reasonable first approximations in the absence of operational nonlinear models. Complete analysis of the impact of nonlinearity was beyond the scope of the Phase III effort, although additional sensitivity analyses using the models and evaluations against measurement data could be expected to shed more light on this matter. For the present, however, it thus becomes subject to individual scientific judgment whether or not nonlinear effects would invalidate the general monthly and annual results of these linear models.

As a group, the simple linear models appear to be able to reproduce the right order of magnitude of the large time and space-scale features of the measured wet sulfur deposition patterns. The Phase III evaluations of the models with observed data showed that collectively, most models performed relatively better in predicting the deposition of sulfur in precipitation than in predicting ambient sulfate concentrations.

Transfer matrices for sulfur species produced by the eight long-range transport models revealed variations among the absolute magnitudes of the transfer matrix elements for a single model and for the same element among different models. It has not been possible to date to choose a best model among the eight nor to produce with confidence a best estimate single transfer matrix for each variable based upon a valid statistical analysis of all model results. However, all eight models predicted generally similar relative impacts on the receptors in terms of ranked order of importance based on the meteorology of one given year.

The diversity of parameterizations in these eight models reflects the fact that they were independently developed. The variations in techniques and parameterizations reflect a breadth of scientific opinions and judgment amongst modelers. It is not at all surprising that models show differences in detail when applied to a single data set. On the contrary, the extent of agreement among the model outputs and between these outputs with observed wet sulfur deposition data is encouraging.

Acknowledgment

This paper is a synopsis of work performed by the following members of the Regional Modeling Subgroup of Work Group 2:

Ball, Richard H.	Olson, Marvin P.	Shannon, Jack D.
Clark, Terry L.	Patterson, David E.	Weisman, Boris
Ley, Barbara	Peck, Eugene L.	Venkatram, Akula
Niemann, Brand L.	Samson, Perry J.	Voldner, Eva C.

REFERENCES

1. F. A. Schiermeier and P. K. Misra, "Regional Modeling Subgroup Final Report," United States/Canada Memorandum of Intent, Report No. 2F-M, 198 pp (1982).

2. H. L. Ferguson and L. Machta, "Atmospheric Sciences and Analysis Work Group 2 Final Report," United States/Canada Memorandum of Intent, Report No. 2F, (1982).

TABLE I. TRANSPORT MODELS ASSEMBLED BY REGIONAL MODELING SUBGROUP

	Model Name	Acronym
1.	Atmospheric Environment Service Long-Range Transport Model	AES
2.	Advanced Statistical Trajectory Regional Air Pollution Model	ASTRAP
3.	Center for Air Pollution Impact and Trends Analysis Monte Carlo Model	CAPITA
4.	Eastern North American Model of Air Pollution	ENAMAP-1
5.	Transport of Regional Anthropogenic Nitrogen and Sulfur Model of Meteorological and Environmental Planning, Ltd.	MEP
6.	Ontario Ministry of Environment Long-Range Transport Model	MOE
7.	University of Illinois Regional Climatological Dispersion Model	RCDM-3
8.	University of Michigan Atmospheric Contributions to Interregional Deposition Model	UMACID

TABLE II. PHASE III SOURCE REGION GROUPINGS

Region Number	Region	Source Areas Included
1	Maritime Provinces	20, 21, 22
2	Quebec	17, 18, 19
3	Ontario	12, 13, 14, 15, 16
4	Western Provinces	10, 11, 23, 24
5	Northeastern States	59, 68, 69, 70
6	Eastern Midwest States	50, 52, 58
7	East Coast States	63, 66
8	Southern and Gulf Coast States	60, 64, 65, 67
9	Central States	51, 53, 54, 56, 57
10	Western Midwest States	55, 61, 62
11	Western States	71, 72, 73, 74

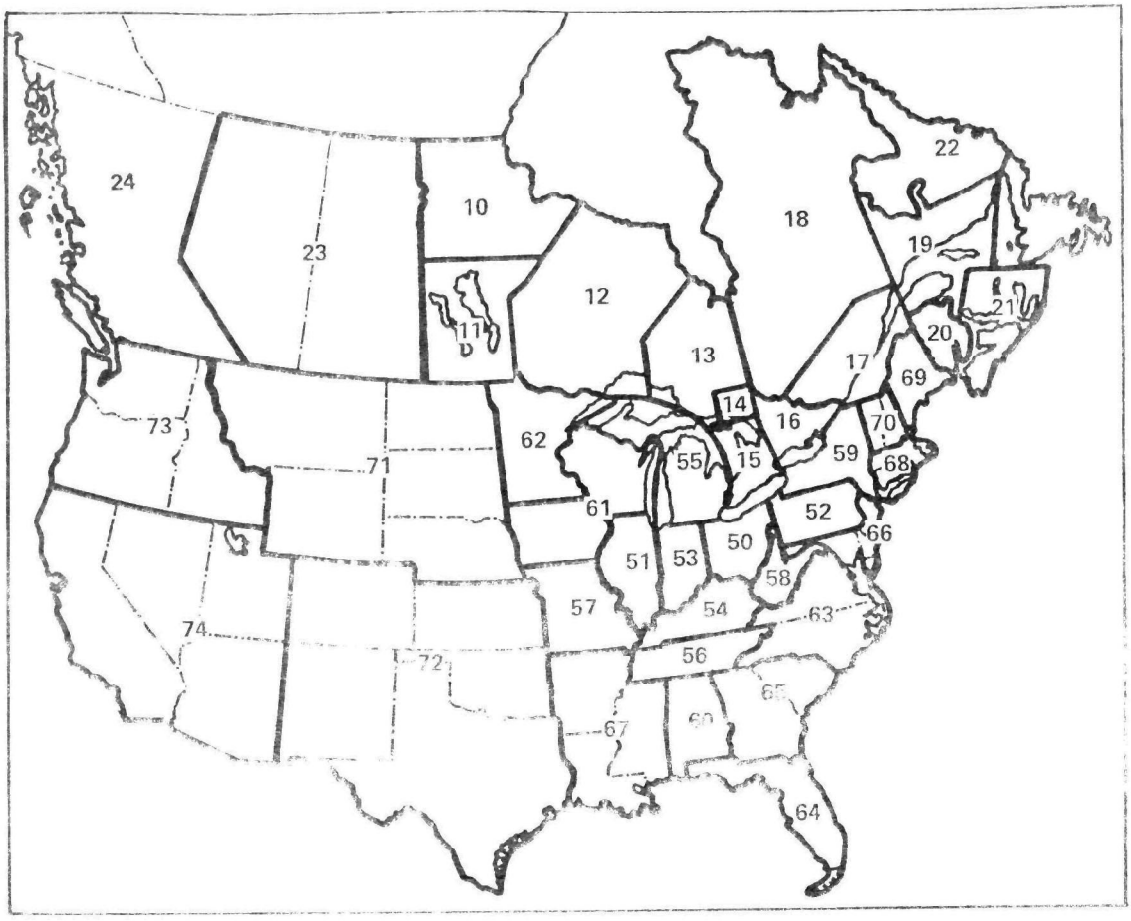

Figure 1. North American emissions source regions.

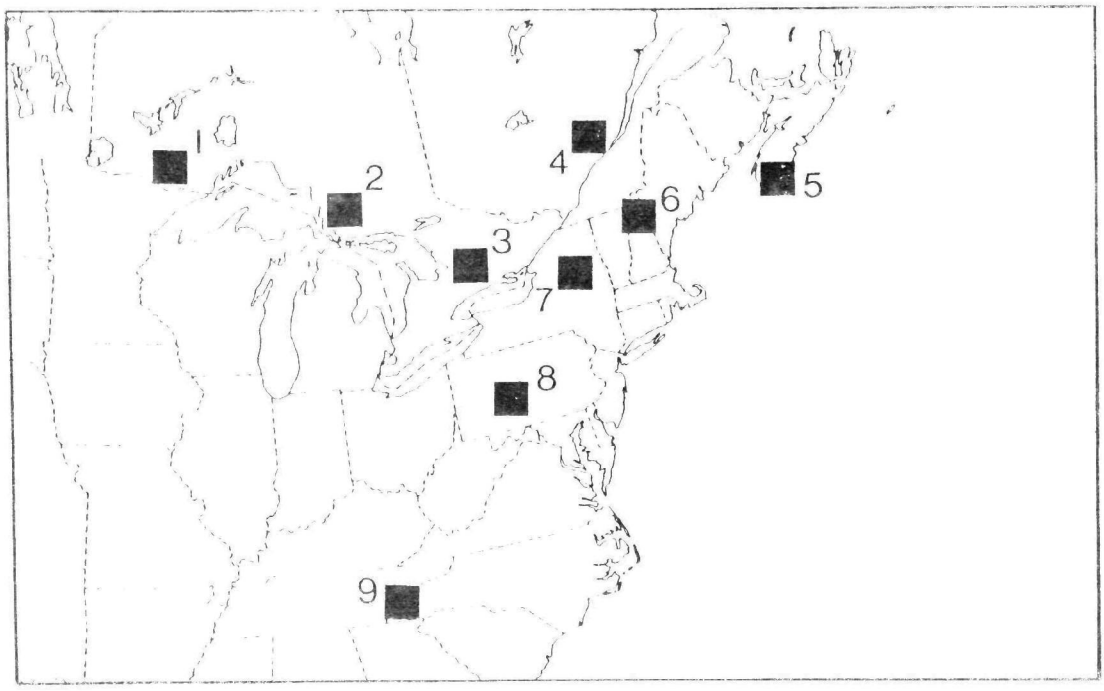

Figure 2. North American targeted sensitive receptor areas.

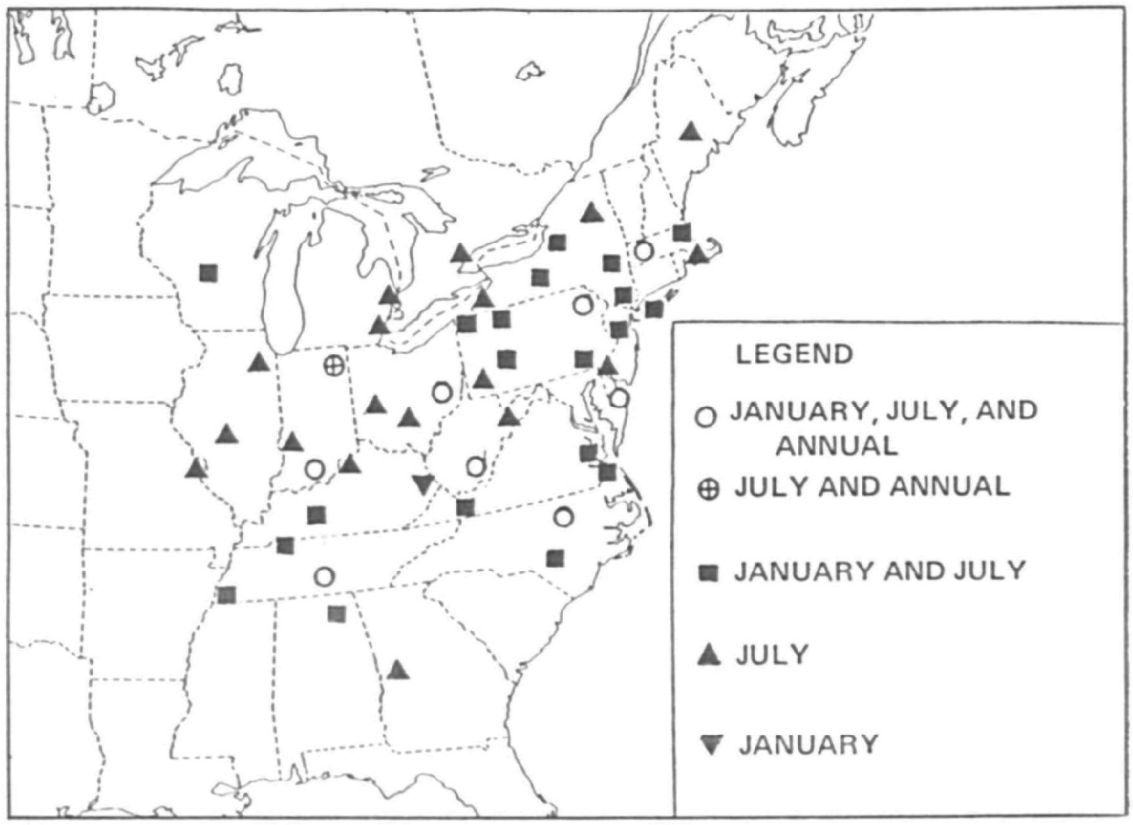

Figure 3. EPRI SURE sites used in Phase III model evaluation.

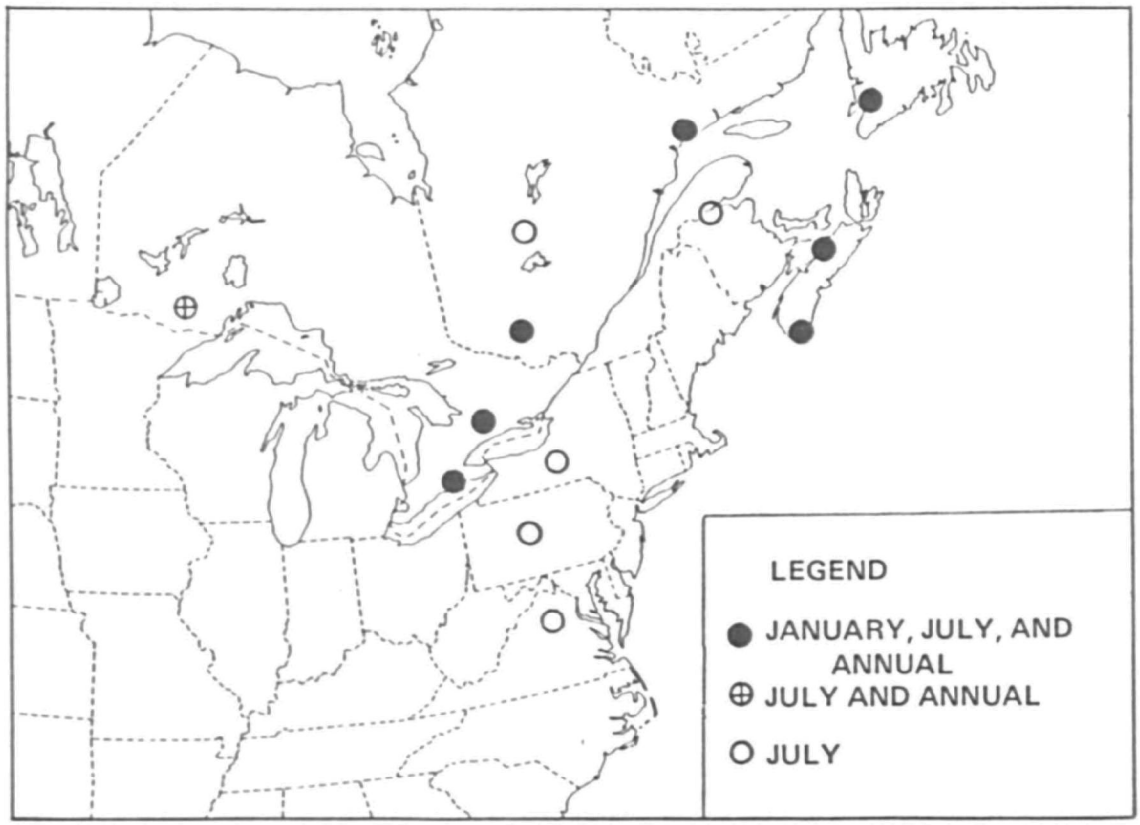

Figure 4. CANSAP and MAP3S sites used in Phase III model evaluation.

FIELD STUDIES ON PHOTOCHEMICAL AIR POLLUTION IN JAPAN

Shinji Wakamatsu
Itsushi Uno
Makoto Suzuki
Yasushi Ogawa

National Institute for
Environmental Studies
P.O. Yatabe, Ibaragi 305
JAPAN

presented by S. Wakamatsu

National Institute for Environmental Studies

Japan EA

1. Introduction

Photochemical oxidants are major air pollutants in Japan. The Japan Environment Agency has been measuring oxidant concentration at more than 900 stations throughout Japan. Especially high concentrations are observed around the Tokyo Metropolitan Area and the Osaka area in the summer season, but high oxidant concentrations, more than 60 ppb, exceeding the environmental standard are also observed in the spring season at many monitoring stations in Japan. In this report, the monitoring data are analyzed statistically to clarify the seasonal variations of oxidant concentration in Japan. The aerial and temporal scales of photochemical air pollution are also analyzed using the data from about 300 monitoring stations and aircraft data covering the Tokyo Metropolitan Area.

2 The seasonal variations of oxidant concentration

The general phenomenon of high photochemical smog when a photochemical oxidant warning is issued usually occurs from May to September. A photochemical oxidant warning is issured by the governor of each prefecture when the hourly averaged oxidant concentration is 120 ppb or higher and when this state is likely to continue from a meteorological viewpoint. If the warning is issued in two prefectures on the same day, it is considered as two warning days. The total number of warning days in 1981 was 59. Of these 41 days were issued from the Tokyo Bay area and 16 days were issued from the Osaka Bay area. In addition, relatively high concentration (exceeding 60 ppb) are observed at many monitoring stations in Japan.

To clarify the seasonal variations of oxidants in Japan, daily maximum oxidant concentration between 1976 and 1980 were averaged monthly. These results are shown in Figure 1. The seasonal variation was classified into three distinct types. The first type shows a peak in the spring season between April and May. This type is mainly observed in northern part of Japan. The second type shows double peaks corresponding to the spring and autumn seasons and this type is mainly observed in southern Japan. In both cases, maximum oxidant concentrations are approximately 60 ppb. In the third type, the maximum peak of oxidants is mainly observed in summer season having a value of approximately 70 ppb. This third type is widely observed near the big city areas, such as Tokyo and Osaka. The former two types are probably due to stratospheric ozone intrusion.[1] The difference in seasons between the southern and northern parts of Japan may correspond to the difference of meteorological conditions. The third type is due to anthropogenic sources. These results shows us that the effects of stratospheric ozone subsidence are significant in the spring season, but negligible in the summer. Next, the aerial and temporal scales of photochemical air pollution from the anthropogenic sources will be analyzed focusing on the Tokyo Metropolitan Area in the summer season.

3. Temporal scale of photochemical smog

The Kanto Plain, where the Tokyo Metropolitan Area is stuated, is one of the biggest plains in Japan. The topography of this area shown in Figure 2. The western and northern sides are walled by mountains, 1,000 to 2,000 meter high. The eastern side is open to the Pacific Ocean, and in the south there are two bays, Tokyo Bay and Sagami Bay. The Keihin Industrial Complex is situated at the western side of Tokyo Bay and the Keiyo Industrial Complex is at the eastern side of this bay. On the southwest side of Sagami Bay, the Izu peninsula projects into the Pacific Ocean.

Generally speaking, when the geostrophic wind velocity is below the level of approximately 6 m/s, five different types of local wind circulations predominate in the summer season and the dynamics of photochemical oxidants are closely connected to them. The sea breeze from Tokyo Bay enter Tokyo as an SE wind. The large-scale sea breeze from Sagami Bay, designated as an S wind, arrives in Tokyo later than the Tokyo Bay breeze. The other large- scale sea breeze is from the Kashima Sea and this is designated as an E wind. The another two local wind circulations are mountain and valley winds. The mountain and valley wind from the western mountain area is seen in the early evening as an W wind and later, large-scale mountain and valley wind from the northern mountain area predomitates as an N, continuing till the early morning. Depending upon the general wind direction and wind speed, these five local wind circulation systems create an extremely complicated wind pattern over the Kanto Plain.

Between 15 July 1981 and 20 July 1981, photochemical smog warnings were issued successsively in the Kanto Plain under such local wind circulating systems. Reports on health injury suspected to be due to photochemical air pollution came from the southern Kanto district betbween 16 July 1981 and 18 July 1981.

On 16 July 1981 and 17 July 1981, three-dimensional observation using two instrumented aircraft were conducted. Upper wind profiles were also measured every hour at 23 stations, and temperature profiles were obtained using a radiosonde at 3 stations. These measurements and data from about 300 ground level monitoring stations provided sufficient information to clarify the mechanism of this episode on 16, 17 July 1981. The arrangement of the pilot-balloon stations, the daily maximum concentration observed in each prefecture and meteorological data observed at the Tokyo Meteorological Obsrvatory are shown in Figure 3. On 16, 17 July 1981, a land breeze predomitated till noon and the wind speed was low, so that high oxidant concentration was observed in the southern part of the Kanto district due to solar radiation and high temperature. From 18-20 July 1981, however, a southerly wind prevailed and relatively high oxidant concentration was observed in the northern prefectures of the Kanto district.

Figure 4a shows the ground level oxidant concentratin pattern at 1500JST which exceeded 100 ppb and the aircraft measurement data at an altitude of 350 m . The southerly Sagami Bay breeze was stopped by the easterly wind from the Kashima Sea and high concentrations were observed in the Sagami Bay sea breeze area. Aircraft data show that the extremely high concentration, exceeding 200 ppb, were observed near the coast side of Sagami Bay between 1450-1455JST. Figure 4b shows the air

trajectory at the altitude of 350 meters calculated from the pilot-balloon data. According to this trajectory analysis the extremely high concentration air mass at 1500JST was transported from the Tokyo Bay industrial area. This air mass was transported inland, and after 2100JST traveled down to the south due to the land breeze. This pattern was also observed on the next day.

Figure 5a shows the air trajectory at an altitude of 150 meter calculated using the 23 point pilot-balloon data on 17 July 1981. The 12 start points of the trajectory were set on an ellipse at 1300JST on the shoreline of Sagami Bay, then the backward and forward trajectories were calculated at one-hour intervals. Trajectory shows the same circulation as on 16 July 1981. Figure 5b shows the Lagrangian variations of NO, NO_2 and Oxidant concentrations along this trajectory line. Concentrations were obtained by interpolating the ground level monitoring station data. In the early morning, NO showed a peak, NO_2 increased corresponding to the NO decrease, and the oxidant concentration peaked in the afternoon. These tendencies coincidence with the smog chamber experiments.[2] The maximum oxidant concentration was observed at 1500JST at a point about 20 km inland from the shoreline of Sagami Bay, and according to the trajectory analysis this high oxidant concentration was mainly caused by emissions from the Tokyo Bay coastal industrial complexes.

To understand the two-dimensional structure along the trajectory line, the Figure 6 was drawn. Trajectory I and II are the averaged trajectory lines between 15 July 1981 and 17 July 1981. It is clear that the high oxidant zones correspond to the sea breeze zone in daytime and the high NO_2 zones correspond to the land breeze zone at nighttime. NO almost reacted with O_3, but on 15 July 1981, the maximum temperature and total solar radiation were not high so that the oxidant concentration was low compared with the other two days, and NO remained at nighttime.

From this analysis, it is clear that the time scale of the photochemical smog in the Tokyo Metropolitan Area is longer than one day, and under the condition of weak atmospheric pressure gradient, polluted air masses circulate for more than three days following the local wind circulation pattern.

4. Aerial scale of photochemical smog

The aerial scale of the photochemical smog covering the Kanto district can be classified according to two types of meteorological condition. The first type is local wind circulation predominant type, and the second is general wind predominant type. These two types are determined using the geostrophic wind calculated from the 700 mb constant pressure gradients. When the geostrophic wind is below 6 m/s, the local wind circulation systems predominate in the Kanto Plain. In this section the dynamics of the three-dimensional distribution under the condition of weak pressure gradient and long distance transportation phenomena in the condition of general wind predominant type are discussed.

Figure 7 shows the vertical cross section measurements using four

instrumented aircraft simultaneously. Figure 7a shows that the primary pollutants were trapped below the inversion layer and aged pollutants were remained above 500 m. having the maximum O concentration of 100 ppb at 800 m. high ,30-40 Km distance from the shore line. According to the sea breeze penetration and development of thermal convective layer NO was transported to the inland and upward as seen in Figure 7b-7c. In the afternoon maximum O was observed in Figure 7c,and in the midnight 140 ppb O remained at 500 m. high, 60-100 Km distance from the shore coast in Figure 7d. In the next morning previous bays O was observed at the upper layer (800-1000 m. high) having the concentration of 140 ppb and this high O area was corresponded to the land breeze zone shown in Figure 7e. Generally speaking under the condition of the weak pressure gradient the local wind circulation predominate and high concentration of secondary pollutants are observed at the upper, outer part of the low level stable zone in the morning and these aged pollutants are involved in accordance with the increase of the thermal mixed layer in the daytime and accelate the formation of the photochenmical oxidants. From five years of aircraft observations conducted by NIES between 1978 and 1981[4],[5], the vertical scale of the phenomenon is approximately within 2-3 km above ground level.

Figures 8 and 9 shows the case of the general wind predominant type. The horizontal distance between Mt.Tsukuba and Makabe is 10 km but the time variation in Figure 8b is quite different at nighttime. This means that the high concentrations of secondary pollutants formed in the metropolitan area were transported traveling above the nighttime radiation inversion area.

When the southerly seasonal wind predominates, pollutants formed in the Kanto district are transported to the Nagano area.[6] Figure 8a shows the movement of the oxidant peak. The peak at Omiya was observed at 1400JST, 15 June 1979 and it traveled 10 hours to Nagano. In this case, the aerial scale of the photochemical smog was more than 200 Km.

When the north-easterly wind predominated, pollutants were transport to Sagami Bay. These phenomena are shown in Figure 9. In this case, pollutants from the Keihin and Keiyo industrial complexes were transported to Izu Peninsla. Pollutants stagnated near the east coast of this peninsla and high ozone levels, above 150 ppb, was observed. Using these data OH radical concentration was estimated to be approximately 0.2-0.4 ppt.[7]

5. Summary and conclusions

Monitoring station data was analyzed statistically to clarify the seasonal variations of oxidant concentration in Japan and the temporal and aerial scales of photochemical air pollution were also analyzed using ground level monitoring station data and aircraft data covering the Tokyo Metropolitan Area. Results are summarized as follows:

(1) The effects of stratospheric ozone subsidence are significant in the spring season, but the effects are negligible in the summer season.

(2) The temporal scale of the photochemical smog formation mechanism is longer than one day, and under the condition of a weak atmospheric pressure gradient, polluted air masses circulate more than three days in the Kanto district following the local wind circulation systems.

(3) At nighttime and early morning, high concentration of secondary pollutants are usually observed in the upper, outer part of the low-level stable zone and these, aged pollutants are involved in accordance with the increase of the thermal mixed layer in daytime.

(4) The scale of the photochemical smog phenomenon in the Tokyo Metropolitan Area is large. When the general wind prevails polluted air masses are transported greater than 200 Km distance from the source area and distributed up to an altitude of 2-3 Km.

These characteristic features of photochemical oxidants in Japan will give us a firm basis for constructing a photochemical smog formation model.

References

(1) Murao,N., Okita,T. and Ohta,S. (1982): Contribution of stratospheric ozone on the ground-level oxidant concentration. (in Japanese) TENKI, Vol.29, No.5, pp. 537-545

(2) Akimoto,H., Bando,H., Sakamaki,F., Inoue,G., Hoshino,M. and Okuda,M. (1979): Photooxidation of the prophylene-nitrogen oxides-air system studied by long-path fourier transform infrared spectrometry. (in Japanese) Reseach Report from the National Institute of Environmental Studies, No.9, pp. 9-27

(3) Uno,I., Wakamatsu,S., Suzuki,M. and Ogawa,Y. (1982): Distribution of photochemical pollutants and their three-dimensional behavior covering the Tokyo Metropolitan Area. Japan-US Joint Conference on Photochemical Air Pollution and Air Pollution-related Meteorology, at Tsukuba, 1-2 December 1982

(4) Wakamatsu,S., Ogawa,Y., Murano,K., Goi,K. and Aburamoto,Y. (1982): Aircraft survey of the secondary photochemical pollutants covering the Tokyo Metropolitan Area. To appear in Atmos. Environ.

(5) Wakamatsu,S., Uno,I., Suzuki,M. and Ogawa,Y. (1982): The Lagrangian observation of polluted air masses using aircraft. Japan-US Joint Conference on Photochemical Air Pollution and Air Pollution-related Meteorology, at Tsukuba, 1-2 December 1982

(6) Kurita,H., Sasaki,S., Hatano,S., Wakamatsu,S., Uno,I. and Ueda,H. (1982): Movement of Oxidant in Inland Area (1) -Relation between Oxidant Concentration in Ueda Basin and Photochemical Oxidant in Kanto District- . (in Japanese) Annual Meeting of Japan Society of Air Pollution, Proceedings, at Miyazaki, 9-11 November 1982

(7) Suzuki,M., Wakamatsu,S., Uno,I. and Ogawa,Y. (1982): Evaluation of OH radical concentration using aircraft data. Japan-US Joint Conference on Photochemical Air Pollution and Air Pollution-related Meteorology, at Tsukuba, 1-2 December 1982

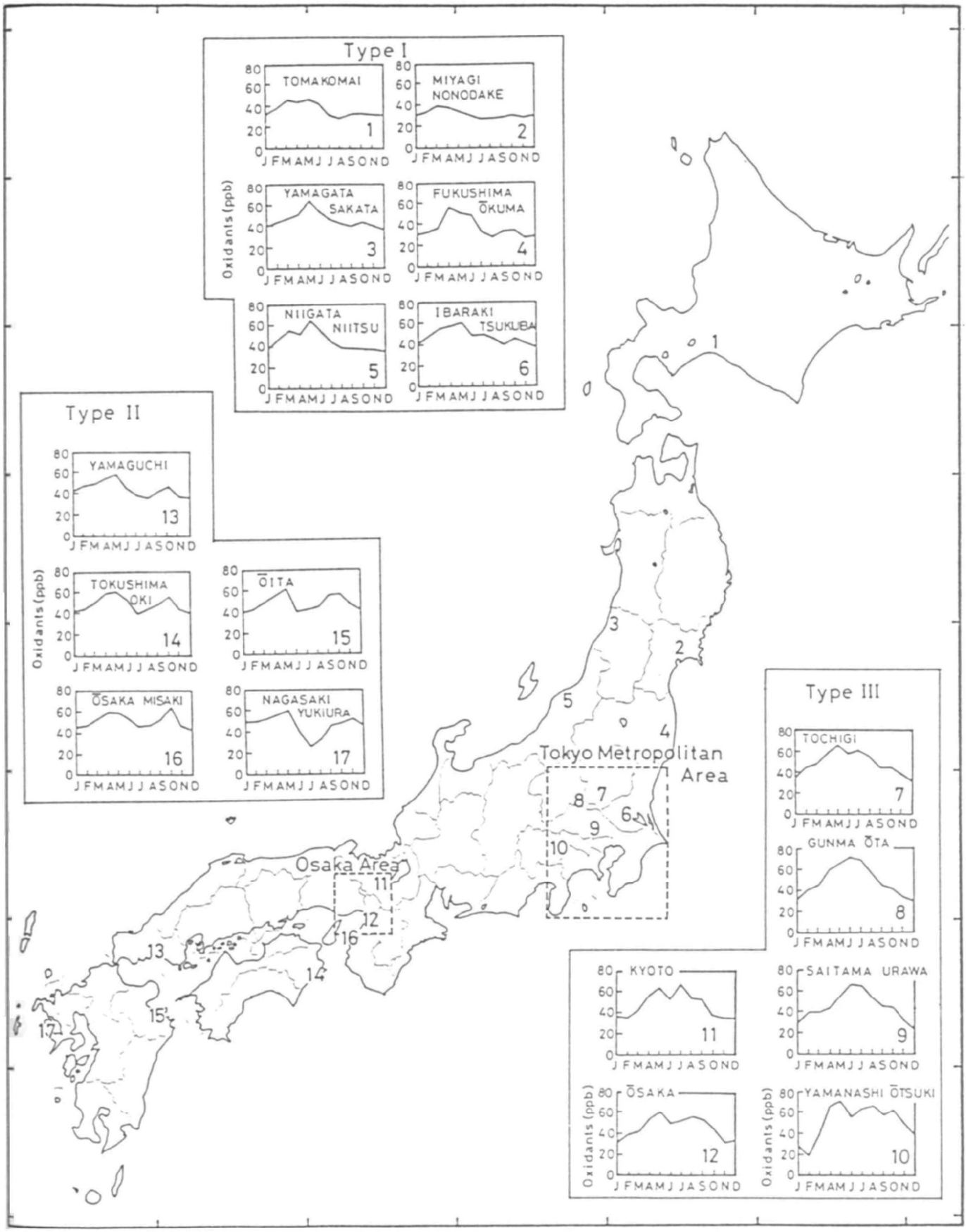

Figure 1. Seasonal variation of oxidants in Japan. Daily maximum oxidant concentration between 1976 and 1980 were averaged monthly. Numeral in the map shows the location of the selected monitoring station.

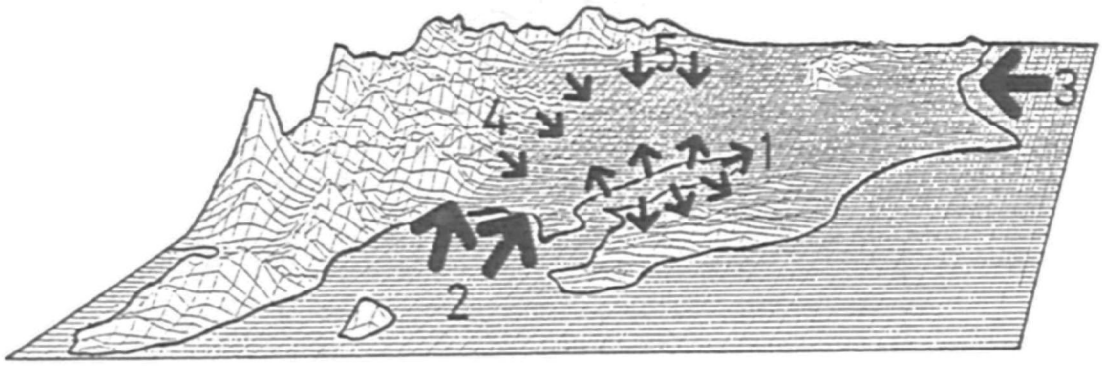

Figure 2. Topography of the Tokyo Metropolitan Area viewed from the south and local wind pattern. Numeral shows following ;

1. Sea and land breezes from Tokyo bay
2. Sea and land breezes from Sagami bay and seasonal wind in the summer
3. Easterly wind from Kashima sea
4. Mountain and valley wind from the western mountain area
5. Mountain and valley wind from the northern mountain area

a

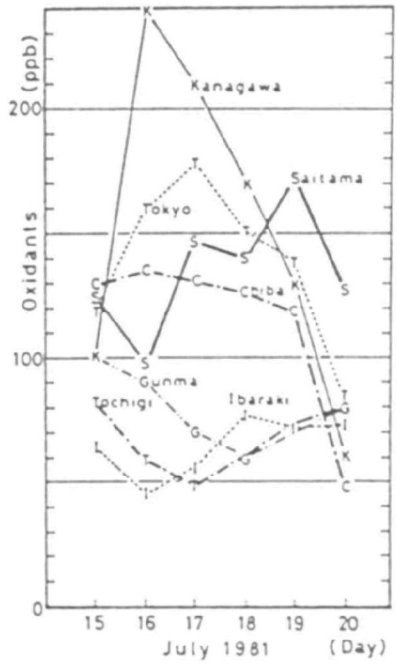

b

July 1981	Wind direction and speed (m/s)			M.T (°C)	T.S.R (MJ/m²)
Date \ Hour	0900JST	1200JST	1500JST	——	——
15	N 2.4	S 3.4	SSE 3.6	31.5	15.4
16	NW 1.3	NNW 2.6	SSE 2.4	34.1	19.7
17	N 1.5	ENE 1.8	SSE 4.4	34.3	20.5
18	N 2.5	SE 3.1	SSE 5.0	33.6	18.5
19	W 0.8	SSE 2.7	SSE 5.6	32.2	17.0
20	SE 2.6	S 4.3	S 6.6	32.4	13.7

M.T: Maximum temperature (°C)
T.S.R: Total solar radiation (MJ/m²)

c

Figure 3. (a) The arrangement of the pilot-balloon station.
(b) The daily maximum oxidant concentration observed in each prefecture in Kanto district
(c) Meteorological data observed at the Tokyo Meteorological Observatory

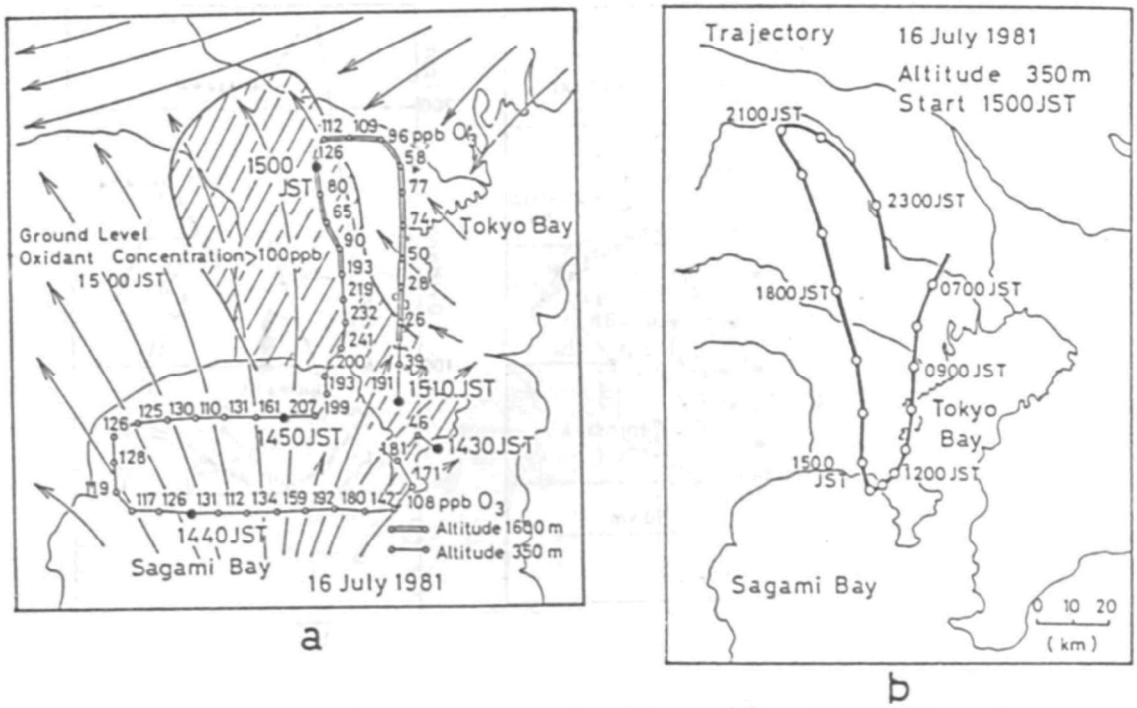

Figure 4. (a) The ground level oxidant concentration pattern at 1500 JST exceeding 100 ppb and the aircraft data at 350 m. on 16 July 1981. (b) The air trajectory at the altitude of 350 m. calculated using 23 pilot-balloon data.

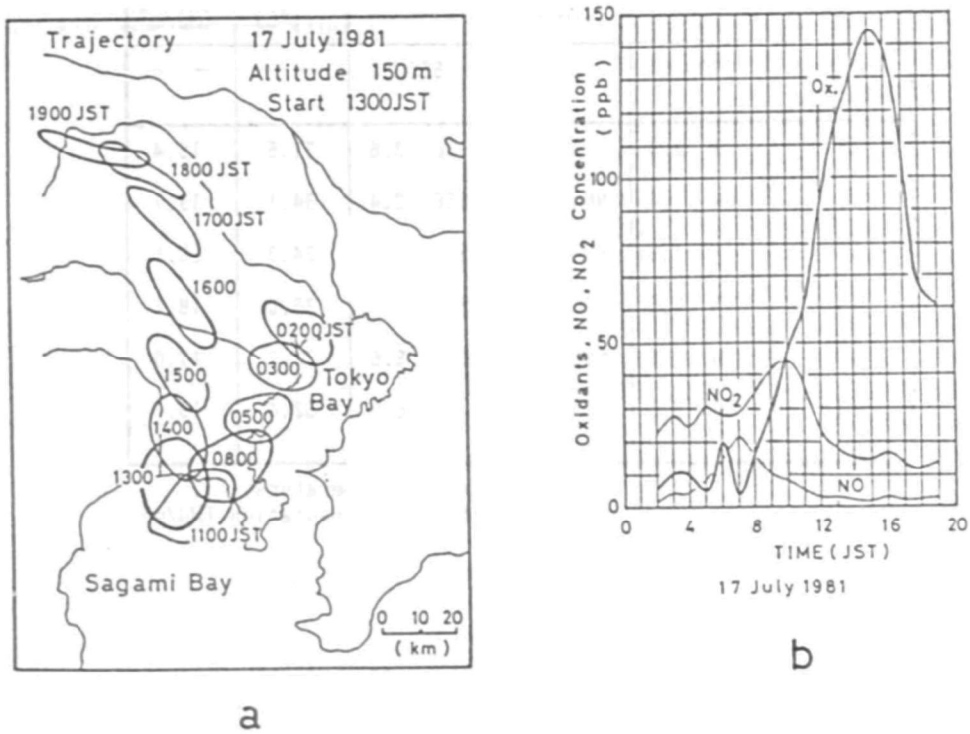

Figure 5. (a) The air trajectory at the altitude of 150 m. calculated using 23 pilot-balloon data on 17 July 1981 (b) The Lagrangian variation of NO, NO_2, and Oxidant concentration along the trajectory line shown in Figure 5(a)

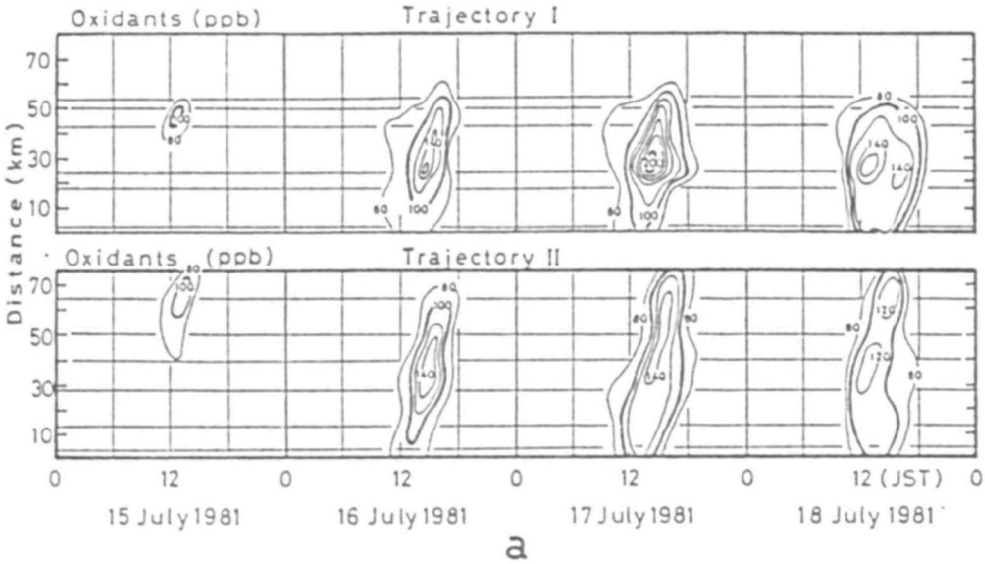

a

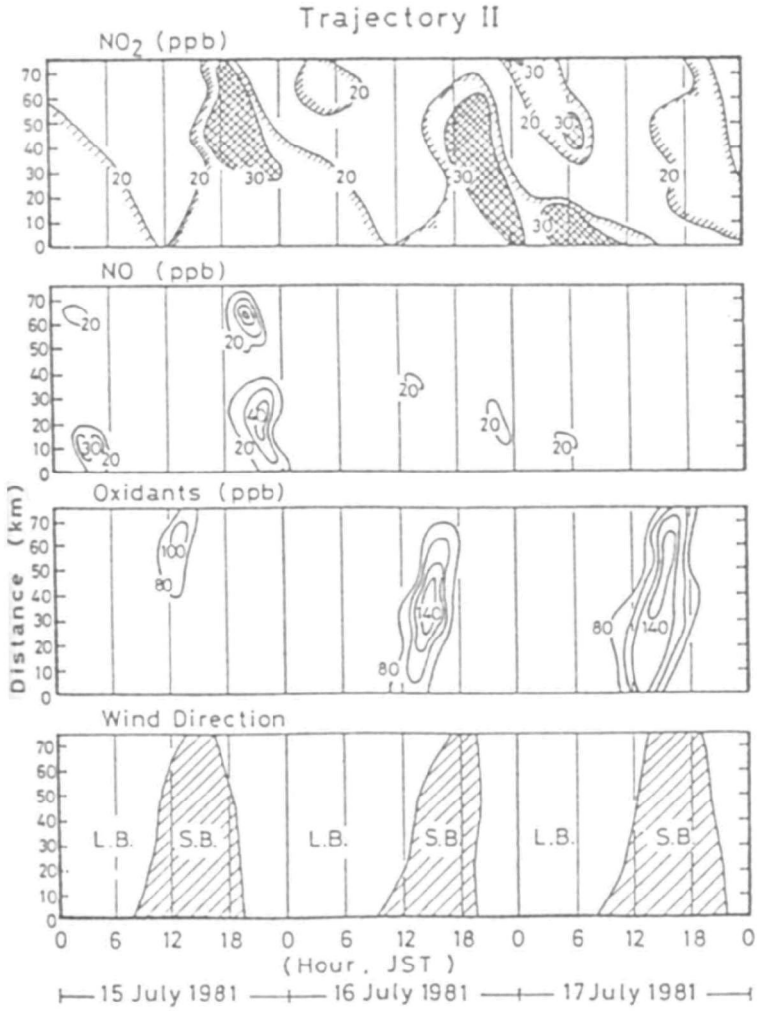

b

July 1981	Wind direction and speed (m/s)			M.T (°C)	T.S.R (MJ/m²)
Date \ Hour	0900JST	1200JST	1500JST	—	—
15	N 2.4	S 3.4	SSE 3.6	31.5	15.4
16	NW 1.3	NNW 2.6	SSE 2.4	34.1	19.7
17	N 1.5	ENE 1.8	SSE 4.4	34.3	20.5
18	N 2.5	SE 3.1	SSE 5.0	33.6	18.5
19	W 0.8	SSE 2.7	SSE 5.6	32.2	17.0
20	SE 2.6	S 4.3	S 6.6	32.4	13.7

M.T: Maximum temperature (°C)
T.S.R: Total solar radiation (MJ/m²)

c

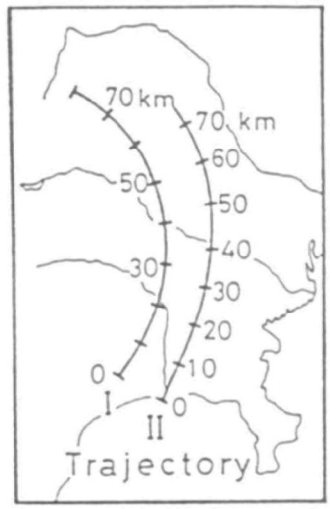

d

Figure 6. (a) The two-dimensional profile of oxidant concentration between 15 July 1981 and 18 July 1981 along the trajectory line shown in Figure 6(d), (b) The two-dimensional profiles of NO, NO_2, Oxidants and wind direction along trajectory II shown in Figure 6(d), (c) Meteorological data observed at the Tokyo Meteorological Observatory, (d) Averaged trajectory lines between 15 July 1981 and 18 July 1981 in the south-west area of Kanto ditrict.

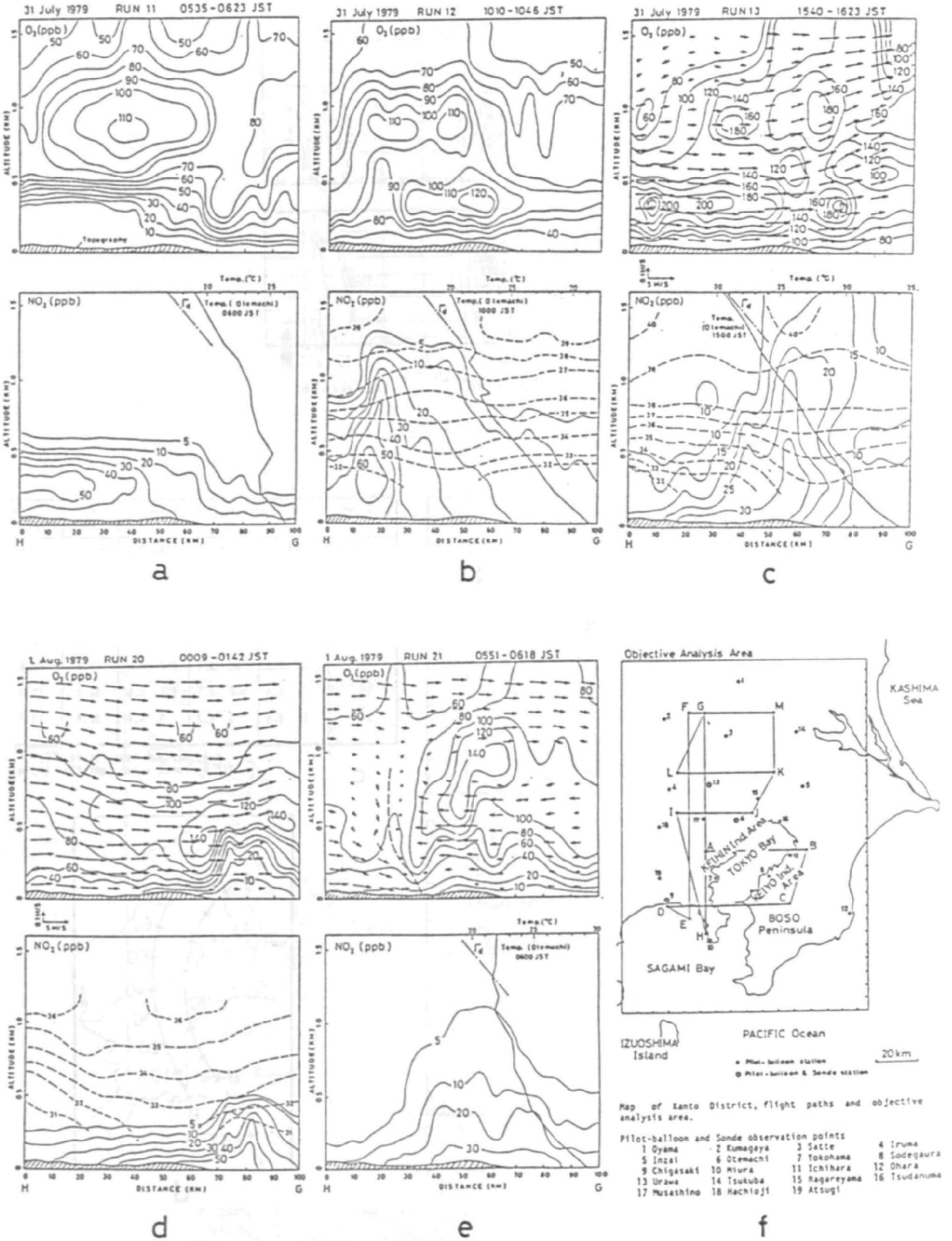

Map of Kanto District, flight paths and objective analysis area.

Pilot-balloon and Sonde observation points

1 Oyama	2 Kumagaya	3 Satte	4 Iruma
5 Inzai	6 Otemachi	7 Tokohama	8 Sodegaura
9 Chigasaki	10 Miura	11 Ichihara	12 Ohara
13 Urawa	14 Tsukuba	15 Nagareyama	16 Tsudanuma
17 Musashino	18 Hachioji	19 Atsugi	

Figure 7(a)-(e). The O_3 and NO_2 distribution on the flight course H-G shown in Figure 7(f) on 31 July 1979 and 1 August 1979 ,using four aircraft simultaniously. Bacically each aircraft flew at the altitude of 350, 650, 900 and 1200 m. respectively and these data was extrapolated. Horizontal and vertical wind shown in Figure 7(c)-(e) are calculated using 19 points pilot balloon data. Dashed line in the Figure (b)-(d) shows a potential temperature. Flight time table are shown as follows;

(a) Run 11 : 0430-0630 JST 31 July 1979
(b) Run 12 : 0945-1130 JST 31 July 1979
(c) Run 13 : 1450-1630 JST 31 July 1979

(d) Run 20: 0000-0145 JST 01 August 1979
(e) Run 21: 0445-0620 JST 01 August 1979

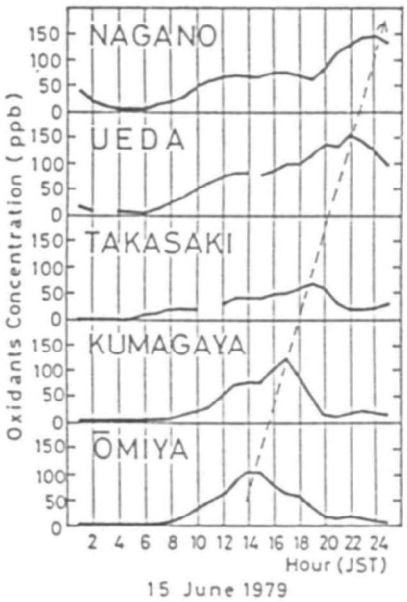

a

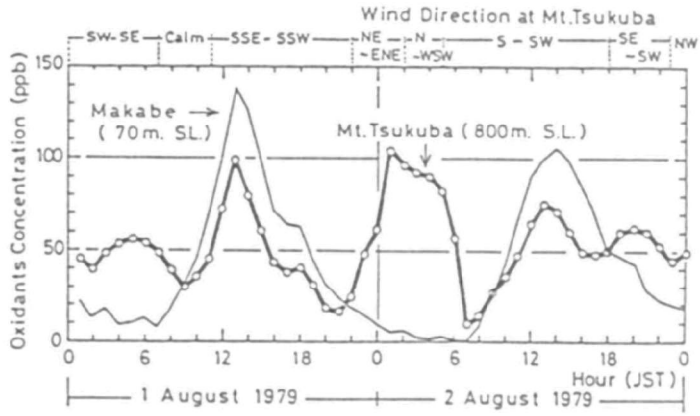

b

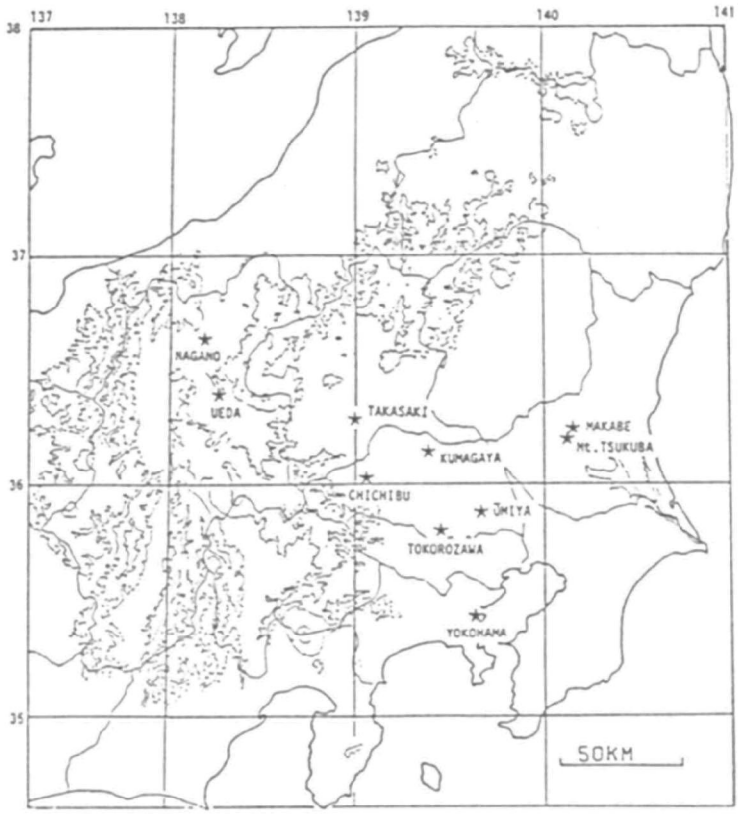

c

Figure 8. (a) The movement of oxidant concentration peak to the inland area ,(b) The diurnal variation of oxidants at Mt.Tsukuba and Makabe , (c) Location of the selected monitoring station.

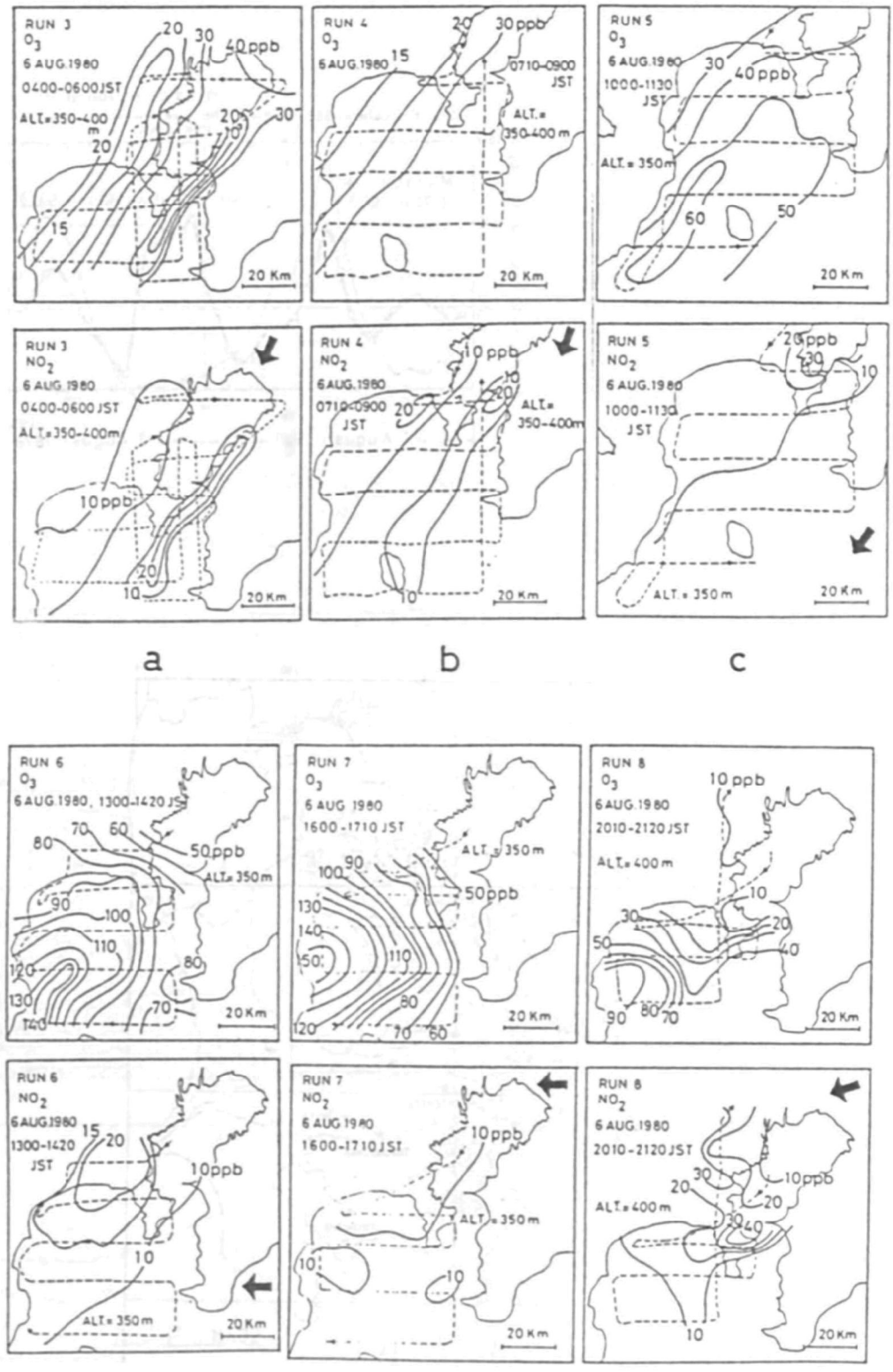

Figure 9.(a)-(f) Horizontal distribution of O_3 and NO_2 at the altitude of 350-400 m. on the Sagami Bay. Arrows in the figure shows a wind direction. Flight time table are shown as follows;

(a)	Run 03:	0400-0600 JST	06 August 1980
(b)	Run 04:	0710-0900 JST	06 August 1980
(c)	Run 05:	1000-1130 JST	06 August 1980
(d)	Run 06:	1300-1420 JST	06 August 1980
(e)	Run 07:	1600-1710 JST	06 August 1980
(f)	Run 08:	2010-2120 JST	06 August 1980

[Ref.]

A Lagrangian Observation of Polluted Air Mass Using Aircraft

by

Shinji Wakamatsu
Itsushi Uno
Makoto Suzuki
Yasushi Ogawa

National Institute for Environmental Studies
P.O. Yatabe, Ibaraki 305
JAPAN

1. Introduction

To understand the photochemical smog formation mechanism in the atmosphere it is necessary to understand the photochemical reaction process. The photochemical reaction process is mainly investigated using smog chamber experiments and these results are useful to understand the fundamental characterstics of the photochemical reaction processes. Nevertheless, these experimental results are not sufficient for the total understanding of the photochemical smog phenomena in the environment. In the case of smog chamber studies (1) pollutants are distributed uniformly (2) light intensity is uniform (3) the effects of atmospheric turbulence is ignored (4) wall effects are not negligible. For these reasons, it is necessary to validate smog chamber results using field observation data.

For this purpose Lagrangian observation is most effective. Calvert et al. (1976) made a Lagrangian observation using two helicopter-tracing tetroons in the Los Angeles area (LARPP). Decker et al. (1977) traced a photochemical reaction process using a balloon near the St. Louis area. (DaVinci II Project)

These are the direct methods of Lagrangian analysis. In this paper we explain an indirect Lagrangian observational system conducted by NIES (National Institute for Environmental Studies) covering the Tokyo metropolitan area during 1980 and 1981. Wakamatsu et al. (1976),(1981) showed the importance of local climatology (sea-land breeze,mountain-vally wind, and urban-rural interaction) in understanding the photochemical smog in the Tokyo metropolitan area. The scale of the phenomenon is approximately 100 km by 100 km with the pollutants distributed three-dimensionally and the time scale of the photochemical smog formation mechanism longer than one day. The aerial scale of the polluted air mass is usually 20-50 km almost corresponding to the aerial distribution of the industrial complexes. In this case, we have to know the averaged three-dimensional wind field and averaged wind trajectory which carries the polluted air mass.

For this purpose, we made a Lagrangian observational system using two instrumented aircraft, 23 pilot-balloons, 4 radio sondes, 100 ground level monitoring stations and two main computer systems.

In this paper, outlines of this system and a summary of the observation are discussed.

2. Instrumentation and Measurement System

The aircraft measurements are performed with a twin-engine Cessna (404-TITAN) and Aero Commander (685). The air sampling tube was set in the nose cone of the aircraft. On the roof of the

aircraft, a UV radiometer was mounted and under the floor, sensors for air temperature and humidity are mounted . These two aircraft had almost identical measuring instruments and flew about two hours alternately along the air trajectory calculated from pilot-balloon data to obtain the photochemical reaction processes in the traced air mass. Aircraft specifications are shown in Table 1. Instrumentation used on the aircraft are shown in Table 2.

(1) Gas measurement

The ozone NO, and NOx monitors were specially designed for this aircraft study. These instruments have high response and controlled to work under the high environmental temperature. Electric power was supplied from the aircraft DC generator and was converted to 400 Hz AC using a rotary inverter. These instruments works on 400 Hz 100V AC and 28 V DC current on the aircraft and easily to change 60-50 Hz 100 V AC for ground calibration. The SO2 monitor used was commercially available equipment.

Pressure test and temperature test were done for all before the observation. They were calibrated in a pressure-controlled chamber and calibration curves were drown for each instrument.

Room temperature and manifold temperature were monitored for the correction of temperature effects on the instruments and air pressure was monitored for the correction of pressure effects. Air samples for the NMHC analyzer and gas chromatographic analysis of hydrocarbons were collected in a 1 liter glass vessel.

This glass vessel has two Teflon valves. Sampled air was collected and pressurized to about 1.4 atm by a Teflon bellows pump and this vessel was connected to the NMHC analyzer after the flight to measure NMHC concentration, and then hydrocarbon species were measured using GC analyzer. About 12-24 samples are obtained in one flight.

(2) Aerosol measurement

Sulfate and nitrate concentrations were measured by ion chromatography of aerosol samples collected on Teflon filters. Sample flow rates were measured with a mass flow meter and recorded on magnetic tape at three-second interval.

(3) Meteorological element, altitude and position measurement

Air temperature, relative humidity, atmospheric pressure and UV radiation were monitored as meteorological elements. Position data was obtained using Loran-C and altitude was calculated from the environmental pressure data.

(4) Data processing

The measured data were averaged over 3-sec intervals and recorded on 1/2 inch magnetic data tape in real time. Data processing system on the aircraft are shown in Table 3(system 0). Three micro computers (Z80A) were used for this airborne system, CPU0 acquired position data from the LORAN-C, CPU1 acquired air pollution data and meteorological data and CPU2 monitored status information of instruments and electric power supply system. These data processing systems are easily operated by one operator.

(5) Calibration

Before the observation, temperature and pressure tests were conducted and calibration curves were obtained for each instrument and these data were used to the data correction.

Before and after each flight, calibration was done using the gas phase titration technique for ozone and NO,NOx analyzer. For the SO2, analyzer zero and span values were checked before and after the flight.

(6) Sampling air flow and electric power supply

Sample air was led through the three Teflon pipes (15 mm ID,TFE Teflon) which projected approximately 0.5 m from the nose cone of the aircraft . The first pipe led into the manifold and delivered the sampling air to the measuring instruments. The second pipe led into the high-volume air sampler to the aerosol sampling on Teflon filter. The third pipe was used for air collection into glass vessels and sampled air was analyzed after the flight. The length of these pipes was approximately 5 m from nose cone. Sampling air was supplied using aircraft dynamic pressure for suction. These sampling air flow patterns are shown in figure 1.

Electric power to the instruments was supplied from aircraft's DC generator. DC current was converted to AC using three rotary inverters. To obtain high efficency, a 400 Hz,100-120 Volt inverter was partly used. The flow of electric power supply is shown in figure 2.

3. Observation system and analysis

Outlines of our Lagrangian observation system are shown in Table 4. Using this system, we are able to know tthe chemical reaction processes in the atmosphere.
An example of data are shown in figure 3. On August 6., 1980 North Easterly general wind prevailed and pollutants from the Keihin and Keiyo industrial complexes are transported to the Sagami Bay Area. These data are very useful to estimate the photochemical reaction processes because of the absence of

additional emission source from the sea area. Using these data Suzuki et al. (1982) estimated OH radical concentration to be approximately 0.2-0.4 ppt

Acknowledgements

The authors wish to express their thanks to the staff of Kimoto Electric Co. Ltd. for valuable cooperation during the aircraft survey. Thanks are also given to Instrumentation & Science Co. Ltd. (ISC) for the measurement of meteorological data and to Institute of JUSE(Union of Japanese Scientist and Engineerers) for the help of data processing.

References

Calvert,J.G. (1976): Test of the theory of ozone generation in Los Angeles atmosphere. Environ. Sci. Technol., 10, 248-256.

Calvert,J.G. (1976b): Hydrocarbon involvement in photochemical smog formation in Los Angeles atmosphere. Environ. Sci. Technol., 10, 256-262.

Decker,C.E. (1977): Ambient monitoring aloft of ozone and precursors near and downwind of St. Louis. EPA-450/3-009.

Suzuki,M., Wakamatsu,S., Uno,I. and Ogawa,Y. (1982): Evaluation of the OH-radical Concentration in the Polluted Atmosphere. Japan-US Conference on Photochemical Air Pollution and Air-Pollution-related Meteorology, December 1-2, 1982, Tsukuba, JAPAN.

Wakamatsu,S and Okita,T. (1976): Vertical and horizontal distribution of ozone covering Kanagawa Prefecture, Japan. Memoirs of the Faculty of Eng., Hokkaido Univ., XIV, 15-24.

Wakamatsu,S., Goi,K., Aburamoto,Y., Hatano,H. and Okuda,M. (1981): Relationship between the areal distribution of photochemical pollutants and local wind flow covering Kanto district.(in Japanese) J. Japan Soc. Air Pollt., 16, 146-157.

Wakamatsu,S., Ogawa,Y., Murano,K., Okuda,M., Tsuruta,H., Goi,K. and Aburamoto,Y. (1981b): Aircraft survey of photochemical smog in Tokyo metropolitan area.(in Japanese) J. Japan Soc. Air. Pollut., 16, 199-214.

環境庁
国立公害研究所
National Institute for Environmental Studies
Japan Environment Agency
Telephone : 0298-51-6111 Cable : KOGAIKENTSUKUBA
P.O. Yatabe Tsukuba Ibaraki 300-21 Japan

AIRCRAFT SPECIFICATIONS

		Cessna (404-TITAN)	Aero Commander (685)
Instrument payload	:	900 kg	550 kg
Available instrument power	:	4.2 kVA at 28 VDC 2.7 kVA at 100 VAC	9.8 kVA at 28 VDC 6.3 kVA at 100 VAC
Sampling speed	:	85 m/s	85 m/s
Navigation system	:	LORAN-C, VOR, DME	LORAN-C, VOR

Table 1 Aircraft specifications

環境庁
国立公害研究所

National Institute for Environmental Studies
Japan Environment Agency

Telephone : 0298-51-6111 Cable : KOGAIKENTSUKUBA P. O. Yatabe Tsukuba Ibaraki 300-21 Japan

Parameter	Analysis Technique	Manufacture and Model	Measurement Ranges	Time Response	Approximate Resolution
Ozone	Chemiluminescence	KIMOTO MCSAM-F	1-2000 ppb (dynamic)	< 3 s (90 %)	1 ppb
N O	Chemiluminescence	KIMOTO MCSAM-F	1-2000 ppb (dynamic)	< 3 s (90 %)	1 ppb
N O X	Chemiluminescence	KIMOTO MCSAM-F	1-2000 ppb (dynamic)	< 3 s (90 %)	1 ppb
S O 2	Fluorescence	Monitor Labs 8850	2-500 ppb	5 s (90 %)	2 ppb
Condensation Nuclei	Light-attenuation	E/one Rich 100	100k CN/cc	3 s (90 %)	1000 CN/cc
Aerosol Size Distribution	Light-scattering	Royco 226	1.0-4.5μm dia.	3 min (periodic)	----
Ambient Temperature	Platinum Resistanse	Deggussa	-50.0-50.0°C	1 s (90 %)	0.1 deg
Ambient Humidity	Electronic Capacity	National Weather Service	20-90 % RH	3 s (90 %)	3 %
Ultraviolet Radiation	Photocell	Eppley UV Radiometer	0-5 mW/cm2	2 s (90 %)	0.002 mW/cm2
Pressure (Altitude)	Bellows Barometer	Tokyo Koku Keiki ATP-20-1	760-380 mmHg (0-5400 gpm)	2 s (90 %)	1 mmHg (10 gpm)
Position	Loran-C	FURUNO LC-30	----	2 s (periodic)	0.03 min (50 m)
Pitching and Rolling	Gyro compass	Tokyo Koku Keiki 230	P ± 15 deg R ∓ 90 deg	----	P 0.1 deg R 0.5 deg

Parameter	Sampling Technique	Manufacture and Model	Analysis Technique	Manufacture and Model	Approximate Resolution
Sulfate Nitrate	Highvolume Sampling on Teflon Filter	KIMOTO 191	Ion-chromatograph	Dionex 10	
non-Methan Hydrocarbon	Compressed Sampling in Glass Vessel		Gas-chromatograph	Simazu GC-	

Table 2 Instrumentation used on the aircraft

庁
立公害研究所

National Institute for Environmental Studies
Japan Environment Agency

lephone : 0298-51-6111 Cable : KOGAIKENTSUKUBA P. O. Yatabe Tsukuba Ibaraki 300-21 Japan

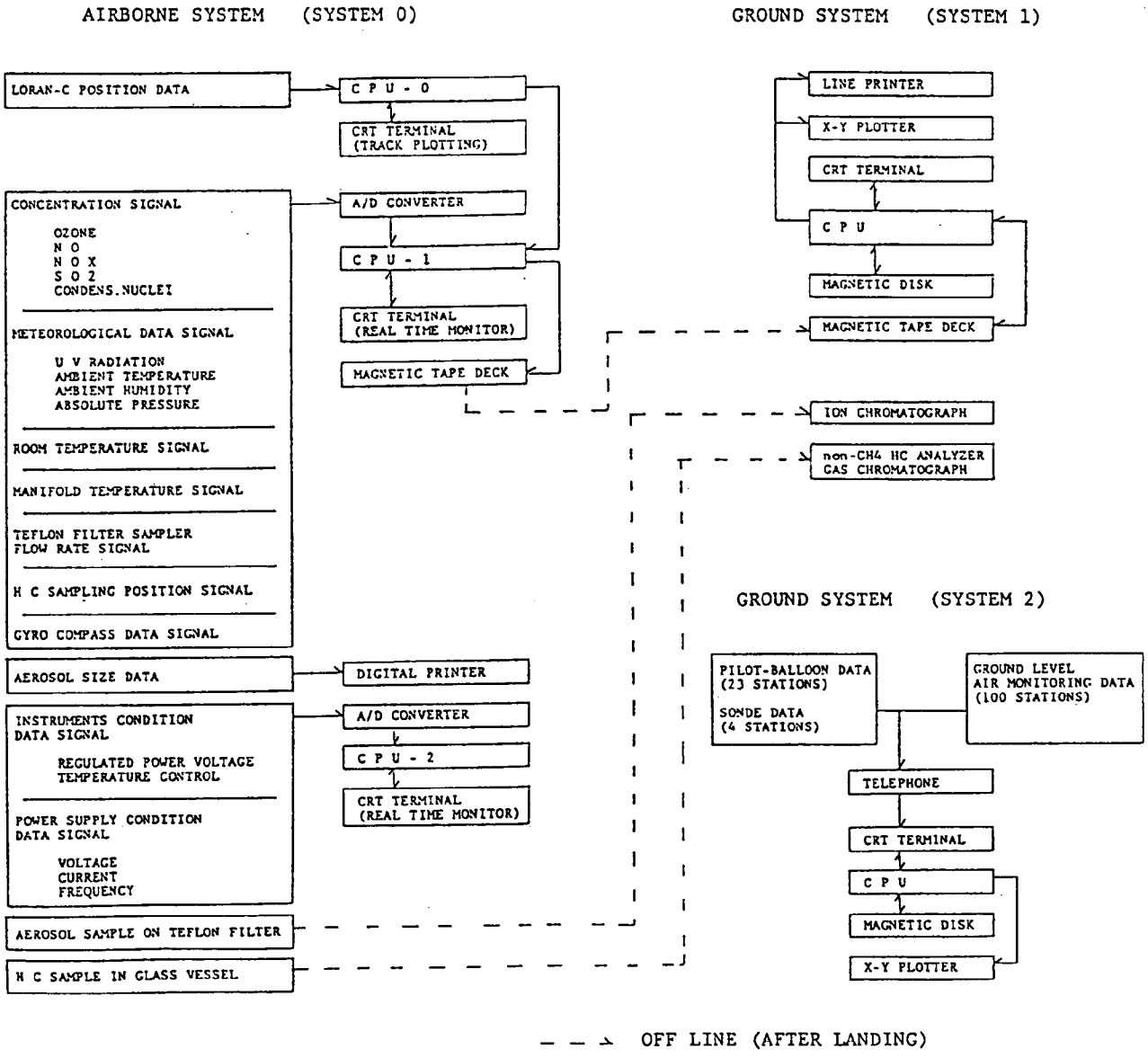

Table 3 Data processing system

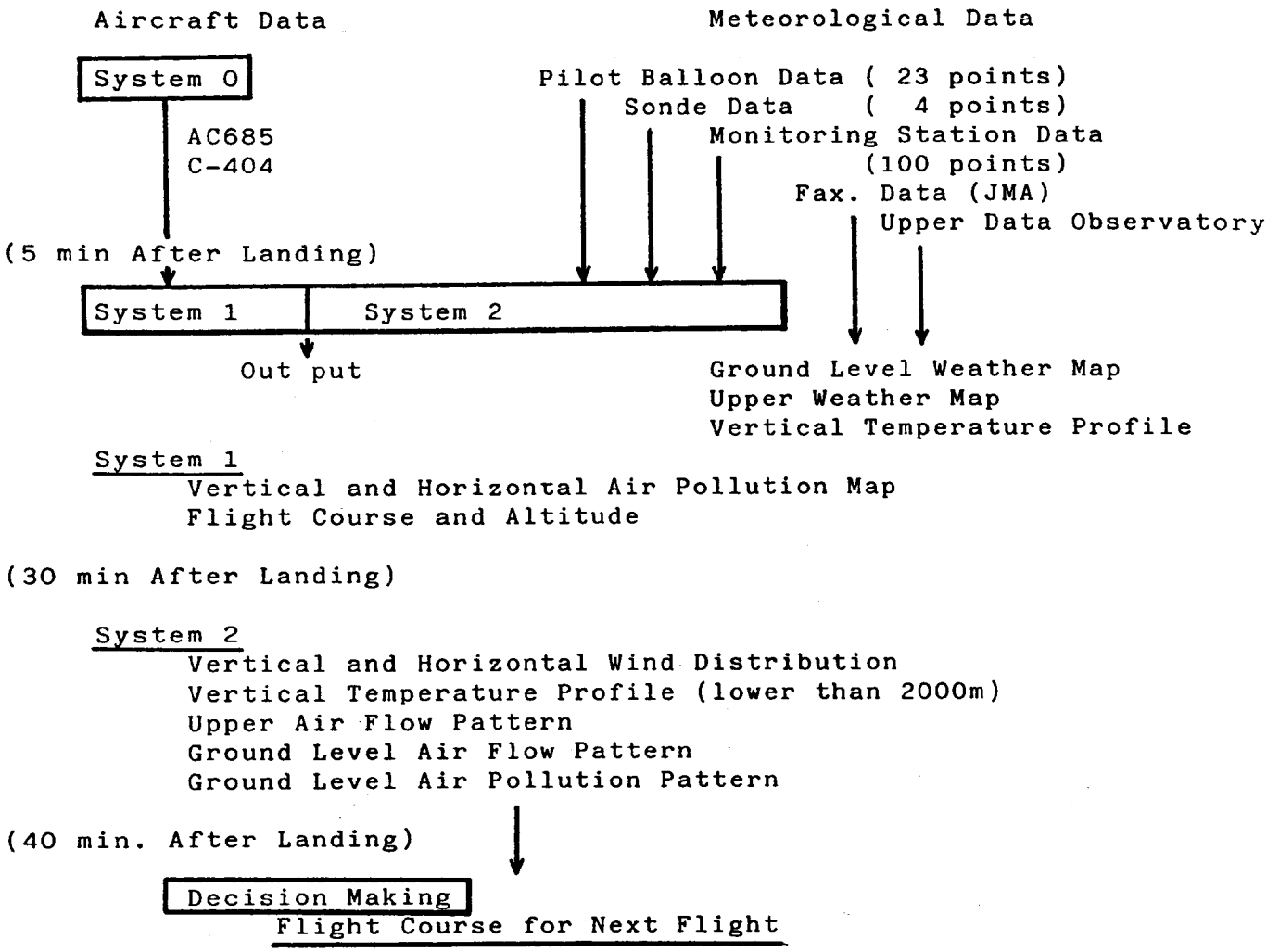

Table 4 Outlines of a Lagrangian observation system

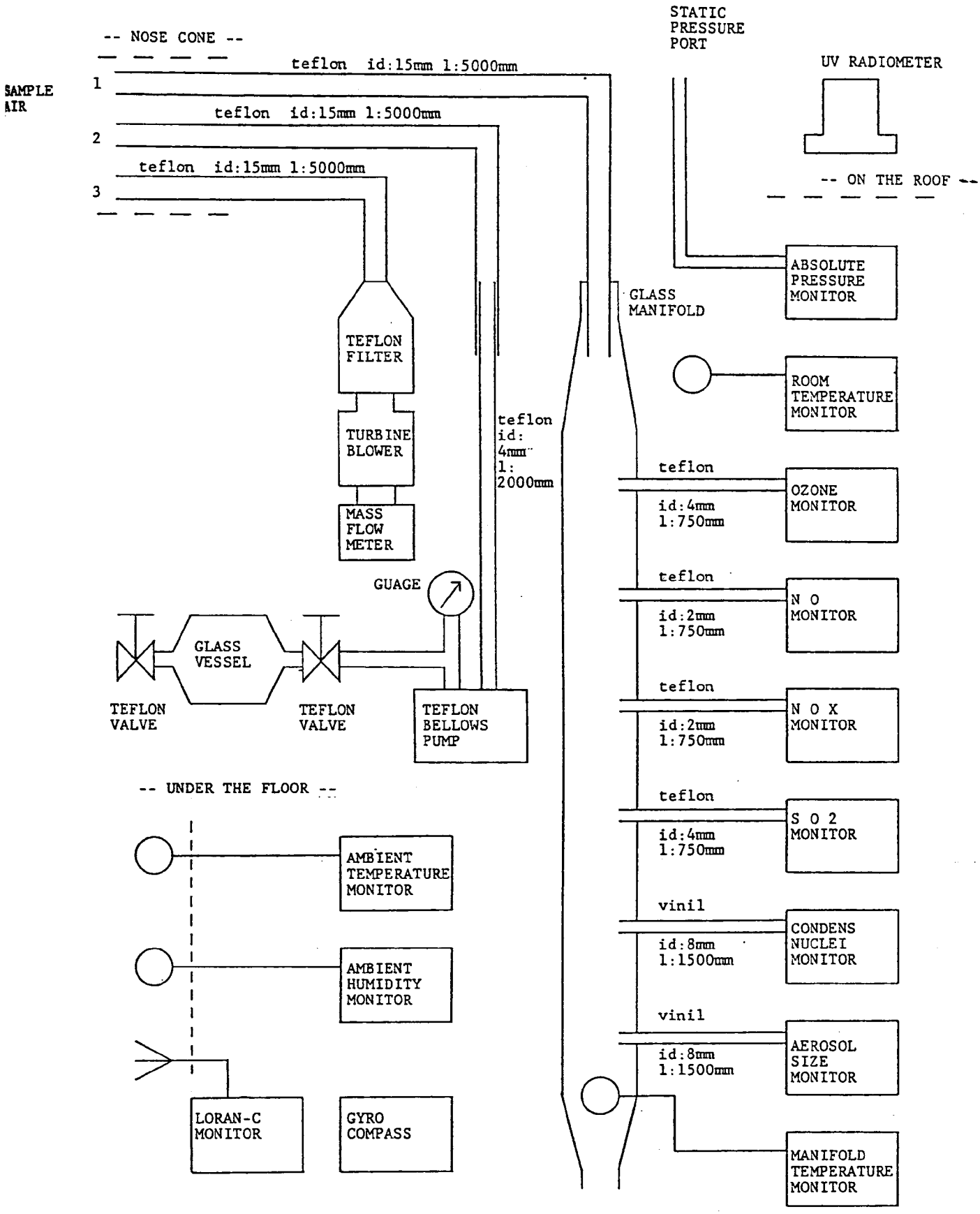

Figure 1 Sampling air flow pattern on the aircraft

環境庁
国立公害研究所

National Institute for Environmental Studies
Japan Environment Agency

Telephone : 0298-51-6111 Cable : KOGAIKENTSUKUBA

P. O. Yatabe Tsukuba Ibaraki 300-21 Japan

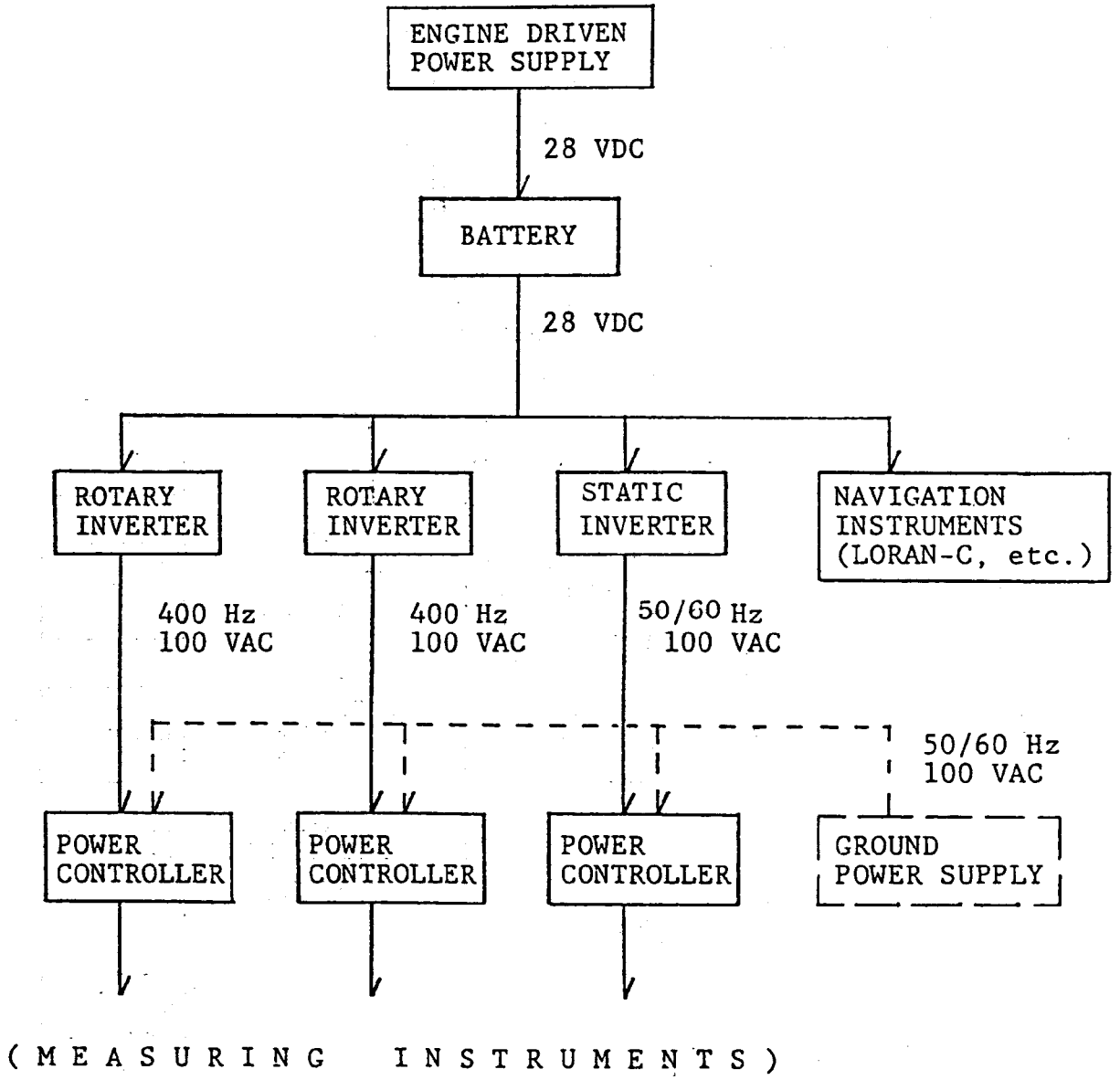

Figure 2 Electric power supply on the aircraft

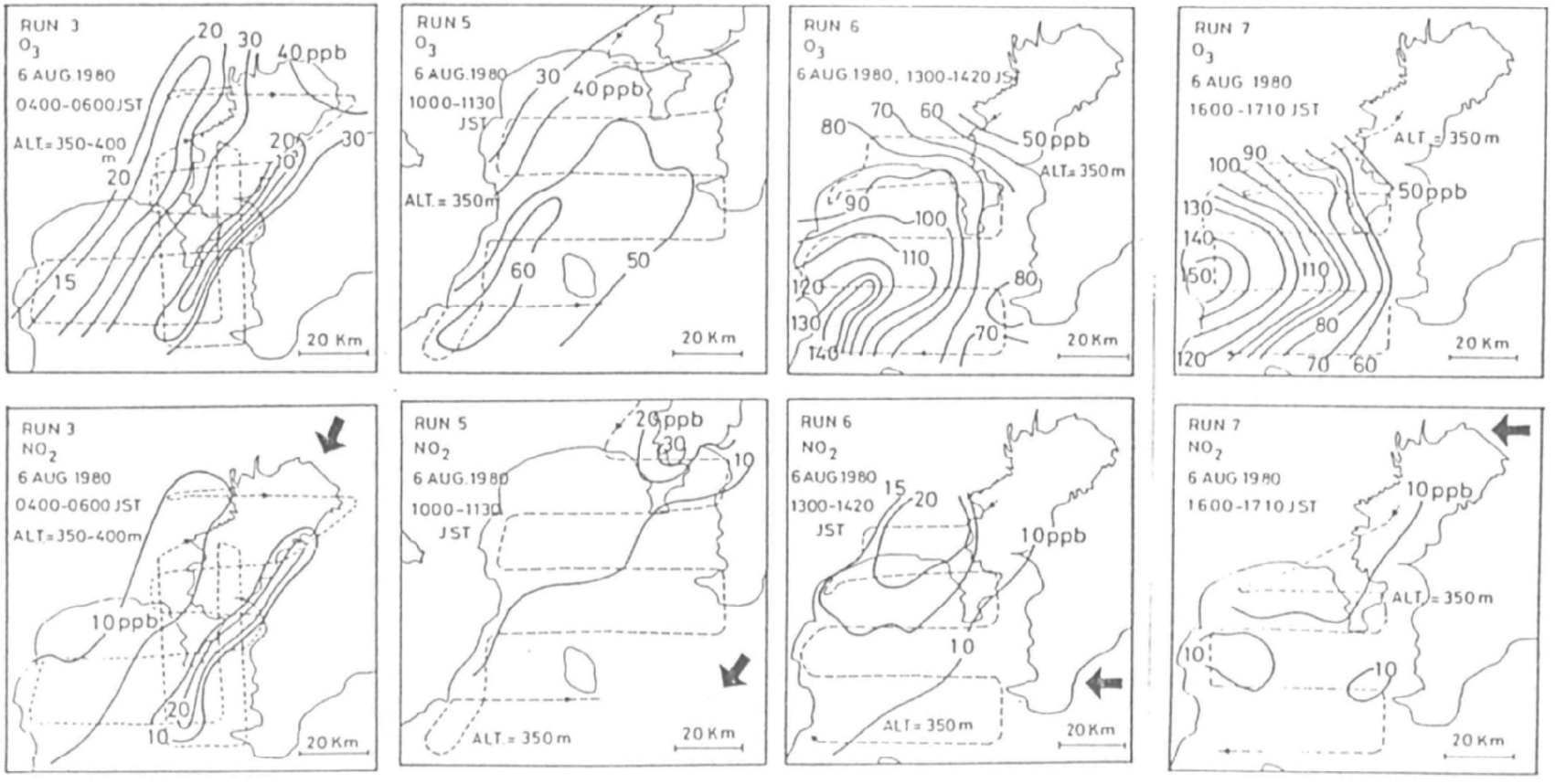

Figure 3. Horizontal distribution of O_3 and NO_2 at the altitude of 350-400 m. on the Sagami Bay. Arrows in the figure shows a wind direction.

[Ref.]

Distribution of Photochemical Pollutants and their Three-Dimensional Behavior covering the Tokyo Metropolitan Area

by

Itsushi Uno, Shinji Wakamatsu, Makoto Suzuki
and Yasushi Ogawa

National Institute for Environmental Studies
P.O. Yatabe, Tsukuba, Ibaraki 305,
JAPAN

ABSTRACT

The spatial distribution and transport process of photochemical pollutants covering the Tokyo Metropolitan Area in Japan were investigated from 31 July to 2 August 1979 using instrumented aircraft. In the experiment, the vertical profiles of pollutants were observed using four instrumented aircraft. This paper mainly considers the transport process of the polluted air mass using three-dimensional trajectory analysis. In this trajectory analysis, we determined the hourly wind field by objective analysis techniques from pilot-balloon observation data.

In the Tokyo Metropolitan Area, the sea-land breeze circulation is an important factor in the photochemical oxidant formation inland, when the geostrophic wind is weak. The nighttime radiation inversion observed in the early morning prevents the mixing of primary pollutant emitted from the big coastal industrial zones around Tokyo Bay. These pollutants were then advected to the Sagami Bay area by the land breeze and the Bay area acts as storage tank for the pollutants. These pollutants were then converted to secondary pollutants resulting in a high ozone air mass inland with the penetration of the sea breeze. The sea breeze layer is thermally stable and inhibts vertical mixing of NOx. On the other hand, at the front of sea breeze zone, a highly turbulent area transports the NOx to 1000-1500 m above mean sea level.

Polluted ozone air masses, whose concentration exceeded 100 ppb, were observed at 500-1000 m on both 31 July and 1 August 1979. It was observed that the maximum ozone concentration on the second day exceeded that on the first day. These ozone air masses contained aged pollutant and they were entrained into the mixing layer in accordance with the elevation of the mixing layer. This accelerated the formation rate of secondary pollutants. These early morning, high ozone concentrations and the storage capacity of the Sagami Bay area are important factors in the time scale of air pollution phenomena in this region.

1. Introduction

Since 1970, complaints of eye irritaton, sore throat and the sensation of suffocation due to the photochemical smog have been reported every summer in Japan. Although the number of the complaints have been decreasing, their number reached more than 1,400 in 1980. Almost all of these complaints came from the vicinity of large cities, such as Tokyo and Osaka. The need to understand the mechanisms of the photochemcal smog phenomena in these areas is urgent. Since the areas are so large, aircraft observation is necessary to this understanding.

A series of aircraft observations were conducted in the Los Angeles Air Basin to understand the photochemical smog behavior (Edinger et al., 1972; Edinger, 1973; Gloria et al., 1974; Husar et al., 1977; Blumenthal et al., 1978). For another area, Lyons and Cole(1976) and Keen and Lyons(1978) investigated the relation between the land-lake breeze at Lake Michigan and the vertical distribution of aerosols, and showed that there was the possibility of re-circulation of pollutants under the land-lake breeze condition. Sexton and Westberg(1980) observed the region downwind of the Chicago-Gary urban complex using aircraft and showed that the transport of pollutants from the Chicago urban complex is the main reason for local high ozone levels. From these investigations, the following has been made clear : 1) there exists a strong relation between the vertical ozone concentration profile and the temperature inversion height (lid), 2) there is a possibility that the layer which contains rich ozone moves along with the terrain or slope, 3) ozone above the lid(i.e., aged ozone) remains a long time compared with that below the lid and affects the higher ozone formation into the next day, 4) a strong vertical and horizontal gradient exists in the concentrations of both primary and secondary pollutants, 5) the sea-breeze is an important factor for the transport and spatial distribution of high concentration pollutant profiles.

These observations are mostly restricted to the qualitative understanding of pollution. As mentioned above, the transport process of photochmical pollutants is very complicated under the local wind circulation system, so it is important to study the relationship between the behavior of the polluted air mass and the three-dimensional wind system. National Institute for Environmental Studies (NIES) has been conducting

summer aircraft surveys since 1978 to understand the photochemical pollutant formation and transport process in the Tokyo Metropolitan Area(Wakamatsu et al., 1982a). To follow the three-dimensional behavior of the polluted air mass, pilot-balloon observation was also conducted at 19 points covering the Tokyo Metropolitan Area beginning 1979.

Tokyo Metropolitan Area is located in the Kanto Plain, which has a complicated topography. The Kanto Plain has a horizontal scale of about 100 km in the east-west direction and 200 km in the north-south direction. Figure 1 shows a perspective view of the Kanto Plain. Figure 2 shows the industrial zone and other topographical information. The topographical characteristics of the Kanto district are as follows: the western and northern sides are walled by mountains 1000 to 2000 m high, the Tokyo and Sagami Bays and the Pacific Ocean are located at the center, south and east sides of the plain, respectively. On the southwest side of Sagami Bay, the Izu Peninsula protrudes into the Pacific Ocean, and this acts as the wall to stop the transport of pollutants from two industrial zones. Two industrial areas are around Tokyo Bay, i.e., the Keihin industrial area(the west side of Tokyo Bay) and the Keiyo industrial area(the east side of Tokyo Bay). A detailed emission map of NOx can be found in Wakamatsu et al.(1982a).

In this paper, we are concerned with the vertical behavior of pollutants based on the three-dimensional wind field. To do this, trajectory analysis is useful. Angell et al.(1972,1973) used tetroons to determine the trajectory over the Los Angeles Basin, and also compared these to the indirect trajectory calculated from surface wind data. They showed that the both methods agreed in their determination of the main paths. In the Los Angeles Reactive Pollutant Program(LARPP), the three-dimensional trajectory was obtained by using three tetroons(Feigley and Jeffries, 1979). In the Tokyo Metropolitan Area, because of the compilicated topography and the restrictions from air-traffic control, it is difficult to use tetroons for measurement, so we determined the three dimensional trajectory from the wind field calculated by an objective analysis procedure. In the following section, we apply the objective analysis technique to the wind data obtained by pilot-balloon observation. Using hourly wind field data, we analyze the vertical distribution of pollutants and the spatial behavior of polluted air mass.

2. Observation data

Aircraft observation was conducted over 3 days from 31 July to 2 August 1979. The four instrumented aircraft were : three twin engine Cessna (C-402 x 2 , C-404) and a twin engine Rockwell Aero Commander (AC-685). Each of the four aircraft flew at a fixed altitude. Four or five runs were performed on each day and the four aircraft measured the vertical cross section at one time, except the runs in the evening and at midnight. In total, 13 runs were conducted. Measured were NO, NOx, ozone, condensation nuclei(CN), hydrocarbons, UV intensity, pressure altitude, temperature, relative humidity and position (Loran-C). Table 1 shows the instrumentation used and the main flight heights. Figure 2 shows the daily flight patterns. The measured data were averaged over 4 sec intervals and recorded on digital cassette tapes. The measurement system is fully described elsewhere (Wakamatsu et al., 1982b). Each run was labeled Run IJK, where the first digit I indicates the day, J is run number in each day, and K means the aircraft identification which corresponds to the operation height. Occasionally, a run was called Run IJ for short to indicate the four flights(Run IJ1 - IJ4) made at one time. The daily flight paths were as follows: in the early morning(Run I1) the path was A-B-C-D-E-F-G-H, near noon(Run I2) E-F-G-H-I-J-K, in the afternoon(Run I3) E-F-M-K-L-G-H, in the evening(Run I4) H-G, and in the midnight is H-G (See Figure 2 for these paths).

Vertical wind profiles were observed at 19 points using a pilot-balloons by the single theodolite method. Data was collected at each 100 m interval above the terrain up to the 3000 m level (Figure 2 shows the points). Also, at 3 additional points, temperature and humidity profiles were measured using the radiosonde at about three hour intervals.

To compare the flight data, we also took into account the hourly surface air quality monitoring stations data (NO, NOx, oxidants, wind speed and wind direction etc.) during the period of the aircraft survey. The ground stations number is about 150 and they are located throughout the Kanto district to follow the behavior of ground level smog phenomena.

3. Vertical distribution and behavior of pollutants

a. Determination of the three-dimensional wind field

The air pollution phenomena in the Tokyo Metropolitan Area cover 100 - 200 km area in horizontal scale and continues for several days(Wakamatsu et al., 1982a). To study these phenomena, it is necessary to understand the transport process of the pollutants. When vertical air motion exists due to the convectional motion or topographical effects, this will become an important factor in the transport process of the pollutant (e.g., see Liu and Seinfeld, 1975)

In general, only the horizontal components of the wind are measured. In addition, the observation points are generally distributed irregularly and sparsely in the region of interest. To use these data, objective analysis is necessary to get the mass-consistent wind field. According to Goodin et al.(1980), the objective analysis of the wind field is defined by a two-step processes. First, interpolation of sparse and discrete measured data to finer mesh data(interpolation step). Second, adjustment of the wind vector at each grid point so as to satisfy an appropriate physical constraint (adjustment step).

In this study, we adopt the MATHEW method to get the three-dimensional wind field. The MATHEW method was proposed by Sherman(1978) based on Sasaki's variational method(Sasaki 1958, 1970). In our application, we modified the vertical coordinate system to a terrain-following one. Using this modified MATHEW method, we could reduce the total divergence to less than one-tenth of the initial value. In the following section, we use this wind field for the detailed analysis of transport process of pollutants.

b. Observation Results

In this section, we show the trajectories and vertical distribution of pollutants and study the transport process of the pollutants. We mainly consider the flights from Run 11(early morning flight of 31 July) to Run 21(early morning flight of 1 August) when the local wind

circulation dominated in the Kanto Plain. Figure 3 shows the geostrophic wind at the 800 mb and 700 mb levels calculated using aerological data from the Japan Meteorological Agency (JMA). This shows that the air pressure gradients were relatively stagnant and wind speed was small on 31 July. Figure 4 shows the diurnal change pattern of wind field at the 350 m height observed from pilot-balloon measurements. In this figure, the typical wind patterns are shown, that is, in the early morning, the land breeze(N or NE direction) covers the whole Kanto plain; in the middle morning the sea breezes from Sagami and Tokyo Bays are detected in the coastal area but in the remaining area the land breezes dominated; in the afternoon the sea breeze from Sagami Bay covers the whole plain and this continues until the late evening; and at midnight, a mountain valley wind and land breeze start and the penetration of the sea breeze decreases. These wind circulation systems complicate the transport process of photochemical pollutants.

The vertical crosssection of pollutants and meteorological elements were observed in several sections(e.g., AB,CD and so on in Figure 2) and complete representation of all this data is outside the scope of this paper. The sea breeze from Sagami Bay has a great effect on the transport process and is a south wind. In addition, in the evening and at midnight, only section H-G was observed by a single aircraft(AC-685), so the south-north crosssection is sufficient to show the details of the pollutant behavior, and we analyzed the section H-G in the following analysis.

In the early morning of 31 July, to observe the initial distribution of photochemical pollutants, the first observation Run 11 was conducted from 0430 to 0630JST. Figure 5 shows a portion of the results(vertical crosssection H-G). The Keihin industrial complex and the Tokyo Metropolitan Area are located in the southern part of section H-G(area covering 0 Km to 40 Km from point H in Figure 5) and in the northern part of this section, no significant NOx emission sources exist. In this figure, the temperature profile at Otemachi(point 6 in Figure 2) is also shown. Otemachi is on the east side(15 Km) of the center of section H-G and this data point represents the typical urban area temperature profile. The ground pollutant level was determined from the ground monitoring stations. Note that oxidant was treated as ozone in the following analysis. The operation heights were at four fixed

levels, so that an isopleth line of pollutant concentration can be drawn by interpolation. The significant temperature inversion layer(lid) was observed about 500 m height at Otemachi. The well-aged ozone layer (the area where the ozone concentration exceeded 100 ppb for about 40 Km) was above the lid and below it , the primary pollutant(NO_2) was trapped(Figure 5). A strong vertical gradient of the pollutants existed at the lid layer. Also, a horizontal gradient of pollutants existed at the industrial area(0-60 Km area in section H-G) and in the rural area(60Km - G). Under the lid, the NO_2 and ozone were inversely related. The NO_2 had a maximum at the 350 m height and this was due to the emission from the stacks of the industrial zone. In Figure 6, we show the prevailing wind direction at 0600JST at the 350 m height and the shaded area indicates that the ozone concentration was less than 10 ppb at the 350 m height. The shaded area was estimated and extrapolated from Run 111(lowest operation height data). The spread of these zones exactly coincided with the downwind areas of the Keihin and Keiyo coastal industrial complexes. The ozone precursors are consistenly transported to the Sagami Bay area along the NE wind(land breeze) and this brings the high ozone concentration inland with the penetration of the sea breeze. The Sagami Bay area plays the part of a storage tank for the ozone precursors. In Figure 6, the Trajectory A which started from 0600JST at the 350 m height is shown. The trajectory was integrated using the three-dimensional wind field data obtained by the modified MATHEW method. In the trajectory analysis, horizontal diffusion is neglected, so to estimate the mean path of the polluted air mass, the calculation area was considered as to be a circle of about 10 Km in radius at start point. The circle line of the trajectory at every hour was distorted by the horizontal wind shear. Trajectory A started at 0600JST coincided with the behavior of pollutants measured in Run 111(the early morning observation). Trajectory A shows the re-circulation of pollutants from the sea area to the inland area. The vertical change of elevation in Trajectory A is not so very significant. Figure 7 shows the surface sea breeze front from 1000JST to 1700JST and the surface oxidant isopleth at 1200, 1300 and 1500JST. On the west side of the Tokyo Metropolitan Area, the oxidant concentration increased rapidly in the afternoon, and its increase exactly coincided with the penetration of the sea breeze front. The Trajectory A in Figure 6 indicates that the early morning's primary pollutant around Tokyo Bay area is the main source of the afternoon's high oxidant pollution.

From 1000JST, the sea breeze was observed at Miura(point 10 in Figure 2) and Chigasaki(point 9), but still the N or NE wind dominated the whole plain(Figure 4). Wind flow at the 350 m level showed no difference from the early morning observation. So until this time, the primary pollutants of two industrial zone were transported into the Sagami Bay area. Run 12 was performed from 0945 to 1130JST(31 July) to observe the middle stage concentration of the photochemical reaction. Figure 8 shows a portion of the results of Run 12(section H-G: NO_2, ozone and potential temperature profile). A lid was observed at about the 1,100 m level at Otemachi. The lid rose about 600 m compared with the level at 0600JST and following this, the high NO_2 area ascended due to mixing. Two high ozone concentration layers were observed at 300 m and 900 m heights. In particular, the upper ozone layer is considered to be an aged layer from trajectory analysis(not shown in the figure) which was entrained into the mixing layer in accordance with the elevation of the lid. The ozone at the lower elevation is considered as a fresh ozone. This shows that aged and fresh pollutants are mixed in the same mixing layer. The potential temperature profile has a relatively high value above the Tokyo Metropolitan Area(10-60 Km area) and the potential temperature has a convex form. The NO_2 profile also has a convex shape and it coincides with the vertical diffusion pattern of NO_2. In Figure 5, Trajectory B started from 1000JST at the 350 m height and shows the backward and forward path. This area is just above Yokohama(point 7 in Figure 2) and above this area, the highest NO_2 (exceeding 60 ppb) was observed in this flight. Trajectory B (backward direction) shows that this air mass has its origin in the Keihin industrial zone. So this high NO_2 area is considered to be the plume from this industrial zone. The vertical section of Trajectory B in Figure 6 indicates that the height of this marked air mass changed rapidly. At the front of sea breeze zone, a small updraft wind exists(Simpson et al., 1978, Mitsumoto et al., 1982), and from 1000JST in the coastal area, the sea breeze began to be observed. So the sudden change of height of Trajectory B was due to the updraft wind of the sea breeze front.

In the afternoon, the sea breeze from Sagami Bay covered the Kanto plain(see Figure 4), and it brought the polluted air mass to the inland area. Figure 9 shows a portion of the results from Run 13 performed

from 1450 to 1630 JST. The period of this observation(Run 13) corresponded to the maximum concentration stage of the photochemical reaction. From the potential temperature profile depicted by the dashed line in Figure 9, the sea breeze layer is easily distinguished. The southern area(0-50 Km from point H) has low potential temperature and is considered to be the sea breeze layer which has a relatively low temperature, while the northern area is considered to be a well-heated and the highly turbulent area. In the sea breeze layer, NO_2 is not diffused vertically, on the other hand, in the well-heated area, NO_2 is transported to more than 1,000 m, which shows that the sea breeze layer became more turbulent as it penetrated inland due to thermal convection and became the cause of high ozone formation in the high altitue layer. In Figure 9, the vertical wind profile(v and w components) at 1500JST obtained by modified MATHEW method are also shown. From this figure, the v component of the wind dominated the whole vertical crosssection. A small updraft wind was detected in the inland area. The distribution of pollutants is very interesting. At the 350 m height, there existed two maximum ozone air masses(10-20 Km area C'and 70-80 Km area D in Figure 9). Above the sea breeze layer(south area) there existed a relatively clean air mass whose ozone concentration was less than 100 ppb. It is considered that there the border of the polluted air mass exists near the 10 ppb isopleth of NO_2. This explains that the borderline of the sea breeze layer ascended with penetration into the inland area. At about the 1,000 m height, high ozone air masses were also detected and belonging in the mixing layer. The highest ozone concentration (exceeding 350 ppb) measured during airborne survey was observed in this run. This high ozone concenration area is labeled as C in Figure 10, which is just to the west side of C' area in Figure 9. The horizontal distance between C and C' is about 10 Km, so the transport pattern is believed to be similar. For the analysis of the transport process of the polluted air mass at 350 m, we selected the two air masses C and D. Figure 10 shows the results of this trajectory analysis. Following this, there exist two types of high ozone concentration air mass. One has an indirect route, that is, its origin is the early morning emissions from the Tokyo Bay coastal industrial zone, which are transported to the Sagami Bay area by the land breeze and penetrate inland due to the sea breeze. The other is almost directly transported from the two industrial zones(Trajectory D) and is well-mixed vertically by thermal convection. These two types penetration pattern are the main reason for the separat-

ion of the polluted ozone air mass. The highest ozone concentration was observed in the former layer, and it most likely that the long photochemical reaction time contributed strongly.

From evening to midnight, the sea breeze from Sagami Bay covered the whole Kanto district(Figure 4) and the polluted air masses were carried inland. The result of Run 14, which was performed in the late evening(1810-1950JST), showed that the relatively clean air mass from Sagami Bay was transported inland(not shown in this paper). In Figure 10, Trajectory E, started at 1830JST at the 350 m height, shows the penetration of pollutants from the Keihin coastal industrial zone in the evening. The primary pollutants were advected to the middle of the Kanto area. This phenomenon continued until the land breeze began at midnight.

The sea breeze from Sagami Bay continued until about 0100JST (1 August) and then the land breeze started gradually down to the southern area. The air pressure gradient became stronger than the previous day and a strong SW wind zone was formed near the line connecting the Izu and Boso Peninsulas. A line of wind discontinuity was formed on this line. Run 20 was conducted from midnight(0000-0145JST , 1 August), and its results showed that the surface pollutants were trapped and diffused slightly to a higher elevation (Figure 11). Sonde observation was not performed at midnight. These high NO_2 areas(40-80 Km) are from the Keihin and Keiyo industrial complexes, and the high ozone concentration layer just covered the NO_2. The rich ozone concentration decreased with the dark reaction with NO. The location of the strong gradients of both pollutants are at that rich NO_2 area. This rich ozone layer remained until the next morning and contributed to the next day's high concentration of pollutants. The vertical wind field at 0100JST 1 August is also shown in Figure 11 with an ozone concentration map. The flow pattern is the same as Figure 9, but in the northern area, the southerly wind decreased.

The early morning flight Run 21 was conducted from 0445 to 0620JST, 1 August 1979. The flight path was the same as Run 11. Figure 12 shows a portion of the result of Run 21. The temperature profile at Otemachi at 0600JST indicated that a weak temperature inversion was located at the 1,000 m height, and the NO_2 distribution(5 ppb line) is coincident at this height. The weak and the strong wind zones are distinguished(dashed

line in Figure 12) and the vertical profiles of ozone are separated in this discontinuity zone(Figure 12). The vertical wind field at 0500JST, 1 August was overlayed on the ozone concentration map. The wind field is very interesting. Near the discontinuity line, a small downdraft wind was detected and this wind would entrain the high ozone air mass from the high altitude to a lower one. The high ozone concentration zone at the 700 to 800 m level is the aged air mass, which was transported from the north by the land breeze; the polluted air was sheared near the strong wind speed area and blown out to the NE direction. The maximum concentration in the aged ozone exceeds 140 ppb and this value is higher than the previous day's early morning observation result(Run 11 in Figure 5). The concentration gradients became stronger. These results indicate that the secondary pollutant concentration level becomes higher than the previous day's maximum under the stagnant pressure condition. On the other hand, the NO_2 maximum in Run 21 was less than the previous day's observation. One reason for this is that on the second day, the wind direction was different so that the emission sources, such as Keihin industrial complex was downwind. The second reason is that lid height was much higher on the second day allowing more mixing.

4. Conclusion and discussion

An aircraft investigation was conducted from 31 July to 2 August 1979 covering the Tokyo Metropolitan Area in Japan. Vertical cross sections of pollutants and wind field were constructed and the transport process of pollutant was studied.

1) From three-dimensional trajectory analysis, it is clear that the complicated air flow pattern due to the local wind circulation is very important in understanding the photochemcial smog phenomena in the Tokyo Metropolitan Area. In particular, the early morning night time radiation inversion inhibits the vertical mixing of primary pollutants and forms a high NO concentration air mass, which is transported to the Sagami Bay area along with the land breeze. These polluted air massses are converted to secondary pollutants and transported inland with the penetration of the sea breeze(Figure 6,10).

2) There exists a strong relation between the penetration pattern of the sea breeze and the photochemical oxidant level on the ground. Blumenthal et al.(1978) reported that the sea breeze transported the clean air inland in Los Angeles, but in the Tokyo Metropolitan Area, Sagami Bay plays an important role in the storage of primary pollutants, which are later converted to secondary pollutants and this leads to the high ozone concentration in the inland area. These continue to bring high ozone concentration inland until the late night. On the other hand, relatively clean air penetrates inland after the midnight. This means that the pollutants stored in Sagami Bay are finally removed.

3) In the early morning in the upper air(500-1,000 m height), an aged ozone layer, whose concentration exceeds 100 ppb, was observed on both days of observation(Figure 5,12). The second day's maximum concentration was higher than the first day's value. From the trajectory analysis, potential temperature profile and sonde observation, the aged ozone air mass was entrained into the mixing layer in accordance with the elevation of the lid(Figure 8). This effect is believed to accelerate the formation of secondary pollutants during the next day.

4) From the potential temperature profile(Figure 10), it is easy to distinguish the marine layer. The marine layer is thermally stable. On the other hand, the air mass ahead of the sea breeze front was turbulent and this layer transported the NO_2 to the 1,000 m level. This is one reason for the high level ozone layer. Edinger et al.(1972) showed that the ozone layer ascends along a slope and breaks through the lid to create a high ozone layer above the lid. However, our results indicate another possibilty for the high levels of ozone. The difference of the density between the marine layer and the surrounding also contributes to these phenomena.

5) The higher concentration of photochemical ozone were observed in the upper air(300-500 m height, i.e., the sea breeze layer) rather than at the ground. In general, except in the midnight and early morning, the oxidant level on the ground was proportional to that in the upper layer. Because of the restriction of air-traffic control, we could not measure below 300 m; however, we can state qualitatively that the upper layer's pollutants affect the levels of ground level pollutant concentrations.

6) We could follow the behavior of the polluted air mass on an urban scale by trajectory analysis. In our next project, the construction of a simulation model of the Tokyo Metropolitan Area, the following must be taken into account :

i) to simulate the photochemical smog phenomena on a scale size of the Kanto Plain, it is necessary to take into account such features as Sagami Bay as a tank and has a time delay effect. Also, the treatment of the local wind circulations are important to the model.

ii) to predict or control the high ozone level in the afternoon, the early morning's meteorological conditions are especially important. For example, the existence of a night-time radiation inversion is an important factor.

Acknowledgements

The authors wish to express their thanks to K.Goi in the Saitama Institute of Environmental Pollution, Y.Aburamoto in the Toyama Environmental Center, and H.Tsuruta in the Yokohama Environment Research Institute for their cooperation in the aircraft field study. Thanks are also given to the staff of Kimoto Electric. Co., Ltd. for their valuable cooperation during the aircraft study.

REFERENCES

Angell,J.K., Pack,D.H., Machta,L., Dickson,C.R. and Hoecker,W.H. (1972): Three-dimensional air trajectories determined from tetroon flights in the planetary boundary layer of the Los Angeles Basin. J. Appl. Meteorol., 11, 451-471.

Angell,J.K., Hoecker,W.H., Dickson,C.R. and Pack,D.H. (1973): Urban influence on a strong daytime air flow as determined from tetroon flights. J. Appl. Meteorol., 12, 924-936.

Blumenthal,D.L., White, W.H. and Smith,T.B. (1978) Anatomy of a smog episode: Pollutant transport in the daytime sea breeze regime. Atmos. Environ., 12, 839-907

Edinger,J.G. (1973): Vertical distribution of photochemical smog in the Los Angeles basin. Environ. Sci. Technol., 7, 247-252.

Edinger,J.G., McCutchan,M.H., Miller,P.R., Ryan,B.C., Schroeder,M.J. and Behar,J.V. (1972): Penetration and duration of oxidant air pollution in the south coast air basin of California. J. Air Pollut. Control Assoc. 22, 882-886

Feigley,C.E. and Jeffries,H.E. (1979): Analysis of processes affecting oxidant and precursors in the Los Angeles reactive pollutant program(LARPP) Operation 33. Atmos. Environ., 13, 1369-1384.

Gloria,H.R., Bradburn,G., Reinisch,R.F., Pitts,Jr.,J.N., Behar,J.V. and Zafonte,L. (1974): Airborne survey of major air basins in California. J. Air Pollut. Control Assoc., 24, 645-652.

Goodin,W.R., McRae,G.J. and Seinfeld,J.H. (1980): An objective analysis tehnique for constructing three-dimensonal urban-scale wind field. J. Appl. Meteorol. 19, 98-108

Husar,R.B., Patterson,D.E., Blumenthal,D.L., Warren,W.H, White,W.H. and Smith,T.B. (1977): Three-dimensional distribution of air pollutants in the Los Angeles basin. J. Appl. Meteorol., 16, 1089-1096.

Keen,C.S. and Lyons,W.A. (1978): Lake/Land breeze circulations on the western shore of Lake Michigan. J. Appl. Meteorol., 17, 1843-1855.

Liu,C.Y. and Seinfeld,J.H. (1975): On the validity of grid and trajectory model of urban air pollution. Atmos, Environ.,9, 555-574.

Lyons,W.A. and Cole,H.S. (1976): Photochemical oxidant transport: Mesoscale lake breeze and synoptic-scale aspects. J. Appl. Meteorol., 15, 733-743.

Mitsumoto,S., Ueda,H. and Ozoe,H. (1982): A laboratory experiment on the dynamics of land and sea breeze. To appear in J. Atmos. Sci.

Sasaki,Y. (1958): An objective analysis based on the variational method. J. Meteorol. Soc. Japan, 36, 77-88.

Sasaki,Y. (1970): Numerical variational analysis under the constraints as determined by longwave equations and lowpass filter. Mon. Wea. Rev., 98, 875-883.

Sexton,K. and Westberg,H. (1980): Elevated ozone concentrations measures downwind of the Chicago-Gary urban complex. J. Air Pollut. Control Assoc., 30, 911-914.

Sherman,C.A. (1978): A mass-consistent model for wind fields over complex terrain, J. Appl. Meteorol., 17, 312-319

Simpson,J.E., Mansfield,D.A. and Milford,J.R. (1977): Inland penetration of sea breeze front. Quart. J. R. Meteorol. Soc., 103, 47-76.

Wakamatsu,S., Ogawa,Y., Murano,K., Goi,K. and Aburamoto,Y. (1982a): Aircrafts survey of the secondary photochemical pollutants covering the Tokyo Metropolitan Area. To appear in Atmos. Environ.

Wakamatsu,S. Uno,I., Suzukis,M. and Ogawa,Y. (1982b): The Lagragian observation of polluted air masses using aircrafts. Japan-US Joint Conference on Photochemical Air Pollution and Air Pollution-related Meteorology, at Tsukuba, 1-2, December 1982

Table 1. Instrumentation for the aircraft

Parameter	Analysis Technique	Resolution	Manufacturer	#1 AC-685	#2 C-404	#3 C-402	#4 C-402
NO/NOx	Chemiluminescence	2-1000 ppb	Kimoto	o	o	o	o
Ozone	Chemiluminescence	1-1000 ppb	Kimoto	o	o	o	o
Condensation Nuclei(CN)	Light attenuation		Environmental One	o	-	-	-
UV Radiation Intensity	UV radiometer		Eppley	o	o	o	o
Aerosol size Distribution	optical particle counter		Rion	o	-	-	-
Humidity	Humicup	0-100 %	Ogasawara	o	-	-	-
Temperature	Platinum resistence	0-50 °C	Kimoto	o	o	o	o
Altitude	Pressure diode		Nissho	o	o	o	o
Nitrate Sulfate	Fluorocarbon filter Ion Chromatography		Dionex	o	-	-	-
Hydrocarbon	Glass vessel Gas Chromatography		Shimadzu	o	-	-	-
Position	LORAN-C		Furuno	o	o	-	-
Operation Height				350m	650m	900m	1200m

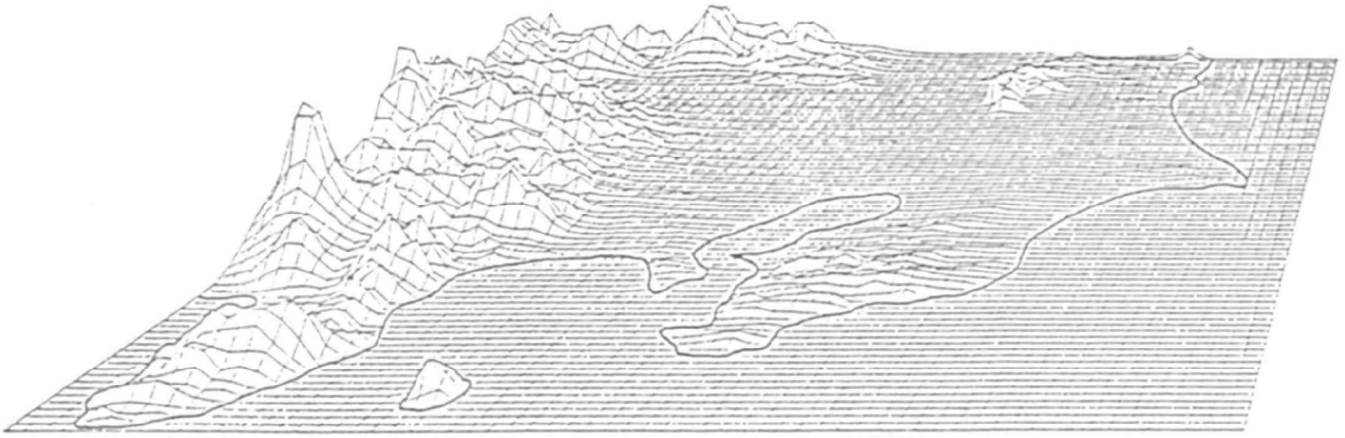

Figure 1. Topography of the Tokyo Metropolitan Area viewed from the south-east.

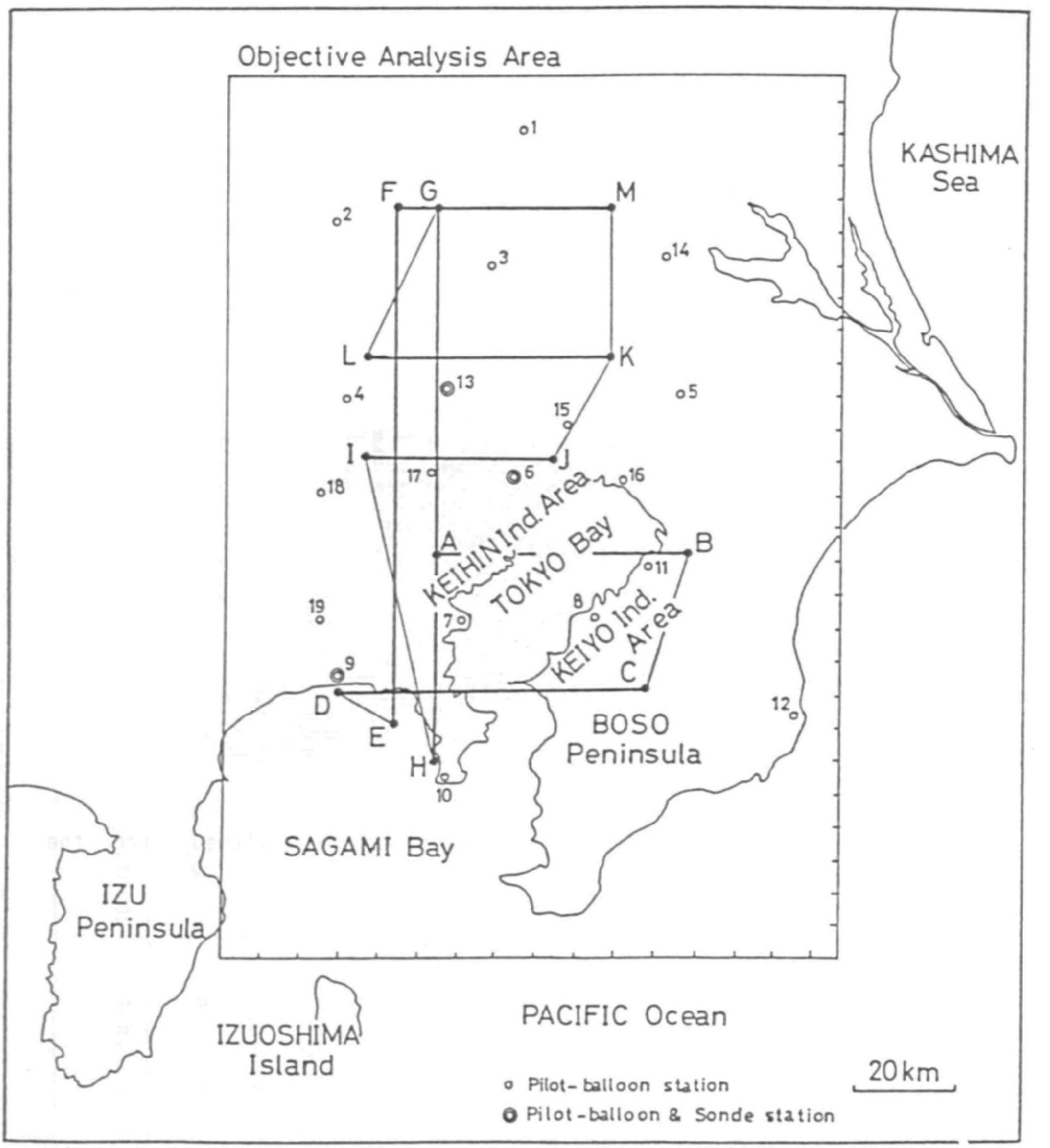

Figure 2. Map of Kanto District, flight paths and objective analysis area.

Pilot-balloon and Sonde observation points

1 Oyama	2 Kumagaya	3 Satte	4 Iruma
5 Inzai	6 Otemachi	7 Yokohama	8 Sodegaura
9 Chigasaki	10 Miura	11 Ichihara	12 Ohara
13 Urawa	14 Tsukuba	15 Nagareyama	16 Tsudanuma
17 Musashino	18 Hachioji	19 Atsugi	

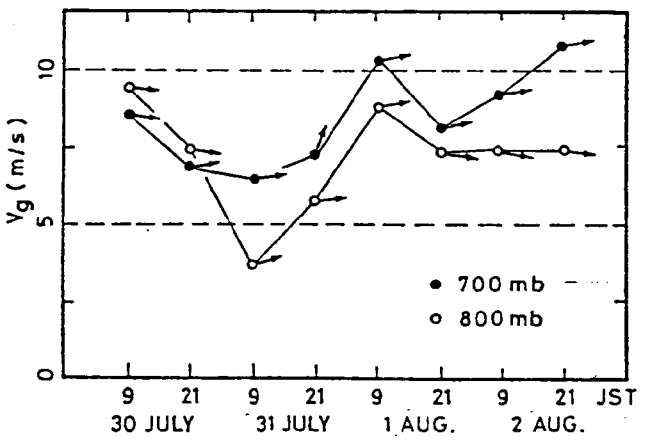

Figure 3. Variation of geostrophic wind during the aircraft survey. Arrows indicate wind directions.

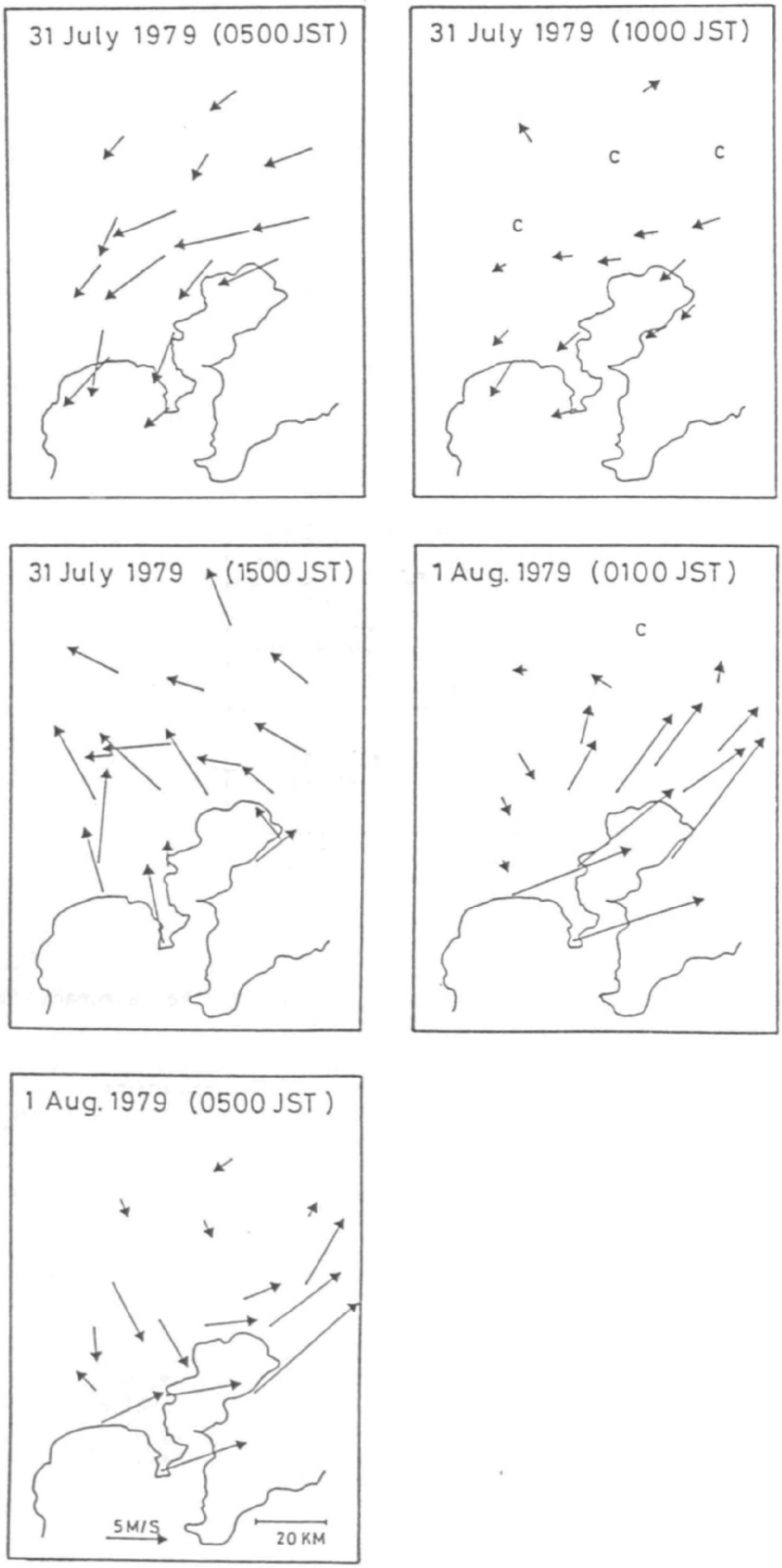

Figure 4. Diurnal change of local wind circulation at 350 m height from 31, July to 1, August.

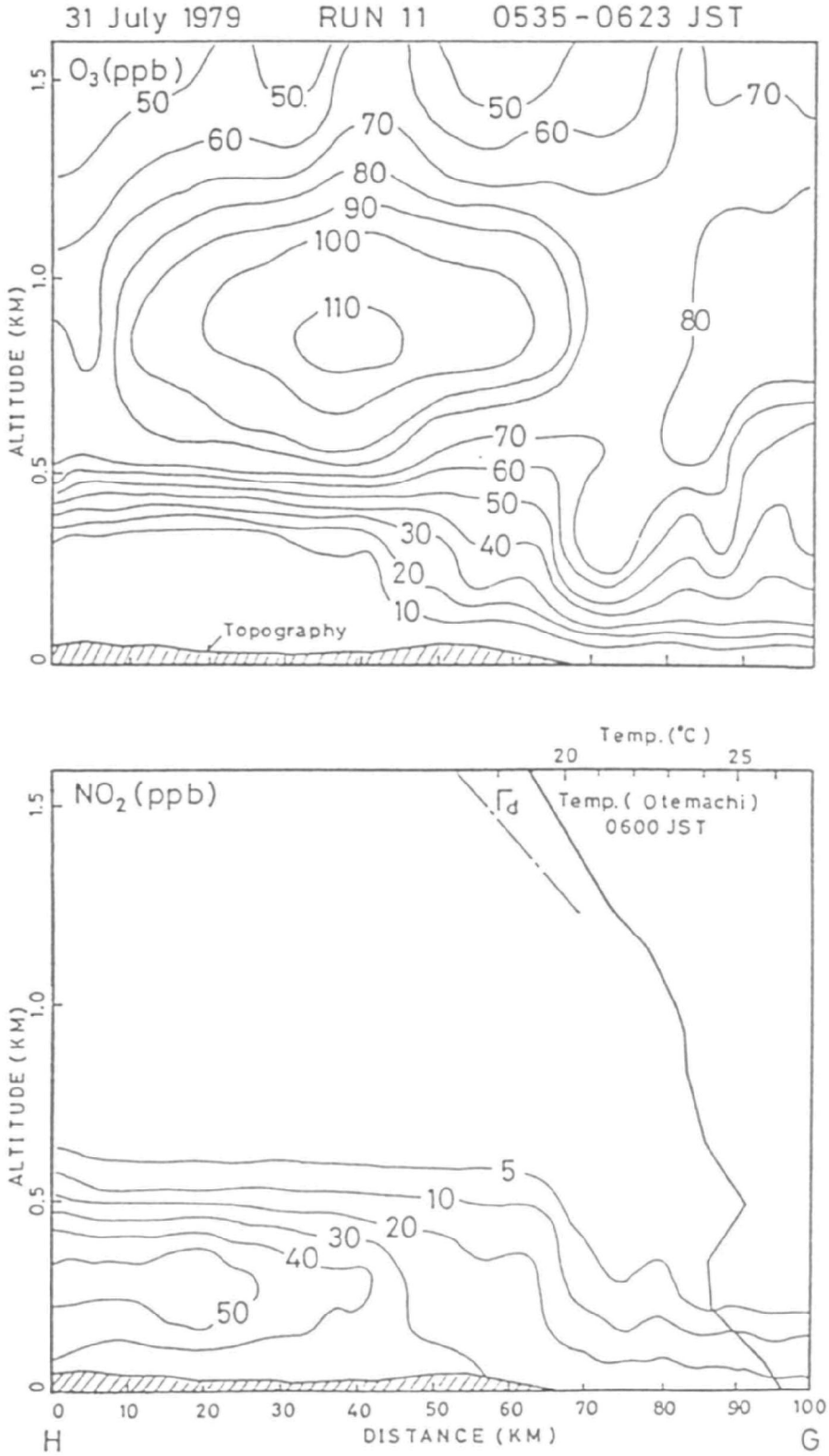

Figure 5. Vertical distribution of pollutants in the early morning of 31 July 1979(RUN 11 : 0430-0630 JST , Crosssection H-G) with vertical temperature profile at Otemachi(0600JST). Night time temperature inversion is observed at about 450 m height. Γ_d is the dry adiabatic lapse rate slope.

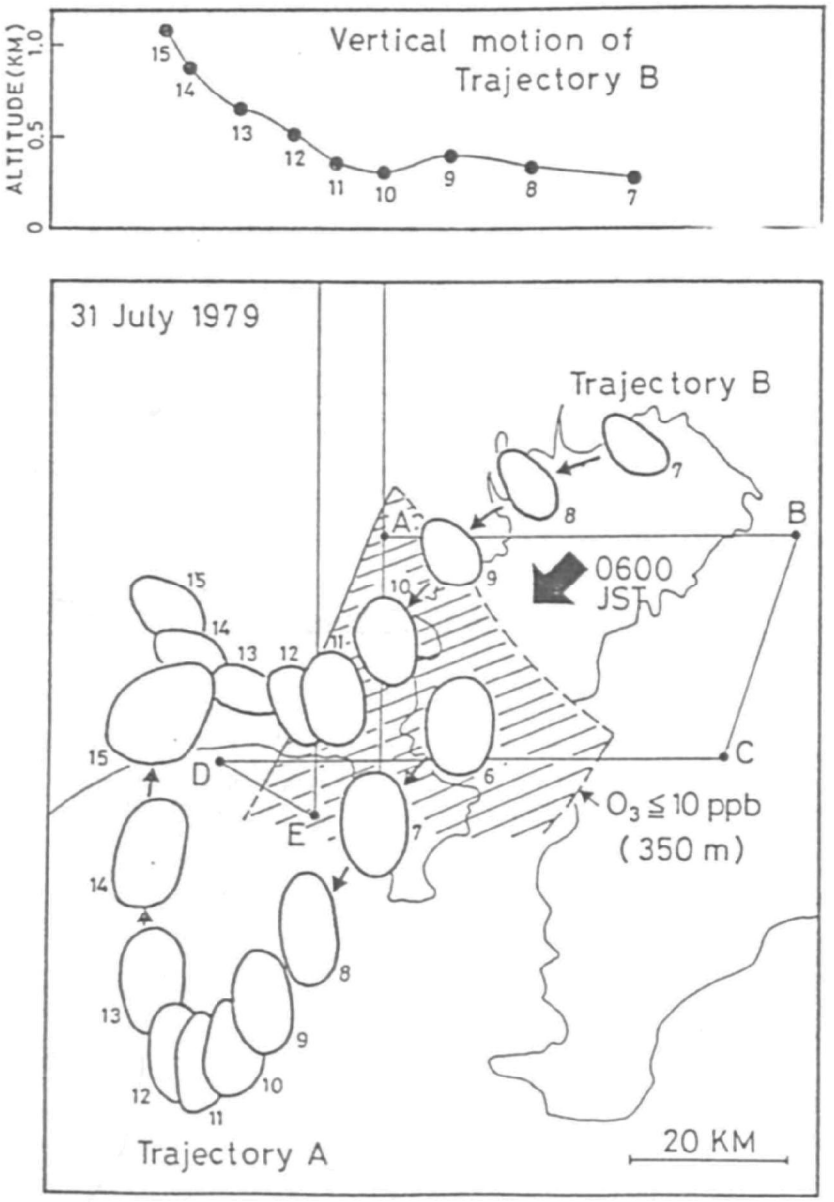

Figure 6. Trajectories of pollutants(31 July 1979): Trajectory A(starting from 0600JST at 350 m level), Trajectory B (starting from 1000JST at 350 m level, forward and backward). The vertical movements of trajectory B are also shown. The shaded area indicates that the ozone concentration was less than 10 ppb estimated from Run 111.

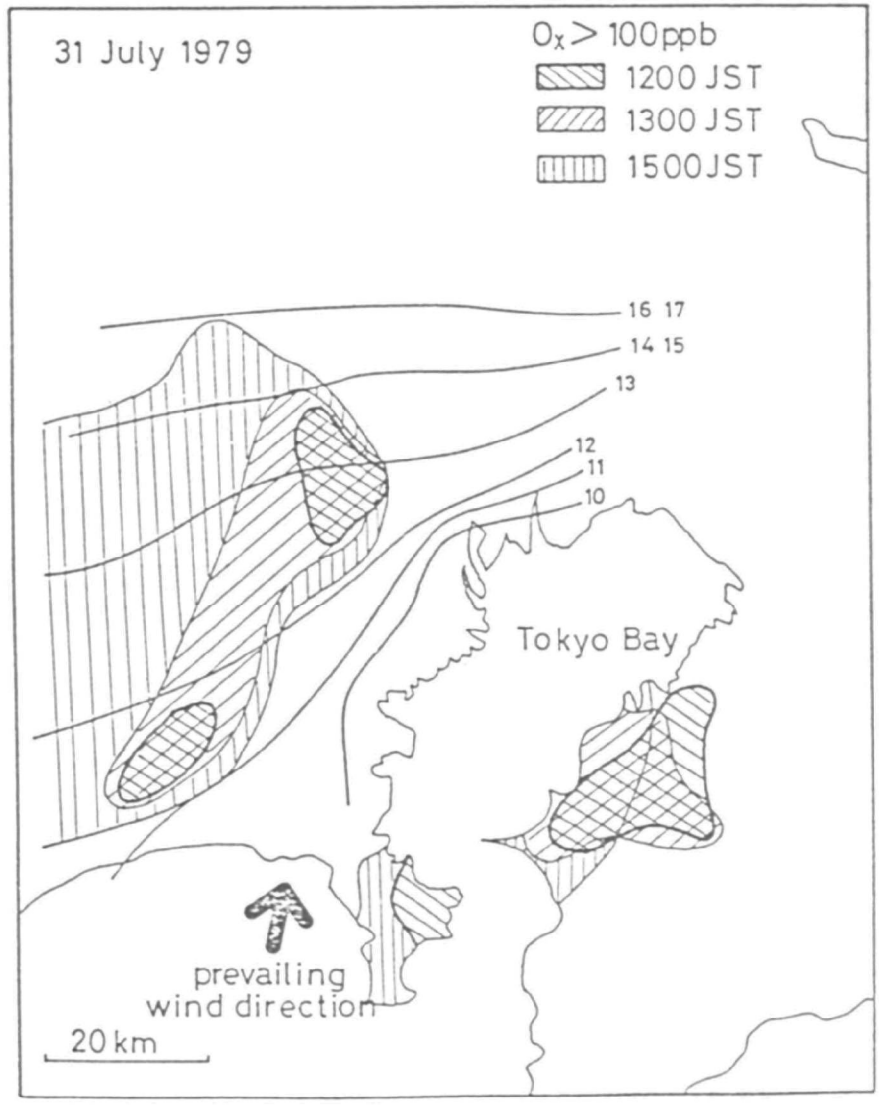

Figure 7. Movement of the heading edge of the sea breeze and ground level oxidant concentration isopleths.

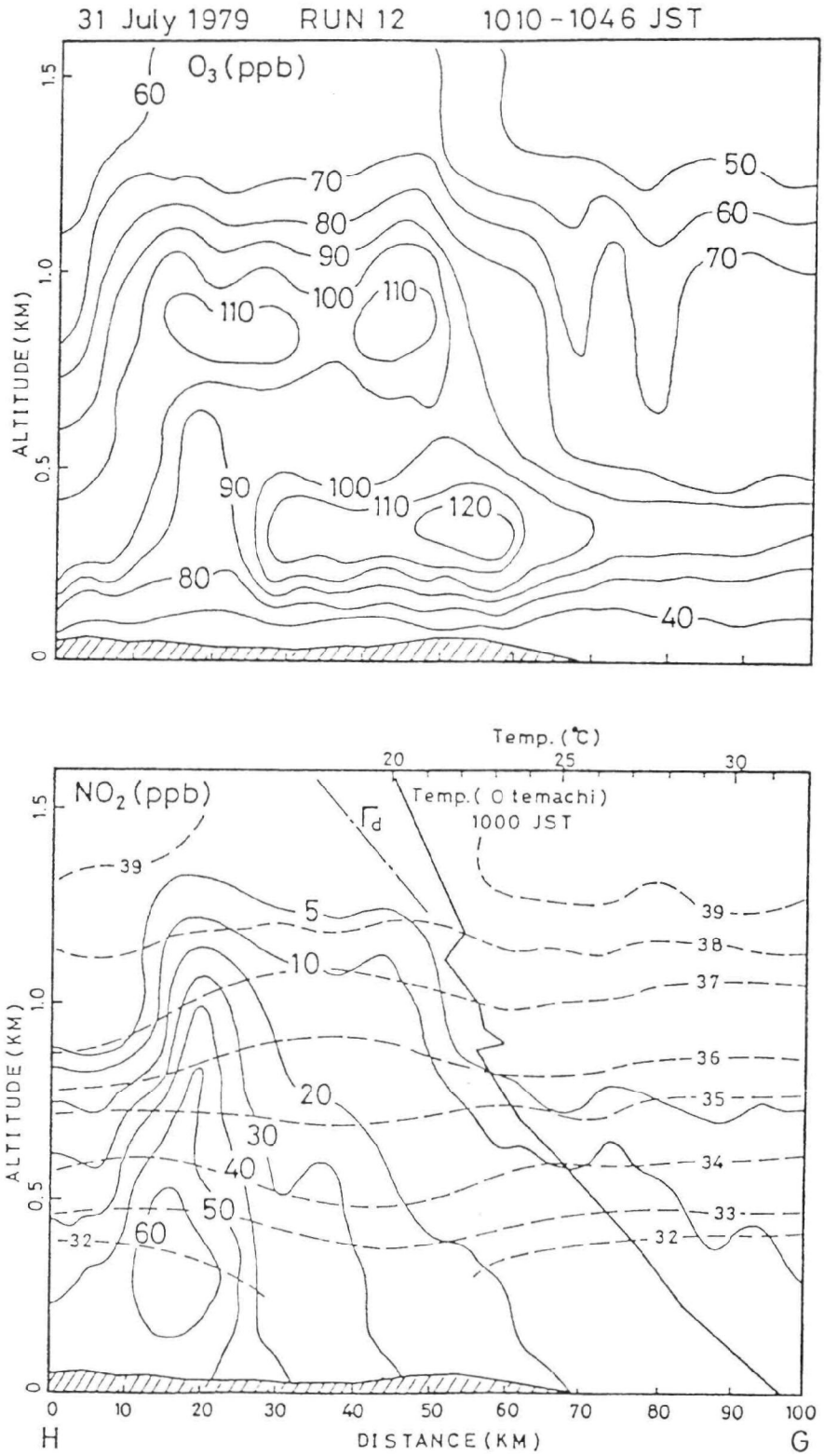

Figure 8. Vertical distribution of pollutants in the midmorning of 31 July 1979 (RUN 12 : 0945-1130 JST , Crosssection H-G) with potential temperature(dashed line) and temperature profile at Otemachi(1000JST). A temperature inversion is observed at about 800 and 1100 m heights.

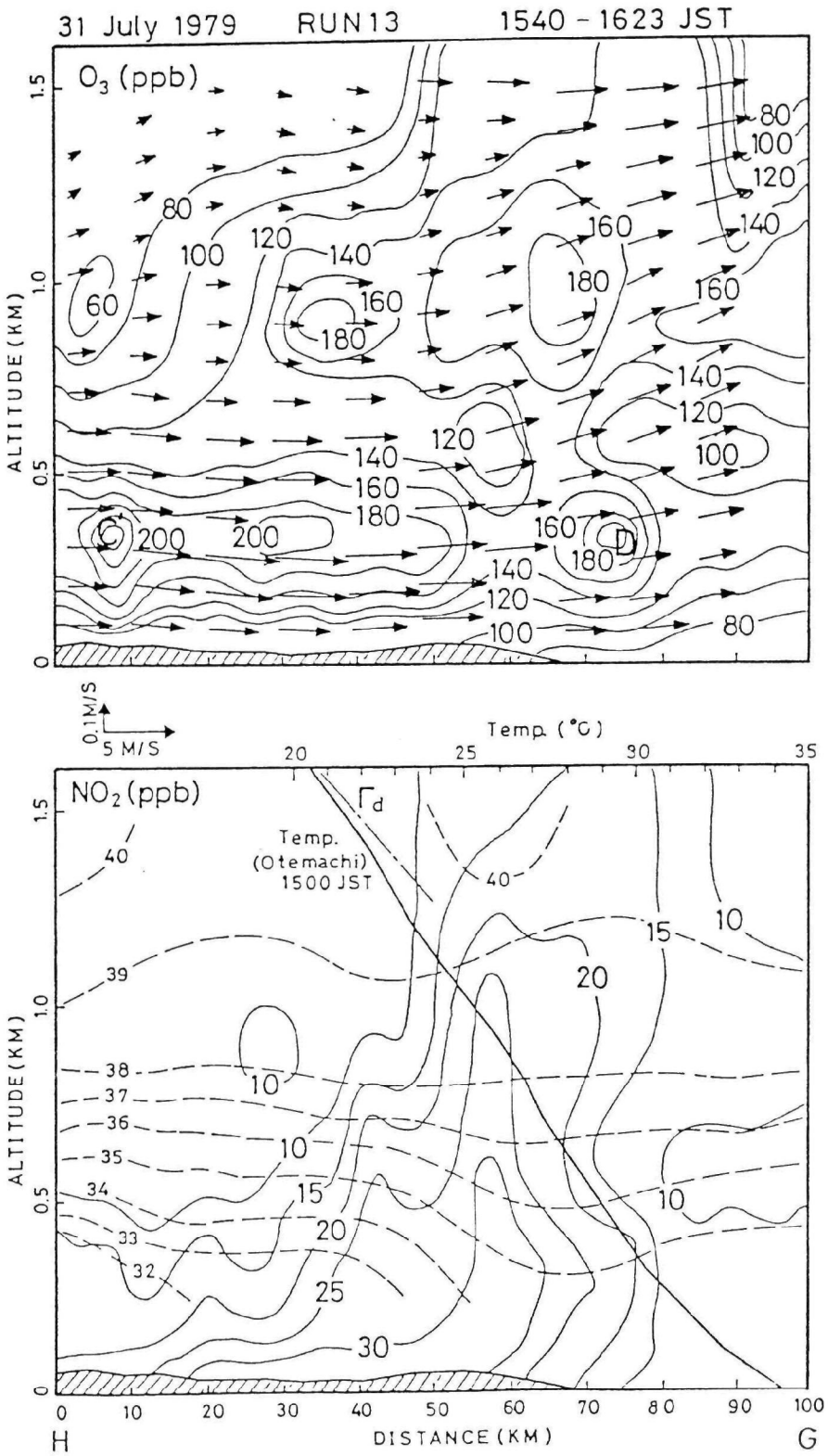

Figure 9. Vertical distribution of pollutants in the afternoon of 31 July 1979 (RUN 13 : 1450-1630 JST, Crosssection H-G) with potential temperature(dashed line) and temperature profile at Otemachi(1500JST). Vertical wind profile(v and w components) is calculated from the modified MATHEW method.

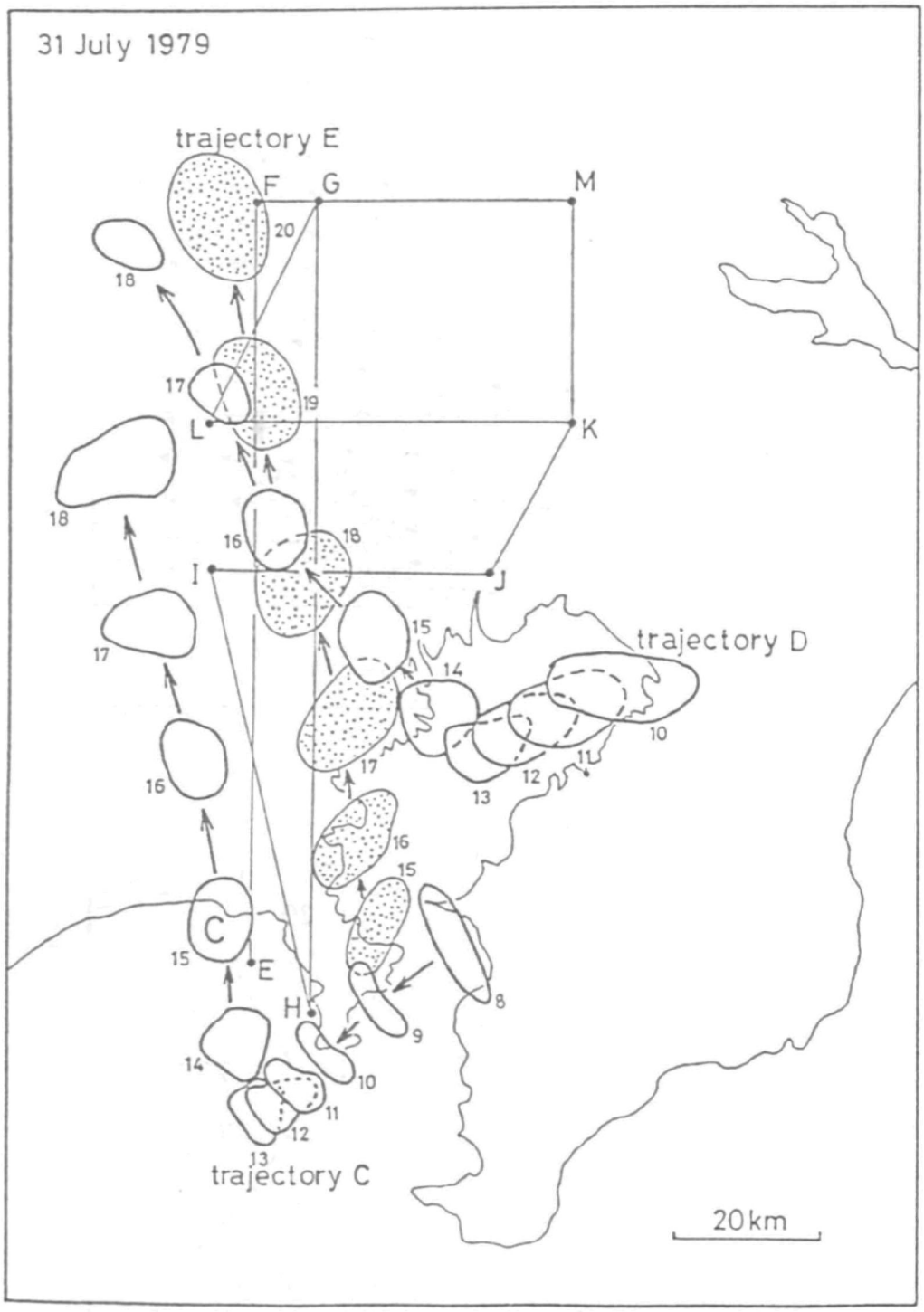

Figure 10. Trajectories of pollutants(31 July 1979): C(starting from 1500JST at 350 m level), D(starting from 1530JST at 350 m level) and E(starting from 1830JST at 350 m level). Calculated in both the forward and backward directions.

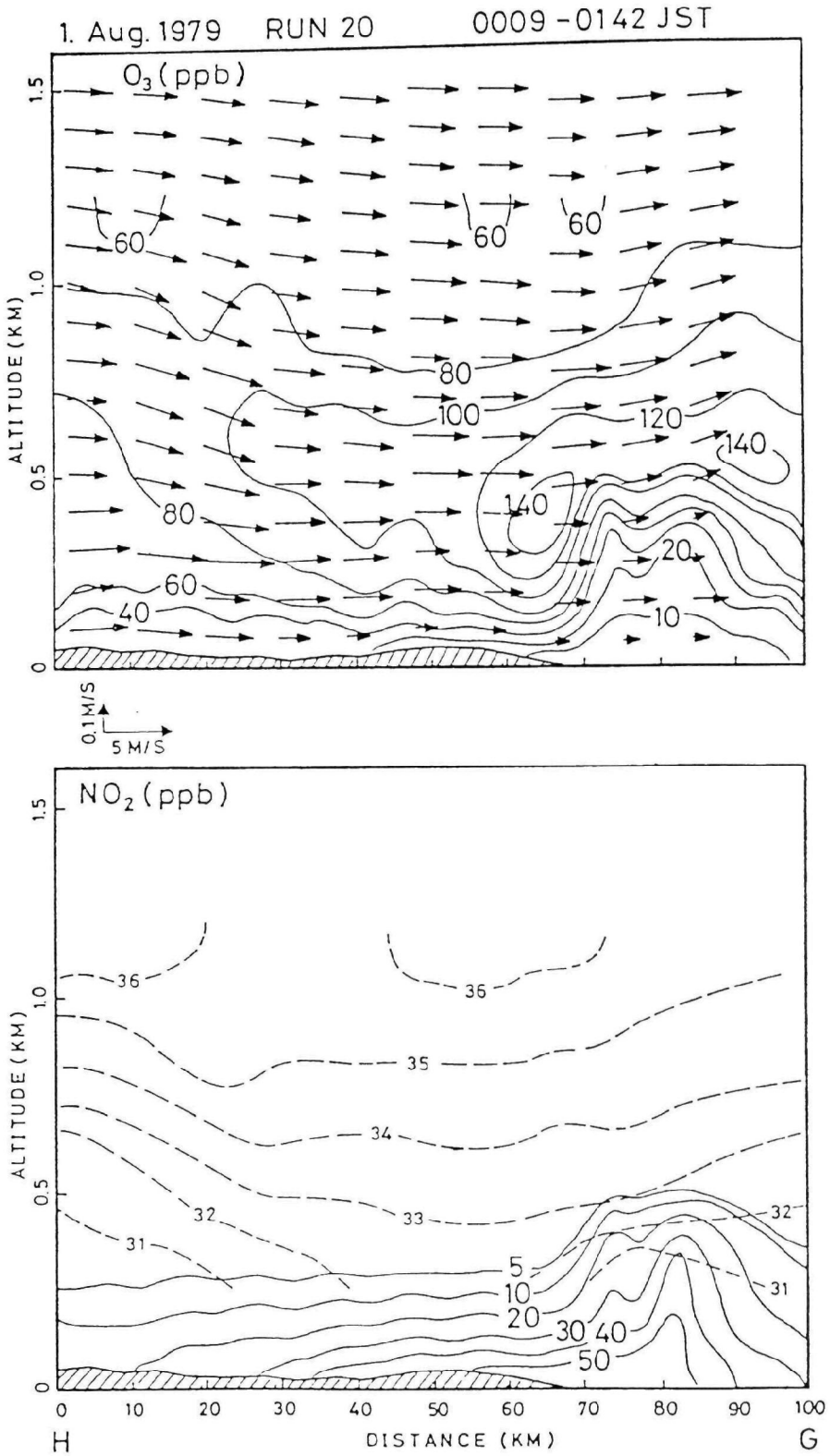

Figure 11. Vertical distribution of pollutants at midnight of 1 August 1979 (RUN 20 : 0000-0145JST , Crosssection H-G). Vertical wind profile is calculated from modified MATHEW method.

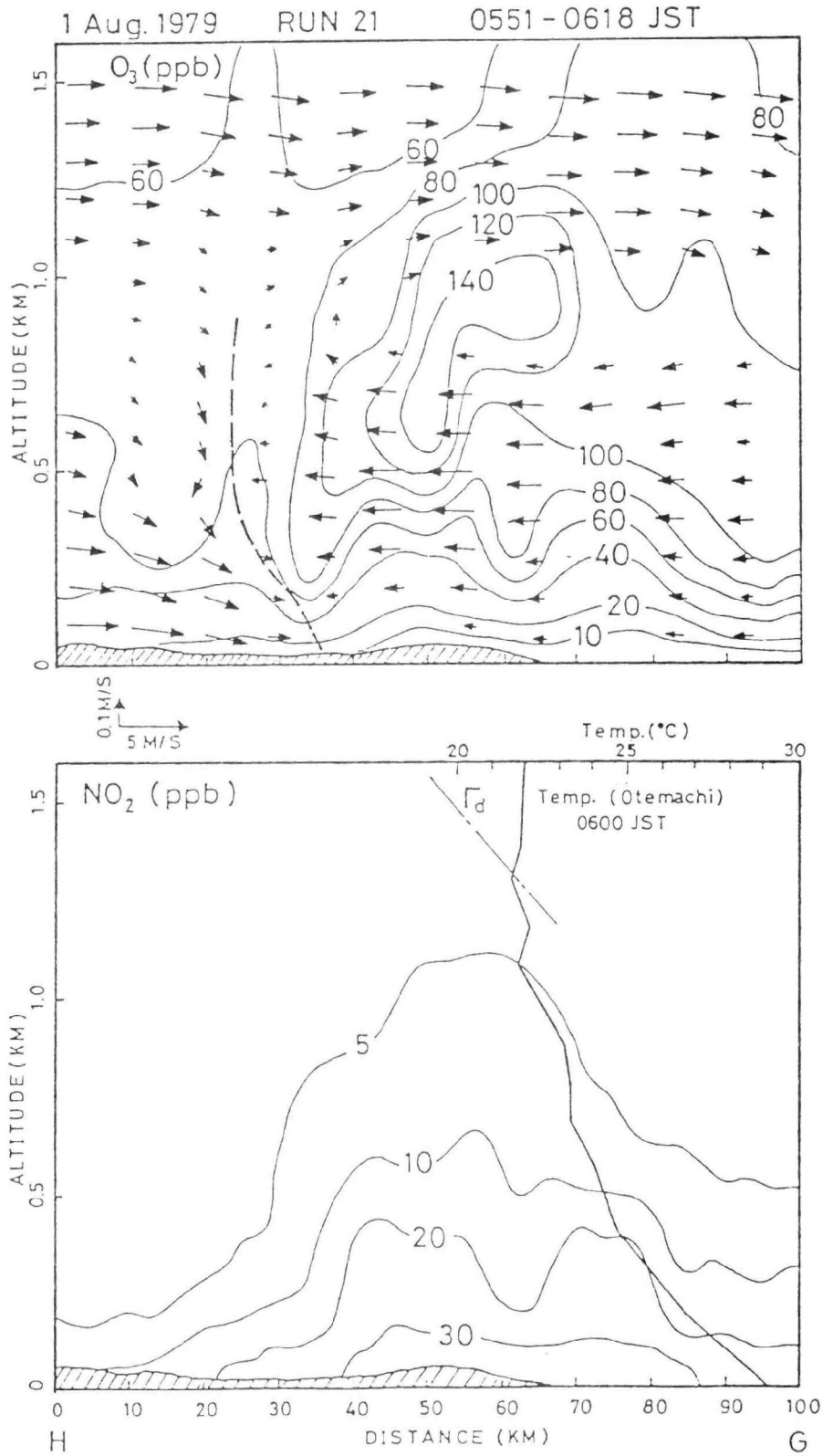

Figure 12. Vertical distribution of pollutants in the early morning of 1 August 1979 (RUN 21 : 0445-0620JST, Crosssection H-G) with temperature profile at Otemachi(0600JST). The hard dashed line indicated the discontinuity line of wind and in the near of this line, the small downdraft wind zone are detected.

US STUDIES ON STRATOSPHERIC OZONE

presented by H. L. Wiser

Environmental Protection Agency
United States

SUMMARY

INTRODUCTION

This report reviews current knowledge about man-made causes of changes in concentrations of stratospheric ozone and the effects of those changes. Recent reports of the National Research Council (NRC 1975, 1976a,b, 1978, 1979a,b) have treated the chemical and physical aspects of potential reductions of stratospheric ozone in detail. Part I of this report reviews recent developments on that subject. Part II deals with the effects of reduction of stratospheric ozone on humans, other animals, and plants, independently of what might cause the reduction.

CHEMISTRY AND PHYSICS OF OZONE REDUCTION

The abundance of ozone in the stratosphere is determined by a dynamic balance among processes that produce and destroy it and transport it to the troposphere. According to current understanding, the most important photochemical reactions regulating ozone involve molecular and atomic oxygen and various radicals containing nitrogen, hydrogen, and chlorine. All of these compounds have natural sources, but their concentrations in the stratosphere can be significantly altered by human activities. The human activities that have thus far been identified as potentially influencing stratospheric ozone are as follows:

- The release of gaseous chlorinated carbon compounds, mainly chlorofluorocarbons (CFCs) and methyl chloroform (CH_3CCl_3). CFCs are used as foam-blowing

agents, as working fluids in refrigeration systems, and as propellants in aerosol sprays. Methyl chloroform is an industrial solvent. These gases decompose in the stratosphere providing a significant source of radicals that contain chlorine.

- The release of nitrous oxide (N_2O) from combustion and its enhanced release from soils and waters as a result of various agricultural and waste management practices. Nitrous oxide decomposes in the stratosphere, introducing radicals that contain nitrogen.
- The direct input of nitrogen radicals to the stratosphere due to nitrogen oxides (NO_x) in aircraft engine exhausts.
- The increased abundance of carbon dioxide (CO_2) in the atmosphere due to combustion of fossil fuels and deforestation. Increased carbon dioxide has a subtle influence, causing the temperature of the stratosphere to decrease, which leads to increased stratospheric ozone, and changing stratospheric concentrations of water vapor.

Key Findings and Conclusions

Over the past several years, research, driven by discrepancies between theory and observation, has led to considerable improvement in our understanding of the effects on stratospheric ozone of releases of CFCs and oxides of nitrogen. As a result, previous discrepancies between the estimates of models of stratospheric processes and observed concentrations of certain important species have been reduced. Important discrepancies still remain, however, which means that there are still uncertainties inherent in the results of modeling exercises.

Current scientific understanding, expressed in both 1- and 2-dimensional models, indicates that if production of two CFCs, CF_2Cl_2 and $CFCl_3$, were to continue into the future at the rate prevalent in 1977, the steady state reduction in total global ozone, in the absence of other perturbations, could be between 5 percent and 9 percent. Comparable results from models prevalent in 1979 ranged from 15 percent to 18 percent. The differences between current findings and those reported in 1979 are attributed to refinements in values of important reaction rates. Also, as an example, if the atmospheric concentration of N_2O were doubled in the absence of other perturbations, total ozone would be reduced by between 10 percent and 16 percent. Although atmospheric concentrations of N_2O appear to be increasing, we cannot reliably project the future course of N_2O emissions. Steady state reductions in both these cases would be reached asymptotically in times on the order of a century, although the assumption of doubling N_2O concentrations is unrealistic on such a time scale. The effects of perturbations by CFCs and N_2O are not additive, so the estimates of effects of combined perturbations require investigation of specific cases.

These results should be interpreted in light of the uncertainties and insufficiencies of the models and observations. For example, other chemicals released from human activities are understood to have the potential for affecting stratospheric ozone. Examples are methyl chloride (CH_3Cl), carbon tetrachloride (CCl_4), and particularly methyl chloroform. Observations of critical species need to be extended and confirmed by a number of measurements using independent techniques. Important assumptions in the models about rate constants, distributions of certain species, and the reactions taking place need to be tested. Furthermore, three important discrepancies between models and observations remain to be resolved: More chlorine monoxide (ClO) is observed at altitudes above 35 km than is predicted, the behavior of NO_x in winter at high latitudes is unexplained, and concentrations of CFCs in the lower stratosphere are lower than the models suggest.

We anticipate that research on these problems in the field, in the laboratory, and in theory currently under way, planned, and proposed will lead to continued improvement in understanding, resulting in further reduction of the remaining discrepancies between theory and observation. In particular, simultaneous measurement of the important chemical species as a function of altitude and latitude by various methods should prove critical to improving understanding during the next several years.

Examination of the historical record of measurements of ozone does not reveal a significant trend in total ozone that can be ascribed to human activities. This observational result is consistent with those of current models, since no detectable trend would be expected on the basis of current theory.

Because data on total global ozone cannot be analyzed to distinguish among causes of ozone changes, total ozone data alone cannot be relied upon for early detection of an anthropogenic change. Measurement of the spatial and

temporal distribution of critical trace species and ozone, together with theoretical modeling taking into account all the major influences on stratospheric ozone, offers promise of understanding the causes of ozone changes and the consequences of alternative actions in response.

Recommendations

1. The national research program, including atmospheric observation, laboratory measurements, and theoretical modeling, should maintain a broad perspective with emphasis on areas of disagreement between theory and observation. Highest priority in research should be given to a coordinated program to understand the spatial and temporal distributions of important species, such as ClO and the hydroxyl radical (OH).

2. The global monitoring effort should include both ground-based and satellite observations of total ozone and concentrations of ozone above 35 km, where theory indicates the largest reductions might occur. Sound, satellite-based systems for stratospheric observations are essential.

3. Potential emissions of N_2O, CO_2, CH_3CCl_3, and other relevant gases should be assessed and their consequences for stratospheric ozone evaluated. Models should be developed to describe the consequences for stratospheric ozone of future emissions of these gases.

BIOLOGICAL EFFECTS OF INCREASED SOLAR ULTRAVIOLET RADIATION

Stratospheric ozone acts as a shield to screen out much of the short-wavelength ultraviolet (UV) in sunlight. Slight changes in this ozone layer may result in large changes in the amount of damaging UV striking the surface of the earth. Living creatures have adapted to the present level of UV and to its fluctuations from season to season and during the day. Part II of this report gives the current state of knowledge about the effects on biological systems of an increase in UV resulting from a decrease in stratospheric ozone concentration.

Each of the findings and conclusions summarized below has important implications for future research--either in efforts to decrease the uncertainty in concepts or in efforts to increase quantitative knowledge. These research implications are spelled out in our list of major recommendations. Recent advances in knowledge since the last NRC report on the subject (NRC 1979a) have clarified our view of the problem but have also pointed out scientific areas not emphasized in earlier reports that confound the simple prediction of the effects of ozone depletion on biological systems. The unraveling of these difficulties will be accomplished only by a research effort directed by knowledgeable scientists, especially photobiologists. In many instances, we are still not sure of the scientific questions to be asked. Similar comments were made in earlier NRC reports (NRC 1975). The fact that they have not been acted on with any reasonable financial commitment accounts for a large part of our inability to make better predictions.

It seems certain that more than 90 percent of skin cancer other than melanoma in the United States is associated with sunlight exposure and that the damaging wavelengths are in the UV-B region (290 nm to 320 nm) of the spectrum. A decrease in ozone will be accompanied by a well-predicted increase in UV-B. We estimate that there will be a 2 percent to 5 percent increase in basal cell skin cancer incidence per 1 percent decrease in stratospheric ozone. The increase in squamous cell skin cancer incidence will be about double that. Where in this range the value falls depends on which theory is used to make the estimate and on the appropriate dosimetric data used. The predicted increases are appreciably greater at lower latitudes than at higher.

Although the incidence of malignant melanoma increases with a decrease in latitude, the degree to which sunlight is responsible is not apparent, and there are few data implicating UV-B as the only responsible wavelength region. Therefore it is not appropriate to make quantitative predictions about the increase in the incidence of this disease associated with a decrease in ozone.

Some of the difficulty in making quantitative predictions about humans comes from uncertainties (even in simple cellular systems) about the effects of interactions among single wavelengths in a broad band, such as in the ultraviolet of sunlight, in producing antagonistic or synergistic effects. Moreover, it has been learned only recently that rapid repair of sunlight damage to human skin takes place during irradiation. An appreciable fraction is photorepair mediated by visible light, and a

similar phenomenon seems to take place in anchovy populations. The quantitative magnitudes of such effects are not known.

The effects of ozone depletion on other animals and plants in the biosphere are as important as the direct effects on human health. However, scientists are still not able to predict quantitative effects on crop plants or ecosystems.

The details of our findings and recommendations are spelled out in Chapters 3, 4, and 5. Key findings and conclusions and major research recommendations have been extracted from the chapters and are listed below. Estimates are given, where possible, of how long the recommended research might take under ideal circumstances.

Key Findings and Conclusions

Molecular and Cellular Studies (Chapter 3)

1. Deoxyribonucleic acid (DNA) is probably the primary target in animal cells for most deleterious effects of UV-B, especially effects involving mutagenesis and neoplastic transformation. Other targets of possible biological significance for UV-B effects include membranes, ribonucleic acid (RNA), and proteins.

2. The spectrum for absorption of energy by DNA for wavelengths in the UV-B region and the spectra for biological damage to DNA as a function of wavelength (action spectra) are known. The absorption spectrum and the action spectra are similar but not identical, probably because long-wavelength light is absorbed in some components of this genetic material that are not effective in changing the structure of DNA. The action spectra in the UV-B region for affecting mammalian cells (killing, mutation, and neoplastic transformation) are similar to those for damaging DNA.

3. The formation of pyrimidine dimers (bonds between pyrimidine residues in one of the two strands of DNA that distort the normal DNA helical structure) appears to be the major injury to DNA from UV-B irradiation.

4. There are major interactions between the effects of UV-A (320 nm to 400 nm) and those of UV-B on DNA in cells. Some of these are antagonisms, whereby UV-A effects significantly reduce or repair the UV-B damage. Except for photoreactivation, which involves enzymic splitting of pyrimidine dimers back to normal single residues mediated by UV-A and visible light, these interactions are still poorly understood.

5. In excision repair, dimers are removed from one strand of a DNA double helix by enzymes that work in the dark, leaving the unaltered strand as a template for reconstitution of a new normal strand. Photoreactivation and excision repair of pyrimidine dimers occurs rapidly in human skin.

Ecosystems and Their Components (Chapter 4)

6. Both UV-A and UV-B have been reported to be detrimental to plant growth and development and to a number of physiological processes of plants, when examined under non-field conditions. The adaptability of plant species appears to be sufficient, under current ambient levels of UV-B, to maintain food crop yields. The potential for further adaptation to predicted increases in ambient UV-B is not known.

7. Ambient UV-B at present levels or similar levels in the laboratory can damage sensitive aquatic organisms or stages in their lifecycles that occur at the water's surface. Natural populations of aquatic organisms have adapted to current UV-B levels so as to maximize reproduction potential. In the case of anchovy larvae, it has been demonstrated that photorepair of UV-B damage is effective even at UV-B levels significantly higher than those that would result from predicted ozone depletions. Photorepair may be a general adaptive mechanism of organisms evolving in the presence of UV-B. Currently, there is no information from which to predict the magnitude of adverse effects of enhanced UV-B on aquatic organisms.

8. From limited field experiments on terrestrial plants and laboratory experiments with captured or cultured aquatic organisms, it appears that different species of both plants and animals have different sensitivities to increases in UV-B above current levels. Changes in species compositions and abundances of organisms have been observed in simulated aquatic ecosystems subjected to enhanced UV-B. Mathematical models show that in systems subject to large natural oscillations in the size of the population, there are severe limitations on the minimum population density needed to maintain a species. However, the data currently available on food chains in the natural

ecosystem are not precise enough or complete enough to be used to predict population dynamics or the displacement of an individual species under current environmental conditions. It is doubtful therefore that a statistically significant causal relationship between increased UV-B levels and food chain success can be predicted in the near future.

9. Only minor effects of increased UV-B levels are predicted for animals used for human food.

Direct Human Health Hazards (Chapter 5)

10. A reduction in the concentration of stratospheric ozone will not create new health hazards, but will increase existing ones.

Effects Other Than Cancer

11. There is evidence that direct acute effects of UV on humans, such as sunburn (acute erythema) and corneal inflammation (photokeratitis), are linked more strongly to UV-B than to UV-A.

12. Acute erythema and photokeratitis can be predicted accurately for a given dose and spectrum of UV-B, since the action spectra, dose-response curves, and intensity-time reciprocity relationships are known.

13. Ultraviolet radiation affects many aspects of the immune system of animals and humans. Allergic contact dermatitis, skin graft rejection, tumor susceptibility, and function and viability of individual circulating and noncirculating cells of the immune system can be altered, primarily by UV-B.

Skin Cancer Other Than Melanoma

14. Data on the relative incidence rates of basal and squamous cell cancers in highly pigmented (black) versus lightly pigmented (white) persons indicate that more than 90 percent of skin cancers other than melanoma in U.S. whites are attributable to sunlight.

15. Molecular, cellular, and whole animal data all implicate UV-B as the major carcinogenic component of sunlight for skin cancers other than melanoma. The evidence is stronger for squamous than basal cell cancers because animals rarely get basal cell cancers. In humans, basal cell cancers are virtually all related to sunlight.

16. Based on animal studies, UV-B is implicated not only as an initiator of carcinogenesis but also as a promoter (in the general sense and via indirect effects) of chemical carcinogenesis. With the current state of knowledge, it is not possible to assess the extent to which increasing exposures to chemicals would result in increases in skin cancers due to synergism, over and above any increase because of increased UV-B exposure alone.

17. A 1 percent reduction in the amount of stratospheric ozone is predicted to give an approximate 2 percent increase in biologically effective UV-B. Epidemiological data suggest that a 2 percent increase in UV-B would give a 2 percent to 5 percent increase in basal cell skin cancers. For squamous cell skin cancers the increase would be about twice these values (4 percent to 10 percent).

18. The risk of developing skin cancers other than melanoma and the increased risk due to increased exposure to UV-B could be mitigated by individuals through changes in lifestyle that would reduce exposure.

Melanoma

19. The incidence of skin melanoma appears to depend on latitude, an indication that sunlight is a contributing factor. Circumstantial evidence such as occupational differences and location of the cancers on the body suggests, however, that exposure to sunlight is only one of several factors. The association between sunlight and melanoma is not strong enough to make a prediction of increased incidence due to increased exposure to UV based on epidemiological data.

20. The only evidence that suggests UV-B causes melanoma in humans comes from studies of people with the inherited disease xeroderma pigmentosum. These people have a known defect in the mechanism that would repair UV-B damage to DNA, and they also have a very high incidence of skin cancers, including melanoma.

21. There are no reliable animal models for light-induced melanoma. The only models currently available are animals with chemically induced, preexisting pigmented lesions that can be made to look like melanoma after UV irradiation.

Major Research Recommendations

The estimates following each recommendation of how long the research might take are educated guesses based on the experience of individual committee members. The estimates provide only a rough idea of how long the research might take under ideal circumstances.

Molecular and Cellular Studies (Chapter 3)

1. An understanding is needed of why broad bands of UV (heterochromatic radiation) often do not act on DNA in vivo and on in vitro cell systems as a simple sum of monochromatic wavelengths.

(a) Studies of interactive effects between UV-A and UV-B are fundamental to understanding the mechanisms of cancer induction by sunlight. Such studies, employing bacteria or cultured mammalian cells, would take about two to five years.
(b) An understanding is needed of UV-A-induced repair systems in bacteria, as a first step in understanding possible similar systems in higher organisms. This would take about two to five years.
(c) Experiments should be conducted to determine the rate and extent of photoreactivation in humans in sunlight. Data are needed on how the level of dimers depends on the relative amounts of UV-A and visible light compared with the amount of dimer-producing UV-B. These experiments would take about two to five years.

2. Data are needed on the rates of repair, in the dark and in laboratory light, of UV-irradiated human skin cells as a function of UV dose. The differences, if any, between acute and chronic irradiations should be determined. One might be able (with informed consent) to study individuals who are exposed to high levels of UV-B as part of phototherapy for psoriasis. The aim of such experiments would be to determine whether the kinetics of dark repair of damage from pyrimidine dimers in human skin show two components, a slow one and a fast one, as is true for human cells irradiated in vitro. The two components represent repair of DNA in different regions of the DNA strands. Equally important questions are, what other types of biologically important damages occur in skin, what are their lifetimes, and are any of them persistent? These data could be obtained in about four or five years.

Ecosystems and Their Components (Chapter 4)

3. Techniques must be developed for simulating changes in UV-B under natural ambient conditions. Only in this way can dose-response relationships be obtained. If these techniques cannot be developed for studies at temperate latitudes, they might best be achieved in a low-latitude (subtropical), minimal-cloud-cover, multiuser facility, which would provide UV-B radiation corresponding to reduced ozone concentrations at more northern latitudes. Priority should be given to screening representative species of important food plant systems for identifying possible adverse effects on crop productivity. Dosimetry and environmental regulation techniques must be developed to ensure optimum experimental conditions--conditions equivalent to the higher latitude ambient field conditions of the plants being tested. Without strict attention to these control conditions, studies will have limited potential for extrapolation or prediction. It would take about three years to develop the facility and another three years to conduct the species screening experiments.

4. The effects of UV dose on elements of aquatic food chains cannot be determined unless (a) the underwater spectral irradiances are integrated over the varying positions of organisms in water columns to obtain the exposures that simulate spectral intensities in the natural systems, and (b) damage to individuals can be related to population dynamics in the natural ecosystem. This would require an integrated research approach involving physical hydrography, physical optics, and organism physiology. It would take about five years to develop this approach and obtain results. Unless UV-B studies are made as a part of an ecosystem study, effects on populations and interactions among populations cannot be predicted. (Testing for whole ecosystem effects is addressed in another NRC report, Testing for Effects of Chemicals on Ecosystems (NRC 1981).)

An attempt to incorporate such an integrated approach was made for anchovy larvae. The interdisciplinary approach used in the anchovy study to assess UV-B damage to food chains, together with the specific laboratory

measurements, should serve as a model for future research proposals.

Direct Human Health Hazards (Chapter 5)

5. Studies (animal and human) should be conducted in the developing field of photoimmunology to determine the magnitude of UV effects on the human immune system, the effective wavelengths, and the dose-response relationship. Results may increase understanding of skin cancer mechanisms, other effects of UV on skin, and certain other diseases. These studies would take about two to five years.

6. Animal studies of UV-induced skin cancers other than melanoma are needed to understand interactions among parameters such as intermittent exposures, different wavelengths, dose rates, chemical carcinogens and promoters, and agents that modify cellular responses to irradiation. These studies would take about two to five years.

7. The Surveillance, Epidemiology, and End Results program of the National Cancer Institute routinely collects data on incidence of melanoma. The incidence of skin cancers other than melanoma should be surveyed every decade at a time coinciding with the population census, so as to determine trends in time. Only a few locations are necessary, but these should be the same as past survey locations. Data should be collected in a way that permits cohort as well as cross-sectional analysis.

8. Animal models for UV- or light-induced melanomas are needed. They would allow studies of action spectra, dose-response curves, waveband interactions, and other parameters. It is not possible to predict how long it would take to develop such models.

9. To determine the association between UV and melanoma, it would be useful to determine the incidence of the various subtypes of melanoma and their dependence on latitude. Although this will be difficult because the majority of melanomas are of the superficial spreading type, the methodology is available. Careful epidemiological studies that are based on reliable clinical and histological studies of subtypes of melanoma are needed.

PART I: CHEMISTRY AND PHYSICS OF OZONE REDUCTION

Chapter 1

CURRENT STATUS

INTRODUCTION

This chapter reviews recent changes in the state of understanding of the chemical and physical processes that determine the effect of human activities on concentrations of stratospheric ozone. The report is motivated by a continuing need to assess the potential effects on stratospheric ozone of chlorofluorocarbons (CFCs) and other chemicals, as prescribed in the Clean Air Act, as amended (42 USC 7450). The topic has been the subject of intense study during the past decade; our report builds on that work, most notably on previous studies by the National Research Council (NRC 1975, 1976b, 1977, 1978, 1979b) and the National Aeronautics and Space Administration (NASA) (Hudson and Reed 1979). To prepare our assessment, we relied on our professional knowledge, on a concurrent technical review prepared under the auspices of NASA, the Federal Aviation Administration, the National Oceanic and Atmospheric Administration, and the World Meteorological Organization (WMO) (Hudson et al. 1982), and on a series of topical reviews prepared at our request by technical consultants. The consultants' reports are contained in Appendixes A to F.

PROCESSES DETERMINING OZONE CONCENTRATIONS

Ozone (O_3) is formed in the stratosphere by reaction of atomic oxygen (O) with diatomic molecular oxygen (O_2). The process is initiated by photolysis of O_2, that is, the dissociation of O_2 into atomic oxygen by absorption of solar ultraviolet radiation at wavelengths below 240 nanometers (nm). Photolysis of O_2 occurs mainly at altitudes above 25 km.

According to current understanding, approximately 1 percent of the ozone created in the stratosphere is removed by transport to the troposphere; the remaining 99 percent is destroyed by chemical reactions in the stratosphere that re-form ozone into O_2. The net effect of these chemical reactions is either the combination of ozone with atomic oxygen to form O_2, represented by the equation

$$O + O_3 \rightarrow 2O_2, \qquad \text{I}$$

or the combination of two ozone molecules represented by

$$O_3 + O_3 \rightarrow 3O_2. \qquad \text{II}$$

These equations represent the net results of a number of complex sets of reactions catalyzed by a variety of gases and chemical radicals present in the stratosphere in trace amounts.

Important examples of sets of reactions summarized by process I are

$$Cl + O_3 \rightarrow ClO + O_2 \qquad (1a)$$
$$ClO + O \rightarrow Cl + O_2, \qquad (1b)$$

$$NO + O_3 \rightarrow NO_2 + O_2 \qquad (2a)$$
$$NO_2 + O \rightarrow NO + O_2, \qquad (2b)$$

$$OH + O_3 \rightarrow HO_2 + O_2 \qquad (3a)$$
$$O + HO_2 \rightarrow OH + O_2. \qquad (3b)$$

Process I may also proceed by the direct path

$$O + O_3 \rightarrow 2O_2. \qquad (4)$$

These reactions are limited by the availability of oxygen atoms and therefore occur mainly at altitudes above 25 km. The reactions that limit the rates at which chains 1, 2, and 3 proceed are (1b), (2b), and (3b), respectively.

Process II summarizes reaction schemes in which atomic oxygen is not limiting, for example,

$$OH + O_3 \rightarrow HO_2 + O_2 \qquad (5a)$$
$$HO_2 + O_3 \rightarrow OH + 2O_2. \qquad (5b)$$

Reactions (5) account for most of the ozone lost below 25 km in current models. The chemistry of the lower stratosphere is complex, however (Appendix A), and one cannot exclude additional reaction schemes involving oxides of nitrogen and chlorine (NO_x, ClO_x) and oxidation products of hydrocarbons such as methane (CH_4).

Ozone removed from the stratosphere by transport to the troposphere is ultimately lost by chemical reactions in the gas phase or at the earth's surface.

The spatial and temporal distribution of the concentration of ozone reflects a dynamic balance among the processes that form and remove ozone (Figure 1.1). According to current understanding, photolysis of O_2 provides a global source of ozone of 50,000 million metric tons per year, with more than 90 percent of this amount formed above 25 km. Most of this ozone is removed by reactions represented by process I. At altitudes between 25 km and 45 km, reaction (2b) accounts for roughly 45 percent of the ozone removed while reactions (1b) and (4) each account for about 20 percent and reaction (3b) for 10 percent (S.C. Wofsy, Harvard University, private communication, 1982). About 1 percent of stratospheric ozone, 600 million metric tons per year, is removed below 25 km by process II, with a similar amount being lost by physical transport to the troposphere.

Only 30 percent of global ozone is stored at altitudes above 25 km, reflecting the relatively short chemical lifetime of ozone at high altitudes. The rest is contained in the region below 25 km, and more than 70 percent of the amount below 25 km is found at latitudes above 30°. The abundance of ozone below 25 km is determined by the balance between transport from the chemically more active region at higher altitudes and losses to the troposphere; its distribution is regulated by atmospheric motions.

Adding to the stratosphere substances that destroy ozone has the effect of creating a new balance between production and removal processes in which the total abundance of ozone is reduced. For example, stratospheric concentrations of chlorine monoxide (ClO) and nitrogen dioxide (NO_2) may be increased as a result of emissions of CFCs and nitrous oxide (N_2O) from human activities. The effects are persistent. A typical CFC molecule, CF_2Cl_2 for example, survives for approximately 75 years in the atmosphere before it is decomposed by sunlight releasing its constituent chlorine atoms in the

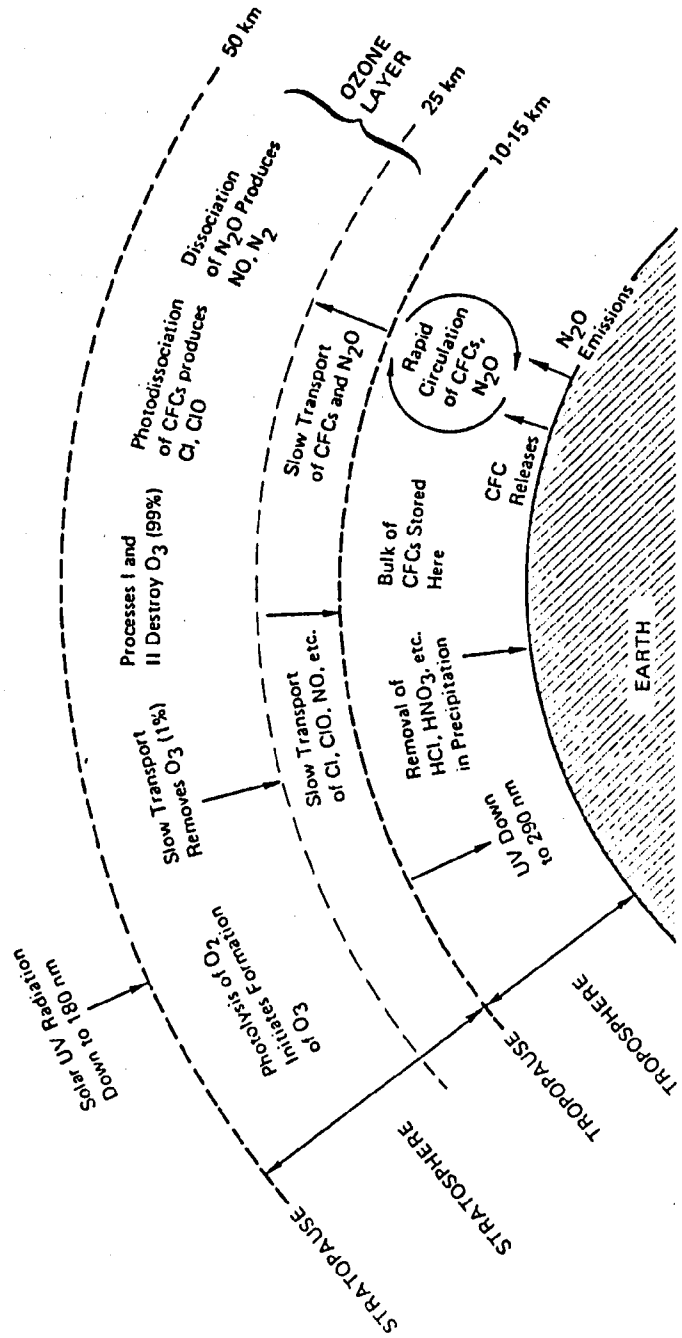

FIGURE 1.1 Representation of the processes that determine the concentration of ozone in the stratosphere.

stratosphere. A chlorine atom can affect recombination of between 10^4 and 10^5 ozone molecules during its lifetime in the stratosphere (on the order of two years) before it returns to the troposphere, mainly as hydrochloric acid (HCl). A similar situation holds for N_2O. Approximately 10 percent of N_2O molecules released to the atmosphere decompose by paths leading to production of stratospheric nitric oxide (NO), and subsequently NO_2, by reaction (2a). The average NO_x molecule also removes between 10^4 and 10^5 ozone molecules before it returns to the troposphere, after its typical two-year residence in the stratosphere. Current theoretical models lead us to conclude that the dependence of ozone concentration on altitude will also change, the net effect being a redistribution of ozone from higher to lower altitudes. Quantitative estimates of these effects have varied somewhat over the past decade (Appendix A).

Perturbations by Chlorine

Currently, approximately 3 parts per billion (ppb) of the lower stratosphere consists of chlorine bound in organic molecules such as methyl chloride (CH_3Cl), carbon tetrachloride (CCl_4), and CFCs (Hudson and Reed 1979, Hudson et al. 1982). Table 1.1 indicates the abundances of the more prevalent species; only methyl chloride is known to have natural origins. The table also shows estimates of current rates of release of man-made compounds found in the lower stratosphere.

Halocarbons decompose under the influence of sunlight at altitudes above 20 km; the fractional abundances (mixing ratios) of halocarbons (in ppb) are observed to decrease with increasing altitude (Appendix C). The chlorine produced by decomposition of halocarbons is converted to inorganic species, including HCl, chlorine nitrate ($ClNO_3$), ClO, and atomic chlorine (Cl). Hydrochloric acid is the major reservoir for chlorine at altitudes above 25 km (Appendix C). Concentrations of Cl, ClO, and HCl have been observed in the stratosphere; observations and predictions of theoretical models are in general agreement, although some difficulties remain (Appendix D), as we shall see.

Computer calculations using current understanding and incorporating new data on rates of several important reactions (Appendixes C and D) suggest that continued release of the CFCs, CF_2Cl_2 and $CFCl_3$, at rates

TABLE 1.1 Concentration in the Lower Stratosphere and Release Rates of Major Sources of Chlorine in the Stratosphere

Compound	Concentration (ppb)[a] Molecular	Concentration (ppb)[a] Chlorine	Rate of Release (million metric tons of Cl per year)
Methyl chloride (CH_3Cl)	0.62	0.62	2[b]
F-12 (CF_2Cl_2)	0.30	0.60	0.19[c]
F-11 ($CFCl_3$)	0.18	0.54	0.20[c]
Carbon tetrachloride (CCl_4)	0.13	0.52	0.053[d]
Methyl chloroform (CH_3CCl_3)	0.11	0.33	0.35[e]

[a]Hudson et al. (1982).
[b]About 85 to 90 percent of CH_3Cl is naturally produced, the remainder being attributed to industrial sources (Cicerone 1981). The total release rate varies slowly in time because of the large contributions of natural sources.
[c]1980 release rate from "World Production and Release of Chlorofluorocarbons 11 and 12 through 1980," Chemical Manufacturers Association Fluorocarbon Program Panel, July 29, 1981. Release rate has decreased by about 20 percent from the peak rate of 1974.
[d]1976 release rate (NRC 1979b). The release rate is apparently relatively constant, although somewhat uncertain.
[e]Neely and Plonka (1978).

prevalent in 1977 would ultimately cause a net decrease of total global ozone roughly between 5 percent and 9 percent assuming no other perturbations (Hudson et al. 1982). We regard a representative result to be 7 percent (Appendix C). This would result in a smaller steady state reduction in ozone than reported in NRC (1979b), which was 16.5 percent with a 95 percent probability that the true value lies between 5 percent and 28 percent. (Other models current in 1979 gave reductions ranging from 15 percent to 18 percent (Hudson and Reed 1979). Estimates have fluctuated between roughly 5 percent and 20 percent over the past eight years as models have been refined (Appendix A).) The steady state reduction would be reached asymptotically in times on the order of a century. Calculations now indicate that the reduction would occur almost entirely at altitudes above 35 km, in the region of the stratosphere where the ozone concentration is determined primarily by chemical processes, with a smaller, partially compensating increase in ozone concentrations at lower altitudes. The current result obtains for both 1- and 2-dimensional models and further differs from that prevalent in 1979 in that earlier calculations showed regions of reduction both above and below 35 km.

The differences between current findings and those reported in 1979 are the result of refinements in the values for the rates of several reactions affecting the concentration of the hydroxyl radical (OH) (Appendixes C and D). The refinements are the result of improved laboratory measurements (Hudson et al. 1982). OH is important because the concentration of ClO in the lower stratosphere is particularly sensitive to it. Results of model calculations using current values for these reaction rates are in good agreement with observations of ClO for altitudes below 35 km (Appendixes C and D), whereas models using the reaction rates favored in 1979 give concentrations of ClO a factor of 3 higher than observed values in this range. The new reaction rates have not changed greatly the results of calculations for altitudes above 35 km, however, so that the amounts of reduction in ozone above 35 km obtained in the 1979 and current models are about the same. The models continue to indicate lower concentrations of ClO in the stratosphere above 40 km than are observed. We shall return to this discrepancy.

Increased attention to effects of releases of methyl chloroform (CH_3CCl_3) on stratospheric ozone is warranted because of the growing use of this compound, an industrial solvent. The release rate increased by a factor of about 50 between 1958 and 1978 (Neely and Plonka 1978).

Perturbations by Oxides of Nitrogen

The chemically active oxides of nitrogen in the stratosphere (such as NO_2) are thought to arise mainly from photooxidation of N_2O. N_2O is formed naturally by bacteria in soil and water. As indicated earlier, reactions involving NO_2 account for about 45 percent of the ozone removed in the stratosphere between 25 km and 45 km.

The human influence on the global cycle of fixed nitrogen is thought to be significant and increasing (NRC 1978). The global atmospheric concentration of N_2O appears to have increased by 2.7 percent (from 292 ppb in 1964 to 300 ppb in 1980) over the past 16 years (Weiss 1981, Weiss and Craig 1976). The concentration of N_2O in the atmosphere is likely to continue to increase with increases in emissions associated with agricultural practices, disposal of human and animal wastes, and possibly combustion; but we cannot say how or on what time scale.

An increase in N_2O concentrations of about 30 percent in the absence of other perturbations could cause a reduction in global ozone of an amount comparable with the 7 percent reduction currently estimated due to continued emissions of CF_2Cl_2 and $CFCl_3$ at 1977 rates, also taken as the sole perturbation. This estimate is based on current model calculations that indicate that, should the concentration of N_2O double in the absence of other perturbations, total global ozone would decline between 10 percent and 16 percent (Hudson et al. 1982).

Early attention to human influences on the stratosphere focused on effects of NO_x released by high-flying aircraft (NRC 1975). Models then and now suggest that an input of NO_x at altitudes above about 20 km should lead to reduction in stratospheric ozone. A source of NO_x at lower altitude, associated for example with subsonic commercial aviation, can modify local chemistry such as to cause an increase in tropospheric ozone. It has been suggested that reductions in the column of ozone above the earth's surface due to reductions in stratospheric ozone may be masked to some extent by increases in tropospheric ozone attributable to subsonic jets and urban smog.

Assessment of the impact on stratospheric ozone due to a combination of perturbations requires investigation of specific cases since the effects are not simply additive. Hudson et al. (1982) report the results of several studies of the effects of doubling atmospheric N_2O concentrations and continuing releases of CFCs at 1977 rates, both separately and in combination. The Lawrence Livermore National Laboratory (LLNL) model, for example, indicated a reduction of 12.5 percent due to doubling N_2O with a reduction of 12.9 percent due to the combination of perturbations. The LLNL model gives a reduction of 5.0 percent for CFC releases alone. Another model, from Atmospheric and Environmental Research, Inc., gives reductions of 9.5 percent for doubling N_2O, 6.1 percent for continuing CFC releases, and 13.0 percent for the combination. The results may be misleading, however, since current trends suggest a considerably longer time scale for doubling atmospheric concentrations of N_2O than for reaching the steady state reduction due to continued emissions of CFCs.

Perturbations by Other Species

Stratospheric ozone may be affected by human activity in a number of other ways. Of greatest potential concern are changes in concentrations of carbon dioxide (CO_2), water vapor (H_2O), and perhaps methane (CH_4).

The well-documented increase in atmospheric concentrations of CO_2 is directly attributable to combustion of fossil fuels and wood. This increase is expected to lead to a global warming of the atmosphere near the surface of the earth but is expected to cause a reduction in the temperature of the stratosphere (Fels et al. 1980).

Lower stratospheric temperatures would have at least two effects. First, the chemical removal processes affecting ozone that were described earlier are sensitive functions of temperature, being less efficient at lower temperature. Consequently, with lower temperature the equilibrium concentration of ozone would be higher. Current models incorporating this effect suggest that the steady state reduction in total ozone due to continuing emissions of CFCs at 1977 rates would change from 5 percent to 9 percent to between 4 percent and 6 percent if global CO_2 were doubled concurrently (Hudson et al. 1982). (Global CO_2 has increased by about 6 percent in the past 22 years.)

The possible second effect of lower statospheric temperatures resulting from increased CO_2 is a thermally driven change in stratospheric water vapor (H_2O) caused by a change in the temperature of the tropical tropopause. Dissociation of H_2O provides the source of hydrogen radicals, and these radicals play a key role in stratospheric chemistry regulating abundances of both active NO_x and Cl_x species in addition to their contributions to reactions (3) and (5). A complete model for stratospheric chemistry should include a description of H_2O interactions, a requirement beyond current capability.

Stratospheric ozone may also vary in response to changes in concentrations of CH_4, which plays an important role in reaction (1b) by regulating the partitioning of chlorine between HCl and ClO (Hudson et al. 1982). Recent reports (Rasmussen and Khalil 1981) suggest increases in global concentrations of CH_4, but likely future changes and their consequences are unknown.

Theoretical models of stratospheric chemistry cannot be validated by measurements of total ozone only, owing to the diversity of factors, natural and man-made, that may affect ozone concentrations. Comparison of calculated and observed values for the concentrations of important trace species and radicals--such as OH, ClO, NO_2, and atomic oxygen--must play a central role in any orderly strategy for validating models.

In general terms, agreement in detail between the predictions of theoretical models and observations is excellent. For example, changes in reaction rates since 1979 have resulted in substantial agreement between theory and observation for ClO below 35 km. There are, however, three areas in which discrepancies remain. The discrepancies may or may not point to significant difficulties in modeling. Similarly, agreement between modeling results and observation of ClO, while encouraging, need not imply validity of the model at lower altitudes.

The improved agreement between observed and calculated concentrations of ClO in the lower stratosphere may be attributed mainly to changes in rate constants for reactions affecting OH. Concentrations of OH in current models are lower than values obtained in 1979, with the result that a larger fraction of Cl_x is now found as HCl. The chemistry of the lower stratosphere is complex, however. Agreement between model and observed values of ClO in the lower stratosphere should be considered necessary but not sufficient for validation. A more extensive and demanding test would require comparison of theoretical and observed profiles of other radicals, particularly OH.

To improve understanding of stratospheric chemistry also requires that attention be directed to the assumptions of the models and to the measurements against which models are tested. High-quality measurements are obviously prerequisite to validation of models. Confidence in observations of critical species is enhanced by using a number of independent, inter-calibrated techniques, each relying on different physical properties. Validation of measurement technique is difficult since concentrations of the important atmospheric species may vary in time and space on scales that are not well understood. Validation procedures involve coordinated studies in the field requiring considerable logistical support.

The assumptions of models are of two types: (1) input data on environmental conditions, reaction rates, and other parameters, and (2) the reaction schemes incorporated into the model. There are still uncertainties about the appropriateness of some assumptions common in current models. For example, the rate for reaction of OH with HO_2, an important path for removal of hydrogen radicals, remains uncertain despite extensive and continuing efforts in the laboratory. There are other reactions in need of similar clarification. Models are sensitive to assumptions about the abundance and distribution of stratospheric H_2O; the underlying physical and chemical processes that regulate this key parameter are not well understood. It is difficult to rule out the possibility of an important role for species not now included in models, and, if history is a guide, there may well be future surprises in this area. Models for the stratosphere have been adjusted over the past decade in just this manner to include gases such as ClO (1974), $ClNO_3$ (1976), and HOCl (1978) (Appendix A, Figure A.1), and there is current discussion of a possible participation of sodium (Kolb and Elgin 1976, Murad et al. 1981). Progress in recognition of missing species or reactions occurs through a combination of laboratory, field, and theoretical studies, the normal practice of validating models and resolving discrepancies.

As was noted earlier, there is reasonable agreement between model calculations and observations for ClO in the lower stratosphere. Currently, however, there is a discrepancy between theory and observation for ClO in the region above 35 km, where chlorine-mediated catalysis is most important. The average value for the concentration of ClO measured by Anderson and co-workers (see Appendix D) near 40 km is almost a factor of 2 larger than the value calculated from models. Furthermore, theory and experiment give different dependences of the concentration of ClO on altitude in the upper stratosphere. The ClO discrepancy is particularly important because it occurs at altitudes where ozone is most sensitive to perturbations caused by CFCs (Appendix D, Figure D.52).

Extensive ground-based observations of NO_2 have been made over a range of latitudes by J. Noxon (see Appendix C), revealing a sharp spatial discontinuity in concentration in the winter with very low concentrations poleward of the discontinuity. Thus far, no theroretical model has been able to explain this phenomenon.

A third area of discrepancy between current models and observations is in concentrations of $CFCl_3$ and CF_2Cl_2 at altitudes above about 20 km (see Appendix C, Figure C.11). Observed values are substantially lower than predicted values. The difference could be due to errors in model simulation of ultraviolet radiance in the lower stratosphere, which, if true, would imply that the CFCs have shorter residence time in the lower stratosphere. The issue is not resolved and requires continuing attention.

Nevertheless, the extent of agreement between measurement and theory is encouragingly good.

MONITORING AND ASSESSMENT OF TRENDS

Measurements of the total amount of ozone above a unit area of the earth's surface (called total column ozone) are essential for assessing the human influence on ozone (as well as the potential effects of changes in ozone on humans and other organisms). As detailed in Appendix A, total column ozone fluctuates on a variety of spatial and temporal scales owing to natural causes; these fluctuations tend to mask possible systematic changes due to man-made perturbations. For example, current models for single and combined perturbations predict a reduction of total column ozone over the past decade of less than 1 percent, but a change of this magnitude cannot be distinguished from fluctuations due to other causes (Appendixes D and E).

Models of the stratosphere predict that the largest reductions in ozone due to releases of CFCs should occur near 40 km. Reductions should therefore be most readily detectable at this altitude. Current models suggest that ozone concentrations at 40 km should have decreased by several percent over the past decade. There have been reports in the press that an effect of this order has been detected in data from satellite experiments (see, for example, Science, Sept. 4, 1981, pp. 1088-1089). The community of atmospheric scientists has not yet had the opportunity to scrutinize this evidence, which must therefore be regarded as preliminary (Appendix F).

Our ability to detect trends in ozone in the future will depend on the availability of consistent, high-quality data taken over long time intervals. Improvements in the current monitoring systems are feasible and clearly needed. For example, it is vitally important to improve and enhance systems for monitoring ozone profiles in the upper stratosphere that could provide a valuable early indication of systematic changes in ozone due to emissions of CFCs or N_2O, but existing data in the upper stratosphere are inadequate for this purpose. It is also imperative to continue, and desirable to expand, the high-quality monitoring of total ozone by Dobson spectrophotometers.

THE QUESTION OF EARLY DETECTION

A notable feature of the ozone issue is that a reduction due to increases in the tropospheric concentrations of CFCs or N_2O, once it has taken place, is expected to persist for more than 100 years even if the practices that caused it are stopped immediately. It is therefore important to detect an anthropogenic effect at the earliest possible time. Three methods currently exist for this purpose.

1. Measurement of total ozone. Relying on measurement of total ozone has the following advantages (Appendix E): There exists a relatively long historical base (30 to 50 years) of data. Ground-based instrumentation is available and may be readily complemented by observations from satellites. Finally, total ozone is most directly related to one of the consequences of depletion that is of concern, the possibility of enhanced exposure to ultraviolet radiation at the ground (Part II). Since, however, the reduction due to CFCs is expected to be concentrated at high altitudes, measurements of total column ozone are less sensitive indicators of an anthropogenic effect than are measurements of ozone profiles.

2. Measurement of ozone at high altitudes. The advantages of this method derive from the theoretical result that changes in ozone due to CFCs are predicted to be largest at high altitudes. Changes in the spatial distribution of ozone may be important for understanding the second major consequence of depletion that is of concern, the possibility of climate change (Appendixes B and C). The disadvantages stem from the difficulty of making the measurements, whose quality and stability are inferior to those of total ozone (Hudson and Reed 1979, Hudson et al. 1982). Satellite data are particularly subject to changes in calibration of instruments, which

cannot be refurbished; ground-based measurements by the Umkehr method give poor height resolution and are subject to perturbations by hazes and stratospheric particulate matter. Partly because of these difficulties, the data base is relatively small and somewhat fragmented (Appendix F). Ozone measurements using satellites would have the desirable attribute of obtaining temporal and spatial distributions that would be useful in validating 2- and 3-dimensional models.

3. Measurement of key radicals involved in chemical removal processes. Measurements of spatial and temporal profiles of important species such as ClO and OH may be combined with chemical models for assessment of trends and their causes, such that the dependence on specific models can be relatively slight. This method is in principle the most sensitive, but it is also the least direct.

The last approach is regarded by many experts as having already shown the effect of chlorine of human origin, mainly connected with emissions of CFCs. But this conclusion would be more firmly established with more direct confirmation, as discussed in the previous section. Ideally, all three types of measurement should be integrated (with due regard to their sensitivity) in a strategy for early detection of anthropogenic effects.

UNCERTAINTY

Quantitative estimates of the uncertainties inherent in current estimates of reductions in ozone due to emissions of CFCs and N_2O are difficult to obtain. The ability to make quantitative estimates of uncertainty depends both on what we know and on what we do not know. Such estimates employ professional judgments about the importance of various factors and the sensitivity of the results to potential changes in understanding.

Our major concern in estimating uncertainties in our understanding of stratospheric ozone is with the possibility that some key process or processes may be missing from current models. In an orderly scientific strategy, continuing development of models on the basis of an ongoing comparison with observational data is expected. Progress is stimulated by the existence of discrepancies or uncertainties and tends to occur in more or less discrete steps rather than uniformly. Our understanding of the lower stratosphere has improved over the past two years as a result of developments that may be attributed at least in part to efforts to resolve earlier (and larger) discrepancies between observed and computed values for the concentration of ClO. Agreement between observed and computed values of ClO is now satisfactory below 35 km, but, as noted earlier, there continues to be a serious discrepancy at higher altitudes. This disagreement illustrates the difficulty of estimating limits of uncertainty for current estimates for reduction in ozone due to CFCs.

For example, observed values of ClO at higher altitudes are larger than calculated values, suggesting that the long-term reduction in ozone could be correspondingly larger. One can, however, conceive of speculative chemical schemes that could suggest a stratosphere less vulnerable to perturbations.

In circumstances such as this, the usual ways of estimating uncertainty (using mathematically rigorous procedures) are not applicable. Instead we rely on professional judgment. The predictions of the current chemical scheme have been cross-checked against observed atmospheric data in many ways, and the agreement in general is quite good. As stated earlier, a representative estimate of potential steady state reduction of global ozone due to continued releases of CFCs at the 1977 rate in the absence of other perturbations is 7 percent. There continue to be, however, important discrepancies between theory and observation.

Our opinions are divided on whether there are sufficient scientific grounds to estimate the effect of resolving one of the discrepancies, that of ClO in the upper stratosphere, on calculations of ozone reduction. We agree that we do not know enough at this time to make a quantitative judgment of the uncertainty associated with the other major discrepancies, NO_2 at high latitudes and lifetime of CFCs in the stratosphere above 20 km.

Those of us who believe there are grounds to judge the effect of resolving the ClO issue conclude that our estimate of ozone reduction from CFC emissions should not change by more than a factor of 2.

Those of us unwilling to offer quantitative estimates of uncertainty hold the conviction that no rigorous scientific basis exists for such statements. We are concerned by implications of the discrepancies noted earlier. These discrepancies should be resolved in the

next few years by orderly application of the scientific method with appropriate interaction between theory and observation. We see no reason to prejudge the result of this process.

Research during the past several years has enhanced our understanding of the factors affecting stratospheric ozone. Development of the field is progressing rapidly. We anticipate further developments in both observation and modeling in the next few years that will result in considerable improvement in our understanding, both clarifying and reducing uncertainties.

FINDINGS

1. Our understanding of the stratosphere has advanced considerably in the past two years. Progress is significant in all areas with improvements in our ability to model the system in more than 1 dimension, with impressive achievements in techniques for measurement of chemical reactions in the laboratory, and with major advances in our ability to measure concentrations of important trace species in the atmosphere. We note here that the success of the research is due in no small part to the breadth of the scientific effort involving scientists from many countries with support from both private and governmental sources. We expect continued improvement in understanding of the chemistry and dynamics of ozone reduction to result from research currently under way, planned, and proposed.

2. The concern regarding the possibility of reduction in stratospheric ozone due to CFCs remains, although current estimates for the effect are lower than results given in NRC (1979b). The change in estimates of ozone reduction reflects improvements in our understanding of chemical processes in the stratosphere below 35 km. There has been no significant change in results obtained by models for the stratosphere above 35 km. The major impact of CFCs is predicted for the height range of 35 km to 45 km.

3. The chlorine species Cl and ClO participate in a series of chemical reactions that destroy ozone. The radical ClO has been measured in the stratosphere in significant amounts and is believed to be primarily of human origin. Our current understanding indicates that if production of CFCs continues into the future at the rate existing in 1977, the steady state reduction in total ozone, in the absence of other perturbations, would be between 5 percent and 9 percent. Previous estimates fluctuate between roughly 5 percent and 20 percent, with those current in 1979 ranging from 15 percent to 18 percent. Latest results also suggest that CFC releases to date should have reduced the total ozone column by less than 1 percent.

4. According to current understanding, increases of N_2O in the stratosphere would result in reductions in total ozone, with the largest effects occurring in the lower stratosphere. Although concentrations of N_2O in the stratosphere appear to be increasing, we cannot reliably project the future course of N_2O sources. If, however, the concentrations of N_2O in the atmosphere were to double, in the absence of other perturbations, current models suggest that the steady state reduction in the total ozone would be between 10 percent and 16 percent.

5. On the whole, there have been substantial improvements in the agreement between model predictions and observed profiles of trace species in the past several years. Three exceptions are still a cause for concern: Above 40 km, more ClO is observed than is predicted by current theory; the behavior of NO_x in winter at near-polar latitudes is unexplained; and concentrations of CFCs in the stratosphere above 20 km are lower than predicted by the models.

6. Examination of historical data (extending back 30 to 50 years) has not yet shown a significant trend in total ozone that can be ascribed to human activities. Current models of combinations of pollutants suggest that a reduction of total ozone to date from human activities would be less than 1 percent. No detectable trend would be expected on the basis of these results.

7. Data on total ozone should not be used alone to guide decisions on whether to take action to prevent future changes in stratospheric ozone. Although an important guide, analysis of trends in total ozone cannot by itself reveal causes of ozone reductions or increases. Such analysis, together with measurement of altitude profiles of trace species and ozone and theoretical modeling, offers promise of understanding causes of ozone changes and the consequences of alternative actions in response.

8. The impact of CFCs should be assessed in the context of a broad understanding of the variety of ways in which human activity can alter stratospheric

composition. Ozone may be reduced by increasing levels of CFCs and N_2O, but reductions might be offset in part by higher concentrations of CO_2 and perhaps CH_4. Human activities have already increased the amounts of CO_2 and CFCs in the atmosphere, and from the known release rates, further increases can be confidently expected. In addition, there is evidence that N_2O and CH_4 concentrations are also increasing. A special reason for concern about perturbations potentially caused by CFCs and N_2O is the long lifetime of these gases in the atmosphere, of the order of 50 to 150 years. Even if the releases of these gases were reduced, the atmosphere would not recover until far in the future.

RECOMMENDATIONS

In light of our findings, we believe it is important to maintain a competent, broadly based research program that includes a long-term commitment to monitoring programs. The research effort should extend over at least two solar cycles (of 11 years each) to distinguish between changes induced by variations in the sun from those associated with man. Accordingly, we make the following recommendations:

1. The national research program, including atmospheric observations, laboratory measurements, and theoretical modeling, should maintain a broad perspective with some focus on areas of discrepancy between theory and observation. A coordinated research program to understand the spatial and temporal distributions of key species and radicals merits highest priority. Observations should be extended to include studies of the equatorial and polar regions.
2. The global monitoring effort should include both ground-based and satellite observations of total ozone and of concentrations of ozone above 35 km, where theory indicates the largest reductions might occur. We also need data to define the variability of stratospheric temperature and water vapor. We regard sound, satellite-based systems for stratospheric observations as essential.
3. Potential emissions of a number of relevant gases, in addition to CFCs and N_2O, and their consequences for stratospheric ozone should be thoroughly evaluated and assessed. It is important that we understand current and potential rates of emissions of these compounds and the effects these emissions might have on ozone in addition to understanding emissions and effects of CFCs. There is observational evidence that atmospheric concentrations of N_2O and CO_2 are increasing. Models should be developed to describe the combined effects on stratospheric ozone of future changes in releases of all relevant gases, such as CFCs, N_2O, CO_2, CH_4, CH_3Cl, and CH_3CCl_3.

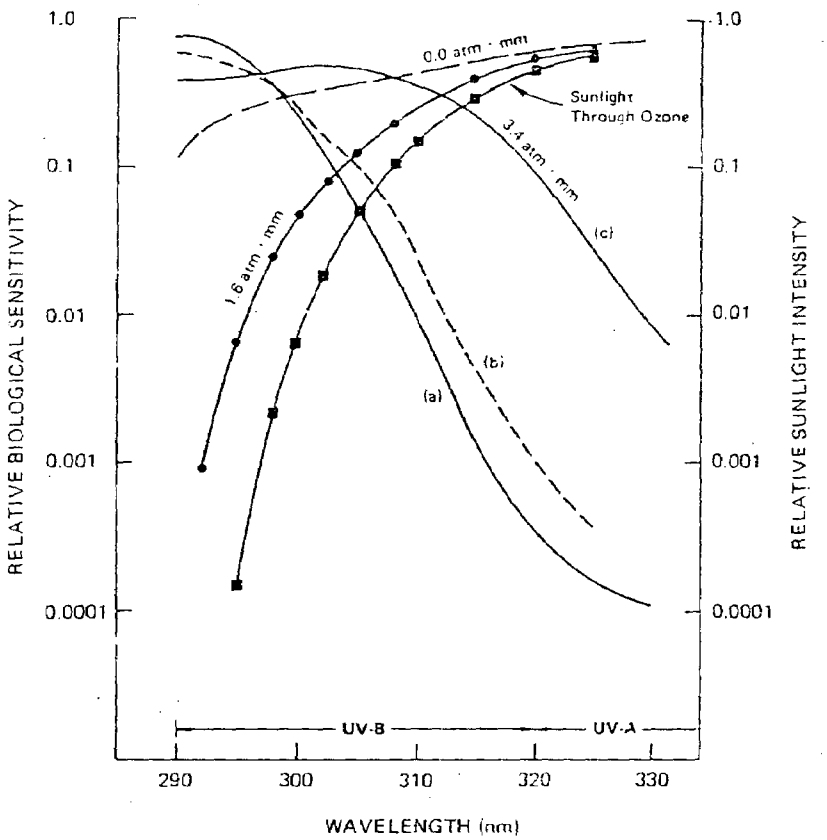

FIGURE 2.2 The relative intensity of sunlight (solar elevation of 60°) reaching the surface of the earth for different amounts of stratospheric ozone (the normal amount is close to 3.4 atmosphere · mm). The shapes of two biological sensitivity curves are also shown: (a) damage to DNA multiplied by the transmission of human epidermis, and (b) human erythema or sunburn. Curve (c) is the response of the Robertson-Berger meter (discussed in Chapter 5). (Source: The three curves of sunlight intensity are from U.S. Congress, Senate (1975); the two biological sensitivity curves are from Setlow (1974) and Scott and Straf (1977); the Robertson-Berger meter curve is from Berger et al. (1975).)

INTRUSION OF STRATOSPHERIC OZONE INTO THE TROPOSPHERE

presented by H. Muramatsu

Meteorological Research Institute

Japan MA

Intrusion of Stratospheric Ozone into the Troposphere

H.Muramatsu,Y.Makino,M.Hirota and T.Sasaki

Meteorological Research Institute, Tsukuba, Japan.

1. Trajectory analysis

1.1 Vertical distribution of ozone

Thin layers which have the maximum ozone mixing ratio are frequently observed below the tropopause especially in spring over Tateno, Tsukuba. The example of the vertical profiles of ozone and temperature obtained by the ozone -sonde is shown in Fig.1 for 28 May 1969. The ozone maximum layer at about 500 mb corresponds to the temperature inversion layer.

Fig.2 shows the vertical cross section along 140° E for the same day of Fig.1. Two jet cores are observed over Sendai and Akita about 250 km and 400 km north of Tateno,respectively. The jet stream front is observed at 550 mb and 430 mb over Tateno, corresponding to the maximum layers of ozone in Fig.1. The relative humidity is below 30 % in the frontal zone (below 10 % in the central part of the frontal zone).

1.2 Isentropic trajectory

The potential temperature at the ozone maximum layer is 325°K. A three-dimensional trajectory on the 325°K surface was traced from the adiabatic assumption. Geostrophic wind was obtained from the isentropic stream-function(Montgomery stream-function), that was calculated from the radiosonde data. From the wind field obtained above, the air parcel was traced backward in time and its location was determined every three hours.

Fig.3 shows the isentropic trajectory on the 325°K surface from 26 May,00Z to 28 May,06Z. The air parcel (which arrived over Tateno on 28 May,06Z) crossed the jet axis over Osaka at 03Z (three hours befre) from the cyclonic side toward the anticyclonic side.

The air parcel is within the stratosphere before 12Z on 27 May,

moving south-westward along the jet axis. After that the air parcel at 300 mb begins to descend from the stratosphere to the troposphere on the southern edge of the cyclone by changing the direction eastward.

The descending velocity of the air parcel shows the maximum value of 17 cm/sec (three hour average) at 00Z on 28 May, when the air parcel crosses the jet axix (Fig.4).

1.3 Frequency of the event

Time cross section of the relative humidity over Tateno for May 1969 is shown in Fig.5. Arrows show the day on which ozone profiles were obtained. Ozone maximum layers (filled circles) are found in area where the relative humidity is less than 20 % (marked by slanting lines). It is also found that the ozone maximum layers are frequently observed around 500 mb. This result is related to the fact that frequency of the appearance of the dry air over Tateno is maximum in late spring at 500 mb level (Fig.6).

2. Aircraft observation

In order to know the mechanism of the intrusion process that was shown in the previous section, the spatial distributions of ozone and other constituents were observed from an aircraft around the tropopause gap and the frontal boundaries.

2.1 Case study : 15 March 1981

(1) Intrusion around the jet axis

There were two jet streams over Japan as shown in Fig.7; subtropical jet at 150 mb and 250 mb and polar front jet at 350mb. Observations were made around the polar front jet along 135°E. Horizontal flight courses are shown by a(5.1 km altitude),b(7.1 km) and c(8.8 km).

The vertical cross section along 135°E is shown in Fig.8. The distribution of ozone(solid lines) around the polar front jet(J) are shown. Strong downward wind (↓ ⇓) was observed at the layers of the maximum ozone concentration and upward wind (↑) was observed on thr north. Low water vapor concentration is observed in the layer of high ozone concentration. Thin broken curves show the range of relative humidity below 20 %; lowest in the frontal boundary shown by heavy broken curves.

It is known that the stratospheric ozone is transported into the troposphere below the polar front jet along the frontal boundary.

(2) Diffusion of ozone

The horizontal distribution of ozone at the altitude of 5.1 km obtained from the south to north flight course is shown in Fig.9. On the north of the high ozone region, the layer of the constant ozone concentration is observed. There is the strong gap of the ozone concentration between them. This gap coincides with the boundary of downward and upward winds. In the region of this constant ozone concentration the strong vibration of the aircrat was recognized.

It is known that the ozone diffuses on the north of the maximum ozone layer by the turbulent air motions whose frequencies are 80 to 180 sec (Fig.10).

(3) Potential vorticity

The variation of the potential vorticity that has the conservative property in the stratosphere was analyzed. The region of the high potential vorticity of stratospheric origin (hatching in Fig.11) is transported downward; southward on 14 and eastward on 15 March. The region of the high potential vorticity decreases rapidly in the troposphere. The total air mass of the high potential vorticity(the air mass of the stratospheric origin) was 11×10^{14} kg at 12 Z on 14 May, and decreased to 5×10^{14}kg at 00 Z on 15 May.

This shows that the potential vorticity is not conserved in the troposphere and has the half-value period of a half day. The decrease of the potential vorticity occurs on the north of the ozone maximum layer as shown in the previous section.

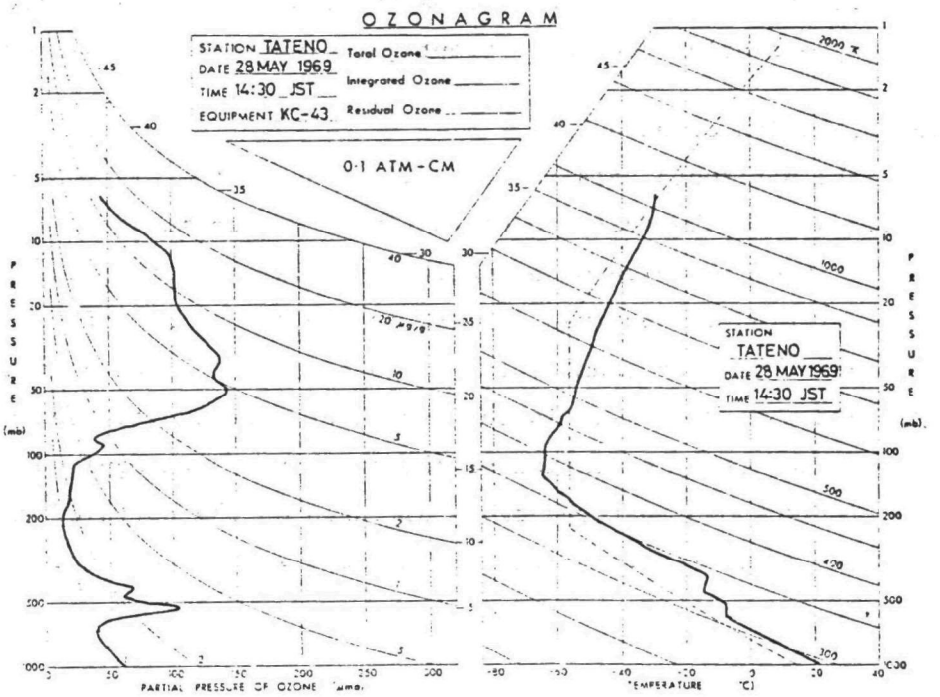

Fig.1 Vertical distributions of ozone and temperature over Tateno,28 May 1969,14:30 JST

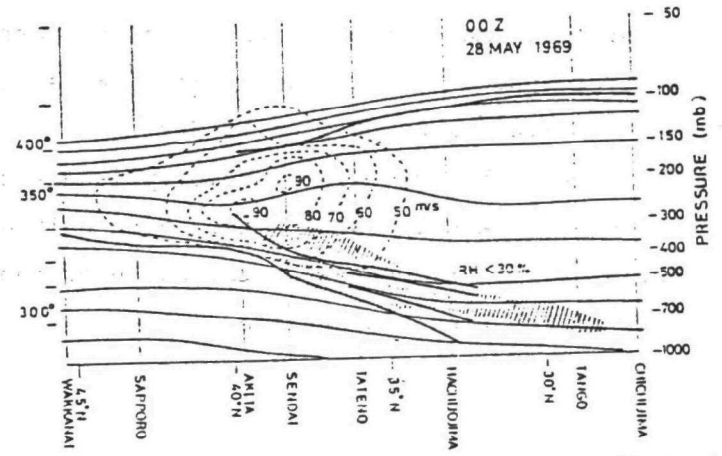

Fig. 2. Vertical cross-section for 28 May 1969, 00Z along 140°E from Wakkanai to Chichijima. Thin lines show potential temperatures (°K); broken lines, isotachs (m/sec); heavy lines, tropopauses and frontal boundaries. The area with relative humidity less than 30% is marked by hatching.

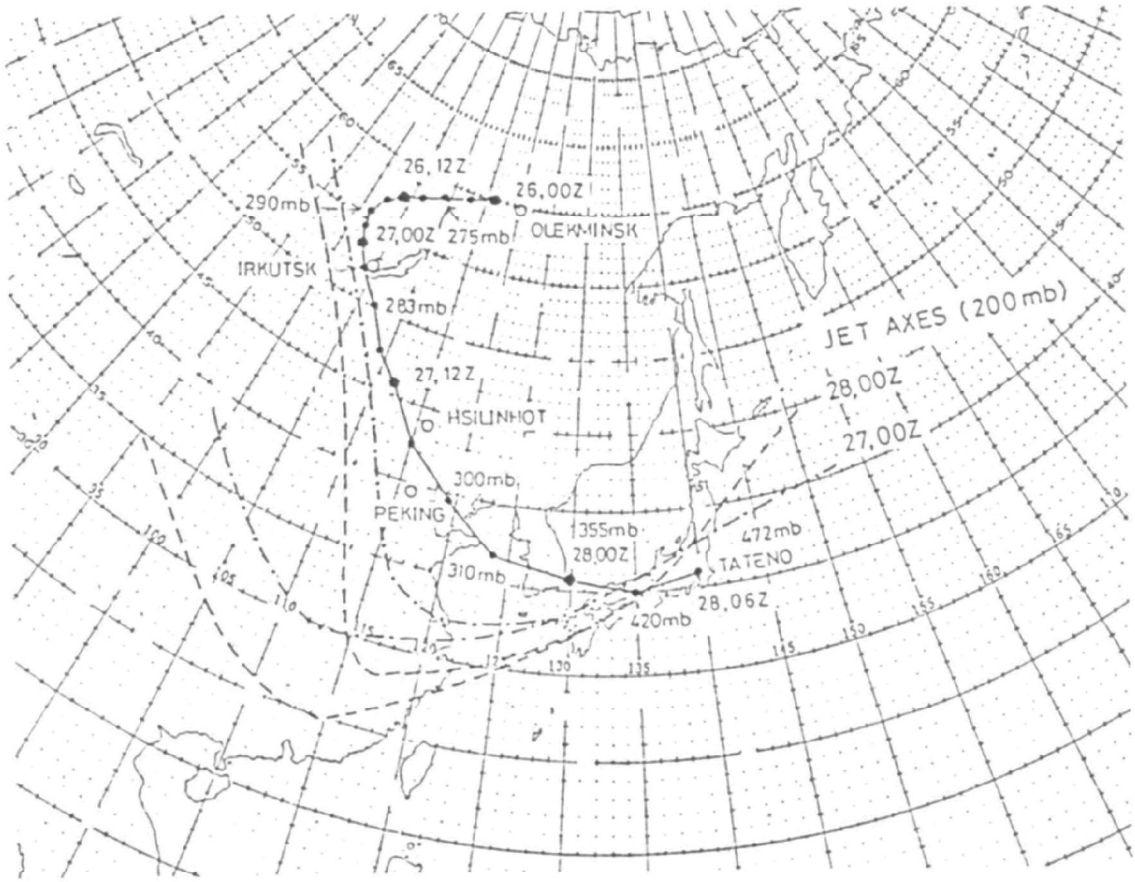

Fig.3 Isentropic trajectory on the 325°K surface from 26 May,00Z to 28 May,06Z, 1969. Jet axes on 200mb surface are indicated for 27 May,00Z (dash-dotted line) and 28 May, 00Z (dashed line)

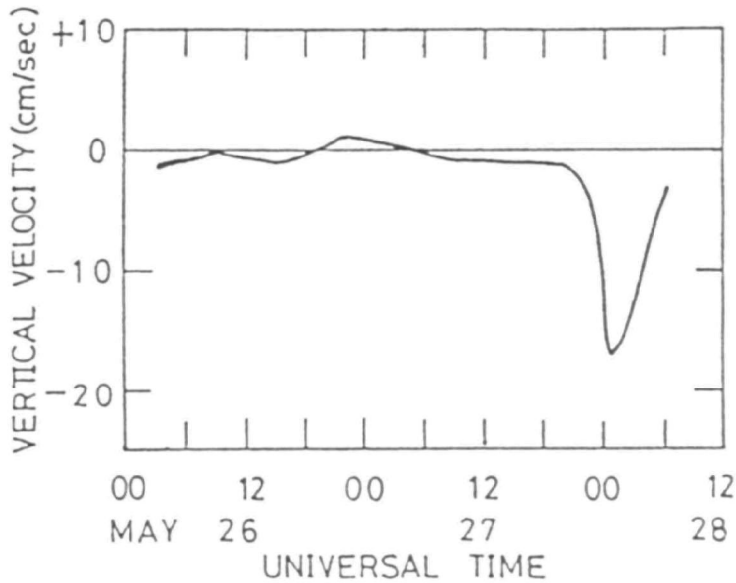

Fig.4 Vertical velocity (three hour average) of the air parcel from 26 May to 28 May 1969

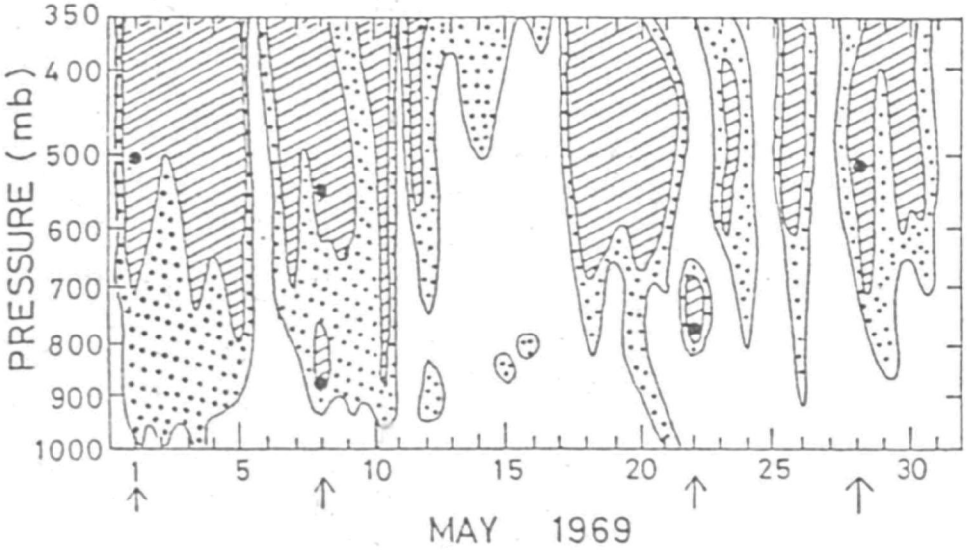

Fig.5 Time section of the relative humidity for Tateno in May 1969. Area with relative humidity less than 20% are marked by slanting lines, those with less rhan 50% but over 20% are stippled. Arrows show the days on which ozone sonde observation was made. Filled circles show the height of the maximum ozone concentration.

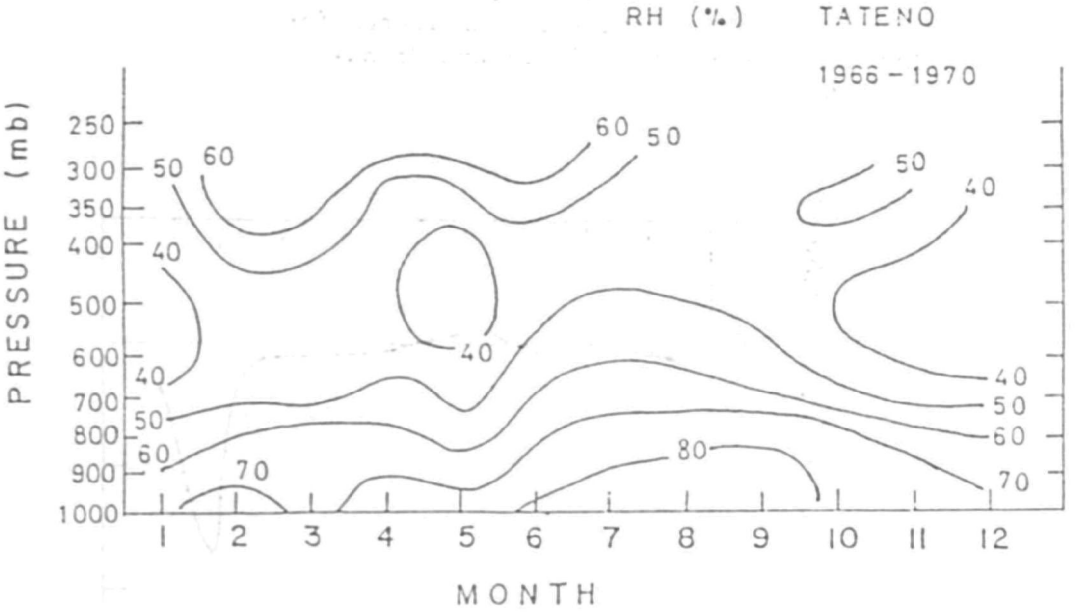

Fig.6 Distribution of the relative humidity(%) over Tateno averaged for the period 1966 to 1970.

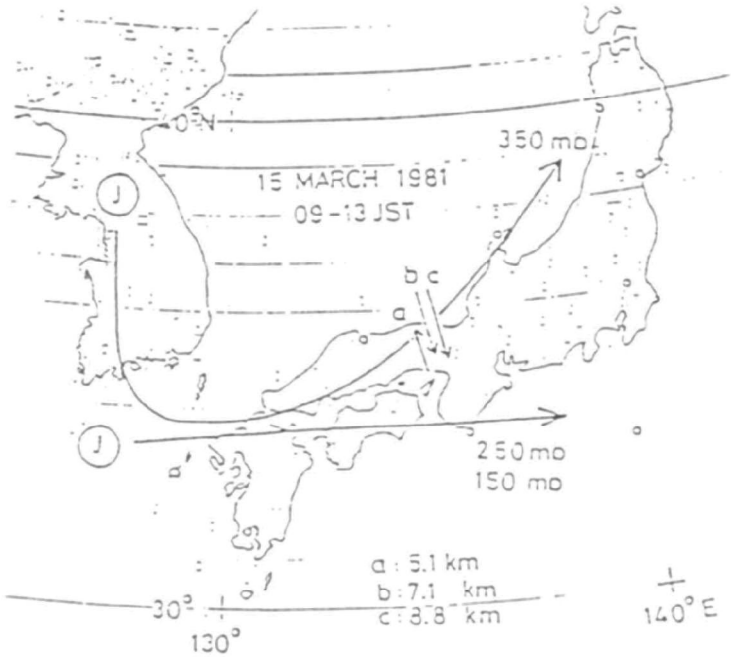

Fig.7

Flight courses and the jet streams

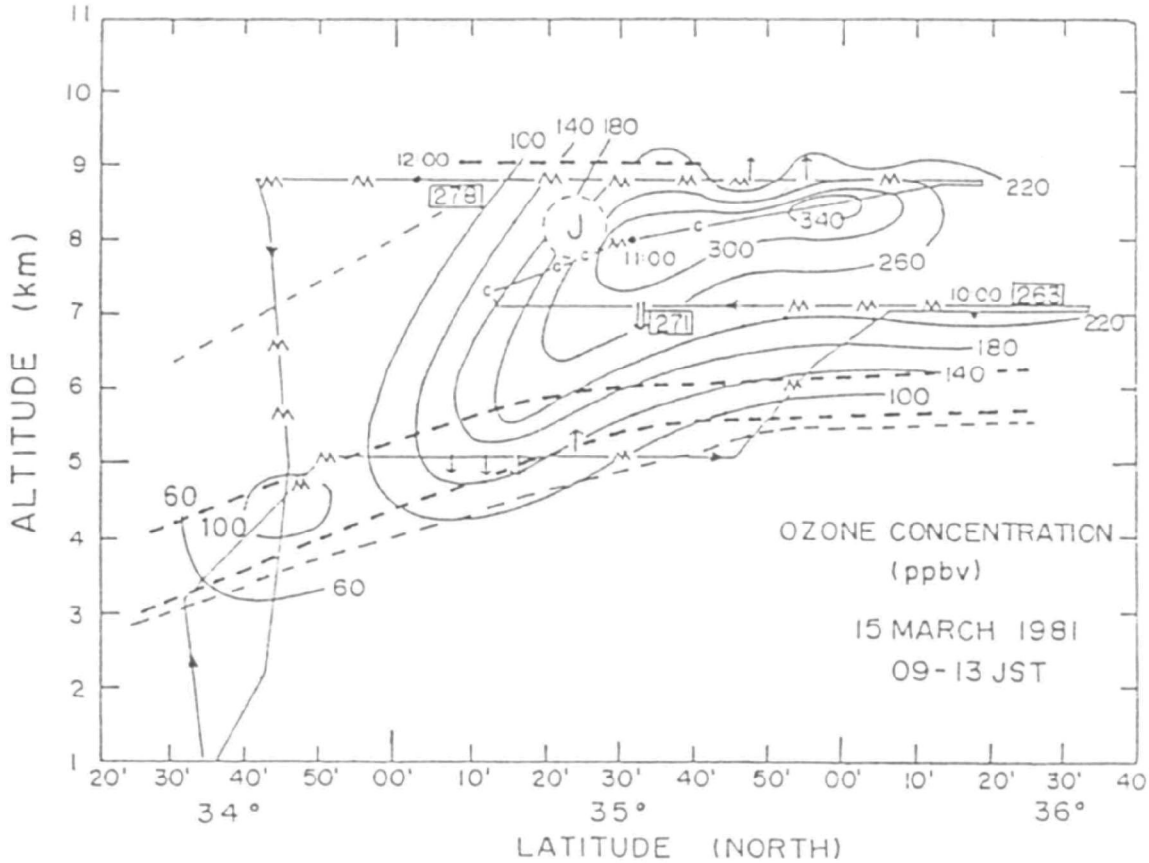

Fig.8 Meridional cross section along 140°E. Solid curves show the ozone concentration (ppbv); heavy broken curves, frontal boundaries and tropopause; solid line with arrows, flight course; ↑ and ↓ show the position of upward and downward winds; ⋀ shows the posotions where the heavy vibration of aircraft was observed; c shows the position of no vibrations; thin broken lines show the boundary of relative humidity below 20%.

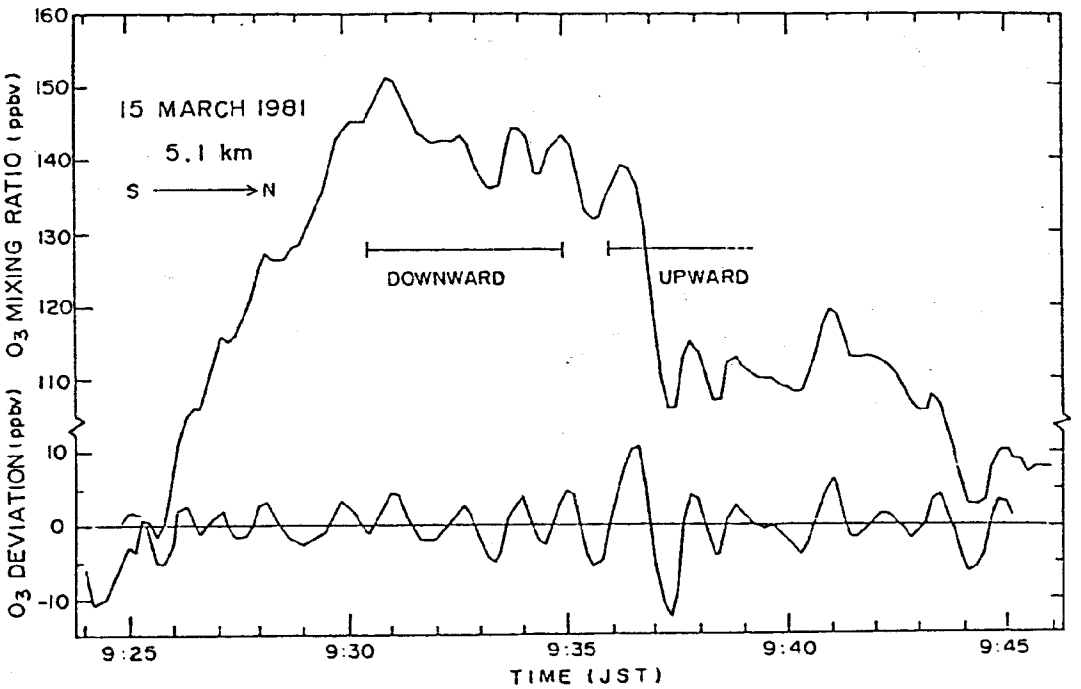

Fig.9 Horizontal ozone distribution and its deviation at 5.1 km across the frontal boundary. DOWNWARD and UPWARD show the region where the downward and upward winds was observed.

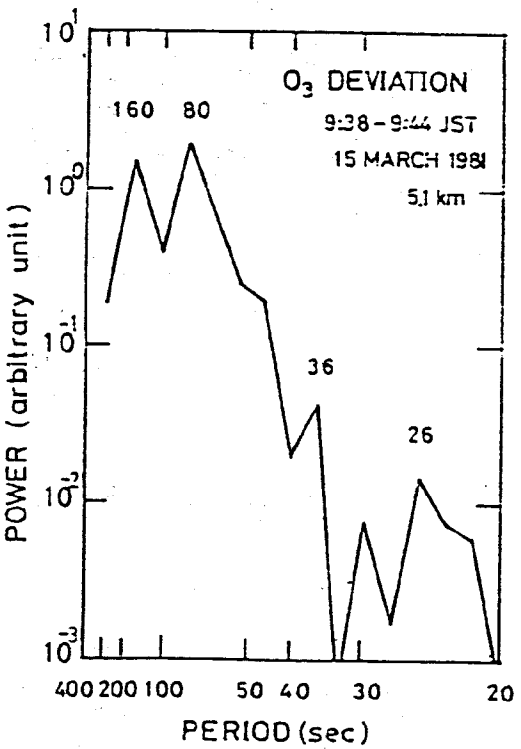

Fig.10 Power spectrum of the ozone deviation on the north of the frontal boundary.

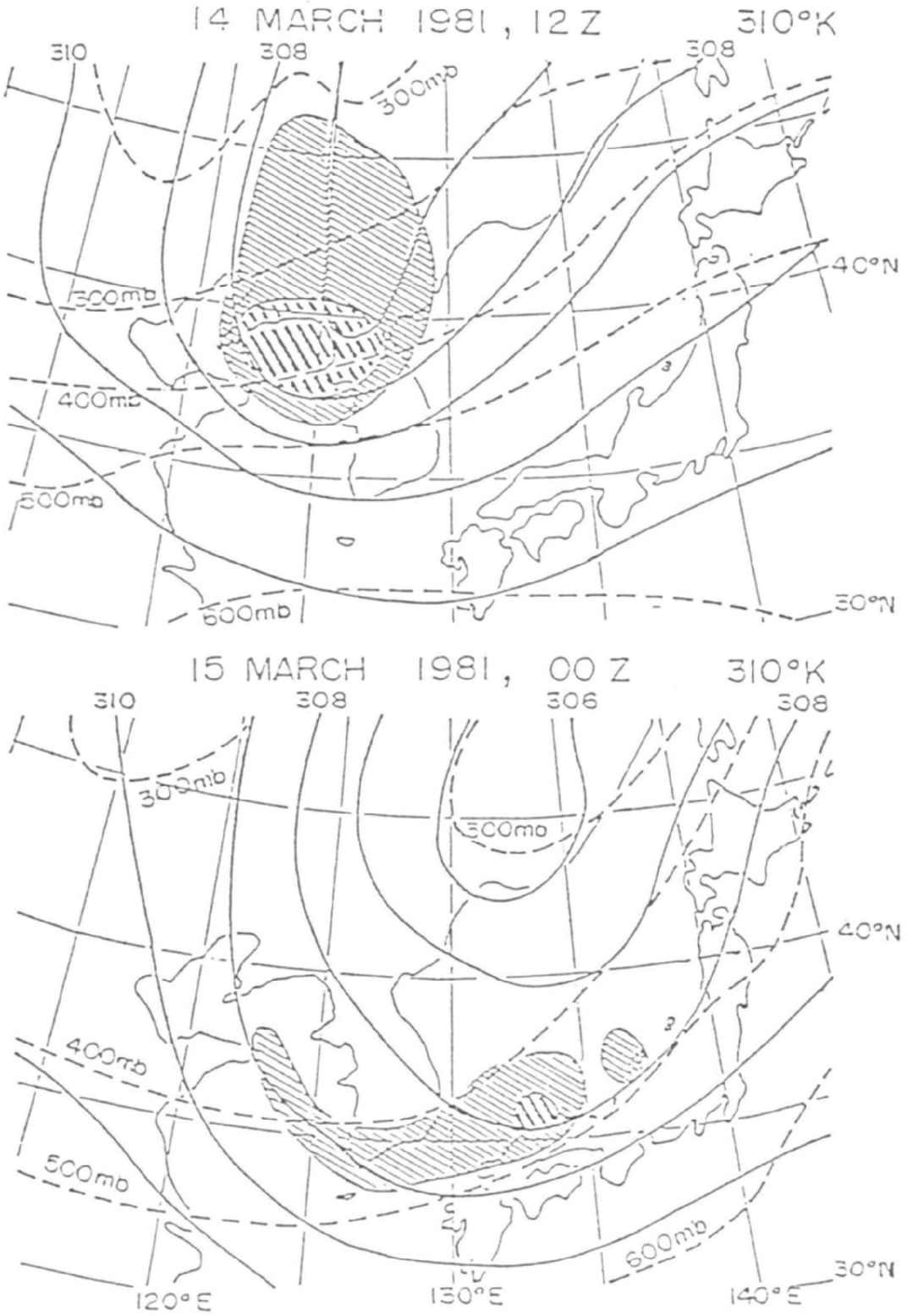

Fig.11 Deviation of the potntial vorticity on the 310°K isentropic surface.
Solid curves show the Montgomery stream function (10^7 erg/g); broken curves, pressure; region of the potential vorticity higher than 6×10^{-5} and 3×10^{-5} °K/mb/sec are shown by heavy and thin slanting lines, respectively.

THE VERTICAL DISTRIBUTION OF CF_2Cl_2, $CFCl_3$ AND N_2O OVER JAPAN

presented by M. Hirota

Meteorological Research Institute

Japan MA

THE VERTICAL DISTRIBUTIONS OF CF_2Cl_2, $CFCl_3$ AND N_2O OVER JAPAN

Michio HIROTA, Hisafumi MURAMATSU, Yukio MAKINO
and Toru SASAKI

Meteorological Research Institute
1-1, Nagamine, Yatabe-machi, Tsukuba-gun, Ibaraki-ken, JAPAN

The atmospheric CF_2Cl_2, $CFCl_3$ and N_2O are thought as the major sources of the stratospheric ClO_x and NO_x respectively. If such species are released in large quantities by man's activity, the natural balance of the stratospheric ozone will be damaged.

It is known that these compounds, especially CF_2Cl_2 and $CFCl_3$, are recently being accumulated in the tropsphere. In order to assess the influence of these compounds on the natural ozone balance, the atmospheric concentrations and distributions of these compounds must be examined.

In this paper, our observations over Japan since 1978 will be reported.

EXPERIMENTAL

Sampling of air and the gas-chromatographic analysis are described in the previous paper(Misaki et al., 1980). In order to return the sampling can on land, collections of the stratospheric air samples were performed only in summer.

RESULTS AND DISCUSSION

Typical vertical profiles of CF_2Cl_2, $CFCl_3$ and N_2O are shown in Fig. 1. These compounds were well mixed in the troposphere except over the urban area up to the altitude of 2 km where the higher mixing ratios of CF_2Cl_2 and $CFCl_3$ were observed. Mean tropospheric mixing ratios for each observation period are summarized in Table 1. All three compounds show increasing trends from 1978 to 1981. Increasing trends of CF_2Cl_2 and N_2O, however, are not clear because only one observation was performed in 1982.

Vertical profiles of CF_2Cl_2, $CFCl_3$ and N_2O in the stratosphere are shown in Figs. 2 - 4. These were observed in summer from 1978 to 1982, and annual variations could not be observed in the range of the experimental error. Vertical profiles of these compounds were compared with those obtained by a one-dimentional photochemical-diffusive model(solid lines in Figs. 2 - 4). In the model calculation, an eddy-diffusion coefficient profile was obtained using vertical profiles of N_2O. Table 2 shows the estimated fractional change in O_3 due to CF_2Cl_2 and $CFCl_3$ in 1980. Total O_3 depletion was 0.6%.

Table 1. Mean volume mixing ratios of CF_2Cl_2, $CFCl_3$ and N_2O in the troposphere

Observation period	Altitude	CF_2Cl_2/ppt*1	$CFCl_3$/ppt*1	N_2O/ppb
Oct. '78 - Mar. '79	→ 7.4 km	28_2(51)*2 SD=2_1	16_2(53)*2 SD=1_9	31_0(90) SD=1_4
Oct. '79 - Feb. '80	→ 13.6 km	29_9(13) SD=2_6	17_9(11) SD=$_7$	32_8(88) SD=1_3
Dec. '80 - Mar. '81	→ 9.3 km	29_4(62) SD=1_0	18_4(12) SD=1_3	32_8(45) SD=1_2
Feb. '82	→ 8.1 km	30_6(17) SD=$_5$	18_8(21) SD=$_5$	33_5(35) SD=$_9$

*1: Values over the urban area up to the altitude of 2 km are excluded.

*2: 4 values obtained in Mar. '78 are included.

SD: standard deviation, number in ( ): number of samples.

Table 2. The fractional change in O_3 due to CF_2Cl_2 and $CFCl_3$ in 1980

Altitude (km)	Fractional change in O_3(%)		
	CF_2Cl_2	$CFCl_3$	CF_2Cl_2+$CFCl_3$
55	-0.59	-0.34	-0.93
51	-1.13	-0.67	-1.76
47	-2.32	-1.44	-3.68
43	-3.80	-2.38	-6.11
39	-2.71	-1.81	-4.43
35	-0.93	-0.70	-1.63
31	-0.09	-0.16	-0.26
27	+0.04	-0.07	-0.04
23	+0.05	-0.03	+0.03
19	+0.15	+0.09	+0.23
15	+0.13	+0.07	+0.23
total	-0.29	-0.26	-0.55

In the calculation of the total O_3 depletion, its effect on the tropospheric O_3 is neglected.

Figure captions

Fig.1 Vertical profiles of CF_2Cl_2, $CFCl_3$ and N_2O in the troposphere

Air samples were collected on Cessna 404.

Flight cource: Haneda - Hachijojima(Feb. 14-16) and Haneda - Sendai(Feb. 18)

Fig.2 Vertical profile of CF_2Cl_2 in the stratosphere

In 1978, air sample was collected in a plastic bag of 250 l.

——: vertical profile calculated from a 1-D model

\\\\: range of the tropospheric mixing ratios

( ): value for which large experimental error was considered

Fig.3 Vertical profile of $CFCl_3$ in the stratosphere

——, \\\\, ( ): same as in Fig.2

Fig.4 Vertical profile of N_2O in the stratosphere

◎ : Ram air was sampled on DC-9, TDA over Osaka on Jan. 8, 1979.

——, \\\\, ( ): same as in Fig.2

Fig. 1

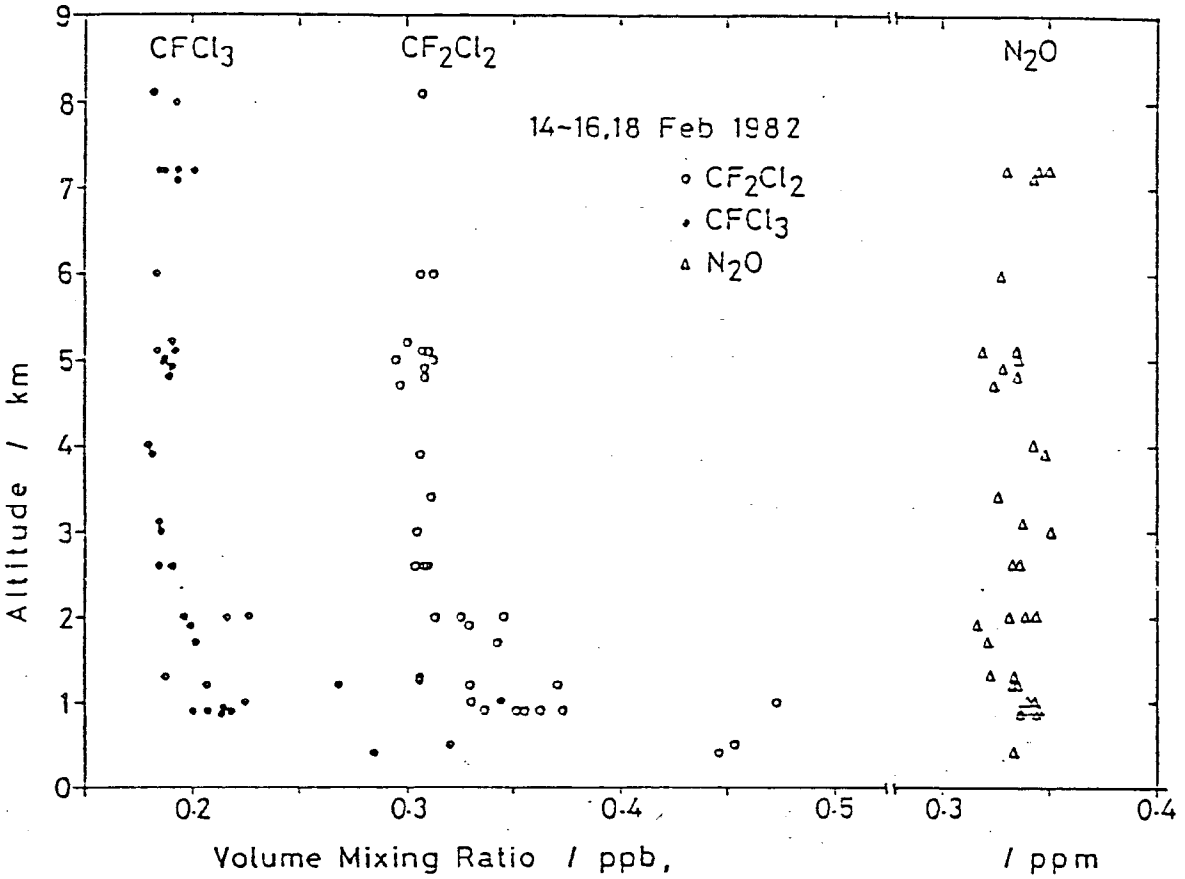
CFCl3
CF2Cl2
N2O
14-16,18 Feb 1982
CF2Cl2
CFCl3
N2O
Altitude / km
Volume Mixing Ratio / ppb,
/ ppm

Fig. 2

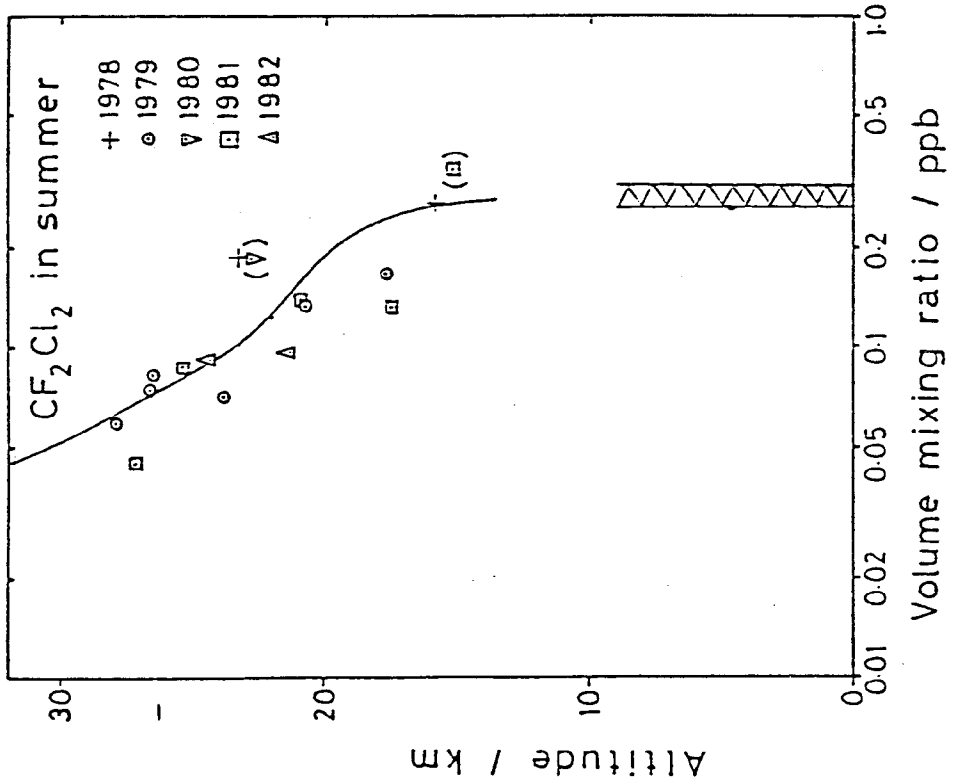
CF2Cl2 in summer
1978
1979
1980
1981
1982
Altitude / km
Volume mixing ratio / ppb

Fig. 4

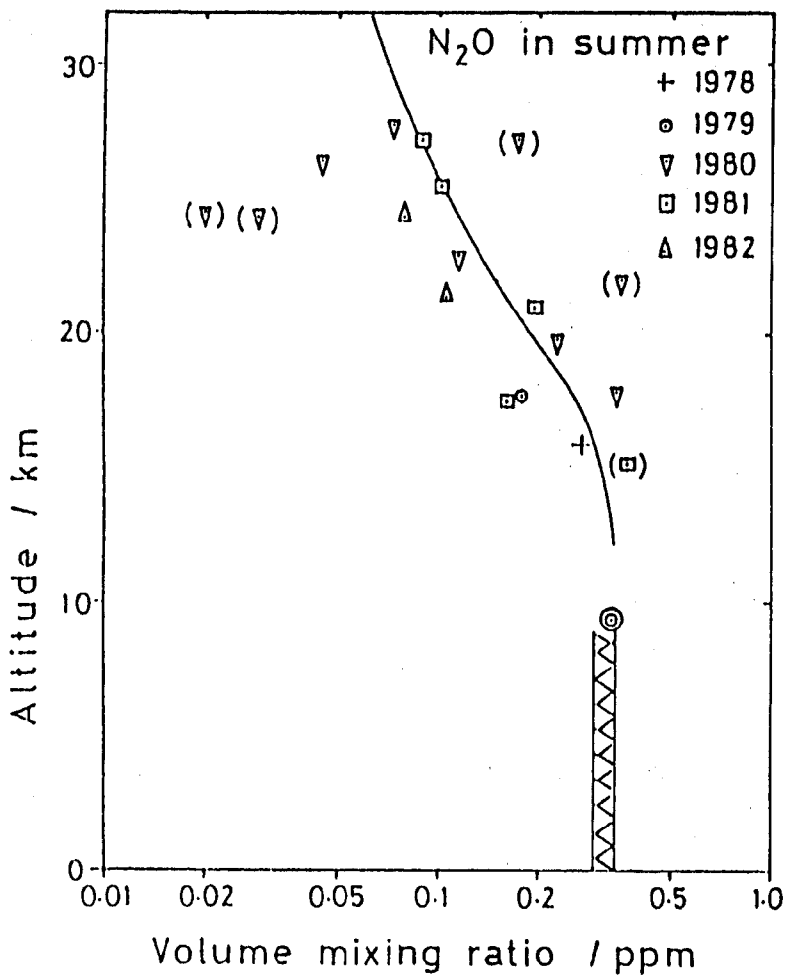
N_2O in summer
+ 1978
⊙ 1979
∇ 1980
⊡ 1981
Δ 1982
Altitude / km
Volume mixing ratio / ppm
0
10
20
30
0·01
0·02
0·05
0·1
0·2
0·5
1·0

Fig. 3

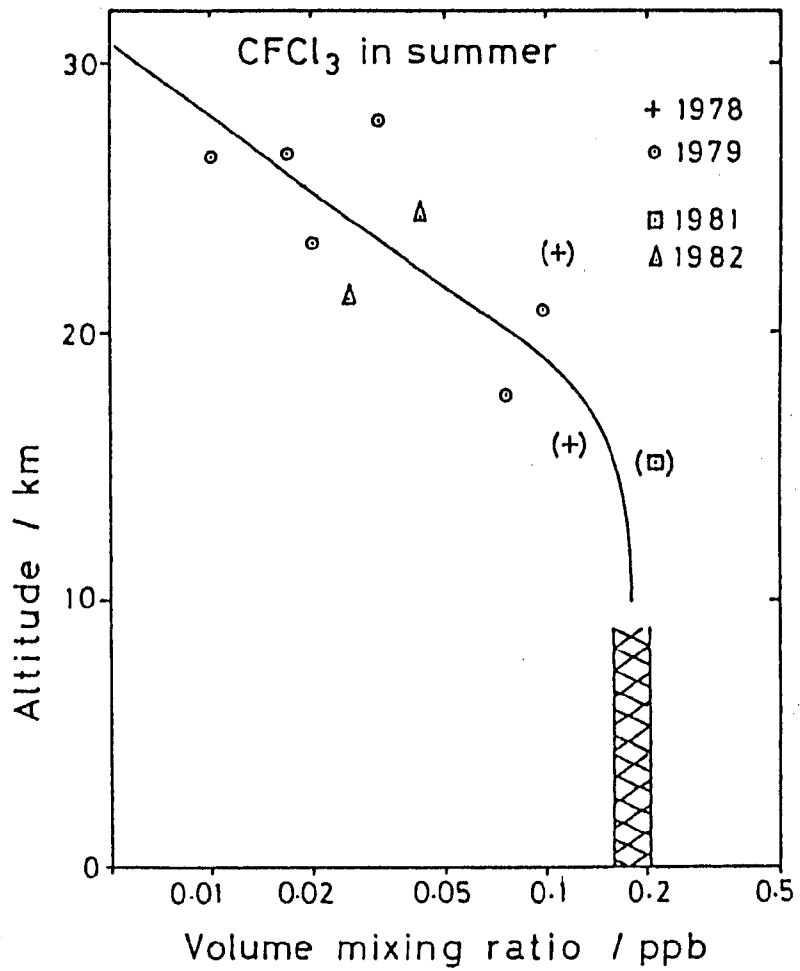
$CFCl_3$ in summer
+ 1978
⊙ 1979
⊡ 1981
Δ 1982
Altitude / km
Volume mixing ratio / ppb
0
10
20
30
0·01
0·02
0·05
0·1
0·2
0·5